Durham E-Theses

Mechanistic studies of azolium ions and their role in organocatalysis

MASSEY, RICHARD,STEPHEN

Mechanistic studies of azolium ions and their role in organocatalysis

RICHARD S. MASSEY

A thesis submitted in partial fulfilment of the requirements for the degree of Doctor of Philosophy

Durham University

Department of Chemistry
Durham University

May 2013

Declaration

The work described in this thesis was carried out at the Department of Chemistry, Durham University, between October 2009 and May 2013, under the supervision of Dr. AnnMarie O'Donoghue. The material contained has not been previously submitted for a degree at this or any other university. All work has been carried out by the author unless otherwise indicated.

R. S. Massey

Copyright

Abstract

Azolium ion precursors to N-heterocyclic carbenes (NHCs) have risen to prominence as versatile organocatalysts for a broad range of synthetic transformations. In recent years, methodologies have been developed for the generation and exploitation of azolium homoenolates, azolium enolates, and acyl azolium intermediates, leading to a diverse range of asymmetric products. It is common in many synthetic procedures to generate the active NHC *in situ* by deprotonation of the parent azolium ion. Knowledge of the kinetic and thermodynamic acidities of these species is therefore an essential first step in understanding their catalytic behaviour.

We have used a kinetic method to determine kinetic acidities and aqueous pK_a values for a set of triazolium, thiazolium and imidazolium ions at the C(3)-H or C(2)-H positions. Using ^{1}H NMR spectroscopy to follow deuterium exchange, pseudo-first-order rate constants for exchange, k_{ex} (s^{-1}), were determined at a range of pDs in D$_2$O at 25 °C and $I = 1.0$ (KCl), from which second-order rate constants for deprotonation by deuteroxide ion, k_{DO} (M^{-1} s^{-1}) could be obtained. By application of a secondary solvent isotope effect ($k_{DO}/k_{HO} = 2.4$), corresponding values of k_{HO} were calculated. General base catalysis experiments support the conclusion that the rate constant for carbene protonation by solvent water is limited by solvent reorganisation, and occurs with a rate constant of $k_{HOH} = k_{reorg} = 10^{11}$ s^{-1}. These values of k_{HO} and k_{HOH} permitted the calculation of carbon acid pK_a values for ionisation of the azolium ion in water. For a homologous series of catalytically-relevant triazolium salts, the effect of the *N*-aryl substituent on values of k_{DO} and pK_a was probed, and comparisons between azolium ion families will be made. The pD-rate profile of an *N*-C$_6$F$_5$ substituted triazolium ion indicates that in acidic media, protonation at the N(1) position may occur to give a dicationic triazolium ion.

Using this methodology, the kinetic acidities of the conjugate acids of 'mesoionic' or 'abnormal' carbenes were also investigated. For a series of 1,2,3-triazolium ions and C(2)-alkylated 1,3-imidazolium ions, rate constants for exchange at the C(4)-H and C(5)-H positions were determined. Our results suggest that these sites are 10^5-fold less acidic than the C(3)-H and C(2)-H positions of 'classical' triazolium and imidazolium ions. To explain the deviation from a first-order dependence on deuteroxide ion for the

imidazolium ions in strong KOD solution, we have proposed a number of exchange pathways that proceed *via* a hydrate. The effects of *N*-aryl substituent and counterion on k_{DO} and pK_a are also discussed.

We have also conducted mechanistic studies of the triazol-3-ylidene-catalysed benzoin condensation. *In situ* ^{1}H NMR spectroscopic studies of the reaction in triethylamine-buffered methanol-d$_4$ at 25 °C show that the 3-(hydroxyaryl)triazolium adduct, generated from addition of the NHC to the aldehyde, is the only intermediate observed over the course of the reaction. Evidence is presented to show that the formation of these intermediates under these conditions is reversible, and reliable equilibrium and rate constants for the formation of these species have been determined using independent approaches. Our results suggest that *N*-mesityl substituents on the catalyst, and *ortho*-alkoxyl groups on the aromatic aldehyde result in significantly enhanced equilibrium concentrations of this intermediate. Slow deprotonation of these intermediates results in the benzoin product. Rate constants for the deprotonation step suggest that electron-deficient adducts result in the fastest rates of deprotonation.

Finally, an initial rates study of the benzoin condensation at catalytic concentrations of azolium ion precatalyst has also been undertaken. An HPLC analysis method was used to determine the concentrations of benzoin and benzaldehyde over the course of the reaction in triethylamine-buffered methanol at 50 °C. Our results suggest that the thiazolium-catalysed reaction is first-order with respect to aldehyde over the full range of benzaldehyde concentrations studied (0.32 – 1.60 M). In contrast, the triazolium-catalysed reaction displays a first-order dependence at low aldehyde concentrations, before changing to a zero-order dependence at higher benzaldehyde concentrations. From the maximum rate of catalysis in this zero-order region, the effect of *N*-aryl substituent on rate of turnover was investigated for a homologous series of triazolium precatalysts.

Contents

Abbreviations

A	absorbance		λ	wavelength
Ac	acetyl		**L**	litre(s)
Ad	adamantyl		**LC-MS**	liquid chromatography with mass spectrometry
Ar	aryl			
aq.	aqueous		**ln**	natural logarithm
br.	broad (spectral)		**log**	logarithm (base 10)
Bu	butyl		**M**	molar (moles/litre)
ºC	degree centigrade		*m-*	*meta*
cm^{-1}	wavenumbers		**m**	multiplet (spectral)
^{13}C NMR	carbon nuclear magnetic resonance		**Me**	methyl
			MeO	methoxy
Cq	quarternary carbon		**m.p.**	melting point
δ	chemical shift		**Mes**	mesityl
d	doublet		**µL**	microlitre(s)
DCM	dichloromethane		**min**	minute(s)
Dipp	diisopropylphenyl		**mL**	millilitre(s)
DMSO	dimethyl sulfoxide		**mmol**	millimole(s)
D$_2$O	deuterium oxide		**mol**	mole(s)
dr	diasteromeric ratio		**m/z**	mass per unit charge
EA	elemental analysis		**NaOH**	sodium hydroxide
ee	enantiomeric excess		**NHC**	N-heterocyclic carbene
Et	ethyl		*o-*	*ortho*
EtOAc	ethyl acetate		*p-*	*para*
eq.	equivalent		**Ph**	phenyl
g	gram(s)		**PhCHO**	benzaldehyde
HCl	hydrochloric acid		**ppm**	parts per million
^{1}H NMR	proton nuclear magnetic resonance		**R**	alkyl substituents
			Rt	retention time
h	hour(s)		**r.t.**	room temperature
HPLC	high performance liquid chromatography		**ρ**	reaction constant
			σ	substituent constant
Hz	hertz		**s**	second(s)
^{i}Pr	isopropyl		**s**	singlet (spectral)
IR	infra red		**t**	triplet (spectral)
J	coupling constant		*t-, tert-*	tertiary
k	rate constant		**THF**	tetrahydrofuran
K	equilibrium constant		**UV**	ultraviolet
K$_a$	acidity constant		**Vis**	visible
kcal	kilocalorie(s)			

CHAPTER   1

Introduction

1.0   Foreword

Beginning with Breslow's groundbreaking mechanistic study of the thiamine-catalysed benzoin condensation in 1958, N-heterocyclic carbenes (NHCs) have long been implicated as important species with organocatalytic potential. For many years, their role as organocatalysts was limited to two reactions – the benzoin condensation and Stetter reaction. However, following the isolation of other stable NHCs in the early 1990s, the past two decades have seen extensive research not only in terms of catalyst design, but also in the breadth of new transformations to which NHCs may be applied. Whilst a large number of very effective triazolylidene catalysts are now available, only a handful of kinetic investigations have been made since Breslow's seminal work.

The main aim of this thesis is to gain a greater understanding of the mechanism of the NHC-catalysed benzoin condensation – a model reaction that involves the generation of intermediates implicated in a range of other NHC-catalysed transformations. This chapter reviews a selection of important reactions that are catalysed by these species, and in particular, studies the progress that has been made towards design of effective azolium ion precatalysts for the benzoin condensation.

1.1   N-Heterocyclic Carbenes: Structure and Isolation

1.1.1   Carbenes

Carbenes are neutral species containing a divalent carbon atom with six valence electrons. Four of these electrons are involved in bonding to the two substituents, while two non-bonding electrons remain on the carbon atom. These non-bonding electrons may be paired in the same orbital (singlet state) or separate orbitals (triplet state). Carbene geometries may be described as bent or linear and are dictated by the degree of hybridisation at the carbon centre (Figure 1.1).[1]

Figure 1.1:   Singlet and triplet carbene states
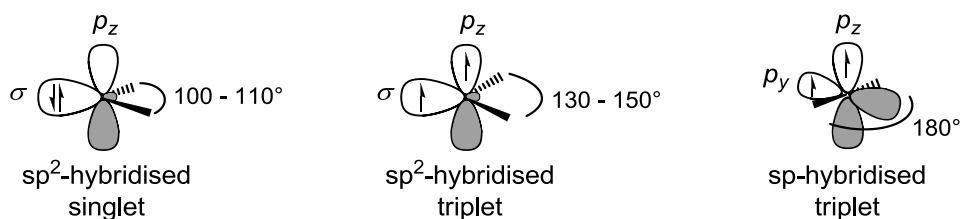
Linear geometries are based on a sp-hybridised carbon, consisting of two bonding σ orbitals and two degenerate non-bonding orbitals (p_y and p_z). As these orbitals are degenerate, the electrons remain unpaired to minimise electronic repulsion. Linear geometry may be considered an extreme case, limited to carbenes sterically restricted by bulky substituents. Most carbenes are based on a trigonal sp^2-hybridised carbon centre, resulting in a bent geometry with bond angles typically in the region of 100 – 150°. In this arrangement, the non-bonding σ and p_z orbitals are no longer degenerate, and the non-bonding electrons may be paired in the same orbital (singlet state) or separate orbitals (triplet state). Ground state multiplicity strongly dictates carbene reactivity, with triplet carbenes expressing diradical behaviour, whilst singlet carbenes – with a filled and vacant orbital – possess ambiphilic character.

The ground state multiplicity of a carbene is determined by the relative energies of the σ and p_z orbitals. Singlet states are preferred where these orbitals are separated by a large energy difference. The size of this σ–p_z gap is strongly influenced by the electronic properties of neighbouring substituents – a combination of inductive and mesomeric effects. Inductively electron-withdrawing groups are known to favour singlet carbenes by stabilising the σ orbital whilst leaving the p_z orbital unaffected, increasing the σ–p_z energy gap and favouring a singlet state. Conversely, inductively donating substituents will stabilise a triplet state by destabilising the σ orbital relative to the p_z orbital. Mesomeric effects, resulting from interactions between the p or π orbitals on substituent atoms and those on the carbene centre, can play an even greater role in dictating carbene geometry and multiplicity. Carbene resonance stabilisation systems can be divided into three main groups depending on the nature of the α-substituents.[2]

Figure 1.2:   Mesomeric stabilisation

(a) diaminocarbenes   (b) diborylcarbenes   (c) phosphinosilylcarbenes
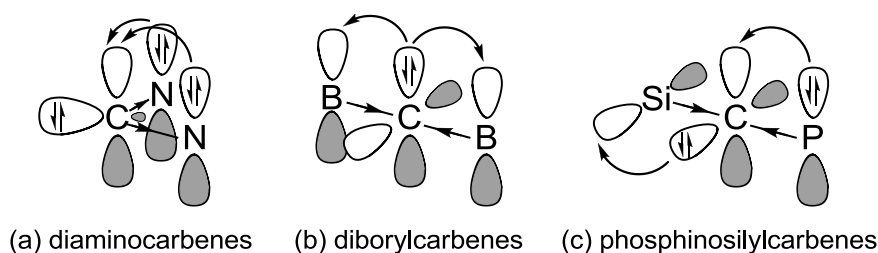
Bent singlet carbenes are strongly stabilised by the interaction between the empty p_z orbital on the carbon and lone-pairs on adjacent atoms (*e.g.* NR_2, OR, F or SR) (Figure 1.2a). π-Donation from atoms adjacent to the carbene centre will increase electron density in the p_z orbital, increasing the σ–p_z energy gap and favouring the singlet ground state. Examples include transient species such as dihalocarbenes[3] and dimethoxycarbenes,[4] which are found to spontaneously dimerise, and the stable diaminocarbenes, including the isolable NHCs that are the focus of this thesis.

Carbenes bearing two π-acceptor substituents (*e.g.* CF_3, BR_2, SiR_3 or PR_3^+) are predicted to have singlet multiplicity with linear geometry. Symmetric interaction between the vacant p orbitals on the α-substituent and filled p orbitals on the carbene breaks the p orbital degeneracy, resulting in a singlet state with a two-electron, three-centre π-resonance system (Figure 1.2b). Such species have never been isolated, although studies of transient dicarbomethoxycarbenes[5] and the reactivity of 'masked' analogues of diborylcarbenes support these predictions.[6]

A combination of π-donor and π-acceptor groups typically results in quasi-linear geometry with singlet multiplicity (Figure 1.2c). Interaction between the filled p orbital on the π-donor group to the vacant p_y orbital on the carbene increases the energy of the p_y orbital, whilst the interaction between the filled p_z orbital on the carbene and the π-acceptor substituent stabilises the p_z orbital. Both of these effects stabilise the singlet state by increasing the energy gap between the p_y and p_z orbitals. Examples of such carbenes include transient halogencarboethoxycarbenes[7] and stable phosphinosilyl- and phosphinophosphonio-carbenes, which have been isolated.[8]

The electronic effects described above demonstrate that it is often easier to design a substitution system to stabilise a singlet rather than a triplet carbene. Indeed, the predominant method for stabilisation of highly reactive triplet carbenes is by means of steric protection, using bulky substituents such as trifluoromethyl groups which confer kinetic stability.

1.1.2   Isolation of NHCs

The investigations detailed in this thesis focus on the chemistry of N-heterocyclic carbenes (NHCs). Four key NHC families **1 – 4** have come to dominate organocatalysis and transition-metal catalysis, and are shown in Figure 1.3.

Figure 1.3:   NHC families

1	**2**	**3**	**4**
thiazol-2-ylidene	imidazol-2-ylidene	imidazolin-2-ylidene	triazol-3-ylidene
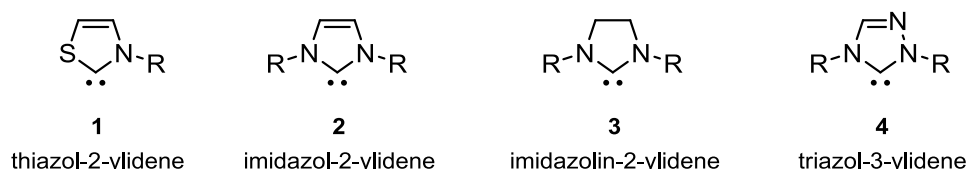
Amongst the earliest evidence for the existence of carbenes may be found in the pioneering work of Curtius and Staudinger in the late 19th and early 20th centuries.[9] Their highly reactive nature prevented isolation and, as such, carbenes were regarded as transient intermediates. Stable NHCs were first proposed in the seminal work of Breslow in the late 1950s, and further research by Wanzlick in the 1960s demonstrated that the stability of singlet carbenes could be significantly enhanced by the presence of α-amino substituents. This increased stability may be explained by the mesomeric-inductive 'push-pull' effects of the nitrogen atoms adjacent to the carbene centre, described in the previous section. Wanzlick's early attempts to isolate dihydroimidazol-2-ylidene **6** by thermal elimination of chloroform from **5** were unsuccessful and resulted in formation of the dimer **7** (Scheme 1.1).[10] However, in 1968 he did achieve the successful synthesis of an imidazol-2-ylidene from an imidazolium ion **8**, albeit as a metal stabilised complex **9** (Scheme 1.2).[11]

Scheme 1.1:
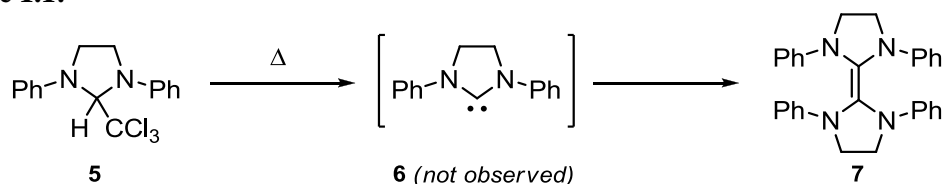
Scheme 1.2:
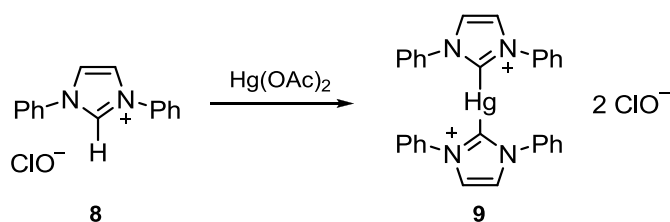
The first examples of stable carbene syntheses are regarded to be those of Bertrand[8a] and Arduengo[12] in 1988 and 1991, respectively. Arduengo's synthesis of imidazol-2-ylidene **11** (Scheme 1.3) from the parent imidazolium chloride salt **10** under anhydrous conditions is widely accepted as the first true stable carbene to be isolated and characterised.

Scheme 1.3:
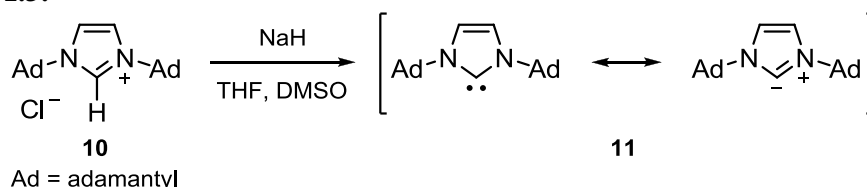
Since this important breakthrough, a large number of NHCs bearing a diverse range of architectures have been prepared by several groups.[1,13] Whilst the most common approach to NHC generation is by deprotonation of the parent azolium ion using a strong base, a number of alternative methods have been reported. In 1993, Kratz and Kuhn demonstrated that imidazol-2-ylidenes, such as **13**, could be generated in near-quantitative yield by reduction of the parent imidazole-2-thione **12** using potassium (Scheme 1.4).[14] Other groups have since applied this approach to the preparation of *N*-substituted imidazolin-2-ylidenes[15] and benzimidazolin-2-ylidenes.[16]

Scheme 1.4:
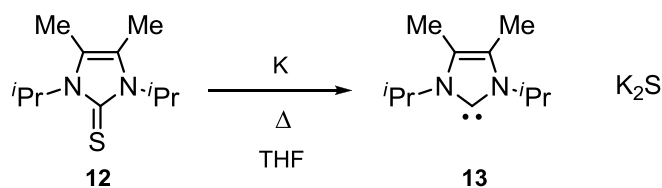
Alternatively, NHCs may be conveniently generated from 'masked carbenes' such as **15** and **17**, by thermal elimination of alcohol. Enders and co-workers first showed that triazolium salts, such as **14**, may be converted to 2-alkoxytriazoles **15** (R = Me, Et) in the presence of the corresponding alcohol under basic conditions (Scheme 1.5).[17] Upon heating, these species were found to generate the triazol-2-ylidene **16** in quantitative yield. Grubbs later adapted this approach to prepare a ruthenium complex incorporating imidazolin-2-ylidene ligand **18** from the parent 2-alkoxy-4,5-dihydroimidazole **17** (R = Me, *t*-Bu) (Scheme 1.6).[18]

Scheme 1.5:
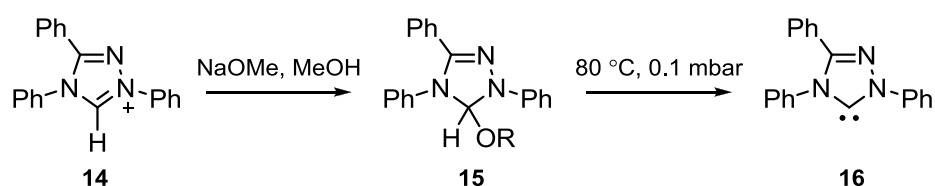
Scheme 1.6:
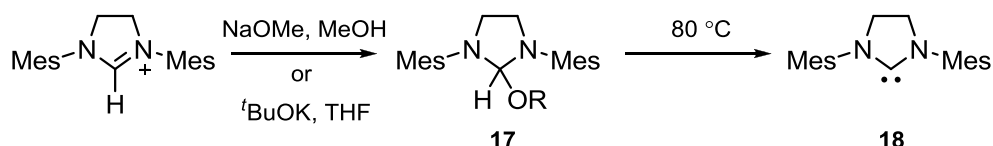
1.2 NHCs in Organocatalysis

1.2.1 Key intermediates

NHCs have long been implicated as organocatalysts for a number of transformations based on the principle of 'Umpolung' (reactions that proceed by reversal of conventional functional group polarity).[19] The groundbreaking developments in the preparation of stable carbenes have led to a rapidly growing interest in the use of these catalysts in a wider range of applications.[20] These reactions typically involve the preparation of the catalytic NHC species by *in-situ* deprotonation of the parent azolium ion by a non-nucleophilic base, followed by reaction of the carbene with an electrophilic substrate. Depending on the nature of the electrophile, one or more of four key reactive intermediates may be generated: the three nucleophilic acyl anion and enolate equivalent species **19 – 21**, and the electrophilic acyl azolium species **22** (Figure 1.4). An overview of typical reactions involving these intermediates will be explored in this section, paying particular attention to the benzoin and Stetter reactions which are the focus of our experimental investigations.

Figure 1.4:   NHC-generated synthons

1.2.2   Acyl anion equivalents (d^1 synthons)

Reaction of an NHC with an aldehyde **23** generates the acyl anion equivalent species **19**, formed from the deprotonation of an initially formed hydroxyaryl adduct **24** (Scheme 1.7). This d^1 synthon, commonly referred to as the 'Breslow intermediate', may react with a second aldehyde **23'** to give an α-hydroxyketone **25** *via* the benzoin condensation. Alternatively, the acyl anion may combine with an α,β-unsaturated ketone **26** (R$_3$ = alkyl) or ester **26** (R$_3$ = alkoxy) to give an 1,4-diketone or 1,4-diketoester **27** *via* the Stetter reaction.

Scheme 1.7:

1.2.2.1   The benzoin condensation

In 1943, Ugai found that the self-condensation of benzaldehyde **28** could be achieved using naturally occurring thiazolium salt thiamine (vitamin B$_1$) **29** in the presence of a mild base.[21] Mizuhara later showed that the compound's catalytic activity was derived from the thiazolium unit,[22] but mechanistic clarity was only brought about in a seminal paper by Breslow published in 1958.[23] Breslow's mechanism (Scheme 1.8), influenced by Lapworth's model of cyanide catalysis,[24] involves deprotonation of the thiazolium salt by a base at the acidic C(2)-H position to generate the catalytically active thiazol-2-

ylidene **30a**, which may be expressed in its ylide **30b** resonance form. This nucleophilic carbene may attack a molecule of benzaldehyde to generate the (α-hydroxybenzyl)thiazolium adduct **32**, which upon deprotonation may form the Breslow intermediate **33**. This species acts as a nucleophilic acylation reagent, and will react towards a second aldehyde molecule. Subsequent proton transfer steps and re-generation of the thiazol-2-ylidene yields benzoin **34**. Further kinetic and mechanistic studies of the benzoin condensation are discussed in detail in Chapter 4.

Scheme 1.8:
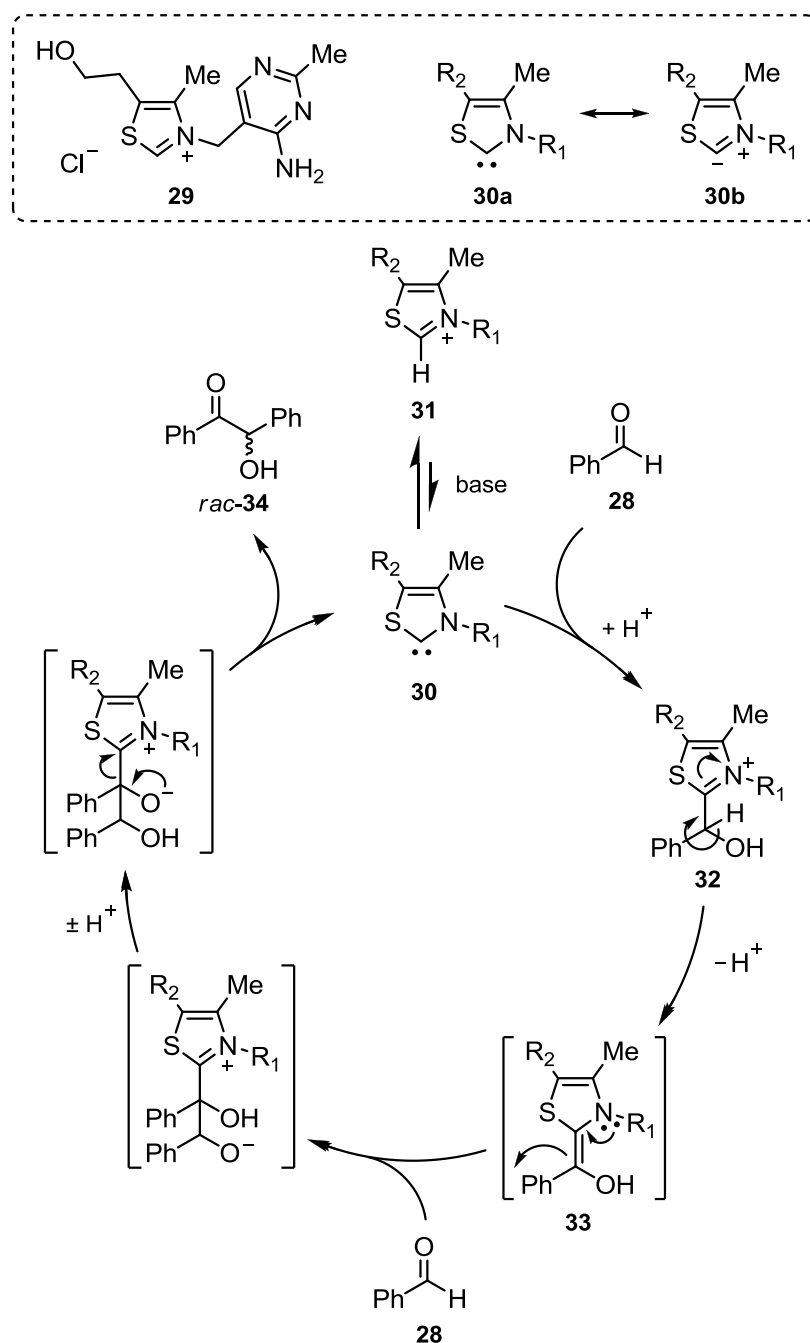
Early catalyst designs were based on chirally modified thiazolium salts, and generally gave poor results (Figure 1.5). In 1966, Sheehan reported the first asymmetric benzoin condensation using thiazolium catalyst **35** to give benzoin in 22% *ee*,[25] although the group later achieved *ee*s of up to 52% using catalyst **36**, albeit in very low yield.[26] Similar compromises between reactivity and enantioselectivity have been observed by other groups, including those of Takagi[27] and Leeper,[28] whose catalysts **37** and **38** also resulted in poor product stereoselectivity, despite their apparent steric bulk.

Figure 1.5:   **Development of asymmetric thiazolium catalysts**
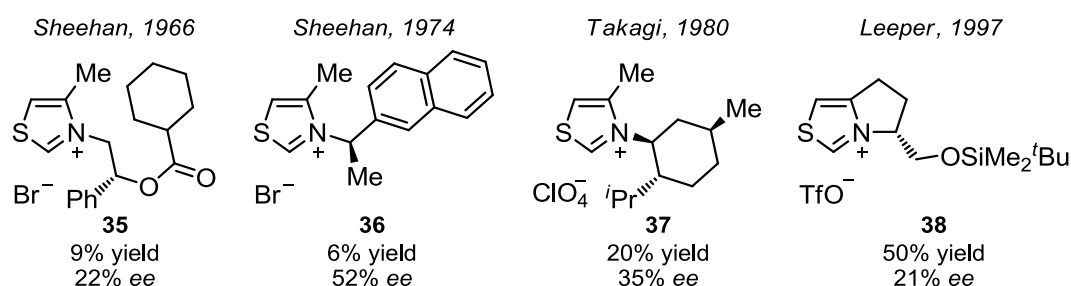
A novel approach towards catalyst design came in 1996 when Enders introduced the first chiral triazolium catalyst **39**, affording benzoin in 75% *ee* and 66% yield (Figure 1.6).[29] Shortly after, Leeper reported a range of bicyclic triazolium catalysts, including **40** and **41**, which selectively generated benzoin in up to 80% *ee*. These developments led to a flurry of novel triazolium salts based on bicyclic architecture, offering yields and enantioselectivities superior to the thiazolium salts used previously. In recent years incremental improvements have been made using catalysts **42 – 44**,[30, 31, 32] with Connon recently reporting benzoin *ee*s of up to 99% in excellent yield (90%) using catalyst **44**.

Figure 1.6:   **Development of asymmetric triazolium catalysts**
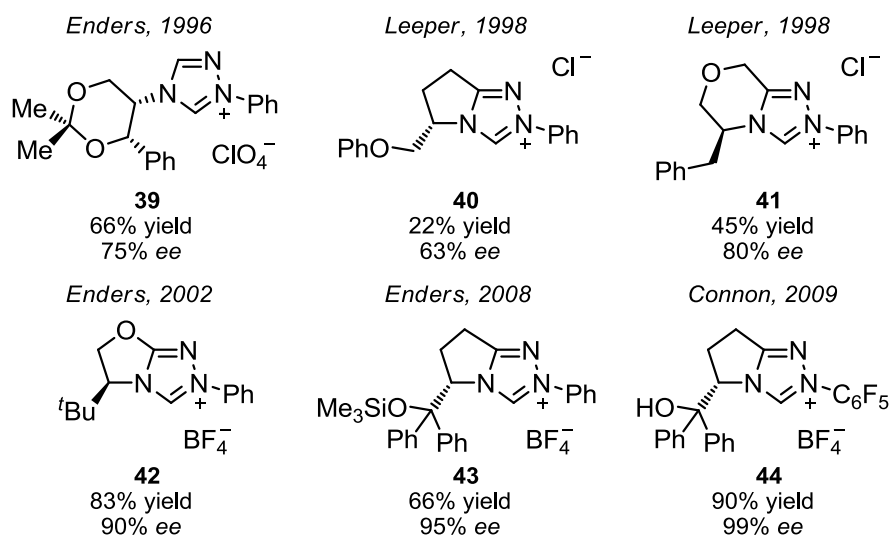
Whilst triazolium pre-catalysts have consistently outperformed related thiazolium salts in terms of both reactivity and enantioselectivity, there is little mechanistic clarity as to why this should be the case. One suggestion, commonly offered in the literature, refers to reports that thiazolium salts are prone to ring opening.[33] Alternatively, it may be that the steric bulk of the *N*-aryl group in bicyclic triazolium species (such as **40** – **44**) offer more enantioselective interaction than the relatively small sulphur atom in structurally similar thiazolium species (such as **38**).

A comparison between these structurally similar triazolium and thiazolium catalysts, performed by Leeper, resulted in divergent stereochemical outcomes.[34] Whilst catalysts **45** and **41** (Figure 1.7) have the same stereochemistry, the benzoin product of **45** is (*R*) and that of **41** is (*S*). This interesting result may be explained by the proposed transition state structures **46‡** and **47‡**, with the steric constraints of the *N*-phenyl substituent on **41** forcing attack at the *re*-face of benzaldehyde.

Figure 1.7: **Leeper's proposed transition state structures for the asymmetric benzoin condensation**
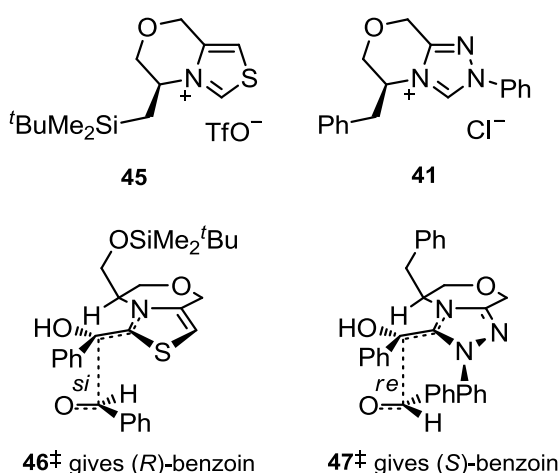
A computational modelling investigation carried out by Dudding and Houk also supports the idea of stereoselective control by avoidance of an unfavourable *N*-aryl interaction.[35] For a sample of chiral triazolium and thiazolium pre-catalysts, including structures **42** and **48**, the group optimised the geometries of the acyl anion-benzaldehyde transition state for *re* and *si* benzaldehyde approaches and *E* and *Z* acyl anion structures. Figure 1.8 shows the two lowest energy transition states in each case.

Figure 1.8: **Proposed transition state structures for the asymmetric benzoin condensation**
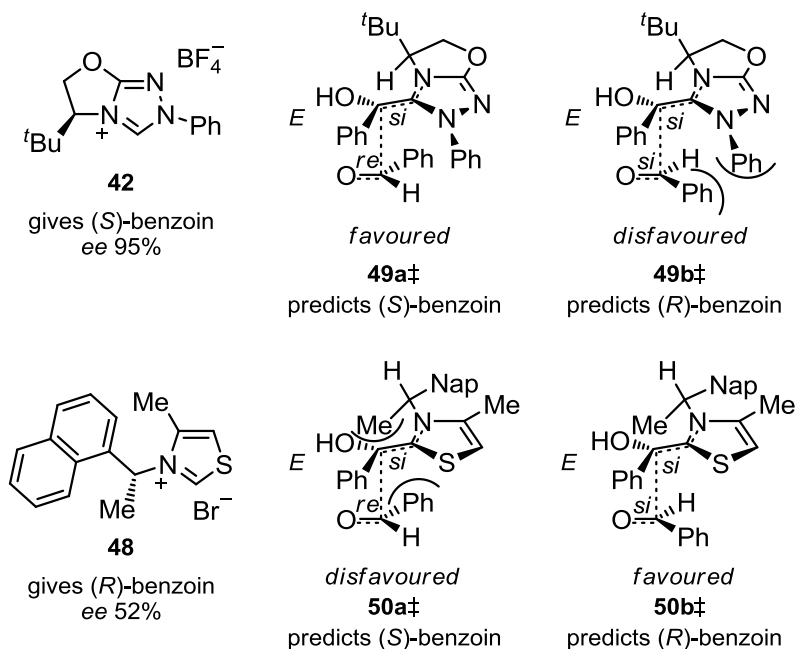
For both of the transition states predicted for catalysts **42** and **48**, the *E* isomer of the acyl anion species is preferred, presumably in order to avoid unfavourable interactions between the phenyl group on the aldehyde and the chiral substituent. For catalyst **42**, (giving transition states **49a‡** and **49b‡**), **49a‡** was lower in energy by 11.7 kJ mol^{-1}, correctly predicting that the experimentally favoured outcome is (*S*)-benzoin. In contrast, the *re* approach of benzaldehyde in transition state **50a‡** for thiazolium catalyst **48** was disfavoured by 7.5 kJ mol^{-1} compared to **50b‡**, correctly predicting predominantly (*R*)-benzoin.

1.2.2.2 The Stetter reaction

The NHC-catalysed addition of an aldehyde **23** to a Michael acceptor **51** *via* an acyl anion equivalent was first reported by Stetter in 1976 (Scheme 1.9).[36] Using thiazolium catalysts **53 – 55**, a wide range of 1,4-bifunctional products **52** were prepared from the reaction of aliphatic and aromatic aldehydes with α,β-unsaturated ketones, esters and nitriles. The reaction was first made asymmetric using Enders' chiral thiazolium catalyst **56**, although poor yields and *ee*s were achieved.[37] Recently, the same group reported *ee*s in the range 56 – 78%, in good yield for a broad range of substrates using chiral triazolium catalyst **57**.[38]

Scheme 1.9:

53 (R = Bn; X = Cl)
54 (R = Me; X = I)
55 (R = Et; X = Br)

56
4% yield
39% *ee*

57
49 - 98% yield
56 - 78% *ee*
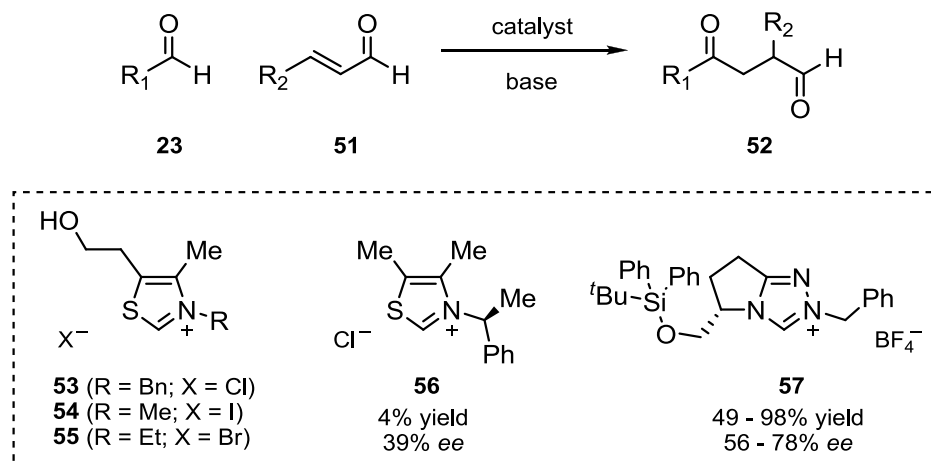
The intramolecular Stetter reactions of salicylaldehyde derived substrates (such as **58**) (Scheme 1.10), initially introduced by Ciganek,[39] are commonly used as benchmarks to test the efficacy of new catalysts. In 1996, Enders reported the first asymmetric version of this reaction using chiral triazolium catalyst **39**, producing a range of chromanones **59** in moderate *ee*s.[40] Rovis and co-workers subsequently improved on these results using several highly effective chiral catalysts based on a number of chiral scaffolds.[41] Triazolium catalysts **60** and **61** afforded excellent product yields and *ee*s for a range of electron rich and poor substrates, with the authors noting that substrates bearing electron donating substituents on the aryl backbone resulted in particularly favourable *ee*s.

Scheme 1.10:

58

(*R*)-**59**

39
69% yield
56% *ee*

60
95% yield
92% *ee*

61
94% yield
94% *ee*
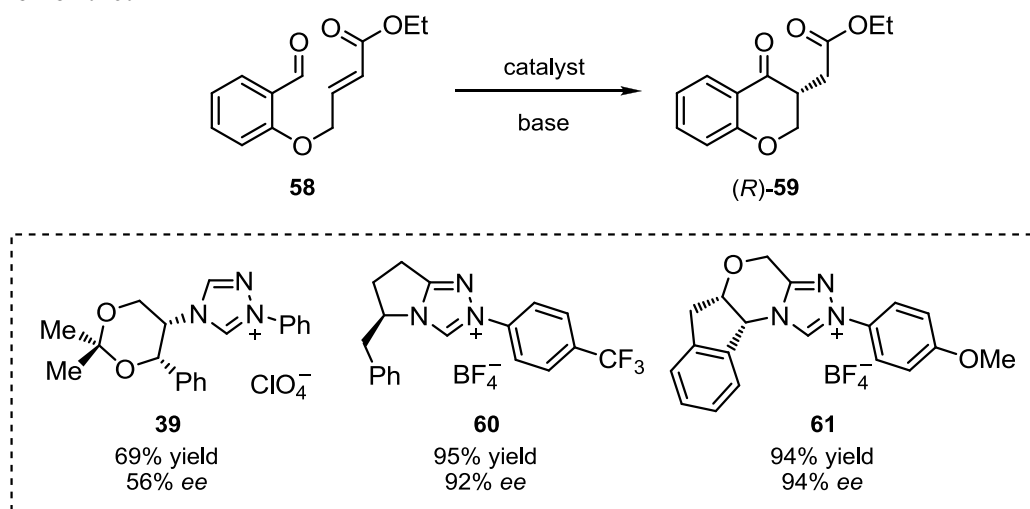
1.2.3   Homoenolates (d³ synthons)

The discovery, by the groups of Glorius[42] and Bode[43] in 2004, that homoenolates **63** may be generated from the reaction an NHC with an α,β-unsaturated aldehyde **62** opened up a new chapter in the field of NHC organocatalysis. Such species are involved in a number of important transformations, including γ-butyrolactone **64** and γ-lactam **65** formation, and redox esterification to give saturated esters **66** (Scheme 1.11). Typically, *N,N*-dimesitylimidazolium catalysts afford optimal yields in these reactions.

Scheme 1.11:
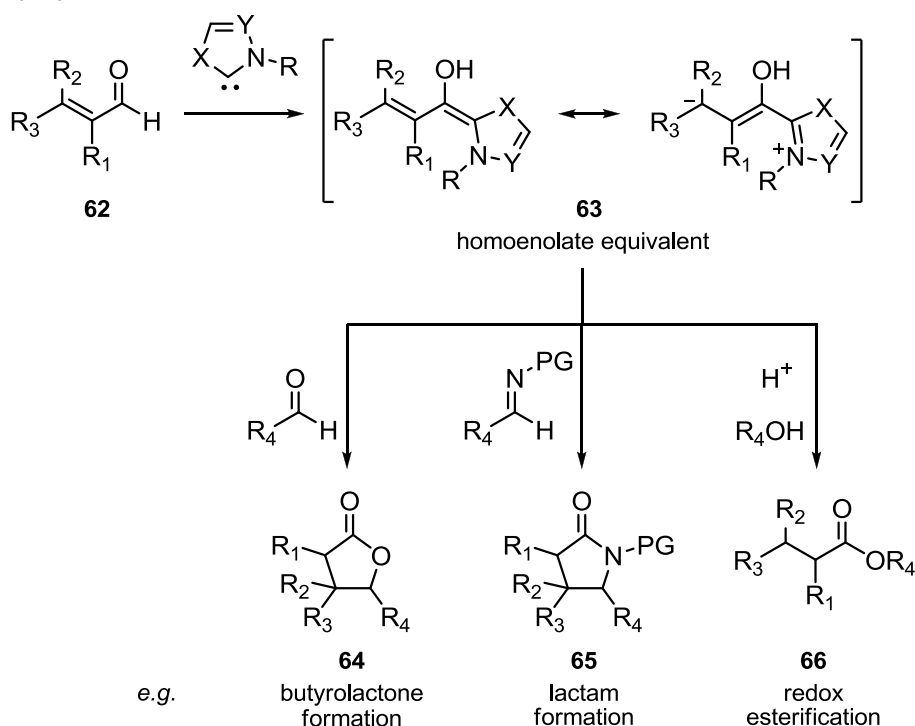
1.2.3.1   Preparation of γ-butyrolactones and γ-lactams

The reaction of a homoenolate with either an aromatic aldehyde or trifluoroketone may result in the formation of a γ-butyrolactone **64**. Glorius *et al.* reported the NHC-catalysed reaction of several α,β-unsaturated aldehydes with trifluoroketone **68** to give the corresponding γ-butyrolactones as a mixture of stereoisomers.[43] In one example, γ-butyrolactones **69a** and **69b** were prepared from cinnamaldehyde **67** in excellent yield using *N,N*-dimesitylimidazolium catalyst **70**, whilst chiral imidazolium catalyst **71** resulted in improved selectivity (Scheme 1.12).

Scheme 1.12:
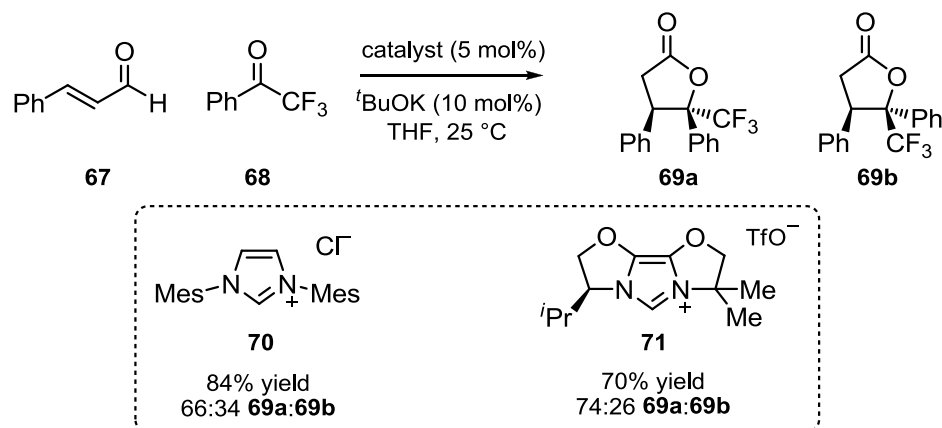
At the same time, Bode reported the NHC-catalysed synthesis of several γ-butyrolactones as a mixture of *cis* and *trans*-isomers from a range of α,β-unsaturated aldehydes **51** and 4-bromobenzaldehyde **72** (Scheme 1.13).[44] Using *N,N*-dimesityl imidazolium catalyst **70**, *cis*-lactone **73a** (R$_1$ = 1-napthyl) was prepared in good yield and high selectivity. Bulkier *N,N*-diisopropylphenyl imidazolium **74** also catalysed the reaction, albeit with loss of selectivity. Imidazolium catalyst **75** was found to be completely unreactive, whilst thiazolium **76** promoted only the benzoin side-reaction.

Scheme 1.13:
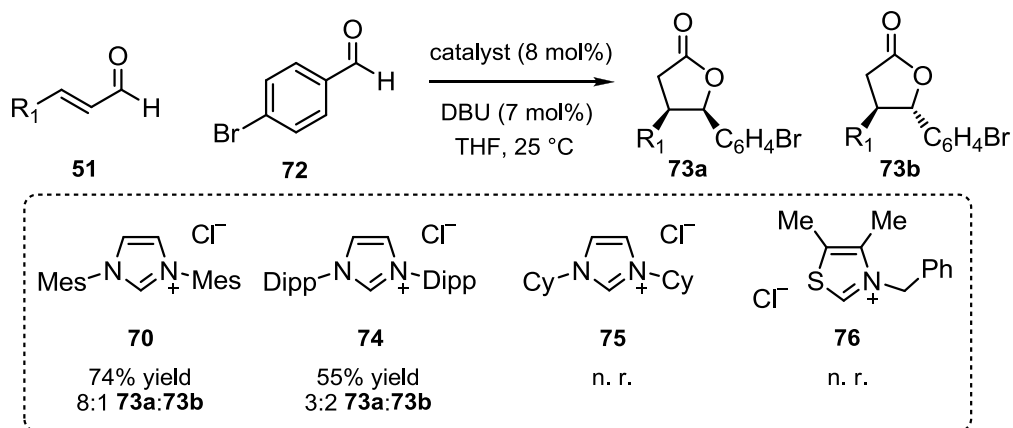
Bode and co-workers later showed that γ-lactams **78** can be prepared from *N*-sulfonylimines **77** using an analogous approach (Scheme 1.14).[44] The choice of protecting group was key to enabling the reactivity of the imine, as *N*-aryl and *N*-alkyl protected imines were unreactive, and more electron-withdrawing *N*-tosyl and *N*-phosphinoyl groups reacted immediately with the NHC. Bode recently applied this principle to the analogous cyclic ketimine **79**, affording the lactam derived product **80** in excellent yields using as little as 0.5 mol% catalyst **81** loadings (Scheme 1.15).[45]

Scheme 1.14:

Ar = 4-MeO-C$_6$H$_4$

50 - 73% yield
1.7:1 - 10:1 *dr*

Scheme 1.15:

55 - 98% yield
1:1 - 6:1 *dr*
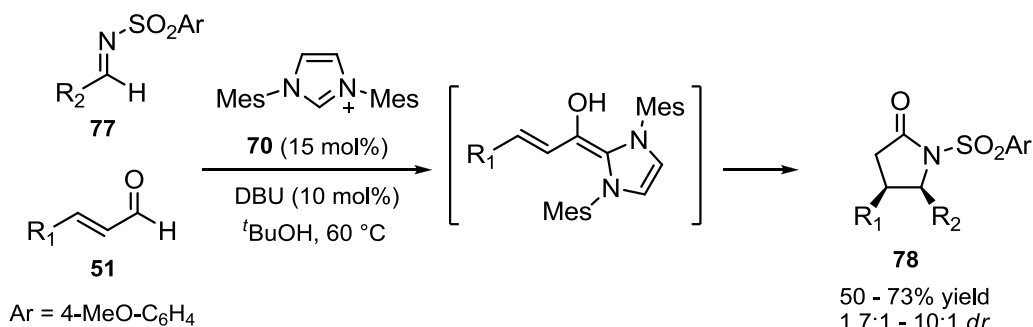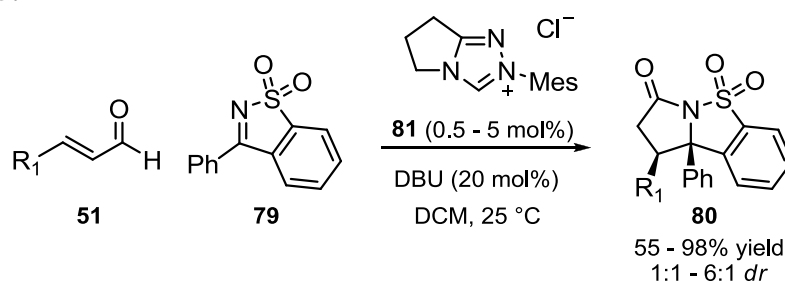
1.2.3.2   Redox esterification

Further efforts to explore homoenolate reactivity led Scheidt and co-workers to develop an NHC-catalysed redox esterification of an α,β-unsaturated aldehyde **62** (Scheme 1.16).[46] Protonation of the homoenolate **82** at the β-position, followed by tautomerisation generates the activated carboxylate **83**. Nucleophilic displacement of the NHC by the alcohol resulted in the saturated ester **66**. Benzimidazolium catalyst **84** demonstrated excellent substrate scope for this reaction, affording the desired product in good-excellent yield.

Scheme 1.16:

56 - 90% yield
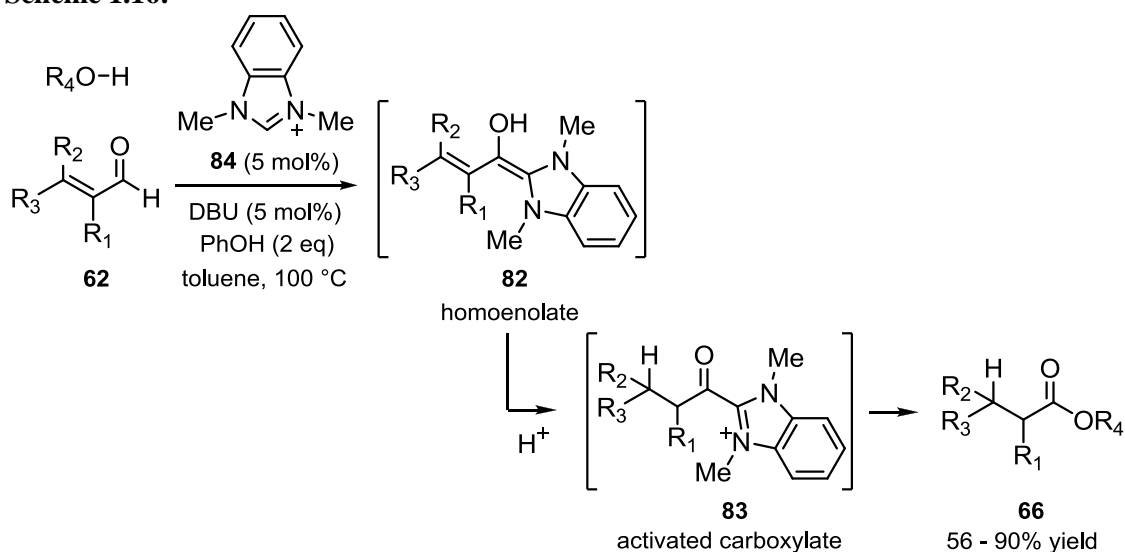
Bode and co-workers subsequently showed that the choice of catalyst and base is important in determining the outcome of the reaction (Scheme 1.17).[47] Less nucleophilic carbenes and mild bases such as diisopropylethylamine (DIPEA) resulted in protonation of the homoenolate, giving exclusively the redox esterification product **85**. Strong bases and more nucleophilic NHCs showed a strong preference for carbon-carbon bond formation, resulting in the self-condensation product **86**.

Scheme 1.17:
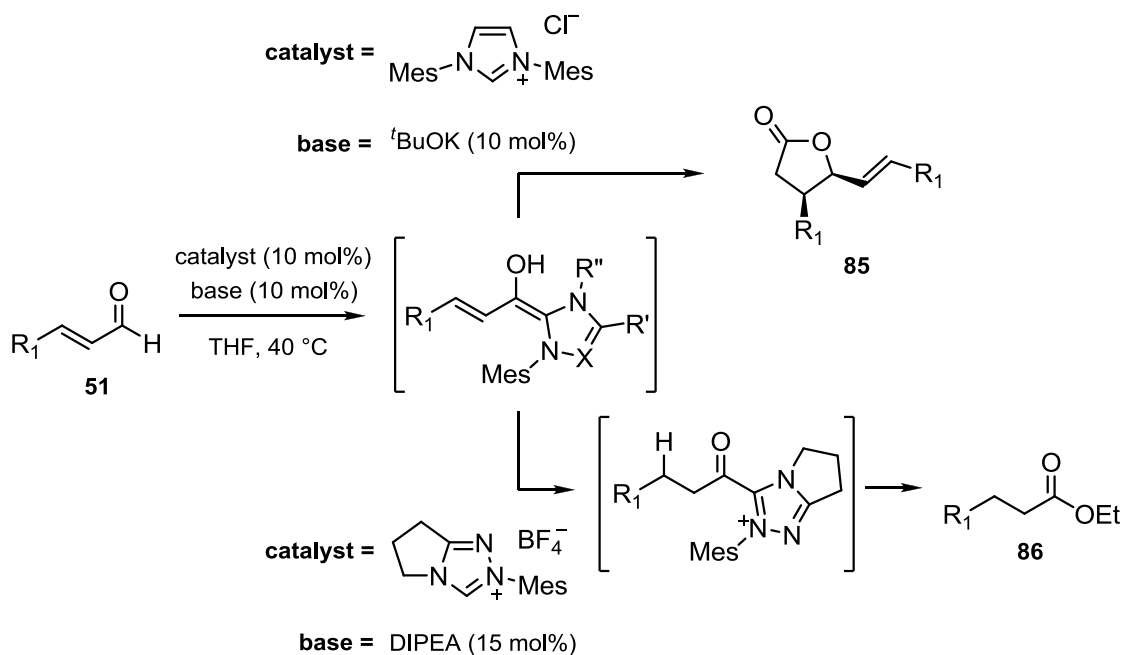
1.2.4   Azolium enolates (d² synthons)

Azolium enolates (d² synthons) **89** may be generated from α,β-unsaturated aldehydes **87** *via* protonation of the homoenolate **88** at the β-position, or alternatively, generated directly from the reaction of an NHC with a ketene **90** (Scheme 1.18). This enolate equivalent may react as a dienophile in [4+2] or [2+2] cycloaddition processes. Catalysts based on triazolium architecture are typically employed for these reactions.

Scheme 1.18:
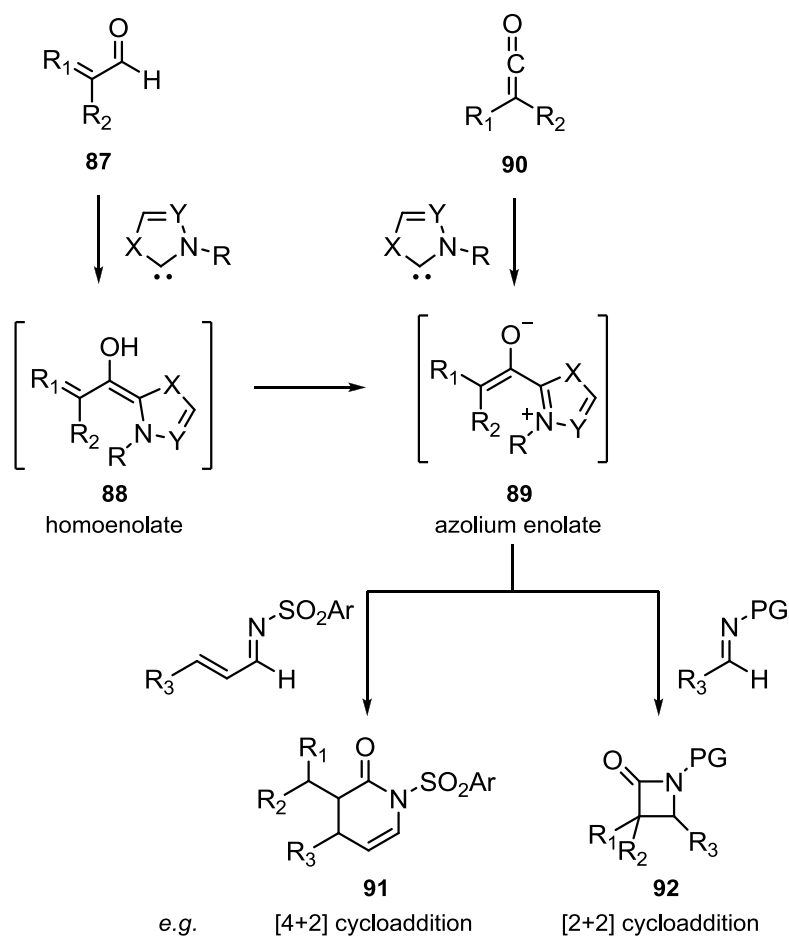
1.2.4.1 Azolium enolate reactions *via* homoenolates

In 2006, Bode and co-workers first harnessed the reactivity of an azolium enolate in a hetero-Diels-Alder transformation (Scheme 1.19).[48] The reaction of an NHC with an enal **93** bearing ester or ketone functionality at the β-position gave a homoenolate with sufficient electron-withdrawing character to protonate at the β-position, generating the enolate equivalent. Reaction with an α,β-unsaturated imine **94** resulted in a range of substituted dihydropyridinones **95**. Initial optimisation studies suggested that homoenolates generated from imidazolium catalysts were relatively unreactive towards β-protonation. *N*-Mesityl substituted triazolium catalysts **81** and **96** proved to be much more effective, with excellent enantioselectivities achieved using chiral catalyst **96**. In contrast, no reaction was observed with the analogous *N*-phenyl and *N-para-*methoxyphenyl substituted triazolium catalysts **97** and **98**.

Scheme 1.19:
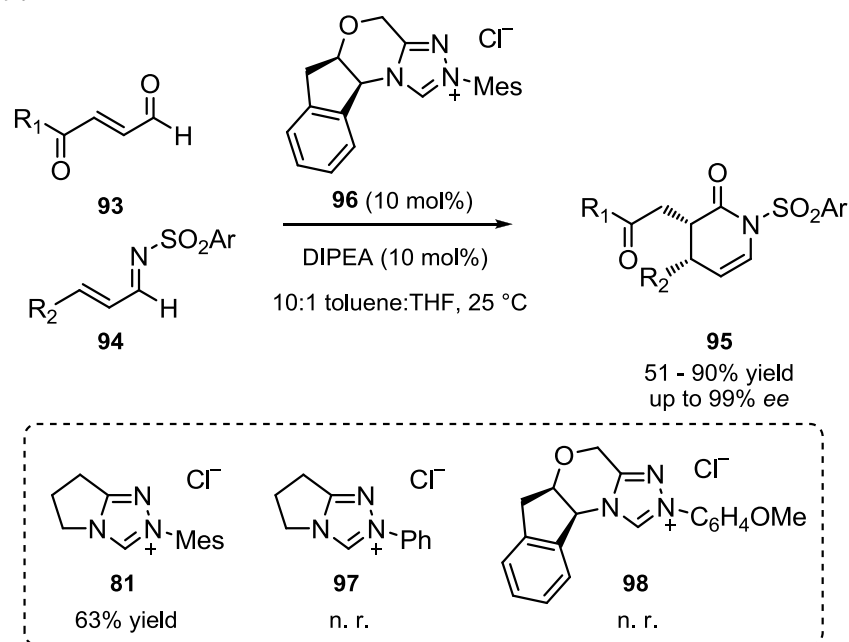
Bode later showed that the reaction of the azolium enolate dienophile with an enone **100** results in an analogous oxodiene Diels-Alder transformation (Scheme 1.20).[49] Using remarkably low loadings of chiral triazolium catalyst **96**, the authors demonstrated that enolate equivalents derived from α-chloroaldehydes **99** were tolerant to a range of enones, giving the corresponding dihydropyranones **101** in up to 99% *ee*.

Scheme 1.20:
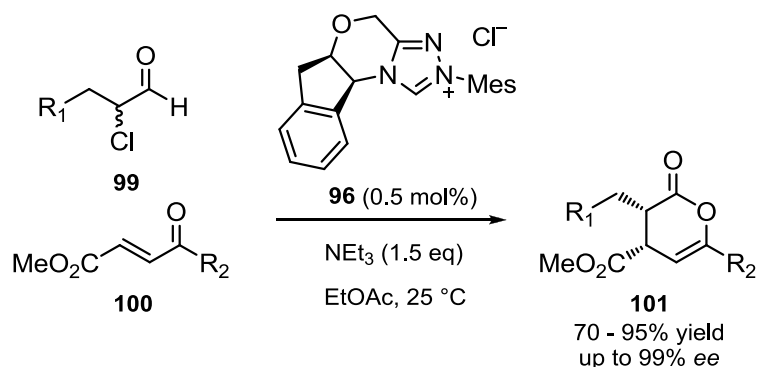
1.2.4.2 Azolium enolates derived from ketenes

Enolate eqivalents may also be generated from the reaction of an NHC with a ketene **90**. In 2008, the groups of Ye[50] and Smith[51] reported the first NHC-catalysed asymmetric Staudinger reactions between a ketene **90** and an imine to give β-lactams. Following optimisation, Ye observed that electron-rich *N-tert*-butoxycarbonyl-protected imines **102** were shown to achieve better stereoselectivity than other protecting groups, with chiral triazolium catalyst **104** affording the *cis* product **103** in good yields and excellent enantioselectivities for a broad range of substrates (Scheme 1.21).

Scheme 1.21:
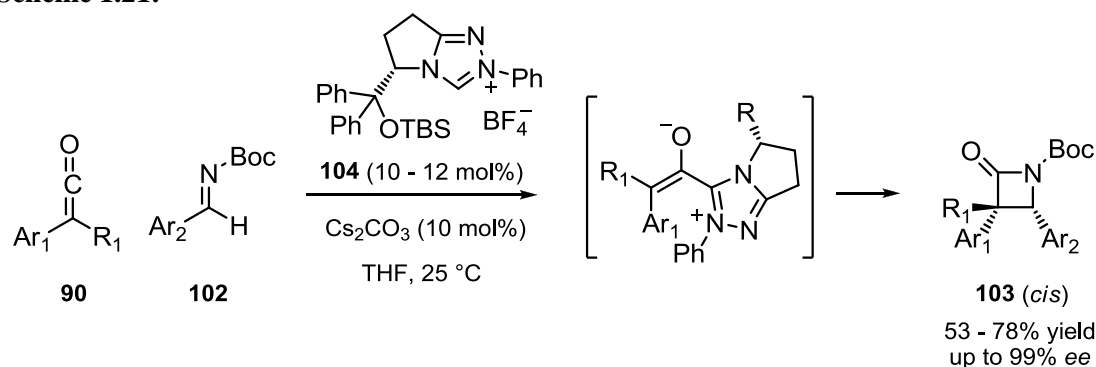
Ye subsequently showed that under similar conditions, ketene-generated azolium enolates may undergo enantioselective [2+2] cycloaddition reactions with 2-oxoaldehydes **105** to give β-lactones **106** (Scheme 1.22)[52] and [4+2] cycloadditions with α,β-unsaturated ketones **107** to give dihydropyranones **108** (Scheme 1.23).[53] Interestingly, *N*-phenyl substituted triazolium species proved to be highly effective catalysts for all of the reactions from ketene starting materials, in contrast to the

reactions proceeding *via* homoenolates which required *N*-mesityl substituents, implying that homoenolate formation is particularly susceptible to the choice of *N*-substiutuent.
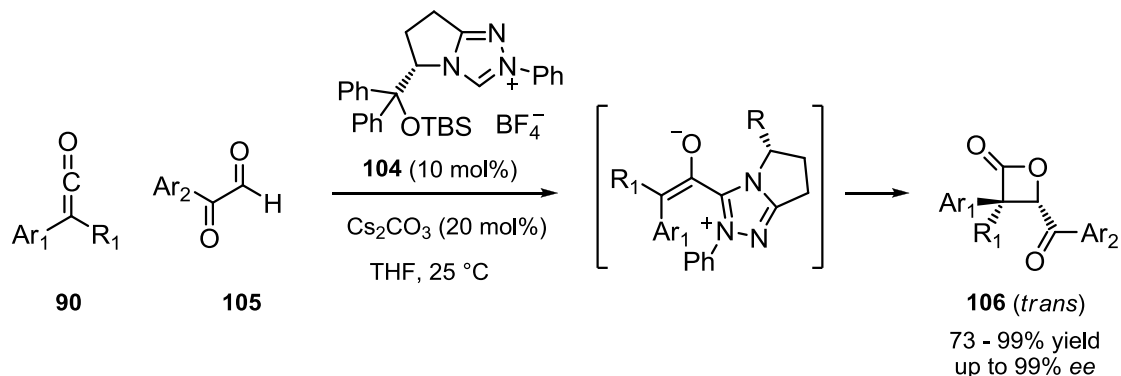
Scheme 1.22:

Scheme 1.23:
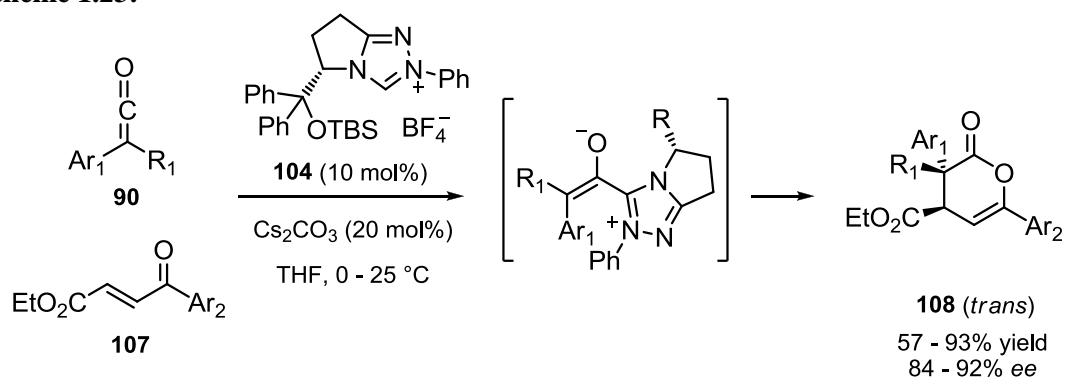
1.2.5 Acyl azolium equivalents (a¹ synthons)

Several NHC-catalysed transformations that proceed *via* acyl azolium equivalents **22** have emerged in the last decade. These intermediates are generated from the nucleophilic addition-elimination reaction between an NHC and an ester.

1.2.5.1 Transesterification reactions

In 2002, the first examples of NHC-catalysed transesterification reactions were reported concurrently by Nolan[54] and Hedrick[55] (Scheme 1.24). Using very low loadings of free NHC, both groups achieved excellent product **109'** yields for a wide selection of alkyl and aryl esters **109** and primary alcohols. Nolan's catalyst screening studies found *N*-mesityl and *N*-cyclohexyl substituted imidazolylidenes to be particularly effective.

Scheme 1.24:
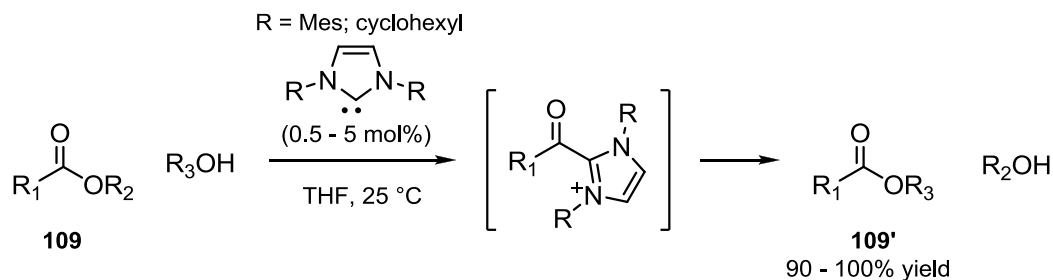
Movassaghi and Schmidt subsequently reported the analogous transformation between esters **109** and 1,2-diaminoalcohols **110** to generate amides **111** in the presence of free *N,N*-dimesitylimidazolylidene **112** (Scheme 1.25).[56] The X-ray crystallographic characterisation of a carbene-alcohol hydrogen bonded species **113** led the authors to propose a base-catalysed mechanism whereby nucleophilic substitution of the alcohol **110** on the ester **109** is assisted by proton-transfer to and from the carbene *via* **114**. Subsequent N → O-acyl transfer on **115** results in the amide product **111**. Computational studies carried out by Hu *et al.* also support the stability of a hydrogen bonded intermediate which assists proton transfer between the alcohol and carbonyl group.[57] This novel mode of catalysis may open up new possibilities for NHCs in organocatalysis.

Scheme 1.25:
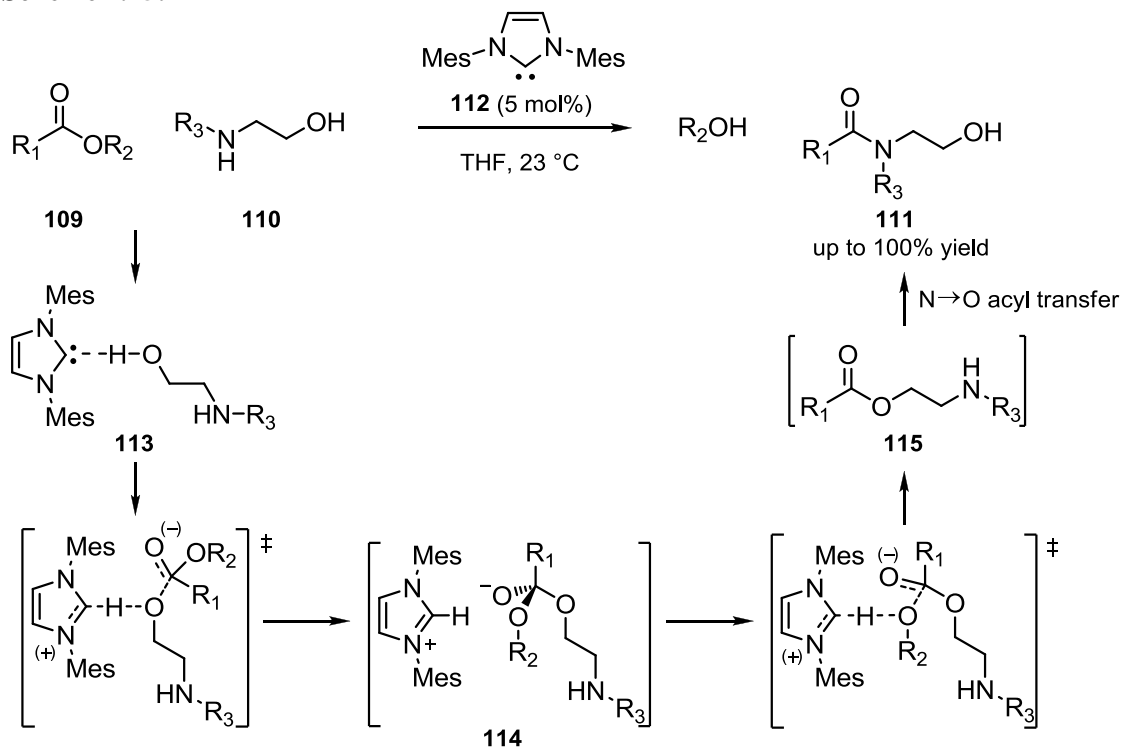
1.2.5.2 Kinetic resolution of alcohols

In 2004, Suzuki and co-workers extended these methods to the kinetic resolution of secondary alcohols.[58] Using chiral imidazolium catalysts such as **119** and vinyl acetate **117**, the selective acylation of a range of aryl methyl alcohols **116** resulted in starting material *ee*s of up to 37% (Scheme 1.26). Maruoka later improved on these results, reaching *ee*s of up to 96% using more hindered acylating agents such as **120**.[59]

Scheme 1.26:
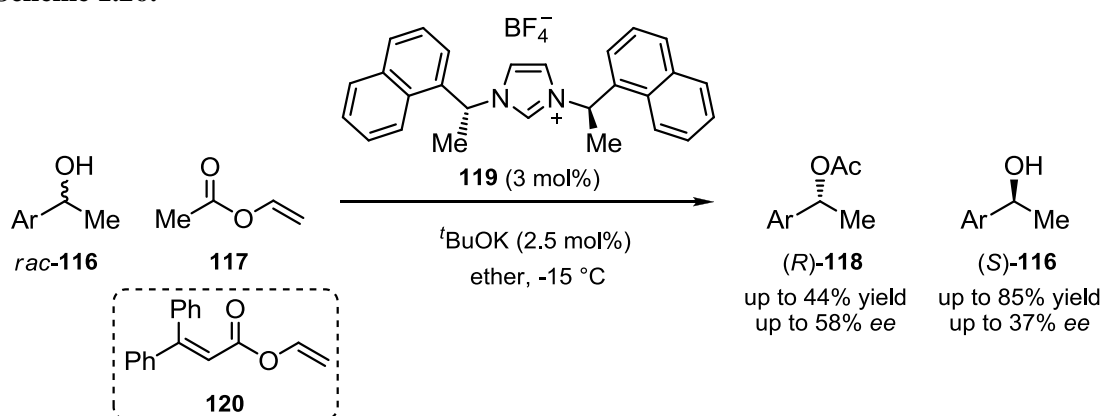
1.2.5.3 O- to C-carboxyl transfer

In 2006, Smith and co-workers demonstrated that NHC organocatalysts also promote the Steglich rearrangement of O-acyl carbonates **121** to C-acyl-azlactones **124** in good yield for a broad range of substrates (Scheme 1.27).[60] The authors proposed a mechanistic pathway *via* acyl azolium intermediate **123**, which facilitates enantioselective acylation of the enolate **122**.

Scheme 1.27:
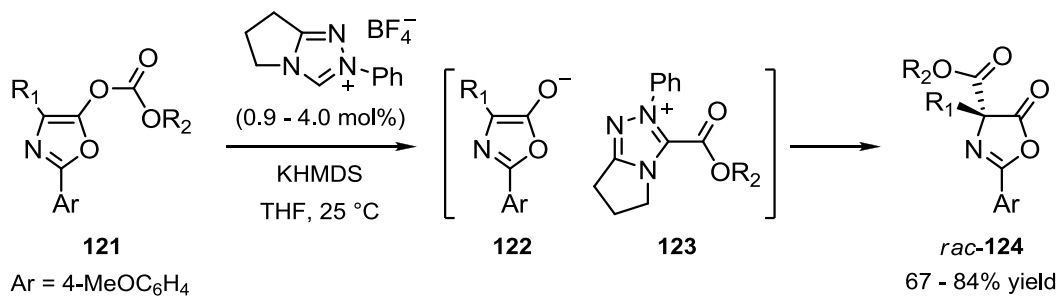
1.3   Summary

Since the isolation of the first stable NHCs two decades ago, the field of NHC organocatalysis has experienced rapid growth, and now encompasses a wide range of asymmetric transformations catalysed by an equally wide range of azolium ion NHC-precursors. The reactivity of four key intermediates (acyl anion, homoenolate, azolium enolate and acyl azolium) has been harnessed to achieve a diverse range of products.

Despite this impressive history, the choice of catalysts for these reactions has been largely based on a 'trial-and-error' approach. Until recently, detailed kinetic studies have been limited to the thiazolium-catalysed benzoin condensation, and have not explored the reactivity of triazolium and imidazolium precatalysts which have become the mainstay of NHC catalysis. These groups of catalysts have been shown to result in contrasting reactivity, and even within these families, divergent reaction outcomes have been achieved using different *N*-substituents.

Based on Breslow's model of thiazolium catalysis, the benzoin condensation involves three key steps common to the vast majority of NHC-catalysed processes: generation of the NHC from the parent azolium ion, nucleophilic addition of the carbene to the carbonyl to generate the initial adduct, and deprotonation of this species to generate the Breslow intermediate.

Using the benzoin condensation as a model reaction, we aim to address three key questions:

1. What are the carbon acid pK_a values for a structurally comparable series of azolium ion NHC-precursors?
2. What are the intermediates involved in the triazolylidene catalysed benzoin condensation?
3. How does the rate-determining step of the reaction change with systematic variation of substituents within a given NHC family, and between NHC families?

References

1   D. Bourissou, O. Guerret, F. P. Gabbaï and G. Bertrand, *Chem. Rev.*, 2000, **100**, 39.

2   G. Bertrand in *Reactive Intermediate Chemistry*, Eds. R. A. Moss, M. S. Platz, M. Jones, John Wiley & Sons, Hoboken, New Jersey, 2004, p. 329.

3   (a) R. A. Mitsch, *J. Am. Chem. Soc.*, 1965, **87**, 758; (b) R. A. Moss and C. B. Mallon, *J. Am. Chem. Soc.*, 1975, **97**, 344; (c) S. Koda, *Chem. Phys. Lett.*, 1978, **55**, 353.

4   R. A. Moss, M. Wlostowski, S. Shen, K. Krogh-Jespersen, A. Matro, *J. Am. Chem. Soc.*, 1988, **110**, 4443; (b) X. M. Du, H. Fan, J. L. Goodman, M. A. Kesselmayer, K. Krogh-Jespersen, J. A. La Villa, R. A. Moss, S. Shen and R. S. Sheridan, *J. Am. Chem. Soc.*, 1990, **112**, 1920.

5   (a) J. L. Wang, J. P. Toscano, J. P. Platz, V. Nikolaev and V. Popik, J. Am. Chem. Soc., 1995, 117, 5477; (b) P. Visser, R. Zuhse, M. W. Wong and C. Wentrup, *J. Am. Chem. Soc.*, 1996, **118**, 12598.

6   (a) A. Berndt, *Angew. Chem. Int. Ed. Engl.*, 1993, **32**, 985; (b) M. Menzel, H. J. Winckler, T. Ablelom, D. Steiner, S. Fau, G. Frenking, W. Massa and A. Berndt, *Angew. Chem. Int. Ed. Engl.*, 1995, **34**, 1340.

7   R. A. Moss, C. B. Mallon and C. T. Ho, *J. Am. Chem. Soc.*, 1977, **99**, 4105.

8   (a) A. Igau, H. Grutzmacher, A. Baceiredo and G. Bertrand, *J. Am. Chem. Soc.*, 1988, **110**, 6463; For elucidation of the bonding in these species see: (b) M. Soleilhavoup, A. Baceiredo, O. Treutler, R. Ahlrichs, M. Nieger and H. Bertrand, *J. Am. Chem. Soc.*, 1992, **114**, 10959; (c) M. Soleilhavoup, G. Alcaraz, R. Réau, A. Baceiredo and G. Bertrand, *Phosphorus Sulfur*, 1993, **76**, 49; (d) T. Kato, H. Gornitzka, A. Baceiredo, A. Savin and G. Bertrand, *J. Am. Chem. Soc.*, 2000, **122**, 998.

9   E. Buchner and T. Curtius, *Ber. Dtsch. Chem. Ges.*, 1885, **8**, 2377; H. Staudinger and O. Kupfer, *Ber. Dtsch. Chem. Ges.*, 1912, **45**, 501.

10   H. W. Wanzlick and H. J. Kleiner, *Angew. Chem.*, 1961, **73**, 493; H. W. Wanzlick, *Angew. Chem. Int. Ed. Engl.*, 1962, **1**, 75; H. W. Wanzlick, F. Esser and H. J. Kleiner, *Chem. Ber.*, 1963, **96**, 1208.

11   H. W. Wanzlick and H. J. Schönherr, *Angew. Chem.*, 1968, **80**, 154; H. J. Schönherr and H. W. Wanzlick, *Chem. Ber.*, 1970, **103**, 1037.

12   A. J. Arduengo, R. L. Harlow and M. Kline, *J. Am. Chem. Soc.*, 1991, **113**, 361.

13   F. E. Hahn and M. C. Jahnke, *Angew. Chem. Int. Ed.*, 2008, **47**, 3122.

14   N. Kuhn and T. Kratz, Synthesis, 1993, 561.

15   M. K. Denk, A. Thadani, K. Hatano and A. J. Lough, *Angew. Chem. Int. Ed.*, 1997, **36**, 2607.

16   F. E. Hahn, L. Wittenbecher, R. Boese and D. Blaster, *Chem. Eur. J.*, 1999, **5**, 1931.

17   D. Enders, K. Breuer, G. Raabe, J. Runsink, J. H. Teles, J-P. Melder, K. Ebel and S. Brode, *Angew. Chem. Int. Ed. Engl.*, 1995, **34**, 1021.

18   M. Scholl, S. Ding, C. W. Lee and R. H. Grubbs, *Org. Lett.*, 1999, **1**, 953.

19   D. Seebach, *Angew. Chem. Int. Ed. Engl.*, 1979, **18**, 239.

20   For a review of NHC applications see: H. U. Vora, P. Wheeler and T. Rovis, *Adv. Synth. Catal.*, 2012, **354**, 1617; J. Douglas, G. Churchill and A. D. Smith, *Synthesis*, 2012, **44**, 2295; D. Enders, O. Niemeier and A. Henseler, *Chem. Rev.*, 2007, **107**, 5606; N. Marion, S. Díez-González and S. P. Nolan, *Angew. Chem. Int. Ed.*, 2007, **46**, 2988; D. Enders and T. Balensiefer, *Acc. Chem. Res.*, 2004, **37**, 534; and references therein.

21   T. Ukai, R. Tanaka and T. A. Dokawa, *J. Pharm. Soc. Jpn.*, 1943, **63**, 296.

22   S. Mizuhara and P. Handler, *J. Am. Chem. Soc.*, 1954, **76**, 571.

23   R. Breslow, *J. Am. Chem. Soc.*, 1958, **80**, 3719.

24   A. Lapworth, *J. Chem. Soc.*, 1903, **83**, 995.

25   J. Sheehan and D. H. Hunnemann, *J. Am. Chem. Soc.*, 1966, **88**, 3666.

26   J. Sheehan and T. J. Hara, J. Org. Chem, 1974, **39**, 1196.

27   W. Tagaki, Y. Tamura and Y. Yano, *Bull. Chem. Soc. Jpn.*, 1980, **53**, 478.

28   R. L. Knight and F. J. Leeper, *Tetrahedron Lett.*, 1997, **38**, 3611.

29   D. Enders, K. Breuer and J. H. Teles, *Helv. Chim. Acta.*, 1996, **79**, 1217.

30   D. Enders and J. Han, *Tetrahedron: Asymmetry*, 2008, **19**, 1367.

31   Catalyst **43** was developed by Y-R. Zhang, L. He, X. Wu, P-L. Shao and S. Ye, *Org. Lett.*, 2008, **10**, 277.

32   Catalysts **43** and **44** were shown to catalyse the benzoin reaction by L. Baragwanath, C. A. Rose, K. Zeitler and S. J. Connon, *J. Org. Chem.*, 2009, **74**, 9214.

33   O. Hollóczki, Z. Kelemen and L. Nyulászi, *J. Org. Chem*, 2012, **77**, 6014.

34   R. L. Knight and F. J. Leeper, *J. Chem. Soc., Perkin Trans. 1*, 1998, 1891.

35   T. Dudding and K. N. Houk, *Proc. Natl. Acad. Sci.*, 2005, **101**, 5770.

36   H. Stetter, *Angew. Chem.*, 1976, **88**, 695.

37   D. Enders in *Stereoselective Synthesis*, Ed. E. Ottow, K. Schoellkopf and B-G. Schulz, Springer-Verlag, Berlin, 1994, p. 63.

38   D. Enders, J. Han and A. Henseler, *Chem. Comm.*, 2008, **34**, 3989.

39   E. Ciganek, *Synthesis*, 1995, **10**, 1311.

40   D. Enders, K. Breuer, J. Runsink and J. H. Teles, *Helv. Chim. Acta.*, 1996, **79**, 1899.

41   M. S. Kerr, J. Read de Alaniz and T. Rovis, *J. Am. Chem. Soc.*, 2002, **124**, 10298.

42   C. Burstein and F. Glorius, *Angew. Chem. Int. Ed.*, 2004, **43**, 6025.

43   S. S. Sohn, E. L. Rosen and J. W. Bode, *J. Am. Chem. Soc.*, 2004, **126**, 14370.

44   M. He and J. W. Bode, *Org. Lett.*, 2005, **7**, 3131.

45   M. Rommel, T. Fukuzumi and J. W. Bode, *J. Am. Chem. Soc.*, 2008, **130**, 17267.

46   A. Chan and K. A. Scheidt, *Org. Lett.*, 2005, **7**, 905.

47   S. S. Sohn and J. W. Bode, *Org. Lett.*, 2005, **7**, 3873.

48   M. He, J. R. Struble and J. W. Bode, *J. Am Chem. Soc.*, 2006, **128**, 8418.

49   M. He, G. J. Uc and J. W. Bode, *J. Am. Chem. Soc.*, 2006, **128**, 15088.

50   Y-R. Zhang, L. He, X. Wu, P-L. Shao and S. Ye, *Org. Lett.*, 2008, **10**, 277.

51   N. Duguet, C. D. Campbell, A. M. Z. Slawin and A. D. Smith, *Org. Biomol. Chem.*, 2008, **6**, 1108.

52   L. He, H. Lv, Y-R. Zhang and S. Ye, *J. Org. Chem.*, 2008, **73**, 8101.

53   Y-R. Zhang, H. Lv, D. Zhou and S. Ye, *Chem. Eur. J.*, 2008, **14**, 8473.

54   G. A. Grasa, R. M. Kissling and S. P. Nolan, *Org. Lett.*, 2002, **4**, 3583.

55   G. W. Nyce, J. A. Lamboy, E. F. Connor, R. M. Waymouth and J. L. Hedrick, *Org. Lett.*, **4**, 3587.

56   M. Movassaghi and M. A. Schmidt, *Org. Lett.*, 2005, **7**, 2453.

57   C-L. Lai, H. M. Lee and C-H. Hu, *Tetrahedron Lett.*, 2005, **46**, 6265.

58   Y. Suzuki, K. Yamauchi, K. Muramatsu, and M. Sato, *Chem. Commun.*, 2004, 2770.

59   T. Kano, K. Sasaki and K. Maruoka, *Org. Lett.*, 2005, **7**, 1347.

60   J. E. Thomson, K. Rix and A. D. Smith, *Org. Lett.*, 2006, **8**, 3785.

CHAPTER   2

*Azolium Ion pK$_a$ Measurements I:
Conjugate Acids of N-Heterocyclic Carbenes*

2.0   Foreword

The first step in NHC organocatalysis, common to all of the reactions detailed in the previous chapter, is the formation of the carbene from the parent azolium ion by deprotonation. Knowledge of the relative acidities of these precatalysts is an essential tool in understanding the reactivities of these species as catalysts. This chapter focuses on work relating to the measurement of azolium ion acidity constants, and is divided into four sections. Section 2.1 presents an overview of literature relating to the measurement of azolium ion pK_as. Section 2.2 details the results of our investigations into the H/D-exchange reactions of triazolium, thiazolium and imidazolium ions. In each case, second-order rate constants for deprotonation by deuteroxide ion, k_{DO} (M^{-1} s^{-1}), have been determined at 25 °C and $I = 1.0$ (KCl). Evidence is presented to show that the reverse rate constant for carbene protonation is equal to the rate constant for solvent reorganisation $k_{HOH} = k_{reorg} = 10^{11}$ s^{-1}. These rate constants are used to calculate carbon acid pK_a values. The results are discussed in Section 2.3 and our conclusions are summarised in Section 2.4.

2.1   Introduction

2.1.1   Acid-base chemistry of azolium ions

In the presence of a base, an azolium ion **125** may be deprotonated to form a carbene (**126a**) – ylide (**126b**) resonance hybrid (Scheme 2.1).

Scheme 2.1:
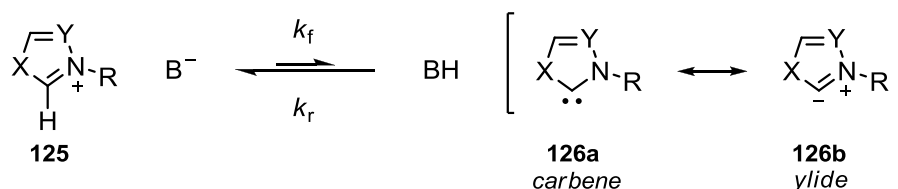
When the role of base is fulfilled by water (*i.e.* B = H$_2$O), the extent of deprotonation at equilibrium may be described by the acid dissociation constant, K_a (Equation 2.1). The acidity constant K_a is more commonly expressed in terms of pK_a (Equation 2.2).

$$K_a = \frac{[126][BH]}{[125]}$$
<div align="right">**Equation 2.1**</div>

$$pK_a = -\log(K_a)$$
<div align="right">**Equation 2.2**</div>

Conventional methods for the determination of pK_a values of strong carbon acids involve measurement of equilibrium concentrations of acid and conjugate base in aqueous solution, often by UV-Vis spectrophotometry or potentiometric techniques. As azolium ions are weak carbon acids, in water this equilibrium lies largely in favour of the acid and direct measurement of a detectable amount of conjugate base cannot generally be made. In such cases, a kinetic approach towards pK_a determination may be adopted. The acidity constant K_a may be written in terms of the rate constants for deprotonation of the azolium ion in the forward direction (k_f, M s^{-1}), and protonation of the carbene in the reverse direction (k_r, s^{-1}) (Equation 2.3).

$$K_a = \frac{k_f}{k_r}$$
<div align="right">**Equation 2.3**</div>

For azolium ions, the rate of deprotonation is relatively slow and their kinetic acidities may be accessed by deuterium exchange. Exchange of a proton for deuterium may be followed by mass spectrometry or ^{1}H NMR spectroscopy – the latter usually a more convenient technique.

2.1.2 Kinetic and thermodynamic acidities of azolium ions in aqueous solution

The earliest systematic study of azolium ion kinetic acidities was made by Haake in 1969,[1] who observed the following trend towards deuteroxide ion-catalysed exchange in D$_2$O at 38 °C: oxazolium **127** > thiazolium **128** > imidazolium **129** (Figure 2.1).

Figure 2.1: **Kinetic acidities of azolium ions reported by Haake**

	127	**128**	**129**
k_{DO} (M^{-1} s^{-1})	C2-H 3.8 × 10^7	C2-H 3.7 × 10^5	C2-H 1.3 × 10^2
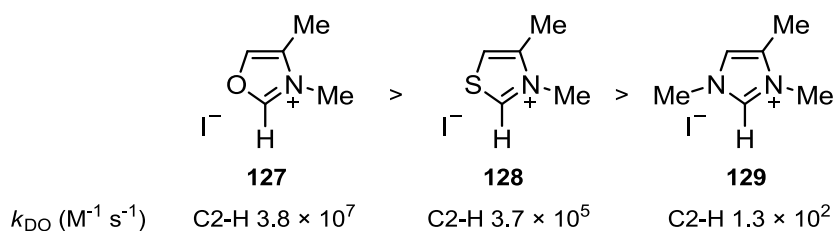
As deprotonation is a thermodynamically unfavourable process, the transition state for carbene formation more closely resembles the carbene than the azolium ion according to the Hammond postulate. The greater kinetic acidity of the oxazolium ion **127** relative to the imidazolium ion **129** may be explained by the presence of the more electron-withdrawing oxygen atom, which destabilises the azolium ion relative to the neutral carbene, resulting in a lower energy barrier for deprotonation.

This inductive effect cannot account for the greater acidity of the thiazolium ion **128** relative to the imidazolium ion **129**, as the greater electronegativity of nitrogen relative to sulfur would predict a less stable azolium ion and increased rate of deprotonation for the imidazolium salt. Several studies have attempted to rationalise the apparent greater stability of the thiazol-2-ylidene relative to the imidazol-2-ylidene. A computational study by Scheffers-Sap suggests that the increased polarisability of the sulfur atom, rather than 3d σ-orbital overlap, better stabilises the negative charge at the C(2) position in the conjugate base of the thiazolium relative to other azolium ions.[2]

However, a study by Amyes and co-workers concluded that the imidazole-2-ylidene is actually more stable than the corresponding thiazol-2-ylidene in water.[3] Scheme 2.2 shows the thermodynamic cycle used to model the 1,2-hydrogen shift. The X-substituent effect on the carbon basicity of the carbene is the sum of the substituent effects on the 1,2-hydrogen shift at the carbene **130** to give the neutral azole **131**, and on azole protonation at nitrogen to give the azolium ion **132**. The difference in pK$_a$s for ionisation between both species (X = S, NH) at carbon ($\Delta\log(K_{\text{CH}})$ = 3.9), and at nitrogen ($\Delta\log(K_{\text{NH}})$ = 4.7), gives the difference in equilibrium constants ($\Delta\log(K)$ = −0.8) for the 1,2-hydrogen shift between the imidazole-2-ylidene and thiazolyl-2-ylidene.

Scheme 2.2:
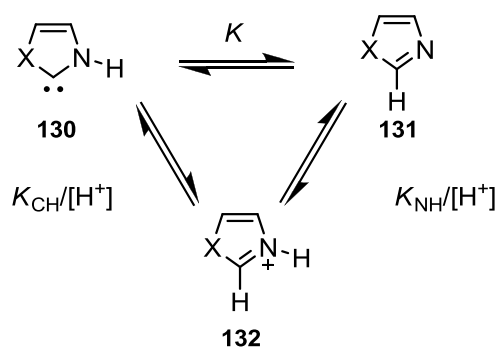
The authors concluded that the 3.9 pK_a unit greater C(2) acidity of the thiazolium ion reflects the 6.4 kcal mol^{-1} greater stabilization of the imidazolium ion than of the thiazolium ion relative to the neutral azole, rather than the greater stability of the thiazol-2-ylidene relative to the imidazole-2-ylidene. In fact, the imidazole-2-ylidene was found to be more stable than the corresponding thiazol-2-ylidene by 1.1 kcal mol^{-1}, relative to the neutral azole (Figure 2.2).

Figure 2.2: **Relative stabilities of imidazole derived species reported by Amyes**
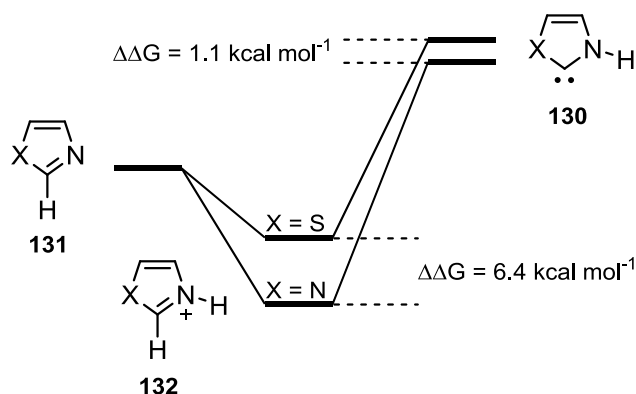
In 1988, Washabaugh and Jencks reported rate constants for deuteroxide ion-catalysed exchange of the C(2)-H for deuterium, k_{DO} (M^{-1} s^{-1}), for a range of thiazolium ions **31**, determined from pD-rate profiles for exchange.[4] Selected results are shown in Table 2.1. The evaluated kinetic acidities were found to be in good agreement with those obtained by Haake, with the observed trends across the series broadly following the inductive properties of the N-substituent. For the thiazolium ions shown, resonance effects do not play a part in stabilisation of the carbene due to the intervening CH$_2$ group on the R$_1$ substituent.

Table 2.1: **Kinetic acidities of thiazolium ions reported by Jencks**

substrate	R$_1$	X	k_{DO}, M^{-1} s^{-1}
	CH$_3$	Cl	4.27×10^5
	CH$_2$CH$_3$	Br	3.24×10^5
	CH$_2$CH$_2$CH$_3$	I	3.80×10^5
	CH$_2$CH$_2$COO$^-$	Br	4.27×10^5
	CH$_2$CH=CH$_2$	Br	9.77×10^5
	CH$_2$CO$_2^-$	Cl	1.07×10^6
	CH$_2$Ph	Cl	2.14×10^6
(R$_2$ = H)	⸨—C$_6$H$_4$—NO$_2$	Br	6.03×10^6
	CH$_2$CO$_2$Et	Br	8.71×10^6
	CH$_2$CN	Cl	4.68×10^7
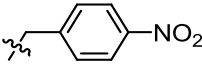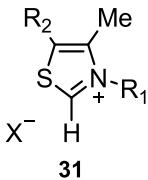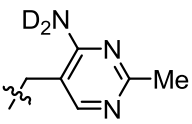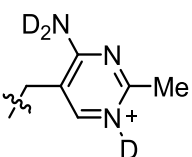
Expanding on this work, Jencks subsequently obtained rate constants for the deuteroxide ion-catalysed exchange of the C(2)-L (L = H, D, T) of three thiazolium ions in a series of kinetic isotope effect experiments.[5] The observation of significant deviations of values of $(k_H/k_T)_{obs}$ and $(k_D/k_T)_{obs}$ from the Swain-Schaad relationship, and an increasing primary kinetic isotope effect with increasing electron-withdrawing substituents, implied significant internal return of the transferred hydron back to the thiazolyl carbene. These results led the authors to conclude that deprotonation of the thiazolium ion **31** to generate the fully solvated carbene **30·DOL** proceeds *via* an Eigen mechanism (Scheme 2.3). In this scheme, proton transfer occurs as a pre-equilibrium K_1, followed by solvent reorganisation k_{reorg}, with both steps partially rate-determining in deuterium exchange. By the Principle of Microscopic Reversibility, protonation of the carbene species by water could be ascribed to the rate constant for solvent reorganisation (*i.e.* occurring at the diffusion-controlled physical transport limit for the encounter of the carbene with the water molecule). Details of these studies will be discussed in the latter part of this chapter, as these results are directly relevant to our own investigation.

Scheme 2.3:
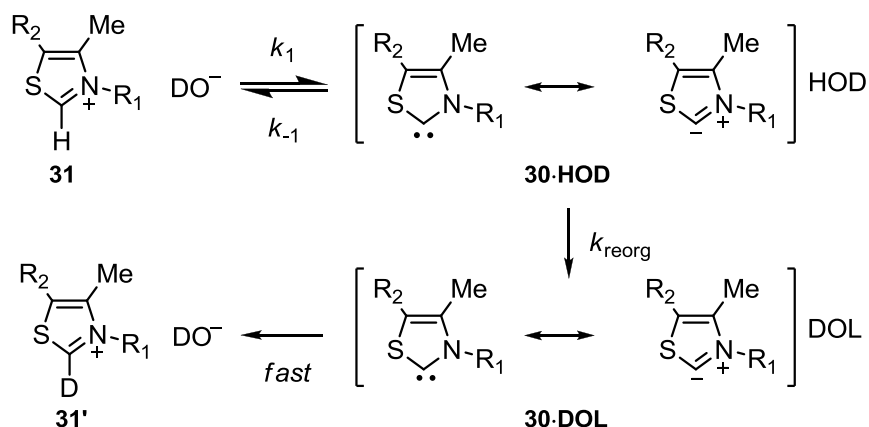
On this basis, carbon acid pK_a values in the range 16.9 – 18.9 were calculated for a set of six thiazolium ions **31** from rate constants for deprotonation by deuteroxide, k_{DO} (M^{-1} s^{-1}), and from solvent, k_{D2O} (s^{-1}), assuming diffusion-controlled protonation of the carbene by water and by hydronium ion, respectively (Table 2.2). Excellent agreement between pK_a values determined using either rate constant k_{DO} or k_{D2O} was observed.
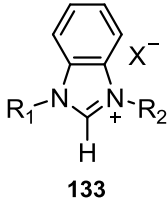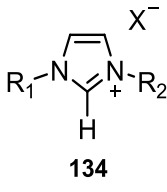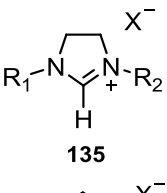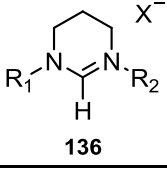
Table 2.2: **Thiazolium ion pK_a values reported by Jencks**

substrate	R$_1$	R$_2$	pK_a (DO⁻)	pK_a (D$_2$O)
	Me	H	18.9	18.7
	CH$_2$Ph	H	18.2	n.d.
		H	17.8	17.8
	CH$_2$CN	H	16.9	16.9
		CH$_2$CH$_2$OH	18.0	n.d.
		CH$_2$CH$_2$OH	17.6	17.7

In 2004, Amyes and co-workers reported second-order rate constants for deuteroxide ion-catalysed exchange of the C(2)-H of four *N*-substituted imidazolium ions **133** (R$_1$ = R$_2$ = Me, (*S*)-1-phenylethyl) and **134** (R$_1$ = R$_2$ = H, Me) in water at 25 °C and fixed ionic strength *I* = 1.0 (KCl) (Table 2.3).[3] These kinetic acidities were consistent with earlier results obtained by Haake.

Given that these rate constants for deuterium exchange were around 10³-fold smaller than those obtained for Jencks' series of thiazolium ions, the authors argued that solvent reorganisation was even more rate-determining for these imidazolium species. Evidence in the form of buffer catalysis experiments supported these conclusions, allowing the authors to obtain pK_a values in the range 21.2 – 23.8.

Table 2.3: **Kinetic acidities and pK_a values of imidazolium and 4,5-dihydroimidazolium and tetrahydropyrimidinium ions**

substrate	R$_1$	X	k_{DO}, M^{-1} s^{-1}	pK_a	Ref.
133	R$_1$ = R$_2$ = Me	I	5.74×10^3	21.6	2
	R$_1$ = R$_2$ = (S)-1-phenylethyl	I	1.48×10^4	21.2	2
134	R$_1$ = R$_2$ = 4-chlorophenyl	Cl	3.92×10^5	19.8	1
	R$_1$ = R$_2$ = 4-methoxyphenyl	Cl	4.80×10^4	20.7	1
	R$_1$ = R$_2$ = 2,4,6-trimethylphenyl	Cl	4.08×10^4	20.8	1
	R$_1$ = R$_2$ = 2,6-di-(i-propyl)phenyl	Cl	2.00×10^4	21.1	1
	R$_1$ = R$_2$ = H	I	3.69×10^1	23.8	2
	R$_1$ = R$_2$ = Me	I	2.47×10^2	23.0	2
	R$_1$ = Me, R$_2$ = Et	Cl	2.29×10^2	23.0	1
	R$_1$ = Me, R$_2$ = n-Bu	PF$_6$	1.07×10^2	23.3	1
	R$_1$ = R$_2$ = t-Bu	Cl	1.69	25.2	1
135	R$_1$ = R$_2$ = 4-methoxyphenyl	Cl	4.26×10^4	20.7	1
	R$_1$ = R$_2$ = 2,4,6-trimethylphenyl	Cl	1.19×10^4	21.3	1
	R$_1$ = R$_2$ = 2,6-di-(i-propyl)phenyl	Cl	8.37×10^3	21.5	1
136	R$_1$ = R$_2$ = Et	PF$_6$	3.48×10^{-3}	27.8	1
	R$_1$ = R$_2$ = i-Pr	PF$_6$	1.48×10^{-3}	28.2	1

Using a similar approach to that of Amyes, O'Donoghue and co-workers recently reported kinetic acidities and carbon acid pK_a values for around twenty imidazolium, 4,5-dihydroimidazolium and tetrahydropyrimidinium ions **134 – 136**.[6] A representative set of results are shown in Table 2.3.

This broad selection of azolium ions allowed for a range of substituent effects to be studied. The largest changes in acidity were found to result from azolium ring size, with 6-membered rings significantly less acidic than 5-membered rings. This observation was rationalised by the established diaminocarbene preference for smaller N-C-N bond angles.[7] The effect of C(4)-C(5) saturation was found to be less significant, with similarly substituted imidazolium and 4,5-dihydroimidazolium ions returning comparable k_{DO} values and pK_as.

Kinetic acidities were reported to increase with the electron withdrawing nature of the *N*-aryl substituent, consistent with the expected destabilisation of azolium cation relative to the neutral carbene upon substitution with more electron-withdrawing groups. Despite the significant changes in electronic properties of the *N*-aryl substituent, only relatively small changes in pK_a were observed. Structural data obtained by X-ray crystallography show that *N,N*-diarylimidazolium rings are not coplanar, implying that electronic changes are largely due to field/inductive effects rather than resonance.

Steric effects were also found to have a significant influence on kinetic and thermodynamic acidities, with bulky *t*-butyl groups resulting in a 2 unit increase in pK_a relative to the *N*-methyl substituted imidazolium ion.

Whilst several studies have now established the position of thiazolium, imidazolium and 4,5-dihydroimidazolium ions on the pK_a scale, relatively little is known about the pK_as of triazolium species. The main focus of the work in this chapter is to determine the pK_as of the triazolium and thiazolium salts that will be used in the mechanistic studies of the benzoin condensation in later chapters.

2.2 Results

2.2.1 Deuterium exchange reactions of 1,2,4-triazolium ions followed by ^{1}H NMR spectroscopy

Deuterium exchange experiments for 1,2,4-triazolium ions **137 – 143** (10 mM) in D₂O at 25 °C and constant ionic strength I = 1.0 (KCl) were performed at a range of pD values.[*] Exchange of a proton for deuterium at the C(3)-H position was followed by ^{1}H NMR spectroscopy (400 and 500 MHz), and resulted in the disappearance of the C(3)-H singlet signal. From this data, first- and second-order rate constants for deuteroxide ion-catalysed exchange, k_{ex} (s^{-1}) and k_{DO} (M^{-1} s^{-1}), were determined. Using these rate constants, carbon acid pK_a values were estimated.

---
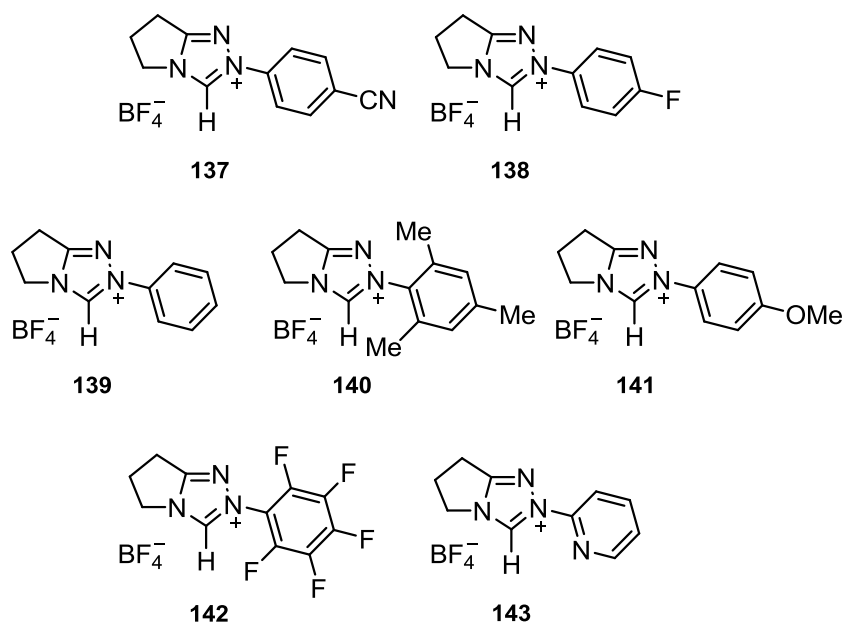
[*]All of the data presented for triazolium salts **137**, **138**, **140** and **143** is newly reported here.

N.B. For three triazolium ions **139**, **141** and **142**, first-order rate constants for exchange, k_{ex}, at five pD values have previously been determined by our laboratory.[8] In earlier work, these measurements were used to obtain second-order rate constants for deuteroxide ion-catalysed exchange (k_{DO}, M^{-1} s^{-1}) of the C(3)-H for deuterium from plots of k_{ex} against [DO^{-}]. Carbon acid pK_a values were estimated using this data. In this thesis, additional exchange data has been obtained for these salts at a wider range of pDs. This new data allows a more complete picture of the pD-rate profile to be established. The existing k_{ex} data has been combined with this new data, and new values of k_{DO} and pK_a for triazolium ions **139**, **141** and **142** have been calculated using an improved fitting model.

2.2.1.1 Determination of pseudo first-order rate constants for exchange (k_{ex})

Deuterium exchange reactions were carried out in D$_2$O solutions of either DCl or acetic acid buffer in the p*D* range 0 – 4.3 at 25 °C and *I* = 1.0 (KCl). Reactions were typically initiated by the addition of buffer (8 mL) containing internal standard, tetramethylammonium deuteriosulfate (~1 mM), to sealed vials containing solid substrate (10 mM). Reactions were incubated in a water bath thermostated at 25 °C. At regular intervals over the course of the reaction, aliquots (0.7 mL) were taken and quenched to p*D* ~0.5 by the addition of 5 M DCl solution to prevent further exchange. These samples were analysed immediately by ^{1}H NMR spectroscopy.

For experiments performed at p*D*s lower than 1.5, quenching by the addition of DCl would not substantially stop the reaction for subsequent analysis by ^{1}H NMR. In these cases, exchange experiments were carried out in capped NMR tubes containing reaction solution (0.7 mL). These reactions were initiated in the same manner and incubated in water baths thermostated at 25 ℃. In cases where reactions were performed at both low p*D* and exhibited half-lives shorter than 4 h, reactions were thermostated at 25 °C directly in the NMR instrument. At regular intervals over the course of the reaction, the samples were analysed by ^{1}H NMR spectroscopy (duration of acquisition ~13 min). Measurement times *t* were calculated from the time at the midpoint of the NMR experiment.

The progress of the deuterium exchange reactions were followed by the decrease in the integrated area of the singlet at approximately 10.0 ppm, corresponding to the C(3)-H of the triazolium ion, relative to that of the fixed peak at approximately 3.1 ppm, corresponding to the twelve non-exchangeable methyl hydrogens of the internal standard. The fraction of protonated substrate remaining *f*(s) was determined using Equation 2.4. Pseudo-first-order rate constants for exchange, k_{ex} (s^{-1}), were determined from semilogarithmic plots of *f*(s) against time (Equation 2.5). These plots were linear for the duration of the reaction (typically three half-lives).

$$f(\text{s}) = \frac{\left(A_{\text{C(3)H}}/A_{\text{std}}\right)_t}{\left(A_{\text{C(3)H}}/A_{\text{std}}\right)_{t=0}}$$

Equation 2.4

$$\ln f(\text{s}) = -k_{ex}\, t$$

Equation 2.5

2.2.1.1a 2-(4-Cyanophenyl)-6,7-dihydro-5*H*-pyrrolo[2,1-c][1,2,4]triazol-2-ium tetrafluoroborate (137)
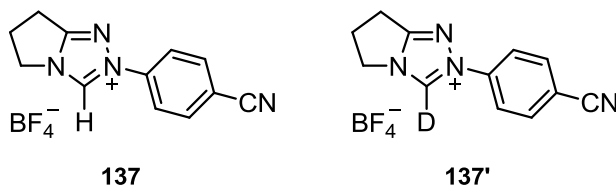
Pseudo-first-order rate constants for the deuteroxide ion-catalysed exchange of the C(3)-H of triazolium ion **137** to form deuterated product **137'** were determined by ^{1}H NMR spectroscopy (400 MHz).

A representative set of spectra taken at three time points during the reaction at p*D* 2.27 (6 mM DCl) is shown in Figure 2.3. Deuterium exchange at the C(3)-H position resulted in the disappearance of the C(3)-H singlet at 10.34 ppm over the course of the reaction. The extent of exchange was measured relative to the 12 equivalent non-exchangeable protons of the internal standard at 3.19 ppm. Signals corresponding to the *ortho*-CH and *meta*-CH groups on the aryl substituent appear as a multiplet at 8.02 – 8.08 ppm. Signals corresponding to the three CH$_2$ groups on the five-membered ring appear as two sets of triplets at 3.30 and 4.56 ppm, and a multiplet at 2.90 ppm. No change was observed in the integrated area of any other peak relative to the internal standard, indicating that deuterium exchange does not occur at any position other than at C(3)-H under these conditions.

Figure 2.3:   **Representative ^{1}H NMR spectra at 400 MHz of triazolium salt (137) (10 mM, pD 2.27), obtained during exchange of the C(3)-H (s, 10.34 ppm) for deuterium in D$_2$O at 25 ºC and I = 1.0 (KCl) [Internal standard, tetramethylammonium deuteriosulfate (s, 3.19 ppm)]**
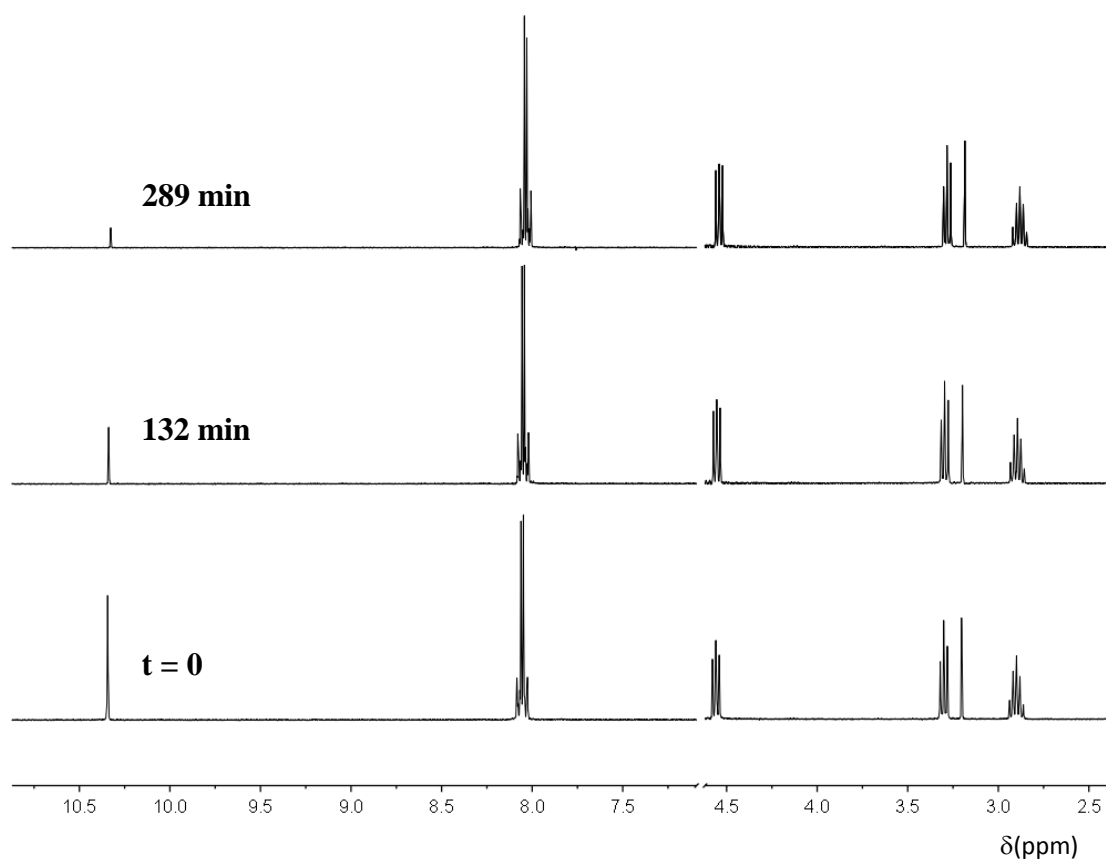
Experimentally observed first-order rate constants for exchange, k_{ex} (s^{-1}), were determined from the slopes of semilogarithmic plots of f(s) against time at each pD (Figures 2.4 – 2.6). Reaction data and values of k_{ex} are presented in Table 2.4.

The concentration of deuteroxide ion is given by Equation 2.6, where K_w is the value for the ion product of D$_2$O at 25 ºC and is equal to $10^{-14.87}$ M^2. A value for the apparent activity coefficient of deuteroxide ion γ_{DO} = 0.73 was determined at I = 1.0 (KCl).[9]

$$[\text{DO}^-] = \frac{10^{(\text{p}D - \text{p}K_W)}}{\gamma_{DO}} \qquad\qquad \textbf{Equation 2.6}$$

Table 2.4: **Reaction data and first-order rate constants for exchange of the C(3)-H of triazolium salt (137) for deuterium in solutions of DCl in D_2O at 25 ºC and $I = 1.0$ (KCl)**

[DCl], M	[DO⁻], M	time, s	f(s)	$\ln f$(s)	k_{ex}, s⁻¹
1.0	2.49×10^{-15} (pD 0.13)	0	1.000	0.000	3.04×10^{-6}
		16140	0.920	-0.084	
		192900	0.537	-0.622	
		270720	0.424	-0.857	
		355860	0.329	-1.113	
		450240	0.248	-1.395	
		604200	0.158	-1.848	
		815940	0.081	-2.508	
0.5	4.33×10^{-15} (pD 0.37)	0	1.000	0.000	4.10×10^{-6}
		61560	0.783	-0.244	
		84540	0.078	-0.345	
		167820	0.503	-0.686	
		244140	0.379	-0.971	
		326160	0.259	-1.350	
0.2	1.04×10^{-14} (pD 0.75)	0	1.000	0.000	6.38×10^{-6}
		60240	0.674	-0.395	
		84720	0.579	-0.547	
		166980	0.336	-1.092	
		240300	0.217	-1.530	
		321960	0.129	-2.049	
		347640	0.107	-2.239	
0.02	1.04×10^{-13} (pD 1.75)	0	1.000	0.000	3.59×10^{-5}
		5760	0.813	-0.207	
		13440	0.615	-0.487	
		16680	0.549	-0.600	
		20220	0.483	-0.727	
		25680	0.401	-0.913	
		32160	0.309	-1.174	
		39600	0.243	-1.413	
0.01	1.98×10^{-13} (pD 2.03)	0	1.000	0.000	6.45×10^{-5}
		5640	0.691	-0.369	
		11400	0.481	-0.733	
		14400	0.394	-0.932	
		16680	0.339	-1.081	
		20040	0.275	-1.291	
		24660	0.206	-1.578	
		30000	0.143	-1.945	
0.008	2.49×10^{-13} (pD 2.13)	0	1.000	0.000	8.14×10^{-5}
		5940	0.626	-0.468	
		9960	0.450	-0.798	
		12300	0.376	-0.978	
		14640	0.307	-1.182	
		16920	0.255	-1.368	
		21360	0.180	-1.712	
		26940	0.111	-2.196	

		0	1.000	0.000	
		6180	0.546	-0.605	
0.006	3.44×10^{-13}	7920	0.452	-0.795	1.03×10^{-4}
	(pD 2.27)	10560	0.342	-1.072	
		12600	0.276	-1.286	
		14940	0.215	-1.538	
		17340	0.172	-1.763	
		20520	0.121	-2.114	
		0	1.000	0.000	
		6240	0.410	-0.892	
0.004	4.86×10^{-13}	7980	0.325	-1.124	1.46×10^{-4}
	(pD 2.42)	9480	0.257	-1.358	
		11400	0.191	-1.653	
		12900	0.154	-1.874	
		14940	0.114	-2.175	
		0	1.000	0.000	
		600	0.733	-0.311	
0.0005	1.93×10^{-12}	1200	0.483	-0.727	6.24×10^{-4}
	(pD 3.02)	1800	0.342	-1.072	
		2400	0.234	-1.451	
		3000	0.161	-1.824	
		4080	0.079	-2.539	

(a) Concentration of deuteroxide ion calculated using Equation 2.6. (b) Fraction of substrate remaining, f(s), calculated using Equation 2.4. (c) Pseudo-first-order rate constant for exchange, k_{ex} (s^{-1}), obtained from the slope of the plot of ln f(s) against time in Figures 2.4 – 2.6.

Figure 2.4: **Semilogarithmic plots of the fraction of unexchanged substrate against time for the deuterium exchange reaction of (137) in solutions of DCl in D$_2$O at 25 ºC and I = 1.0 (KCl)**
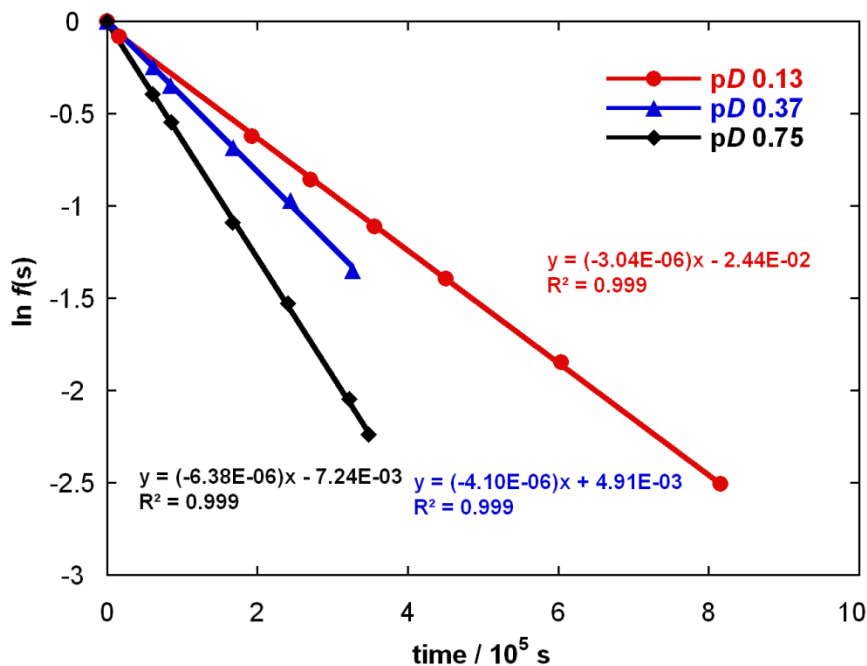
Figure 2.5: Semilogarithmic plots of the fraction of unexchanged substrate against time for the deuterium exchange reaction of (137) in solutions of DCl in D$_2$O at 25 ºC and I = 1.0 (KCl)
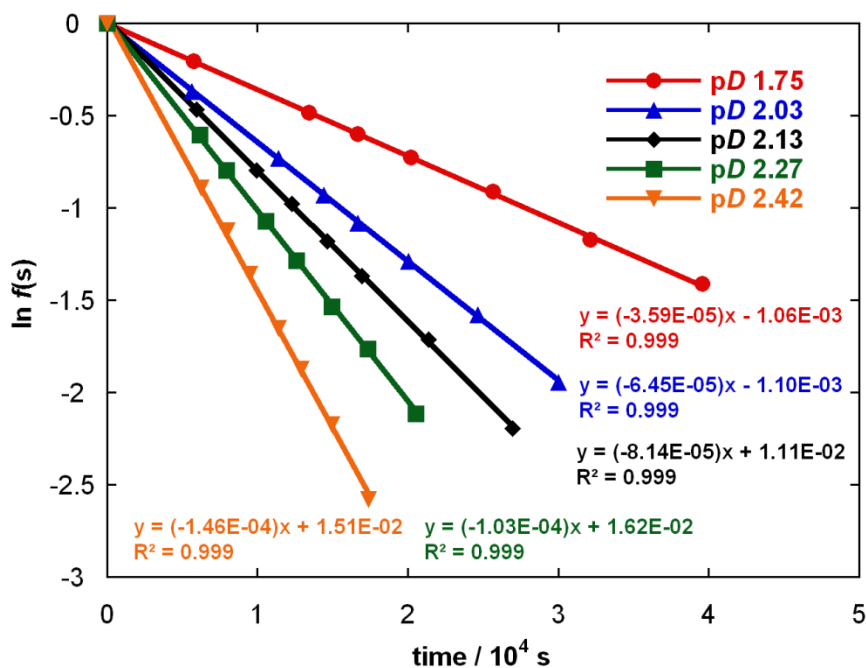
Figure 2.6: Semilogarithmic plots of the fraction of unexchanged substrate against time for the deuterium exchange reaction of (137) in solutions of DCl in D$_2$O at 25 ºC and I = 1.0 (KCl)
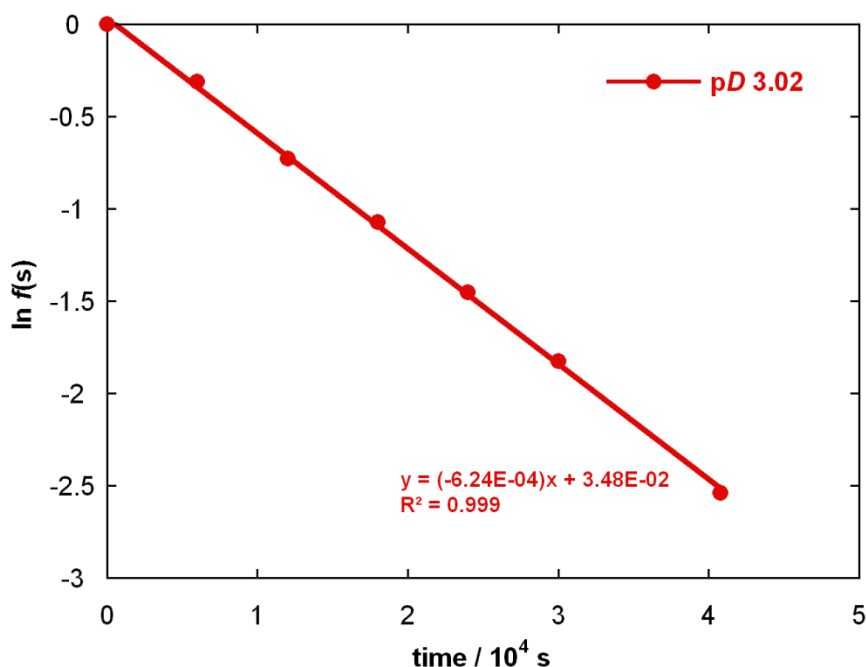
2.2.1.1b 2-(4-Fluorophenyl)-6,7-dihydro-5*H*-pyrrolo[2,1-c][1,2,4]triazol-2-ium tetrafluoroborate (138)
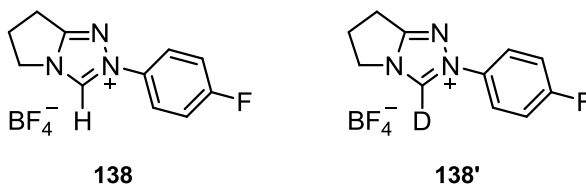
Pseudo-first-order rate constants for the deuteroxide ion-catalysed exchange of the C(3)-H of triazolium ion **138** to form deuterated product **138'** were determined by ^{1}H NMR spectroscopy (400 MHz).

A representative set of spectra taken at three time points during the reaction at p*D* 2.27 (6 mM DCl) is shown in Figure 2.7. Deuterium exchange at the C(3)-H position resulted in the disappearance of the C(3)-H singlet at 9.98 ppm over the course of the reaction. The extent of exchange was measured relative to the 12 equivalent non-exchangeable protons of the internal standard at 3.09 ppm. Signals corresponding to the *ortho*-CH and *meta*-CH groups on the aryl substituent appear as a triplet and multiplet at 7.29 and 7.71 ppm respectively. The signals corresponding to the three CH_2 groups on the five-membered ring appear as two sets of triplets at 3.15 and 4.40 ppm, and a multiplet at 2.76 ppm. No change was observed in the integrated area of any other peak relative to the internal standard, indicating that deuterium exchange does not occur at any position other than at C(3)-H under these conditions.

Figure 2.7:   **Representative ^{1}H NMR spectra at 400 MHz of triazolium salt (138) (10 mM, p*D* 2.27), obtained during exchange of the C(3)-H (s, 9.98 ppm) for deuterium in D$_2$O at 25 ºC and *I* = 1.0 (KCl) [Internal standard, tetramethylammonium deuteriosulfate (s, 3.09 ppm)]**

Experimentally observed first-order rate constants for exchange, k_{ex} (s^{-1}), were determined from the slopes of semi-logarithmic plots of *f*(s) against time at each p*D*. Reaction data and values of k_{ex} are presented in Appendix A (Table A1, Figures A1 – A3).

2.2.1.1c 2-Phenyl-6,7-dihydro-5*H*-pyrrolo[2,1-c][1,2,4]triazol-2-ium tetrafluoroborate (139)

139 **139'**

Pseudo-first-order rate constants for the deuteroxide ion-catalysed exchange of the C(3)-H of triazolium ion **139** to form deuterated product **139'** were determined by ^{1}H NMR spectroscopy (400 MHz).

A representative set of spectra taken at three time points during the reaction at p*D* 0.13 (1 M DCl) is shown in Figure 2.8. Deuterium exchange at the C(3)-H position resulted in the disappearance of the C(3)-H singlet at 9.67 ppm over the course of the reaction. The extent of exchange was measured relative to the 12 equivalent non-exchangeable protons of the internal standard at 2.74 ppm. Signals corresponding to the *ortho*-CH, *meta*-CH and *para*-CH groups on the phenyl substituent appear as a pair of multiplets at 7.20 and 7.35 ppm respectively. The signals corresponding to the three CH$_2$ groups on the five-membered ring appear as two sets of triplets at 4.06 and 2.81 ppm, and a multiplet at 2.43 ppm. No change was observed in the integrated area of any other peak relative to the internal standard, indicating that deuterium exchange does not occur at any position other than at C(3)-H under these conditions.

Figure 2.8:   Representative ^{1}H NMR spectra at 400 MHz of triazolium salt (139) (10 mM, p*D* 0.13), obtained during exchange of the C(3)-H (s, 9.67 ppm) for deuterium in D$_2$O at 25 ºC and *I* = 1.0 (KCl) [Internal standard, tetramethylammonium deuteriosulfate (s, 2.74 ppm)]

Experimentally observed first-order rate constants for exchange, k_{ex} (s^{-1}), were determined from the slopes of semi-logarithmic plots of *f*(s) against time at each p*D*. Reaction data and values of k_{ex} are presented in Appendix A (Table A2, Figures A4 – A5).

2.2.1.1d   2-(1,3,5-Trimethylphenyl)-6,7-dihydro-5*H*-pyrrolo[2,1-c][1,2,4]triazol-2-ium tetrafluoroborate (140)

140   **140'**

Pseudo-first-order rate constants for the deuteroxide ion-catalysed exchange of the C(3)-H of triazolium ion **140** to form deuterated product **140'** were determined by ^{1}H NMR spectroscopy (500 MHz).

A representative set of spectra taken at three time points during the reaction at p*D* 2.27 (6 mM DCl) is shown in Figure 2.9. Deuterium exchange at the C(3)-H position resulted in the disappearance of the C(3)-H singlet at 9.92 ppm over the course of the reaction. The extent of exchange was measured relative to the 12 equivalent non-exchangeable protons of the internal standard at 3.25 ppm. A signal corresponding to the two equivalent *meta*-CH protons on the mesityl substituent appears as a singlet at 7.24 ppm, and those corresponding to the CH_3 groups are present as two singlets at 2.42 and 2.12 ppm. The signals corresponding to the three CH_2 groups on the five-membered ring appear as two sets of triplets at 3.34 and 4.61 ppm, and a multiplet at 2.96 ppm. No change was observed in the integrated area of any other peak relative to the internal standard, indicating that deuterium exchange does not occur at any position other than at C(3)-H under these conditions.

Figure 2.9:   **Representative ^{1}H NMR spectra at 500 MHz of triazolium salt (140) (10 mM, p*D* 2.27), obtained during exchange of the C(3)-H (s, 9.92 ppm) for deuterium in D$_2$O at 25 ºC and *I* = 1.0 (KCl) [Internal standard, tetramethylammonium deuteriosulfate (s, 3.25 ppm)]**
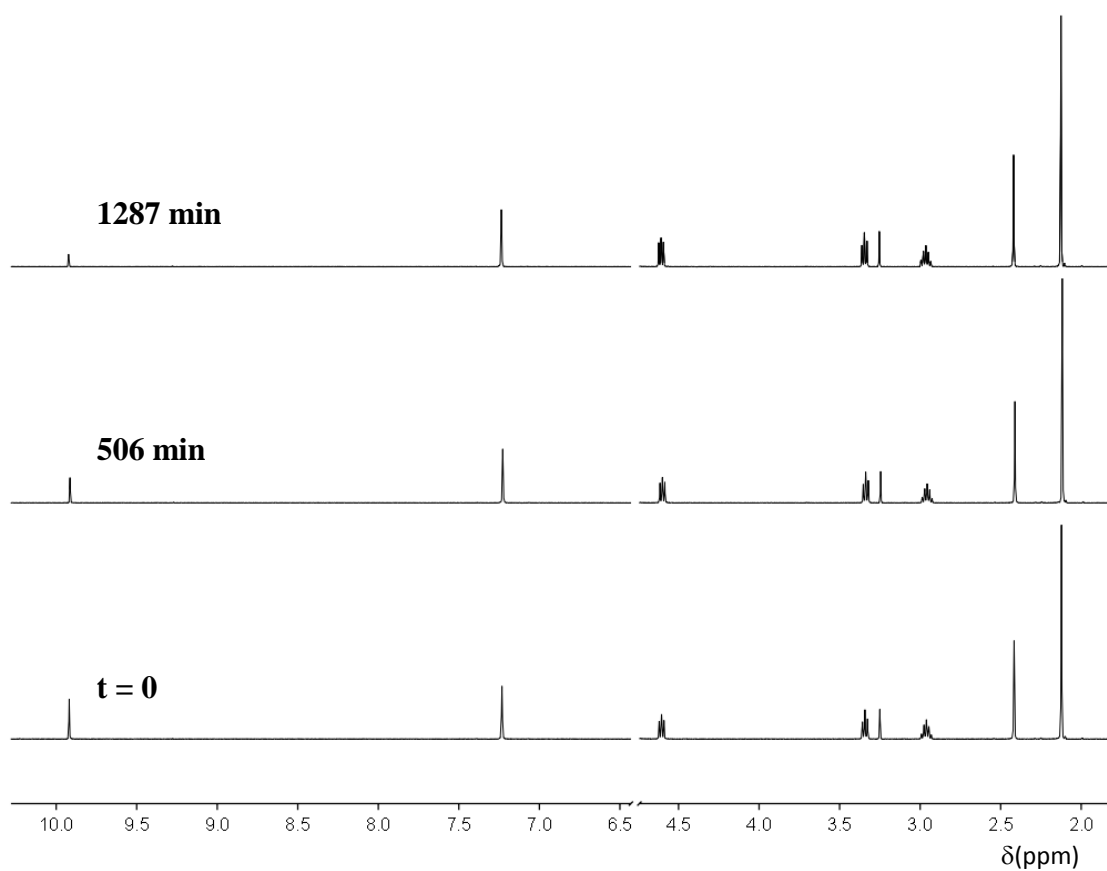
Experimentally observed first-order rate constants for exchange, k_{ex} (s^{-1}), were determined from the slopes of semi-logarithmic plots of *f*(s) against time at each p*D*. Reaction data and values of k_{ex} are presented in Appendix A (Table A3, Figures A6 – A8).

2.2.1.1e   2-(4-Methoxyphenyl)-6,7-dihydro-5*H*-pyrrolo[2,1-c][1,2,4]triazol-2-ium tetrafluoroborate (141)

141   **141'**

Pseudo-first-order rate constants for the deuteroxide ion-catalysed exchange of the C(3)-H of triazolium ion **141** to form deuterated product **141'** were determined by ^{1}H NMR spectroscopy (400 MHz).

A representative set of spectra taken at three time points during the reaction at p*D* 0.13 (1 M DCl) is shown in Figure 2.10. Deuterium exchange at the C(3)-H position resulted in the disappearance of the C(3)-H singlet at 9.55 ppm over the course of the reaction. The extent of exchange was measured relative to the 12 equivalent non-exchangeable protons of the internal standard at 2.73 ppm. Signals corresponding to the *ortho*-CH and *meta*-CH groups on the aryl substituent appear as a pair of doublets at 7.27 and 6.74 ppm respectively. A singlet corresponding to the CH$_3$ group on the methoxy substituent appears at 3.45 ppm. The signals corresponding to the three CH$_2$ groups on the five-membered ring appear as two sets of triplets at 4.04 and 2.79 ppm, and a multiplet at 2.41 ppm. No change was observed in the integrated area of any other peak relative to the internal standard, indicating that deuterium exchange does not occur at any position other than at C(3)-H under these conditions.

Figure 2.10: Representative ^{1}H NMR spectra at 400 MHz of triazolium salt (141) (10 mM, p*D* 0.13), obtained during exchange of the C(3)-H (s, 9.55 ppm) for deuterium in D$_2$O at 25 ^{o}C and *I* = 1.0 (KCl) [Internal standard, tetramethylammonium deuteriosulfate (s, 2.73 ppm)]
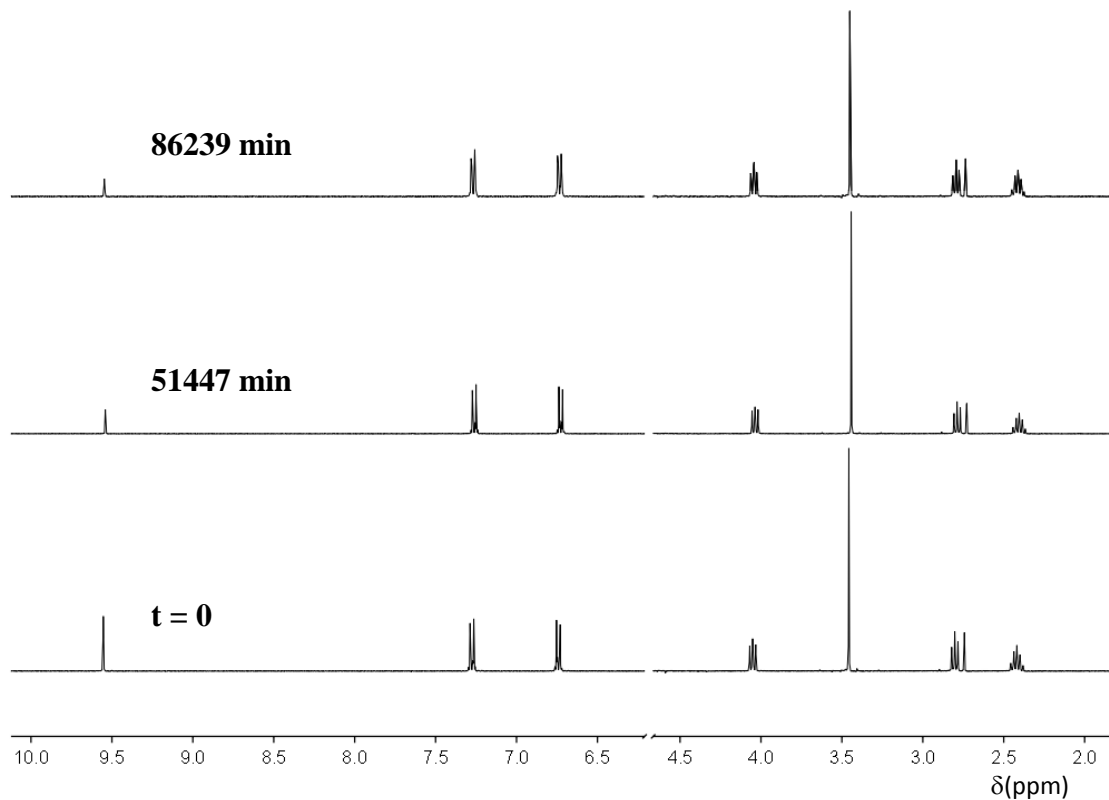
Experimentally observed first-order rate constants for exchange, k_{ex} (s^{-1}), were determined from the slopes of semi-logarithmic plots of *f*(s) against time at each p*D*. Reaction data and values of k_{ex} are presented in Appendix A (Table A4, Figures A9 – A10).

2.2.1.1f 4-Pentafluorophenyl-6,7-dihydro-5*H*-pyrrolo[2,1-c][1,2,4]triazol-2-ium tetrafluoroborate (142)
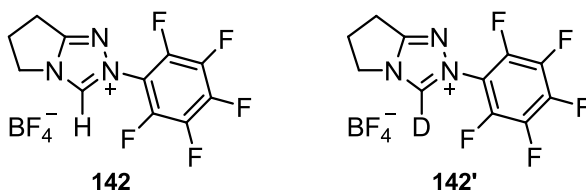
142   **142'**

Pseudo-first-order rate constants for the deuteroxide ion-catalysed exchange of the C(3)-H of triazolium ion **142** to form deuterated product **142'** were determined by ^{1}H NMR spectroscopy (400 MHz).

A representative set of spectra taken at three time points during the reaction at p*D* 0.37 (0.5 M DCl) is shown in Figure 2.11. Deuterium exchange at the C(3)-H position resulted in the disappearance of the C(3)-H singlet at 10.05 ppm over the course of the reaction. The extent of exchange was measured relative to the 12 equivalent non-exchangeable protons of the internal standard at 3.01 ppm. Signals corresponding to the three CH$_2$ groups on the five-membered ring appear as two sets of triplets at 3.12 and 4.39 ppm, and a multiplet at 2.90 ppm. No change was observed in the integrated area of any other peak relative to the internal standard, indicating that deuterium exchange does not occur at any position other than at C(3)-H under these conditions.

Figure 2.11: Representative ^{1}H NMR spectra at 400 MHz of triazolium salt (142) (10 mM, p*D* 0.37), obtained during exchange of the C(3)-H (s, 10.05 ppm) for deuterium in D$_2$O at 25 °C and *I* = 1.0 (KCl) [Internal standard, tetramethylammonium deuteriosulfate (s, 3.01 ppm)]
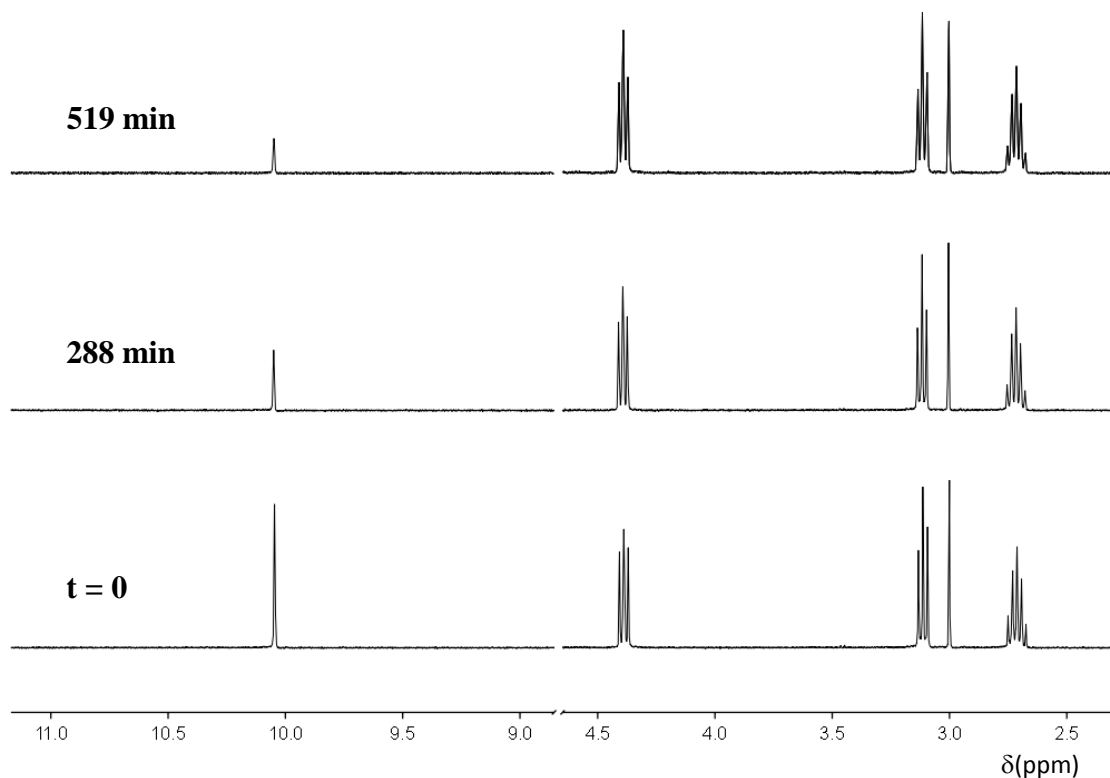
Experimentally observed first-order rate constants for exchange, k_{ex} (s^{-1}), were determined from the slopes of semi-logarithmic plots of *f*(s) against time at each p*D*. Reaction data and values of k_{ex} are presented in Appendix A (Table A5, Figures A11 – A12).
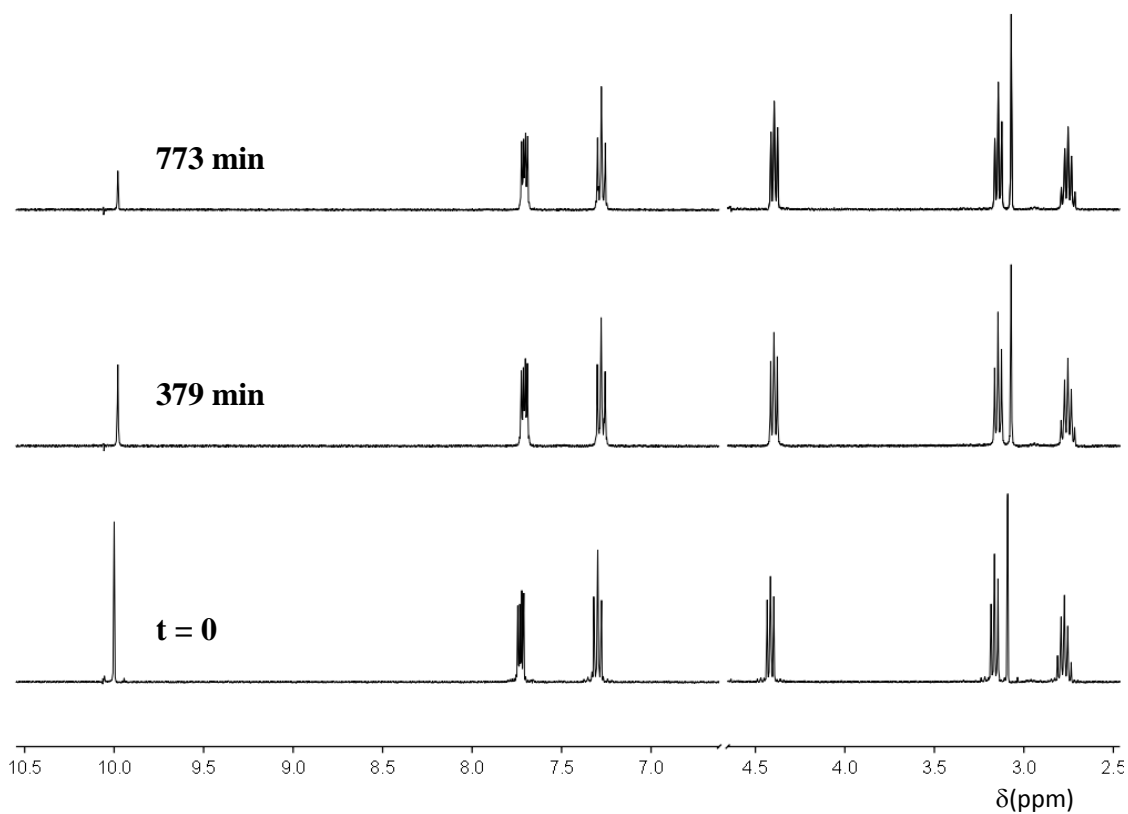
2.2.1.1g   2-(2-Pyridyl)-6,7-dihydro-5*H*-pyrrolo[2,1-c][1,2,4]triazol-2-ium tetrafluoroborate (143)
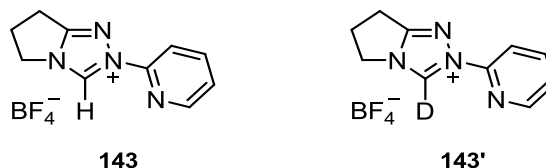
Pseudo-first-order rate constants for the deuteroxide ion-catalysed exchange of the C(3)-H of triazolium ion **143** to form deuterated product **143'** were determined by ^{1}H NMR spectroscopy (400 MHz).
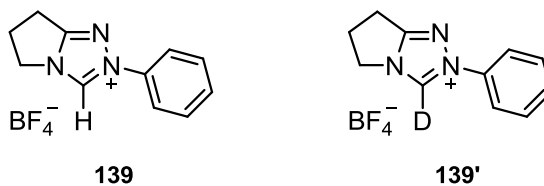
A representative set of spectra taken at three time points during the reaction at p*D* 2.05 (10 mM DCl) is shown in Figure 2.12. Deuterium exchange at the C(3)-H position resulted in the disappearance of the C(3)-H singlet at 10.34 ppm over the course of the reaction. The extent of exchange was measured relative to the 12 equivalent non-exchangeable protons of the internal standard at 3.17 ppm. Signals corresponding to the *ortho*-CH and *para*-CH groups on the pyridyl ring appear as a doublet at 8.57 ppm and a triplet at 7.64 ppm respectively. Those corresponding to the *meta*-CH groups appear as a triplet at 8.15 ppm and a doublet at 7.98 ppm. Signals corresponding to the three CH$_2$ groups on the five-membered ring appear as two sets of triplets at 4.53 and 3.27 ppm, and a multiplet at 2.88 ppm. No change was observed in the integrated area of any other peak relative to the internal standard, indicating that deuterium exchange does not occur at any position other than at C(3)-H under these conditions.

Figure 2.12: Representative ^{1}H NMR spectra at 400 MHz of triazolium salt (143) (10 mM, pD 2.05), obtained during exchange of the C(3)-H (s, 10.34 ppm) for deuterium in D$_2$O at 25 ºC and I = 1.0 (KCl) [Internal standard, tetramethylammonium deuteriosulfate (s, 3.17 ppm)]
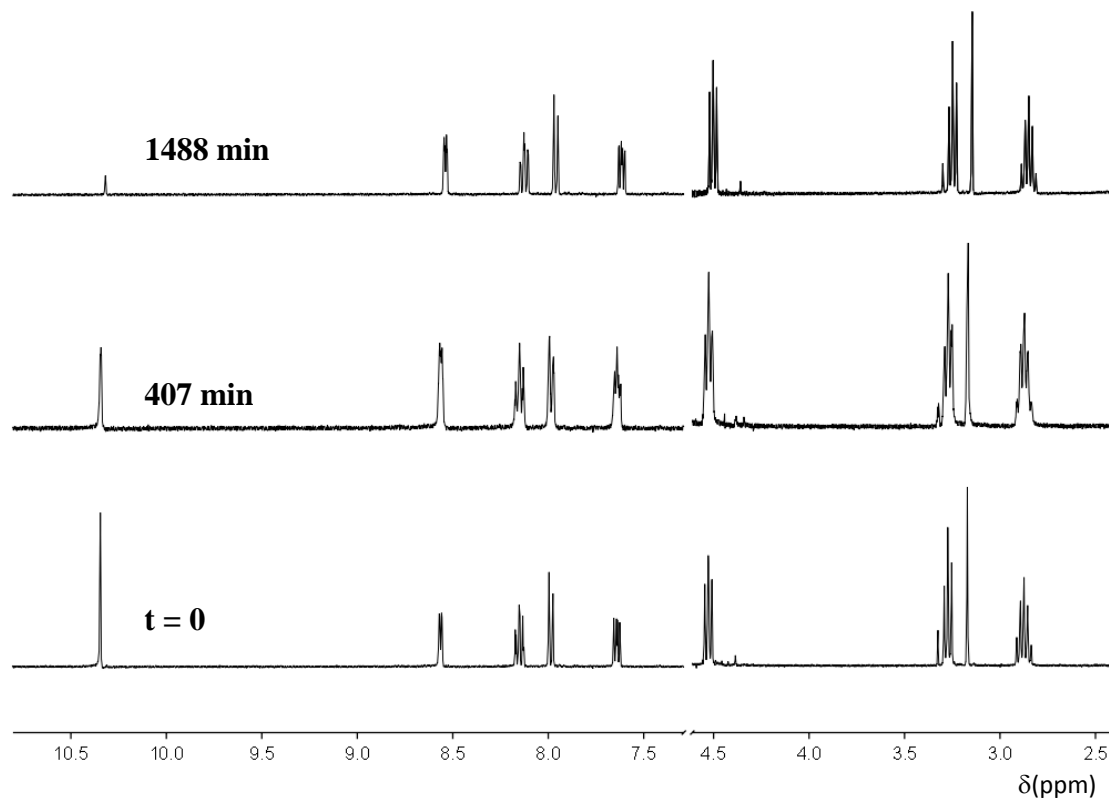
Experimentally observed first-order rate constants for exchange, k_{ex} (s^{-1}), were determined from the slopes of semi-logarithmic plots of f(s) against time at each pD. Reaction data and values of k_{ex} are presented in Appendix A (Table A6, Figures A13 – A14).
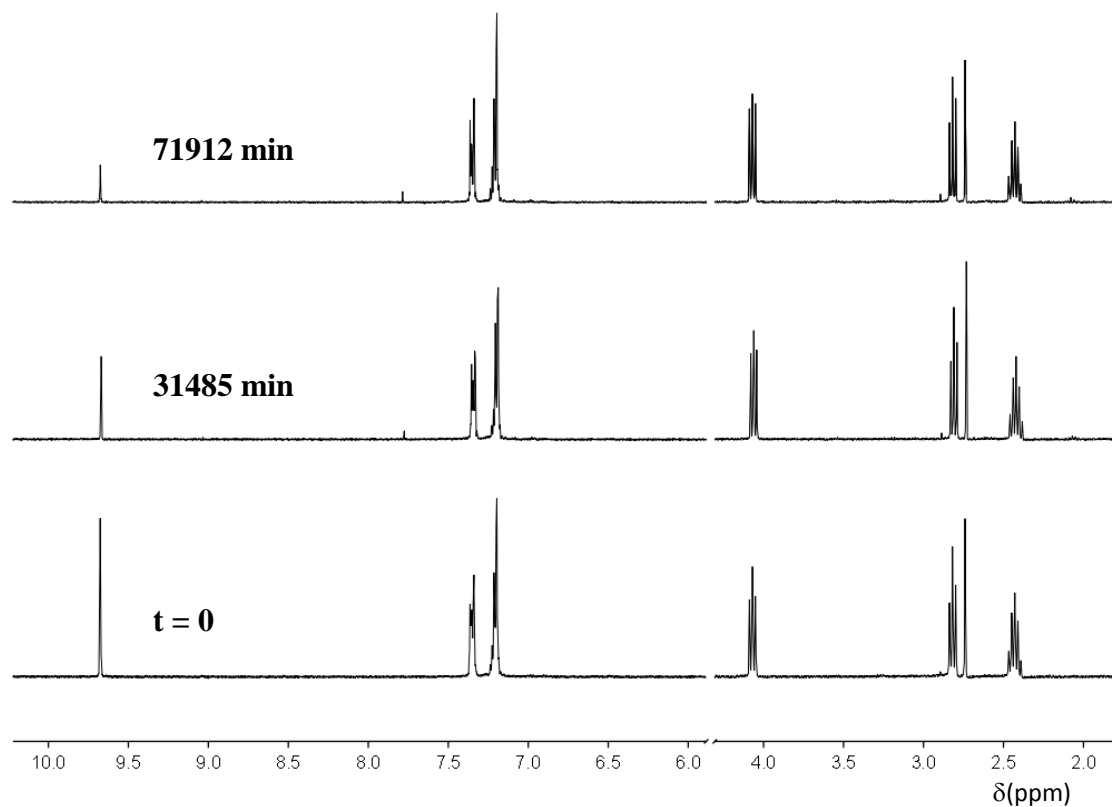
2.2.1.2 Determination of second-order rate constants for deuteroxide ion-catalysed exchange (k_{DO})

The experimentally observed pseudo-first-order rate constants for exchange, k_{ex} (s^{-1}), determined in the previous section, include terms for deuteroxide ion ($k_{DO}[DO^-]$), and potentially, solvent (k_{D2O}) and buffer base ($k_B[B]$) (Equation 2.7). The extent of contributions from the latter two species will be assessed in this section.

$$k_{ex} = k_{DO}[DO^-] + k_{D2O} + k_B[B] \qquad \textbf{Equation 2.7}$$

In the majority of cases, exchange reactions of triazolium ions **137** – **143** were performed in solutions of DCl in the absence of buffer base. However, for measurements in acetic acid buffers, general base catalysis by acetate ion may contribute to the experimentally observed rate constant for exchange, k_{ex} (s^{-1}). To determine the extent of general base catalysis, exchange experiments were performed at a fixed concentration of deuteroxide ion, but with varying concentrations of buffer base. This was achieved by using a fixed buffer ratio (*i.e.* pD was maintained), whilst varying the total concentration of buffer. The presence of general base catalysis of exchange would result in an increase in the experimentally observed pseudo-first-order rate constant for exchange, k_{ex} (s^{-1}), as the concentration of buffer base is increased.

General base catalysis of exchange can be observed when deprotonation of the substrate by deuteroxide ion is rate-determining for the overall deuteroxide ion-catalysed exchange reaction. The low reactivity of the lyoxide ion (LO$^-$) towards proton transfer to and from carbon is known as the 'lyoxide ion anomaly'. Brønsted bases (*i.e.* buffer bases) are significantly more reactive, and will result in an increase in the rate of the deprotonation step. However, in cases where reprotonation of the carbene by solvent is so fast that the solvent reorganisation step is rate-determining overall, then general base catalysis will not be observed as there is no mechanism by which a Brønsted base may lower the energy barrier for this step. Thus, the absence of general base catalysis of exchange allows a value of $k_{reorg} = 10^{11}$ s^{-1} to be assigned as the rate constant for the reverse protonation of the carbene. This requirement will be discussed in more detail in Section 2.3.

The contribution of general base catalysis to exchange of the C(3)-H for deuterium was assessed for representative triazolium ion **138**, and these results are presented below.
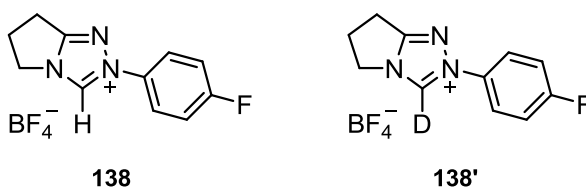
138 **138'**

First-order rate constants for deuteroxide ion-catalysed exchange of the C(3)-H of triazolium ion **138** to form deuterated product **138'** were dete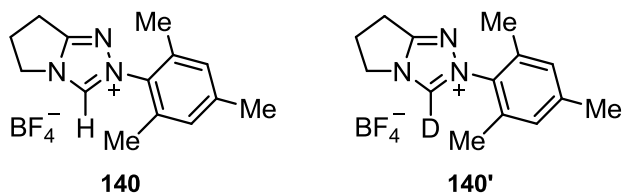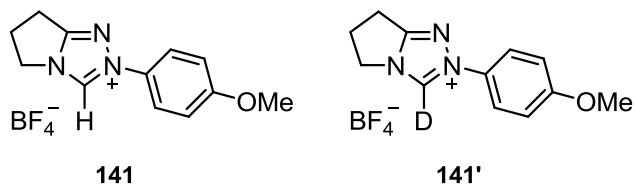rmined by ^{1}H NMR spectroscopy (400 MHz). Experiments were performed in acetic acid buffers at a fixed buffer ratio. ^{1}H NMR spectral details have been described previously for **138**.

Experimentally observed first-order rate constants for exchange, k_{ex} (s^{-1}), were determined from the slopes of semi-logarithmic plots of *f*(s) against time at five total buffer concentrations ([Buffer]$_{tot}$ = 0.1 − 1.0 M) (Figure 2.13). Reaction data for these experiments and values of k_{ex} at each buffer concentration are presented in Table 2.5.

Figure 2.13: **Semilogarithmic plots of the fraction of unexchanged substrate against time for the H/D-exchange reaction of triazolium ion (138) in acetic acid buffer solutions (10% *f*$_B$) at buffer base concentrations 0.01 M (◯), 0.015 M (□), 0.02 M (◇), 0.025 M (△) and 0.1 M (▽) in D$_2$O at 25 ºC and *I* = 1.0 (KCl)**
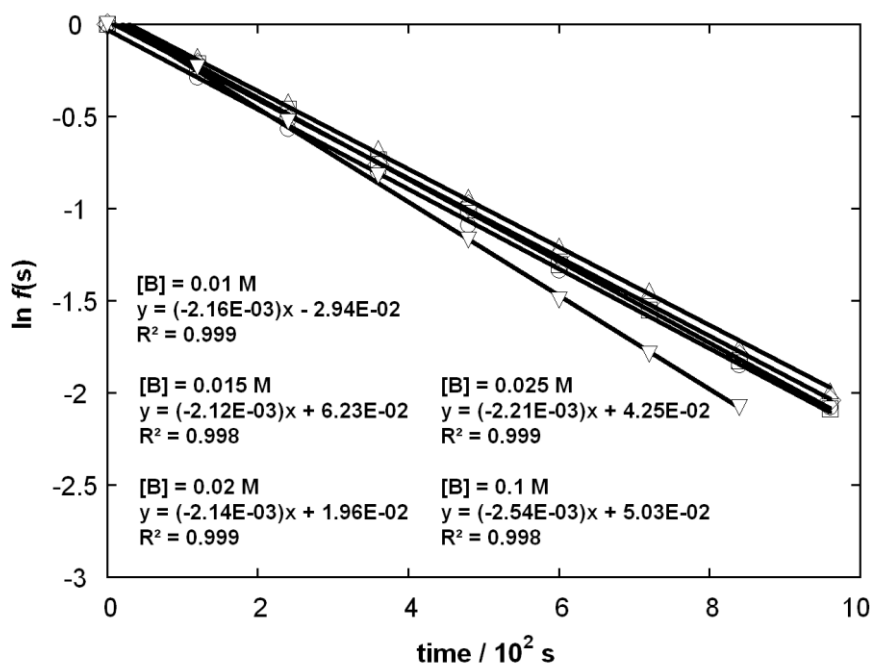
Table 2.5: **Reaction data and pseudo-first-order rate constants for exchange, k_{ex} (s^{-1}), of the C(3)-H of triazolium ion (138) for deuterium in 10% f_B acetic acid buffered solutions of D$_2$O at 25 °C and $I = 1.0$ (KCl)**

[buffer]$_{tot}$, M^a	[DO$^-$], M	time, s	f(s)^d	ln f(s)	k_{ex}, s^{-1}
		0	1.000	0.000	
		120	0.748	-0.290	
0.10	2.61 × 10^{-11}	240	0.567	-0.567	2.16 × 10^{-3}
	(pD 4.15)	360	0.447	-0.805	
		480	0.336	-1.091	
		600	0.263	-1.336	
		840	0.157	-1.852	
		960	0.125	-2.079	
		0	1.000	0.000	
		120	0.839	-0.176	
0.15	2.55 × 10^{-11}	240	0.658	-0.419	2.12 × 10^{-3}
	(pD 4.14)	360	0.510	-0.673	
		480	0.391	-0.939	
		600	0.300	-1.204	
		720	0.236	-1.444	
		840	0.174	-1.749	
		960	0.137	-1.988	
		0	1.000	0.000	
		120	0.809	-0.212	
0.20	2.55 × 10^{-11}	240	0.599	-0.512	2.14 × 10^{-3}
	(pD 4.14)	360	0.468	-0.759	
		480	0.375	-0.981	
		600	0.286	-1.252	
		720	0.222	-1.505	
		840	0.166	-1.796	
		960	0.130	-2.040	
		0	1.000	0.000	
		120	0.809	-0.212	
0.25	2.55 × 10^{-11}	240	0.631	-0.460	2.21 × 10^{-3}
	(pD 4.14)	360	0.479	-0.736	
		480	0.366	-1.005	
		600	0.271	-1.306	
		720	0.212	-1.551	
		840	0.161	-1.826	
		960	0.124	-2.087	
		0	1.000	0.000	
		120	0.790	-0.236	
1.00	2.70 × 10^{-11}	240	0.589	-0.529	2.53 × 10^{-3}
	(pD 4.16)	360	0.439	-0.823	
		480	0.311	-1.168	
		600	0.224	-1.496	
		720	0.167	-1.790	
		840	0.125	-2.079	

(a) Total concentration of acetic acid buffer [CH$_3$CO$^-$K$^+$]+[CH$_3$COD]; (b) Concentration of deuteroxide ion calculated using Equation 2.6, where $\gamma_{DO} = 0.73$; (c) Concentration of deuteroxide ion calculated using Equation 2.6, where $\gamma_{DO} = 0.72$; (d) Fraction of unexchanged substrate remaining, f(s), calculated using Equation 2.4; (e) Pseudo-first-order rate constant for exchange, k_{ex} (s^{-1}), obtained from the slope of the plot of ln f(s) against time in Figure 2.13.

Values of k_{ex} (s^{-1}) as a function of the concentration of buffer base are shown in Table 2.6. The ratio of rate constants, k_{rel}, obtained using Equation 2.8, is a measure of the relative difference in the experimentally observed rate constant for exchange, k_{ex} (s^{-1}), and contribution to rate from deuteroxide ion-catalysed exchange, k_{DO}[DO$^-$] (s^{-1}), where k_{DO} (M^{-1} s^{-1}) is determined from rate measurements in un-buffered solution.

Table 2.6: **Pseudo-first-order rate constants for exchange, k_{ex} (s^{-1}), of the C(3)-H of triazolium ion (138) for deuterium in 10% f_B acetic acid buffered solutions of D$_2$O at 25 °C and I = 1.0 (KCl)**

[B], M ^{a}	[B]/[DO$^-$] ^{b}	k_{ex}, s^{-1}	k_{rel}
0.010	3.83×10^8	2.16×10^{-3}	1.08
0.015	5.88×10^8	2.12×10^{-3}	0.96
0.020	7.84×10^8	2.14×10^{-3}	0.96
0.025	9.80×10^8	2.21×10^{-3}	0.97
0.100	3.70×10^9	2.53×10^{-3}	1.08

(a) Concentration of free base (CH$_3$CO$^-$) form of buffer. (b) Ratio of concentrations of CH$_3$CO$^-$ to deuteroxide ion. (c) Experimentally observed pseudo-first-order rate constant for exchange of C(3)-H of triazolium **138**, (d) Ratio of first-order rate constant for exchange of C(3)-H (k_{ex}) to first-order rate term for deuteroxide ion-catalysed exchange only (k_{DO}[DO$^-$]), as described in Equation 2.8, where $k_{DO} = 8.66 \times 10^7$ M^{-1} s^{-1}.

Figure 2.14 shows a plot of k_{rel} against ([B]/[DO$^-$]), which corrects for the small changes in pD that occur upon dilution of a buffer solution at constant ionic strength. The ratio of second-order rate constants for buffer base catalysed exchange to deuteroxide ion catalysed exchange, k_B/k_{DO}, may be obtained as the slope this plot according to Equation 2.8. In the absence of general base catalysis of exchange, this ratio should be close to zero.

$$k_{rel} = \frac{k_{ex}}{k_{DO}[DO^-]} = \frac{(k_{DO}[DO^-] + k_B[B])}{k_{DO}[DO^-]} = 1 + \frac{k_B[B]}{k_{DO}[DO^-]} \qquad \textbf{Equation 2.8}$$

Figure 2.14: Plot of the ratio of rate constants k_{rel} against ([B]/[DO$^-$])
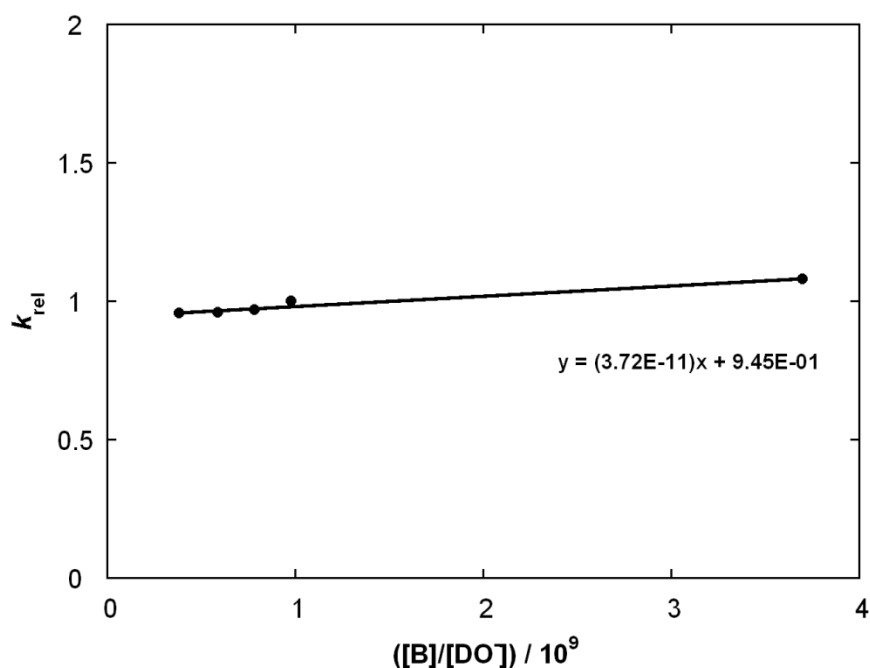
From the slope of this plot, the ratio k_B/k_{DO} was found to be equal to 3.72×10^{-11}. This value is small relative to the changes in concentration of buffer base, and falls well within the 6% experimental error limits associated with values of k_{DO} (M^{-1} s^{-1}) (treatment of errors in exchange reactions is discussed in Appendix A2). As such, general base catalysis is judged to be insignificant for 1,2,4-triazolium ions **137 – 143**, and the buffer catalysis term may be removed from Equation 2.7.

The significance of the contribution from the solvent reaction (k_{D2O}) will be discussed in Section 2.3.1, following our analysis of the pD-rate profiles for exchange.

The p*D*-rate profiles for exchange of the C(3)-H of triazolium ions **137** – **142** for deuterium are shown in Figure 2.15.

Figure 2.15: **p*D*-rate profiles for exchange of the C(3)-H of triazolium ions (137) – (142) for deuterium in D$_2$O at 25 ^{o}C and *I* = 1.0 (KCl)**
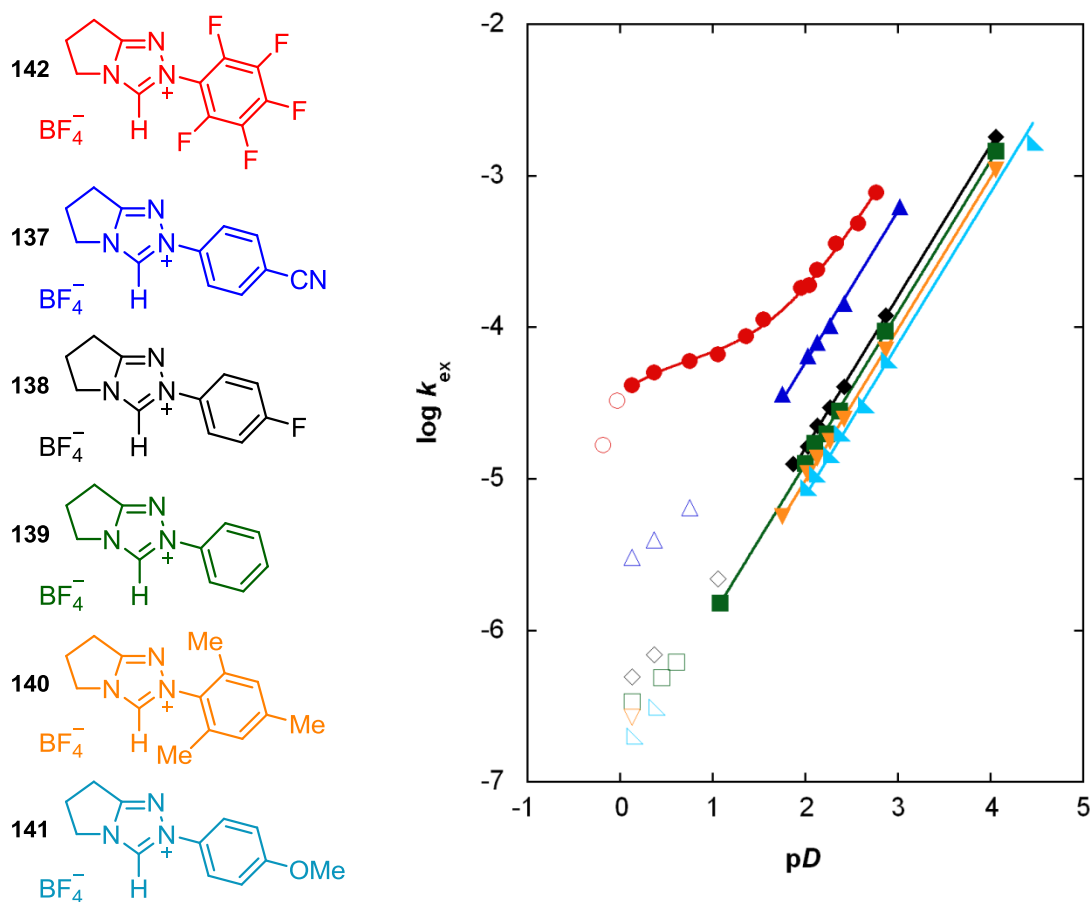
For triazolium ions **137** – **141**, values of log k_{ex} were found to increase with p*D* in the range 0 – 4.5. The solid lines through the p*D*-rate profiles for triazolium ions **137** – **141** show the fit of this data to Equation 2.9, derived from Equation 2.10, where k_{DO} is the second-order rate constant for deuteroxide ion-catalysed exchange, $K_W = 10^{-14.87}$ is the ionic product for D$_2$O at 25 °C, and γ_{DO} is the activity coefficient for deuteroxide ion determined under our reaction conditions. These fits were linear and are consistent with deuteroxide ion-catalysed exchange *via* pathway A (Scheme 2.4) as the dominant mechanism for H/D-exchange.

$$\log k_{ex} = \log \left(\frac{k_{DO} K_W}{\gamma_{DO}} \right) + pD \qquad \textbf{Equation 2.9}$$

$$k_{ex} = k_{DO}[DO^-] \qquad \textbf{Equation 2.10}$$

Scheme 2.4:
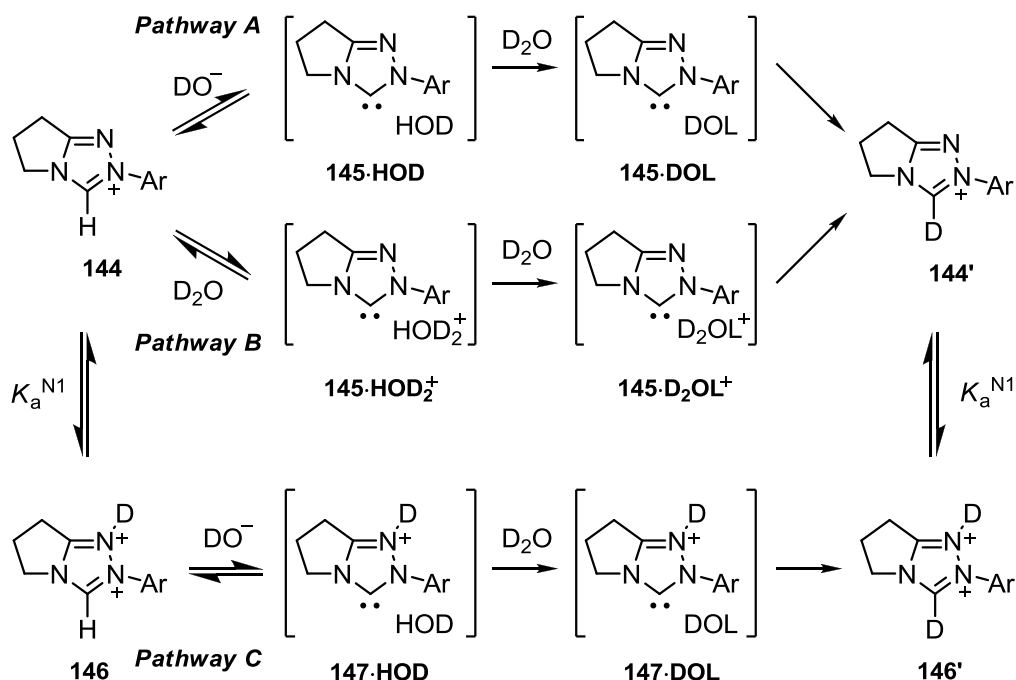
In Pathway A, deprotonation of triazolium ion **144** by deuteroxide ion gives **145·HOD** (an intimately bound complex of triazolylidene **145** and a molecule of HOD). Solvent reorganisation results in the replacement of HOD with a molecule of DOL (L = H or D) to form **145·DOL**, where the molecule of DOL is in a position to deliver a deuterium ion to the C(3) position. This solvent reorganisation step could involve rotation of the original molecule of HOD within the complex to give **145·DOL** (L = H), or alternatively, rotation could be accompanied by proton transfer with bulk solvent (L = D). As the concentration D$_2$O is present in vast excess of protonated substrate (10 mM), deuteration to form the exchanged product **144'** is essentially irreversible.

The pD-rate profiles of triazolium ions **137 – 141** deviate upwards from the linear fit to Equation 2.10 upon moving to lower pDs, implying that additional H/D-exchange pathways begin to compete under more acidic conditions. This deviation may be explained by H/D-exchange *via* one or both of pathways B and C, which are discussed in detail below. As a result, these data points (*i.e.* points that resulted in errors greater than 3% in the linear fit) were not included in fits of the pD-rate data to Equation 2.10 and are indicated by open symbols in the pD-rate profile. Values of the second-order rate constant for deuteroxide ion-catalysed exchange k_{DO} (M^{-1} s^{-1}) determined from the fits of the pD-rate profiles to Equation 2.10 are summarised in Table 2.7.

The p*D*-rate profile for triazolium ion **142** shows significant deviation from a slope of 1, and only the data above p*D* 2 fits well to Equation 2.10. In addition to the upward deviation in log k_{ex} observed between p*D* 0.5 and 1.5, a further decrease in log k_{ex} is observed at lower p*D*s. This altered dependence on p*D* cannot be attributed to a medium effect as ionic strength was maintained at $I = 1.0$ (KCl) above p*D* 0. Additional data points at 1.24 M DCl and 2.0 M DCl support the existence of this downward trajectory, although the ionic strength is higher in these cases.

The changes in the dependence of log k_{ex} on p*D* suggest competition from one or more additional deuterium exchange pathways at lower p*D*s. One possible mechanism, Pathway B, involves deprotonation of triazolium ion **144** by a molecule of solvent (D$_2$O), rather than deuteroxide ion, resulting in exchange product **144'** *via* the complex **145·HOD$_2$$^+$**. However, as the p*D*-rate profile does not become fully p*D*-independent, the occurrence of Pathways A and B alone are not sufficient to explain all of the data. Thus, an additional deuterium exchange pathway must be considered to explain the further decrease in log k_{ex} upon moving to lower p*D*s.

Protonation of the triazolium ion at N(1) would result in a dicationic species **146** and reduce the amount of monocationic **144** available for exchange *via* Pathways A and B. Alternatively, deprotonation of dicationic species **146** by deuteroxide ion (Pathway C) would result in carbene/ylide complex **147·HOD**, leading to the dicationic exchange product **146'**. Although the concentration of deuteroxide ion is considerably smaller than that of D$_2$O at these p*D*s, the 10^{19}-fold greater reactivity of the deuteroxide ion means that deprotonation by DO$^-$ is still possible.[10]

Equation 2.12, derived from Equation 2.13, allows for the dependence of Pathway A on the ionisation constant for protonation at N(1), $K_a^{N(1)}$, but does not take into account deprotonation *via* pathways B or C. The poor fit of Equation 2.12 to the p*D*-rate data for triazolium ion **1** indicates that one or both of competing pathways B and C are also necessary to account for the non-linear dependence of log k_{ex} on p*D*.

$$\log k_{ex} = \log \left[\frac{K_a^{N(1)}\left(\left(\frac{k_{DO}K_W}{\gamma_{DO}}\right)10^{pD}\right)}{K_a^{N(1)}+10^{-pD}} \right] \qquad \textbf{Equation 2.11}$$

$$k_{ex} = f_{T+}(k_{DO}[DO^-]) \qquad \textbf{Equation 2.12}$$

Equations 2.13 and 2.15 take into account Pathways A and B, and Pathways A and C respectively, in addition to N(1)-protonation at lower p*D*s. These kinetically equivalent equations are derived from Equations 2.14 and 2.16 respectively, and include terms for the pseudo-first-order rate constant for C(3)-H exchange of triazolium ion **144** by solvent, k_{D2O} (s^{-1}), and second-order rate constant for deuteroxide ion-catalysed C(3)-H exchange of dicationic triazolium ion **146**, k_{DO}' (M^{-1} s^{-1}). Both equations fit equally well to the p*D*-rate data for triazolium ion **142** (Figure 2.15), implying that pathway A is the predominant mechanism for H/D-exchange at higher p*D*s, and that one or both of pathways B and C are involved at lower p*D*s. As Equations 2.13 and 2.15 are kinetically indistinguishable, it is not possible to determine the extent to which pathway B or C contribute at lower p*D*s on the basis of overall kinetic fitting.

$$\log k_{ex} = \log \left[\frac{K_a^{N(1)}\left(\left(\frac{k_{DO}K_W}{\gamma_{DO}}\right)10^{pD}\right)+\left(K_a^{N(1)}k_{D2O}\right)}{K_a^{N(1)}+10^{-pD}} \right] \qquad \textbf{Equation 2.13}$$

$$k_{ex} = f_{T+}(k_{DO}[DO^-] + k_{D2O}) \qquad \textbf{Equation 2.14}$$

$$\log k_{ex} = \log \left[\frac{K_a^{N(1)}\left(\left(\frac{k_{DO}K_W}{\gamma_{DO}}\right)10^{pD}\right)+\left(\frac{k'_{DO}K_W}{\gamma_{DO}}\right)}{K_a^{N(1)}+10^{-pD}} \right] \qquad \textbf{Equation 2.15}$$

$$k_{ex} = f_{T+}(k_{DO}[DO^-]) + f_{T2+}(k'_{DO}[DO^-]) \qquad \textbf{Equation 2.16}$$

Identical values for the second-order rate constant for deuteroxide ion-catalysed exchange, k_{DO} (M^{-1} s^{-1}), and ionisation constant $K_a^{N(1)}$ were obtained using fitting Equations 2.14 and 2.16. Values for the pseudo-first-order rate constant for H/D-exchange of triazolium ion **142** by solvent, k_{D2O} (s^{-1}), and second-order rate constant for deuteroxide ion catalysed H/D-exchange of the dicationic form, k_{DO}' (M^{-1} s^{-1}), assume extremes of either pathway B or pathway C using Equations 2.13 and 2.15 respectively. By consideration of the magnitude of these rate constants, the likelihood of pathways B and C may be assessed, and this will be discussed in Section 2.4. Rate constants determined in the fits of triazolium ion **142** to Equations 2.13 and 2.15, and triazolium ions **137 – 141** to Equation 2.10, are summarised in Table 2.7.

Table 2.7: **Rate constants for exchange of the C(3)-H of triazolium salts (137) – (142) for deuterium in D$_2$O at 25 °C and *I* = 1.0 (KCl)**

substrate	
142	$k_{DO} = 6.82\ (\pm\ 0.25) \times 10^8\,M^{-1}\,s^{-1}$ [a] $k_{D2O} = 6.1\ (\pm\ 0.36) \times 10^{-5}\,s^{-1}$ [a] $k_{DO}' = 4.8\ (\pm\ 1.0) \times 10^{10}\,M^{-1}\,s^{-1}$ [a] $K_a^{N(1)} = 1.5\ (\pm\ 0.4)$ [a]
137	$k_{DO} = 3.18\ (\pm\ 0.08) \times 10^8\,M^{-1}\,s^{-1}$ [b]
138	$k_{DO} = 8.66\ (\pm\ 0.11) \times 10^7\,M^{-1}\,s^{-1}$ [b]
139	$k_{DO} = 6.82\ (\pm\ 0.13) \times 10^7\,M^{-1}\,s^{-1}$ [b]
140	$k_{DO} = 5.29\ (\pm\ 0.07) \times 10^7\,M^{-1}\,s^{-1}$ [b]
141	$k_{DO} = 4.20\ (\pm\ 0.23) \times 10^7\,M^{-1}\,s^{-1}$ [b]

(a) Obtained from fitting of the p*D*-rate profile to kinetically equivalent Equation 2.14 or Equation 2.16.
(b) Obtained from fitting of the p*D*-rate profile to Equation 2.10.

The pD-rate profile for exchange of the C(3)-H of triazolium ion **143** for deuterium is shown in Figure 2.16. Values of log k_{ex} were found to increase linearly with pD in the range 1.3 – 4, consistent with deuteroxide ion-catalysed exchange *via* Pathway A.

Figure 2.16: **pD-rate profile for exchange of the C(3)-H of triazolium ion (143) for deuterium in D₂O at 25 ºC and I = 1.0 (KCl)**


The presence of the pyridyl *N*-substituent in triazolium ion **143** must account for the increase in log k_{ex} below pD ~1.3. Two interpretations are proposed below.

In the first scenario, the nitrogen on the pyridyl ring may be protonated under acidic conditions according to Scheme 2.5a. This protonated structure may benefit from intramolecular hydrogen-bond stabilisation afforded by the proximal triazolium ring nitrogen N(1), as in **148**, or may simply exist as dicationic species **149**. Solvent-mediated exchange of the dication at the C(3)-H position would be expected to occur faster than the reaction of the monocationic azolium ion **143**. Once the pD-dependent term corresponding to Pathway A becomes negligible, an increase in log k_{ex} upon moving to lower pDs would be expected as the fraction of the more reactive dicationic substrate increases.

Scheme 2.5a:

Scheme 2.5b:

Alternatively, protonation at N(1) may occur to generate dicationic species **150**, as shown by Scheme 2.5b. Assisted deprotonation at the C(3)-H position by solvent water using the pyridyl nitrogen lone pair will result in H/D-exchange that may occur faster than that of unassisted deprotonation by solvent. These interpretations will be discussed in more detail in Section 2.3, paying particular attention to the differences between postulated Pathways C, D and E which all proceed *via* dicationic species.

Equation 2.17 describes both of the mechanistic scenarios proposed in Scheme 2.5. Pathways D and E are kinetically indistinguishable and the likelihood of either pathway cannot be judged by fitting alone. From the fit of the p*D*-rate data to Equation 2.18, derived from Equation 2.17, values of $k_{DO} = 1.10 \times 10^8$ M^{-1} s^{-1} and $K_a^N = 1.2$ ($\pm$ 0.6) were obtained. A value for the pseudo-first-order rate constant for deprotonation of the generic dicationic species (**148** – **150**) by solvent, $k_{D2O}' = 1.75 \times 10^{-4}$ s^{-1}, was also determined.

$$k_{ex} = f_{T+}(k_{DO}[DO^-]) + f_{T2+}(k_{D2O}')$$

Equation 2.17

$$\log k_{ex} = \log \left[\frac{K_a^N\left(\left(\frac{k_{DO}K_W}{\gamma_{DO}}\right)10^{pD}\right) + k_{D2O}' \cdot 10^{-pD}}{K_a^N + 10^{-pD}} \right]$$

Equation 2.18

In an attempt to obtain alternative estimates of the pK_a for the dicationic species, the effect of pD on UV-Vis absorbance was probed. UV-Vis spectra of **143** (0.25 mM) were obtained in aqueous solutions of HCl at constant ionic strength, $I = 1.0$ (KCl), in the pD range $0 - 2$ (Figure 2.17). Unfortunately, no significant change in absorbance was observed.

Figure 2.17: UV-Vis spectrum of (143) in solutions of HCl in H$_2$O at 25 °C and $I = 1.0$ (KCl)

The effect of a change in pD on ^{1}H chemical shifts was also assessed. The difference in ^{1}H chemical shift between the doublet corresponding to the *ortho*-CH group on the pyridyl ring, relative to the singlet corresponding to the four equivalent CH$_3$ groups on the internal standard, is presented in Table 2.8. Across the full pD range studied, no significant change in chemical shift is observed (<0.005 ppm).

Table 2.8: Variation of *ortho*-CH ^{1}H chemical shift relative to tetramethyl ammonium deuteriosulfate with pD, in solutions of DCl in D$_2$O at $I = 1.0$ (KCl) for (143)

[DCl], M	pD	$\Delta \delta_H$, ppm [a]
0.01	2.05	5.393
0.02	1.75	5.393
0.05	1.34	5.393
0.10	1.03	5.393
0.20	0.76	5.393
0.50	0.38	5.391
1.00	0.13	5.392

(a) Chemical shift difference between δ_H (*ortho*-CH) and δ_H (internal standard CH$_3$)

The combined UV-Vis and ^{1}H NMR data does not provide any additional evidence for N-protonation at lower pD values. However, from the fit of the pD-rate data to Equation 2.10, the error in K_a is relatively large ($\pm 50\%$), potentially yielding a value of p$K_a^{N(pyr)}$ as low as -0.25. The fraction of protonated species at pD 0.13 could therefore be as low as 30% and would be significantly smaller at higher pDs, and may explain these results.

Alternative estimates of the second-order rate constant for deuteroxide ion-catalysed exchange at the C(3)-H position, k_{DO} (M^{-1} s^{-1}), may be obtained from the slope of a plot of k_{ex} against deuteroxide ion concentration (*via* Equation 2.9). The y-axis intercept may potentially be assigned to the contribution from the uncatalysed solvent reaction, k_{D2O} (s^{-1}). Plots of k_{ex} against deuteroxide ion concentration for 1,2,4-triazolium ions **137**, **138**, **140** and **143** are shown in Figure 2.18. Values of k_{DO} and y-intercept values are summarised in Table 2.9. Values of k_{DO} for triazolium ions **139**, **141** and **143** have been determined previously using this method and are included in the discussion at the end of this chapter for comparison.

Figure 2.18: **Plots of k_{ex} against [DO⁻] for the H/D-exchange reaction of triazolium ions (137) (○), (138) (□), (140) (◇) and (143) (△) in D₂O at 25 ºC and *I* = 1.0 (KCl)**

Table 2.9: **Rate constants for exchange of the C(3)-H of 1,2,4-triazolium salts (137), (138), (140) and (143) for deuterium in D$_2$O at 25 °C and I = 1.0 (KCl)**

substrate	
137	k_{DO} = 2.84 (± 0.08) × 10^8 M^{-1} s^{-1} [a] **intercept** = 7.72 (± 2.48) × 10^{-6} s^{-1} [b]
138	k_{DO} = 8.17 (± 0.27) × 10^7 M^{-1} s^{-1} [b] **intercept** = 1.16 (± 0.82) × 10^{-6} s^{-1} [b]
140	k_{DO} = 4.96 (± 0.14) × 10^7 M^{-1} s^{-1} [b] **intercept** = 8.65 (± 4.14) × 10^{-7} s^{-1} [b]
143	k_{DO} = 9.50 (± 0.26) × 10^7 M^{-1} s^{-1} [b] **intercept** = 5.37 (± 0.56) × 10^{-6} s^{-1} [b]

(a) Obtained from the slope of a plot of k_{ex} against [DO$^-$] (Figure 2.18).
(b) Obtained from the y-intercept of a plot of k_{ex} against [DO$^-$] (Figure 2.18).

2.2.1.3 Estimation of k_{HOH}, k_{HO} and pK_a

The second-order rate constants for deuteroxide ion-catalysed exchange, k_{DO} (M^{-1} s^{-1}), determined in the previous section for triazolium ions **137** − **143** may be used to estimate carbon acid pK_a values. By combining the equations for the reaction of triazolium ion **144** with hydroxide and the self-ionization of water (Scheme 2.6), we obtain an equation which relates the acid dissociation constant K_a to rate constants k_{HO} and k_{HOH}, and the ionic product of water K_w (Equation 2.20).

Scheme 2.6:

$$pK_a = pK_W + \log_{10}\left(\frac{k_{HOH}}{k_{HO}}\right)$$

Equation 2.19

Scheme 2.4 outlined the steps involved in deuteroxide ion-catalysed exchange of the C(3)-H of triazolium ion **144** for deuterium. Buffer catalysis experiments performed on triazolium ion **138** show that deprotonation by deuteroxide ion is not rate-determining where $k_{DO} \leq 8.17 \times 10^{-7}$ M^{-1} s^{-1}, as no significant general base catalysis of exchange is observed. As solvent reorganisation cannot be catalysed by a general base mechanism, this step is therefore rate-determining for deuteroxide ion-catalysed exchange and the proton transfer step exists as a pre-equilibrium.

A value for the analogous second-order rate constant for deprotonation by hydroxide ion, k_{HO} (M^{-1} s^{-1}), may be obtained from k_{DO} (M^{-1} s^{-1}) using the secondary solvent isotope effect relationship, $k_{DO}/k_{HO} = 2.4$, where proton transfer occurs as a pre-equilibrium.[11] This secondary solvent isotope effect is caused by the higher basicity of deuteroxide ion in D$_2$O compared to hydroxide ion in H$_2$O.

As solvent reorganisation is rate-determining for deprotonation of the azolium ion, the 'principle of microscopic reversibility' dictates that solvent reorganisation will also be rate-determining for protonation of the carbene/ylide. Thus, the rate constant for solvent reorganisation may be assigned to the rate constant for protonation of the carbene/ylide by water, according to Equation 2.21.

$$k_{HOH} = k_{reorg} \approx 10^{11} \text{ s}^{-1}$$

Equation 2.20

These values of k_{HO} (M^{-1} s^{-1}) and k_{HOH} (s^{-1}) may be combined with Equation 2.20 to estimate carbon acid pK_a values. The term pK_w = 14 is derived from the ion product of water, K_w = 10^{-14} M^2. Values of k_{HO} and pK_a determined using this method are summarised at the end of this section.

If we consider that the intercepts of the plots of k_{ex} against deuteroxide ion concentration correspond to the term for the solvent reaction, k_{D2O}, an alternative estimate of pK_a may also be obtained. The merits of this assumption will be discussed in Section 2.3.1. A corresponding value of k_{H2O} may be calculated using the secondary solvent isotope relationship, k_{H2O}/k_{D2O} = 2.6.[4] Scheme 2.7 and Equation 2.22 relate k_{HO} to K_a.

Scheme 2.7:

$$K_a = \frac{k_{H2O}}{k_{H3O}}$$
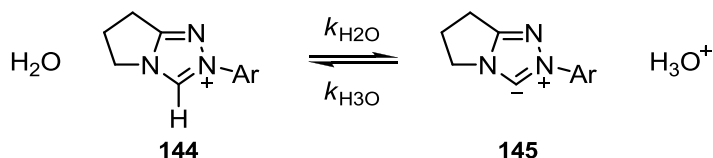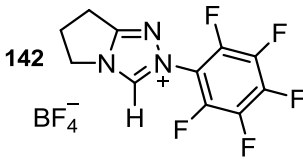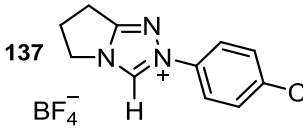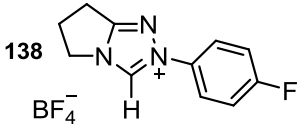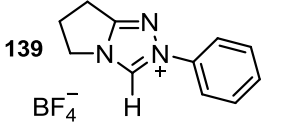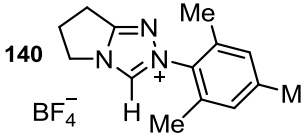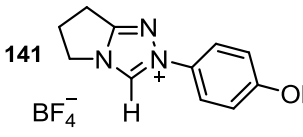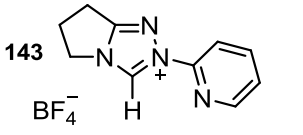
Equation 2.21

In the reverse direction, the rate constant for protonation of the carbene/ylide by hydronium ion, k_{H3O} (M^{-1} s^{-1}), is assumed to be equal to the rate constant for diffusion (k_{H3O} = 2 × 10^{10} M^{-1} s^{-1}). A summary of the rate constants and pK_a values obtained for triazolium salts **137** – **143** are shown in Table 2.10. Values quoted in italics have been reported previously and are shown for comparison. An estimate of the error in pK_a values was found to be ±0.08 units based on reported error in k_{DO} from fitting of the pD-rate data.

Table 2.10:   Summary of rate constants and pK$_a$ values for triazolium salts (137) – (143)

substrate	k_{HO}, M^{-1}s^{-1}	pK$_a$	k_{H2O}, s^{-1} [c]	pK$_a$
142	2.84×10^8 *2.69×10^8*	**16.5** [a] ***16.6*** [b]	1.59×10^{-4} *1.87×10^{-4}*	**14.1** [d] ***14.0*** [e]
137	1.33×10^8 1.18×10^8	**16.9** [a] **16.9** [b]	2.01×10^{-5}	**15.0** [e]
138	3.61×10^7 3.40×10^7	**17.4** [a] **17.5** [b]	1.16×10^{-6}	**15.8** [e]
139	2.84×10^7 *2.65×10^7*	**17.5** [a] ***17.6*** [b]	*1.84×10^{-6}*	***16.0*** [e]
140	2.20×10^7 2.07×10^7	**17.7** [a] **17.7** [b]	2.25×10^{-6}	**15.9** [e]
141	1.75×10^7 *1.53×10^7*	**17.8** [a] ***17.8*** [b]	*6.32×10^{-6}*	**15.5** [e]
143	4.60×10^7 3.96×10^7	**17.3** [a] **17.4** [b]	1.40×10^{-5}	**15.2** [e]

(a) The second-order rate constant, k_{HO}, and associated pK$_a$ were obtained from fitting of the p*D*-rate profile. (b) The second-order rate constant, k_{HO}, and associated pK$_a$ were obtained from the slope of the plot of k_{ex} against [DO$^-$]. (c) Value of k_{H2O} obtained from the intercept of a plot of k_{ex} against [DO$^-$]. The validity of this assumption is discussed in Section 2.3. (d) The second-order rate constant, k_{H2O}, and associated pK$_a$ was obtained from fitting of the p*D*-rate profile. (c) The second-order rate constant, k_{H2O}, and associated pK$_a$ were obtained from the y-intercept of the plot of k_{ex} against [DO$^-$].

2.2.2 Deuterium exchange reactions of thiazolium ions and imidazolium ions followed by ^{1}H NMR spectroscopy

Deuterium exchange experiments for thiazolium salts **53** and **151** (10 mM) and imidazolium salts **152** and **153** (10 mM) in D$_2$O at 25 °C and constant ionic strength $I =$ 1.0 (KCl) were performed in acetic acid buffers at a range of pD values in an analogous manner to the experiments described in Section 2.2.1. Exchange of the proton for deuterium at the C(2)-H position was followed by ^{1}H NMR spectroscopy (400 MHz), and resulted in the disappearance of the C(2)-H singlet signal. From this data, first- and second-order rate constants for deuteroxide ion-catalysed exchange, k_{ex} (s^{-1}) and k_{DO} (M^{-1} s^{-1}), were determined. Using these rate constants, carbon acid pK_a values were estimated.

53   **151**   **152**   **153**
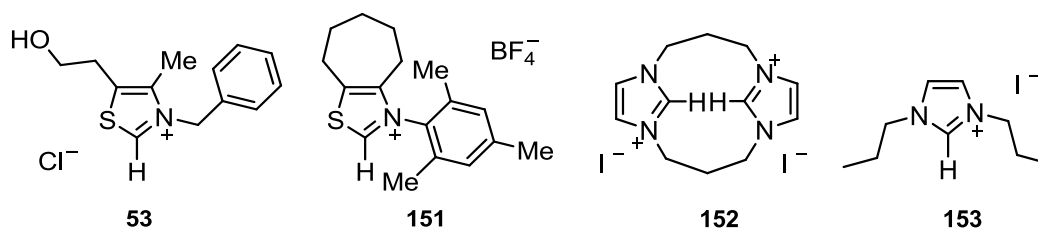
2.2.2.1 Determination of pseudo-first-order and second-order rate constants for exchange (k_{ex} and k_{DO})

In Section 2.2.1 we discussed that the first-order rate constant for deuteroxide ion-catalysed exchange, k_{ex} (s^{-1}), is equal to the sum of the contributions from all potentially catalytic species in solution, and may include terms for deuteroxide ion (k_{DO}[DO$^-$]), solvent (D$_2$O), and buffer base (k_B[B]). Washabaugh and Jencks have previously shown that acetic acid buffers do not catalyse the H/D-exchange reaction of a range of substituted thiazolium ions. Likewise, the results of buffer catalysis experiments performed by Amyes and co-workers, and by our laboratory, show that acetic acid buffers do not catalyse the H/D-exchange reaction of a range of substituted thiazolium ions. This evidence will be discussed in considerable detail in Section 2.3. Thus, for the thiazolium and imidazolium ions described below the contribution from buffer base (k_B[B]) may be neglected.

Thiazolium and imidazolium salts are known to be significantly less acidic than the triazolium ions described in Section 2.2.1, and values of k_{D2O} may be expected to be correspondingly smaller. Indeed, Washabaugh and Jencks obtained values of $k_{D2O} = 1.6$

$\times 10^{-9} - 9.4 \times 10^{-8}$ s^{-1} for a range of thiazolium ions, although these measurements were obtained from pD-rate profiles from exchange which gives a more precise measurement of k_{D2O}. Full pD-rate profiles were not obtained for the azolium ions described in this section and second-order rate constants for deuteroxide ion-catalysed exchange of the C(2)-H for deuterium for thiazolium and imidazolium salts **53** and **151 – 153** are obtained from the slopes of plots of k_{ex} against deuteroxide ion concentration. The contribution to k_{ex} from k_{D2O} is likely to be small and within the error of the plots of k_{ex} against deuteroxide ion, and may be neglected. As such, Equation 2.7 may be further simplified to Equation 2.11, shown previously.

2.2.2.1a 3-Benzyl-5-(2-hydroxyethyl)-4-methylthiazolium chloride (53)
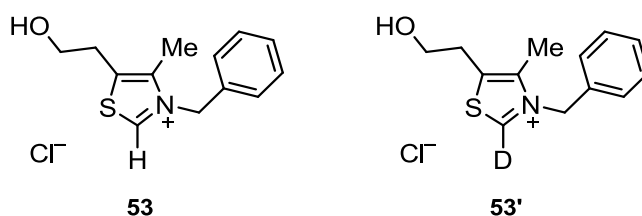
53   **53'**

Pseudo-first-order rate constants for the deuteroxide ion-catalysed exchange of the C(2)-H of thiazolium salt **53** to form deuterated product **53'** were obtained by ^{1}H NMR spectroscopy (400 MHz).

A representative set of spectra taken at three time points during the reaction in acetic acid buffer at pD 4.07 (10% f_B) is shown in Figure 2.19. Deuterium exchange at the C(2)-H position resulted in the disappearance of the C(2)-H singlet at 9.69 ppm over the course of the reaction. The extent of exchange was measured relative to the 12 equivalent non-exchangeable protons of the internal standard at 3.21 ppm. Signals corresponding to the *ortho*-CH, *meta*-CH and *para*-CH groups on the benzyl substituent appear as two sets of multiplets at 7.52 and 7.37 ppm. Singlets corresponding to the methyl CH$_3$ group and benzyl CH$_2$ group appear at 2.45 and 5.70 ppm respectively. Signals corresponding to the two CH$_2$ groups on the hydroxyethyl substituent appear as two sets of triplets at 3.87 and 3.16 ppm. No change was observed in the integrated area of any other peak relative to the internal standard, indicating that deuterium exchange does not occur at any position other than at C(2)-H under these conditions.

Figure 2.19: Representative ^{1}H NMR spectra at 400 MHz of thiazolium salt (53) (10 mM, pD 4.07), obtained during exchange of the C(2)-H (s, 9.69 ppm) for deuterium in D$_2$O at 25 ºC and I = 1.0 (KCl) [Internal standard, tetramethylammonium deuteriosulfate (s, 3.21 ppm)]
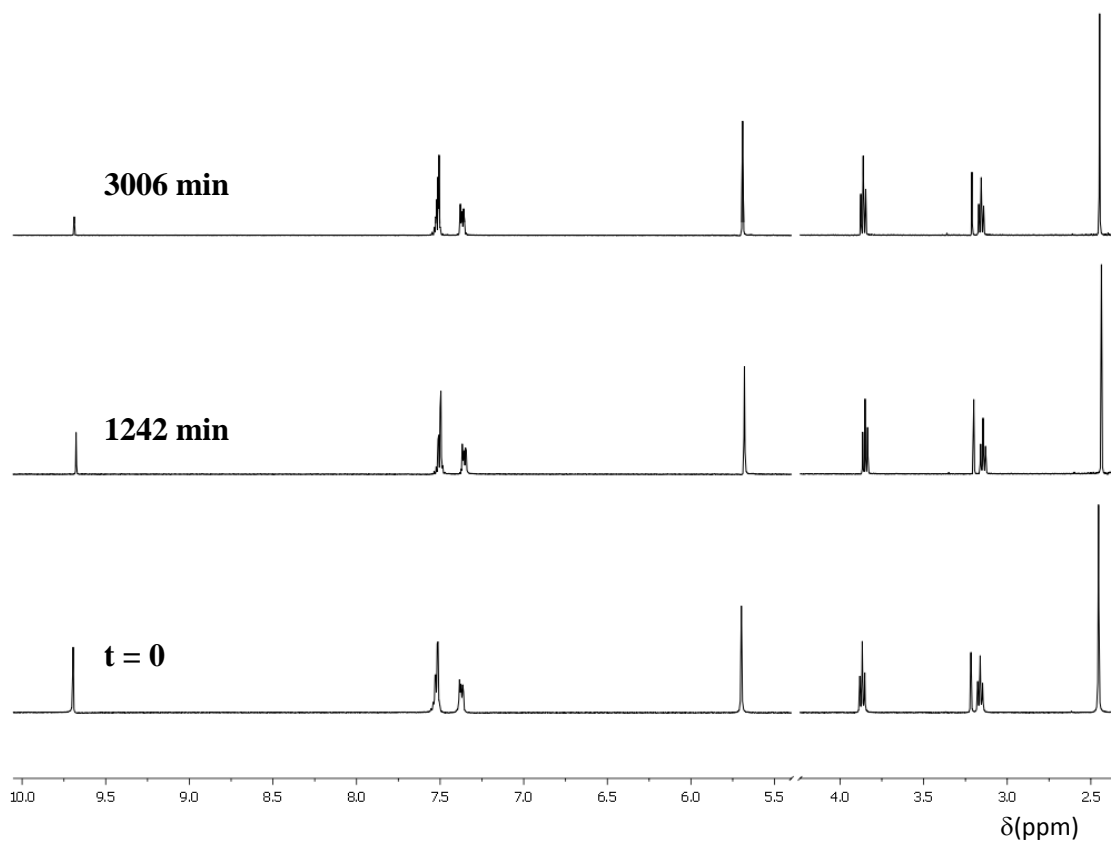
Experimentally observed first-order rate constants for exchange, k_{ex} (s^{-1}), were determined from the slopes of semi-logarithmic plots of f(s) against time at each pD. Reaction data and values of k_{ex} are presented in Appendix A (Table A7, Figure A15).

A value of 3.03 × 10^5 M^{-1} s^{-1} for the second-order rate constant for deuteroxide ion-catalysed exchange, k_{DO}, was obtained from the slope of a plot of k_{ex} against deuteroxide ion concentration (Figure 2.20).

Figure 2.20: Plot of k_{ex} against [DO$^-$] for the H/D-exchange reaction of thiazolium salt (53) in D$_2$O at 25 °C and $I = 1.0$ (KCl)
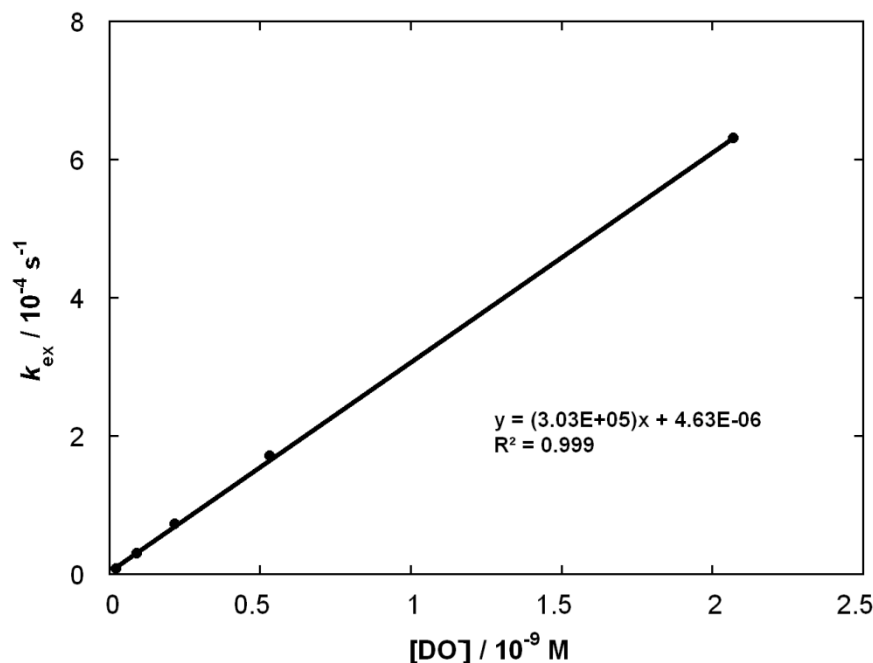
2.2.2.1b   3-Mesityl-5,6,7,8-tetrahydro-4*H*-cycloheptathiazolium perchlorate (151)
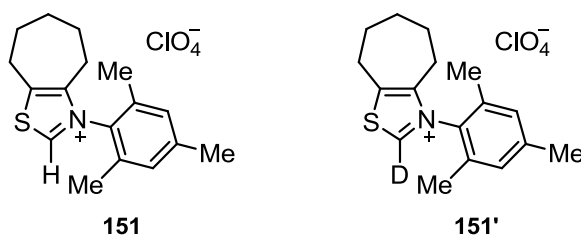
Pseudo-first-order rate constants for the deuteroxide ion-catalysed exchange of the C(2)-H of thiazolium salt **151** to form deuterated product **151'** were determined by ^{1}H NMR spectroscopy (400 MHz).

A representative set of spectra taken at three time points during the reaction in acetic acid buffer at pD 4.13 (10% f_B) is shown in Figure 2.21. Deuterium exchange at the C(2)-H position resulted in the disappearance of the C(2)-H singlet at 9.68 ppm over the course of the reaction. The extent of exchange was measured relative to the 12 equivalent non-exchangeable protons of the internal standard at 3.22 ppm. A signal corresponding to the two equivalent *meta*-CH protons on the mesityl substituent appears as a singlet at 7.23 ppm, and those corresponding to the CH$_3$ groups are present as two singlets at 2.39 and 1.97 ppm. The signals corresponding to the five CH$_2$ groups

on the seven-membered ring appear as multiplets at 3.14, 2.62, 1.93, 1.86 and 1.66 ppm. No change was observed in the integrated area of any other peak relative to the internal standard, indicating that deuterium exchange does not occur at any position other than at C(2)-H under these conditions.

Figure 2.21: **Representative ^{1}H NMR spectra at 400 MHz of thiazolium salt (151) (10 mM, pD 4.13), obtained during exchange of the C(2)-H (s, 9.68 ppm) for deuterium in D$_2$O at 25 ºC and I = 1.0 (KCl) [Internal standard, tetramethylammonium deuteriosulfate (s, 3.22 ppm)]**
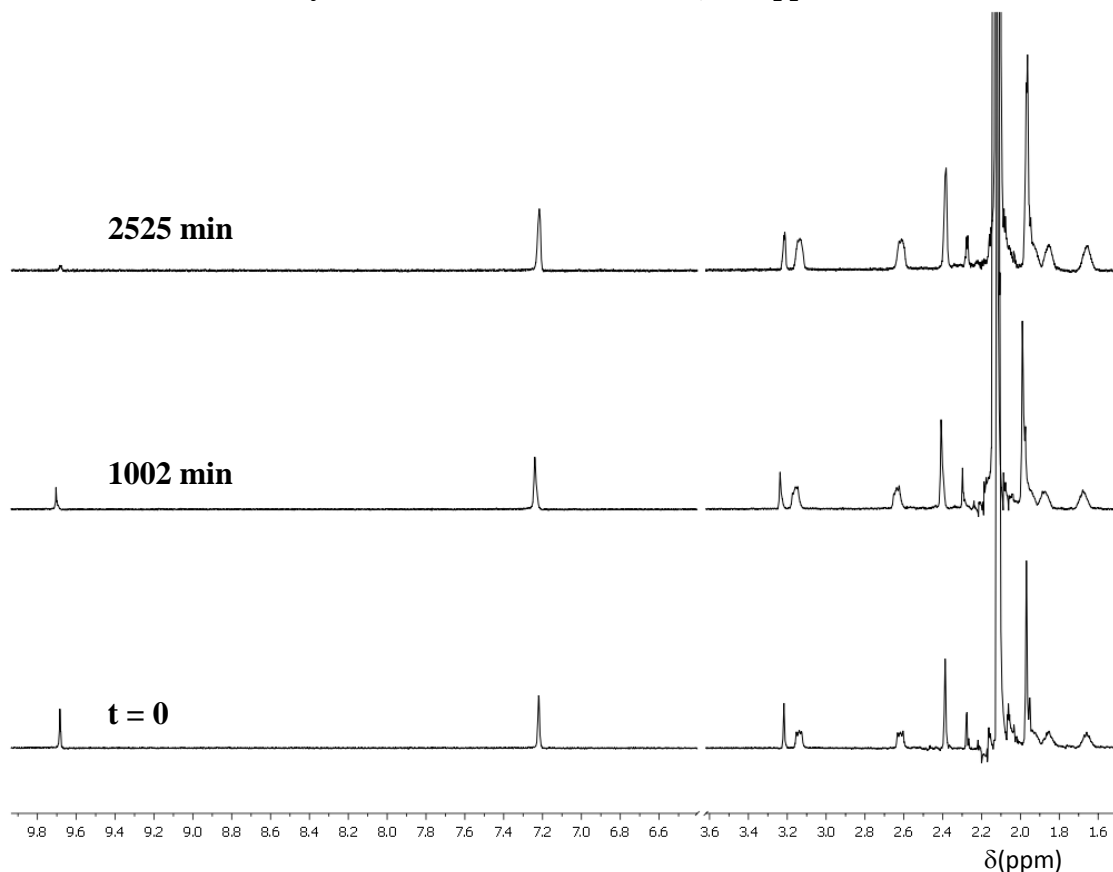
Experimentally observed first-order rate constants for exchange, k_{ex} (s^{-1}), were determined from the slopes of semi-logarithmic plots of f(s) against time at each pD. Reaction data and values of k_{ex} are presented in Appendix A (Table A8, Figure A16).

A value of 5.17 × 10^5 M^{-1} s^{-1} for the second-order rate constant for deuteroxide ion-catalysed exchange, k_{DO}, was obtained from the slope of a plot of k_{ex} against deuteroxide ion concentration (Figure 2.22).

Figure 2.22: **Plot of k_{ex} against [DO$^-$] for the H/D-exchange reaction of thiazolium salt (151) in D$_2$O at 25 °C and I = 1.0 (KCl)**

y = (5.17E+05)x - 3.14E-06
R² = 0.998
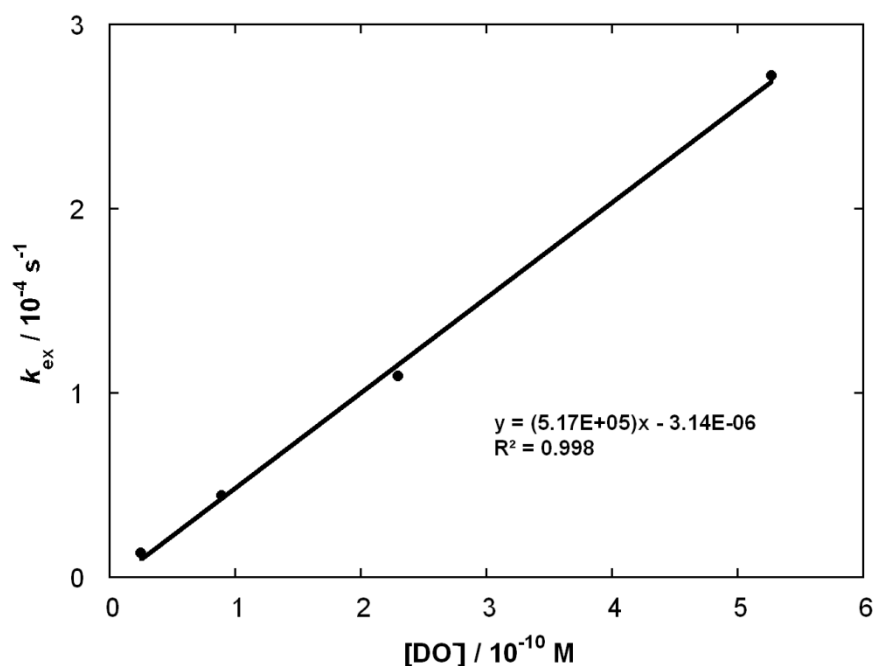
2.2.2.1c   Bridged *bis*-propyl *bis*-imidazolium diiodide (152)

152   **152''**
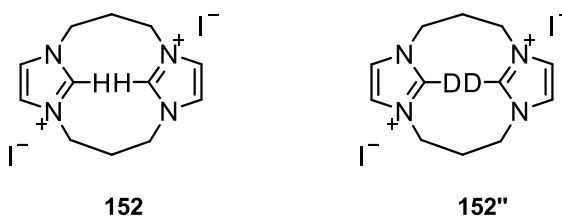
Pseudo-first-order rate constants for the deuteroxide ion-catalysed exchange of the two C(2)-H groups of imidazolium salt **152** to form di-deuterated product **152''** were determined by ^{1}H NMR spectroscopy (400 MHz).

A representative set of spectra taken at three time points during the reaction in acetic acid buffer at p*D* 5.46 (70% f_B) is shown in Figure 2.23. Deuterium exchange at the two C(2)-H positions resulted in the disappearance of the C(2)-H singlet at 8.99 ppm over the course of the reaction. The extent of exchange was measured relative to the 12 equivalent non-exchangeable protons of the internal standard at 3.24 ppm. A singlet corresponding to the four equivalent C(4)-H and C(5)-H protons appears at 7.56 ppm. Signals corresponding to the four CH$_2$ groups adjacent to the nitrogen atoms on the propyl linkers appear as triplets at 4.77, 4.73, 4.65 and 4.61 ppm. Signals corresponding to the remaining two CH$_2$ groups on the propyl linkers appear as a set of

multiplets at 2.63 – 2.73 ppm. No change was observed in the integrated area of any other peak relative to the internal standard, indicating that deuterium exchange does not occur at any position other than at C(2)-H under these conditions.

Figure 2.23: **Representative ^{1}H NMR spectra at 400 MHz of imidazolium salt (152) (10 mM, pD 5.46), obtained during exchange of the C(2)-H (s, 8.99 ppm) for deuterium in D$_2$O at 25 °C and I = 1.0 (KCl) [Internal standard, tetramethylammonium deuteriosulfate (s, 3.24 ppm)]**
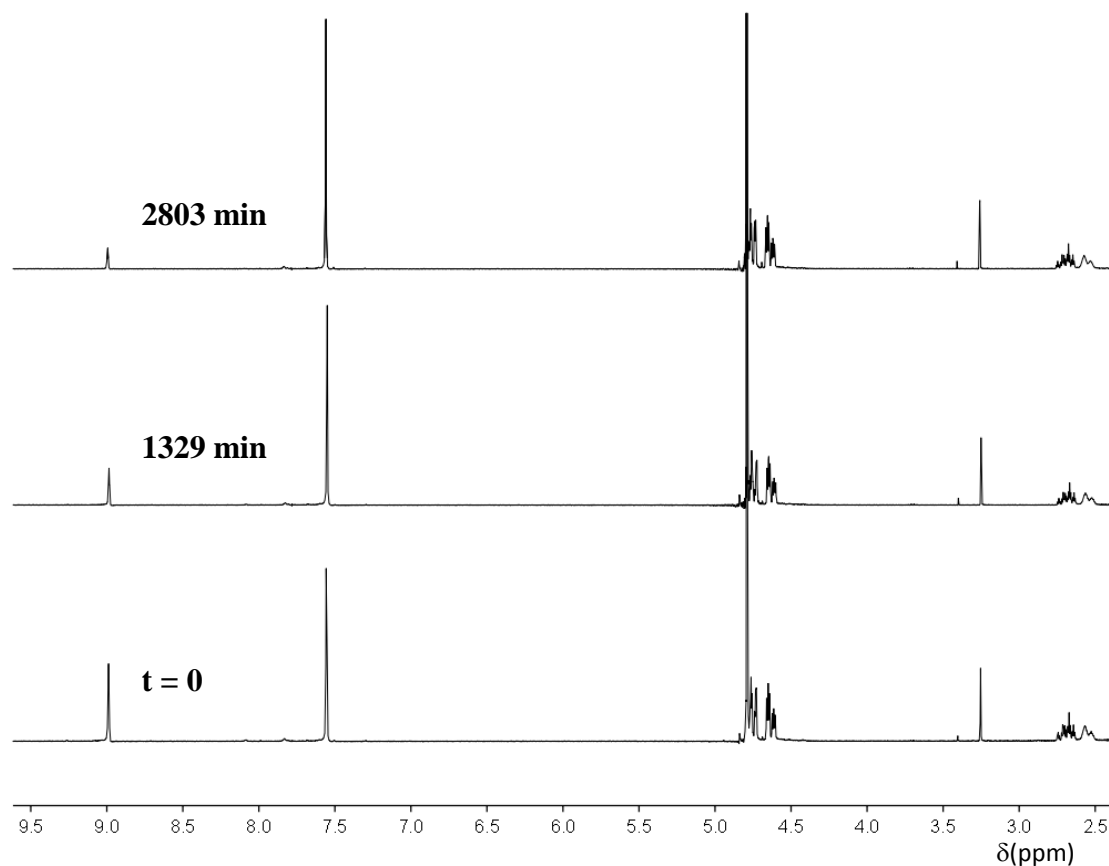
Experimentally observed first-order rate constants for exchange, k_{ex} (s^{-1}), were determined from the slopes of semi-logarithmic plots of f(s) against time at each pD. Reaction data and values of k_{ex} are presented in Appendix A (Table A9, Figure A17).

A value of 1.37×10^4 M^{-1} s^{-1} for the second-order rate constant for deuteroxide ion-catalysed exchange, k_{DO}, was obtained from the slope of a plot of k_{ex} against deuteroxide ion concentration (Figure 2.24).

Figure 2.24: **Plot of k_{ex} against [DO⁻] for the H/D-exchange reaction of imidazolium salt (152) in D₂O at 25 ºC and I = 1.0 (KCl)**
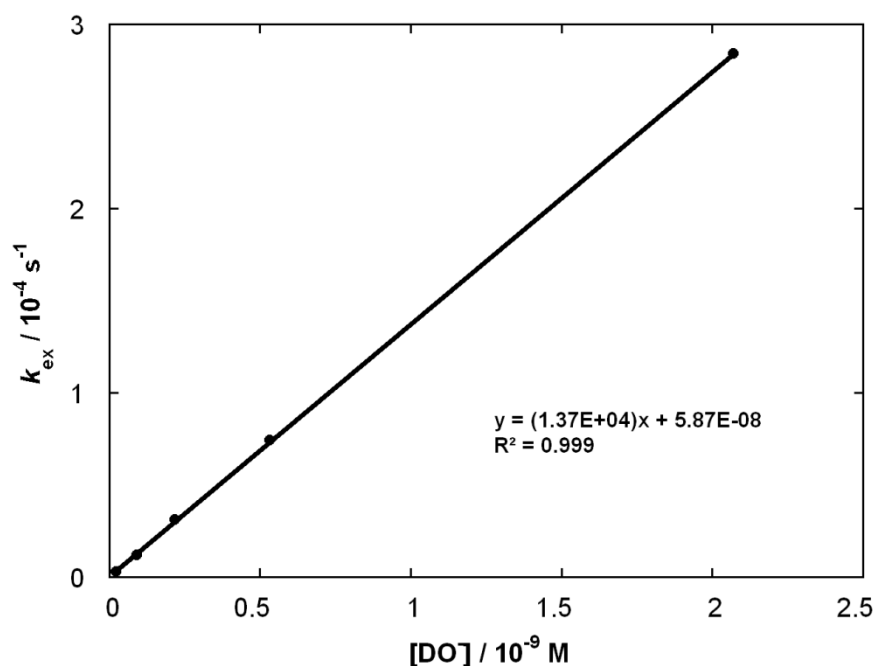
2.2.2.1d   1,3-Dipropylimidazolium iodide (153)
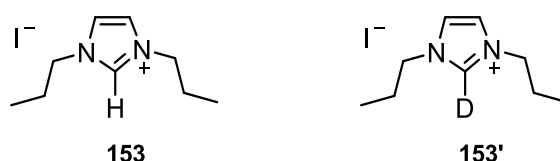
153   **153'**

Pseudo-first-order rate constants for the deuteroxide ion-catalysed exchange of the C(2)-H of imidazolium salt **153** to form deuterated product **153'** were obtained by ^{1}H NMR spectroscopy (400 MHz).

A representative set of spectra taken at three time points during the reaction in acetic acid buffer at pD 4.07 (10% f_B) is shown in Figure 2.25. Deuterium exchange at the C(2)-H position resulted in the disappearance of the C(2)-H singlet at 8.81 ppm over the course of the reaction. The extent of exchange was measured relative to the 12 equivalent non-exchangeable protons of the internal standard at 3.20 ppm. A singlet corresponding to two equivalent C(4)-H and C(5)-H protons appears at 7.51 ppm. Signals corresponding to the two CH₂ groups on the propyl linker appear as a triplet and multiplet at 4.16 and 1.89 ppm respectively, and the signal corresponding to the CH₃ group appears as a triplet at 0.91 ppm. No change was observed in the integrated

area of any other peak relative to the internal standard, indicating that deuterium exchange does not occur at any position other than at C(2)-H under these conditions.

Figure 2.25: Representative ^{1}H NMR spectra at 400 MHz of imidazolium salt (153) (10 mM, pD 6.05), obtained during exchange of the C(2)-H (s, 8.81 ppm) for deuterium in D$_2$O at 25 ºC and I = 1.0 (KCl) [Internal standard, tetramethylammonium deuteriosulfate (s, 3.20 ppm)]
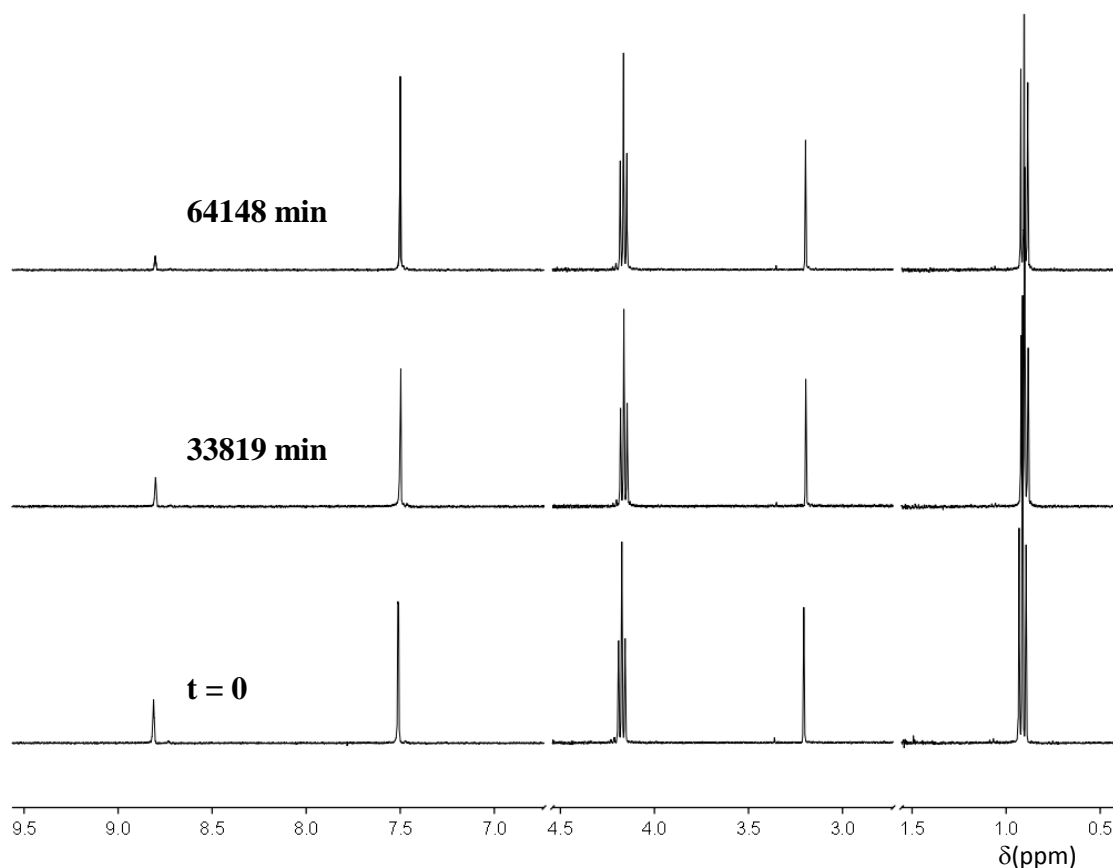
Experimentally observed first-order rate constants for exchange, k_{ex} (s^{-1}), were determined from the slopes of semi-logarithmic plots of f(s) against time at each pD. Reaction data and values of k_{ex} are presented in Appendix A (Table A10, Figure A18).
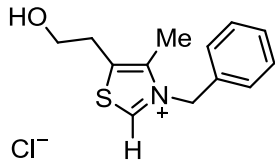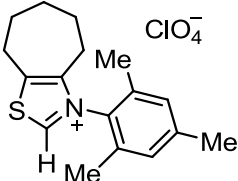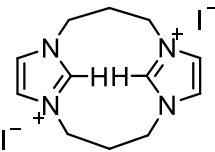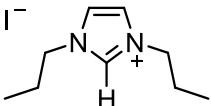
A value of 1.79×10^2 M^{-1} s^{-1} for the second-order rate constant for deuteroxide ion-catalysed exchange, k_{DO}, was obtained from the slope of a plot of k_{ex} against deuteroxide ion concentration (Figure 2.26).

Figure 2.26: **Plot of k_{ex} against [DO$^-$] for the H/D-exchange reaction of imidazolium salt (153) in D$_2$O at 25 ºC and I = 1.0 (KCl)**
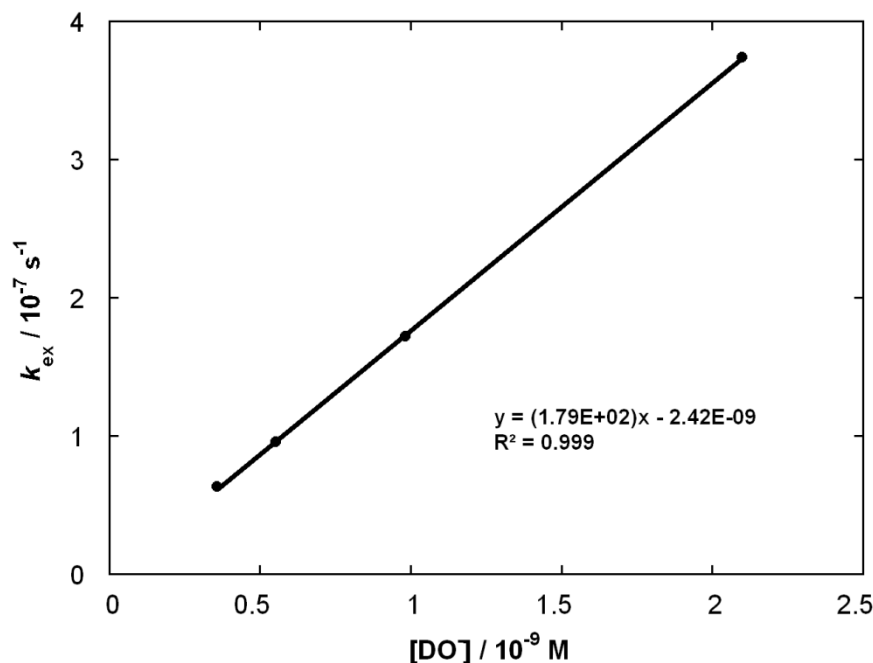
2.2.2.2 Estimation of k_{HOH}, k_{HO} and pK_a

Washabaugh and Jencks have shown that solvent reorganisation is the rate-determining step in the H/D-exchange reactions of a series of thiazolium ions. Likewise, the results of buffer catalysis experiments performed by Amyes and co-workers, and by our laboratory, provide strong evidence to support the conclusion that solvent reorganisation is also rate-determining for H/D-exchange of imidazolium ions. This evidence is discussed in detail in Section 2.3. We may therefore assume that for the thiazolium and imidazolium salts presented in this section, solvent reorganisation is rate-determining in both the forward and reverse directions, and the rate constant for carbene protonation by water, k_{HOH} (s^{-1}), may be equated to k_{reorg} = 10^{11} s^{-1}. Following the treatment described for the 1,2,4-triazolium salts described in Section 2.2.1, second-order rate constants for deuteroxide ion-catalysed exchange, k_{DO} (M^{-1} s^{-1}), may be used to obtain rate constants for deprotonation by hydroxide ion, k_{HO} (M^{-1} s^{-1}), using the secondary solvent isotope relationship k_{DO}/k_{HO} = 2.4. By combining values of k_{HO} and k_{HOH} in Equation 2.20, carbon acid pK_a values may be estimated. These results are summarised in Table 2.11.

Table 2.11: Rate constants for exchange of the C(2)-H of thiazolium salts (53) and (151) and imidazolium salts (152) and (153), and carbon acid pK_a values for deuterium in D$_2$O at 25 °C and I = 1.0 (KCl)

substrate	k_{DO}, M^{-1} s^{-1}	k_{HO}, M^{-1} s^{-1}	pK_a
53	3.03×10^5	1.26×10^5	**19.9**
151	5.17×10^5	2.15×10^5	**19.7**
152	1.37×10^4	5.71×10^3	**21.2**
153	1.79×10^2	7.46×10^1	**23.1**

2.3   Discussion

2.3.1   Deuterium exchange reactions

The H/D-exchange reactions of triazolium salts **137 – 143**, thiazolium salts **53** and **151**, and imidazolium salts **152** and **153** were followed by ^{1}H NMR spectroscopy (400 and 500 MHz) in solutions of D_2O at 25 °C and $I = 1.0$ (KCl), as described in Section 2.2. The mechanism for deuteroxide ion-catalysed exchange for general azolium ion **125** is shown in Scheme 2.8.

Scheme 2.8:
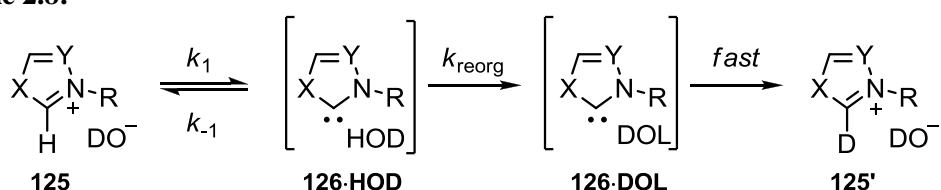
Deprotonation of azolium species **125** by deuteroxide ion yields an intimately bound complex of carbene/ylide **126** and a molecule of HOD (k_1). This step is reversible, and transfer of the proton back to the carbene/ylide may regenerate the azolium ion (k_{-1}). Alternatively, solvent reorganisation will result in complex **126·DOL**, where the DOL molecule is positioned to deliver a deuteron to the carbene (k_{reorg}). Deuteration to form the exchanged product **125'** is essentially irreversible: under these conditions, bulk solvent D_2O is present in vast excess of substrate (10 mM).

Rate constants for the protonation of singlet diphenylcarbene from neat alcohol solvents have been determined using femtosecond laser flash photolysis.[12] These rate constants correlate well with the dielectric relaxation time of the solvent. For example, the rate constant for proton transfer from methanol, k_{MeOH}, was found to be 1.1×10^{11} s^{-1}, corresponding to a reaction time τ of 9 ps. This value is close to the solvation time of methanol ($\tau = 6.8$ ps), indicating that protonation of carbenes in hydroxylic solvents is limited by solvent reorganisation, with a rate constant on the order of 10^{11} s^{-1}.

Rate-determining solvent reorganisation in the forward direction permits us to equate the rate constant for solvent reorganisation to the rate constant for carbene protonation by the Principle of Microscopic Reversibility ($k_{reorg} = k_{HOH} = 10^{11}$ s^{-1}). Figure 2.27 shows an energy profile for the mechanism shown in Scheme 2.8. Existing evidence for

the rate-determining solvent reorganisation step for H/D-exchange of imidazolium and thiazolium ions is discussed below, followed by an assessment of our buffer catalysis experiments for H/D-exchange of 1,2,4-triazolium ions, which also show solvent reorganisation to be rate-determining.

Figure 2.27:   Energy profile for H/D-exchange of azolium ions
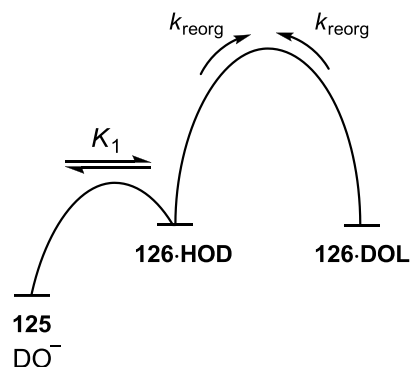
2.3.1.1   Existing evidence for rate-determining solvent reorganisation in the H/D-exchange reactions of imidazolium and thiazolium ions

A number of authors have presented strong evidence to support rate-limiting solvent reorganisation in the deuteroxide ion-catalysed H/D-exchange reactions of imidazolium ions. Amyes and co-workers have shown for representative imidazolium salt **154** that a 2-fold increase in the concentration of phosphate buffer at constant pD results in no significant change in the first-order rate constant for exchange, k_{ex} (s^{-1}), outside of experimental error (±10%).[3] Moreover, O'Donoghue and co-workers recently reported that a 2-9-fold change in the concentration of buffer base at constant pD resulted in no significant change in k_{ex} for imidazolium salts **155** and **156**.[6] As there is no mechanism by which solvent reorganisation may be catalysed by a Brønsted base, the absence of general base catalysis implies that proton transfer is not rate determining for imidazolium ions in Scheme 2.8.
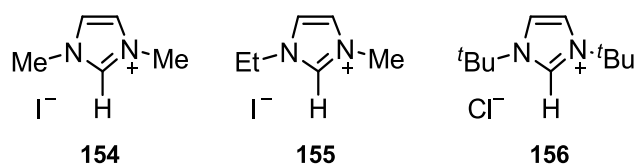
Based on these results, we may assume that solvent reorganisation is also rate-determining for imidazolium salts **152** and **153** detailed in Section 2.2. The values of k_{DO} determined for these species are smaller than the value of k_{DO} determined by Amyes for imidazolium ion **154** ($k_{DO} = 2.47 \times 10^2$ M^{-1} s^{-1}), and therefore reprotonation of the carbene/ylide species generated from imidazolium ions **152** and **153** will be equal to or faster than the rate of reprotonation of the carbene/ylide generated for Amyes' imidazolium ions.

Detailed studies by Jencks and co-workers also indicate that solvent reorganisation is rate-determining in the H/D-exchange reaction of thiazolium ions.[5] Jencks determined second-order-rate constants for exchange of the C(2)-L (L = H, D, T) by hydroxide or deuteroxide ion at 30 °C and $I = 2.0$ (NaCl) for a series of thiazolium ions **157 – 159** (Figure 2.28). These reactions showed primary kinetic isotope effects that increased over the range $(k_H/k_T)_{obs} = 2.9 - 14.7$ with increasing acidity of the thiazolium ion.

Figure 2.28: **Thiazolium ions studied by Jencks at 30 °C and $I = 2.0$ (NaCl)**

		157	**158**	**159**
L = H	k_{DO} / M^{-1} s^{-1}	4.27×10^5	2.14×10^6	4.62×10^7
	(k_H/k_T)	2.94	6.37	14.7
	(k_{-1}/k_{reorg})	3.3	1.1	0.29

Furthermore, these values of $(k_H/k_T)_{obs}$ and $(k_D/k_T)_{obs}$ were found to deviate significantly from the Swain-Schaad[13] relationship (Equation 2.22). For reactions where proton transfer is clearly rate-determining overall, the observed primary kinetic isotope effects $(k_H/k_T)_{obs}$ and $(k_D/k_T)_{obs}$ are maximised, and the Swain-Schaad relationship is obeyed. As solvent reorganisation becomes more rate-determining relative to deprotonation, the ratio k_{-1}/k_{reorg} increases and the amount of internal return of the transferred hydron becomes more significant. Thus, deviation from the Swain-Schaad relationship provides good evidence that reprotonation of the carbene/ylide (k_{-1}) and solvent reorganisation (k_{reorg}) occur at similar rates.

$$\log(k_H/k_T)_{obs} = 3.34 \times \log(k_D/k_T)_{obs}$$

Equation 2.22

As the values of k_{DO} determined for thiazolium ions **53** and **151** in Section 2.1 are smaller than the value of $k_{DO} = 4.27 \times 10^5$ M^{-1} s^{-1} determined for Jencks' thiazolium ion **157**, we may assume that solvent reorganisation is more rate-determining for our species.

2.3.1.2   Evidence for rate-determining solvent reorganisation in the H/D-exchange of reactions of 1,2,4-triazolium ions

The fast rates of exchange observed for the three most acidic triazolium ions **137**, **142** and **143** would not permit us to follow exchange in acetic acid buffers for these species. Buffer catalysis experiments are presented in Section 2.1 for triazolium ion **138**.

The results of these experiments indicate that general base catalysis of exchange is not significant for triazolium salt **138**. As described in Section 2.1, the term ([B]/[DO$^-$]) corrects for the small changes in pD that occur upon dilution at constant ionic strength. Values of k_{rel} remain constant within experimental error (6%) and do not significantly deviate from unity over a 10-fold range of buffer base concentrations. Thus, for triazolium ions **138** – **141** where second-order rate constants for exchange are less than or equal to 8.66×10^7 M^{-1} s^{-1}, solvent reorganisation is rate-determining overall.

For salts **138**, **142** and **143** which have associated values of k_{DO} that are above the tested limit for general base catalysis, Jencks' thiazolium studies enable us to estimate how much the rate constant for protonation may potentially differ from k_{reorg}. Within Jencks' thiazolium series, the increase in k_{DO} from least acidic *N*-methyl thiazolium **157** to most acidic *N*-cyanomethyl **159** is 108-fold, and the decrease in the internal return ratio, k_{-1}/k_{reorg}, is approximately 11-fold. The value of $k_{DO} = 6.82 \times 10^8$ M^{-1} s^{-1} for triazolium **142** is 14.4-fold larger than that of thiazolium **159**, and on this basis, the internal return ratio should be 1.5-fold smaller, giving a value of $k_{-1}/k_{reorg} = 0.19$ for **142**. Based on this estimate, the rate constant for protonation of **138**, **142** and **143** should be no more than ~6-fold smaller than the value of $k_{reorg} = 10^{11}$ s^{-1} used for the remaining triazolium salts that do not show buffer catalysis.

2.3.2   Acidities of 1,2,4-triazolium ions

2.3.2.1   Substituent effects on C(3)-H kinetic acidities towards deuteroxide ion, k_{DO} (M^{-1} s^{-1})

The kinetic acidities of triazolium ions **137 – 143** towards deuteroxide ion at 25 °C and I = 1.0 (KCl) are considerably greater than those of imidazolium, 4,5-dihydroimidazolium and thiazolium ions reported both previously and in these investigations. For instance, the value of k_{DO} determined for *N*-mesityl substituted triazolium ion **140** is around 1300-fold larger than for *N,N*-dimesityl substituted imidazolium ion **70** (k_{DO} = 4.08 × 10^4 M^{-1} s^{-1}), and over 4400-fold larger than 4,5-dihydroimidazolium ion **160** (k_{DO} = 1.19 × 10^4 M^{-1} s^{-1}). A more accurate comparison of the effect of the additional ring nitrogen may be made with 4,5-dihydroimidazolium ion **161** (k_{DO} = 3.45 × 10^2 M^{-1} s^{-1}), which incorporates a single *N*-mesityl substituent and two alkyl groups at the N(4) and C(5) positions.[14] The value of k_{DO} obtained for triazolium **140** is approximately 1.5 × 10^5 times greater than for **161**, and demonstrates the acidifying effect of the additional electron withdrawing nitrogen atom – which destabilises the positively charged azolium ion relative to the more neutral carbene-like transition state.
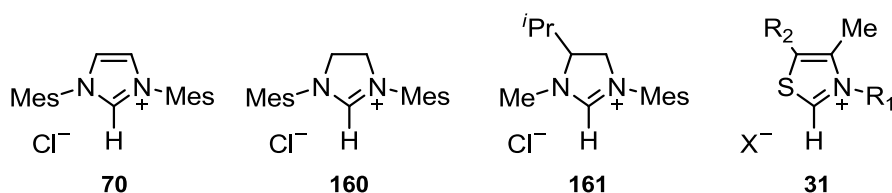
Triazolium ions **137 – 143** are also more acidic than the thiazolium ions reported in this investigation and in the literature. *N*-mesityl substituted triazolium ion **140** is over 100 times more reactive towards deprotonation by deuteroxide ion than the *N*-mesityl substituted thiazolium ion **151** (k_{DO} = 5.17 × 10^5 M^{-1} s^{-1}) determined in Section 2.2.2. Jencks and co-workers have reported values of k_{DO} for several thiazolium ions **31** in the range 3.23 × 10^5 M^{-1} s^{-1} – 2.14 × 10^6 M^{-1} s^{-1}, which are between 20 and 130-fold slower than even the least reactive *N*-C$_6$H$_4$OMe triazolium ion **141**.

Within the series of triazolium ions studied, a 16-fold difference in k_{DO} was observed between the most acidic species (*N*-C$_6$F$_5$ triazolium ion **142**) and least acidic species (*N*-C$_6$H$_4$OMe triazolium ion **141**). More electron-withdrawing *N*-substituents were found to result in larger values of k_{DO}. This trend is consistent with observations made

for an imidazolium series reported by O'Donoghue and co-workers,[6] and qualitative observations of the extent of triazolium deprotonation reported by Bode.[15] This trend may be rationalised by considering the stability of the azolium ion conjugate acid. Electron withdrawing substituents result in a destabilisation of the positively charged triazolium ion relative to the neutral carbene, leading to a smaller energy barrier for deprotonation.

The 16-fold difference observed across this series is surprisingly small, given the large difference in the electronic properties of the aryl substituents. A similarly small *N*-substituent effect was observed for the imidazolium ions studied previously by O'Donoghue and co-workers, and this was attributed to the non-planar orientation of the aryl rings. This effect, whilst significant for the di-substituted imidazolium ions, is less likely to contribute for the singly substituted triazolium ions. A more significant effect may arise from the dual electronic nature of the carbene/ylide species (Scheme 2.9). For more electron withdrawing triazolium ions, the transition state for deprotonation may more closely resemble the neutral carbene resonance structure **145a**, resulting in a more favourable energy barrier to overcome. Conversely, for electron donating species the transition state may more closely resemble ylide **145b**, where a positive charge is formally located on N(2). This 'dampening' effect may reduce the overall observed *N*-substituent effect.

Scheme 2.9:

145a   **145b**
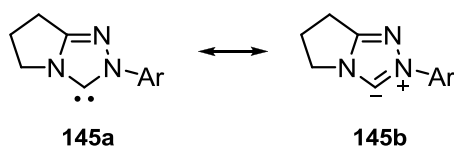
2.3.2.2   Substituent effects on C(3)-H carbon acid p*K*$_a$ values

Carbon acid p*K*$_a$ values were estimated for triazolium ions **137** – **143** from second-order rate constants for deuteroxide ion-catalysed exchange, k_{DO} (M^{-1} s^{-1}) determined in Section 2.1. These values range from 16.5 – 17.8 and are reported in Table 2.10. The p*K*$_a$ values calculated from values of k_{DO} determined from both p*D*-rate profiles and linear plots of k_{ex} against deuteroxide concentration are in excellent agreement. This reflects the good agreement of k_{DO} values determined by these two approaches.

Accordingly, pK_a values for these triazolium ions are significantly lower than those recorded for analogous thiazolium and imidazolium ions. For instance, the pK_a of triazolium **140** (pK_a = 17.7) is 2 pK_a units more acidic than *N*-mesityl substituted thiazolium ion **151** (pK_a = 19.7). The 3.1 unit difference between *N,N*-dimesityl imidazolium **70** (pK_a = 20.8) and triazolium **140** illustrates the effect of the additional electron withdrawing nitrogen atom present in the aryl ring, consistent with the reduced stabilisation of the positively charged triazolium ion relative to the neutral carbene. Within the series, triazolium ions bearing electron withdrawing *N*-aryl substituents resulted in more acidic pK_a values. The narrow span of 1.2 pK_a units across this series reflects the relatively small changes in values of k_{DO} discussed previously.

Buffer catalysis experiments performed on *N*-C$_6$H$_4$F substituted triazolium ion **138** suggest that for values of $k_{DO} \leq 8.66 \times 10^7$ M^{-1} s^{-1}, solvent reorganisation is rate-determining and a value for the rate constant for carbene protonation by water, $k_{HOH} = k_{reorg} = 10^{11}$ s^{-1}, may be used to estimate pK_a. The errors in pK_a, obtained from the error associated with k_{DO} from fitting of the pD-rate profile, were found to be no greater than 0.08 units. Exchange of triazolium salts **137**, **142** and **143** in acetic acid buffer was too fast to measure, and the extent of general base catalysis of exchange could not be determined. Earlier, it was argued that k_{HOH} may be up to 6-fold smaller, and accordingly these pK_a values may be up to 1 unit lower.

2.3.2.3   Evaluation of additional pathways and protonation at N(1)

An exchange pathway involving protonation at the N(1) position is necessary to explain the downward deviation of the pD-rate profile for triazolium ion **142** at lower pDs. In the absence of N(1)-protonation, exchange *via* Pathways A and B alone would result in a fully pD independent region at more acidic pDs, resulting in a 'levelling off' of the pD-rate profile. Indeed, Washabaugh and Jencks observed the onset of a fully pD-independent region in the pD-rate profile of the C(2)-H of thiazolium ion **162** (Figure 2.29a). The levelling off of the profile below pD -1.0 was attributed to the solvent reaction (analogous to Pathway B in Scheme 2.4), resulting in a value of $k_{D2O} = 1.5 \times 10^{-8}$ s^{-1}. Similarly, the onset of a pD-independent region was also observed for thiazolium ion **159**, returning an estimate of $k_{D2O} = 9.4 \times 10^{-8}$ s^{-1} (Figure 2.29b).

Figure 2.29: **p*D*-Rate profiles for the H/D-exchange reaction of the C(2)-H of thiazolium ions (162) and (159) in D$_2$O at 30 °C.**
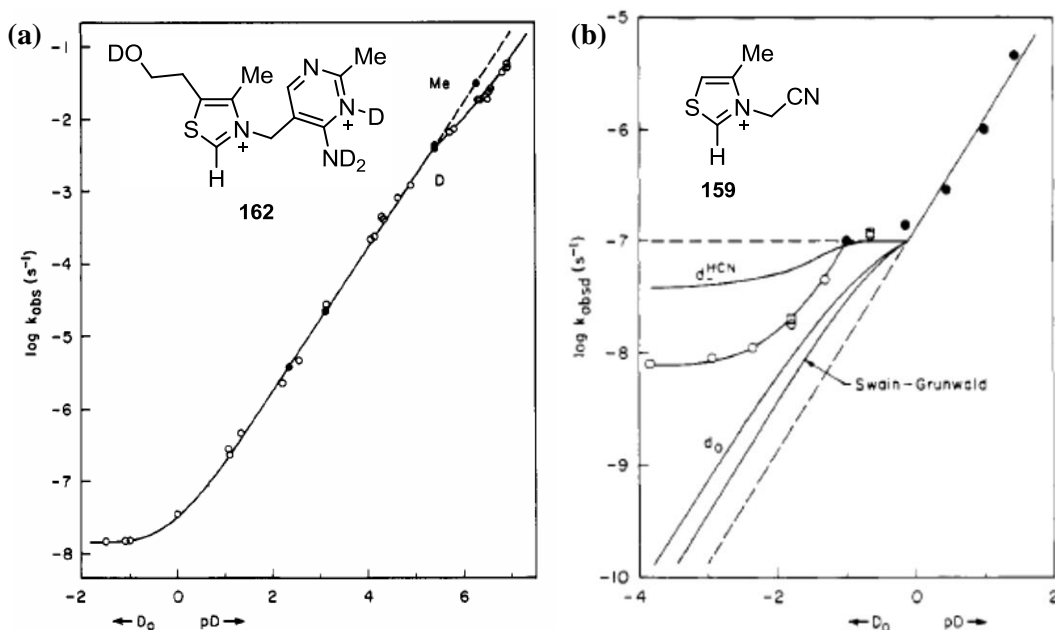
(Reproduced with permission of ACS publications. Copyright © 2001 American Chemical Society)

In the latter case, a further decrease in log k_{ex} was observed upon moving to strongly acidic solutions (>5 M DCl), which the authors attribute to acid inhibition of ionisation caused by acidity function effects. This explanation stems from the large increase in hydronium ion activity in strong acid solutions, which would be expected to shift the equilibrium shown in Scheme 2.10 towards the protonated substrate. It is unlikely that the significant downward deviation in the p*D*-rate profile for triazolium ion **142** below p*D* 1.5 results from similar acidity function effects, as the onset of altered dependence begins in more dilute DCl solutions (<1 M DCl), and these inhibition effects should be similar for triazolium and thiazolium species. Thus, a combination of N(1)-protonation and Pathways A and B, and/or Pathways A and C, are required to fit the data.

Scheme 2.10:
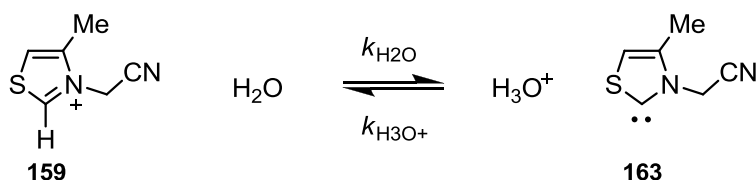
By combining the values of k_{DO} and k_{D2O} obtained from the p*D*-rate profile for thiazolium ion **159** with values for the reverse rate constants for protonation by water

and hydronium ion respectively, using a similar method to that described for our data in Section 2.2, Jencks determined identical estimates of pK_a = 16.9. This identical outcome, reached by two independent methods, strongly supports the conclusion that H/D-exchange for Jencks' thiazolium ions occurs exclusively *via* mechanisms analogous to Pathways A and B.

In contrast, the pK_a values estimated from k_{DO} (pK_a = 16.5) and k_{D2O} (pK_a = 14.1) for triazolium **142** are in poor agreement, implying that the value of k_{D2O} obtained from Equation 2.14 is overestimated. In other words, if the value of k_{D2O} = 6.1 × 10^{-1} s^{-1} gleaned from Equation 2.14 is to be used, an impossibly large value of k_{H3O+} = 5 × 10^{12} s^{-1} is required to obtain a pK_a of 16.5. This conclusion is supported by comparing the relative rates of k_{DO} and k_{D2O} obtained by Jencks' for thiazolium **159**. The value of k_{DO} for triazolium **142** is around 15-fold larger than that for thiazolium **159**, whereas the values of k_{D2O} differ by over 5000-fold. Whilst it is possible that this difference may be partly due to errors in fitting of the pD-rate data, it is more likely that exchange does not occur *via* Pathway B.

A similarly large difference is observed between the pK_a values obtained from the slopes (k_{DO}) and intercepts (k_{D2O}) of plots of k_{ex} against deuteroxide concentration. Whilst the values of k_{D2O} obtained from these plots are affected by a large degree of error associated with extrapolating to the y-axis, it is likely that these values are overestimated and do not correspond to a rate constant for Pathway B.

From the fitting of the pD-rate data to kinetically equivalent Equations 2.14 and 2.16, a value of -0.2 is estimated for p$K_a^{N(1)}$. To the best of our knowledge, no literature pK_a data for protonation at the N(1) position of a triazolium ion is available. However, using the Cox-Yates excess acidity method, aqueous pK_a values of -0.43 and -1.66 have been obtained for the second protonations of adenine **164** and purine **165**, and a value of -1.23 has been determined for dicationic species **166**[16] – all of which share similar charge separation to the proposed dicationic triazolium species **146**. Although the value of p$K_a^{N(1)}$ calculated for triazolium ion **142** is determined from an incomplete titration curve, these literature values support the validity of this estimate. In addition, the synthesis and characterisation of several trialkylated triazolium ions **167** (R = Me, Et and ^{i}Pr) reported by the groups of Curphey[17] and Bertrand[18] further support the existence of dicationic triazolium ions under acidic conditions.

164 **165** **166** **167**
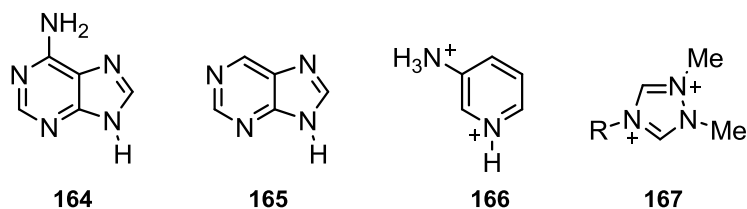
Fitting of the p*D*-rate data to Equation 2.16 allows us to obtain a value for the second-order rate constant for deprotonation of the dication **146** at the C(3)-H position by deuteroxide ion ($k_{DO}' = 4.8 \times 10^{10}$ M^{-1} s^{-1}). The bimolecular diffusion of small molecules in water occurs with a rate constant $k_d = 5 \times 10^9$ M^{-1} s^{-1}, and for facilitated diffusion, as observed for the hydronium ion, $k_d = 2 \times 10^{10}$ M^{-1} s^{-1}. Under normal circumstances, bimolecular rate constants should not exceed these diffusional limits. The value of k_{DO}' determined for **142** is just outside of these limits, however, the large errors associated with both k_{DO}' and $K_a^{N(1)}$ may justify the conclusion that deprotonation of the dication occurs at the diffusion limit. Given that the value of k_{DO}' is more reasonable than the likely overestimated value of k_{D2O}, these observations support the conclusion that exchange is more likely to occur *via* Pathways A and C rather than *via* Pathways A and B.

The observation that the rate constant for C(3)-H deprotonation of the dication, k_{DO}' (M^{-1} s^{-1}), is larger than the rate constant for C(3)-H deprotonation of the monocationic triazolium ion, k_{DO} (M^{-1} s^{-1}), is unsurprising. The additional charge located on the azolium ring would further destabilise the positively charged azolium ion relative to deprotonation transition state, resulting in a more acidic species.

2.3.2.4   p*D*-rate profile of *N*-pyridyl triazolium salt (143)

The p*D*-rate profile for triazolium ion **143** is consistent with deuteroxide ion-catalysed exchange *via* Pathway A above p*D* ~1.5, changing to a formal acid-dependent reaction at lower p*D*s. One explanation for this upward deviation is a solvent-mediated pathway involving protonation of the pyridyl ring nitrogen under acidic conditions to generate a dicationic species **148** or **149** *via* Pathway D (Scheme 2.5a). Alternatively, protonation at the triazolium N(1) position will also generate a dication **150**, analogous to that proposed for the *N*-C$_6$F$_5$ triazolium ion **142** (Scheme 2.5b). Deprotonation of this species by solvent *via* Pathway E, which involves assistance from the pyridyl nitrogen,

may result in the exchange product **150'**. Exchange of either of the proposed dicationic species **148/149** or **150** would be expected to occur faster than that of the monocationic azolium ion **143** due to charge destabilisation. Once the pD-dependent term corresponding to Pathway A becomes negligible, an increase in log k_{ex} upon moving to lower pDs would be expected as the fraction of the more reactive dicationic substrate increases. Pathways D and E are kinetically indistinguishable as both involve protonation to form a dication, which undergoes solvent-mediated deprotonation. By fitting the pD-rate data to Equation 2.19, a pK_a value of -0.1 was obtained for the proposed dicationic species. A pK_a value of 5.2 has been reported for the conjugate acid of pyridine **168**,[19] and it would be expected that the additional positive charge on the dicationic species would contribute to its ~5 pK unit increase in acidity. This pK_a is also consistent with that obtained for the N(1) position of N-C$_6$F$_5$ triazolium ion **142**, and thus this estimated value does not eliminate Pathway D or E from consideration.
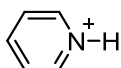
168

Given that we are attributing both the downward deviation in the pD-rate profile of N-C$_6$F$_5$ triazolium ion **142**, *and* the upward deviation in the pD-rate profile of N-pyridyl triazolium ion **143** to the formation of dicationic species, we must pose the question: *Why should protonation of the pyridyl nitrogen result in upward deviation in the pD-rate profile, whilst protonation at the N(1) position result in downward deviation?*

The two proposed dicationic species **169** and **148/149** may in theory undergo exchange at the C(3)-H *via* a combination of Pathway C (deprotonation by deuteroxide ion) and Pathway D (deprotonation by solvent), as illustrated in Scheme 2.11.

Scheme 2.11:
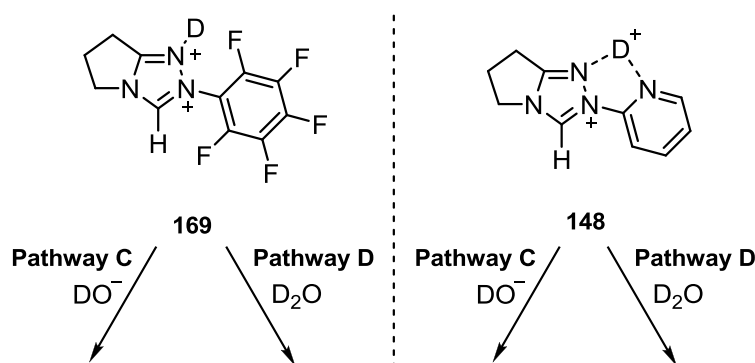
To explain the p*D*-rate profile of *N*-pyridyl triazolium ion **143**, the increase in log k_{ex} upon moving to lower p*D*s requires that the contribution of the solvent reaction (Pathway D) to exchange of **148/149** is significantly greater than for **169**. Furthermore, the p*D*-rate data for **143** does not fit to Equation 2.19, which does not include a term for the solvent reaction of the dication. Using this fitting equation, the p*D*-rate profile requires a decrease in log k_{ex} at lower p*D*s as the deuteroxide ion-catalysed term is the significant pathway for exchange of dication **169**. Based on these results we may conclude that the solvent reaction is the dominant contribution to exchange of **148/149**. Conversely, the p*D*-rate profile of *N*-C$_6$F$_5$ triazolium ion **142** does not fit to Equation 2.19 – values of log k_{ex} decrease as a result of the greater impact of the decrease in concentration of deuteroxide ion. In other words, solvent-mediated exchange of *N*-C$_6$F$_5$ dication **169** *via* Pathway D is significantly slower than for *N*-pyridyl dication **148/149**.

The cause of the difference in the rate of the solvent exchange reaction is unclear, and should be the focus of further investigation. One possible explanation is the existence of an intramolecular hydrogen bond between the triazolium N(1) and pyridyl nitrogen. For this effect to enhance the rate of deprotonation of the dication by solvent, the hydrogen bond strength should be greatest at the transition state, thus stabilising the positive charge and lowering the barrier to deprotonation.

Pathway E may more conveniently explain why solvent-mediated deprotonation is significantly faster in the case of the *N*-pyridyl dication. Assisted deprotonation at the C(3)-H position by solvent using the lone pair on the pyridyl nitrogen would result in faster rates of solvent-mediated exchange for dication **150** (Scheme 2.12). Exchange *via* Pathway E does not involve an appreciable amount of pyridyl nitrogen protonation, and may explain the absence of significant change in the UV-Vis spectra of **143**.
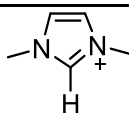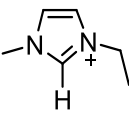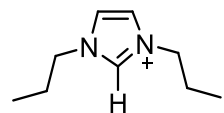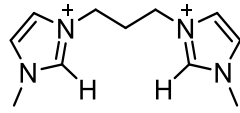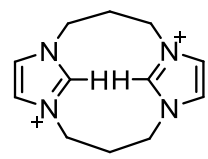
Scheme 2.12:
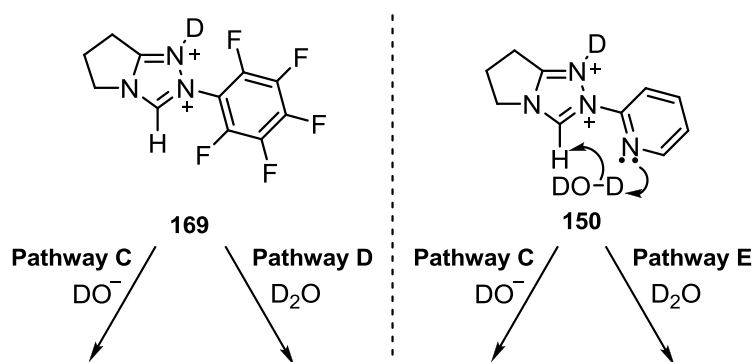
2.3.3   Acidities of imidazolium ions

The kinetic acidities of imidazolium ions **152** and **153** towards deuteroxide ion at 25 °C and $I = 1.0$ (KCl) are presented in Table 2.12, alongside literature data for related imidazolium salts which are included for discussion.

Table 2.12:   **Kinetic and thermodynamic acidities of structurally similar bis-imidazolium salts, determined at 25 °C and $I = 1.0$ (KCl)**

	substrate	k_{DO}, M^{-1} s^{-1}	pK_a [a]	Ref.
154		2.47×10^2	**23.0**	3
155		2.29×10^3	**23.0**	6
153		1.83×10^2	**23.1**	this work
170		1.30×10^3	**22.3**	6
152		1.37×10^4	**21.2**	this work

2.3.3.1   Effect of propyl linker on acidity

O'Donoghue and co-workers have previously reported kinetic acidities and associated aqueous pK_a values for a series of *N*-methyl, *N*-alkyl imidazolium ions, and found that the *N*-alkyl chain length does not substantially affect C(2)-H acidities.[6] The value of k_{DO} determined for **153** is within 25% of the values determined for similarly substituted 1-ethyl-3-methylimidazolium chloride **155**, reported by O'Donoghue, and 1,3-dimethylimidazolium chloride **154** reported by Amyes,[3] consistent with these conclusions. Accordingly, the value of pK_a determined for **153** is within 0.1 units of **154** and **155**.

Comparing monomeric 1,3-dipropylimidazolium salt **153** and singly linked bis-imidazolium salt **170**, the addition of the second imidazolium unit results in a 7-fold increase in k_{DO} and a 0.8 unit decrease in pK_a. This increase in acidity is likely due to the additional presence of positive charge on the dicationic conjugate acid, resulting in destabilisation of the azolium ion relative to the neutral carbene.

An even larger 10-fold increase in kinetic acidity is observed upon addition of the second propyl linker (*i.e.* **152**), corresponding to a 1.1 unit decrease in pK_a. This further increase in acidity may be due to the more favourable formation of a intermolecular hydrogen bonded structure **171** between the ylide and adjacent C(2)-H position brought about by the more rigid linkages between the imidazolium units. This structure may stabilise the energy of the carbene/ylide, assisting exchange. An alternative explanation may be that the more rigid structure of **152** may force the two positive charges on the nitrogen into a more unfavourable position compared to the singly linked bis-imidazolium **170**, which is less sterically constrained and would be more able to maximise the distance between positive charges. Surprisingly, the observed increase in acidity is in contrast to the potential influence of the greater steric bulk of the second imidazolium unit, which would be expected to result in a decrease in kinetic acidity.
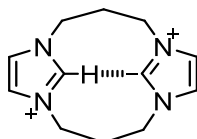
171

2.3.3.2 Dimerisation

Doubly bridged carbene **172** is known to undergo dimerisation to generate **173** in non-protic solvents (*e.g.* DMF or NH₃ (l)) containing strong base.[20] In previous work by our laboratory, no evidence for carbene dimerisation (Scheme 2.13) was observed during the H/D-exchange reactions of singly linked *bis*-imidazolium ion **170**. We hypothesised that the more rigid structure and close proximity of the imidazolium C(2)-H positions in *bis*-linked *bis*-imidazolium **152** would facilitate dimerisation. However, no evidence for **173** was found even under long reaction times (up to 13 days). We may conclude that dimerisation occurs with a rate constant significantly slower than that of carbene protonation ($k_{dimer} \ll 10^{11}$ s^{-1}).

Scheme 2.13:
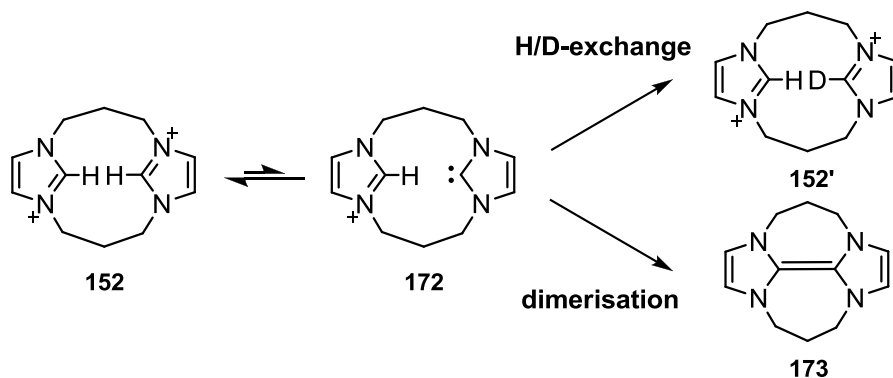
2.4   Summary

Azolium ions are weak carbon acids, and aqueous pK_a values cannot be determined using conventional equilibrium methods. In these investigations, carbon acid pK_a values for several triazolium, thiazolium and imidazolium ions in aqueous solution have been estimated using a kinetic method, based on methodology initially adopted by Jencks. The kinetic acidities of these azolium ions towards deuteroxide ion at 25 °C and $I = 1.0$ (KCl) were determined in a series of H/D-exchange experiments by ^{1}H NMR spectroscopy. Second-order rate constants for deuteroxide ion-catalysed exchange, k_{DO} (M^{-1} s^{-1}), were obtained by fitting of the pD-rate profiles for exchange, or from the slopes of second-order plots of k_{ex} (s^{-1}) against deuteroxide ion concentration.

Our results show that the kinetic acidities of triazolium ions towards deuteroxide ion (k_{DO}) are 10^3-fold greater than for thiazolium ions and 10^5-fold greater than for imidazolium ions. This 10^5-fold difference highlights the effect of the additional electron-withdrawing nitrogen atom in the azolium ring, which destabilises the triazolium ion relative to the neutral carbene/ylide. Within the homologous series studied, a 16-fold difference in k_{DO} was observed as a result of changes to the *N*-aryl ring, with electron-withdrawing substituents resulting in an increase in k_{DO}.

The absence of general base catalysis of exchange for triazolium salt **138** strongly suggests that solvent reorganisation is the rate-determining step for exchange of these species, where $k_{DO} \leq 8.66 \times 10^7$ M^{-1} s^{-1}. This conclusion allows us to calculate carbon acid pK_a values using a rate constant for carbene protonation of $k_{HOH} = k_{reorg} = 10^{11}$ s^{-1}. In acetic acid buffer, deuterium exchange of triazolium salts **137**, **142** and **143** was too fast to measure, and the extent of general base catalysis experiments could not be

determined. However, we estimate that the value of k_{HOH} for species **137**, **142** and **143** is no greater than ~5-fold smaller than k_{reorg}, and therefore the 'true' pK_as for these acidic triazolium ions may be up to 1 unit lower than the values presented in Table 2.10.

The sigmoidal p*D*-rate profile obtained for *N*-C_6F_5 substituted triazolium salt **142** requires that the mechanism for H/D-exchange involves protonation at the N(1) position to form a dicationic triazolium ion. By fitting the p*D*-rate data to a mechanistic scenario that takes into account H/D-exchange of this dicationic species, a value of -0.2 was estimated for p$K_a^{N(1)}$. This estimate is consistent with those of structurally similar dicationic nitrogen acids, supporting this conclusion.

In a separate investigation, the H/D-exchange reaction of a doubly propyl bridged bis(imidazolium) salt **152** was also studied. Based on the absence of dimer **173**, we may conclude that in aqueous solution, dimerisation occurs with a rate constant well below that of NHC protonation by solvent water ($k_{dimer} << 10^{11}$ s^{-1}).

References

1   P. Haake, L. P. Bausher and W. P. Miller, *J. Am. Chem. Soc.*, 1969, **91**, 1113.

2   M. M. E. Scheffers-Sap and H. M. Buck, *J. Am. Chem. Soc.*, 1979, **101**, 4807.

3   T. L. Amyes, S. T. Diver, J. P. Richard, F. M. Rivas and K. Toth, *J. Am. Chem. Soc.*, 2004, **126**, 4366.

4   M. W. Washabaugh and W. P. Jencks, *Biochemistry*, 1988, **27**, 5044.

5   (a) M. W. Washabaugh and W. P. Jencks, *J. Am. Chem. Soc.*, 1989, **111**, 674; (b) M. W. Washabaugh and W. P. Jencks, *J. Am. Chem. Soc.*, 1989, **111**, 683.

6   E. M. Higgins, J. A. Sherwood, A. G. Lindsay, J. Armstrong, R. S. Massey, R. W. Alder and A. C. O'Donoghue, *Chem. Commun.*, 2011, **47**, 1559.

7   The NCN bond angle in imidazolium ion **134** (R$_1$ = R$_2$ = *t*-Bu) is 109.6° (see (a)), whereas in the free imidazol-2-ylidene it is 102.2° (see (b)): (a) P. A. Chase and D. W. Stephan, *Angew. Chem. Int. Ed.*, 2008, **47**, 7433; (b) A. J. Arduengo, H. Bock, H. Chen, M. Denk, D. A. Dixon, J. C. Green, W. A. Herrmann, N. L. Jones, M. Wagner and R. West, *J. Am. Chem. Soc.*, 1994, **116**, 6641.

8   A. G. Lindsay, A. C. O'Donoghue, Ph.D. Thesis, Durham University, Durham, 2010.

9   Over the course of these investigations two p*H* electrodes were used. Values of γ_{DO} = 0.73 and γ_{DO} = 0.72 were determined for each, and used appropriately. See Chapter 6 for details of γ_{DO} = 0.72 measurement.

10   pK_a (D$_2$O) = 16.6, pK_a (D$_3$O$^+$) ≈ –2

11   A. J. Kresge, R. A. M. O'Ferrall and M. F. Powell, in *Isotopes in Organic Chemistry*, E. Buncel, C. C. Lee, Eds., Elsevier, New York, 1987, Vol. 7.

12   J. Peon, R. Pottel and A. Schumacher, *J. Phys. Chem.*, 1992, **96**, 6017.

13   C. G. Swain, E. C. Stivers, J. F. Reuwer and L. J. Schaad, *J. Am. Chem. Soc.*, 1958, **80**, 5885; The equation used by Jencks and quoted in Equation 2.22 is from A. Streitwieser, W. B. Hollyhead, A. H. Pudjaatmaka, P. H. Owens, T. L. Kruger, P. A. Rubenstein, R. A. MacQuarrie, M. L. Brokaw, W. K. C. Chu and H. M. Niemeyer, *J. Am. Chem. Soc.*, 1971, **93**, 5088.

14   E. M. Higgins, A. C. O'Donoghue, Ph.D. Thesis, Durham University, Durham, 2007.

15   J. Mahatthananchai and J. W. Bode, *Chem. Sci.*, 2012, **3**, 192.

16   R. L. Benoit and M. Frechette, *Can. J. Chem.*, 1984, **62**, 995.

17   T. J. Curphey and K. S. Prasad, *J. Org. Chem.*, 1972, **37**, 2259.

18   O. Guerret, S. Sole, H. Gornitzka, G. Trinquier and G. Bertrand, *J. Organomet. Chem.*, 2000, **600**, 112.

19   R. A. Kenneth, *J. Phys. Chem. A*, 2002, **106**, 11963.

20   (a) J. A. Murphy, S. Zhou, D. W. Thomson, F. Schoenebeck, M. Mahesh, S. R. Park, T. Tuttle and L. E. A. Berlouis, *Angew. Chem. Int. Ed.*, 2007, **46**, 5178; (b) F. Schoenebeck, J. A. Murphy, S. Zhou, Y. Uenoyama, Y. Miclo and T. Tuttle, *J. Am. Chem. Soc.*, 2007, **129**, 13368.

CHAPTER 3

Azolium Ion pK$_a$ Measurements II:
Conjugate Acids of Mesoionic Carbenes

3.0   Foreword

This chapter builds on the investigations into azolium ion acidity discussed in Chapter 2, and details the results of kinetic acidity and pK_a measurements of the C(5)-H of 1,2,3-triazolium ions and C(4/5)-H of imidazolium ions – the conjugate acids of mesoionic carbenes. Section 3.1 provides a brief historical introduction on abnormal carbenes. Section 3.2 presents the results of the kinetic experiments, the outcome of which are discussed in Section 3.3. These results are summarised in Section 3.4.

3.1   Introduction

3.1.1   Overview

The N-heterocyclic carbenes discussed up to this point may be described as 'normal' or classical NHCs, in the sense that the carbene centre is located between the heteroatoms and may be generated by deprotonation of the parent azolium ion at the acidic C(2)-H or C(3)-H positions. The organometallic chemistry of classical NHCs has been intensively studied and extensively reviewed, particularly in the last two decades, aided in no small part by the pioneering research of Arduengo and others.

A new class of NHC species have recently risen to prominence – of which imidazol-4/5-ylidenes **174** and 1,2,3-triazol-5-ylidenes **175** are amongst the most widespread – where the carbene is stabilised by a single heteroatom only. Originally described as 'abnormal' carbenes[1] by reference to the surprising ligand binding position in transition metal complexes, the term 'mesoionic' carbene (MIC)[2] is now more commonly used, and stems from the inability to draw the free carbene without additional formal charges in the resonance structure (Scheme 3.1). The classification of these species as carbenes is somewhat controversial,[3] as the description of carbene implies that the ligand is a neutral donor. Clearly, the borderline between one canonical representation and the other is continuous, and the issue of whether or not a carbene is more like structure **174a** or **174b**/**174c** may become a matter of semantics.

Scheme 3.1:

| 174a | 174b | 174c |

| 175a | 175b | 175c |
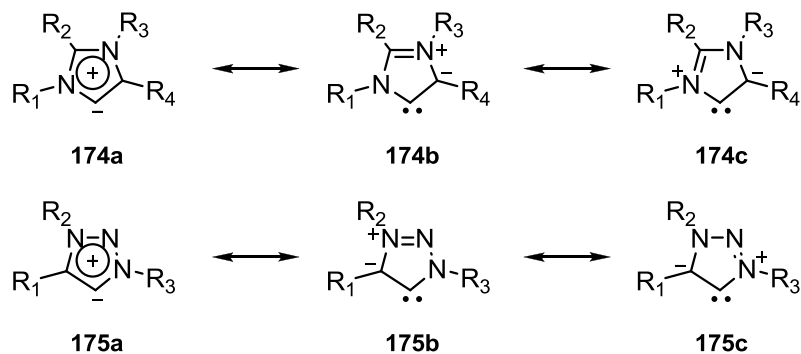
3.1.2   Mechanistic rationale for 'abnormal' binding

In 2001, Crabtree and co-workers reported the observation of the first 'abnormal' NHC-metal complex **177**, in which the imidazolylidene ligand was co-ordinated at the C(4) position rather than at C(2) (Scheme 3.2).[1] The reaction of pyridine substituted imidazolium ion **176** (X = BF$_4$) with IrH$_5$(PPh$_3$)$_2$ resulted in a stable C(4)-coordinated imidazolylidene complex – characterised unambiguously by X-ray diffraction – which showed no signs of rearrangement even upon heating.

Scheme 3.2:

176 R = ^{t}Bu, ^{i}Pr   **177** L = PPh$_3$
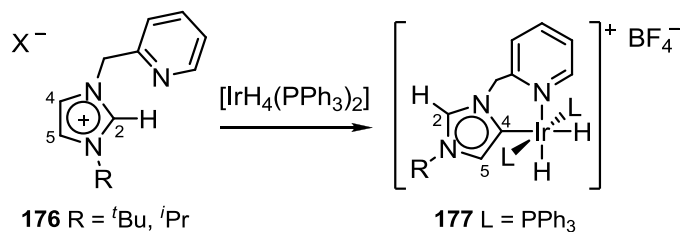
The observation of metallation at the C(4), rather than C(2) position is surprising, given the difference in acidity between the two positions. Indeed, a computational study by Yates has estimated the acidity of the C(4/5)-H (pK$_a$ = 33) to be 8 pK$_a$ units higher than that of the C(2)-H (pK$_a$ = 25).[4] Synthetic protocols to these species attest to this difference. Normal C(2)-bound complexes are typically generated from the free carbene – formed by deprotonation of the parent azolium salt using a strong base. Few reports suggest complexes of mesoionic carbenes are generated in this manner – in most cases C(4/5)-metallation is unanticipated.

Investigations undertaken by Crabtree indicate that binding occurs *via* competing mechanisms from the imidazolium ion – by heterolytic cleavage of the C(2)-H bond, or C(4/5)-H oxidative addition, and that this preference is dependent upon a number of factors. Computational[5] and experimental[6] studies into the effect of counterion on the reactivity of **176** suggest that the interaction between anion and C(2)-H plays an important role in directing the binding position (Scheme 3.3). Small anions such as Br⁻ may significantly weaken the C(2)-H bond through hydrogen bonding, strongly directing proton migration from the imidazolium ion to the hydride *via* heterolytic cleavage (**178**). In contrast, large, non-polarisable ions interact more weakly, favouring an oxidative addition pathway towards C(4/5)-metallation (**177**).

Scheme 3.3:
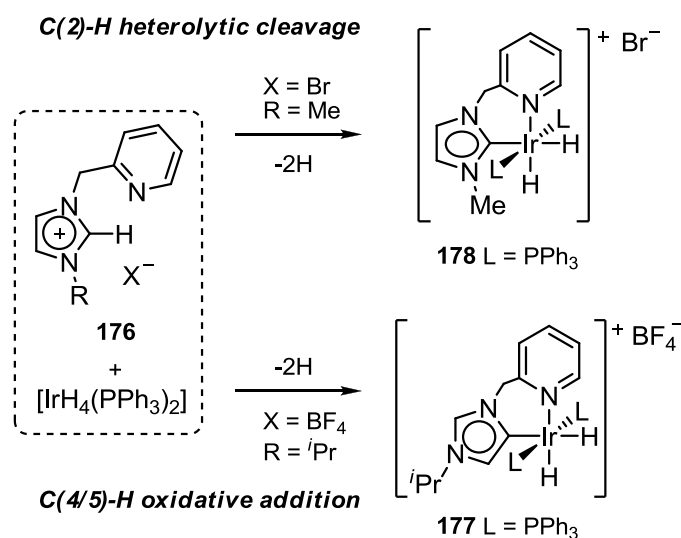
More recent studies by Esteruelas and co-workers also support these conclusions.[7] By analysing the distribution of coordination products (**180** and **181**) of the reaction between Crabtree's imidazolium ion **176** and $OsH_6(P^iPr_3)_2$, a preference for 'abnormal' binding was observed in the order $BPh_4^- > BF_4^- > Br^-$, with C(2) isomer formation rising with increasing coordinating power of the anion (Scheme 3.4a).

Scheme 3.4a:
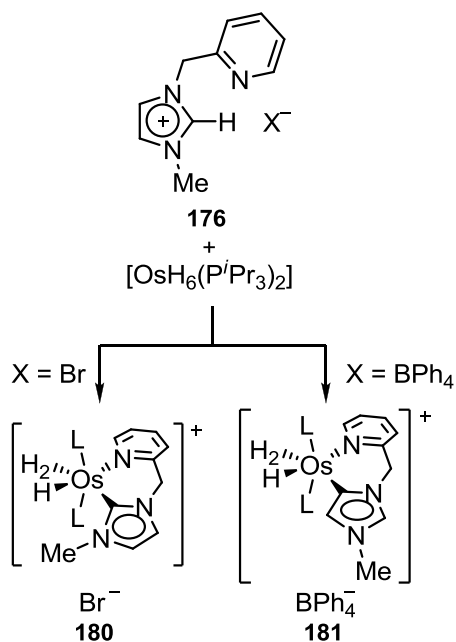
Scheme 3.4b:
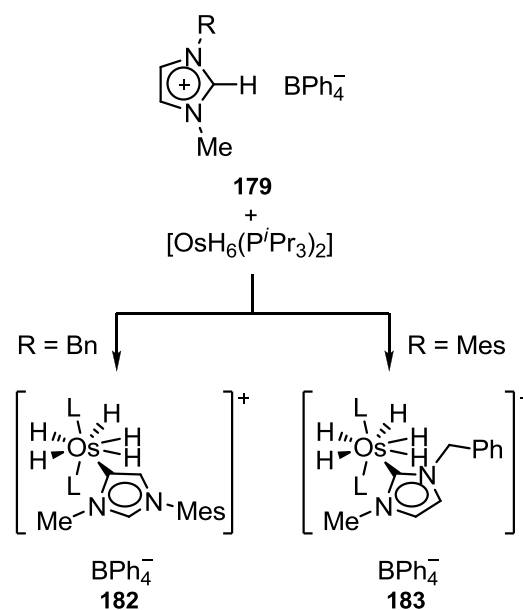
Steric effects can also play a significant role in determining the regioselectivity of binding. Experimental studies by Crabtree found that *iso*-propyl *N*-substituents direct towards the C(5)-metallation product **177**, whereas smaller methyl *N*-groups favour the C(2) complex **178** (Scheme 3.3). Similarly, a comparison of *N*-mesityl and *N*-benzyl groups on the complexation of methylimidazolium ion **179** with [OsH$_6$(P^{i}Pr$_3$)$_2$] found that C(5) binding (**182**) was preferred in the case of the more sterically hindered mesityl complex, to minimise unfavourable interactions between the tertiary phosphine ligands (Scheme 3.4b).[8]

In the last five years a number of other metallated MIC complexes have been prepared. In 2008, Albrecht and co-workers reported the first palladated 1,2,3-triazolylidene complex **184**, generated from the parent azolium ion by oxidative addition.[9] In 2010, the same group prepared a palladated isoxazolylidene complex **185**, this time generated from a 4-iodoisoxazolium salt by oxidative addition.[10] Using a similar method, Huynh and Han prepared a palladium complex **186**, incorporating a pyrazolin-4-ylidene ligand generated from the oxidative addition of C(4)-I bond.[11]
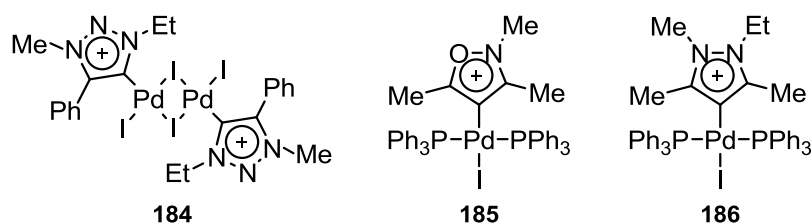
In 2009, Bertrand and co-workers reported the isolation of the first stable crystalline MIC.[12] By applying a similar deprotonation approach used in the preparation of classical NHCs, MIC **188** was generated from imidazolium salt **187** by deprotonation at the C(5)-H position using potassium hexamethyldisilazide (Scheme 3.5). Bulky 2,6-diisopropylphenyl (Dipp) and phenyl substituents were incorporated into the parent structure, offering kinetic protection to the C(5) position, and blocking the more acidic C(2) position which would otherwise be deprotonated first.

Scheme 3.5:
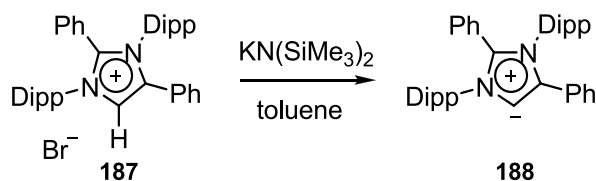
The scope of abnormally-bound carbene containing complexes in catalysis covers a wide range of applications, including C-C cross coupling reactions, hydrogenation reactions, and olefin metathesis, and these areas have been extensively reviewed.[13] Given the nature of these transformations, the majority of these catalysts are based on palladium metal centres; however, ruthenium and nickel complexes have recently become more widespread.

Mandal and co-workers recently demonstrated the first organocatalytic application of an uncomplexed MIC in the ring opening polymerisation of cyclic esters.[14] Using imidazol-4-ylidene **188**, rates of polymerisation were reportedly over 20-fold faster than previously obtained using classical NHCs.[15] Density Functional Theory studies carried out by the group suggest that the nucleophilic character at the carbene centre of imidazol-4-ylidene is much greater than for the corresponding imidazol-2-ylidene, which the authors speculate may account for this difference in reactivity.

3.1.3 Ligand donor ability

The ligand donor ability and basicity of NHCs often follow similar trends. As discussed above, MICs are most widely used as ligands in catalysis, and their basicity is of considerable importance in tuning their reactivity towards a given transformation. Work carried out by a number of groups indicates that abnormal carbenes are significantly stronger σ-donors than their 'normal' counterparts.

Ligand donor ability is often assessed by studying the effect of a ligand's coordination to a metal centre on a second, standard, ligand bound to the same metal centre. Changes in the bonding of the second ligand are measured spectroscopically. One of the most widely used scales is Tolman's electronic parameter (TEP), which compares the A$_1$ vibrational mode of the C≡O bond in the infrared spectrum of a [Ni(CO)$_3$(L)] complex.[16] As the donating power of the ligand under investigation increases, the electron density on the metal centre increases, resulting in increased π-backbonding to the vacant π* anti-bonding orbital on the CO ligand (Figure 3.1). Thus, the triple-bond character of the CO species decreases, resulting in lower A$_1$ stretching frequencies.

Figure 3.1: **Tolman's electronic parameter**
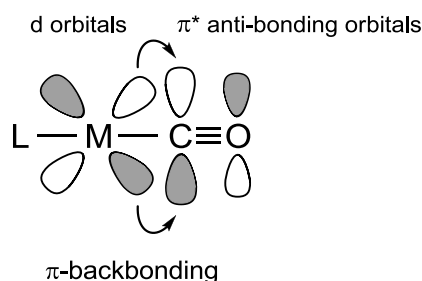
In 2004, Crabtree reported CO stretching frequencies for four *cis*-[Ir(CO)$_2$Cl(L)] complexes **189 – 192** containing classical and mesoionic NHC ligands.[17] Two stretching frequencies were observed in the infrared spectrum, consistent with *cis* geometry, which were averaged to give values of v_{av}(CO), shown in Figure 3.2. The value of v_{av}(CO) determined for the abnormal NHC complex **189** was found to be substantially lower than for the classical NHC species **190 – 192**, inferring that C(5)-bound imidazolylidenes are significantly stronger ligand donors than structurally similar C(2)-bound species. A corresponding TEP value (N.B. a scale based on nickel-centred complexes) for the mesoionic NHC was also estimated from the value of v_{av}(CO) obtained for the iridium-based **189** by extrapolating from a linear correlation of v_{av}(CO)-TEP data determined in earlier studies for a series of phosphine and NHC complexes.[18] The authors note that the estimated value of 2039 cm^{-1} is extremely low for a neutral ligand, with normal NHCs typically giving TEP values in the range 2048 – 2051 cm^{-1}.

Figure 3.2:   **Averaged CO stretching frequencies for [Ir(CO)$_2$(Cl)(L)] complexes**

	189	**190**	**191**	**192**
v_{av}(CO) / cm^{-1}	2003	2017	2017	2019
TEP / cm^{-1}	2039	2048	2048	2050

Investigations by Huynh into the ligand donor properties of normal and abnormal carbenes in palladium complexes also support these conclusions. Using ^{13}C NMR spectroscopy, the authors devised a scale of carbon chemical shifts for the C(2) position of benzimidazole ligand **193** in a range of [PdBr$_2$(**193**)(L)] complexes, where L took the form of tertiary phosphines, imidazoles and NHCs **194 – 197** (Figure 3.3).[19] The carbon chemical shift at the C(2) position of a carbene-metal complex is highly sensitive to changes in the Lewis acidity of the metal centre, a property influenced by the donor abilities of the surrounding ligands. As the ligand donor strength of the *trans* ligand L increases, the Lewis acidity of the metal centre decreases, and the δ_C of NHC **193** was found to move downfield.
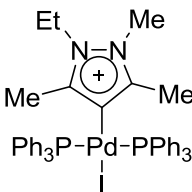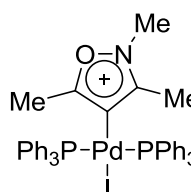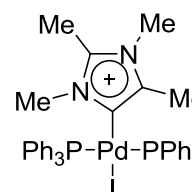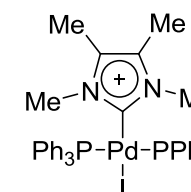
Figure 3.3:   **Values of δ_C for the C(2) position of NHC (193) in [PdBr$_2$(194)(L)] determined by ^{13}C NMR spectroscopy**

L =	**194**	**195**	**196**	**197**
C(2) δ_C / ppm	176.6	179.0	181.9	182.4

From this data, imidazol-4-ylidene **196** was found to be a stronger donor than imidazol-2-ylidene **195**, in agreement with Crabtree's study. The newly isolated pyrazolin-4-ylidene **197** was found to be more basic still. Expanding on this work, Albrecht has recently constructed a ligand basicity series for a selection of sterically similar palladated-MIC complexes **198 – 201**, determined by ^{31}P NMR spectroscopy (Figure

3.4).[20] The phosphorus chemical shifts of the two equivalent phosphine ligands were shown to undergo a solvent-independent move upfield as the donor strength of the NHC increased, enabling NHC-ligand basicity to be probed. On this scale, imidazol-5-ylidenes were found to be stronger σ-donors than analogous 'normal' imidazol-2-ylidenes, with isoxazol-4-ylidenes and pyrazol-4-ylidenes more basic still, in agreement with both Huynh's earlier work, and calculated TEP measurements made by Gusev.[21]

Figure 3.4: **CO stretching frequencies for [Pd(PPh$_3$)$_2$(I)(L)][CF$_3$SO$_3$] complexes in CDCl$_3$**

	198	**199**	**200**	**201**
δ$_P$ / ppm	22.56	21.28	20.48	18.76
TEP / cm^{-1} (calc)	2035	2042	2040	2065

3.1.4 Proton affinity measurements

Whilst the ligand donor properties of NHCs typically mirror basicity, these scales often fail when ligands become increasingly sterically hindered. In Chapter 2 we showed that the acid-base properties of classical NHCs have now been quantitatively studied by a number of groups. In contrast, estimates of mesoionic NHC basicities are limited to only a handful of computational estimates and no experimental pK$_a$ measurements have been determined in any solvent. Given that MICs have now been isolated independently from metal bound complexes and applied as organocatalysts in their own right, it is important that their acid-base properties are established.

Yates has obtained estimates of pK$_a$ for the C(2)-H and C(4/5)-H of parent imidazolium ion **134** (R$_1$ = R$_2$ = H) using computational methods. The pK$_a$ of the C(2)-H was found to be 24.9, in reasonable agreement with experimental measurements of 23.8 determined by Amyes.[22] A pK$_a$ of 33.0 was evaluated for the C(4/5)-H. Similar calculations returned proton affinities of 250.3 and 269.0 kcal mol^{-1} for the 'normal' and 'abnormal' positions respectively, indicating that the C(2)-localised anion is 18.7 kcal mol^{-1} more basic than the C(4/5)-localised anion.

Frenking has also reported proton affinities for a series of *N*-substituted abnormal imidazolylidenes **202** using computational methods (Table 3.1).[23] These proton affinities, which are 12 – 17 kcal mol^{-1} higher than for their classical counterparts **203**, further support the conclusion that imidazol-5-ylidenes are more basic than imidazol-2-ylidines. Structures of the conjugate acids of normal carbenes **203** are indistinguishable from those of abnormal carbenes **202**, thus the difference in proton affinity represents the energy difference between the carbene tautomers.

Across the *N*-alkyl series (R = H, Me, *t*-Bu), more electron-rich substituents lead to increases in proton affinity, consistent with trends in aqueous pK_a reported for the acidic C(2)-H positions of imidazolium ions.[24] However, for both the NHC **203** and MIC **202** species, *N*-aryl substituents result in a small increase in basicity relative to the *N,N*-dimethyl imidazolylidene, in contrast to the decrease in values of pK_a observed for similar parent imidazolium ions in aqueous solution. Bertrand *et al.* recently reported proton affinities for a number of 1,2,3-triazol-5-ylidenes **176** determined computationally (Table 3.2).[25] The proton affinity of the parent 1,2,3-triazol-5-ylidene **176** (R$_1$ = R$_2$ = R$_3$ = H) is around 18 kcal mol^{-1} lower than the corresponding imidazol-4/5-ylidene **202** (R = H), illustrating the effect of the additional electron-withdrawing nitrogen atom.

Table 3.1: **Proton affinities for abnormal and normal imidazolylidene calculated at the MP2/TZVPP//BP86/SVP level of theory**
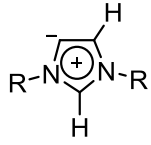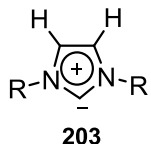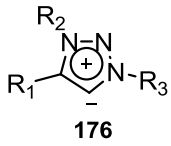
carbene		PA, kcal mol^{-1}	ΔPA(203 – 202), kcal mol^{-1}
202	R = H	270.9	16.7
	R = Me	278.3	16.0
	R = *t*-Bu	283.0	12.4
	R = Ph	279.7	15.0
	R = Mes	284.4	14.0
203	R = H	254.2	
	R = Me	262.3	
	R = *t*-Bu	270.6	
	R = Ph	264.7	
	R = Mes	270.4	

Table 3.2:   Proton affinities for 1,2,3-triazol-5-ylidenes calculated at the MP2/TZVPP//BP86/SVP level of theory

carbene		PA, kcal mol⁻¹
176	$R_1 = R_2 = R_3 = H$	252.8
	$R_1 = Dipp; R_2 = Me; R_3 = Ph$	272.5
	$R_1 = R_2 = Dipp; R_3 = t\text{-}Bu$	275.2

In this chapter, we will apply the same kinetic method used to determine the kinetic acidities and pK_as of the C(3)-H of 1,2,4-triazolium salts and C(2)-H of imidazolium salts discussed in Chapter 2, to the conjugate acids of triazol-5-ylidenes and imidazol-4/5-ylidenes. Within these families, the effect of *N*-aryl and *N*-alkyl substituents on acidity will be assessed.

3.2   Results

3.2.1   Deuterium exchange reactions of 1,2,3-triazolium ions followed by ¹H NMR spectroscopy

Proton-deuterium exchange experiments for 1,2,3-triazolium salts **204 − 207** (5 mM) in D₂O at 25 °C and constant ionic strength $I = 1.0$ (KCl) were performed at a range of pDs in an analogous manner to those described in Chapter 2. Exchange of the proton for deuterium at the C(5)-H position was followed by ¹H NMR spectroscopy (400 MHz), and resulted in the disappearance of the C(5)-H singlet signal. From this data, first- and second-order rate constants for deuteroxide ion-catalysed exchange, k_{ex} (s⁻¹) and k_{DO} (M⁻¹ s⁻¹), were determined. Using these rate constants, carbon acid pK_a values were estimated.

204	**205**	**206**	**207**
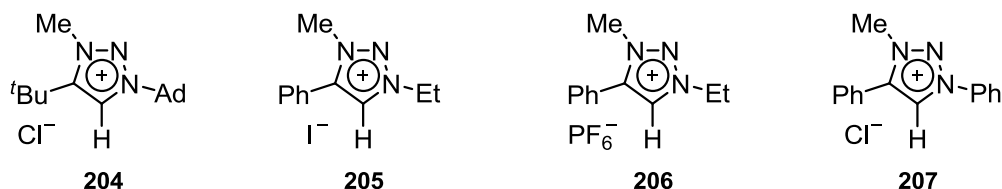
3.2.1.1 Determination of pseudo-first-order rate constants for exchange (k_{ex})

3.2.1.1a 1-Adamantyl-3-methyl-4-(*tert*-butyl)[1,2,3]triazolium chloride (204)
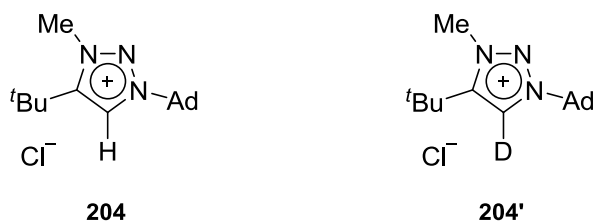
Pseudo-first-order rate constants for the deuteroxide ion-catalysed exchange of the C(5)-H of triazolium ion **204** to form deuterated product **204'** were determined by ^{1}H NMR spectroscopy (400 MHz).

A representative set of spectra taken at three time points during the reaction at 0.01 M KOD is shown in Figure 3.5. Deuterium exchange at the C(5)-H position resulted in the disappearance of the C(5)-H singlet at 8.69 ppm over the course of the reaction. The extent of exchange was measured relative to the 12 equivalent non-exchangeable protons of the internal standard at 3.18 ppm. Signals corresponding to the adamantyl β-CH$_2$, γ-CH and δ-CH$_2$ groups appear as a quartet at 1.73 ppm, singlet at 2.19 ppm and singlet at 2.22 ppm respectively. Signals corresponding to the methyl CH$_3$ group and nine equivalent methyl hydrogens on the *tert*-butyl group appear as singlets at 4.28 and 1.39 ppm respectively. No change was observed in the integrated area of any other peak relative to the internal standard, indicating that deuterium exchange does not occur at any position other than at C(5)-H under these conditions.

Experimentally observed first-order rate constants for exchange, k_{ex} (s^{-1}), were determined from the slopes of semi-logarithmic plots of f(s) against time at each pD. Reaction data and values of k_{ex} are presented in Appendix A (Table A11, Figure A19).

Figure 3.5:   Representative ^{1}H NMR spectra at 400 MHz of triazolium salt (204) (5 mM, 0.01 M KOD), obtained during exchange of the C(5)-H (s, 8.31 ppm) for deuterium in D$_2$O at 25 ^{o}C and *I* = 1.0 (KCl) [Internal standard, tetramethylammonium deuteriosulfate (s, 3.13 ppm)]
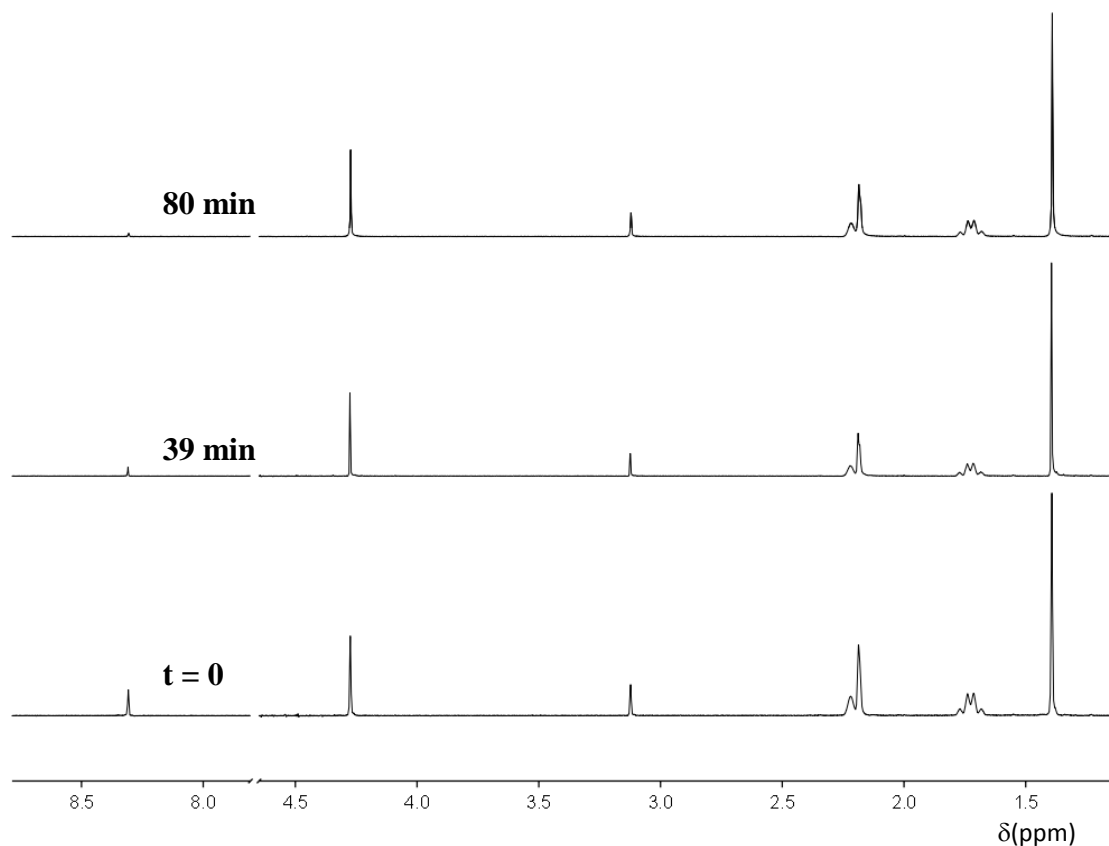
3.2.1.1b   1-Ethyl-3-methyl-4-phenyl[1,2,3]triazolium iodide (205)
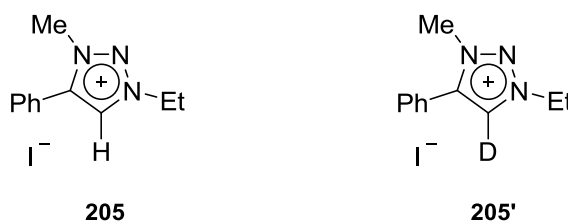
Pseudo-first-order rate constants for the deuteroxide ion-catalysed exchange of the C(5)-H of triazolium ion **205** to form deuterated product **205'** were determined by ^{1}H NMR spectroscopy (400 MHz).

A representative set of spectra taken at three time points during the reaction at p*D* 7.05 (40% *f*$_B$, phosphate buffer) is shown in Figure 3.6. Deuterium exchange at the C(5)-H position resulted in the disappearance of the C(5)-H singlet at 8.69 ppm over the course of the reaction. The extent of exchange was measured relative to the 12 equivalent non-exchangeable protons of the internal standard at 3.18 ppm. Signals corresponding to the

phenyl *ortho*-CH, *meta*-CH and *para*-CH groups appear as overlapping multiplets in the range 7.58 – 7.73 ppm. A signal corresponding to the methyl CH$_3$ group appears as a singlet at 4.26 ppm, and signals corresponding to the CH$_3$ and CH$_2$ protons on the ethyl substituent appear as a triplet at 1.65 ppm and a quartet at 4.69 ppm respectively. No change was observed in the integrated area of any other peak relative to the internal standard, indicating that deuterium exchange does not occur at any position other than at C(5)-H under these conditions.

Experimentally observed first-order rate constants for exchange, k_{ex} (s^{-1}), were determined from the slopes of semi-logarithmic plots of f(s) against time at each pD. Reaction data and values of k_{ex} are presented in Appendix A (Table A12, Figure A20).

Figure 3.6: **Representative ^{1}H NMR spectra at 400 MHz of triazolium salt (205) (5 mM, pD 7.75), obtained during exchange of the C(5)-H (s, 8.68 ppm) for deuterium in D$_2$O at 25 ºC and I = 1.0 (KCl) [Internal standard, tetramethylammonium deuteriosulfate (s, 3.18 ppm)]**
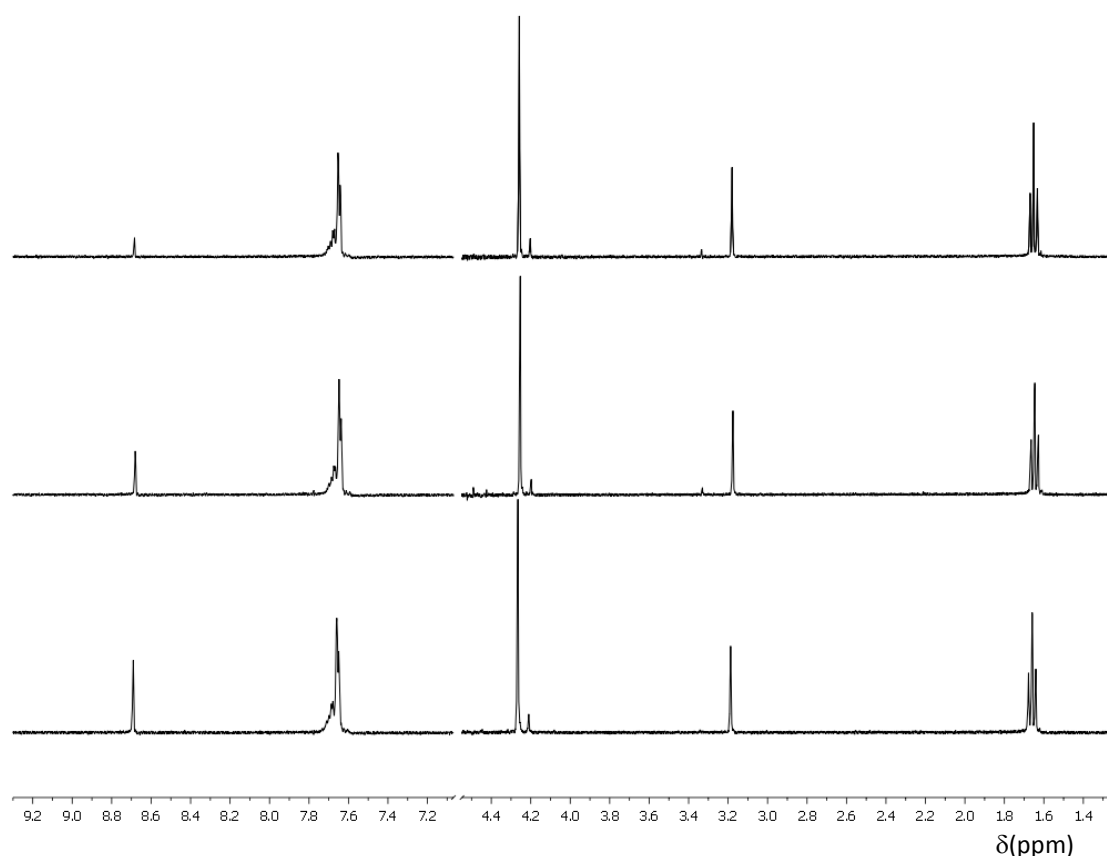
3.2.1.1c   1-Ethyl-3-methyl-4-phenyl[1,2,3]triazolium hexafluorophosphate (206)
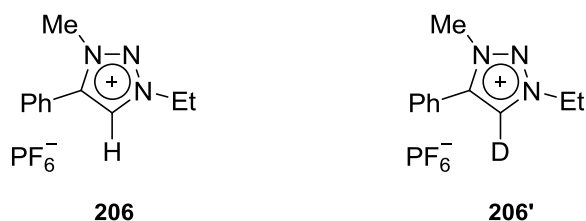
Pseudo-first-order rate constants for the deuteroxide ion-catalysed exchange of the C(5)-H of triazolium ion **206** to form deuterated product **206'** were determined by ^{1}H NMR spectroscopy (400 MHz).

A representative set of spectra taken at three time points during the reaction at pD 7.50 (70% f_B, phosphate buffer) is shown in Figure 3.7. Deuterium exchange at the C(5)-H position resulted in the disappearance of the C(5)-H singlet at 8.68 ppm over the course of the reaction. The extent of exchange was measured relative to the 12 equivalent non-exchangeable protons of the internal standard at 3.18 ppm. Signals corresponding to the phenyl *ortho*-CH, *meta*-CH and *para*-CH groups appear as overlapping multiplets in the range 7.58 – 7.73 ppm. A signal corresponding to the methyl CH$_3$ group appears as a singlet at 4.26 ppm, and signals corresponding to the CH$_3$ and CH$_2$ protons on the ethyl substituent appear as a triplet at 1.65 ppm and a quartet at 4.69 ppm respectively. No change was observed in the integrated area of any other peak relative to the internal standard, indicating that deuterium exchange does not occur at any position other than at C(5)-H under these conditions.

Experimentally observed first-order rate constants for exchange, k_{ex} (s^{-1}), were determined from the slopes of semi-logarithmic plots of f(s) against time at each pD. Reaction data and values of k_{ex} are presented in Appendix A (Table A13, Figure A21).

Figure 3.7: Representative ^{1}H NMR spectra at 400 MHz of triazolium salt (206) (5 mM, p*D* 7.50), obtained during exchange of the C(5)-H (s, 8.68 ppm) for deuterium in D_2O at 25 °C and *I* = 1.0 (KCl) [Internal standard, tetramethylammonium deuteriosulfate (s, 3.18 ppm)]
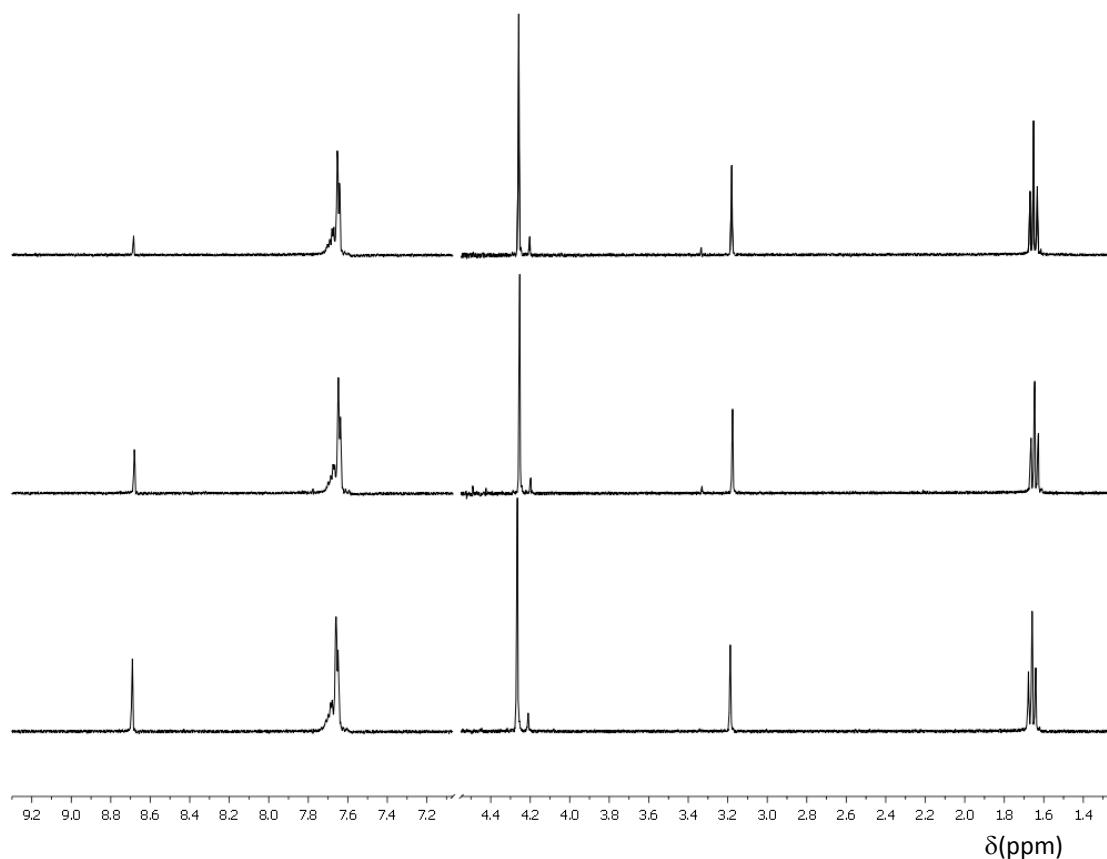
3.2.1.1d 1,4-Diphenyl-3-methyl[1,2,3]triazolium chloride (207)
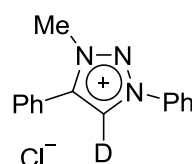
Pseudo-first-order rate constants for the deuteroxide ion-catalysed exchange of the C(5)-H of triazolium ion **207** to form deuterated product **207'** were determined by ^{1}H NMR spectroscopy (400 MHz).

A representative set of spectra taken at three time points during the reaction in phosphate buffer at p*D* 7.52 (70% f_B) is shown in Figure 3.8. Deuterium exchange at the C(5)-H position resulted in the disappearance of the C5-H singlet at 9.23 ppm over the course of the reaction. The extent of exchange was measured relative to the 12 equivalent non-exchangeable protons of the internal standard at 3.19 ppm. Signals

corresponding to the phenyl *ortho*-CH groups appear as a doublet at 7.97 ppm, those corresponding to the *meta*-CH and *para*-CH groups as overlapping multiplets at 7.66 – 7.77 ppm. A signal corresponding to the methyl CH_3 group appears at 4.41 ppm. No change was observed in the integrated area of any other peak relative to the internal standard, indicating that deuterium exchange does not occur at any position other than at C(5)-H under these conditions.

Experimentally observed first-order rate constants for exchange, k_{ex} (s^{-1}), were determined from the slopes of semi-logarithmic plots of *f*(s) against time at each p*D*. Reaction data and values of k_{ex} are presented in Appendix A (Table A14, Figure A22).

Figure 3.8: **Representative ^{1}H NMR spectra at 400 MHz of triazolium salt (207) (5 mM, p*D* 7.50), obtained during exchange of the C(5)-H (s, 8.68 ppm) for deuterium in D$_2$O at 25 ºC and *I* = 1.0 (KCl) [Internal standard, tetramethylammonium deuteriosulfate (s, 3.18 ppm)]**
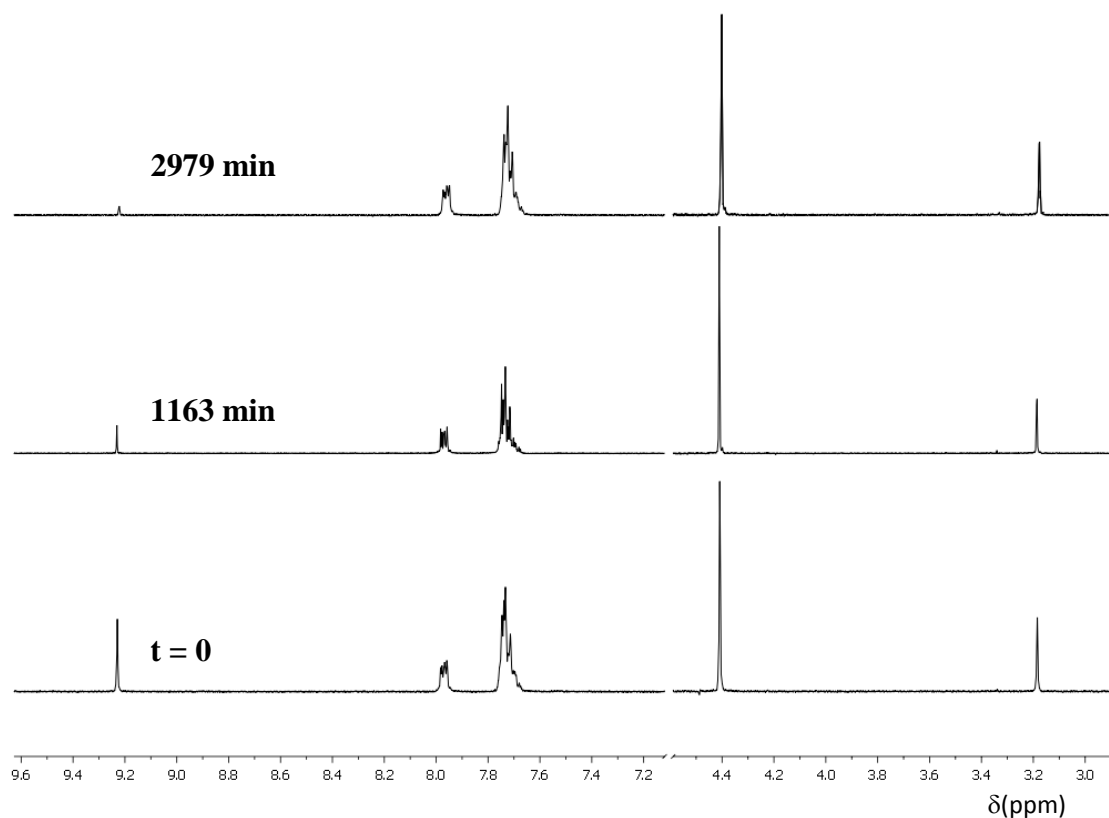
3.2.1.2 Determination of second-order rate constants for exchange (k_{DO})

In Chapter 2, we described that the experimental pseudo-first-order rate constants for exchange (k_{ex}) may comprise terms for all potentially catalytic species in the reaction. In our experiments, these contributions come from deuteroxide ion ($k_{DO}[DO^-]$), and potentially, solvent (k_{D2O}) and buffer base ($k_B[B]$) (Equation 2.7).

$$k_{ex} = k_{DO}[DO^-] + k_{D2O} + k_B[B] \qquad \textbf{Equation 3.1}$$

The extent of general base catalysis of exchange for these 1,2,3-triazolium species has not previously been investigated. Therefore, the contribution of general base catalysis to exchange of the C(5)-H for deuterium was assessed for representative triazolium ion **207**, and these results are presented below.

207   **207'**

Pseudo-first-order rate constants for the deuteroxide ion-catalysed exchange of the C(5)-H of representative triazolium ion **207** to form deuterated product **207'** were determined by ¹H NMR spectroscopy (400 MHz). Experiments were performed in phosphate buffers at a fixed buffer ratio (70% f_B). ¹H NMR spectral details have been described previously for **207**.

Experimentally observed first-order rate constants for exchange, k_{ex} (s⁻¹), were determined from the slopes of semi-logarithmic plots of f(s) against time at five total buffer concentrations ([Buffer]$_{tot}$ = 0.1 − 0.4 M). Reaction data for these experiments and values of k_{ex} at each buffer concentration are presented in Appendix A (Table A15, Figure A23). Values of k_{ex} (s⁻¹) as a function of the concentration of buffer base are shown in Table 3.3. The ratio of rate constants, k_{rel}, obtained using Equation 2.8, is a measure of the relative difference in the experimentally observed rate constant for exchange, k_{ex} (s⁻¹), and contribution to rate from deuteroxide ion-catalysed exchange, $k_{DO}[DO^-]$ (s⁻¹), where k_{DO} (M⁻¹ s⁻¹) is determined from rate measurements in un-buffered solution.

Table 3.3: **First-order rate constants, k_{ex} (s^{-1}), for deuterium exchange of the C(5)-H of (207) in phosphate buffers (70% f_B) in D$_2$O at 25 ºC and I = 1.0 (KCl)**

[B], M [a]	pD	[B]/[DO$^-$] [b]	k_{ex}, s^{-1} [c]	k_{rel} [d]
0.070	7.49	1.21×10^6	1.16×10^{-5}	0.92
0.140	7.51	2.31×10^6	1.32×10^{-5}	1.00
0.175	7.52	2.82×10^6	1.28×10^{-5}	0.95
0.210	7.55	3.16×10^6	1.45×10^{-5}	1.00
0.280	7.58	3.94×10^6	1.57×10^{-5}	1.01

(a) Concentration of free base (PO$_4$H^{2-}) form of buffer. (b) Ratio of concentrations of PO$_4$H^{2-} to deuteroxide ion. (c) Experimentally observed pseudo-first-order rate constant for exchange of C(5)-H of triazolium **207**. (d) Ratio of first-order rate constant for exchange of C(5)-H (k_{ex}) to first-order rate term for deuteroxide ion-catalysed exchange only (k_{DO}[DO$^-$]), as described in Equation 2.8, where $k_{DO} = 2.10 \times 10^2$ M^{-1} s^{-1}.

Figure 3.9 shows a plot of k_{rel} against ([B]/[DO$^-$]), which corrects for the slight changes in pD that occur upon dilution of a buffer solution at constant ionic strength. The ratio of second-order rate constants for buffer base catalysed exchange to deuteroxide ion catalysed exchange, k_B/k_{DO}, may be obtained as the slope this plot according to Equation 2.8. In the absence of general base catalysis of exchange, this ratio should be close to zero.

Figure 3.9: **Plot of the ratio of rate constants k_{rel} against ([B$^-$]/[DO])**

$y = (3.08E\text{-}08)x + 8.94E\text{-}01$
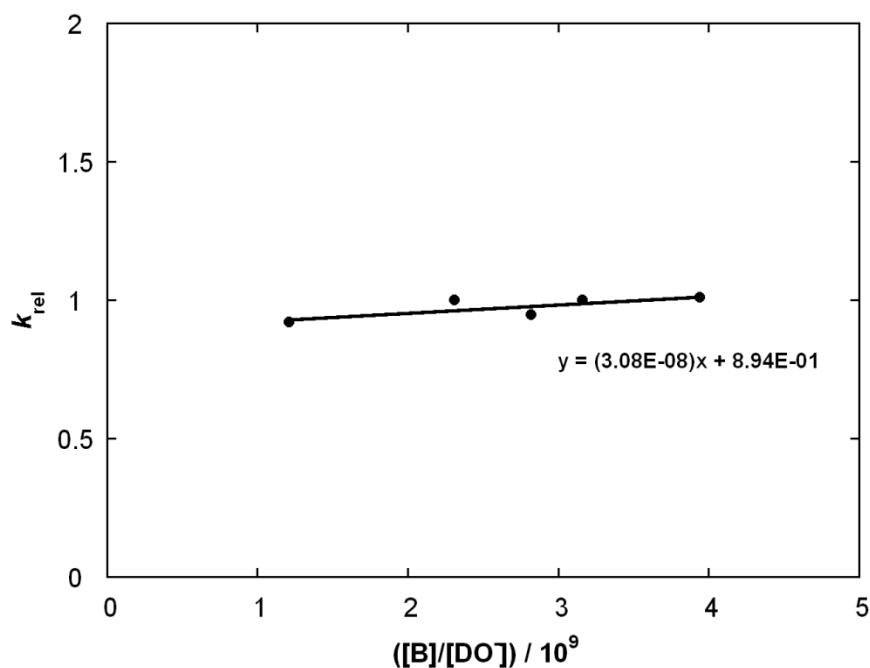
From the slope of this plot, the ratio k_B/k_{DO} was found to equal 3.08×10^{-8}. This value is small relative to the changes in concentration of buffer base, and falls well within the 6% experimental error limits associated with values of k_{DO} (M^{-1} s^{-1}) (Appendix A). As such, general base catalysis is judged to be insignificant for 1,2,3-triazolium ions **204 – 207**, and the buffer catalysis term in Equation 3.1 may be neglected.

Plots of k_{ex} against deuteroxide ion concentration for 1,2,3-triazolium ions **204 – 207** are shown in Figures 3.10 – 3.13. Table 3.4 summarises the y-intercept values obtained from these plots, expressed as a percentage of the range of k_{ex} measured experimentally. As the experimental error in k_{ex} is estimated to be around 6%, these negative y-intercept values are well within this experimental error and are judged to be insignificant. Therefore, second-order rate constants for deuteroxide ion-catalysed exchange, k_{DO} (M^{-1} s^{-1}), may be obtained from the slopes of plots of k_{ex} against deuteroxide ion concentration according to Equation 3.2. Values of k_{DO} are summarised in Table 3.5.

$$k_{ex} = k_{DO}[DO^-]$$

Equation 3.2

Table 3.4: **Evaluation of the significance of y-intercept values as a percentage of the range of k_{ex} obtained**
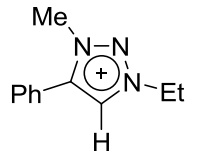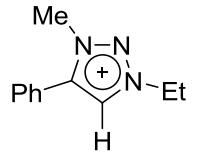
substrate		y-intercept, s⁻¹	k_{ex} range, s⁻¹	%
204	Cl⁻	-3.60×10^{-5}	1.85×10^{-3} $(4.20 \times 10^{-4} - 2.27 \times 10^{-3})$	1.9%
205	I⁻	-2.47×10^{-8}	2.71×10^{-6} $(2.42 \times 10^{-7} - 2.95 \times 10^{-6})$	0.9%
206	PF₆⁻	-1.38×10^{-9}	7.01×10^{-7} $(2.04 \times 10^{-8} - 7.21 \times 10^{-7})$	0.2%
207	Cl⁻	-2.28×10^{-7}	1.25×10^{-5} $(3.06 \times 10^{-7} - 1.28 \times 10^{-5})$	1.8%

Figure 3.10: Plot of k_{ex} against [DO$^-$] for the H/D-exchange reaction of triazolium ion (204) in D$_2$O at 25 ºC and $I = 1.0$ (KCl)

Figure 3.11: Plot of k_{ex} against [DO$^-$] for the H/D-exchange reaction of triazolium ion (205) in D$_2$O at 25 ºC and $I = 1.0$ (KCl)

Figure 3.12: Plot of k_{ex} against [DO⁻] for the H/D-exchange reaction of triazolium ion (206) in D$_2$O at 25 ºC and I = 1.0 (KCl)

y = (1.23E+01)x - 5.62E-10
R² = 0.997

Figure 3.13: Plot of k_{ex} against [DO⁻] for the H/D-exchange reaction of triazolium ion (207) in D$_2$O at 25 ºC and I = 1.0 (KCl)

y = (2.10E+02)x - 2.28E-07
R² = 0.999
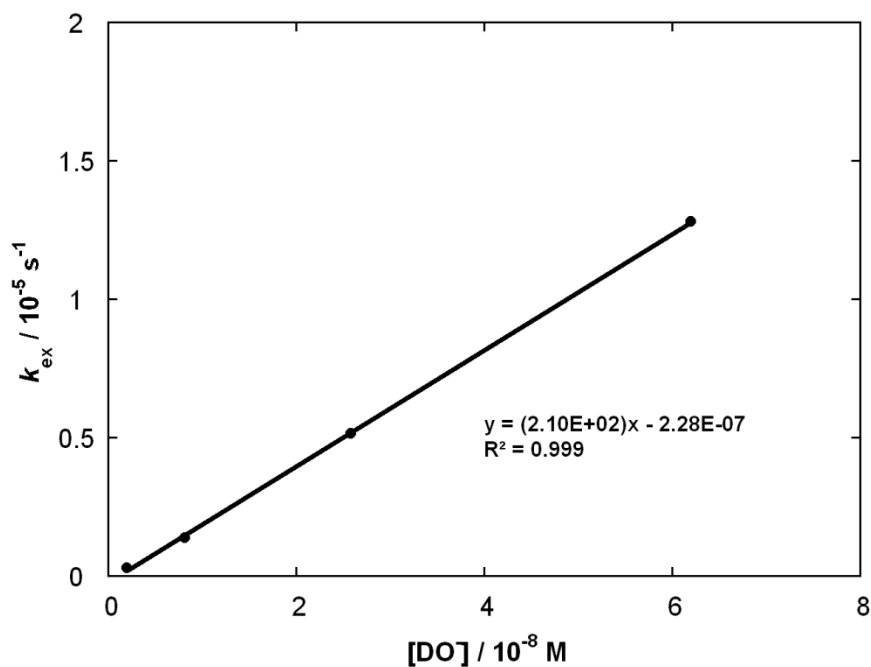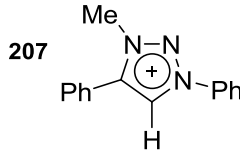
Table 3.5: **Second-order rate constants for deuteroxide ion-catalysed exchange (k_{DO}, M^{-1} s^{-1}) of the C(5)-H of 1,2,3-triazolium salts (204) – (207) for deuterium in D$_2$O at 25 °C and I = 1.0 (KCl)**

substrate	k_{DO}, M^{-1} s^{-1} [a]
204	4.61×10^{-2}
205	1.25×10^{1}
206	1.24×10^{1}
207	2.10×10^{2}

(a) Obtained from the slope of a plot of k_{ex} against [DO$^-$] (Figures 3.10 – 3.13).

3.2.2 Deuterium exchange reactions of 1,3-imidazol-4,5-ium ions followed by ^{1}H NMR spectroscopy

Proton-deuterium exchange experiments for imidazolium salts **208** – **210** (5 mM) in D$_2$O at 25 °C and constant ionic strength I = 1.0 (KCl) were performed at a range of pDs in an analogous manner to the experiments described in Chapter 2. Exchange of the proton for deuterium at the C(4/5)-H position was followed by ^{1}H NMR spectroscopy (400 MHz), and resulted in the disappearance of the C(4/5)-H singlet signal(s). From this data, first- and second-order rate constants for deuteroxide ion-catalysed exchange, k_{ex} (s^{-1}) and k_{DO} (M^{-1} s^{-1}), were determined. Using these rate constants, carbon acid pK_a values were estimated.

208 **209** **210**
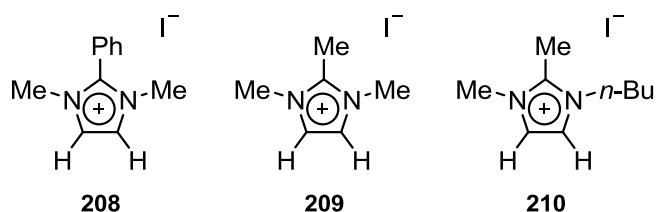
3.2.2.1   Determination of pseudo first-order rate constants for exchange (k_{ex})

3.2.2.1a   1,3-Dimethyl-2-phenyl[1,3]imidazolium iodide (208)

Pseudo-first-order rate constants for the deuteroxide ion-catalysed exchange of the C(4)-H and C(5)-H of imidazolium ion **208** to form deuterated product **208'** were determined by ^{1}H NMR spectroscopy (400 MHz).
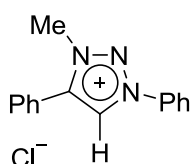
A representative set of spectra taken at three time points during the reaction at 0.1 M KOD is shown in Figure 3.14. The signals shown in these spectra are broad, possibly as a result of the difficulty in shimming these more concentrated, viscous solutions of KOD. Deuterium exchange at the equivalent C(4)-H and C(5)-H positions resulted in the disappearance of the C(4/5)-H singlet at 7.58 ppm over the course of the reaction. The extent of exchange was measured relative to the 12 equivalent non-exchangeable protons of the internal standard at 3.25 ppm. Signals corresponding to the *ortho*-CH, *meta*-CH and *para*-CH groups on the phenyl substituent appear as a broad asymmetric doublet at 7.69 ppm, and as two broad asymmetric triplets at 7.77 and 7.82 ppm respectively. A singlet corresponding to the two equivalent *N*-methyl groups appears at 3.78 ppm. No change was observed in the integrated area of any other peak relative to the internal standard, indicating that deuterium exchange does not occur at any position other than at C(4)-H and C(5)-H under these conditions.

Experimentally observed first-order rate constants for exchange, k_{ex} (s^{-1}), were determined from the slopes of semi-logarithmic plots of f(s) against time at each deuteroxide ion concentration. Reaction data and values of k_{ex} at each pD are presented in Appendix A (Table A16, Figure A24).

Figure 3.14: Representative ^{1}H NMR spectra at 400 MHz of imidazolium salt (208) (5 mM, 0.1 M KOD), obtained during exchange of the C(4/5)-H (s, 7.58 ppm) for deuterium in D$_2$O at 25 ºC and I = 1.0 (KCl) [Internal standard, tetramethylammonium deuteriosulfate (s, 3.25 ppm)]
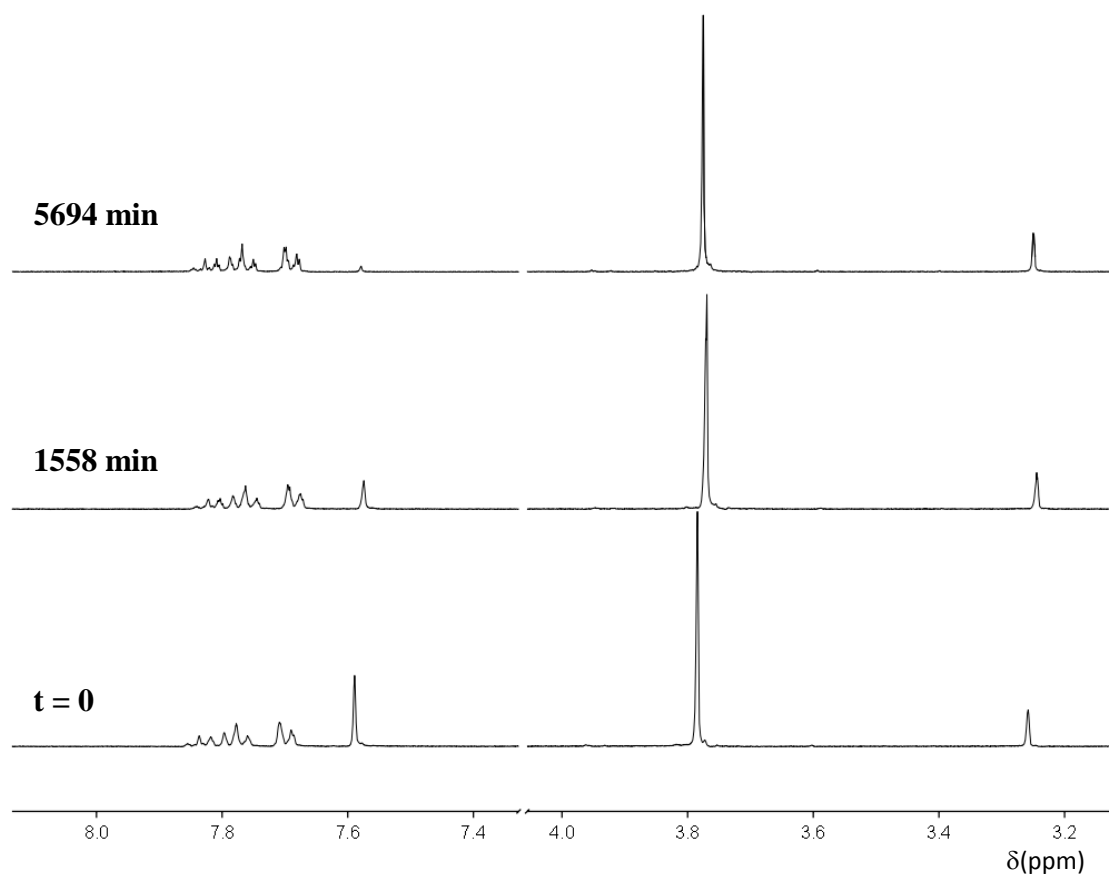
3.2.2.1b   1,2,3-Trimethyl[1,3]imidazolium iodide (209)
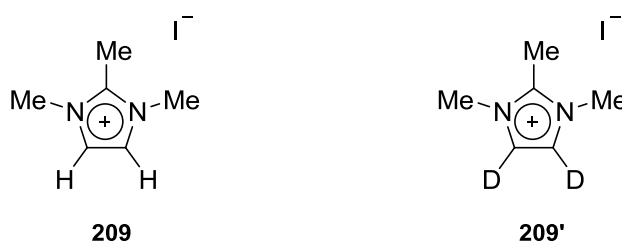
209   **209'**

Pseudo-first-order rate constants for the deuteroxide ion-catalysed exchange of the C(4)-H and C(5)-H of imidazolium ion **209** to form deuterated product **209'** were determined by ^{1}H NMR spectroscopy (400 MHz).

A representative set of spectra taken at three time points during the reaction at 0.4 M KOD is shown in Figure 3.15. The signals shown in these spectra are broad, possibly as a result of the difficulty in shimming these more concentrated, viscous solutions of KOD. Deuterium exchange at the equivalent C(4)-H and C(5)-H positions resulted in the disappearance of the C(4/5)-H singlet at 7.30 ppm over the course of the reaction.

The extent of exchange was measured relative to the 12 equivalent non-exchangeable protons of the internal standard at 3.22 ppm. A singlet corresponding to the two equivalent *N*-methyl groups appears at 3.78 ppm, and a singlet corresponding to the C(2)-methyl group appears initially at 2.58 ppm. In addition to exchange at the C(4)-H and C(5)-H positions, exchange of the protons on the C(2)-methyl was also observed. Under these conditions C(2)-methyl exchange was rapid, and was not studied in further detail.

Experimentally observed first-order rate constants for exchange, k_{ex} (s^{-1}), were determined from the slopes of semi-logarithmic plots of *f*(s) against time at each deuteroxide ion concentration. Reaction data and values of k_{ex} are presented in Appendix A (Table A17, Figure A25).

Figure 3.15: **Representative ^{1}H NMR spectra at 400 MHz of imidazolium salt (209) (5 mM, 0.4 M KOD), obtained during exchange of the C(4/5)-H (s, 7.30 ppm) for deuterium in D$_2$O at 25 ºC and *I* = 1.0 (KCl) [Internal standard, tetramethylammonium deuteriosulfate (s, 3.22 ppm)]**
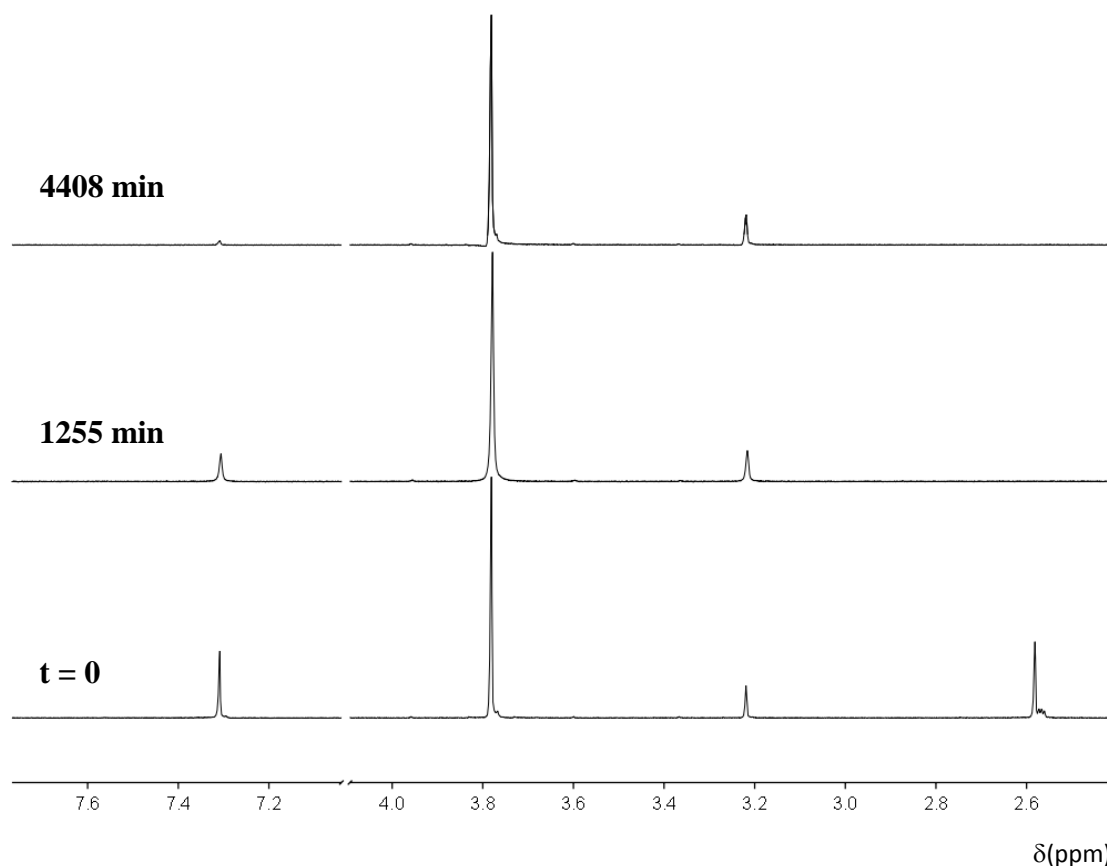
3.2.2.1c   1-Butyl-2,3-dimethyl[1,3]imidazolium iodide (210)
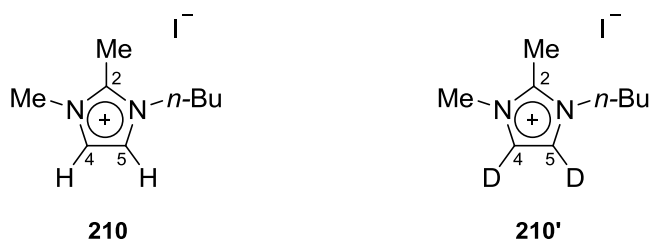
Pseudo-first-order rate constants for the deuteroxide ion-catalysed exchange of the C(4)-H and C(5)-H of imidazolium ion **210** to form deuterated product **210'** were determined by ^{1}H NMR spectroscopy (400 MHz).

A representative set of spectra taken at three time points during the reaction at 0.2 M KOD is shown in Figure 3.16. Deuterium exchange at the C(4)-H and C(5)-H positions resulted in the disappearance of the C(4)-H and C(5)-H doublets at 7.35 and 7.39 ppm respectively, over the course of the reaction. ^{1}H-NOESY, ^{1}H,^{13}C-HSQC and ^{1}H,^{13}C-HMBC NMR experiments confirm that the more downfield signal (7.39 ppm) corresponds to the C(5)-H position, proximal to the *n*-butyl substituent. The extent of exchange was measured relative to the 12 equivalent non-exchangeable protons of the internal standard at 3.23 ppm. Signals corresponding to the three CH$_2$ groups on the *N*-butyl chain appear as a triplet at 4.13 ppm and multiplets at 1.81 and 1.35 ppm, and a triplet corresponding to the terminal CH$_3$ group appears at 0.95 ppm. A singlet corresponding to the *N*-methyl group appears at 3.80 ppm, and a singlet corresponding to the C(2)-methyl group appears initially at 2.62 ppm. In addition to exchange at the C(4)-H and C(5)-H positions, exchange of the protons on the C(2)-methyl was also observed. Under these conditions C(2)-methyl exchange was rapid, and was not studied in further detail.

Experimentally observed first-order rate constants for exchange, k_{ex} (s^{-1}), were determined from the slopes of semi-logarithmic plots of *f*(s) against time at each deuteroxide ion concentration. Reaction data and values of k_{ex} are presented in Appendix A (Table A18, Figure A26 – A27).

Figure 3.16: Representative ^{1}H NMR spectra at 400 MHz of imidazolium salt (**210**) (5 mM, 0.2 M KOD), obtained during exchange of the C(4)-H (d, 7.35 ppm) and C(5)-H (d, 7.39 ppm) for deuterium in D$_2$O at 25 °C and *I* = 1.0 (KCl) [Internal standard, tetramethylammonium deuteriosulfate (s, 3.23 ppm)]
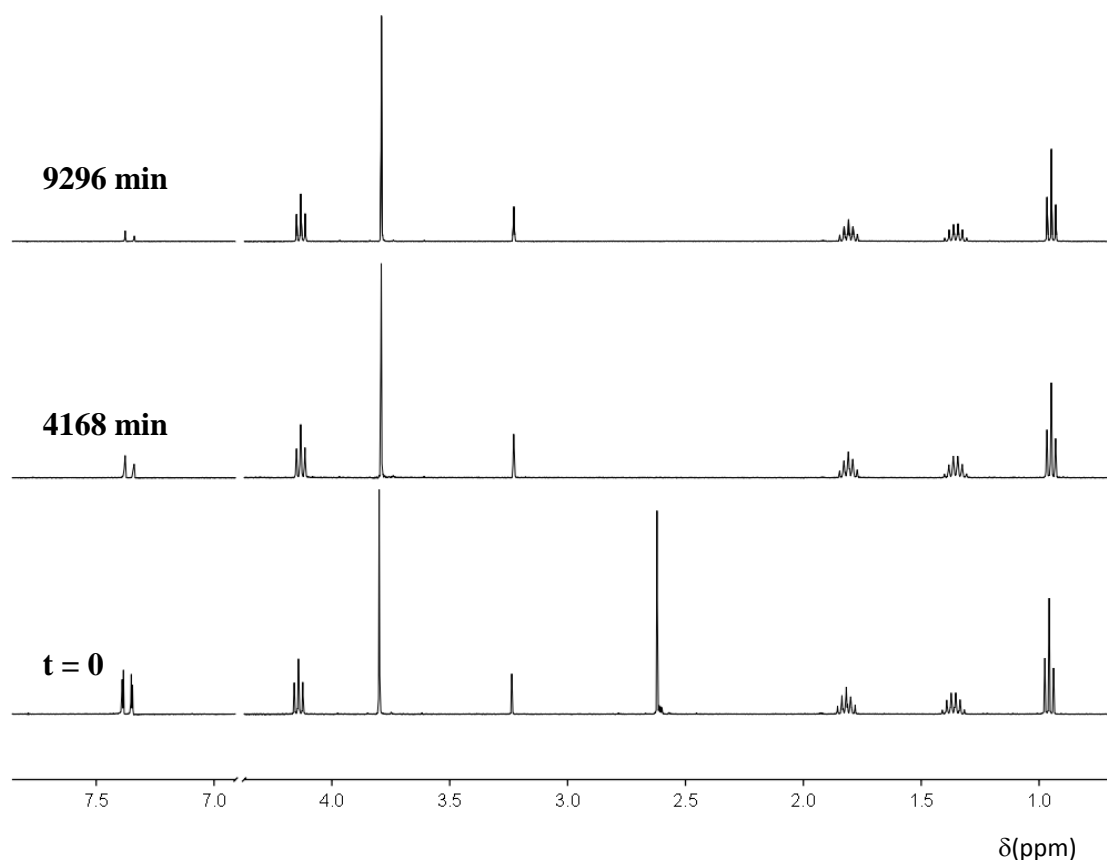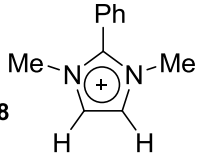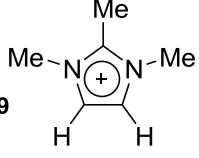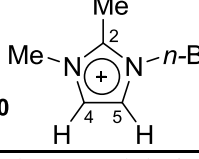
3.2.2.2   Determination of second-order rate constants for exchange (k_{DO})

As described earlier, experimental pseudo-first-order rate constants for exchange (k_{ex}) comprise terms for deuteroxide ion ($k_{DO}[DO^-]$), and potentially, solvent (k_{D2O}) and buffer base ($k_B[B]$) (Equation 3.1). The exchange reactions of imidazolium ions **208 – 210** were performed in solutions of KOD, and therefore, the buffer term may be neglected.

Figures 3.16 – 3.18 show plots of k_{ex} against deuteroxide ion concentration for imidazolium salts **208 – 210**. Potentially, the slopes of these plots may be used to obtain second-order rate constants for deuteroxide ion-catalysed exchange, k_{DO} (M^{-1} s^{-1}), according to Equation 3.2. Table 3.6 summarises the y-intercept values obtained from these plots, expressed as a percentage of the range of k_{ex} measured experimentally. In all cases, however, a significant negative y-intercept is observed which falls outside of experimental error (6%).

Table 3.6: Evaluation of the significance of y-intercept values as a percentage of the range of k_{ex} obtained
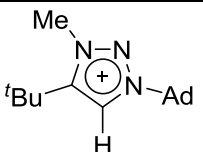
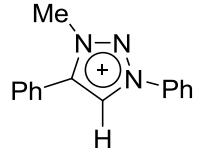| substrate		y-intercept, s^{-1}	k_{ex} range, s^{-1}	%
208		-2.44×10^{-6}	2.95×10^{-5} $(7.51 \times 10^{-6} - 3.71 \times 10^{-5})$	8.3%
209		-1.13×10^{-6}	1.50×10^{-5} $(2.24 \times 10^{-6} - 1.72 \times 10^{-5})$	7.6%
210	C(4)-H	-3.26×10^{-5}	2.59×10^{-5} $(3.83 \times 10^{-6} - 2.97 \times 10^{-5})$	126% [a]
	C(5)-H	-2.62×10^{-5}	2.08×10^{-5} $(2.99 \times 10^{-6} - 2.38 \times 10^{-5})$	126% [a]

(a) The upward deviation from the linear fit of the data to $k_{ex} = k_{DO}[DO^-]$, implied by all of these plots, will be greater at higher deuteroxide ion concentrations. Therefore, the apparent greater % y-intercepts for **210** is likely due to the greater range of measurement points obtained in this case (0.8 M and 1.0 M KOD).
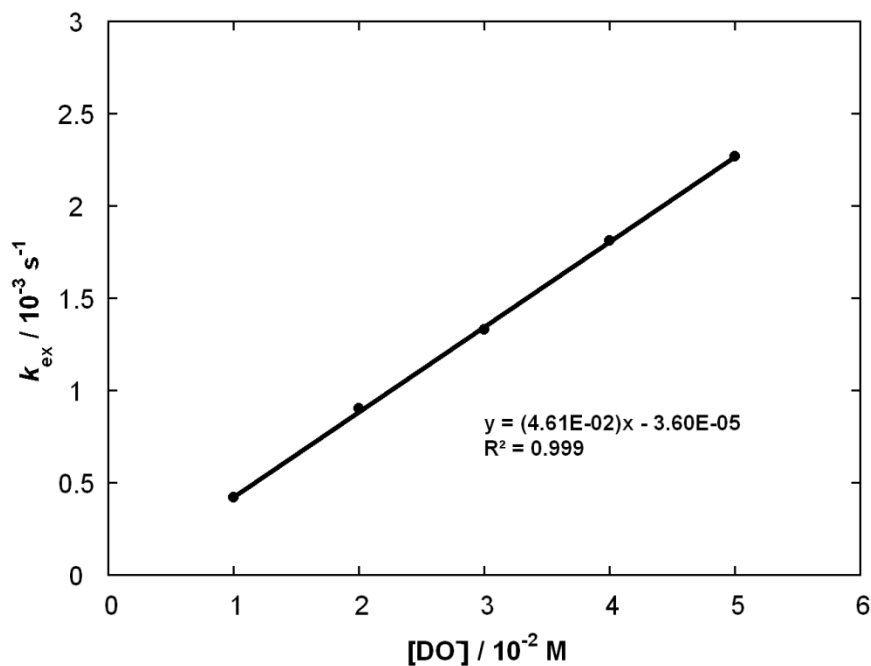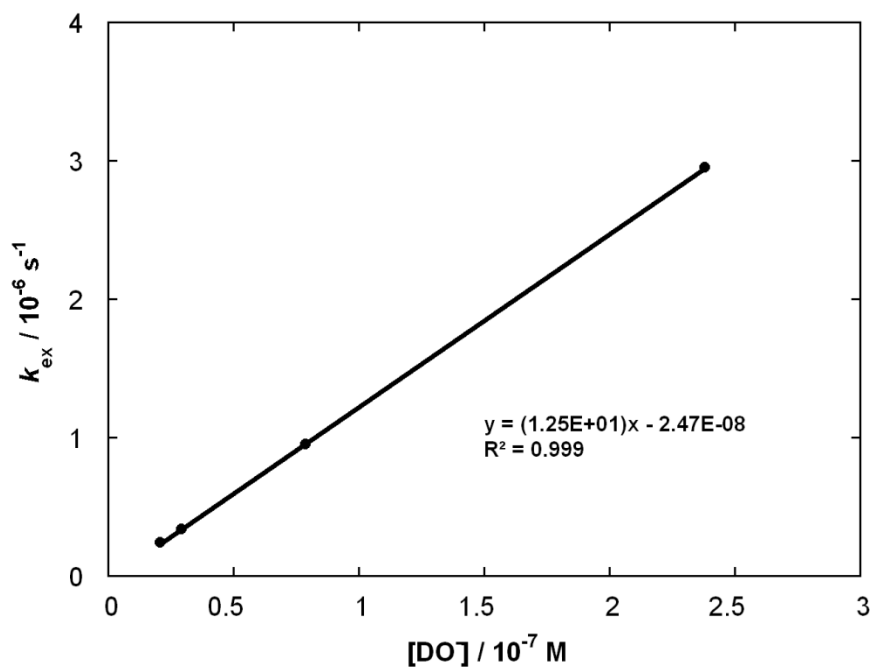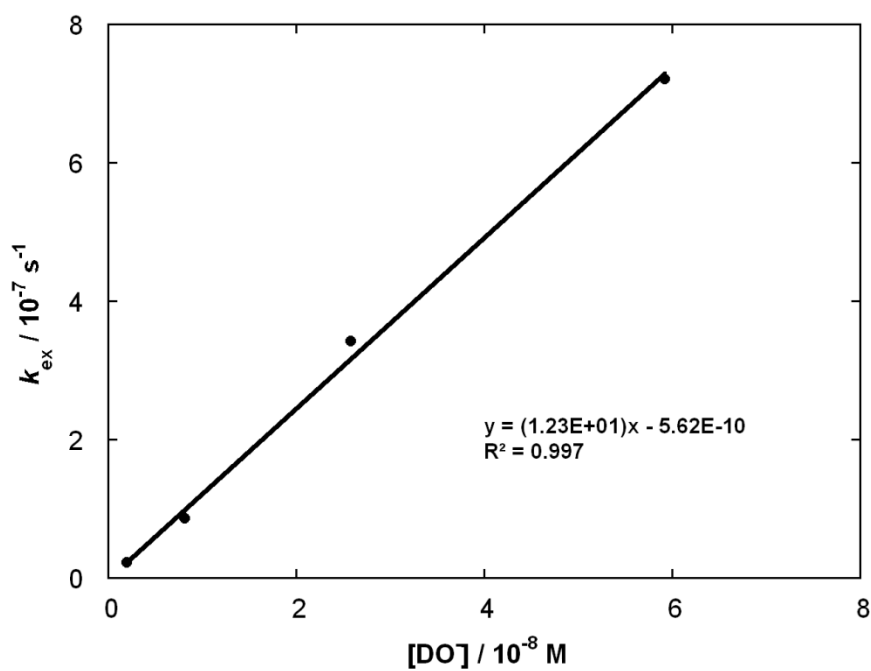
Figure 3.16: Plot of k_{ex} against $[DO^-]$ for the H/D-exchange reaction of imidazolium ion (208) in D$_2$O at 25 °C and $I = 1.0$ (KCl)
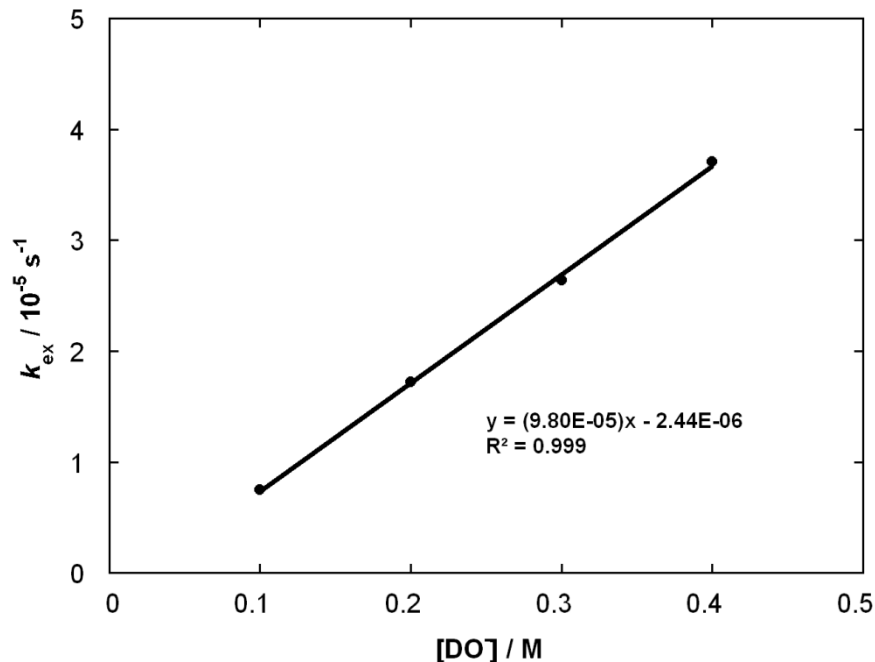
Figure 3.17: Plot of k_{ex} against [DO⁻] for the H/D-exchange reaction of imidazolium ion (209) in D$_2$O at 25 ºC and I = 1.0 (KCl)
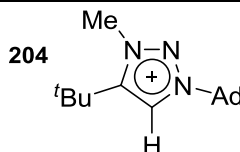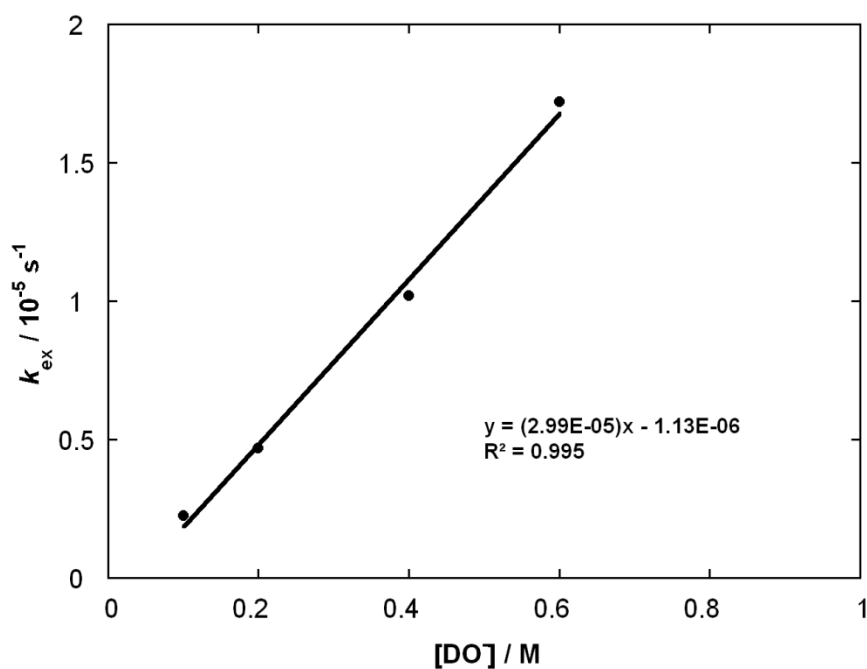

Figure 3.18: Plot of k_{ex} against [DO⁻] for the H/D-exchange reaction of imidazolium ion (210) in D$_2$O at 25 ºC and I = 1.0 (KCl)
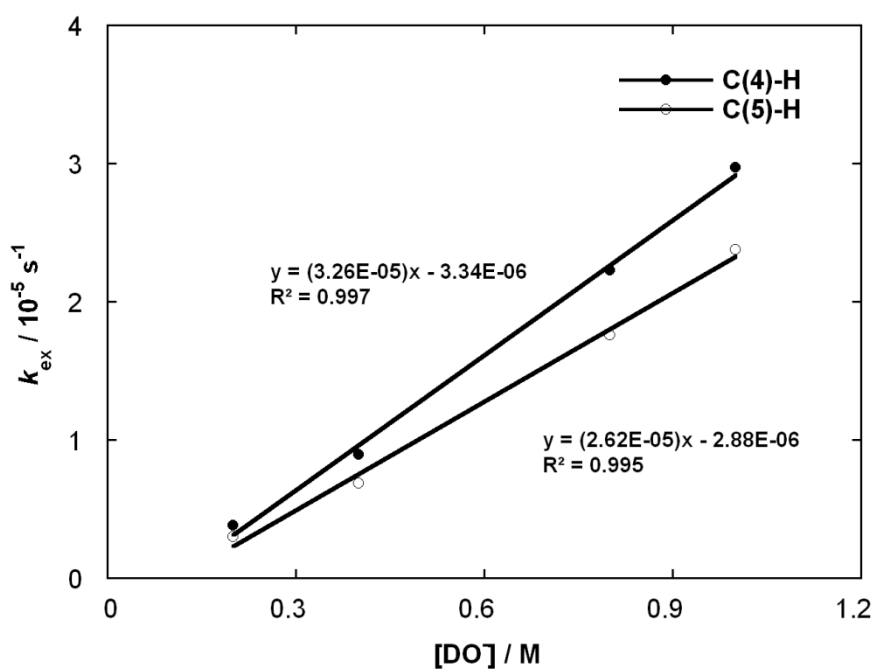
The observation of a significant negative intercept in plots of k_{ex} against deuteroxide ion concentration is inconsistent with a first-order dependence on deuteroxide ion, and the implication of this negative intercept will be discussed further in Section 3.3. Collett and Smith (whom we are collaborating with on this project) have also observed large negative intercepts in their C(4/5)-H exchange studies of similar 'abnormal' C(2)-alkylated imidazolium ions in solutions of KOD.[26]

The concentrations of deuteroxide ion reported for the reactions performed in solutions of KOD were obtained by titration against standard solutions of HCl. To establish whether the large negative intercept resulted from experimental errors in calculating the concentration of deuteroxide ion, the p*D*s of the reaction solutions containing internal standard and substrate were checked using a p*H* meter. The p*D*s of these solutions were found to be within ±0.03 of the predicted p*D*, although at these high p*D*s, small changes in p*D* correspond to large changes in deuteroxide ion concentration. We therefore believe it is unlikely that this negative intercept results from a systematic error in the measurement of [DO⁻], and we must consider a mechanistic explanation.

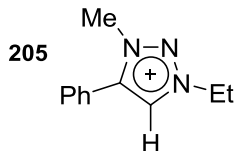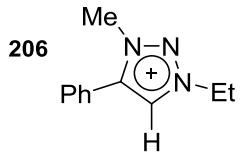Equation 3.3 describes a mechanistic scenario where the experimentally observed first-order rate constant for exchange, k_{ex} (s^{-1}), corresponds to the sum of the second-order rate constant for deuteroxide ion-catalysed exchange, k^2_{DO} (M^{-1} s^{-1}), and a third-order term, k^3_{DO} (M^{-2} s^{-1}), corresponding to an additional deuteroxide ion-catalysed pathway.

$$k_{\text{ex}} = k^2_{\text{DO}}[\text{DO}^-] + k^3_{\text{DO}}[\text{DO}^-]^2 \qquad \textbf{Equation 3.3}$$

$$k_{\text{ex}}/[\text{DO}^-] = k^2_{\text{DO}} + k^3_{\text{DO}}[\text{DO}^-] \qquad \textbf{Equation 3.4}$$

Values of k^2_{DO} (M^{-1} s^{-1}) may be obtained as the y-intercept of a plot of ($k_{\text{ex}}/[\text{DO}^-]$) against deuteroxide ion concentration, whilst values of k^3_{DO} may be obtained as the slope of this plot (Equation 3.4). Plots of ($k_{\text{ex}}/[\text{DO}^-]$) against deuteroxide ion concentration are shown for imidazolium salts **208 – 210** in Figures 3.19 – 3.21. Corresponding values of k^2_{DO} and k^3_{DO} are summarised in Table 3.7, alongside the values of k_{DO} obtained from the slopes of plots of k_{ex} against deuteroxide ion concentration (Figures 3.16 – 3.18). This data will be discussed further in Section 3.3.

Figure 3.19: Plot of (k_{ex}/[DO$^-$]) against [DO$^-$] for the H/D-exchange reaction of triazolium ion (208) in D$_2$O at 25 °C and I = 1.0 (KCl)
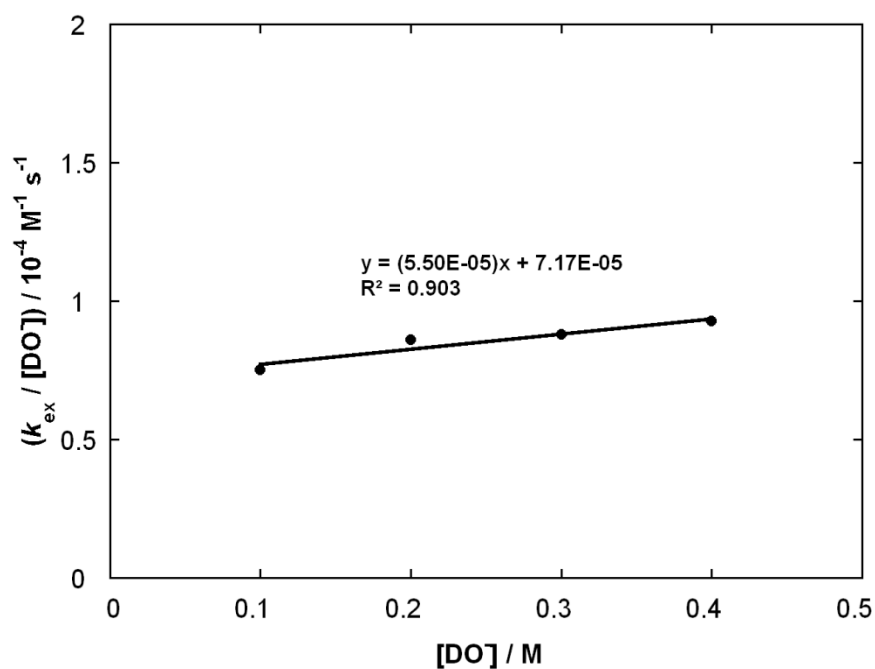
Figure 3.20: Plot of (k_{ex}/[DO$^-$]) against [DO$^-$] for the H/D-exchange reaction of triazolium ion (209) in D$_2$O at 25 °C and I = 1.0 (KCl)
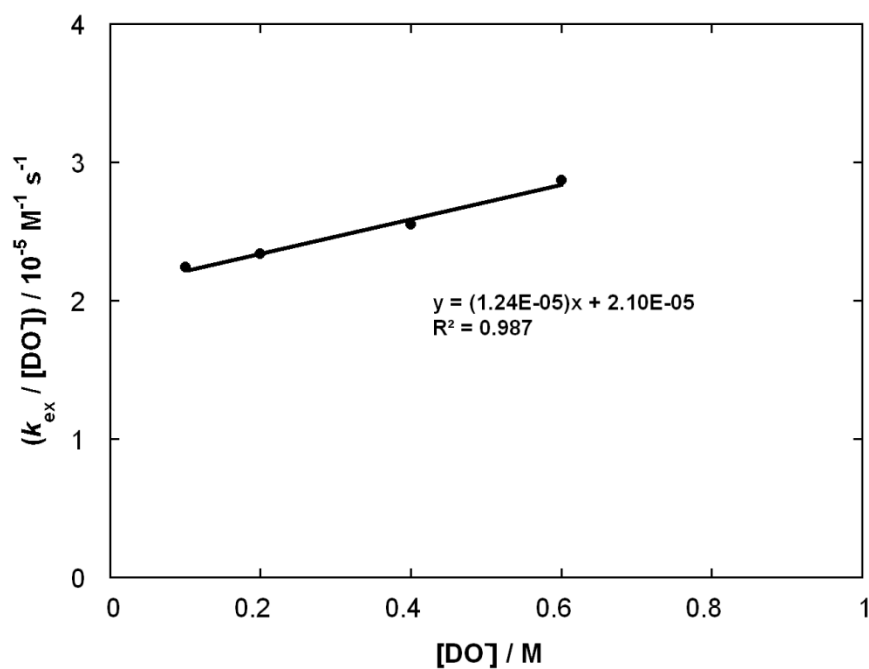
Figure 3.21: Plot of k_{ex} against [DO$^-$] for the H/D-exchange reaction of triazolium ion (210) in D$_2$O at 25 °C and I = 1.0 (KCl)
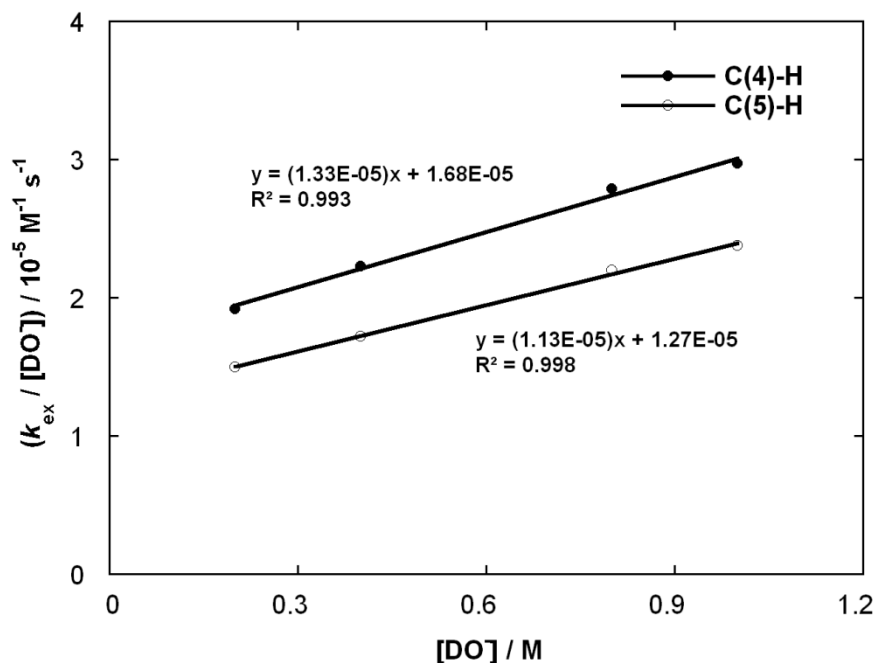
Table 3.7: Rate constants for deuteroxide ion-catalysed exchange (k_{DO}, M^{-1} s^{-1}) of the C(4/5)-H of imidazolium salts (208) – (210) for deuterium in D$_2$O at 25 °C and I = 1.0 (KCl)

substrate		k^2_{DO}, M^{-1} s^{-1}	k^3_{DO}, M^{-2} s^{-1}
208	C(4/5)-H	7.17×10^{-5} [a] (9.80×10^{-5}) [c]	5.50×10^{-5} [b]
209	C(4/5)-H	2.10×10^{-5} [a] (2.99×10^{-5}) [c]	1.24×10^{-5} [b]
210	C(4)-H	1.68×10^{-5} [a] (3.26×10^{-5}) [c]	1.33×10^{-5} [b]
	C(5)-H	1.27×10^{-5} [a] (2.62×10^{-5}) [c]	1.13×10^{-5} [b]

(a) Obtained from the y-intercept of a plot of (k_{ex}/[DO$^-$]) against [DO$^-$] (Figures 3.19 – 3.21)
(b) Obtained from the slope of a plot of (k_{ex}/[DO$^-$]) against [DO$^-$] (Figures 3.19 – 3.21)
(c) Obtained from the slope of a plot of k_{ex} against [DO$^-$] (Figures 3.16 – 3.18).

3.3   Discussion

3.3.1   Mechanism for deuterium exchange of 1,2,3-triazolium ions and estimation of carbon acid pK$_a$ values

The H/D-exchange reactions of 1,2,3-triazolium salts **204 – 207** were followed by ^{1}H NMR spectroscopy (400 MHz) in solutions of D$_2$O at 25 °C and I = 1.0 (KCl), as described in Section 3.2. The proposed mechanism for deuteroxide ion-catalysed exchange of the C(5)-H of generic 1,2,3-imidazolium ion **211** for deuterium is shown in Scheme 3.6.

Scheme 3.6:
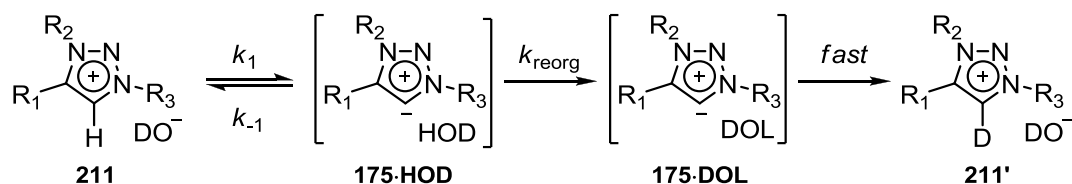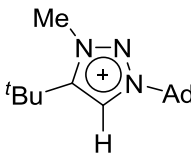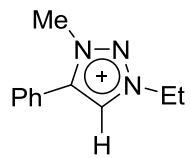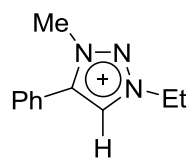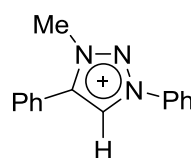
Deprotonation of 1,2,3-triazolium species **211** by deuteroxide ion yields an intimately bound complex of ylide **175** and a molecule of HOD (k_1). This step is reversible, and transfer of the proton back to the ylide may regenerate the triazolium ion (k_{-1}). Alternatively, solvent reorganisation will result in complex **175·DOL**, where the DOL molecule is positioned to deliver a deuteron to the C(5) position (k_{reorg}). Deuteration to form the exchanged product **211'** is essentially irreversible: under these conditions, bulk solvent D$_2$O is present in vast excess of substrate (5 mM).

Buffer catalysis experiments are presented in Section 3.2 for representative 1,2,3-triazolium salt **207**. The results of these experiments indicate that general base catalysis of exchange is not significant for this species. The term ([B]/[DO$^-$]) corrects for the changes in pD that occur upon dilution at constant ionic strength. Values of k_{rel} remain constant within experimental error (6%) and do not significantly deviate from unity across a 4-fold range of buffer base concentrations. As there is no mechanism by which the solvent reorganisation step may be catalysed by a Brønsted base, the observation of buffer catalysis of exchange would imply that the deprotonation step is rate-determining for deuteroxide ion-catalysed exchange. Thus, the absence of general base catalysis strongly indicates that deprotonation by deuteroxide ion is not rate-determining overall, and solvent reorganisation must be the rate-determining step in

Scheme 3.6. To further support this conclusion, we refer to the earlier H/D-exchange studies of Washabaugh and Jencks described earlier. For thiazolium ion **157**, Jencks observed significant internal return of the transferred hydron to the thiazolylidene ($k_{-1}/k_{\text{reorg}} \approx 3.3$), showing that solvent reorganisation is rate-determining for H/D-exchange of the thiazolium species. Values of the second-order rate constant for deuteroxide ion-catalysed exchange of the C(5)-H for deuterium, k_{DO} (M^{-1} s^{-1}), for 1,2,3-triazolium salts **204 – 207** are at least 2×10^3-fold smaller than the value of $k_{\text{DO}} = 4.27 \times 10^5$ M^{-1} s^{-1} reported for thiazolium **157**. Therefore, exchange of these 1,2,3-triazolium ions should be even more limited by the solvent reorganisation step.

In parallel with the treatment described for the 1,2,4-triazolium salts in Chapter 2, second-order rate constants for deuteroxide ion-catalysed exchange, k_{DO}, may be used to obtain rate constants for deprotonation by hydroxide ion, k_{HO}, using the secondary solvent isotope relationship $k_{\text{DO}}/k_{\text{HO}} = 2.4$, where deprotonation occurs as a pre-equilibrium. Previously, we showed that if solvent reorganisation is rate-limiting for H/D-exchange, by the Principle of Microscopic Reversibility this step must also be rate-determining for protonation of the free carbene. Solvent reorganisation is estimated to occur with a first-order rate constant $k_{\text{HOH}} = 10^{11}$ s^{-1}, corresponding to the dielectric relaxation of water. By combining the values of k_{HO} and k_{HOH} in Equation 2.8, carbon acid pK_a values may be estimated, and these results are summarised in Table 3.8. These results will be discussed in the final part of the discussion.

Table 3.8: **Kinetic acidities towards lyoxide ion and evaluated pK$_a$s of the C(5)-H of triazolium salts (204) – (207) in water at 25 °C and I = 1.0 (KCl)**

	substrate		k_{DO}, M^{-1} s^{-1} [a]	k_{HO}, M^{-1} s^{-1}	pK$_a$
204		Cl$^-$	4.61×10^{-2}	1.92×10^{-2}	**26.7**
205		I$^-$	1.25×10^{1}	5.21×10^{0}	**24.3**
206		PF$_6^-$	1.23×10^{1}	5.13×10^{0}	**24.3**
207		Cl$^-$	2.10×10^{2}	8.75×10^{1}	**23.1**

(a) The value of the second-order rate constant for deuteroxide ion-catalysed exchange (k_{DO}, M^{-1} s^{-1}) was determined from the slope of a plot of k_{ex} against [DO$^-$] in Figures 3.10 – 3.13.

3.3.2   Possible mechanisms for deuterium exchange of imidazolium ions

The H/D-exchange reactions of imidazolium salts **208** – **210** were followed by ^{1}H NMR spectroscopy (400 MHz) in solutions of D$_2$O at 25 °C and I = 1.0 (KCl), as described in Section 3.2. Unlike any of the other H/D-exchange studies of azolium ions presented in this thesis, plots of k_{ex} against [DO$^-$] resulted in significant negative y-intercepts that were inconsistent with a first-order dependence on deuteroxide ion. This unusual behaviour was also observed by Collett and Smith for exchange at the C(4/5)-H position for a similar set of 'abnormal' C(2)-alkylated imidazolium ions.[26a] In earlier work our group have followed exchange at the C(4/5)-H position of a 'classical' imidazolium salt **67** in solutions of KOD, and a significant negative intercept was observed in this case, upon revisiting the data (Figure 3.22).[26b]

Upon examination of all data obtained previously by our laboratory for exchange reactions of a range of azolium ions at pDs 0 – 12, these negative intercepts are only significant for exchange reactions performed in concentrated deuteroxide solution.

Figure 3.22:   Plot of k_{ex} against [DO$^-$] for the H/D-exchange reaction at the C(4/5)-H position of imidazolium ion (67) in D$_2$O at 25 ºC and I = 1.0 (KCl)
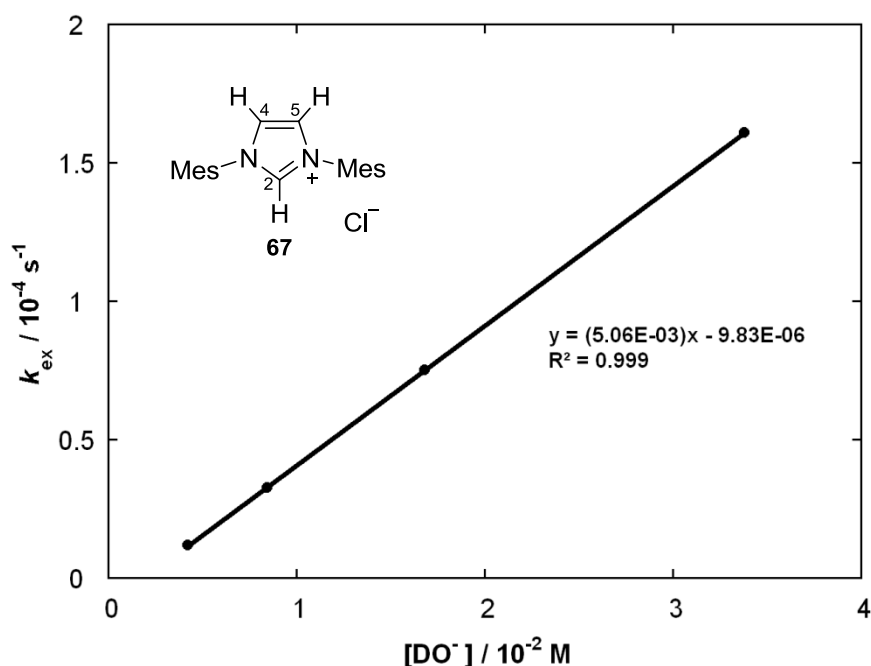
Non-mechanistic explanations were initially considered. To avoid errors associated with the measurement of pD in solutions of KOD, the concentrations of deuteroxide ion in these experiments were obtained by titration against standard solutions of HCl.

Given the high concentrations of deuteroxide ion used in these experiments, variations in viscosity should also be considered. According to the Stokes-Einstein relationship (Equation 3.5), reaction rate constants are inversely proportional to solution viscosity (η). Stanley and co-workers have reported aqueous viscosities as a function of sodium hydroxide concentration at constant ionic strength I = 3.0 (KCl), and found that viscosity increases with mol% NaOH.[27] Solution viscosity cannot explain the apparent upward deviation from the linear fit of the data to Equation 3.2, as the more viscous solutions would be expected to result in slower rates of exchange.

$$k_{rxn} \propto \frac{1}{\eta} \qquad\qquad \textbf{Equation 3.5}$$

We therefore believe that this behaviour results from possible additional contributions to exchange at high DO$^-$ concentrations. This data was fitted to third-order plots of (k_{ex}/[DO$^-$]) against deuteroxide ion concentration (Figures 3.19 – 3.21). The reasonable fit of this data to these plots is consistent with a second-order dependence on

deuteroxide ion. Scheme 3.7 describes several alternative pathways that may result in deuterium exchange at the C(4/5)-H position of representative imidazolium ion **209** in strong KOD solutions.

Scheme 3.7:
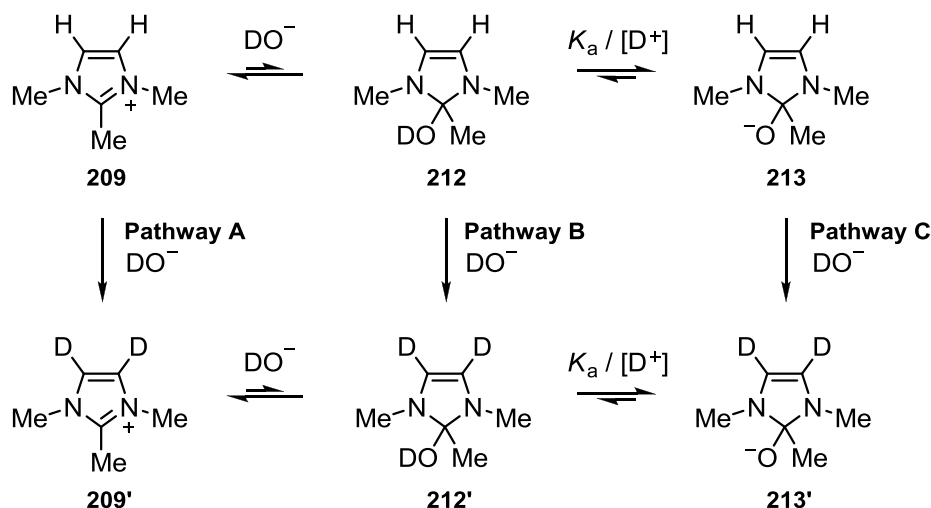
Pathway A describes H/D-exchange *via* the conventional mechanism, described earlier in Scheme 3.6 for the 1,2,3-triazolium ions in Section 3.3.1. As the kinetics of exchange for these imidazolium ions do not appear to follow a first-order dependence on deuteroxide ion at higher concentrations, additional pathways must be considered.

Pathways B and C consider the possibility of exchange *via* a hydrate (**212**). Our laboratory have extensively studied H/D-exchange for a range of imidazolium and 4,5-dihydroimidazolium ions in phosphate and quinuclidinone buffers up to p*D* ~9. In all cases, a single set of peaks were observed (which we have attributed to the azolium ion). Only for 6-membered membered imidazolinium salts **214** and **217**, were signals due to hydrolysis products observed at any point during the reaction.[28] For these species, a decrease in the initial C(2)-H singlet was accompanied by one or more decomposition products in the ^{1}H NMR spectra over time (Scheme 3.8, L = H/D). In the case of **214**, two new sets of signals appeared at a fixed ratio over the course of the reaction, which were attributed to the simultaneous formation of hydrate **215** and hydrolysis product **216** in equilibrium. For **217**, the appearance of only one new set of signals was rationalised by an equilibrium which strongly favoured **219**. This interpretation will subsequently be revised following consideration of the data obtained in these investigations.

Scheme 3.8:

not detected
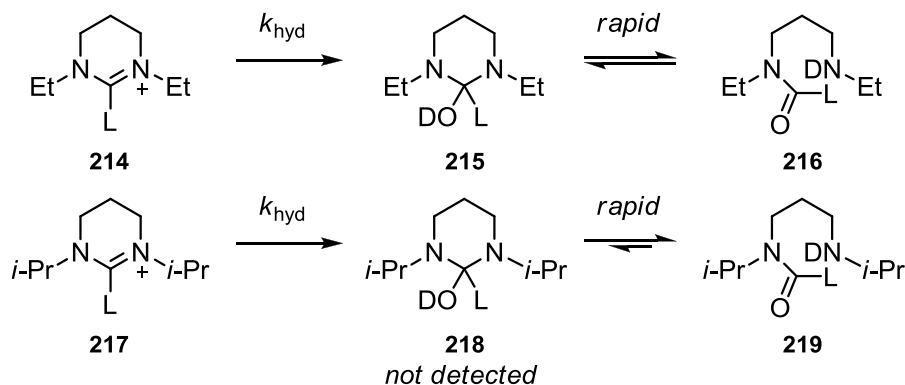
In the present studies, a single set of signals were observed in the ^{1}H NMR spectra of **208 – 210** throughout the reaction. Only the signal at ~7.4 ppm decays to zero, consistent with H/D-exchange at the C(4)-H and C(5)-H positions. With respect to possible hydrate formation, this observation implies one of three scenarios: (i) imidazolium-hydrate interconversion is slow on the NMR time scale (*i.e.* a lifetime >0.2 s)[29] and largely favours hydrate **212**; (ii) imidazolium-hydrate interconversion is slow on the NMR time scale and largely favours imidazolium ion **209**; or (iii) imidazolium-hydrate interconversion is fast on the NMR time scale and an averaged set of unresolved signals are observed.

Hydration of propanal, iso-butyraldehyde and pivaldehyde by hydroxide ion occur with second-order rate constants of 2.35×10^3, 1.77×10^3 and 6.33×10^3 M^{-1} s^{-1} at °0 C (these rate constants would be expected to be ~10-fold higher at 25 °C).[30] For these aldehydes, distinct signals for hydrate and free aldehyde were observed in concentrated hydroxide solutions at 0 °C. Corresponding rate constants for our imidazolium species would be expected to fall well below the values for the relatively electrophilic aldehydes discussed above. It is therefore unlikely that scenario (iii) is viable, and any hydrate formation should be slow on the NMR time scale. It follows that separate signals for hydrate and azolium ion should be observed in the ^{1}H NMR spectrum, particularly upon a decrease in deuteroxide ion concentration.

For aldehydes, singlet signals corresponding to the aldehydic proton typically appear at 9 – 10 ppm in the ^{1}H NMR spectrum, and those of the hydrate proton appear at approximately 5 – 6 ppm. For our substrates, and for all other imidazolium salts studied previously by our group at a wide range of pDs, only a single set of signals is observed throughout the reaction. The imidazolium ions described in this investigation are

alkylated at the C(2) position, however, the observation of a singlet at approximately 9 – 10 ppm for the other 'classical' imidazolium ions studied by our laboratory is consistent with an azolium ion C(2)-H rather than a hydrate.

Likewise, for the triazolium ions described in the previous chapter, only one singlet was observed at around 10 ppm in the ^{1}H NMR spectra, consistent with the non-hydrate assignment. Considering scenario (i), where this signal is due to hydrate and has been mis-interpreted as triazolium ion (*i.e.* hydrate is present in >99%), it is possible to calculate a 'true' rate constant for deuteroxide ion-catalysed exchange from the relationship described by Equation 3.6, where f_{az} is the fraction of azolium ion. For the triazolium ions **137** – **143**, observed rate constants for deuteroxide ion-catalysed exchange of triazolium ions are in the order of $\sim 10^8$ M^{-1} s^{-1}. Assuming that the fraction of azolium ion is no greater than 0.1 – 1%, 'true' values for k_{DO} would be on the order of 10^{10} – 10^{11} M^{-1} s^{-1}. Rate constants for exchange on this magnitude are unrealistic, and strongly suggest that consumption of the azolium ion *via* hydrate formation is not occurring in the case of 1,2,4-triazolium ions, and the signal under investigation is due to the azolium ion C(3)-H. Thus, the most likely scenario to explain the imidazolium data is that the level of hydration is small and undetectable by NMR (*i.e.* scenario (ii)).

$$k_{DO}^{obs} = f_{az} \times k_{DO}^{true}$$
<div align="right">**Equation 3.6**</div>

To accommodate these new observations, the original hydrolysis pathways of 6-membered imidazolium salts **214** and **217** have been re-evaluated. We now propose that the appearance of additional peaks in the ^{1}H NMR spectra of **214** and **217** are consistent with the formation of the final hydrolysis product only (**216** and **219**), and *not* hydrates **215** or **218**. The appearance of two peaks in the case of **214** may be due to two rotational isomers of **216**, due to the partial double-bond character of the amide bond. The bulky isopropyl substituents may prevent rotation about this bond, resulting in one isomer only. To confirm this hypothesis, it will be necessary to prepare structure **216** and obtain NMR spectra in a non-aqueous solvent, which would allow the observation of rotational isomers but prevent hydrate equilibration.

Following hydrate formation, Pathway B involves deprotonation of the hydrate **212** by deuteroxide ion to generate the exchange product **212'**. In order for exchange *via* Pathway B to significantly affect the overall rate (given that the imidazolium-hydrate

equilibrium lies largely towards imidazolium ion) C(4/5)-H deprotonation of the hydrate **212** must occur faster than C(4/5)-H deprotonation of the azolium ion. Hydrate **212** is non-aromatic, and would be predicted to be less acidic, although the electron-withdrawing deuteroxide group would off-set some of this difference. Higher deuteroxide ion concentrations would increase the rate of hydrate formation and amount of hydrate present in equilibrium, promoting exchange. Pathway B would result in a second-order dependence on deuteroxide ion, and may account for the higher order dependence indicated by Figures 3.19 – 3.21.

To fully assess the contribution to the observed rate of exchange from Pathway B (*i.e.* exchange of **212** to give di-deuterated **212'**), it may be necessary to prepare a structurally similar compound such as **220** or **221**. As mentioned in Chapter 1, triazole and 4,5-dihydoimidazole analogues of **220** have been prepared by Enders and Grubbs from the parent azolium ion and corresponding alcohol (R = Me, Et, *t*-Bu) under basic conditions.[31] Markovnik has reported the synthesis of benzimidazole **222** from *N,N*-dimethyl-1,2-diaminobenzene and propanone under acidic conditions.[32] The absence of a hydroxyl group at the C(2) position would prevent equilibration with the azolium ion, allowing a rate constant for exchange, if observable, to be obtained.

220   **221**   **222**   **223**

pK_a = 14.8
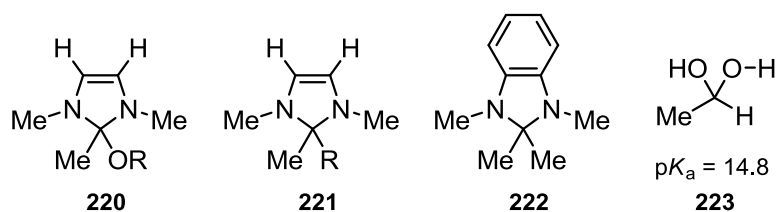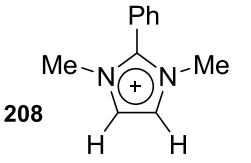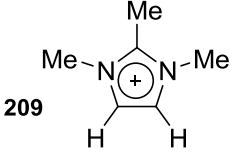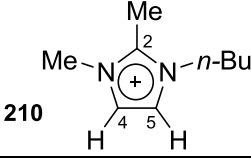
Alternatively, deprotonation of the hydrate at the C(2)-OH position by deuteroxide ion may occur (Pathway C). Hydroxyl pK_a values for hydrates such as **223** have been reported in the range 12 – 15,[33] and under the highly basic conditions used for the exchange measurements, an appreciable amount of the deprotonated species would be likely to form. Deprotonation of species **213** at the C(4/5)-H positions by deuteroxide ion and subsequent deuteration by solvent would result in exchange product **213'**.

From the third-order plots of (k_{ex}/[DO$^-$]) against deuteroxide ion concentration shown in Figures 3.19 – 3.21, second-order rate constants for deuteroxide ion-catalysed exchange (k^2_{DO}) have been determined from the y-intercept. Corresponding rate constants for deprotonation by hydroxide ion (k^2_{HO}) were obtained using the secondary

solvent isotope effect $k_{DO}/k_{HO} = 2.4$, and these values were used to estimate pK_as. These rate constants and pK_as are summarised in Table 3.9. The second-order rate constants for deuteroxide ion-catalysed exchange, k_{DO} (M^{-1} s^{-1}), obtained from the slopes of plots of k_{ex} against time and corresponding pK_a values are also shown alongside in brackets. The values obtained from the two methods are in close agreement, suggesting that the contribution from Pathways B or C is relatively small.

Table 3.9: **Kinetic acidities towards lyoxide ion and evaluated pK_as of the C(4/5)-H of imidazolium salts (208) – (210) in water at 25 °C and *I* = 1.0 (KCl)**

substrate		k^2_{DO}, M^{-1} s^{-1} (k_{DO}, M^{-1} s^{-1})	k^2_{HO}, M^{-1} s^{-1} (k_{HO}, M^{-1} s^{-1})	pK_a
208	C(4/5)-H	$7.17 \times 10^{-5\ a}$ (9.80×10^{-5}) ^{b}	2.99×10^{-5} (4.08×10^{-5})	**29.5** **(29.4)**
209	C(4/5)-H	$2.10 \times 10^{-5\ a}$ (2.99×10^{-5}) ^{b}	8.75×10^{-6} (1.25×10^{-5})	**30.1** **(29.9)**
210	C(4)-H	$1.68 \times 10^{-5\ a}$ (3.26×10^{-5}) ^{b}	7.00×10^{-6} (1.36×10^{-5})	**30.2** **(29.9)**
	C(5)-H	$1.27 \times 10^{-5\ a}$ (2.62×10^{-5}) ^{b}	5.29×10^{-6} (1.09×10^{-5})	**30.3** **(30.0)**

(a) The second-order rate constant for deuteroxide ion-catalysed exchange, k^2_{DO}, was obtained from the y-intercept of a plot of $k_{ex}/[DO^-]$ against $[DO^-]$ in Figures 3.19 – 3.21. (b) The second-order rate constant for deuteroxide ion-catalysed exchange, k_{DO}, was obtained from the slope of a plot of k_{DO} against $[DO^-]$ in Figures 3.16 – 3.18.

3.3.3 Substituent effects on 1,2,3-triazolium and imidazolium ion acidities

3.3.3.1 Substituent effects on 1,2,3-triazolium ion C(5)-H kinetic acidities towards deuteroxide ion, k_{DO} (M^{-1} s^{-1}), and pK_a values
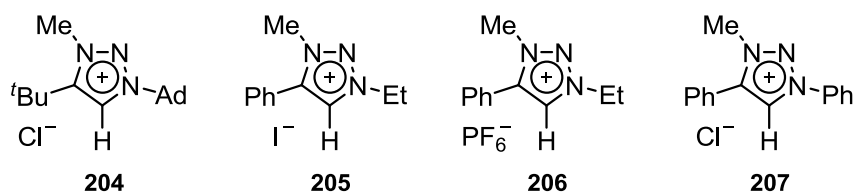
Kinetic acidities at the C(5)-H position of 1,2,3-triazolium salts **204 – 207** range from $4.61 \times 10^{-2} – 2.10 \times 10^2$ M^{-1} s^{-1}, and are at least 10^5-fold smaller than those at the C(3)-H position of 1,2,4-triazolium salts **137 – 143**. For example, the value of k_{DO} obtained for **205** is around 5×10^6 times smaller than the value of $k_{DO} = 6.8 \times 10^7$ M^{-1} s^{-1}

determined for *N*-phenyl triazolium salt **139**, which also bears alkyl and phenyl substituents adjacent to the site of deprotonation. This difference may be rationalised by considering the proximity of the electron-withdrawing nitrogen atom to the site of deprotonation. Relocation of the nitrogen atom results in a more stable cation relative to the formally neutral carbene/ylide, resulting in a less acidic triazolium species.

Within the series shown in Table 3.8, triazolium ions bearing aryl substituents at the C(4) position are at least 270-fold more reactive towards deuteroxide ion and 2.4 pK_a units more acidic than related alkyl substituted species (*cf.* **204** and **205**). Furthermore, replacement of an ethyl substituent with a phenyl substituent at the N(1) position results in an additional 17-fold increase in k_{DO} and 1.2 unit decrease in pK_a (*cf.* **205** and **207**). These changes mirror the decrease of at least 1.9 pK_a units observed upon moving from *N,N*-dialkyl to *N,N*-diaryl substituted imidazolium salts, reported previously by our group, and are in contrast to the apparent increase in proton affinity mentioned in the introduction to this chapter. Proton affinities are, however, measures of gas-phase stability, and aqueous solvent effects often play a significant role in carbocation stabilisation.

3.3.3.2 Counterion effects on 1,2,3-triazolium ion C(5)-H kinetic acidities towards deuteroxide ion, k_{DO} (M^{-1} s^{-1}), and pK_a values

The effect of counterion on triazolium ion acidity is essentially negligible, as shown by the near identical values of k_{DO} obtained for salts **205** and **206**. The small increase in k_{DO} upon moving from a phosphorus hexafluoride to an iodide counterion may be rationalised in terms of the potential for increased hydrogen bonding between the iodide anion and the C(5)-H, although the observed difference (2%) falls within experimental error (6%). Our laboratory reported a similarly small difference in k_{DO} between the chloride and tetrafluoroborate salts of the *N*-phenyl substituted 1,2,4-triazolium ion (salts **95** and **139** respectively).

3.3.3.3 Substituent effects on imidazolium ion C(4/5)-H kinetic acidities towards deuteroxide ion, k_{DO} (M^{-1} s^{-1})
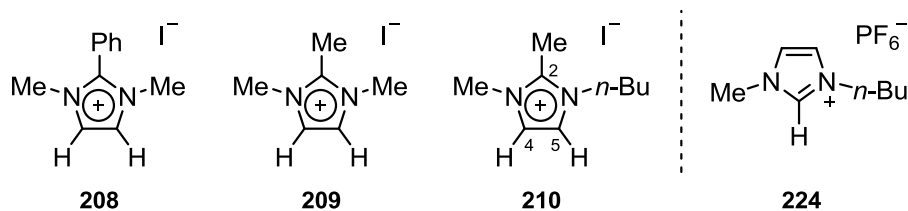
Kinetic acidities at the C(4)-H and C(5)-H positions of imidazolium ions **208** – **210** range from 1.27×10^{-5} – 7.17×10^{-5} M^{-1} s^{-1}, and are substantially less reactive towards deprotonation by deuteroxide ion than at the C(2)-H position. For example, the values of k^2_{DO} obtained for deprotonation at the C(4)-H and C(5)-H positions for *N*-butyl imidazolium salt **210** are around 6×10^6-fold smaller than the value of $k_{DO} = 1.1 \times 10^2$ M^{-1} s^{-1} reported by our laboratory for deprotonation at the C(2)-H position of imidazolium **224**. This difference is largely due to the cation-stabilising effect of moving the electron-withdrawing nitrogen away from the site of deprotonation.

Varying the *N*-alkyl substituent results in a much smaller effect, characterised by the 1.7-fold difference in k_{DO} between *N*-methyl and *N*-butyl substituted species **209** and **210**. This observation is consistent with an earlier study of *N*-methyl *N*-alkyl imidazolium salts carried out by our group, which revealed that changes in alkyl chain length resulted in no more than a 2-fold difference in kinetic acidity.[24]

More interestingly, for asymmetric imidazolium ion **210**, the C(4)-H and C(5)-H positions experience different rates of deprotonation. ¹H-NOESY, ¹H,¹³C-HSQC and ¹H,¹³C-HMBC NMR experiments confirm that the more downfield signal corresponds to the C(5)-H position, proximal to the more electron rich *n*-butyl substituent. Deprotonation at the C(4)-H position is around 18% faster than at the C(5)-H position, consistent with earlier observations that more electron deficient azolium ions are more acidic. This difference may in part be due to the increase steric bulk of the butyl chain.

3.4 Summary

The kinetic acidities of the conjugate acids of four mesoionic triazolylidenes and three mesoionic imidazolylidenes were measured in a series of H/D-exchange experiments at 25 °C and $I = 1.0$ (KCl). Using ^{1}H NMR spectroscopy, pseudo-first-order rate constants for deuteroxide ion-catalysed exchange of the C(4)-H and C(5)-H of 1,2,3-triazolium and imidazolium salts for deuterium, k_{ex} (s^{-1}), were obtained.

For the 1,2,3-triazolium salts, second-order rate constants for deuteroxide ion-catalysed exchange, k_{DO} (M^{-1} s^{-1}), were determined from slopes of second-order plots of k_{ex} against deuteroxide ion concentration. To our surprise, similar plots of the imidazolium exchange data (performed in 0.1 – 1.0 M KOD solutions) returned significant negative intercepts that suggested the presence of an additional higher order exchange reaction at these high p*D*s. Second-order rate constants were instead obtained from the y-intercepts of third-order plots of (k_{ex}/[DO$^-$]) against deuteroxide ion concentration. To account for this behaviour, two competing pathways that stem from the formation of a small, undetectable, level of hydrate have been considered. Further work is necessary to determine rate constants for exchange of analogues of the hydrate species. For both azolium ion families, values of k_{DO} were converted into second-order rate constants for deprotonation by hydroxide ion, k_{HO} (M^{-1} s^{-1}), using a secondary solvent isotope relationship ($k_{DO}/k_{HO} = 2.4$). These rate constants were combined with the first-order rate constant for carbene protonation ($k_p = k_{reorg} = 10^{11}$ s^{-1}) to obtain estimates of p*K*$_a$.

In both cases, rate constants for deprotonation at the 'abnormal' C(4)-H or C(5)-H position were around 10^5-fold smaller that at the 'classical' C(3)-H or C(2)-H positions. This difference may be rationalised by the relocation of the electron-withdrawing nitrogen atom away from the site adjacent to that of deprotonation, which stabilises the positively charged azolium ion relative to the neutral carbene/ylide. The values of k_{DO} obtained for exchange at the C(4/5)-H positions of imidazolium ions **208 – 210** are amongst the least acidic of all azolium ion acidity measurements studied to date.

Replacement of alkyl for aryl substituents results in an increase in k_{DO} and decrease in p*K*$_a$. This increase in acidity is in contrast to the apparent increase in proton affinity reported by Frenking and Bertrand, although solvent effects that are not accounted for in the gas phase may be responsible for this difference. The effect of counterion on

acidity was found to be negligible, based on the essentially identical values of k_{DO} and pK_a obtained for a common triazolium ion.

References

1   S. Gründemann, A. Kovacevic, M. Albrecht, J. W. Faller and R. H. Crabtree, *Chem. Commun.*, 2001, 2274.

2   S. Araki, Y. Wanibe, F. Uno, A. Morikawa, K. Yamamoto, K. Chiba and Y. Butsugan, *Chem. Ber.*, 1993, **12**, 1149.

3   O. Schuster, L. Yang, H. G. Raubenheimer and M. Albrecht, *Chem. Rev.*, 2009, **109**, 3445.

4   A. M. Magill and B. F. Yates, *Aust. J. Chem.*, 2004, **57**, 1205.

5   L. N. Appelhans, D. Zuccaccia, A. Kovacevic, A. R. Chianese, J. R. Miecznikowski, A. Macchioni, E. Clot, O. Eisenstein and R. H. Crabtree, *J. Am. Chem. Soc.*, 2005, **127**, 16299.

6   A. Kovacevic, S. Gründemann, J. R. Miecznikowski, E. Clot, O. Eisenstein and R. H. Crabtree, *Chem. Commun.*, 2002, 2580.

7   M. Baya, B. Eguillor, M. A. Esteruelas, M. Oliván and E. Oñate, *Organometallics*, 2007, **26**, 6556.

8   B. Eguillor, M. A. Esteruelas, M. Oliván and M. Puerta, *Organometallics*, 2008, **27**, 445.

9   P. Mathew, A. Neels and M. Albrecht, *J. Am. Chem. Soc.*, 2008, **130**, 13534.

10   M. Iglesias and M. Albrecht, *Dalton Trans.*, 2010, **39**, 5213.

11   Y. Han and H. V. Huynh, *Dalton Trans.*, 2011, **40**, 2141.

12   E. Aldeco-Perez, A. J. Rosenthal, B. Donnadieu, P. Parameswaran, G. Frenking and G. Bertrand, *Science*, 2009, **326**, 556.

13   (a) O. Schuster, L. Yang, H. G. Raubenheimer and M. Albrecht, *Chem. Rev.*, 2009, **109**, 3445; (b) P. L. Arnold and S. Pearson, *Coordination Chem. Rev.*, 2007, **251**, 956.

14   T. K. Sen, S. C. Sau, A. Mukherjee, A. Modak, S. K. Mandal and D. Koley, *Chem. Commun.*, 2011, **47**,11972.

15   (a) E. F. Connor, G. W. Nyce, M. Myers, A. Mock and J. L. Hedrick, *J. Am. Chem. Soc.*, 2002, **124**, 914; (b) M. K. Kiesewetter, E. J. Shin, J. L. Hedrick and R. M. Waymouth, *Macromolecules*, 2010, **43**, 2093.

16   C. A. Tolman, *Chem. Rev.*, 1977, **77**, 313.

17   A. R. Chianese, A. Kovacevic, B. M. Zeglis, J. W. Faller and R. H. Crabtree, *Organometallics*, 2004, **23**, 2461.

18   A. R. Chianese, X. W. Li, M. C. Janzen, J. W. Faller and R. H. Crabtree, Organometallics, 2003, **22**, 1663.

19   H. V. Huynh, Y. Han, R. Jothibasu and J. A. Yang, *Organometallics*, 2009, **28**, 5395.

20   M. Iglesias and M. Albrecht, *Dalton. Trans.*, 2010, **39**, 5213.

21   D. Gusev, *Organometallics*, 2009, **28**, 6458.

22   T. L. Amyes, S. T. Diver, J. P. Richard, F. M. Rivas and K. Toth, *J. Am. Chem. Soc.*, 2004, **126**, 4366.

23   R. Tonner, G. Heydenrych and G. Frenking, *ChemPhysChem*, 2008, **9**, 1474.

24   E. M. Higgins, J. A. Sherwood, A. G. Lindsay, J. Armstrong, R. S. Massey, R. W. Alder and A. C. O'Donoghue, *Chem. Commun.*, 2011, **47**, 1559.

25   J. Bouffard, B. K. Keitz, R. Tonner, G. Guisado-Barrios, G. Frenking, R. H. Grubbs and G. Bertrand, *Organometallics*, 2011, **30**, 2617.

26   (a) C. J. Collett and A. D. Smith have observed negative y-intercepts of a similar magnitude in plots of k_{ex} against [DO$^-$] for other 'abnormal' imidazolium ions in solutions of KOD. (b) J. Sherwood, A. C. O'Donoghue, M.Sc. Thesis, 2007, Durham University.

27   G. Hefter, P. M. May, P. Sipos and A. Stanley, *J. Mol. Liquids*, 2003, **103**, 261.

28   Supporting information, ref. 23; J. A. Sherwood, A. C. O'Donoghue, Ph.D. Thesis, University College Dublin, Dublin, 2004.

29   Interconversion once every 0.25 s, assuming 0.1 ppm (*i.e.* 4 Hz) separation for distinguishable signals on a 400 MHz instrument at 25 °C.

30   (a) Y. Pocker and D. G. Dickerson, *J. Phys. Chem.*, 1969, **73**, 4005; (b) G. Daw, A. Regan, I. F. Watt and E. Wood, *in communication*.

31   (a) D. Enders, K. Breuer, G. Raabe, J. Runsink, J. H. Teles, J-P. Melder, K. Ebel and S. Brode, *Angew. Chem. Int. Ed. Engl.*, 1995, **34**, 1021; (b) M. Scholl, S. Ding, C. W. Lee and R. H. Grubbs, *Org. Lett.*, 1999, **1**, 953.

32   A. S. Markovnik, *Zhurnal Obschei Khimi*, 1989, **59**, 446.

33    $pK_a(CH_2OCH_2(O\text{-}H)) = 14.8$.

CHAPTER   4

Mechanistic Studies of the N-Heterocyclic Carbene-Catalysed Benzoin Condensation

4.0   Foreword

The benzoin condensation is a useful model reaction to study the kinetics of many of the NHC-catalysed reactions described in the introduction. This chapter brings together our mechanistic studies of this reaction, and is divided into six sections. Section 4.1 summarises the progress that has already been made towards understanding the NHC-catalysed benzoin and Stetter reactions and highlights a number of questions that remain unsolved. Section 4.2 describes our efforts to characterise intermediates in the benzoin condensation and study their stabilities. Section 4.3 presents our studies of the benzoin condensation in triethylamine buffered methanol-d_4, followed by ^{1}H NMR spectroscopy, to yield concentration profiles for a range of catalysts and substrates. The methods used to obtain this data and our proposed mechanism are discussed. Section 4.4 focuses on our attempts to evaluate microscopic rate constants for several of the steps highlighted in this mechanism using the data in the reaction profiles, which includes a global fitting approach. The results of these combined investigations are discussed in Section 4.5 and our conclusions are summarised in Section 4.6.

4.1   Introduction

4.1.1   Early studies: Establishing the 'Breslow mechanism'

Reports of the self-condensation of benzaldehyde date back to 1832, when Wöhler and Liebig first described the formation of benzoin from benzaldehyde in the presence of cyanide.[1] In 1903, Lapworth proposed a viable mechanism for this process, involving the formation of a carbanion **226** with inverted polarity at the carbonyl group (Scheme 4.1).[2] This reactive acyl anion equivalent can subsequently react with a second aldehyde molecule to generate the acyloin product.

Scheme 4.1:
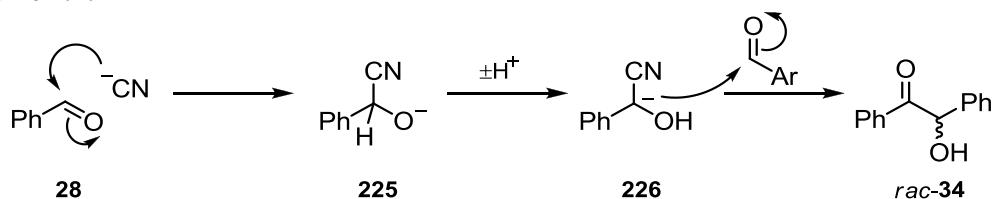
In 1943, Ugai observed that the benzoin condensation could be catalysed by naturally occurring thiazolium salt thiamine (vitamin B₁) **29** in the presence of a mild base.[3] Mizuhara later showed that the compound's catalytic reactivity was derived from the thiazolium unit.[4] However, mechanistic clarity was finally achieved in 1958, in a seminal paper by Breslow.[5] From the observation of deuterium exchange at the C(2)-H position, Breslow concluded that the thiazolium ion **31** is in reversible equilibrium with its conjugate base – the catalytically active thiazol-2-ylidene **30**. His proposed mechanism (Scheme 1.5), an adaptation of Lapworth's model of cyanide catalysis, involves nucleophilic addition of this carbene/ylide to the aldehyde to generate the 2-(hydroxybenzyl)thiazolium intermediate **32**, which upon deprotonation may form enolamine **33**, often referred to as the 'Breslow intermediate'. This species acts as a nucleophilic acylation reagent towards a second aldehyde molecule. Subsequent proton transfer steps and re-generation of the thiazol-2-ylidene yields benzoin **34**.

Whilst Breslow's model of the thiazolium ion-catalysed benzoin condensation is generally accepted as the most likely mechanism of catalysis, several alternative proposals involving the formation of bis(thiazolin-2-ylidene) dimers briefly found favour with some authors. The formation of thiazolylidene dimers (**227**) by nucleophilic attack of the carbene/ylide **30** on its parent thiazolium ion **31** is known to occur in non-aqueous solvents under basic conditions (Scheme 4.2).[6] In a number of cases these dimers have been observed to act as catalysts in the benzoin condensation.[7]

Scheme 4.2:
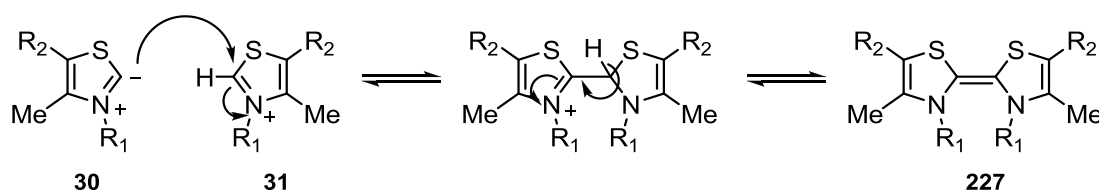
The observation of a bis(thiazolin-2-ylidene) **227**-catalysed reaction led Lopez-Calahorra *et al.* to suggest a number of controversial alternative pathways involving dimer formation as an essential first step (Scheme 4.3).[8] In Pathway A, formation of the 2-(hydroxybenzyl)thiazolium adduct or Breslow intermediate are avoided, and instead the reaction proceeds *via* the rather unlikely deprotonation of **228** to give tetrahedral anion intermediate **229**, which has no notable features for charge stabilisation. Perhaps

unsurprisingly, this unorthodox mechanism was strongly derided by Breslow,[9] who referred to several sources of data showing a first-order dependence with respect to the total concentration of thiazolium ion – ruling out Lopez-Calahorra's dimer model. Breslow and other groups[10] have since detected formation of the 2-(hydroxybenzyl)thiazolium adduct.

Scheme 4.3:
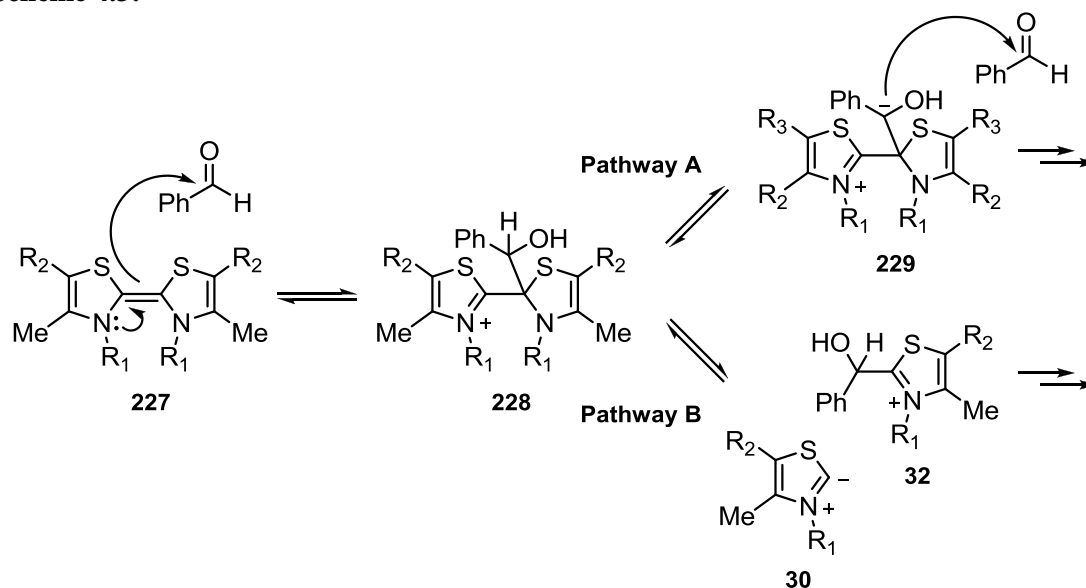
Lopez-Calahorra's alternative pathway (Pathway B), based on earlier studies by Lemal,[11] involves dissociation of **228** to form the same 2-(hydroxybenzyl)thiazolium intermediate **32** involved in Breslow's model. As the proposed mechanism would result in the formation of the 2-(hydroxybenzyl)thiazolium adduct **32** which goes on to react in a rate-determining step, the observance of first-order kinetics with respect to thiazolium ion would not unambiguously rule out the dimer pathway. However, by studying the rate of oxidation of **32** by ferricyanide from its formation from aldehyde and thiazolium ion, Breslow demonstrated that the reaction had a first-order dependence with respect to both aldehyde and thiazolium ion, convincingly ruling out a bis(thiazolin-2-ylidene) catalysed mechanism.[9a]

4.1.2   Isolation of intermediates

Experimental and computational investigations of the thiazolium-catalysed reaction support the identity of several of the intermediates proposed in Breslow's model, however, the isolation of the elusive Breslow intermediate has become a key challenge in contemporary mechanistic studies of the benzoin and Stetter reactions. Berkessel *et*

al. have prepared a ketone tautomer **231** of a triazolium-derived Breslow intermediate, formed from the direct addition of an equimolar amount of triazolylidene **16** to propionic aldehyde **230** in anhydrous solvent (Scheme 4.4).[12] The catalytically relevant benzylic species **232**, generated from benzaldehyde **28**, was also observed by ^{1}H and ^{13}C NMR. For both species however, attempts to observe the enol tautomer **233** (*i.e.* the acyl anion) directly, or prepare the analogous silyl ether **234** were unsuccessful.

Scheme 4.4:
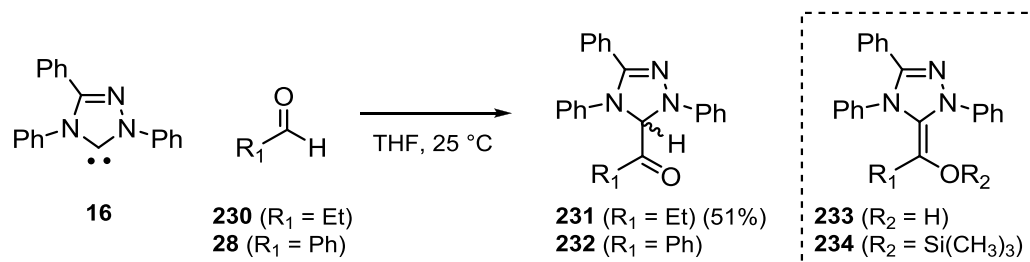
Further studies implicated a previously unreported spirocyclic orthoamide species **236** in the NHC-catalysed aliphatic benzoin condensation. Using stoichiometric concentrations of free NHC **16** and propionic aldehyde **230**, signals corresponding to the orthoamide were initially formed, before converting to the ketone tautomer of the Breslow intermediate **231**. However, in excess of aldehyde, the reaction led exclusively to the orthoamide **236**, *via* the reversible mechanism shown in Scheme 4.5. DFT studies support the proposal that the spirocyclic orthoamide species is the resting state of the system, and that cleavage of this species is necessary to enter the catalytic cycle.

Scheme 4.5:
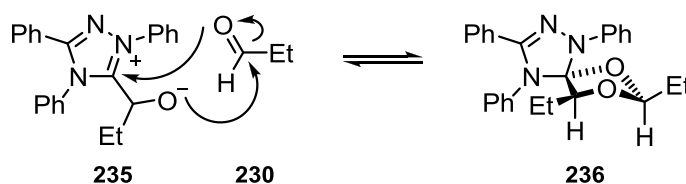
In 2012, Rovis and co-workers reported the isolation and characterisation of a nitrogen analogue of the triazolylidene-derived Breslow intermediate.[13] By replacing aldehyde **28** with an iminium ion **237**, a more chemically inert Breslow intermediate **238** with enamine – rather than enol – functionality could be prepared (Scheme 4.6). In the presence of weak acid this species was shown to regenerate the triazolium ion **239** and catalyse the Stetter reaction, demonstrating the reversibility of this process.

Scheme 4.6:
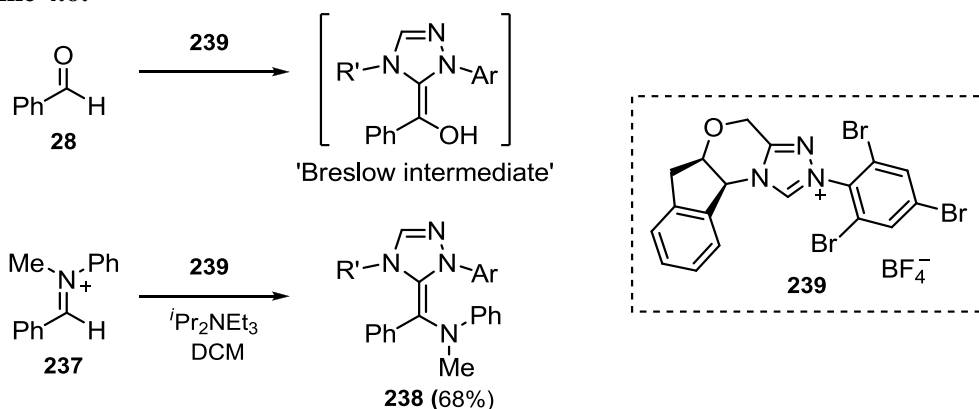
The first 'true' Breslow intermediate was finally prepared by Berkessel and co-workers in 2012.[14] The authors reported the isolation of several 2,2-diamino enols **241** from *N,N*-dimesityl and -diisopropylphenyl substituted 4,5-dihydroimidazol-2-ylidenes **3** and a range of aldehyde substrates **23** under rigorously dry conditions (Scheme 4.7a). These species were unambiguously confirmed by NMR spectroscopy, and X-ray structural information was obtained for a number of related enol ethers, such as **240**. Crucially, the role of these species in catalysis was confirmed by following the reaction of enol **242** with aldehydes **28** and **243** (Scheme 4.7b). Rapid equilibration of **242** to **244** was observed, demonstrating the reversibility of acyl anion formation. Interestingly, only the cross-benzoin product **245** was formed – alternative product **246** was not observed.

Scheme 4.7a:
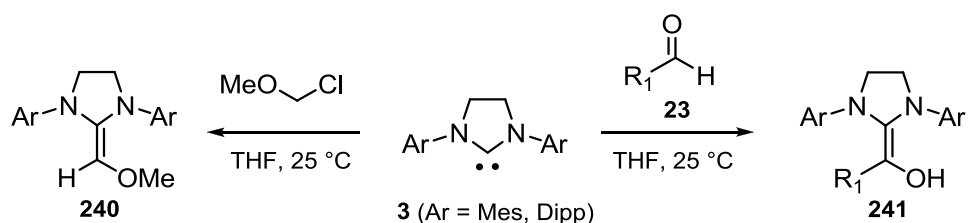
Scheme 4.7b:
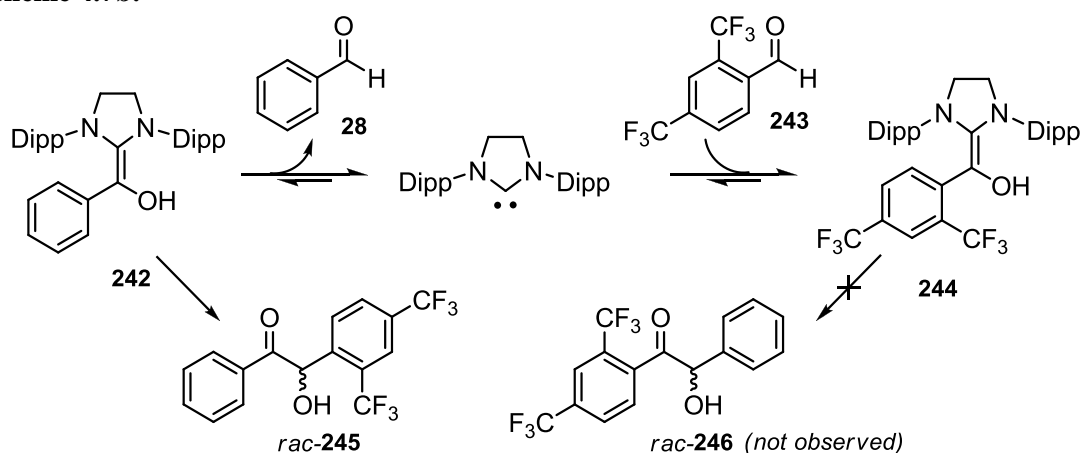
Whilst attempts to prepare the acyl anion have received significant attention in recent years, the initial adduct – formed from the reaction between the free NHC and aldehyde – has been somewhat overlooked, particularly for the more synthetically relevant triazolylidene-derived species. This is surprising, as this important intermediate is common to all of the NHC-catalysed reactions described in Chapter 1. Several thiazolylidene-derived examples were isolated by the groups of Spiegelberg[15] and Sable[16] in the late 1960s, and a number of groups have studied the kinetic acidity of these species at the $C(\alpha)$-H position by deuterium exchange experiments.[17]

In contrast, little information has been gleaned about the analogous triazolylidene-derived adduct. To the best of our knowledge, no structural information exists for this important species, and no detailed kinetic studies have been made regarding the acidity of this species. One of the aims of this investigation is to prepare and estimate the acidity of these species, in order to better understand their role in NHC organocatalysis.

4.1.3   Kinetic studies: NHC families

In 2001, Leeper and White undertook a detailed mechanistic study of the benzoin condensation catalysed by thiazolium precatalyst **247**.[10] Building on Breslow's mechanism, the authors probed the kinetics of the reaction using catalytic concentrations of **247** and under pre-steady-state conditions (*i.e.* stoichiometric concentrations of aldehyde and catalyst) in order to identify and determine rate constants for the key steps in the reaction. Leeper's steady-state initial rates work will be discussed separately in the following chapter.

The reaction was followed by ^{1}H NMR spectroscopy at stoichiometric concentrations of catalyst and benzaldehyde in triethylamine-buffered methanol-d_4 at 27 °C. The only intermediate observed over the course of the reaction was the initially-formed 2-(hydroxybenzyl)thiazolium adduct **248**. The absence of signals corresponding to the Breslow intermediate **249** or any of the other proposed intermediates that follow it indicated that steps subsequent to the formation of **249** were relatively fast. Consolidation of these steps resulted in the simplified mechanism shown in Scheme 4.8. Leeper assumed that interconversion between the thiazolium salt and thiazol-2-ylidene was rapid under these conditions, and did not need to be considered as a separate step. H/D-exchange studies by Jencks[18] and our laboratory show this to be the case.

Scheme 4.8:
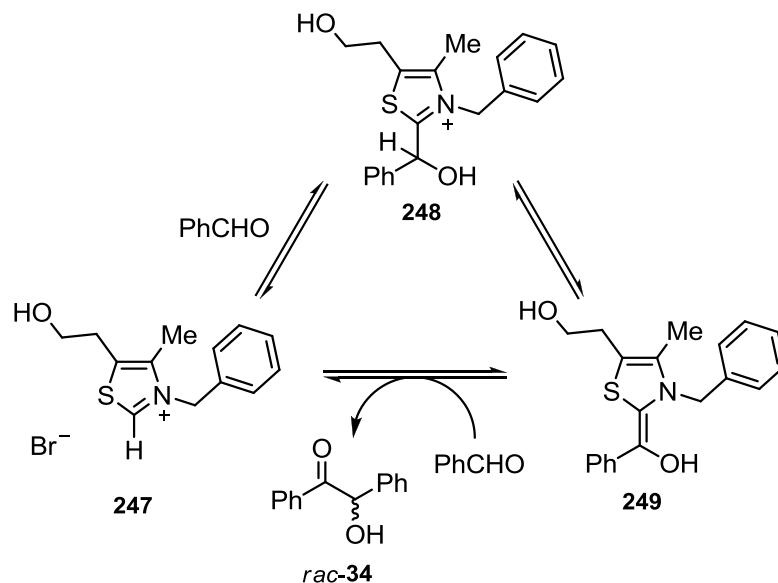
Integration of proton signals from benzaldehyde, benzoin and adduct **248**, relative to those of the free precatalyst **247**, enabled the concentrations of each species over the course of the reaction to be determined. By fitting the measured concentrations to rate equations, rate constants for the kinetically significant steps identified in Scheme 4.8 could be estimated. No single step was fully rate-determining: all three steps contributed to the overall rate. From these rate constants, free energies of activation could be determined and a free energy profile constructed (Figure 4.1). The energy of the Breslow intermediate **249** could not be accessed from the fitting of the experimental data, and was calculated from estimates of pK_a for a methylated analogue of the adduct **250** ($pK_a = 15.5$)[19] at the effective pH of the reaction conditions (pH 11.3).

Figure 4.1: **Free energy profile for the self-condensation of benzaldehyde (1 M), catalysed by (247) at 27 °C [free energies shown in kcal mol^{-1}]**
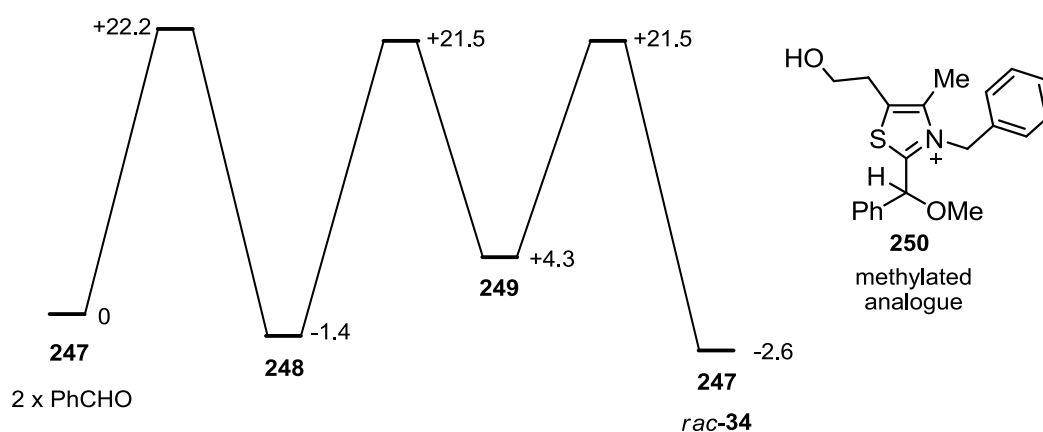
Holloczki recently published a theoretical study of reaction energy profiles for the benzoin condensation of formaldehyde, acetaldehyde and benzaldehyde, catalysed by imidazol-2-ylidene, thiazol-2-ylidene and triazol-3-ylidene species (**126**). Using the mechanism proposed in Scheme 4.9 (updated for the 'resting states' **256** and **257** observed by Berkessel), the energies of the stationary points and transition states involved in the reaction were calculated using B3LYP/6-311+G** level of theory. An additional hydrogen-bonded state **253·28** was incorporated into the pathway to minimise entropic contributions that may complicate comparisons between three catalyst families.

Scheme 4.9:
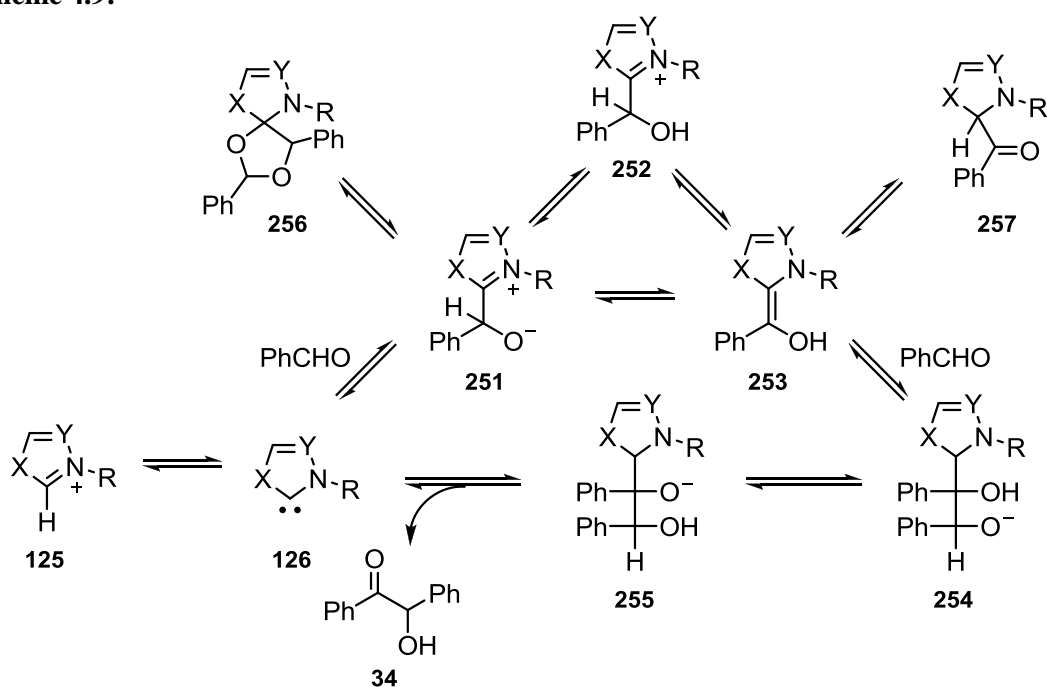
In all cases the reaction was found to be exothermic overall, with the reaction of benzaldehyde having the lowest exothermicity – consistent with the known reversibility of the reaction of aromatic aldehydes. The energy profiles for the reaction of benzaldehyde with the three common NHC families **258 – 260** are shown in Figure 4.2. The first step of the reaction to give the (hydroxybenzyl)azolium adduct was found to proceed through a low energy barrier. As the reaction was modelled for the gas phase, conversion of the adduct to the Breslow intermediate by a 1,2-hydrogen shift was accompanied by a substantial energy barrier. In solution however, this step may be achieved *via* a much easier protonation/deprotonation pathway, and the authors note that the protonation energies for species **251** and **253** are comparable to those of the

carbenes themselves, suggesting that in the reaction mixture, both of these species exist in the protonated form **252**. For all carbenes and aldehydes studied, resting state **257** was found to be significantly more stable than the parent Breslow intermediate.

Figure 4.2: **Energy profile for the self-condensation of benzaldehyde, catalysed by NHCs (258) – (260) [selected relative energies (kcal mol⁻¹) shown]**
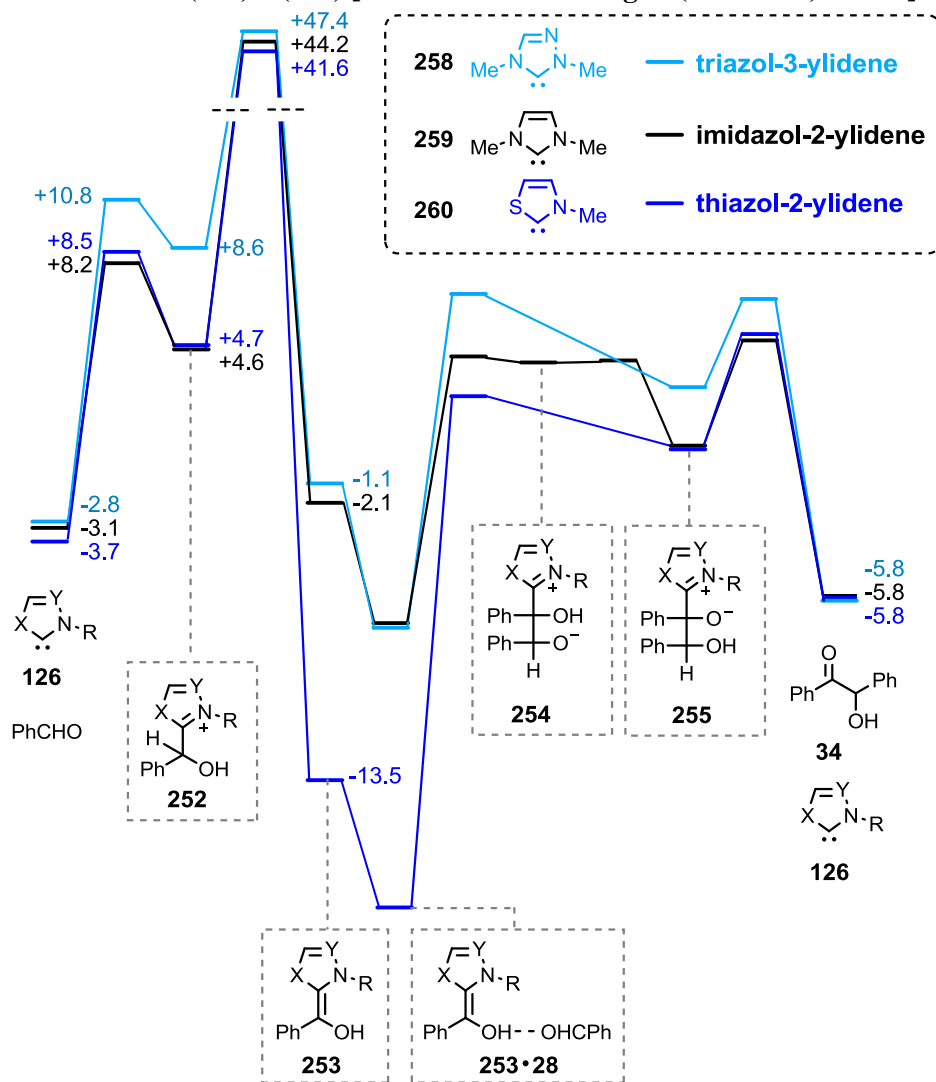
Interestingly, the Breslow intermediates derived from thiazol-2-ylidene **260** was found to be over 10 kcal mol⁻¹ more stable than those from triazol-2-ylidene **258** or imidazol-2-ylidene **259**. Thus, for the coupling step between the hydrogen-bonded Breslow intermediate and second aldehyde, imidazole and triazole-based catalysts were found to benefit from a relatively low energy barrier (14 – 16 kcal mol⁻¹ in the case of benzaldehyde). This barrier was significantly higher for thiazol-2-ylidene **260**. In several cases, structures resembling those of **254** could not be located on the potential energy surface, and formation of **255** proceeded directly from **253·28**. Energies for the final product forming step were found to transition *via* a low energy barrier.

4.1.4   The effect of the *N*-aryl substituent

One final mechanistic question posed by synthetic observations of the benzoin condensation and Stetter reaction focuses on the effect of the *N*-aryl substituent. In the introduction, we summarised a range of NHC-catalysed reactions and described suitable catalysts for each transformation. There exists a clear superiority for *N*-mesityl substituted NHCs in reactions involving α,β-unsaturated aldehydes, whereas transformations involving formation of the acyl anion (*i.e.* the benzoin and Stetter reactions) proceed more effectively using *N*-C_6F_5 architectures.

Bode recently noted that the redox esterification of cinnamaldehyde **67** to saturated ester **261** with methanol (Scheme 4.10) proceeds to completion using *N*-mesityl substituted triazolium precatalyst **81**, even in the absence of base.[20] By contrast, the reaction using the *N*-C_6F_5 catalyst **142** gave no product in the absence of base and slower rates of reaction when base was added. Clearly, this result cannot be rationalised in terms of azolium ion acidities – less of the *N*-mesityl NHC would be present under common conditions.

Scheme 4.10:
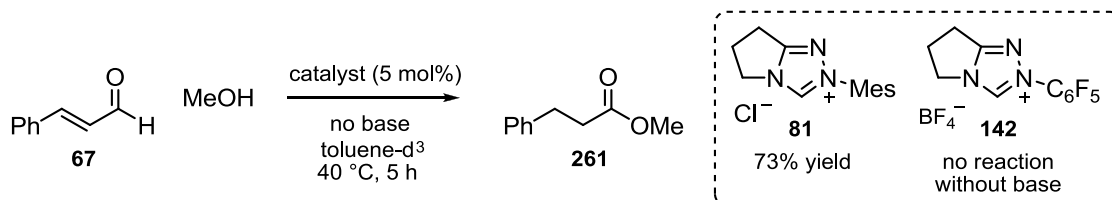
Following a series of insightful experiments,[21] Bode and co-workers recently ascribed this difference to the irreversible addition of the *N*-mesityl NHC to the aldehyde, which may accelerate the formation of the homoenolate. From the absence of H/D-exchange at the aldehydic position of D-cinnamaldehyde in the presence of a proton source, Bode concluded that the formation of a homoenolate from either *N*-mesityl or *N*-C_6F_5 triazolium catalysts is irreversible – in contrast to accounts of the benzoin and Stetter reactions.

By studying the rates of product formation for a number of related reactions that diverged from a common pathway at different points, the authors determined that formation of the homoenolate was the origin of the reactivity difference between *N*-

C_6F_5 and *N*-mesityl catalysts, leading to the mechanistic proposal shown in Scheme 4.11. Interestingly, for several reactions that proceed *via* this intermediate (oxidative esterification, ynal redox esterification and enone redox esterification) the reactivity of catalysts **262**, **142**, **263** and **81** (which possess a full matrix of steric and electronic substitutions) followed the order shown below. The fact that bulky catalysts **81** and **263** resulted in faster rates of conversion than electron-rich **262** suggested that sterics, rather than electronic effects lead to the proposed irreversibility of adduct formation. Based on inductive effects, the NHC derived from **142** would be expected to be a better leaving group than **263**, facilitating the reverse reaction.

Scheme 4.11:
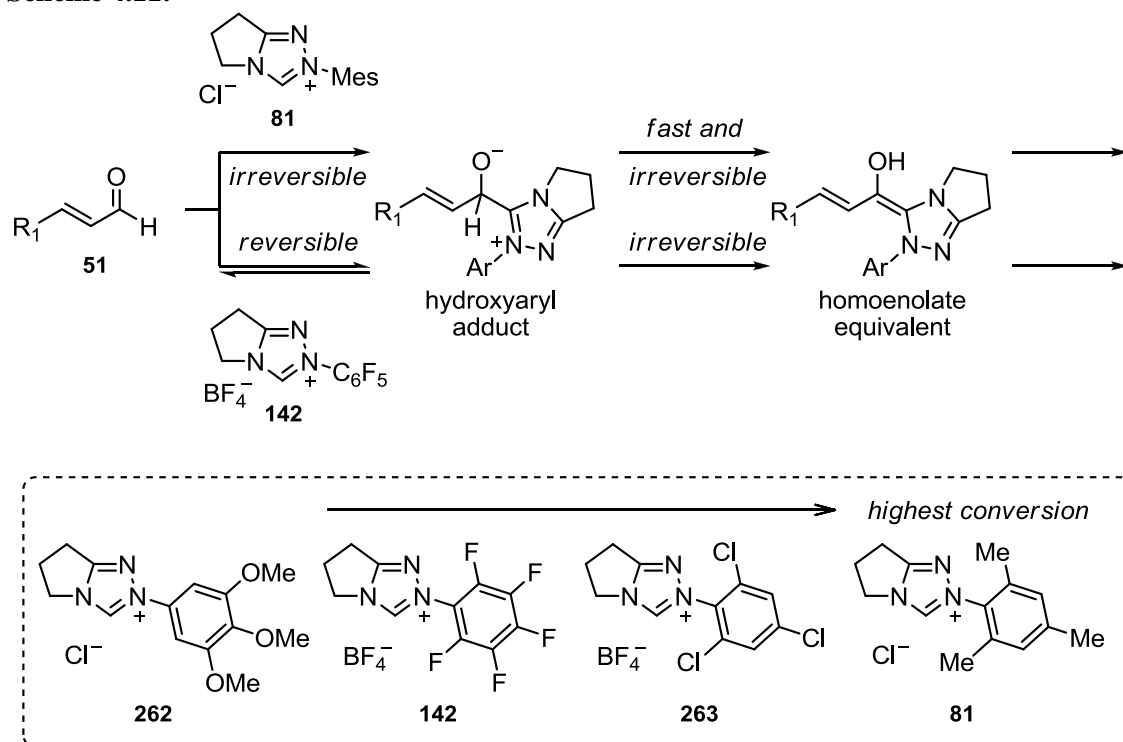
A tangible explanation for the behaviour of the bulky *N*-mesityl substituent is still a key challenge to a more complete understanding of these NHC-catalysed processes, and a detailed mechanistic study of the effect of the *N*-mesityl substituent on saturated aldehydes that proceed *via* acyl anion equivalents (*i.e.* the benzoin condensation) would complement Bode's study of homoenolate reactions.

4.2 *In situ* NMR Studies of the Benzoin Condensation and Isolation and Studies of Intermediates

4.2.1 Preliminary reaction studies by ^{1}H NMR spectroscopy

In order to guide the mechanistic studies that follow, an example of an NHC-catalysed benzoin condensation is outlined below.

The self-condensation of benzaldehyde **28** to give benzoin **34**, catalysed by triazolium salt **139** in triethylamine buffered methanol-d_4 (Scheme 4.12) was followed by ^{1}H NMR spectroscopy (500 MHz). The reaction was initiated by the addition of benzaldehyde **28** (0.08 M) to a solution of triazolium precatalyst **139** (0.08 M), NEt_3 (0.107 M) and $NEt_3 \cdot HCl$ (0.053 M) in methanol-d_4 (0.75 mL) in an NMR tube. The reaction was thermostated at 25°C in the NMR instrument.

Scheme 4.12:
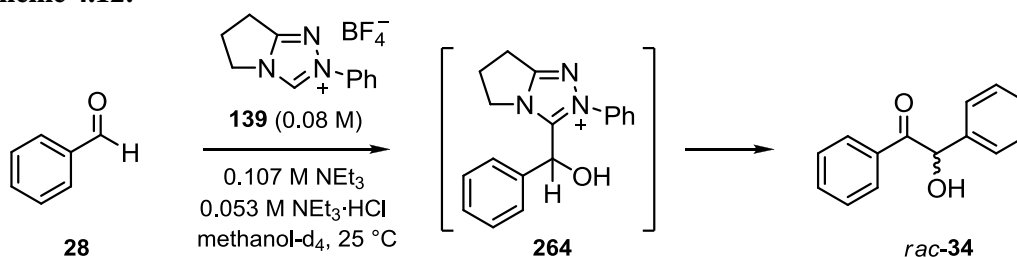
These relatively large stoichiometric concentrations of catalyst and aldehyde would aid the observation of any intermediates that may be formed over the course of the reaction. Substrate concentrations of 0.08 M were chosen, as this was within the limit of solubility of the catalyst. The choice of triethylamine buffer and methanol solvent were guided by a literature precedent for these conditions.[22] Previous studies by Leeper have used these buffer and solvent conditions, allowing comparisons to be made with this work.

A representative set of spectra taken at three time points during the reaction, alongside reactants, intermediates and product, is shown in Figure 4.3.

Figure 4.3: Representative ^{1}H NMR spectra at 500 MHz of the benzoin condensation of benzaldehyde (28), catalysed by triazolium salt (139), in methanol-d_4 at 25 ºC and 0.16 M triethylamine buffer (66% f_B). Spectra of benzaldehyde (28), adduct (264), and benzoin (34) in buffered methanol-d_4 are shown for comparison.
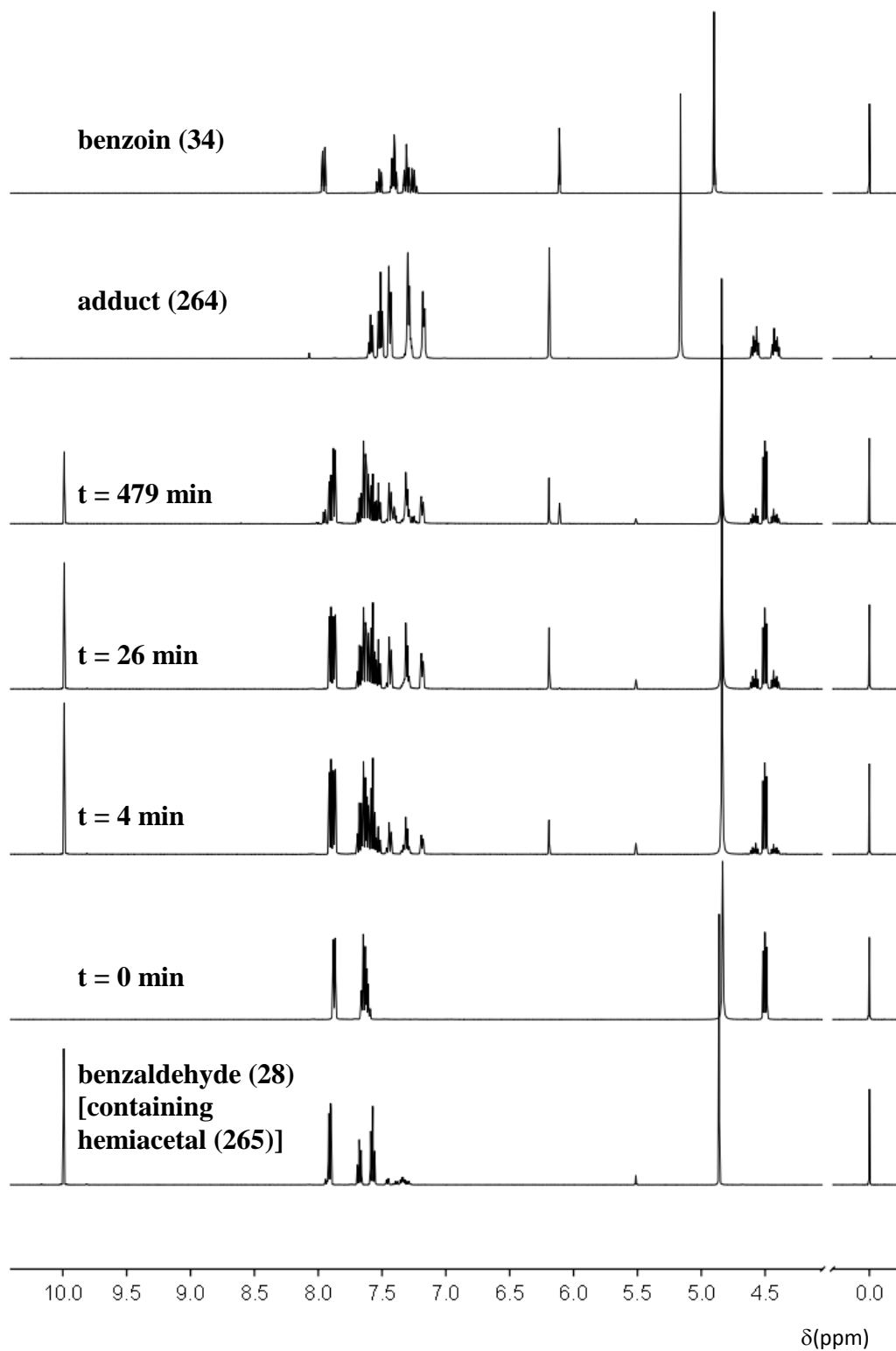
Initially, only C(3)-deuterated catalyst is present. No signal corresponding to the C(3)-H was observed due to exchange under the basic conditions employed. Benzaldehyde **28**, as with all of the aromatic aldehydes used in these studies, was found to equilibrate with its methanol-derived hemiacetal **265** (Scheme 4.13). This interconversion is slow on the NMR timescale but rapid relative to the kinetics of the benzoin condensation, and is discussed in more detail in Section 4.3. The appearance of peaks consistent with those of the benzoin product could be detected as the reaction progressed. In contrast, no hemiacetal formation could be detected for a reference solution of benzoin under the reaction conditions. A more detailed description of signals used to study the kinetics of the reaction is presented in Section 4.3.

Scheme 4.13:
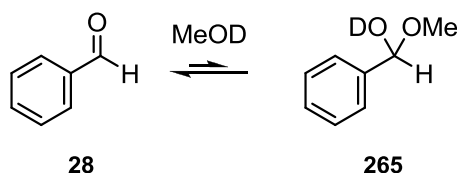
Immediately following the addition of benzaldehyde to catalyst, a set of peaks corresponding to an unidentified species appeared. Based on ^{1}H NMR investigations performed by Leeper and White, we believed this species to be the 3-(hydroxybenzyl)triazolium adduct **264** formed from the initial addition of triazol-3-ylidene to the aldehyde. The isolation and studies of this intermediate are the focus of the following section.

4.2.2   Isolation of 3-(hydroxybenzyl)triazolium intermediates

A range of substituted 3-(hydroxybenzyl)triazolium adducts **264** and **269 – 272** were prepared from equimolar amounts of triazolium ion and aldehyde in the presence of triethylamine base (Scheme 4.14). Compounds **264** and **269 – 271** were found to be unstable in non-acidified solvents, dissociating back to aldehyde and catalyst within 2-3 hours. For these species, separation by column chromatography proved to be unsuccessful; however, clean separation was achieved using a Liquid Chromatography Mass Spectrometry (LCMS) method, albeit in poor yield. The presence of an *ortho*-methoxy substituent on the aldehyde ring resulted in increased stability, and isolation of compound **272** was achieved by column chromatography.

Scheme 4.14:

28 R = H
266 R = 4-F
267 R = 4-Me
268 R = 2-OMe

139 Ar = Ph
140 Ar = Mes

NEt$_3$ (2 eq.)
DCM / MeOH

264 Ar = Ph, R = H (3%)
269 Ar = Ph, R = 4-F (2%)
270 Ar = Ph, R = 4-Me (3%)
271 Ar = Mes, R = H (9%)
272 Ar = Ph, R = 2-OMe (24%)
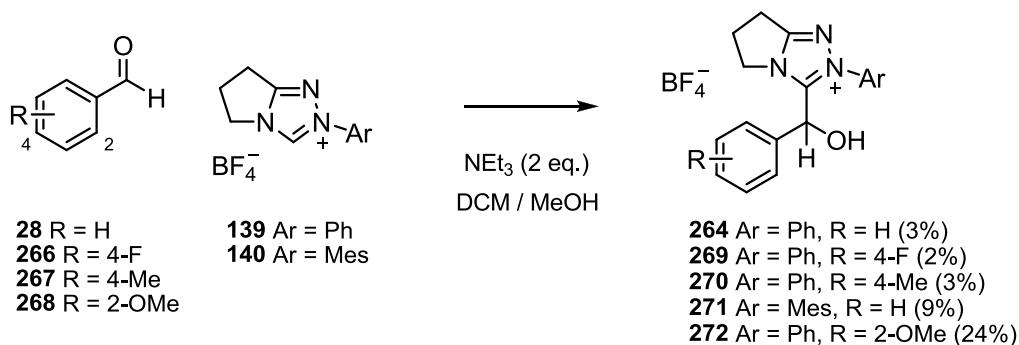
Berkessel has reported NMR chemical shifts for the ketone tautomer **232** of the triazolium-derived Breslow intermediate, mentioned in the introduction to this chapter. By chance, the ^{1}H chemical shifts of the postulated C(α)-H in our products (such as **264**) were identical or close to the value for the C(3)-H in **232** (Figure 4.4), and it was necessary to confirm the identity of our isolated species using an alternative approach. Using ^{1}H,^{13}C-HSQC NMR spectroscopy, the C(α) ^{13}C chemical shift in **264** was assigned, and was found to lie significantly upfield from Berkessel's Breslow tautomer. The environment of the C(3) in **232** consists of two adjacent electron-withdrawing nitrogen atoms and a carbonyl group, and would likely give a more downfield signal than in our species **264**.

Figure 4.4: **[1]H and ^{13}C chemical shifts of intermediates in the benzoin condensation**
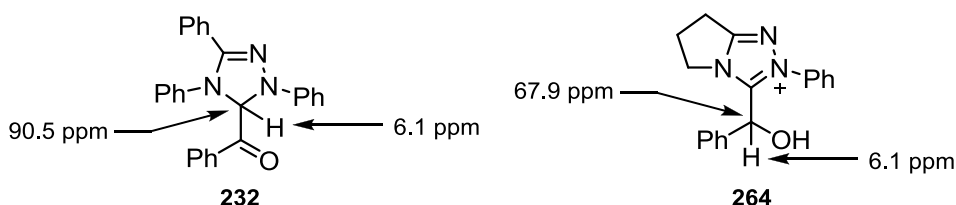
For practical reasons, the majority of isolated adducts were prepared in dichloromethane solvent. To confirm whether the formation of **264** and **269 – 272** were as a result of solvent, adduct **264** was also prepared in methanol, affording the same species. Furthermore, a ^{1}H,^{13}C-HSQC spectrum was taken midway through the reaction in triethylamine-buffered methanol-d$_4$, and corresponded exactly with isolated **264**.

Finally, for species **264**, **269** and **270**, crystallisation from solutions of DCl (~0.1 M) in D$_2$O enabled unambiguous structural determination of the corresponding chloride salts by X-ray crystal structure analysis (Figure 4.5). Unfortunately, it was not possible to obtain suitable crystals for the *N*-mesityl substituted adduct **271**.

Figure 4.5: **Representations of the X-ray crystal structures of the chloride salts of 3-(hydroxybenzyl)triazolium adducts (264), (269) and (270)**

264

269   270
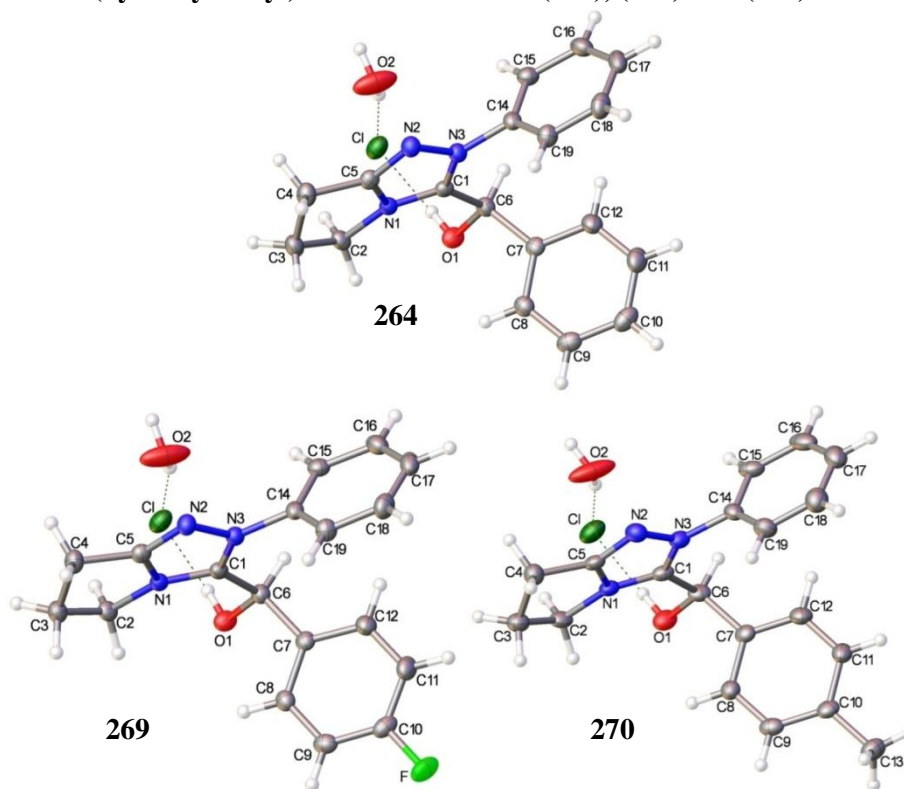
4.2.3 Adduct dissociation: Kinetic studies

The kinetics of 3-(hydroxybenzyl)triazolium adduct decomposition were studied in triethylamine buffered methanol-d_4 at 25 °C. This decomposition highlights the reversibility of the first addition step in the benzoin mechanism. Adduct dissociation to triazolium ion precatalyst and aldehyde was followed by ^{1}H NMR spectroscopy (500 MHz), and resulted in the disappearance of signals corresponding the adduct, and formation of signals corresponding to aldehyde and catalyst. From this data, equilibrium constants for the reaction shown in Scheme 4.15 were estimated.

Scheme 4.15:
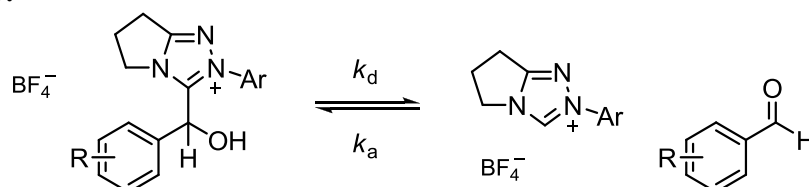
Reactions were initiated by the addition of a 0.6 - 0.7 mL solution of buffer (0.107 M NEt$_3$, 0.053 M NEt$_3$·DCl, unless otherwise stated) in methanol-d_4 (containing 0.01% TMS) to an NMR tube containing dried substrate (0.04 M). The capped NMR tube was

inverted to ensure complete dissolution. Reactions were thermostated at 25 °C directly in the NMR instrument. The instrument was pre-shimmed on a blank solution of buffer in order to maximise the measurement time at the start of the reaction. At regular intervals over the course of the reaction the composition of the solution was analysed by ^{1}H NMR spectroscopy (duration of acquisition ~4 min).

4.2.3.1   2-Phenyl-3-(α-hydroxybenzyl)-6,7-dihydro-5*H*-pyrrolo[2,1-c][1,2,4]triazol-2-ium tetrafluoroborate (264)

Scheme 4.16:
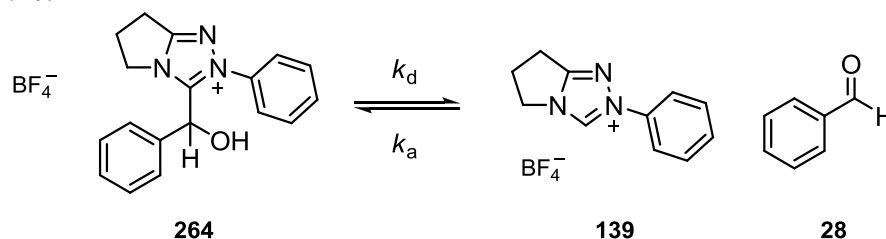
264   **139**   **28**

A representative set of spectra taken at three time points over the course of the reaction is shown in Figure 4.6. Dissociation of adduct **264** resulted in the disappearance of the pair of multiplet signals at 4.60 (*A1*) and 4.42 ppm (*A1'*), corresponding to the non-equivalent CH$_2$ protons on the five-membered ring of the adduct **264**, and appearance of the triplet at 4.51 ppm (*C1*), corresponding to the same protons on the catalyst **139**. The integrated areas of these signals were measured relative to the singlet signal at 0.0 ppm corresponding to the internal standard, TMS. Additionally, the extent of H/D-exchange at the α-CH position was monitored by following the singlet signal at 6.20 ppm (*A2*), relative to the non-exchangeable CH$_2$ signals (*A1* and *A1'*). The fast decomposition of adduct under these conditions did not permit measurement of the aforementioned CH$_2$ integrals on adduct **264** at $t = 0$. However, no significant formation of benzoin (~3% conversion), or any other intermediate, were observed. Therefore, the sum of the integrals corresponding to the CH$_2$ protons on catalyst **139** (*C1*) and adduct **264** (*A1* and *A1'*) at any time should correspond to the integrated area of the CH$_2$ protons on adduct **264** present initially, as described by Equation 4.1. In this manner, the integrals of adduct **264** at $t = 0$ were calculated from the average of the sum of the integrals of *A1*, *A1'* and *C1*, over the whole reaction.

$$\left\{A_{(A1+A1')}\right\}_0 \equiv \left\{A_{(A1+A1'+C1)}\right\}_{avg} \approx \left\{A_{(A1+A1')}\right\}_t + \left\{A_{(C1)}\right\}_t \qquad \textbf{Equation 4.1}$$

Figure 4.6: Representative ^{1}H NMR spectra at 500 MHz showing dissociation of adduct (264) to form catalyst (139) and benzaldehyde (28) in methanol-d$_4$ at 25 ºC and 0.16 M triethylamine buffer (66% f_B)
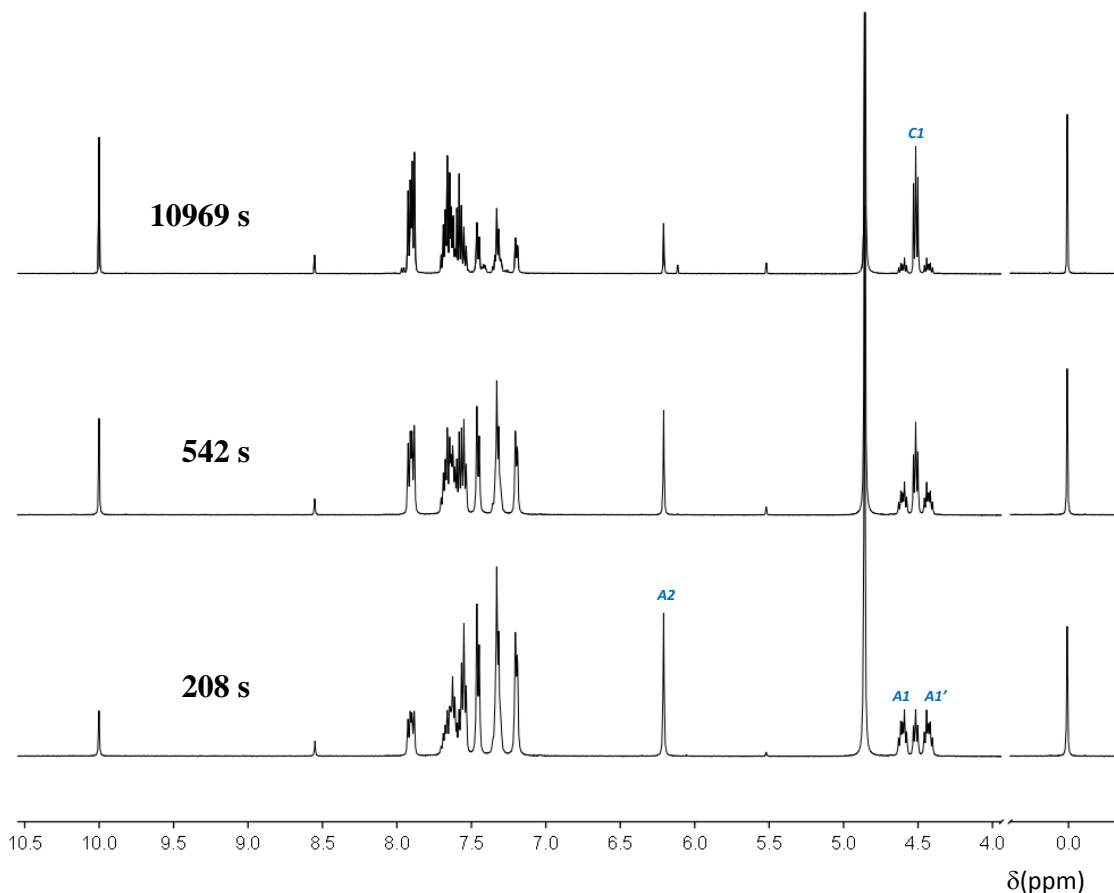
The concentration of adduct at the beginning of the reaction, equal to the averaged sum of signals *A1*, *A1'* and *C1*, was known to be 0.04 M. The concentrations of adduct and catalyst during the reaction could be calculated from integrated area of these signals at time *t* relative to the integrated area corresponding to adduct at the start of the reaction, shown by Equations 4.2 and 4.3. To determine the extent of exchange at the C(α)-H position on **264**, the concentration of protonated adduct was also calculated using signal *A2* by Equation 4.4. Figure 4.7 shows a concentration profile for the reaction.

$$[\text{adduct (tot)}]_t = \frac{\left\{A_{(A1+A1')}\right\}_t}{\left\{A_{(A1+A1'+C1)}\right\}_{avg}} \times 0.04 \qquad \textbf{Equation 4.2}$$

$$[\text{catalyst}]_t = \frac{\left\{A_{(C1)}\right\}_t}{\left\{A_{(A1+A1'+C1)}\right\}_{avg}} \times 0.04 \qquad \textbf{Equation 4.3}$$

$$[\text{adduct (H)}]_t = \frac{\left\{A_{(A2)}\right\}_t}{\left\{A_{(A1+A1'+C1)}\right\}_{avg}} \times 0.04 \qquad \textbf{Equation 4.4}$$

Figure 4.7: Concentration profile showing dissociation of 0.04 M adduct (264) (C(α)-L, L=H/D ●, L=H ○) to triazolium precatalyst (139) (♦) in 0.107 M NEt$_3$ and 0.053 M NEt$_3$·DCl in methanol-d$_4$ at 25 °C
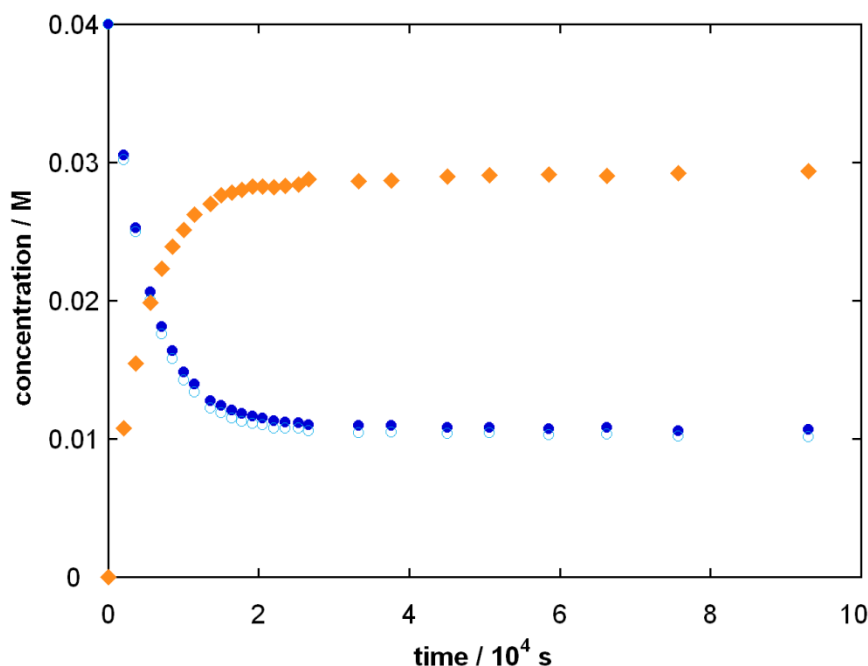
Dissociation of adduct to catalyst and benzaldehyde was observed to reach equilibrium after approximately 55 min. An equilibrium constant, K_1 (M), for the reaction shown in Scheme 4.16 was calculated from the concentrations of adduct and catalyst at equilibrium, shown by Equation 4.5. As adduct decomposition results in the formation of one molecule of aldehyde and one molecule of catalyst, and no significant benzoin formation was encountered, it was assumed that the equilibrium concentration of aldehyde corresponded to that of catalyst. The concentrations used to calculate K_1 were taken from the first point at which equilibrium had been reached (*i.e.* at 55 min). Equilibrium constants determined in this section are summarised in Table 4.1.

$$K_1 = \frac{k_d}{k_a} = \frac{[\text{cat}]_e \times [\text{ald (tot)}]_e}{[\text{add (tot)}]_e} = \frac{([\text{cat}]_e)^2}{[\text{add (tot)}]_e} \qquad \textbf{Equation 4.5}$$

According to the mechanism proposed in Scheme 4.16, a first-order rate constant for adduct dissociation to precatalyst and aldehyde, k_d (s^{-1}), may be obtained from the consumption of adduct in the period leading to equilibrium, where onward benzoin formation is negligible. The expression for the concentration of adduct is given in Equation 4.6, which may be rewritten as Equation 4.7 (where [cat] = [ald]).

$$\frac{d[add]}{dt} = -k_d[add] + k_a[cat][ald] \qquad \textbf{Equation 4.6}$$

$$\frac{d[add]}{dt} = -k_d[add] + k_d \frac{[add]_e}{([add]_0-[add]_e)^2} ([add]_0 - [add])^2 \quad \textbf{Equation 4.7}$$

If the initial concentrations are $[add]_0 = a$ and $[cat]_0 = [ald]_0 = 0$, then Equation 4.7 may be integrated to give the rate equation shown in Equation 4.8, where $x = ([add]_0 - [add])$ and $x_e = ([add]_0 - [add]_e)$.[23] Thus, a value of k_d may be obtained from the slope of a semilogarithmic plot of $[(ax_e + x(a - x_e))/(a(x_e - x))]$ against time (Figure 4.8).

$$\frac{x_e}{(2a-x_e)} \ln \frac{ax_e+x(a-x_e)}{a(x_e-x)} = k_d t \qquad \textbf{Equation 4.8}$$

Similar plots for the dissociation of other adducts presented in this section are shown in Appendix C. These plots were linear and were followed over the first three half-lives. Values of k_d obtained by this method are summarised in Table 4.1.

Figure 4.8:   **Semilogarithmic plot of $[(ax_e + x(a - x_e))/(a(x_e - x))]$ against time for the reaction of (264) in 0.107 M NEt$_3$ and 0.053 M NEt$_3$·DCl in methanol-d$_4$ at 25 ºC**
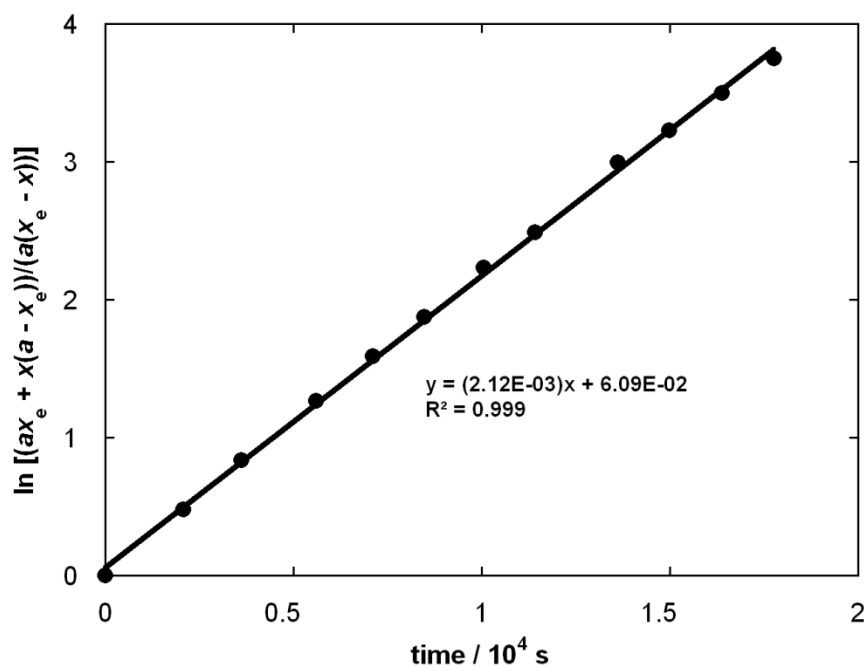
y = (2.12E-03)x + 6.09E-02
R² = 0.999

time / 10⁴ s

4.2.3.2 2-Phenyl-3-(α-hydroxy(*para*-methylbenzyl))-6,7-dihydro-5*H*-pyrrolo[2,1-c][1,2,4]triazol-2-ium tetrafluoroborate (270)

Scheme 4.17:
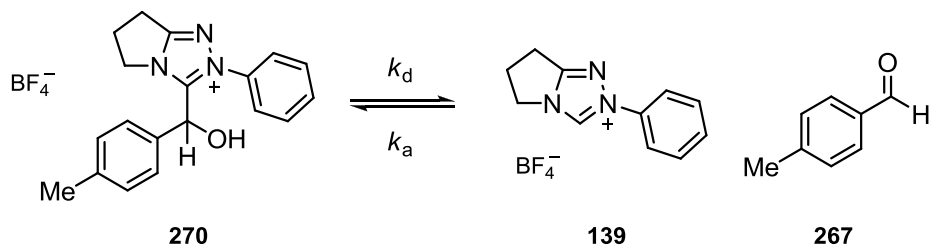
A representative set of spectra taken at three time points over the course of the reaction is shown in Figure 4.9. Dissociation of adduct **270** resulted in the disappearance of the pair of multiplet signals at 4.75 (*A1*) and 4.69 ppm (*A1'*), corresponding to the non-equivalent CH$_2$ protons on the five-membered ring of the adduct **270**, and appearance of the triplet at 4.54 ppm (*C1*), corresponding to the same protons on the catalyst **139**. The integrated areas of these signals were measured relative to the singlet signal at 0.0 ppm corresponding to the internal standard TMS. Additionally, the extent of H/D-exchange at the C(α)-H position was monitored by following the singlet signal at 5.80 ppm (*A2*), relative to the non-exchangeable CH$_2$ signals (*A1* and *A1'*). As described previously for adduct **264**, the integrals of adduct **270** at $t = 0$ were calculated from the average of the sum of the integrals of *A1*, *A1'* and *C1*, over the whole reaction. Concentrations of adduct and catalyst were calculated according to Equations 4.1 – 4.4. A concentration profile for the reaction is shown in Figure 4.10.

Dissociation of adduct to catalyst and aldehyde was observed to reach equilibrium after approximately 62 min. An equilibrium constant, K_1 (M), for the reaction (Scheme 4.17) was calculated from the concentrations of adduct and catalyst at equilibrium, shown by Equation 4.5. As adduct decomposition results in the formation of one molecule of aldehyde and one molecule of catalyst, and no significant benzoin formation was encountered, it was assumed that the equilibrium concentration of aldehyde corresponded to that of catalyst. The concentrations used to calculate K_1 were taken from the first point at which equilibrium had been reached (*i.e.* at 62 min). Equilibrium constants determined in this section are summarised in Table 4.1. A first-order rate constant for adduct decomposition, k_d (s^{-1}), was obtained from the slope of a semilogarithmic plot of $[(ax_e + x(a - x_e))/(a(x_e - x))]$ against time (Appendix C, Figure C5).

Figure 4.9: Representative ^{1}H NMR spectra at 500 MHz showing dissociation of adduct (270) to form precatalyst (139) and *para*-methylbenzaldehyde (267) in methanol-d_4 at 25 °C and 0.16 M triethylamine buffer (66% f_B)

Figure 4.10: Concentration profile showing dissociation of 0.04 M adduct (270) (C(α)-L, L=H/D ●, L=H ○) to triazolium precatalyst (139) (◆) in 0.107 M NEt$_3$ and 0.053 M NEt$_3$·DCl in methanol-d_4 at 25 °C
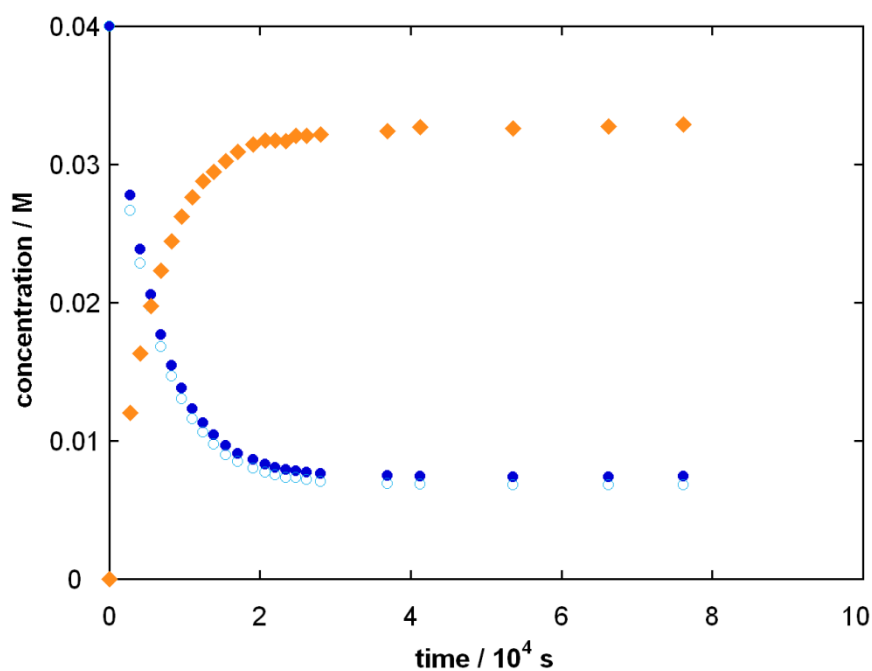
4.2.3.3   2-Phenyl-3-(α-hydroxyl(*para*-fluorobenzyl))-6,7-dihydro-5*H*-pyrrolo[2,1-c][1,2,4]triazol-2-ium tetrafluoroborate (269)

Scheme 4.18:
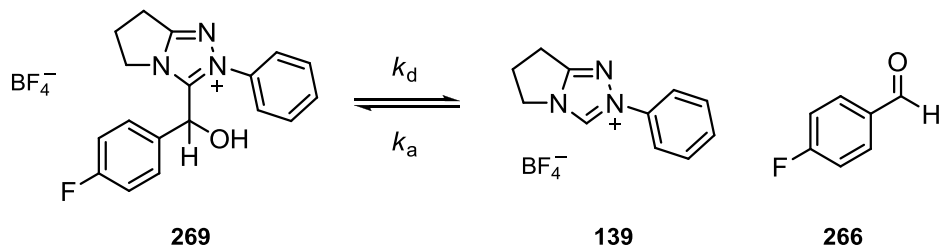
A representative set of spectra taken at three time points over the course of the reaction is shown in Figure 4.11. Dissociation of adduct **269** resulted in the disappearance of the pair of multiplet signals at 4.75 (**A1**) and 4.69 ppm (**A1'**), corresponding to the non-equivalent CH_2 protons on the five-membered ring of the adduct **269**, and appearance of a triplet at 4.54 ppm (**C1**), corresponding to the same protons on the catalyst **139**. The integrated areas of these signals were measured relative to the singlet signal at 0.0 ppm corresponding to the internal standard TMS. Signals **C1** and **A1'** overlapped, so the integrated area of the **C1** signal was calculated by subtracting the integrated area of the **A1** signal from the sum of the **C1** and **A1'** signals. Additionally, the extent of H/D-exchange at the C(α)-H position was monitored by following the singlet signal at 5.80 ppm (**A2**), relative to the non-exchangeable CH_2 signals (**A1**). As described previously for **264**, the integrals of adduct **269** at $t = 0$ were calculated from the average of the sum of the integrals of **A1**, **A1'** and **C1** over the whole reaction. Concentrations of adduct and catalyst were calculated according to Equations 4.1 – 4.4. A concentration profile for the reaction is shown in Figure 4.12.

Dissociation of adduct to catalyst and aldehyde was observed to reach equilibrium after approximately 60 min. An equilibrium constant, K_1 (M), for the reaction (Scheme 4.18) was calculated from the concentrations of adduct and catalyst at equilibrium using Equation 4.5. As adduct decomposition results in the formation of one molecule of aldehyde and one molecule of catalyst, and no significant benzoin formation was encountered, it was assumed that the equilibrium concentration of aldehyde corresponded to that of catalyst. The concentrations used to calculate K_1 were taken from the first point at which equilibrium had been reached (*i.e.* at 60 min). Equilibrium constants determined in this section are summarised in Table 4.1. A first-order rate constant for adduct decomposition, k_d (s^{-1}), was obtained from the slope of a semilogarithmic plot of $[(ax_e + x(a - x_e))/(a(x_e - x))]$ against time (Appendix C, Figure C6).

Figure 4.11: Representative ^{1}H NMR spectra at 500 MHz showing dissociation of adduct (269) to form precatalyst (139) and *para*-fluorobenzaldehyde (266) in methanol-d$_4$ at 25 ºC and 0.16 M triethylamine buffer (66% f_B)
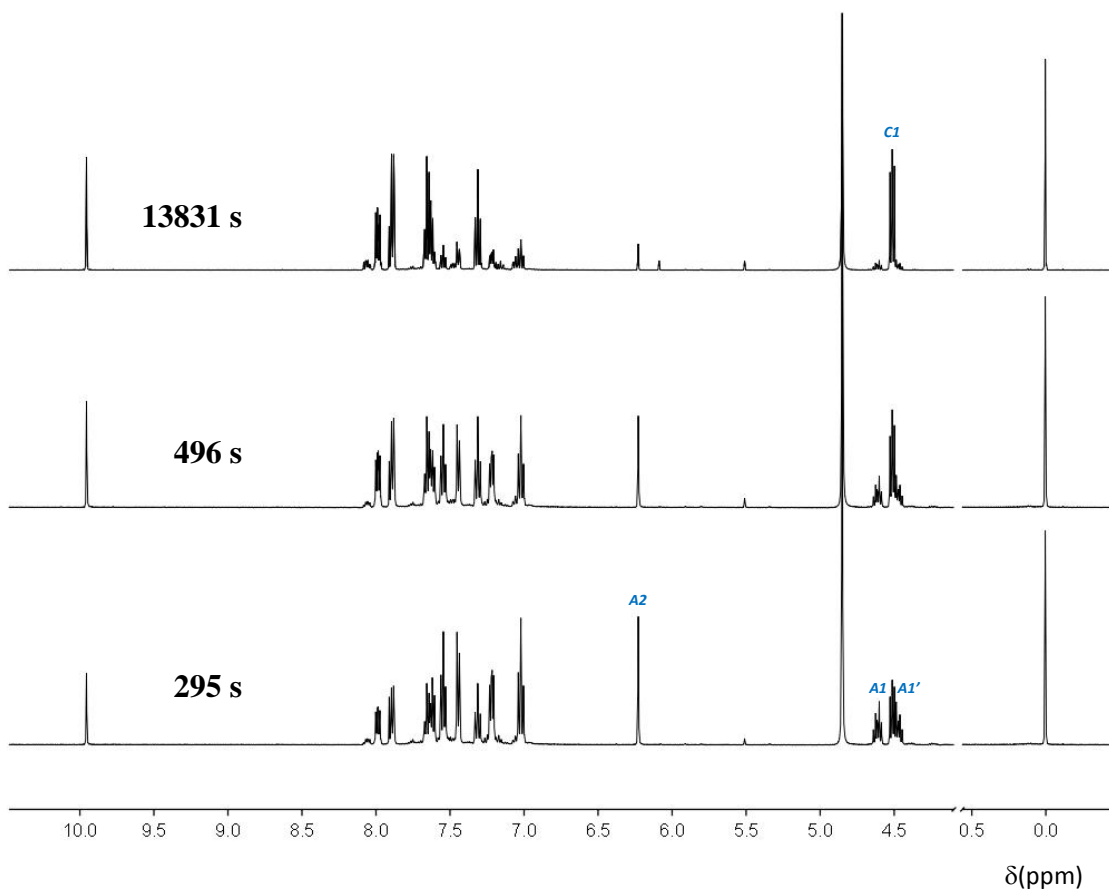

Figure 4.12: Concentration profile showing dissociation of 0.04 M adduct (269) (C(α)-L, L=H/D ●, L=H ○) to triazolium precatalyst (139) (◆) in 0.107 M NEt$_3$ and 0.053 M NEt$_3$·DCl in methanol-d$_4$ at 25 °C
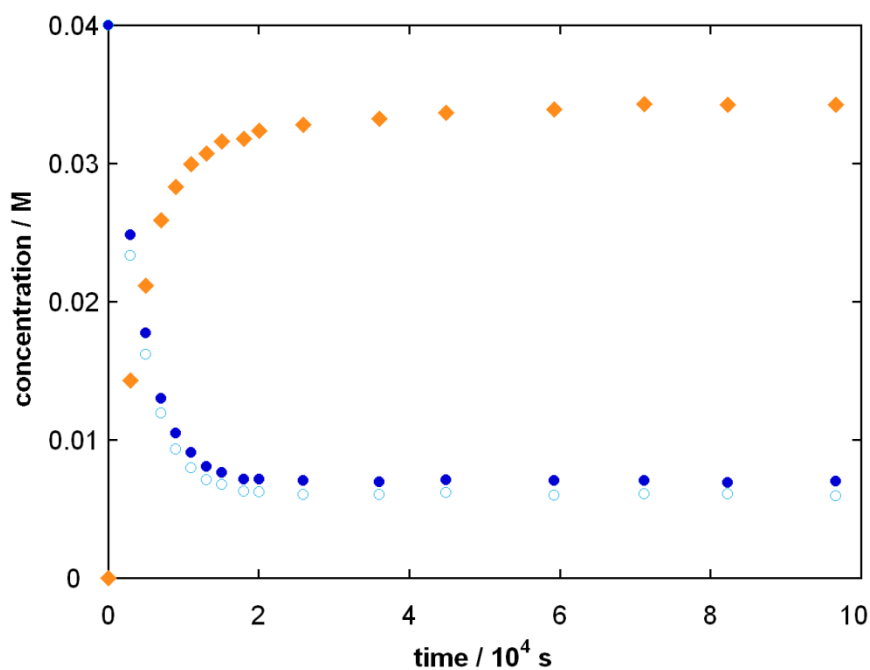
4.2.3.4 2-Phenyl-3-(α-hydroxy(*ortho*-methoxybenzyl)-6,7-dihydro-5*H*-pyrrolo[2,1-c][1,2,4]triazol-2-ium tetrafluoroborate (272)

Scheme 4.19:
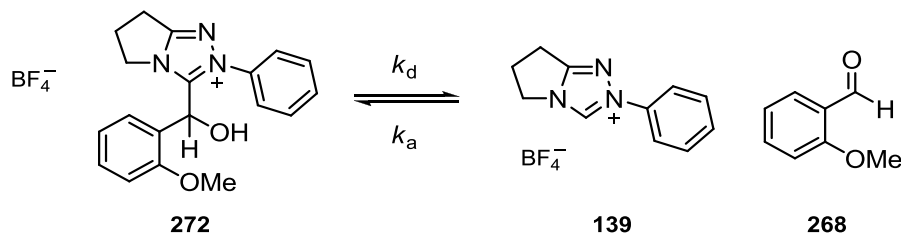
A representative set of spectra taken at three time points over the course of the reaction is shown in Figure 4.13. Dissociation of adduct **272** resulted in the disappearance of the pair of multiplet signals at 4.75 (**A1**) and 4.69 ppm (**A1'**), corresponding to the non-equivalent CH$_2$ protons on the five-membered ring of the adduct **272**, and appearance of the triplet at 4.54 ppm (**C1**), corresponding to the same protons on the catalyst **139**. The integrated areas of these signals were measured relative to the singlet signal at 0.0 ppm corresponding to the internal standard TMS. Additionally, the extent of H/D-exchange at the C(α)-H position was monitored by following the singlet signal at 5.80 ppm (**A2**), relative to the non-exchangeable CH$_2$ signals (**A1** and **A1'**). As described previously for adduct **264**, the integrals of adduct **272** at $t = 0$ were calculated from the average of the sum of the integrals of **A1**, **A1'** and **C1**, over the whole reaction. Concentrations of adduct and catalyst were calculated according to Equations 4.1 – 4.4. A concentration profile for the reaction is shown in Figure 4.14.

Dissociation of adduct to catalyst and aldehyde was observed to reach equilibrium after approximately 68 min. An equilibrium constant, K_1 (M), for the reaction (Scheme 4.19) was calculated from the concentrations of adduct and catalyst at equilibrium, shown by Equation 4.5. As adduct decomposition results in the formation of one molecule of aldehyde and one molecule of catalyst, and no significant benzoin formation was encountered, it was assumed that the equilibrium concentration of aldehyde corresponded to that of catalyst. The concentrations used to calculate K_1 were taken from the first point at which equilibrium had been reached (*i.e.* at 68 min). Equilibrium constants determined in this section are summarised in Table 4.1. A first-order rate constant for adduct decomposition, k_d (s^{-1}), was obtained from the slope of a semilogarithmic plot of $[(ax_e + x(a - x_e))/(a(x_e - x))]$ against time (Appendix C, Figure C7).

Figure 4.13: Representative ^{1}H NMR spectra at 500 MHz showing dissociation of adduct (272) to form precatalyst (139) and *ortho*-methoxybenzaldehyde (268) in methanol-d$_4$ at 25 ºC and 0.16 M triethylamine buffer (66% f_B)
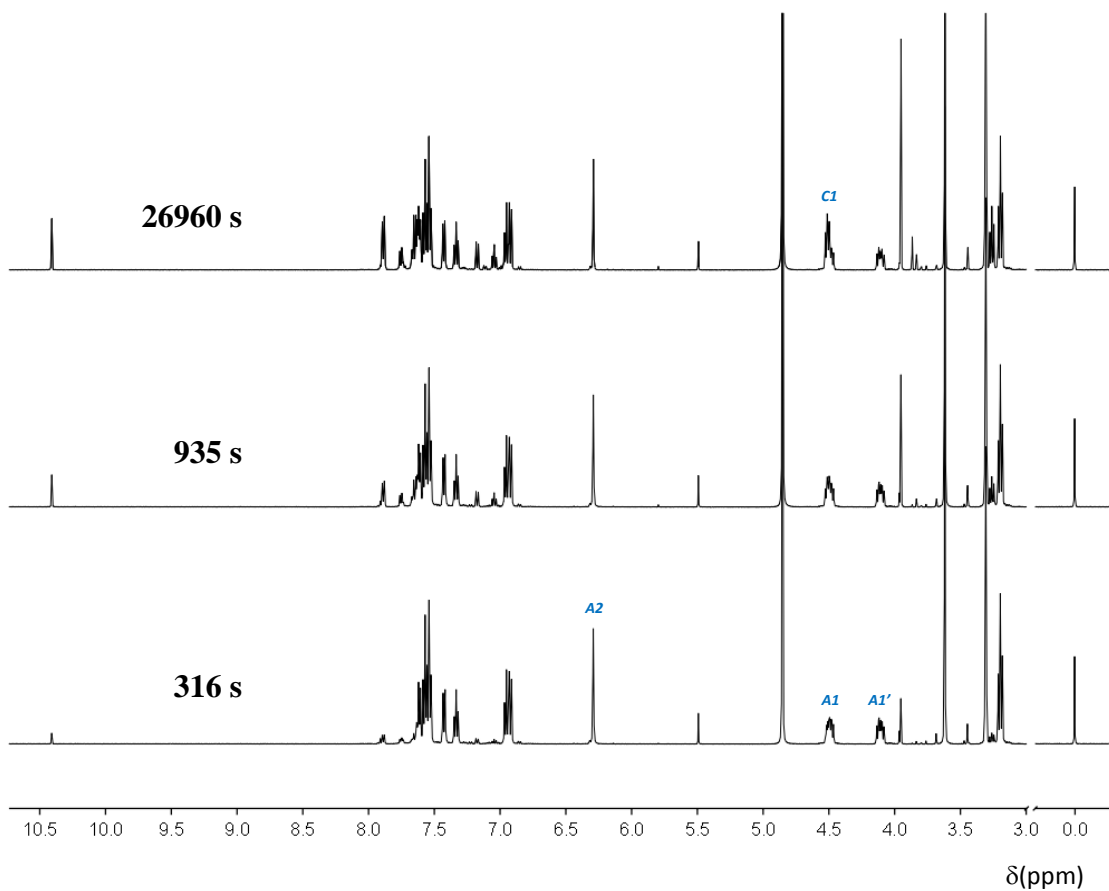
Figure 4.14: Concentration profile showing dissociation of 0.04 M adduct (272) (C(α)-L, L=H/D ●, L=H ○) to triazolium precatalyst (139) (◆) in 0.107 M NEt$_3$ and 0.053 M NEt$_3$·DCl in methanol-d$_4$ at 25 °C
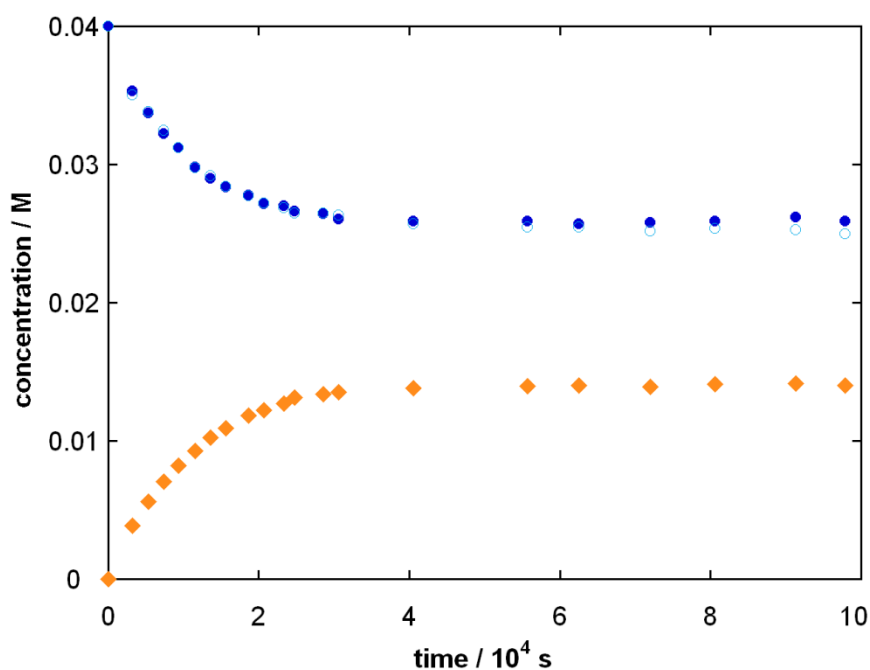
4.2.3.5 2-Mesityl-3-(α-hydroxybenzyl)-6,7-dihydro-5*H*-pyrrolo[2,1-c][1,2,4]triazol-2-ium tetrafluoroborate (271)

Scheme 4.20:
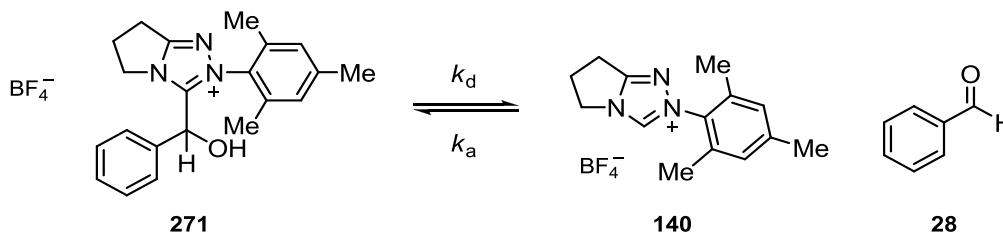
The dissociation reaction of **271** was studied in a range of buffer conditions. A representative set of spectra taken at three time points over the course of the reaction (buffer: 0.107 M NEt$_3$; 0.053 M NEt$_3$·DCl) is shown in Figure 4.15. Dissociation of adduct **271** resulted in the disappearance of the pair of multiplet signals at 4.75 (**A1**) and 4.69 ppm (**A1'**), corresponding to the non-equivalent CH$_2$ protons on the five-membered ring of the adduct **271**, and appearance of the triplet at 4.54 ppm (**C1**), corresponding to the same protons on the catalyst **140**. Signals **A1** and **A1'** overlapped with the solvent signal, and could not be used to follow the reaction. Instead, the singlet signals at 7.17 (**A3**) and 6.92 ppm (**A3'**), corresponding to the non-equivalent *meta*-CH protons on the adduct *N*-mesityl substituent, and the singlet signal at 7.13 ppm (**C2**) corresponding equivalent *meta*-CH protons on the catalyst were used to follow the reaction. The integrated areas of these signals were measured relative to the singlet signal at 0.0 ppm corresponding to the internal standard TMS. Additionally, the extent of H/D-exchange at the C(α)-H position was monitored by following the singlet signal at 5.80 ppm (**A2**), relative to the *meta*-CH signals (**A3** and **A3'**). In a similar manner to that described previously for adduct **264**, the integrals of adduct **271** at *t* = 0 were calculated from the average of the sum of the integrals of **A3**, **A3'** and **C2**, over the whole reaction.

For each set of buffer conditions, concentrations of adduct and catalyst were calculated according to Equations 4.1 – 4.4. Concentration profiles for these reactions are shown in Figures 4.16 – 4.18, and give essentially the same equilibrium constant under all three conditions.

Figure 4.15: Representative ^{1}H NMR spectra at 500 MHz showing dissociation of adduct (271) to form precatalyst (140) and benzaldehyde (28) in methanol-d$_4$ at 25 ºC and 0.16 M triethylamine buffer (66% f_B)
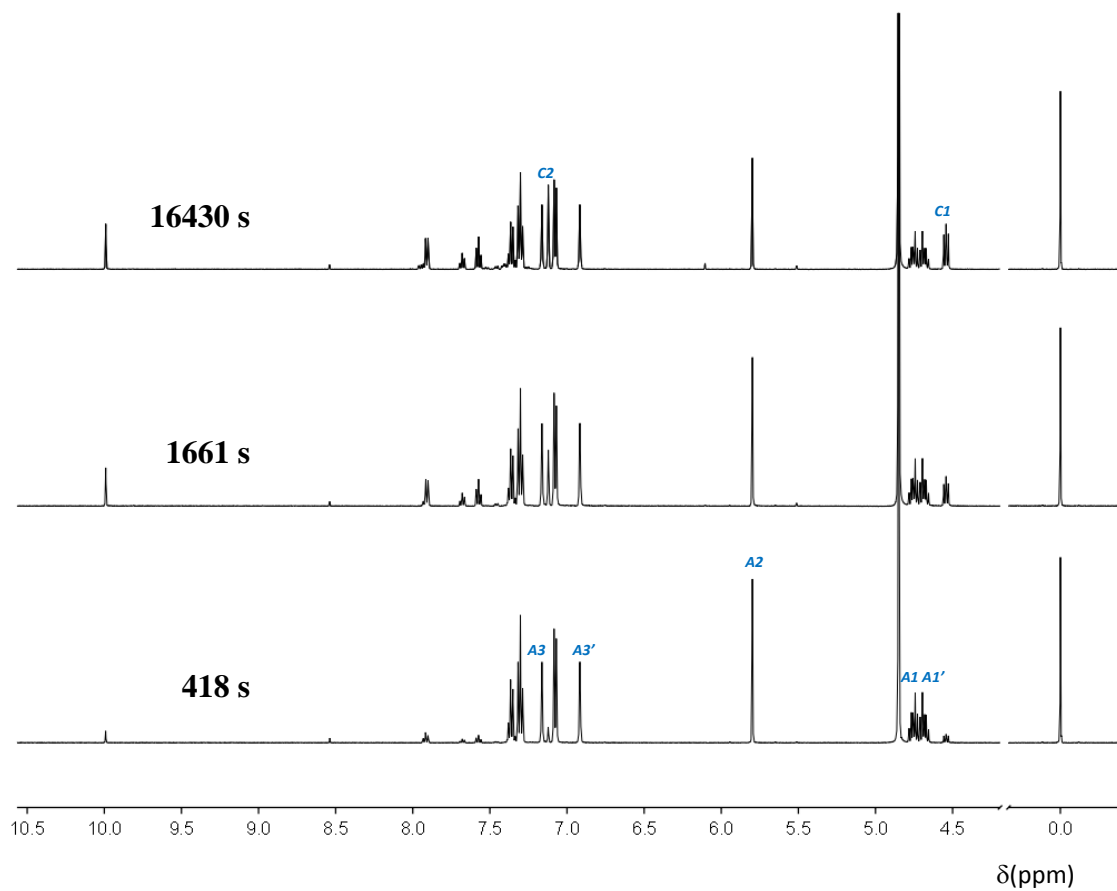
Figure 4.16: Concentration profile showing dissociation of 0.04 M adduct (271) (C(α)-L, L=H/D ●, L=H ○) to triazolium precatalyst (140) (◆) in 0.107 M NEt$_3$ and 0.053 M NEt$_3$·DCl in methanol-d$_4$ at 25 °C
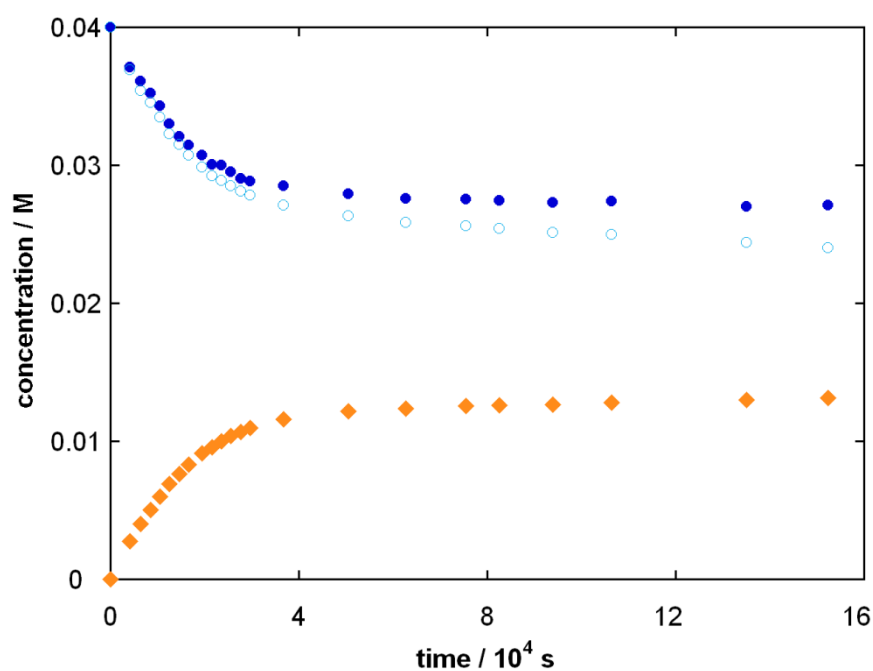
Figure 4.17: Concentration profile showing dissociation of 0.04 M adduct (271) (C(α)-L, L=H/D ●, L=H ○) to triazolium precatalyst (140) (◆) in 0.053 M NEt₃ and 0.053 M NEt₃·DCl in methanol-d₄ at 25 °C
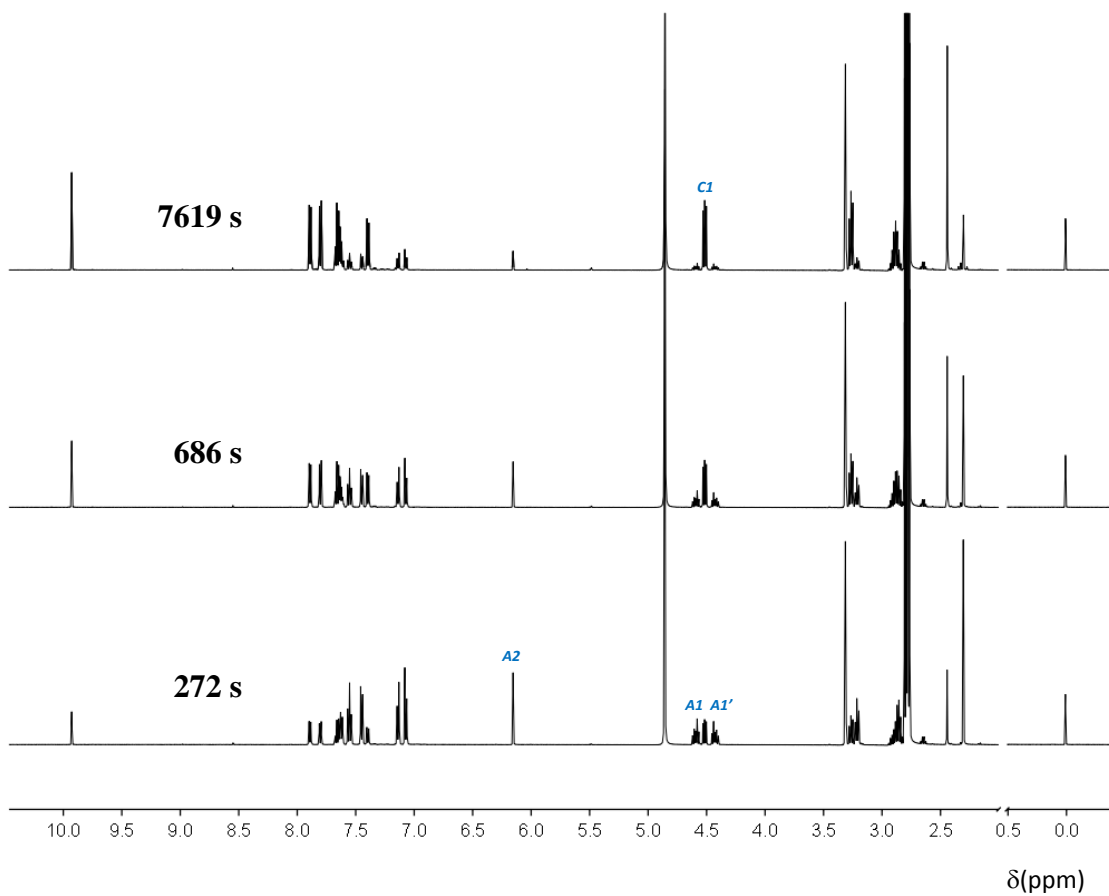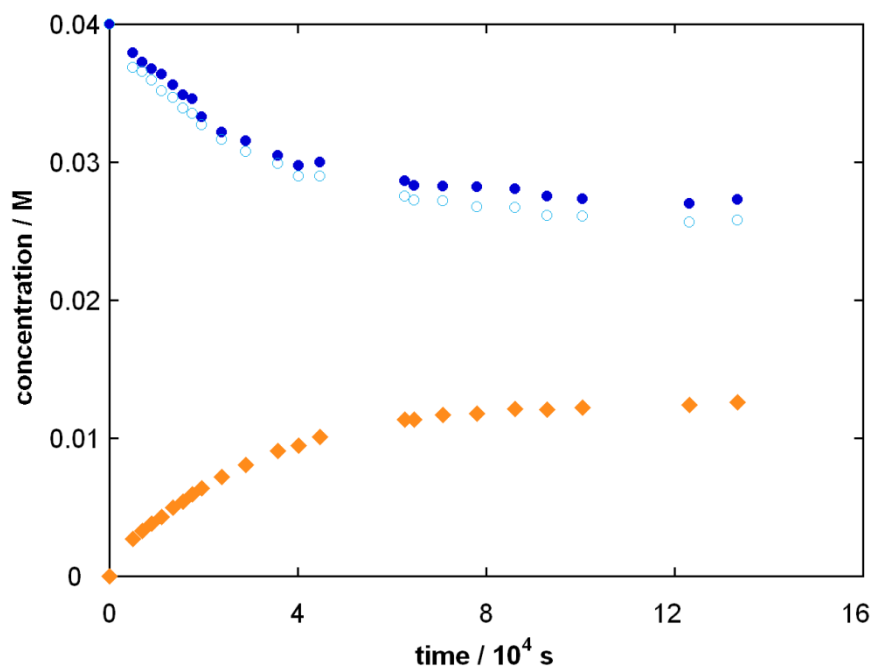

Figure 4.18: Concentration profile showing dissociation of 0.04 M adduct (271) (C(α)-L, L=H/D ●, L=H ○) to triazolium precatalyst (140) (◆) in 0.107 M NEt₃ and 0.107 M NEt₃·DCl in methanol-d₄ at 25 °C
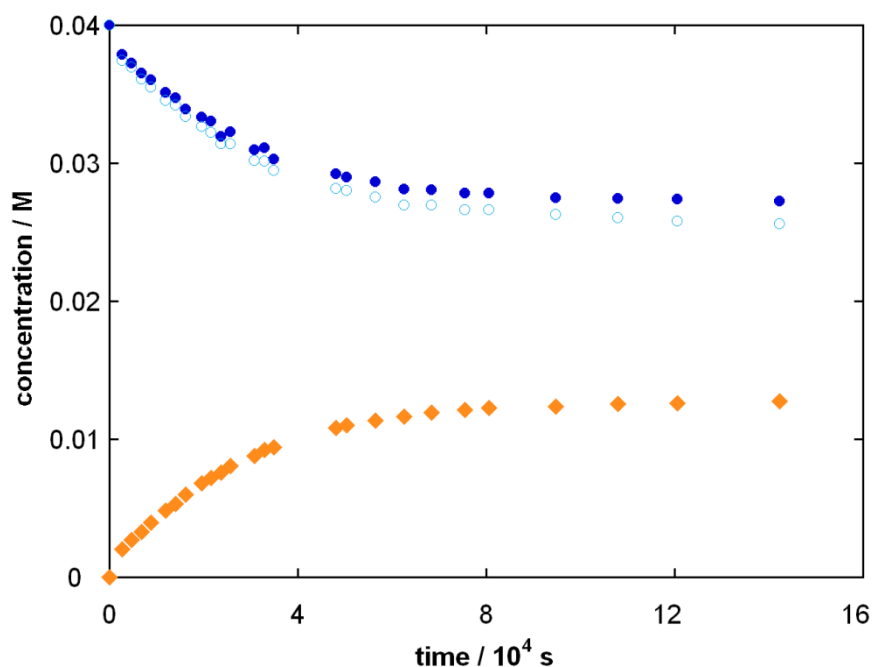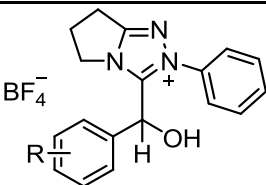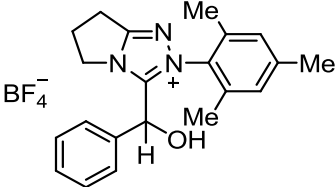
The dissociation of adduct to catalyst and benzaldehyde was observed to reach equilibrium after approximately 84 min. An equilibrium constant, K_1 (M), for the reaction shown in Scheme 4.20 was calculated from the concentrations of adduct and catalyst at equilibrium, shown by Equation 4.5. As adduct decomposition results in the formation of one molecule of benzaldehyde and one molecule of catalyst, and no significant benzoin formation was encountered, it was assumed that the equilibrium concentration of benzaldehyde corresponded to that of catalyst. The concentrations used to calculate K_1 were taken from the first point at which equilibrium had been reached (*i.e.* at 84 min).

For each set of buffer conditions, a first-order rate constant for adduct decomposition, k_d (s^{-1}) was obtained from the slope of a semilogarithmic plot of $[(ax_e + x(a - x_e))/(a(x_e - x))]$ against time (Appendix C, Figure C8).

Equilibrium constants, K_{eq} and rate constant for equilibration are summarised in Table 4.1. The inverse of K_{eq} (*i.e.* $1/K_{eq}$) gives the equilibrium constant in terms of adduct formation from aldehyde and catalyst, which will be used to compare against values obtained from fitting of the reaction profiles in Sections 4.3 and 4.4.

Table 4.1:   Summary of equilibrium constants and rate constants

substrate	buffer NEt$_3$; NEt$_3$·DCl	K_{eq}, M ^{a}	$1/K_{eq}$, M^{-1}	k_d, s$^{-1 b}$
269 R = 4-F	0.107 M; 0.053 M	**0.158**	**6.33**	1.92×10^{-3}
264 R = H	0.107 M; 0.053 M	**0.075**	**13.3**	1.21×10^{-3}
270 R = 4-Me	0.107 M; 0.053 M	**0.140**	**7.14**	1.27×10^{-3}
271 R = 2-OMe	0.107 M; 0.053 M	**0.0074**	**136**	2.76×10^{-4}
272	0.107 M; 0.053 M	**0.0056**	**180**	1.64×10^{-4}
	0.053 M; 0.053 M	**0.0053**	**189**	8.22×10^{-5}
	0.107 M; 0.107 M	**0.0056**	**179**	9.40×10^{-5}

(a) Estimated from the equilibrium concentrations of [add (tot)] and [cat], using Equation 4.5.
(b) Determined from the slope of a semilogarithmic plot of $[(ax_e + x(a - x_e))/(a(x_e - x))]$ against time using Equation 4.8.

4.3 Concentration Profiles by ^{1}H NMR Spectroscopy

The benzoin condensation was followed by ^{1}H NMR spectroscopy at stoichiometric initial concentrations of aldehyde and azolium precatalyst in triethylamine-buffered (2:1 NEt$_3$: NEt$_3$·HCl) methanol-d$_4$. These relatively large concentrations of catalyst would allow for the detection of the formation and decay of intermediates such as the proposed Breslow intermediate or 3-(hydroxyaryl)azolium adduct. Concentration profiles have been obtained for the reaction of five triazolium precatalysts **138 – 141** and **143** (0.08 M) with up to six substituted aromatic aldehydes **28**, **266 – 268**, **273** and **274** (0.08 M). The reactions of thiazolium precatalysts **53** and **151**, imidazolium precatalysts **70**, **74** and **156**, and 4,5-dihydroimidazolium precatalyst **275** (0.3 M) with benzaldehyde **28** (0.3 M) were also investigated for comparison.

Two representative methods for determining the concentration of species over the course of the reaction are shown for the self-condensation of benzaldehyde **28**, catalysed by *N*-phenyl triazolium salt **139** and thiazolium salt **53**.

4.3.1 2-Phenyl-6,7-dihydro-5*H*-pyrrolo[2,1-c][1,2,4]triazol-3-ium tetrafluoroborate (139) and benzaldehyde (28)
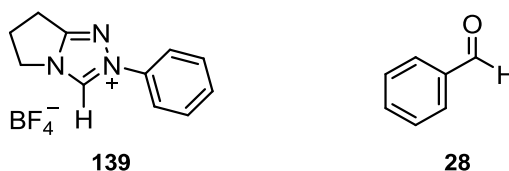
A 0.75 mL solution of triazolium salt **139** (0.08 M), NEt$_3$ (0.107 M), NEt$_3$·HCl (0.053 M), in methanol-d$_4$ (containing 0.01% TMS) was transferred to an NMR tube. The reaction was initiated by addition of benzaldehyde **28** (0.08 M, 6.1 μL) and inverted to ensure complete mixing. The reaction was thermostated at 25 °C directly in the NMR instrument. At regular intervals over the course of the reaction the composition of the solution was analysed by ^{1}H NMR spectroscopy (duration of acquisition ~4 min). A concentration of 0.08 M was chosen as this was close to the limit of solubility for the catalyst. A representative set of spectra taken at three time points during the reaction is shown in Figure 4.19.

Figure 4.19: Representative ^{1}H NMR spectra at 500 MHz showing progress of the benzoin condensation of benzaldehyde (28), catalysed by triazolium salt (139), in triethylamine buffered methanol-d_4 at 25 °C
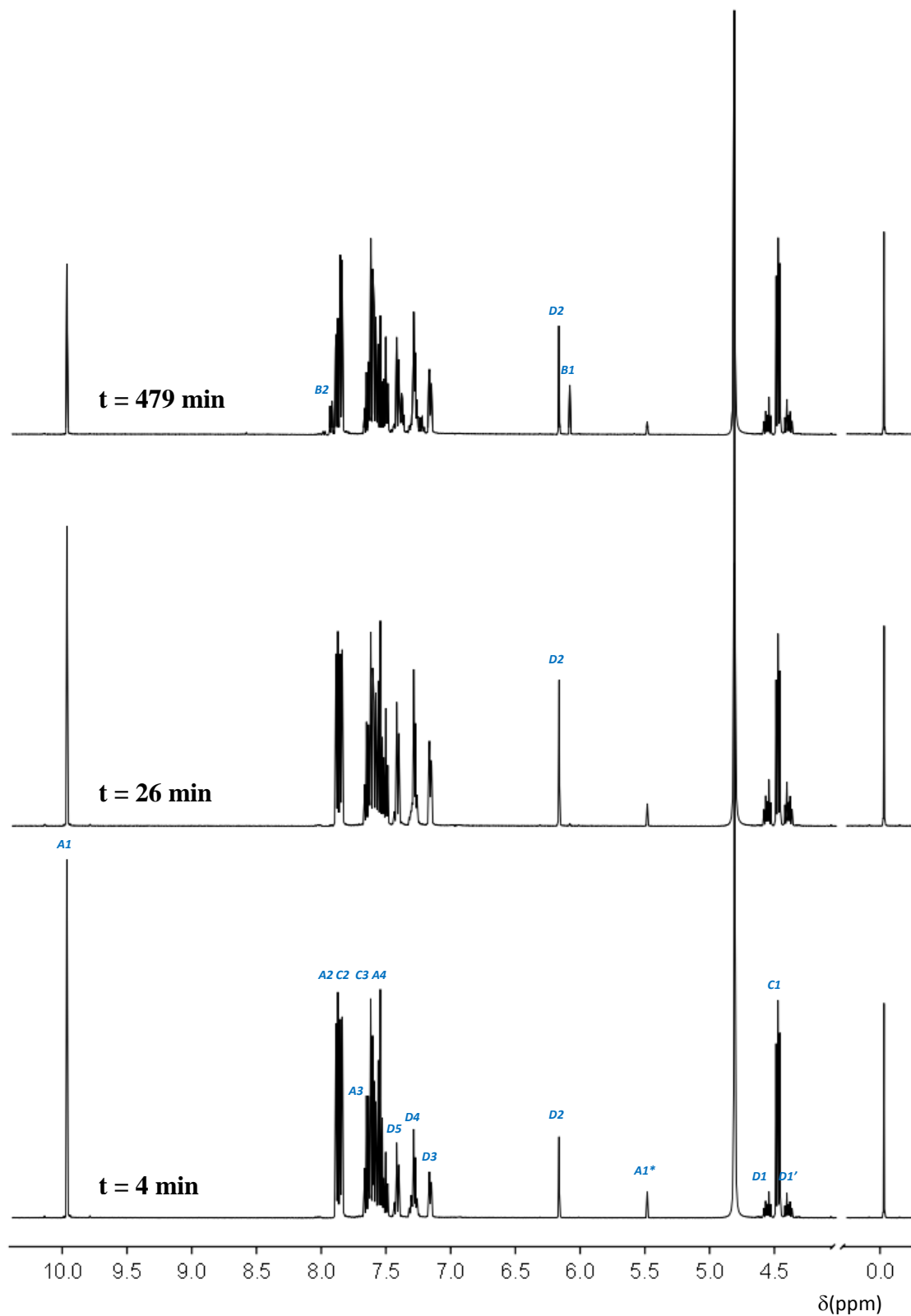
In triethylamine-buffered methanol-d$_4$, the C(3)-H on the triazolium ion rapidly undergoes H/D-exchange to give precatalyst **139'**. Upon addition of benzaldehyde **28**, signals corresponding to the triazolium precatalyst and aldehyde decreased, and signals consistent with the 3-(hydroxybenzyl)triazolium adduct **264**, appeared (spectroscopic evidence for this and other substituted adduct species were presented in the previous section). Under these conditions, the only intermediate detected by ^{1}H NMR was the adduct **264** – no other intermediates were observed. Formation of benzoin **34** was observed at later time points.

A mechanistic pathway for the benzoin condensation in methanol-d$_4$, catalysed by a generic triazolium species **144'** is proposed in Scheme 4.21. From the decomposition experiments described in the previous section, adduct formation is reversible for both the *N*-phenyl and *N*-mesityl substituted triazolium precatalysts **139** and **140**. Although the Breslow intermediate **277** was not observed directly in any of the reactions, the formation of deuterated adduct **276D** and deuterated aldehyde **23D** in several cases, provide indirect evidence that the reaction proceeds *via* the Breslow intermediate **277**. The integrals of various ^{1}H NMR signals corresponding to protons on these species were used to determine the concentrations of each species, analogous to the treatment described below for the reaction of *N*-phenyl triazolium salt **139** with benzaldehyde **28**.

Scheme 4.21:
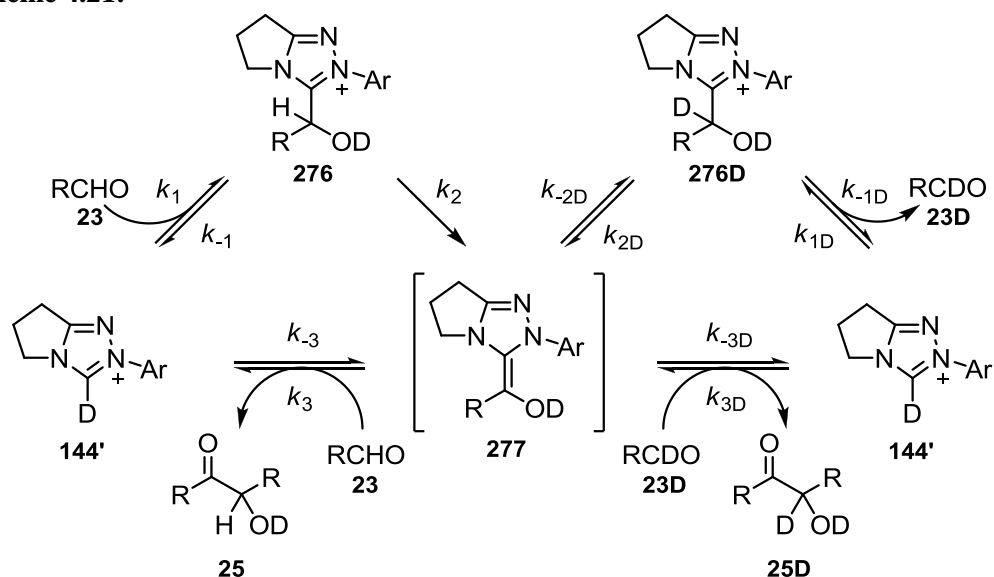
The triplet signal at 4.50 ppm (**C1**), corresponding to the pair of CH_2 protons on the five membered ring (adjacent to the N(4) atom) was used to calculate the concentration of precatalyst (Equation 4.9). Signals corresponding to the other CH_2 peaks on the five-membered ring could not be used, as these overlapped with signals corresponding to the triethylamine buffer. The doublet at 7.87 ppm (**C2**) and triplet at 7.78 ppm (**C3**) assigned to the two pairs of *ortho-* and *meta*-protons on the catalyst phenyl ring integrated equivalently to the **C1** triplet throughout the duration of the experiment. For the majority of the triazolium ion-catalysed reactions these aryl signals were not used to calculate catalyst concentrations, with the exception of the *N*-mesityl triazolium ion-catalysed reaction.

$$[\text{catalyst}] = \frac{(A_{C1}/2)}{((A_{C1}+A_{D1}+A_{D1'})/2)} \times 0.08 \qquad \textbf{Equation 4.9}$$

Upon initiation of the reaction, two multiplet signals at 4.42 (**D1**) and 4.58 ppm (**D1'**) appeared in the ^1H NMR spectrum. The preparation of several 3-(hydroxybenzyl)triazolium adducts allow us to assign these signals to the CH_2 protons adjacent to the N(4) position. In other words, the catalyst CH_2 signal **C1** is split into two diasterotopic signals **D1** and **D1'** upon formation of the adduct. As the triazolium species was present in solution only as the free triazolium precatalyst **139D** or the 3-(hydroxybenzyl)triazolium adduct **264** (or **264D**), the sum of these integrals at any time during the reaction must correspond to the concentration of precatalyst present initially (*i.e.* 0.08 M). Thus, the sum of the integrals for **D1** and **D1'** was used to calculate the concentration of total 3-(hydroxybenzyl)triazolium adduct in solution, relative to the sum of **D1**, **D1'** and **C1**, which corresponded to the total concentration of triazolium species in adduct and precatalyst form (Equation 4.10).

$$[\text{adduct (tot)}] = \frac{((A_{D1}+A_{D1'})/2)}{((A_{C1}+A_{D1}+A_{D1'})/2)} \times 0.08 \qquad \textbf{Equation 4.10}$$

The singlet at 6.11 ppm (**D2**) corresponds to the exchangeable $C(\alpha)$-H on the adduct **264**. Using this signal, the concentration of protonated adduct **264** was determined relative to the sum of the integrals of signals **D1**, **D1'** and **C1** (Equation 4.11). Furthermore, the concentration of deuterated adduct **264D** was gleaned from the difference in concentration between the total and protonated species (Equation 4.12).

$$[\text{adduct (H)}] = \frac{A_{D2}}{((A_{C1}+A_{D1}+A_{D1\prime})/2)} \times 0.08 \qquad \textbf{Equation 4.11}$$

$$[\text{adduct (D)}] = [\text{adduct (tot)}] - [\text{adduct(H)}] \qquad \textbf{Equation 4.12}$$

Benzaldehyde **28**, along with all of the other aromatic aldehydes used in these experiments, exists in equilibrium with its methanol adduct or hemiacetal **265** (Scheme 4.13). A singlet at 5.52 ppm (**A1***) corresponding to the hemiacetal proton is present in methanolic solutions of benzaldehyde, and under our reaction conditions. Additionally, an analogous set of hemiacetal phenyl signals are observed in the aromatic region. By contrast, benzoin does not exist in equilibrium with a methanol adduct.

From the ratio of integrals of the aldehyde and hemiacetal proton, values for the equilibrium coefficient K_{add} and the fraction of aldehyde present f_{ald}, were determined by application of Equations 4.13 and 4.14. This data is summarised in Table 4.2.

$$K_{\text{add}} = \frac{A_{A1*}}{A_{A1}} = \frac{[\text{hemiacetal}]}{[\text{aldehyde}]} \qquad \textbf{Equation 4.13}$$

$$f_{\text{ald}} = \frac{A_{A1*}}{(A_{A1*}+A_{A1})} = \frac{[\text{aldehyde}]}{([\text{aldehyde}]+[\text{hemiacetal}])} \qquad \textbf{Equation 4.14}$$

Table 4.2:   **Equilibrium constants for aldehyde hydrate formation**

aldehyde		K_{add}	f_{ald}
	266 R = 4-F	0.103	0.907
	28 R = H	0.095	0.913
	267 R = 4-Me	0.040	0.962
	273 R = 4-OMe	0.010	0.990
	274 R = 2-Me	0.083	0.923
	268 R = 2-OMe	0.064	0.940

In order to create an accurate description of speciation over time, a correction should be made for f_{ald} in the case of each aldehyde concentration. In Leeper's studies of the thiazolium ion-catalysed benzoin condensation, the authors did not make a correction for this equilibrium. The proportions of total aldehyde and benzoin were calculated from the doublet signals at 7.91 (*A2*) and 7.95 ppm (*B2*) corresponding to the *ortho*-aryl CH protons, and converted to concentrations relative to the sum of the *D1*, *D1'* and *C1* signals. Triplet signals at 7.68 (*A3*) and 7.57 ppm (*A4*) corresponding to the *para*- and *meta*-aryl CH protons on benzaldehyde were not used to calculate concentrations over the course of the reaction in this instance, however, for some aldehyde and precatalyst combinations, *A3* and *A4* signals were used to obtain concentrations where signal overlap restricted the use of the *ortho- C2* signal.

Concentrations of protonated benzaldehyde **28** and benzoin **34** were determined from the singlet signals at 9.99 (*A1*) and 6.11 ppm (*B1*) corresponding to the aldehydic hydrogen and the C(α)-H on benzoin. Concentrations of deuterated species **28D** and **34D** were determined from the difference in concentration between total and protonated species. Equations 4.15 – 4.20 summarise how these concentrations were calculated.

$$[\text{aldehyde (tot)}] = \frac{1}{f_{ald}} \times \frac{(A_{A2}/2)}{((A_{C1}+A_{D1}+A_{D1'})/2)} \times 0.08 \qquad \textbf{Equation 4.15}$$

$$[\text{aldehyde (H)}] = \frac{1}{f_{ald}} \times \frac{A_{A1}}{((A_{C1}+A_{D1}+A_{D1'})/2)} \times 0.08 \qquad \textbf{Equation 4.16}$$

$$[\text{aldehyde (D)}] = [\text{aldehyde (tot)}] - [\text{aldehyde(H)}] \qquad \textbf{Equation 4.17}$$

$$[\text{benzoin (tot)}] = \frac{(A_{B2}/2)}{((A_{C1}+A_{D1}+A_{D1'})/2)} \times 0.08 \qquad \textbf{Equation 4.18}$$

$$[\text{benzoin (H)}] = \frac{A_{B1}}{((A_{C1}+A_{D1}+A_{D1'})/2)} \times 0.08 \qquad \textbf{Equation 4.19}$$

$$[\text{benzoin (D)}] = [\text{benzoin (tot)}] - [\text{benzoin (H)}] \qquad \textbf{Equation 4.20}$$

4.3.2 3-Benzyl-5-(2-hydroxyethyl)-4-methylthiazol-2-ium chloride (53) and benzaldehyde (28)
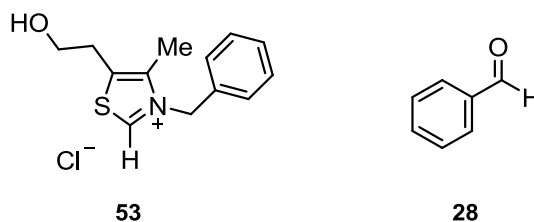
A 0.75 mL solution of thiazolium salt **53** (0.3 M), NEt$_3$ (0.107 M), NEt$_3$·HCl (0.053 M), in methanol-d$_4$ (containing 0.01% TMS) was transferred to an NMR tube. The reaction was initiated by addition of benzaldehyde **28** (0.3 M, 23 μL) and inverted to ensure complete mixing. The reaction was thermostated at 25 °C directly in the NMR instrument. At regular intervals over the course of the reaction the composition of the solution was analysed by ^{1}H NMR spectroscopy (duration of acquisition ~4 min). A concentration of 0.3 M was chosen to compare against similar experiments performed by Leeper. A representative set of spectra taken at three time points during the reaction is shown in Figure 4.20.

The integrals of various ^{1}H NMR signals corresponding to protons on these species were used to determine the concentrations of each species, according to the treatment described below.

In triethylamine buffered methanol-d$_4$, the C(2)-H on the thiazolium ion rapidly exchanges to give precatalyst **53'**. Upon addition of aldehyde, signals corresponding to the thiazolium precatalyst and aldehyde decreased, and signals consistent with the 3-(hydroxybenzyl)thiazolium adduct **278** appeared. The identity of this species was confirmed using an independently prepared sample based on a literature procedure.[24] As with the triazolium precatalysts described earlier, the only intermediate detected by ^{1}H NMR was the adduct **278** – no other intermediates were observed under our conditions. Formation of benzoin was observed at later time points.

Figure 4.20: Representative ^{1}H NMR spectra at 500 MHz showing progress of the benzoin condensation of benzaldehyde (28), catalysed by thiazolium salt (53), in triethylamine buffered methanol-d$_4$ at 25 °C
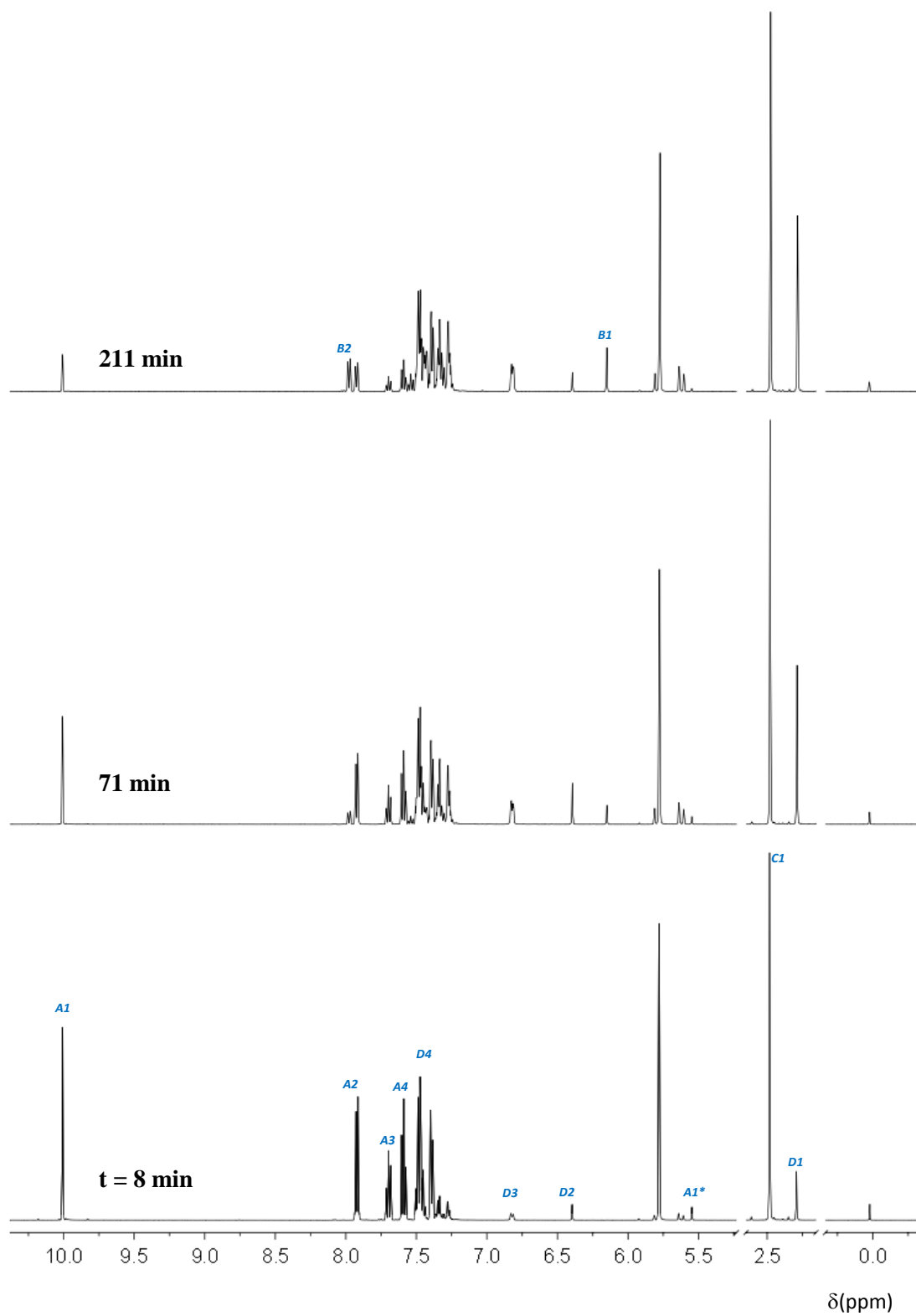
A mechanistic pathway for the benzoin condensation in methanol-d$_4$, catalysed by thiazolium species **53** is proposed in Scheme 4.22. This scheme is identical to that employed by Leeper in his studies of the analogous bromide salt **247**. Decomposition studies of the thiazolium adduct **278** have been undertaken by our laboratory, and show that adduct formation is reversible. Although the Breslow intermediate is not observed directly, the formation of significant amounts of deuterated adduct **278D** and deuterated benzaldehyde **28D**, provide indirect evidence that the reaction proceeds *via* the Breslow intermediate **279**. The integrals of various ^{1}H NMR signals corresponding to protons on these species were used to determine the concentrations of each species, according to the treatment described below.

Scheme 4.22:
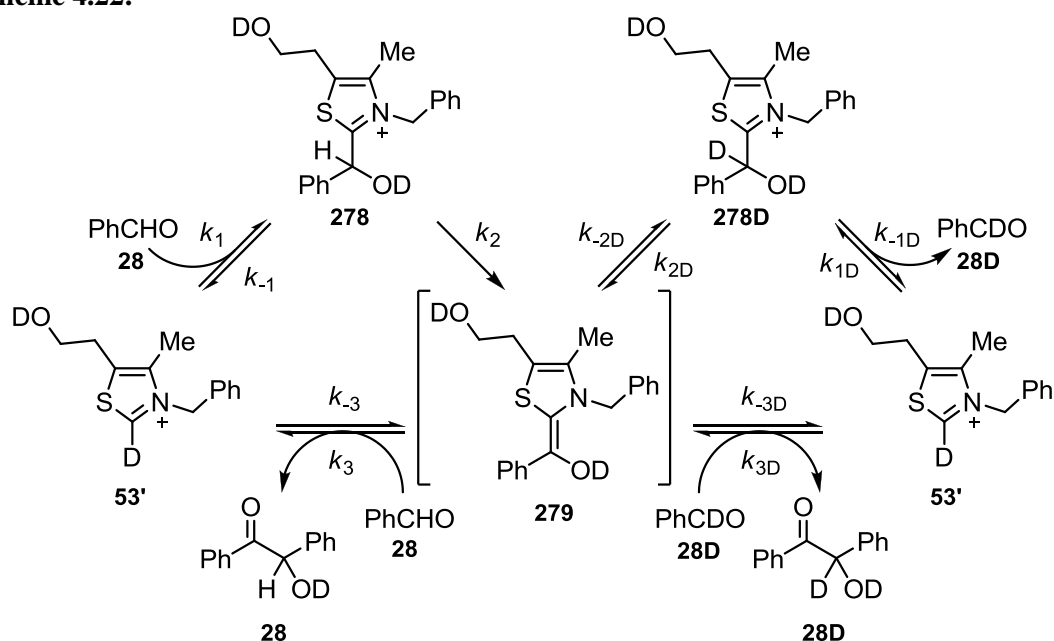
The singlet signals at 2.49 (***C1***) and 2.29 ppm (***D1***), corresponding to the 4-methyl substituent on the thiazolium ring of the free precatalyst and adduct, respectively, were used to calculate the concentration of precatalyst (Equation 4.21) and adduct (Equation 4.22). As the thiazolium species was present in solution only as the free precatalyst **53** or the 3-(hydroxybenzyl)thiazolium adduct **278**, the sum of these integrals at any time during the reaction must correspond to the concentration of precatalyst present initially (*i.e.* 0.3 M). Accordingly, these peaks were used to calculate the concentrations of the various species over the course of the reaction.

$$[\text{catalyst}] = \frac{(A_{C1}/3)}{((A_{C1}+A_{D1})/3)} \times 0.3 \qquad \textbf{Equation 4.21}$$

$$[\text{adduct (tot)}] = \frac{(A_{D1}/3)}{((A_{C1}+A_{D1})/3)} \times 0.3 \qquad \textbf{Equation 4.22}$$

The singlet at 6.40 ppm (**D2**) corresponds to the exchangeable C(α)-H on the adduct. Using this signal, the concentration of protonated adduct **278** was determined relative to the sum of the integrals of signals **D1** and **C1** (Equation 4.23). The concentration of deuterated adduct **278D** was calculated from the difference in concentration between the total and protonated species (Equations 4.24).

$$[\text{adduct (H)}] = \frac{A_{D2}}{((A_{C1}+A_{D1})/3)} \times 0.3 \qquad \textbf{Equation 4.23}$$

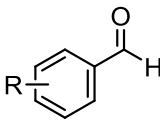$$[\text{adduct (D)}] = [\text{adduct (tot)}] - [\text{adduct(H)}] \qquad \textbf{Equation 4.24}$$

The concentrations of total benzaldehyde **28** and benzoin **34** over the course of the reaction were obtained in a similar manner to that described for the reaction catalysed by 2-phenyl-6,7-dihydro-5*H*-pyrrolo[2,1,c][1,2,4]triazol-3-ium tetrafluoroborate **1**. The *ortho*-aryl CH signals at 7.91 (**A2**) and 7.95 ppm (**B2**) were used to calculate concentrations of total aldehyde and benzoin respectively, relative to the integrated areas of signals **C1** and **D1**, and correcting for the fraction of hydrate in the case of benzaldehyde. Concentrations of protonated aldehyde and benzoin were determined from the singlet signals at 9.99 (**A1**) and 6.11 ppm (**B1**) respectively. Concentrations of deuterated species **28D** and **34D** were calculated from the difference between the concentrations of total and protonated species. Equations 4.25 – 4.30 summarise how these concentrations were calculated.

$$[\text{aldehyde (tot)}] = \frac{1}{f_{\text{ald}}} \times \frac{(A_{A2}/2)}{((A_{C1}+A_{D1})/3)} \times 0.3 \qquad \textbf{Equation 4.25}$$

$$[\text{aldehyde (H)}] = \frac{1}{f_{\text{ald}}} \times \frac{A_{A1}}{((A_{C1}+A_{D1})/3)} \times 0.3 \qquad \textbf{Equation 4.26}$$

$$[\text{aldehyde (D)}] = [\text{aldehyde}]_{\text{tot}} - [\text{aldehyde(H)}] \qquad \textbf{Equation 4.27}$$

$$[\text{benzoin (tot)}] = \frac{(A_{B2}/2)}{((A_{C1}+A_{D1})/3)} \times 0.3 \qquad \textbf{Equation 4.28}$$
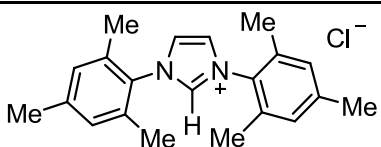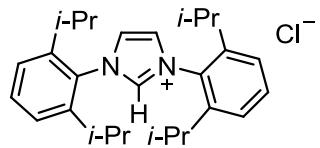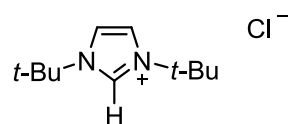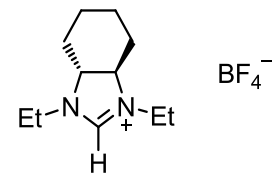
$$[\text{benzoin (H)}] = \frac{A_{B1}}{((A_{C1}+A_{D1})/3)} \times 0.3 \qquad \textbf{Equation 4.29}$$

$$[\text{benzoin (D)}] = [\text{benzoin (tot)}] - [\text{benzoin(H)}] \qquad \textbf{Equation 4.30}$$

4.3.3 Reactions of imidazolium and 4,5-dihydroimidazolium precatalysts

The reactions of a sample of imidazolium and 4,5-dihydroimidazolium precatalysts (0.3 M) with benzaldehyde (0.3 M) were studied in triethylamine-buffered (0.107 M NEt$_3$, 0.053 NEt$_3$·HCl) methanol-d$_4$. These reactions were initiated in the manner described previously for thiazolium precatalyst **53**. The outcomes of these reactions are summarised in Table 4.3, alongside aqueous pK_a values, where available.[25] These reactions were substantially less reactive than the triazolium and thiazolium-catalysed reactions, presumably as a result of the markedly lower concentration of NHC present in solution due to the reduced acidity of the azolium ion. Concentration profiles were not generated in these cases.

Table 4.3: Observations for the reactions of imidazolium and 4,5-dihydroimidazolium precatalysts (0.3 M) with benzaldehyde (0.3 M) in triethylamine buffered methanol-d$_4$

	catalyst	pK_a (aq.)	observations
70		**20.8**	Fully exchanged at t = 1 Adduct formation observed No benzoin formation after 24 h
74		**21.1**	Fully exchanged at t = 1 No adduct formation after 24 h No benzoin formation after 24 h
156		**25.2**	Slow C(2)-H exchange over 4 h No adduct formation after 4 h No benzoin formation after 4 h
275		**n.d.**	Fully exchanged at t = 1 No adduct formation after 4 h No benzoin formation after 4 h

4.3.3   Concentration profiles

As representative examples, concentration profiles for the self-condensation of benzaldehyde are shown for the reactions catalysed by *N*-phenyl and *N*-mesityl substituted triazolium precatalysts **139** (Figure 4.21) and **140** (Figure 4.22), and *N*-benzyl and *N*-mesityl substituted thiazolium precatalysts **53** (Figure 4.23) and **151** (Figure 4.24). Profiles for all other reactions are presented in Appendix B.

For all reactions, the starting concentration of aldehyde used in the profiles was adjusted to reflect the slight variation from the 'true' concentration of 0.08 M due to experimental error in adding aldehyde to the reaction. In other words, the difference between aldehyde and catalyst concentration at the first measurement point t = 1 was used to correct the aldehyde concentration at t = 0. Catalyst concentration at t = 0 was kept constant at 0.08 M or 0.3 M. In all cases this difference was small and no more than ±5% of the expected starting concentration.

Figure 4.21: **Concentration profile for the self-condensation of benzaldehyde (28) (0.08 M), catalysed by *N*-phenyl triazolium precatalyst (139) (0.08 M), in 0.107 M NEt$_3$ and 0.107 M NEt$_3$·DCl in methanol-d$_4$**
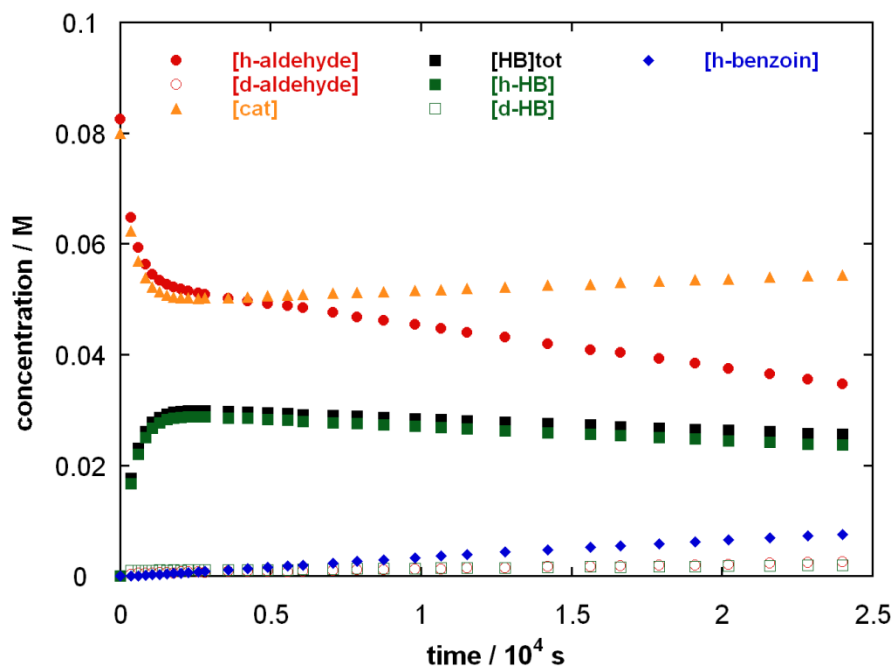
Figure 4.22: **Concentration profile for the self-condensation of benzaldehyde (28) (0.08 M), catalysed by *N*-mesityl triazolium precatalyst (140) (0.08 M), in 0.107 M NEt$_3$ and 0.107 M NEt$_3$·DCl in methanol-d$_4$**
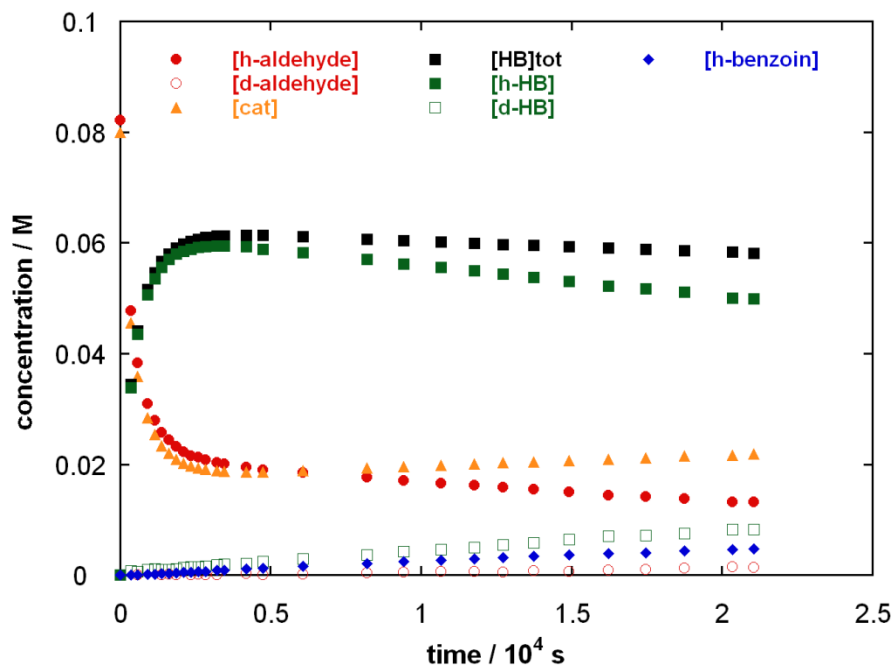
Figure 4.23: **Concentration profile for the self-condensation of benzaldehyde (28) (0.30 M), catalysed by thiazolium precatalyst (53) (0.30 M), in 0.107 M NEt₃ and 0.107 M NEt₃·DCl in methanol-d₄**
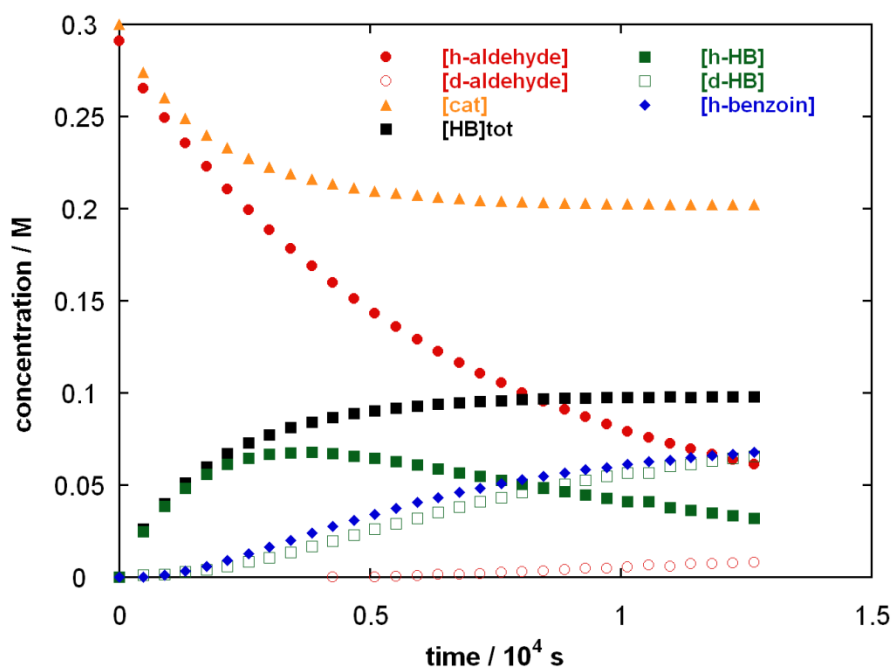
Figure 4.24: **Concentration profile for the self-condensation of benzaldehyde (28) (0.3 M), catalysed by thiazolium precatalyst (151) (0.3 M), in 0.107 M NEt₃ and 0.107 M NEt₃·DCl in methanol-d₄**
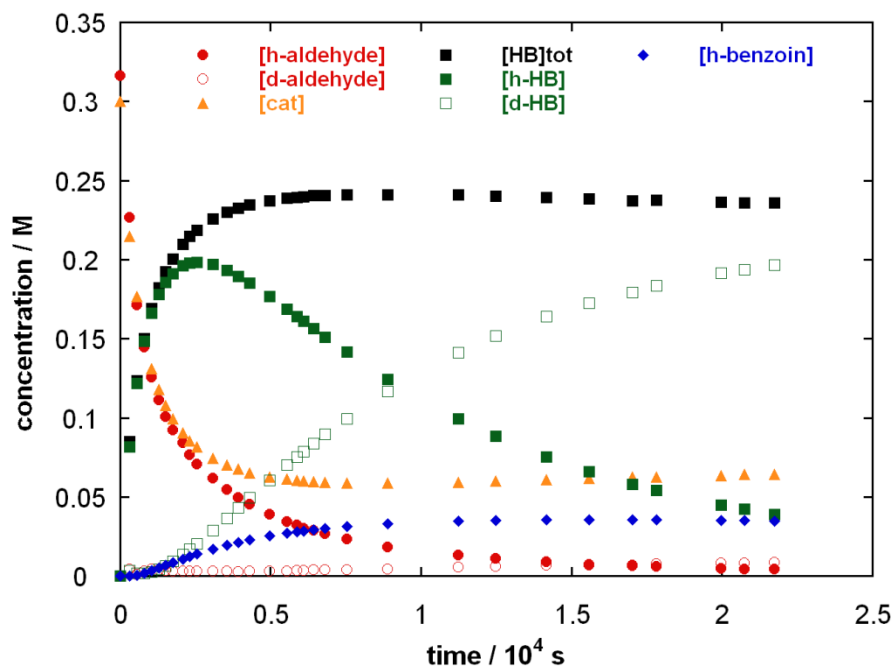
4.4 Determination of Rate Constants for Individual Steps

4.4.1 Triazolium precatalysts: Determination of k_1, k_{-1} and K_1

Scheme 4.23:
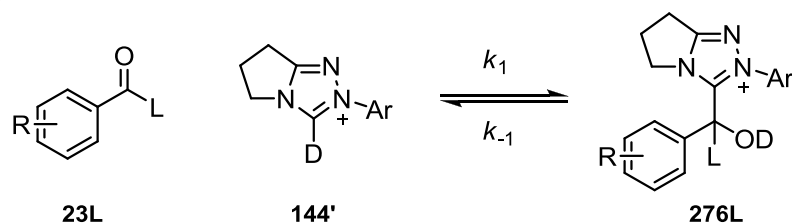
According to Scheme 4.23, a second-order rate constant for adduct formation from precatalyst and aldehyde, k_1 (M^{-1} s^{-1}), may be obtained from the consumption of catalyst in the period leading to equilibrium, where onward benzoin formation is negligible. The expression for the consumption of catalyst is given in Equation 4.31, which may be rewritten as Equation 4.32 (where [cat] = [ald]).

$$\frac{d[\text{cat}]}{dt} = -k_1[\text{cat}][\text{ald}] + k_{-1}[\text{add}]$$ **Equation 4.31**

$$\frac{d[\text{cat}]}{dt} = -k_1[\text{cat}]^2 + k_1 \frac{[\text{cat}]_e^2}{([\text{cat}]_0 - [\text{cat}]_e)}([\text{cat}]_0 - [\text{cat}])$$ **Equation 4.32**

If the initial concentrations are $[\text{add}]_0 = 0$ and $[\text{cat}]_0 = [\text{ald}]_0 = b$, then Equation 4.33 may be integrated to give the rate equation shown in Equation 4.33, where $y = ([\text{cat}]_0 - [\text{cat}]) = ([\text{ald}]_0 - [\text{ald}])$ and $y_e = ([\text{cat}]_0 - [\text{cat}]_e) = ([\text{ald}]_0 - [\text{ald}]_e)$. Thus, a value of k_1 may be obtained from the slope of a semilogarithmic plot of $(y_e(b^2 - yy_e)/(b^2(y_e - y))$ against time, using the concentration of catalyst in the approach towards equilibrium.

$$\frac{y_e}{(b^2 - y_e^2)} \ln \frac{y(b^2 - yy_e)}{b^2(y_e - y)} = k_1 t$$ **Equation 4.33**

Plots for the reaction of the *N*-phenyl triazolium catalyst with a variety of substituted benzaldehyde substrates are shown in Figure 4.25. Similar plots for reactions of other catalysts are shown in Appendix C. These plots were linear and were followed over the first three half-lives. Values of k_1 obtained by this method are summarised in Table 4.4.

Figure 4.25: Semilogarithmic plots of $[y_e(b^2 - yy_e)/(b^2(y_e - y))]$ against time for the reactions of a range of substituted aromatic aldehydes with *N*-phenyl triazolium precatalyst (**139**)
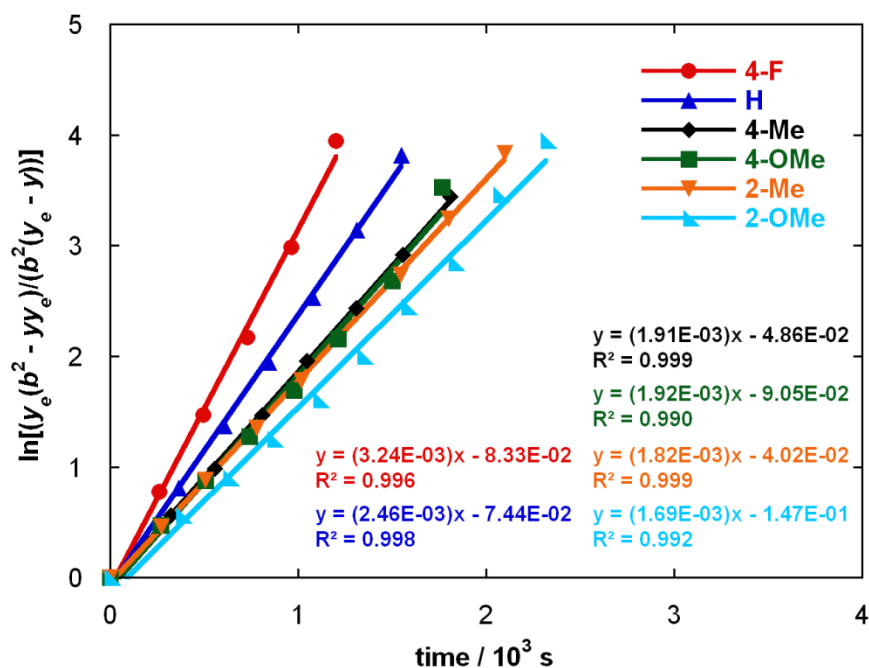
Values of k_d obtained in the studies of adduct decomposition to free catalyst and aldehyde in the previous section provide an alternative estimate of the first-order rate constant for decomposition of adduct to starting materials, k_{-1} (s^{-1}), expressed by Equation 4.34. By combining these values of k_1 and k_{-1} in Equation 4.35, equilibrium constants for adduct formation, K_1 (M^{-1}), may be obtained. This value will be termed K_1^{calc} to distinguish it from other methods that will subsequently be used to estimate K_1. These rate constants and equilibrium constants are summarised in Table 4.4.

$$k_d = k_{-1} \qquad \qquad \textbf{Equation 4.34}$$

$$K_1 = \frac{k_1}{k_{-1}} \qquad \qquad \textbf{Equation 4.35}$$

Rate constants k_1 and k_{-1} were also estimated by fitting the concentrations of catalyst, total aldehyde and total adduct in the time period leading up to equilibrium using global fitting software (Berkeley Madonna, Version 8.3.18). The rate equation used in the fitting model, which is based on Scheme 4.23, is given in Equation 4.36. The values of k_1 and k_{-1} shown in Table 4.4 were used as starting estimates in the software, but even when these starting figures were changed, consistent output values were recorded.
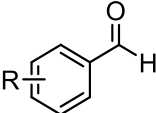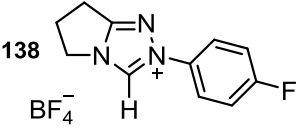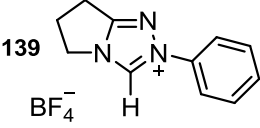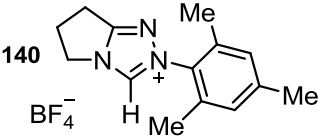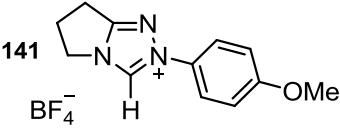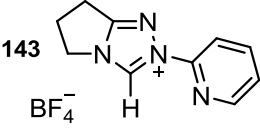
$$\frac{d[\text{add (tot)}]}{dt} = k_1[\text{ald (tot)}][\text{cat}] - k_{-1}[\text{add (tot)}] \qquad \textbf{Equation 4.36}$$

Values of K_1^{fit} were obtained from the values of k_1 and k_{-1} obtained from the fitting software using Equation 4.35.

Finally, alternative estimates of K_1^{con} were obtained from the concentrations of total adduct, total aldehyde and catalyst at equilibrium according to Equation 4.37. Rate constants k_1 and k_{-1}, and equilibrium constants K_1^{fit} and K_1^{con} are summarised in Table 4.4.

$$K_1^{\text{con}} = \frac{[\text{add (tot)}]_e}{[\text{cat}]_e \times [\text{ald (tot)}]_e}$$

Equation 4.37

Table 4.4: **Rate constants and equilibrium constants for step 1 determined by 'manual' fitting**

catalyst	aldehyde	k_1, M^{-1} s^{-1} [a]	k_{-1}, s^{-1} [b]	K_1^{calc}, M^{-1} [c]
138	**266** R = 4-F	3.39×10^{-2}	-	-
	28 R = H	2.83×10^{-2}	-	-
	267 R = 4-Me	1.70×10^{-2}	-	-
139	**266** R = 4-F	1.29×10^{-2}	1.92×10^{-3}	**6.72**
	28 R = H	1.33×10^{-2}	1.21×10^{-3}	**11.0**
	267 R = 4-Me	6.71×10^{-3}	1.27×10^{-3}	**5.28**
	273 R = 4-OMe	2.86×10^{-3}	-	-
	274 R = 2-Me	1.15×10^{-2}	-	-
	268 R = 2-OMe	3.44×10^{-2}	2.76×10^{-4}	**115**
140	**266** R = 4-F	3.83×10^{-2}	-	-
	28 R = H	3.29×10^{-2}	1.64×10^{-4}	**201**
	267 R = 4-Me	1.62×10^{-2}	-	-
141	**266** R = 4-F	8.79×10^{-3}	-	-
	28 R = H	9.11×10^{-3}	-	-
	267 R = 4-Me	4.76×10^{-3}	-	-
143	**28** R = H	1.10×10^{-2}	-	-

(a) Obtained from the slope of a semilogarithmic plot of $(y_e(b^2 - yy_e)/(b^2(y_e - y))$ against time using Equation 4.33. (b) Values of k_d (s^{-1}) obtained from fitting the decomposition of adduct in Table 4.1 are re-quoted as values of k_{-1} (s^{-1}) in Table 4.4. (c) Calculated from values of k_1 (M^{-1} s^{-1}) and k_{-1} (s^{-1}) in Table 4.4.

Table 4.5: Rate constants and equilibrium constants for step 1, determined from fitting up to equilibrium, and from equilibrium concentrations

catalyst	aldehyde	k_1, M⁻¹ s⁻¹ [a]	k_{-1}, s⁻¹ [a]	K_1^{fit}, M⁻¹ [b]	K_1^{con}, M⁻¹ [c]
138	**266** R = 4-F	3.11×10^{-2}	3.70×10^{-3}	**8.41**	**8.58**
	28 R = H	2.59×10^{-2}	1.65×10^{-3}	**15.7**	**15.5**
	267 R = 4-Me	1.57×10^{-2}	1.84×10^{-3}	**8.53**	**8.52**
139	**266** R = 4-F	1.11×10^{-2}	1.60×10^{-3}	**6.91**	**6.88**
	28 R = H	1.16×10^{-2}	1.01×10^{-3}	**11.5**	**11.4**
	267 R = 4-Me	6.22×10^{-3}	1.01×10^{-3}	**6.16**	**6.02**
	273 R = 4-OMe	2.59×10^{-3}	1.32×10^{-3}	**1.96**	**1.92**
	274 R = 2-Me	1.07×10^{-2}	7.03×10^{-4}	**15.2**	**14.7**
	268 R = 2-OMe	2.78×10^{-2}	2.26×10^{-4}	**123**	**118**
140	**266** R = 4-F	2.73×10^{-2}	2.61×10^{-4}	**105**	**86.8**
	28 R = H	2.76×10^{-2}	1.64×10^{-4}	**168**	**160**
	267 R = 4-Me	1.45×10^{-2}	1.47×10^{-4}	**98.6**	**89.0**
141	**266** R = 4-F	7.12×10^{-3}	6.32×10^{-4}	**11.3**	**10.8**
	28 R = H	7.92×10^{-3}	4.42×10^{-4}	**17.9**	**17.0**
	267 R = 4-Me	4.39×10^{-3}	4.38×10^{-4}	**10.0**	**9.95**
143	**28** R = H	1.06×10^{-2}	9.64×10^{-4}	**11.0**	**10.7**

(a) Obtained by global fitting according to Equation 4.36, using concentrations of [add (tot)], [ald (tot)] and [cat]. (b) Calculated using values of k_1 and k_{-1} in Table 4.5. (c) Estimated from equilibrium concentrations of [add (tot)], [ald (tot)] and [cat] using Equation 4.37.

4.4.2 Triazolium precatalysts: Determination of k_2 and the partitioning ratio k_3/k_{-2D}

Scheme 4.24:
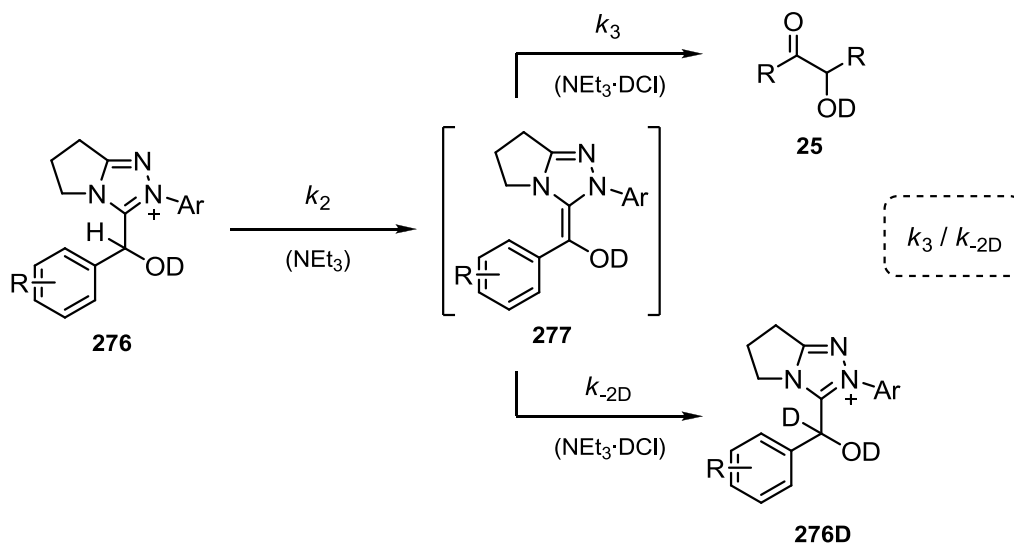
According to Scheme 4.24, a pseudo-first-order rate constant for adduct deprotonation to give the transient Breslow intermediate, k_2 (s^{-1}), may be estimated from the consumption of protonated adduct **276**, once a significant equilibrium concentrations of the species have been reached. In methanol-d_4, formation of the Breslow intermediate **277** from **276** is essentially irreversible and subsequent reactions lead to deuterated adduct **276D** or product **25**. The expression for the rate of adduct consumption is given in Equation 4.38 and the integrated rate equation is shown in Equation 4.39.

$$-\frac{d[\text{add (H)}]}{dt} = k_2[\text{add(H)}] \qquad\qquad \textbf{Equation 4.38}$$

$$[\text{add (H)}] = [\text{add (H)}]_0 e^{-k_2 t} \qquad\qquad \textbf{Equation 4.39}$$

A value of k_2 may be obtained from the slope of a semilogarithmic plot of the concentration of the respective protonated form of the adduct **276** against time. Plots for the reaction of the *N*-phenyl triazolium precatalyst with a variety of substituted benzaldehyde substrates are shown in Figure 4.26. Similar plots for reactions of other catalysts are shown in Appendix C. Values of k_2 obtained by this method are summarised in Table 4.6.

Figure 4.26: **Semilogarithmic plots of [adduct (H)] against time for the reactions of a range of substituted aromatic aldehydes with *N*-phenyl triazolium precatalyst (139)**
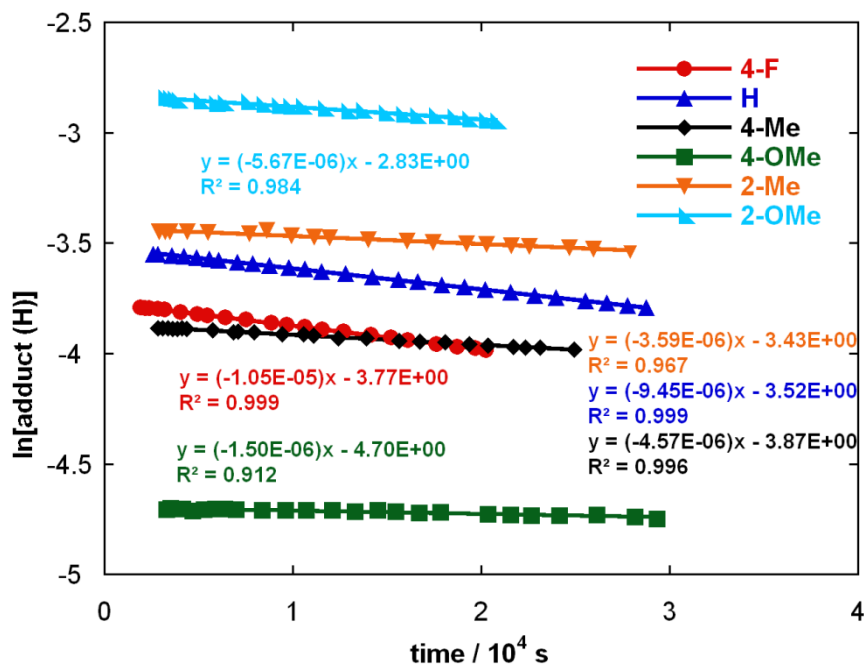
The Breslow intermediate partitioning ratio, k_3/k_{-2D}, describes the ratio of rate constants for onward benzoin formation (k_3) and the reverse reaction back to deuterated adduct (k_{-2D}), illustrated by Scheme 4.24.

In his studies of the thiazolium **249**-catalysed benzoin condensation, Leeper obtained estimates of this ratio from the rates of formation of product and deuterated adduct. For the triazolylidene-catalysed reactions, rates of product formation, v_{prod} (M s^{-1}), and formation of deuterated adduct, v_{deut} (M s^{-1}), were obtained from the slopes of plots of product or deuterated adduct concentration against time, once an equilibrium concentration of adduct had been established. Where possible, the same time period used to follow the formation of benzoin was used to follow adduct deuteration. Figure 4.27 shows plots of product formation as a function of time for a selection of substituted aromatic aldehydes catalysed by *N*-phenyl triazolium salt **139**, and Figure 4.28 shows a similar plot for the formation of deuterated adduct. Similar plots for other reactions are presented in Appendix C. Values of v_{prod} and v_{deut} are summarised in Table 4.6, alongside calculated k_3/k_{-2D} ratios.

Figure 4.27: Plots of acyloin product concentration against time for the self-condensations of a range of substituted aromatic aldehydes catalysed by *N*-phenyl triazolium salt (**139**)
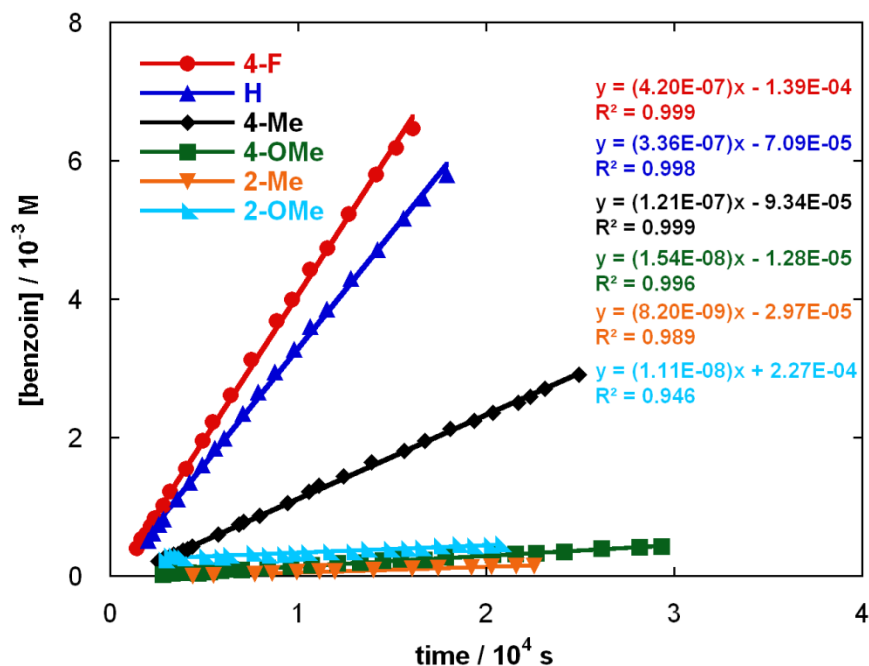
Figure 4.28: Plots of deuterated adduct concentration against time for the self-condensation of a range of substituted aromatic aldehydes catalysed by *N*-phenyl triazolium salt (**139**)
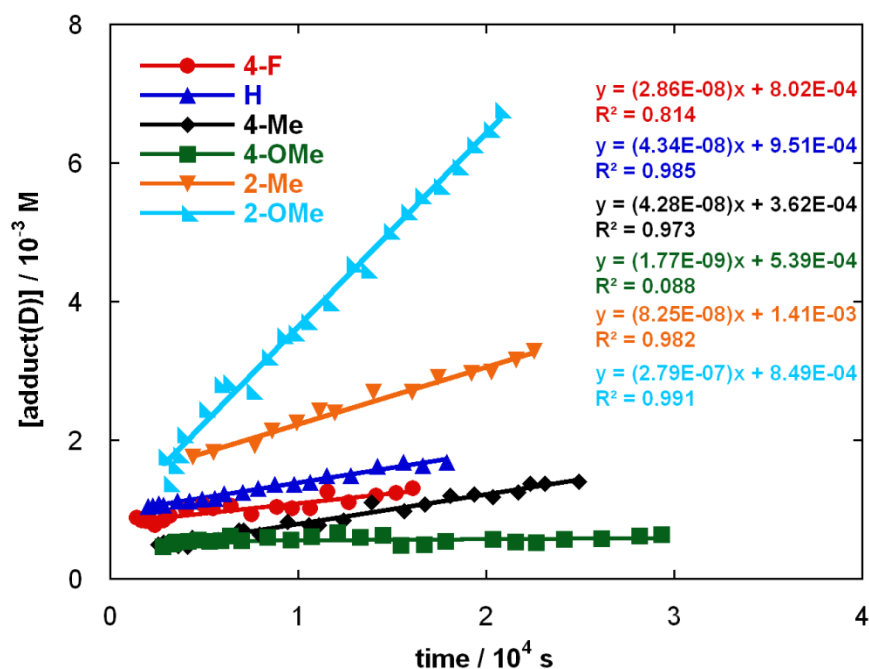
Table 4.6: Values of k_2, and values of v_{prod} and v_{deut} used to obtain partitioning ratio k_3/k_{-2D}

catalyst	aldehyde	k_2 s^{-1} [a]	v_{prod}, M s^{-1} [b]	v_{deut}, M s^{-1} [c]	k_3/k_{-2D} [d]
138	**266** R = 4-F	2.47×10^{-5}	9.71×10^{-7}	1.26×10^{-7}	7.7
	28 R = H	2.19×10^{-5}	8.41×10^{-7}	1.54×10^{-7}	5.5
	267 R = 4-Me	1.04×10^{-5}	3.71×10^{-7}	4.87×10^{-8}	7.6
139	**266** R = 4-F	1.05×10^{-5}	4.20×10^{-7}	2.86×10^{-8}	14.7
	28 R = H	9.45×10^{-6}	3.36×10^{-7}	4.34×10^{-8}	7.7
	267 R = 4-Me	4.57×10^{-6}	1.21×10^{-7}	4.28×10^{-8}	2.8
	273 R = 4-OMe	1.50×10^{-6}	1.54×10^{-8}	1.77×10^{-9}	8.7
	274 R = 2-Me	3.59×10^{-6}	8.20×10^{-9}	8.25×10^{-8}	0.1
	268 R = 2-OMe	5.67×10^{-6}	1.11×10^{-8}	2.79×10^{-7}	0.0
140	**266** R = 4-F	2.03×10^{-5}	5.87×10^{-7}	5.20×10^{-7}	1.1
	28 R = H	1.03×10^{-5}	2.38×10^{-7}	3.89×10^{-7}	0.6
	267 R = 4-Me	5.58×10^{-6}	1.00×10^{-7}	2.01×10^{-7}	0.5
141	**266** R = 4-F	9.73×10^{-6}	3.76×10^{-7}	5.76×10^{-8}	6.5
	28 R = H	7.96×10^{-6}	2.56×10^{-7}	5.36×10^{-8}	4.8
	267 R = 4-Me	3.18×10^{-6}	1.09×10^{-7}	1.74×10^{-8}	6.3
143	**28** R = H	9.54×10^{-6}	2.82×10^{-7}	1.25×10^{-7}	2.3

(a) Obtained from the slope of a semilogarithmic plot of [adduct(H)] against time. (b) Obtained from the slope of a plot of [benzoin(H)] against time. (c) Obtained from the slope of [adduct(D)] against time. (d) Calculated from v_{prod}/v_{deut}.

4.4.3 Triazolium precatalysts: global fitting to obtain values of k_2, k_{-2D}, k_3, k_{1D} and k_{-1D}

Using the mechanisms described in Schemes 4.21 and 4.22 as a starting point, the concentration profiles for the reactions described in Section 4.3 were fitted using global fitting software (Berkeley Madonna, Version 8.3.18). Scheme 4.25 describes the simplified mechanism used in the model.

Scheme 4.25:
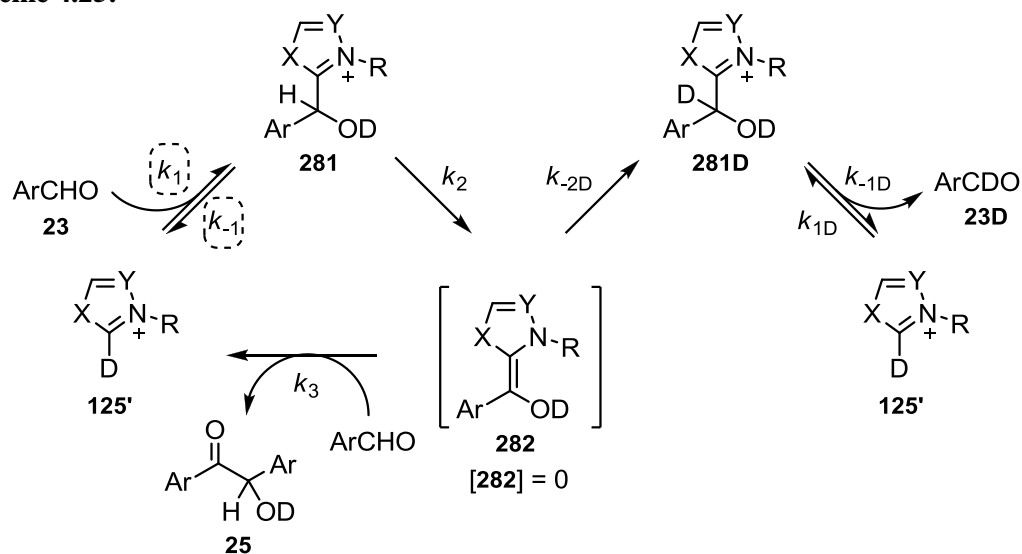
In order to simply the fitting model, a number of modifications were made to the proposed mechanisms shown in Schemes 4.21 and 4.22:

(i) Whilst the benzoin condensation is known to be reversible over long reaction times, in independent experiments we did not observe the formation of aldehyde or any intermediate for any of the precatalysts over the time period for which these experiments were performed. Accordingly, steps corresponding to the addition of the catalyst **125'** to acyloin **25** were removed from the scheme ($k_{-3} = k_{-3D} = 0$).

(ii) For all reactions studied, the concentration of deuterated acyloin product **25D** was negligible, and was removed from the model.

(iii) Deprotonation of the deuterated adduct **281D** to form the Breslow intermediate **282** will be affected by a large primary kinetic isotope effect ($k_2/k_{2D} \approx 9$). From the estimates of k_2, this would result in values of k_{2D} on the order of 10^{-7} s^{-1}. A smaller secondary isotope effect will affect k_{-1D}, which is already significantly faster (10^{-3} s^{-1}).

The partitioning of **281D** between deprotonation (k_{2D}) and decomposition (k_{-1D}) will strongly favour decomposition, and step 2D was removed from the scheme.

(iv) The Breslow intermediate is a transient species and was not observed in the studies by ^{1}H NMR spectroscopy. To accommodate this in the model, **282** was described as an intermediate but was fitted to a fixed concentration of zero for the full duration of the reaction. The fitted concentration predicted by the software was equal to zero in all cases (*i.e.* **282** was correctly predicted as a transient species from the fits).

(v) In bulk deuterated solvent, protonation of the Breslow intermediate **282** to give protonated adduct **281** (k_{-2}) is negligible. Thus, the deprotonation step (k_2) is essentially irreversible in the proposed 'true' mechanism and in the fitting model.

Values of k_1 and k_{-1}, obtained from the partial fits of the profiles in the period leading up to equilibrium concentrations of catalyst and adduct, were incorporated into the fitting model as fixed values. Values for the remaining five rate constants, k_2, k_{-2D}, k_3, k_{1D} and k_{-1D} were obtained simultaneously from the global fitting software. In general, curve-fitting resulted in good-excellent visual correlation with the concentration data. Berkeley Madonna does not permit a quantitative assessment of fitting. Representative results for the reactions of *N*-phenyl and *N*-mesityl precatalysts with benzaldehyde are shown in Figures 4.29 and 4.30. Other reaction profiles are presented in Appendix C.

Output values for k_2 remained relatively constant despite changes in the starting estimates used in the fitting routine. Furthermore, these rate constants are relatively consistent with the values obtained from semilogarithmic plots of [adduct (H)] against time. We are therefore confident that these values reflect the rate constant for step 2, and these values will be discussed further in Section 4.4. The other rate constants were less reliable, and varied significantly depending on the starting values. This is unsurprising given the error associated with the formation of small concentrations of species (*i.e.* benzoin, adduct (D) and aldehyde (D)). The output values of k_2 are summarised in Table 4.7.

Figure 4.29: Concentration profile for the self-condensation of benzaldehyde (28) (0.30 M), catalysed by thiazolium precatalyst (53) (0.30 M), in 0.107 M NEt₃ and 0.107 M NEt₃·DCl in methanol-d₄, fitted using Berkeley Madonna global fitting software
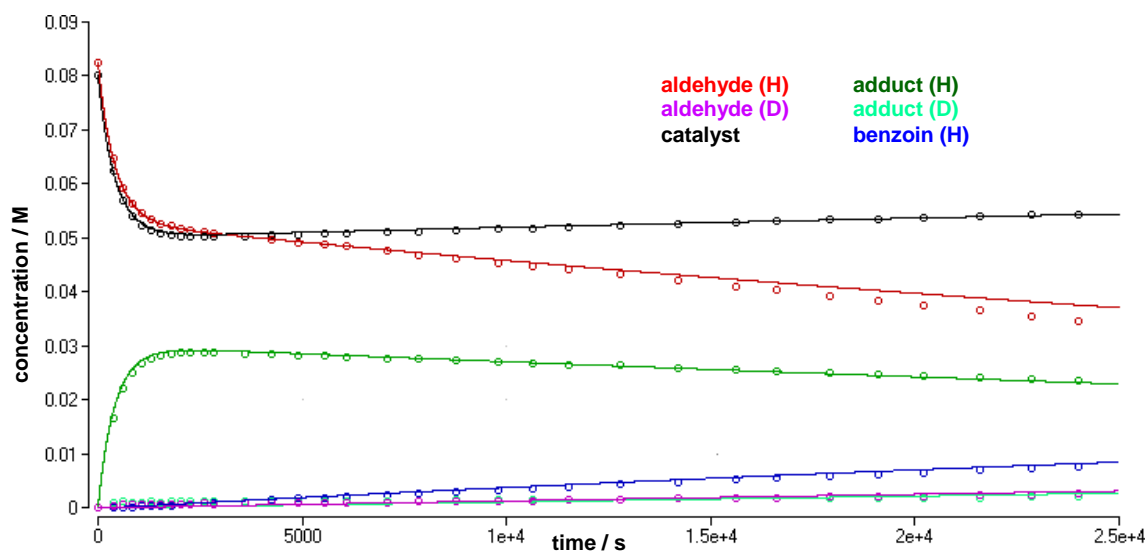
Figure 4.30: Concentration profile for the self-condensation of benzaldehyde (28) (0.08 M), catalysed by triazolium precatalyst (151) (0.08 M), in 0.107 M NEt₃ and 0.107 M NEt₃·DCl in methanol-d₄, fitted using Berkeley Madonna global fitting software
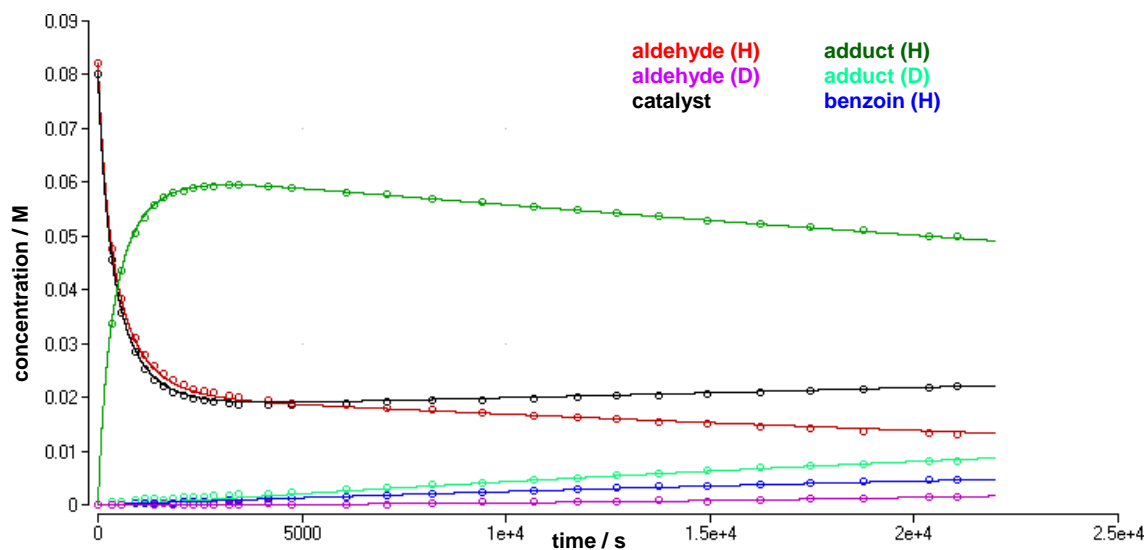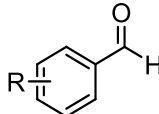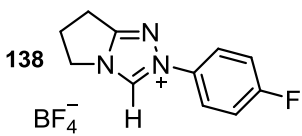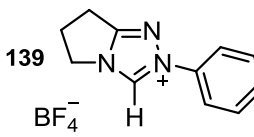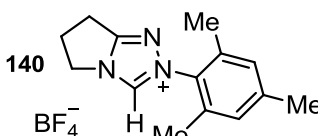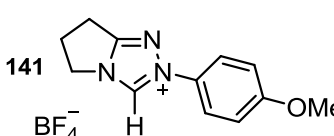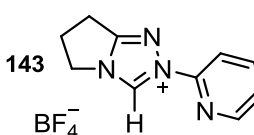
Table 4.7:   **Rate constants and values obtained from global fitting**

catalyst	aldehyde	k_2, s^{-1}
138	**266** R = 4-F	4.99×10^{-5}
	28 R = H	3.79×10^{-5}
	267 R = 4-Me	3.07×10^{-5}
139	**266** R = 4-F	3.34×10^{-5}
	28 R = H	2.19×10^{-5}
	267 R = 4-Me	1.48×10^{-5}
	273 R = 4-OMe	7.92×10^{-6}
	274 R = 2-Me	1.35×10^{-5}
	268 R = 2-OMe	8.87×10^{-6}
140	**266** R = 4-F	2.37×10^{-5}
	28 R = H	1.27×10^{-5}
	267 R = 4-Me	6.95×10^{-6}
141	**266** R = 4-F	2.01×10^{-5}
	28 R = H	1.37×10^{-5}
	267 R = 4-Me	8.42×10^{-6}
143	**28** R = H	2.34×10^{-5}

4.4.4   Thiazolium precatalysts: global fitting to obtain values of k_1, k_{-1}, k_2, k_{-2D}, k_3, k_{1D} and k_{-1D}

Unlike the reactions catalysed by the triazolium ions studied in the previous section, the reactions of the thiazolium precatalysts did not show a clear pre-equilibrium formation of adduct. Significant conversion to benzoin and deuterated adduct were encountered well before the concentrations of adduct and catalyst had reached equilibrium. As a result, 'manual fitting' of the kind used for the triazolium precatalysts proved difficult, given that these methods assume a distinct equilibration period prior to onward reaction. Thus, estimates of k_1, k_{-1} and k_2 could not be independently measured prior to global fitting.

The concentrations profiles for thiazolium catalysts **53** and **151** were fitted using global fitting software in the same manner described for the triazolium reactions in Section 4.4.1. Importantly, as independent estimates of k_1 and k_{-1} had not previously been obtained these were included in the fitting routine along with the other unknown rate constants.

Curve-fitting resulted in excellent visual correlation with the concentration profiles, and the results for the reactions of *N*-benzyl and *N*-mesityl precatalysts with benzaldehyde are shown in Figures 4.31 and 4.32 (N.B. shown on same scale). Values of k_1, k_{-1}, K_1 and k_2 obtained from the fits are presented in Table 4.8. As with the triazolium-catalysed reactions, rate constants for the steps following adduct deprotonation gave unreliable output values that varied depending on initial starting estimates and these will not be discussed in detail.

Figure 4.31: **Concentration profile for the self-condensation of benzaldehyde (28) (0.30 M), catalysed by thiazolium precatalyst (53) (0.30 M), in 0.107 M NEt$_3$ and 0.107 M NEt$_3$·DCl in methanol-d$_4$, fitted using Berkeley Madonna global fitting software**
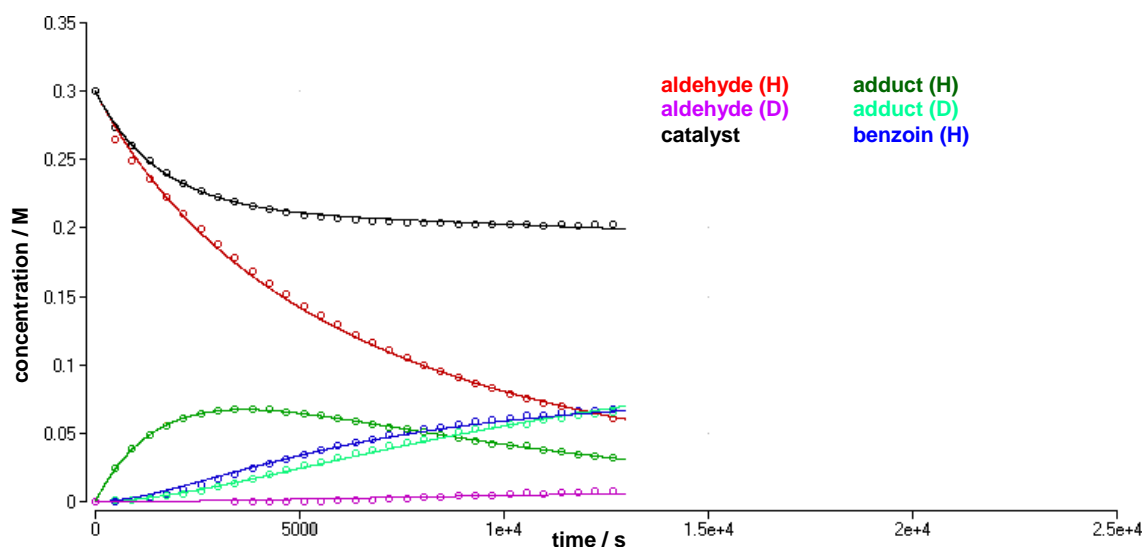
Figure 4.32: Concentration profile for the self-condensation of benzaldehyde (28) (0.30 M), catalysed by thiazolium precatalyst (151) (0.30 M), in 0.107 M NEt₃ and 0.107 M NEt₃·DCl in methanol-d₄, fitted using Berkeley Madonna global fitting software
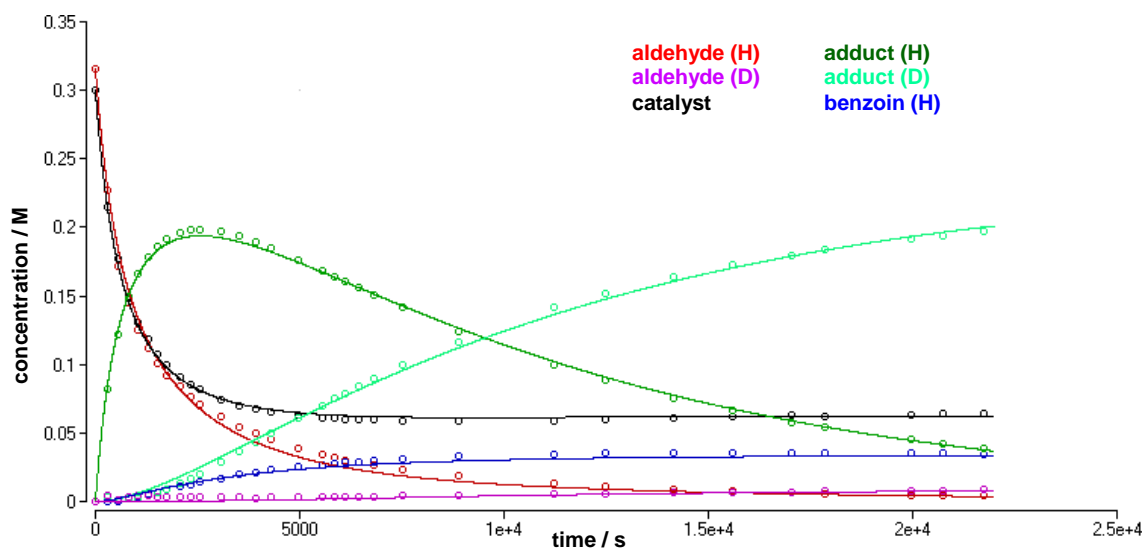
Table 4.8: Rate constants for steps following Breslow intermediate formation obtained from global fitting [*Values in brackets are quoted for Leeper's experiments under identical conditions, and will be discussed in Section 4.5*]

catalyst	k_1, M^{-1} s^{-1} [a]	k_{-1}, s^{-1} [b]	K_1 M^{-1} [c]	k_3/k_{-2D} [c]	k_2, s^{-1} [d]
53	6.47×10^{-4}	1.34×10^{-4}	**4.83**		2.20×10^{-4}
	(7.66×10^{-4})	(7.17×10^{-5})	**(10.7)**	(1.0)	(3.20×10^{-4})
151	4.28×10^{-3}	1.89×10^{-5}	**226**		1.01×10^{-4}

(a) Obtained from the slope of a plot of [benzoin(H)] against time. (b) Obtained from the slope of [adduct(D)] against time. (c) Calculated from k_{prod}/k_{deut}. (d) Obtained from global fitting method.

4.5 Discussion

4.5.1 *In situ* ^{1}H NMR studies

The NHC-catalysed benzoin condensation of a range of aromatic aldehydes in triethylamine buffered methanol-d_4 at 25 °C was followed by ^{1}H NMR spectroscopy. For all of the reactions catalysed by triazolium and thiazolium salts, formation of an (hydroxyaryl)azolium adduct – generated from the addition of the NHC to the aldehyde – was observed.

For the triazolium-catalysed reactions, adduct formation was fast and reversible. This pre-equilibrium was followed by relatively slow deprotonation of the adduct at the C(α)-H position to yield the acyloin product. For the thiazolium-catalysed reactions, the rate constants for adduct formation, decomposition and onward reaction were relatively similar, and did not result in a clear pre-equilibrium formation of adduct.

For a representative cross-section of samples, this intermediate was isolated and characterised by spectroscopic and X-ray crystallographic techniques. Decomposition studies under equivalent reaction conditions show that the formation of this intermediate is reversible in all cases. No other intermediates were observed over the course of the reaction. Although the Breslow intermediate was not observed by ^{1}H NMR spectroscopy (500 MHz), the formation of deuterated adduct and aldehyde in a number of cases provides indirect evidence that the reaction does proceed *via* this transient intermediate.

Fitting of the reaction profiles, both manually and using global fitting software, allow us to estimate values for several microscopic rate constants corresponding to steps in Scheme 4.25. The effects of the *N*-aryl substituent on the catalyst, aryl substituent on the aldehyde, and differences in NHC family are discussed below.

4.5.2   Substituent effects on microscopic rate constants

4.5.2.1   Formation of (hydroxyaryl)azolium adduct (K_1, k_1 and k_{-1})
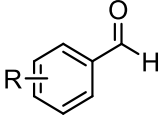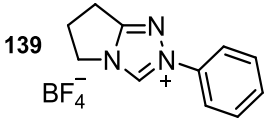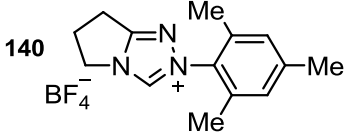
Establishing reversibility and evaluation of methods used to obtain rate constants:
For the triazolium precatalysts, formation of an equilibrium mixture of aldehyde, catalyst and 3-(hydroxyaryl)triazolium adduct was observed, before relatively slow onward reaction to give the benzoin product. The observation of adduct decomposition to reactants in triethylamine-buffered methanol-d_4, for both the *N*-phenyl and *N*-mesityl precatalysts, highlights the reversibility of this first step.

Although the reversibility of step 1 in the thiazolium-catalysed reaction is suggested by the small increase in the concentration of deuterated aldehyde over the course of the reaction, similar adduct decomposition studies performed by other members of our group clarify that in triethylamine buffered methanol-d_4, adduct **278** regenerates benzaldehyde and thiazolium salt **53**.[24]

Four separate estimates for the equilibrium constant for step 1, K_1 (M^{-1}), have been obtained from two sets of experimental data (Table 4.9): (i) from the equilibrium concentrations of adduct and catalyst resulting from adduct decomposition ($1/K_{eq}$), (ii) from the values of k_1 and k_{-1} obtained using the rate equations (K_1^{calc}), (iii) from the values of k_1 and k_{-1} obtained using global fitting software (K_1^{fit}), and (iv) from the equilibrium concentrations of catalyst, aldehyde and adduct determined in the forward benzoin condensation (K_1^{con}). Pleasingly, the resulting equilibrium constants are in good agreement and follow the same trends. At worst, the maximum difference in values is 35% (for the reaction between *N*-phenyl precatalyst **139** and *para*-methylbenzaldehyde **267**). This provides strong evidence to suggest that the rate constants and equilibrium constants derived from fitting are realistic, and may be used to probe the substituent effects for the wider range of substrates described below.

Table 4.9: **Summary of equilibrium constants for step 1**

precatalyst	aldehyde	$1/K_{eq}$, M^{-1} [a]	K_1^{calc}, M^{-1} [b]	K_1^{fit}, M^{-1} [c]	K_1^{con}, M^{-1} [d]
139	**266** R = 4-F	6.33	6.72	6.91	6.88
	28 R = H	13.3	11.0	11.5	11.4
	267 R = 4-Me	7.14	5.28	6.16	6.02
	268 R = 2-OMe	136	115	123	118
140	**28** R = H	180	201	168	160

(a) Estimated from the equilibrium concentrations of [add (tot)] and [cat], using Equation 4.5 (from decomposition experiments). (b) Calculated from the values of $k_{-1} = k_d$ (determined by fitting [add (tot)] decomposition data using Equation 4.8) and k_1 (determined by fitting [cat] forward reaction data using Equation 4.33). (c) Calculated from the values of k_1 and k_{-1} obtained by global fitting from the concentrations of [ald (H)], [cat] and [add (H)] in the initial build-up to equilibrium (from forward reaction). (d) Estimated from the equilibrium concentrations of [ald (tot)], [cat] and [add (tot)], using Equation 4.37 (from forward reaction).

Furthermore, the rate constants (k_1 and k_{-1}) obtained from fitting the forward and reverse approaches to equilibrium using the integrated rate equation and by global fitting are in good agreement. For instance, the value of $k_1 = 1.16 \times 10^{-2}$ M^{-1} s^{-1} obtained by global fitting of the reaction of *N*-phenyl precatalyst with benzaldehyde is with 15% of the value obtained using the integrated rate equation ($k_1 = 1.33 \times 10^{-2}$ M^{-1} s^{-1}). Reassuringly, the value of $k_{-1} = 1.01 \times 10^{-3}$ s^{-1} obtained from global fitting in the forward reaction is within 20% of the value obtained by manually fitting the consumption of adduct in the independent decomposition studies ($k_{-1} = 1.21 \times 10^{-3}$ s^{-1}). Therefore, we are confident that the general trends indicated by these values are representative of the substituent effects on the catalyst and aldehyde.

From the studies of *N*-mesityl adduct equilibration under differing buffer conditions, the 2-fold decrease in k_d upon halving the concentration of triethylamine shows that the rate of adduct decomposition towards aldehyde and catalyst is proportional to the concentration of buffer base. However, the consistency of the values of K_{eq} obtained under three buffer ratios strongly suggests that triethylamine does not appear in the expression for K_1, implying that base is regenerated, presumably as a result of carbene protonation (Scheme 4.26).

Scheme 4.26:
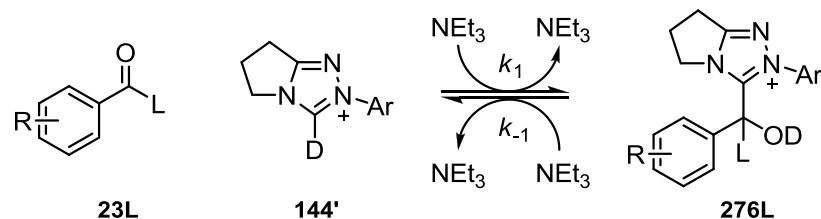
Therefore, strictly speaking, both the forward and reverse rates of step 1 are dependent on the concentration of free triethylamine. In these investigations, we have chosen to include this concentration term within the rate constant. Thus, values of k_1 and k_{-1} should be more correctly termed pseudo-second-order and pseudo-first-order rate constants respectively. All of the reactions in these investigations were performed under the same buffer conditions, and a comparison between substrates may be made without delineating triethylamine. Trends in the rate constants and equilibrium constants obtained by fitting (*i.e.* those used to obtain K_1^{fit}) are discussed below.

Rate constants k_1 and k_{-1}:

Moving up the triazolium precatalyst series in order of increasing electron-withdrawing nature of the aryl substituent (N-C$_6$H$_4$OMe, N-phenyl, N-C$_6$H$_4$F), a small increase in k_1 is observed. Addition of triazolium precatalyst to aldehyde to generate adduct (k_1) is composed of two separate equilibria (Scheme 4.27): deprotonation of the triazolium ion to give the carbene, and nucleophilic addition of the carbene to the aldehyde to generate the 3-(hydroxy)benzyl triazolium adduct. From the pK_a studies described in the previous chapter, electron-deficient N-aryl substituents on the triazolium ion have been shown to favour deprotonation to give free carbene, whilst the same electron-deficient nature would reduce the nucleophilicity of the carbene. Using the benzaldehyde reaction as a representative example, the 3-fold decrease in the overall rate constant for adduct formation upon moving from the electron-withdrawing N-C$_6$H$_4$F substituted triazolium ion to the electron-donating N-C$_6$H$_4$OMe species indicates that the deprotonation equilibrium is the dominant factor in adduct formation for the simple *para-* substituted catalysts.

Comparing the reactivities of *para-* substituted aldehydes with any given catalyst, more electron-rich aldehydes result in slower rates of addition. For example, the rate constant for addition of N-phenyl triazolium precatalyst **139** to *para*-methylbenzaldehyde **267** is around 2-fold smaller than for benzaldehyde **28**, whilst the value for *para-*

methoxybenzaldehyde **273** is a further 2-fold lower again. This is consistent with expected trends based on carbonyl electrophilicties.

Scheme 4.27:
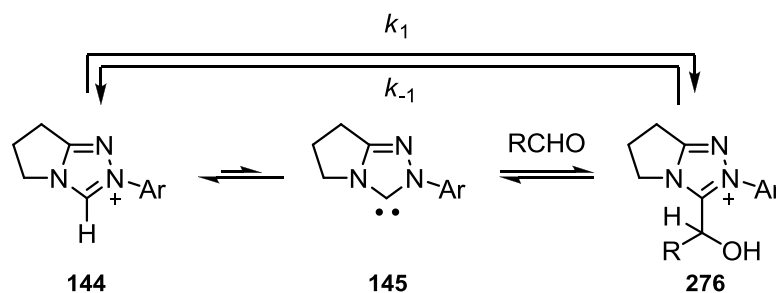
Electron-withdrawing groups on the catalyst *N*-aryl substituent result in larger rate constants for adduct dissociation towards reactants (k_{-1}). Across the series *N*-C$_6$H$_4$F **138**, *N*-phenyl **139**, *N*-C$_6$H$_4$OMe **141**, a small 4-fold decrease is observed for the reaction with benzaldehyde. This is consistent with the expected trend based on leaving group ability of the free carbene/ylide, which will be stabilised by electron-deficient substituents.

In contrast, the reactivity of the *N*-mesityl triazolium catalyst **140** is significantly different to those of the *para*-substituted precatalysts, based on its electronic properties and pK_a. The pK_a of **140** (17.7) lies between those of **139** (17.5) and **140** (17.8), however, its rate constant for adduct formation (k_1) is 7% greater than the value obtained for the most acidic catalyst **138** (17.4). We may conclude that nucleophilic addition of the free *N*-mesityl carbene to the aldehyde is intrinsically fast relative to other NHCs, to make up for the fact that less of the free carbene is present in solution. Similarly, the rate constant for adduct decomposition (k_{-1}) is much reduced suggesting that the *N*-mesityl adduct is particularly stable. The combined *N*-mesityl effect on k_1 and k_{-1} (*i.e.* K_1) and possible structural explanations for this will be discussed further below.

Equilibrium constant K_1:
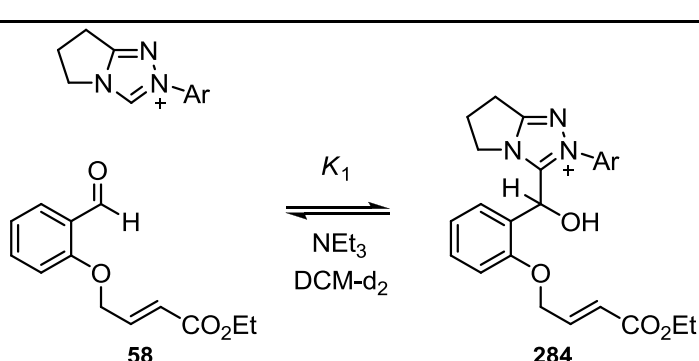
The equilibrium constants for step 1, K_1 (M^{-1}), reflect the relative stabilities of the hydroxybenzyl adducts in relation to the starting materials. Notably, equilibrium constants for the formation of *N*-mesityl adducts are over 10-fold greater than those derived from *N*-phenyl or *N*-*para*-aryl substituted precatalysts. This large difference suggests that, compared to reactants, *N*-mesityl adducts are substantially more stable

than those without 2,6-substituents on the *N*-aryl ring. It is reasonable to assume that this effect is not limited to triazolium salts, as the value of $K_1 = 226$ for the reaction of *N*-mesityl thiazolium salt **151** is of a similar order of magnitude to **140**, and around 50-fold greater than that of *N*-benzyl substituted thiazolium **53**.

X-ray crystal structure data obtained for adducts **264**, **269** and **270** show that the *N*-aryl ring adopts a near-orthogonal orientation with respect to the triazole unit. Indeed, for all of the adducts, we would predict that the *N*-aryl ring would be non-coplanar in order to minimise unfavourable 1,2-interactions. Therefore, NHCs containing large 2,6-substituents may force the *N*-aryl ring to adopt a near-perpendicular conformation, which may better accommodate the 3-hydroxybenzyl group. Unfortunately, an X-ray crystal structure for an *N*-mesityl-substituted adduct could not be obtained, however, computational and X-ray crystallographic structural data reported by Mayr and co-workers show that the *N*-mesityl substituent on the free carbene prefers to adopt an almost perpendicular conformation in a range of imidazolylidene and triazolylidenes.[26]

Similar experiments by Collett and Smith, with whom we have been collaborating with on this project, have shown that other 2,6-aryl substituted precatalysts (*i.e.* **140**, **263** and **283**) also result in enhanced values of K_1.[27] Table 4.10 presents analogous equilibrium constants for the addition of catalyst to aldehyde **58** in the first step of the intramolecular Stetter reaction, obtained in dichloromethane-d$_2$.

Table 4.10:   **Intramolecular Stetter reaction: equilibrium constants for step 1**

precatalyst	K_1, M^{-1} [a]
263 Ar = 2,4,6-ClC$_6$H$_2$	**336**
138 Ar = 4-FC$_6$H$_4$	**28**
139 Ar = Ph	**27**
140 Ar = Mes	**140**
141 Ar = 4-OMeC$_6$H$_4$	**31**
283 Ar = 2,6-OMeC$_6$H$_3$	**1283**

(a) Estimated from the equilibrium concentrations of [ald (tot)], [cat] and [add (tot)], using Equation 4.37.

Glorius has suggested that *ortho-* substituted *N*-aryl substituents would destabilise the 3-(hydroxybenzyl)azolium adduct due to steric effects.[28] Our combined results do not appear to support this statement for 'smaller' 2,6-substituents (mesityl, C_6F_5 etc.), however, the results of our experiments using imidazolium precatalysts indicate that very large substituents may be detrimental to adduct formation. A comparison between *N,N*-dimesitylimidazolium **70** and *N,N*-di(diisopropylphenyl)imidazolium **74** resulted in the appearance of adduct only in the case of the mesityl precatalyst. No reaction was observed for the more bulky diisopropylphenyl species.

In addition to the effect of the precatalyst *N*-aryl substituent, a second, separate, equilibrium-shifting effect was also observed using *ortho*-methoxybenzaldehyde **268**. Relative to benzaldehyde **28**, a 10-fold increase in the equilibrium constant for adduct formation was observed for the reaction of **268** using precatalyst **139**. To probe the origin of this increase, a study of *ortho-* and *para*-substituted aldehydes was made. The value of K_1 obtained for *ortho*-methylbenzaldehyde **274** is 2-fold larger than for *para*-methylbenzaldehyde **267**, and this small difference may be attributed to steric effects. In contrast, the same positional change for methoxy substituted aldehydes **268** and **273** results in a 60-fold increase in K_1. This behaviour may result from the formation of an intramolecular hydrogen bond between the lone pair on the *ortho*-methoxy substituent and the α-OH group on **272** (Figure 4.33), and has the potential to enhance the rate of turnover in future reaction design. However, part of this increase in K_1 may also stem from electronic effects, as moving a methoxy group from *para-* position to the *ortho*-position would be expected to result in more electrophilic aldehyde.

Figure 4.33: Proposed intramolecular hydrogen bond

272
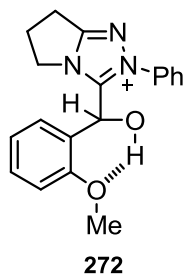
Similar studies of the intramolecular Stetter reaction of **58** by Smith and Collett show that values of K_1 for the adduct-forming step are around $10 - 20$-fold larger than for the benzoin condensation, under identical conditions of triethylamine-buffered methanol-d$_4$ at 25 °C.[26b] Intrinsic to the commonly studied Stetter substrate **58** is a 2-alkoxy substituent, which may also form an adduct-stabilising hydrogen bond.

To further examine this effect, we obtained an equilibrium constant for the formation of adduct from an *N*-pyridyl substituted precatalyst **143**, developed by Ukaji and co-workers.[29] The authors proposed that the pyridyl nitrogen may induce an intramolecular hydrogen bond in the Breslow intermediate, forming a conformationally rigid structure which would promote enantioselective benzoin formation. Indeed, *ee*s of up to 65% were obtained using similar precatalyst **285**, compared with 8% for the reaction using the *N*-phenyl variant **286**.
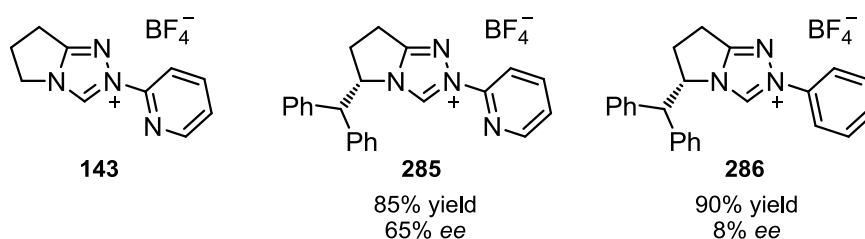
We hypothesised that this *N*-pyridyl substituent could also induce a stabilising intramolecular hydrogen bond between the nitrogen and α-OH proton in the adduct. Disappointingly, no additional increase in K_1 was observed relative to the *N*-phenyl catalyst (in fact, a 4% decrease in K_1 was observed). Based on the crystal structures obtained for other adducts, it is likely that the *N*-pyridyl ring occupies a non-planar conformation with respect to the azolium ring, resulting in an unfavourable orientation of the lone pair on the pyridyl nitrogen for hydrogen bond formation. The proposed hydrogen bond derived from the pyridyl nitrogen would also result in a 7-membered ring, which would be less likely to form than the more stable 6-membered ring proposed for the *ortho*-alkoxyl species.

4.5.2.2   Deprotonation of (hydroxyaryl)azolium adduct (k_2)

Substituent effects on values of k_2:

Pseudo-first-order rate constants for deprotonation of the 3-(hydroxylbenzyl)triazolium adducts, k_2 (s^{-1}), were estimated from the slopes of semilogarithmic plots of protonated adduct concentration against time, and also from fitting of the reaction profile data using global fitting software. To simplify the fitting model, values of k_1 and k_{-1} shown in Table 4.4 (obtained from fitting the initial equilibration period) were used as fixed values in the fitting routine.

The good first-order fits of the [adduct(H)] data to the semilogarithmic plots discussed in Section 4.4.1 (and presented in Appendix C) indicate that pseudo-first-order rate constants may be obtained for the adduct deprotonation step. In Leeper's studies of the thiazolium-catalysed reaction under similar conditions, the rate constant for adduct deprotonation was also expressed as a pseudo-first-order rate constant (s^{-1}). Clearly, base is consumed during deprotonation at the $C(\alpha)$-H position, and regenerated upon protonation of the carbene following elimination of benzoin (step 3). However, as the reaction solution is buffered, and in the case of the triazolium reactions, buffer base is present in 2-3-fold excess of the peak concentration of adduct, the concentration of base is unlikely to significantly change over the course of the reaction. It is therefore unnecessary to model the reaction with triethylamine as a separate reagent.

Data obtained by both methods show that more electron-deficient adducts result in larger rate constants for deprotonation. For instance – using the rate constants obtained from global fitting – the value of k_2 determined for the reaction between *N*-phenyl precatalyst **139** and *para*-fluorobenzaldehyde **266** is 3.5-fold larger than that for the reaction with *para*-methoxybenzaldehyde **273**. Similarly, the value of k_2 for the reaction of benzaldehyde **28** catalysed by the *N*-C_6H_4F precatalyst **138** is 3-fold larger than with the *N*-C_6H_4OMe precatalyst **141**. This trend is consistent with the expected $C(\alpha)$-H acidities of the adduct, and may be rationalised by considering the potential for stabilisation of the electron-rich deprotonation transition state. In general, values of k_2 obtained from the fitting model are around 2-3-fold larger than those obtained from the 'manual' approach. The largest discrepancy between the two evaluated rate constants is for the reaction between *N*-phenyl catalyst **139** and 4-methoxybenzaldehyde **273**, where a 5-fold difference is observed.

The trend in acidity of the hydroxybenzyl adducts derived from the N-C$_6$H$_4$F, N-phenyl and N-C$_6$H$_4$OMe triazolium salts is the same from both methods, and follows the order of acidity of the respective precatalysts. However, the two approaches place the acidity of the N-mesityl-derived adduct slightly differently. By 'manual' fitting, the rate constant for deprotonation of the N-mesityl adduct is around 10% larger than the value for the N-phenyl adduct. By contrast, from the global fitting approach, the value of k_2 for the N-mesityl adduct is approximately 10% smaller than the N- C$_6$H$_4$OMe adduct. Neither approach places the acidity of the N-mesityl adduct between the N-phenyl and N-C$_6$H$_4$OMe, as may be expected based on precatalyst acidities. However, the rate constants for these three adducts are relatively similar, particularly for the N-methoxy and N-mesityl adducts, and for these adducts this ordering will be sensitive to experimental error. Despite this slight ambiguity, the N-mesityl group does not result in significantly altered values of k_2 to the extent observed for step 1, and we may conclude that the largest influence on rates of adduct deprotonation are of an electronic nature.

The value of k_2 obtained for the reaction of N-phenyl triazolium catalyst **139** with *ortho*-methylbenzaldehyde is smaller than the reaction of *para*-methylbenzaldehyde (20% or 9% depending on whether the value from manual fitting or global fitting method is used, respectively). This small decrease is consistent with a small degree of steric hindrance close to the site of deprotonation. In contrast, moving the methoxy group from the para- to the ortho- position results in an increase in k_2. The magnitude of this change is unclear, from global fitting this increase is around 12%, whereas from manual fitting this difference is much larger – around 400%.

Rovis has proposed for the Stetter reaction that the ethereal oxygen promotes the adduct deprotonation step, *via* the intramolecular pathway shown in Scheme 4.27. In a competition experiment between Stetter substrates **58** and **288**, Rovis found that the rate of consumption of oxygen-bearing **58** was over 10-fold faster than that of **288**, which the author concluded was as a result of intramolecular deprotonation *via* species **287**. However, given that our experiments show that the ethereal oxygen would likely accelerate substrate consumption by the enhancement of rate of formation of the 3-(hydroxyaryl)triazolium adduct, Rovis' conclusion – based on the faster disappearance of aldehyde – is not necessarily correct.

Scheme 4.27:
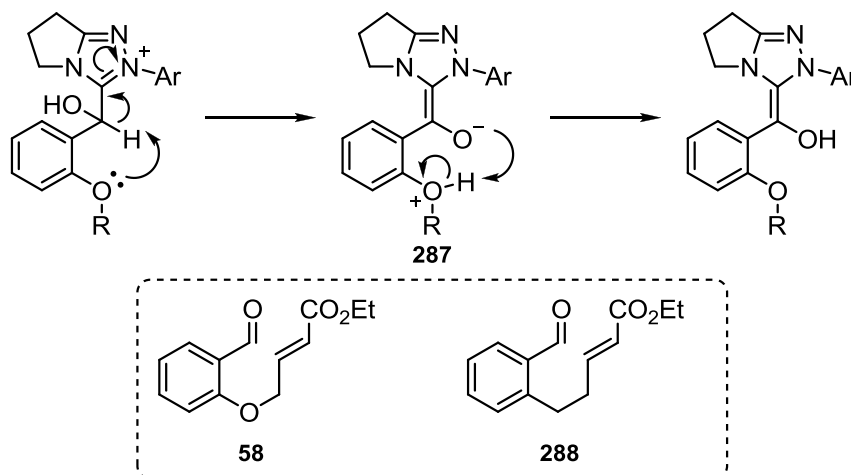
Furthermore, whilst our results do show that the presence of an *ortho*-alkoxyl group does enhance the rate of adduct deprotonation, this difference may be due to electronic effects – the electron-withdrawing inductive effect of the ortho-alkoxyl group would be greater in the *ortho-* position, whilst the conjugative electron-donating effect would remain relatively constant.

Rate-determining step: a comparison between triazolium and thiazolium salts:

Qualitatively, the appearance of equilibrium concentrations of the 3-(hydroxyaryl)triazolium adduct prior to product formation is consistent with adduct deprotonation as the rate-determining step. The adduct partitioning ratios (k_2/k_{-1}) for the reactions of triazolium salts **138 – 141** range from 0.02 – 0.07, and support the conclusion that onward adduct deprotonation is slow relative to decomposition back to reactants. From the Breslow intermediate partitioning ratios (k_3/k_{-2D}), benzoin formation is clearly favoured over the reverse reaction to adduct, indicating that adduct deprotonation is rate-determining.

The fact that a clear pre-equilibrium was not observed for the thiazolium-catalysed reactions suggest that the rates of adduct formation and deprotonation are more similar. For thiazolium salt **53**, the adduct partitioning ratio (k_2/k_{-1}) and Breslow intermediate partitioning ratio (k_3/k_{-2D}) are 1.6 and ~1.0 respectively, indicating that no single step is clearly rate-determining.

4.5.2.3 Breslow intermediate partitioning ratio (k_3/k_{-2D})

The ratio of rate constants k_3/k_{-2D} describes the partitioning of the Breslow intermediate between onward benzoin formation (k_3) and deuteration back to adduct (k_{-2D}). This ratio may be estimated from the slopes of zero-order plots of benzoin and deuterated adduct against time, and has also been estimated from the rate constants obtained by global fitting.

From visual inspection of the concentration profiles, it is clear that accumulation of benzoin is strongly favoured over deuterated adduct for the majority of triazolium precatalysts. In contrast, the rates of formation of benzoin and deuterated adduct for the reaction of thiazolium precatalyst **53** are approximately equal, and for the reaction of thiazolium precatalyst **151** partitioning favours deuterated adduct. This difference may help to explain why triazolium salts typically offer improved yields in the benzoin condensation over thiazolium salts. In addition, *N*-mesityl substituted thiazolium and triazolium precatalysts show significant deuteration of adduct. This is likely to result from the increased thermodynamic stability of the adduct, which will manifest itself in a more favourable return to adduct rather than onward benzoin formation.

Unfortunately, the values of k_3 and k_{-2D} obtained from global fitting do not result in realistic ratios of k_3/k_{-2D} based on evidence from the rates of product or deuterated adduct formation. Given that the concentrations of these species are small and in several cases do not significantly increase over the course of the reaction, the rate constants associated with these values would be expected to experience a large degree of error. However, the fact that the calculated values of k_3/k_{-2D} for the triazolium-catalysed reactions are around 10-fold larger than those of the thiazolium-catalysed reactions supports the conclusions described above.

4.6 Summary

The appearance and consumption of reactants, intermediates and products in the NHC-catalysed benzoin condensation was monitored *in situ* by ^{1}H NMR spectroscopy, at 25 °C in triethylamine-buffered methanol-d$_4$. For the reactions of a range of triazolium precatalysts, our studies indicate that the 3-(hydroxyaryl)triazolium adduct (generated by addition of the free NHC to the aldehyde) is the only intermediate observed over the

course of the reaction under these conditions. Relatively slow deprotonation of this intermediate yields product. Several examples of these adducts have been isolated and structures unambiguously confirmed by NMR and crystallographic techniques.

Under our conditions, formation of the 3-(hydroxyaryl)triazolium is reversible, irrespective of *N*-aryl substitution pattern. However, studies of the equilibrium between aldehyde, precatalyst and adduct reveal that 2,6-substituents on the *N*-aryl result in substantially larger values of K_1 (a ~10-fold increase) relative to the *N*-phenyl substituted catalyst. These equilibrium values from the forward reaction were confirmed by independent studies of adduct decomposition, giving alternative estimates of K_1 that were in excellent agreement. Based on our interpretation of available crystallographic data, we propose that this equilibrium effect may result from a sterically-enforced orthogonal *N*-aryl ring orientation on the NHC, which may better accommodate the 3-hydroxybenzyl group relative to unsubstituted aryl rings.

Reactions of *ortho*-alkoxyl-substituted aromatic aldehydes also resulted in enhanced equilibrium concentration of adduct. We believe that this increase in adduct stability may be due to the formation of an intramolecular hydrogen bond between the lone pair on the *ortho*-alkoxyl substituent and the hydrogen on the α-hydroxyl group. We had hypothesised that a similar hydrogen bond may result from use of a *N*-pyridyl catalyst, however no such effect was observed.

Under the conditions employed, adduct deprotonation was found to be rate-determining. Pseudo-first-order rate constants for deprotonation at the C(α)-H position (k_2) were estimated from first-order plots of protonated adduct concentration against time and from global fitting. Variation of aryl substituents on the catalyst and aldehyde show that electron-deficient adducts result in larger rate constants, presumably as a result of the increased acidity of the C(α)-H position.

We may conclude that electron-withdrawing 2,6-aryl substituted catalysts will benefit from increased values of both K_1 and k_2, resulting in faster rates of product formation. Unfortunately, the reaction of the *N*-C_6F_5 substituted precatalyst was too fast to study under these conditions. It would be useful to perform similar experiments on this precatalyst under milder conditions which would allow a sufficient adduct equilibration period. Furthermore, it would also be beneficial to prepare a trifluoromethyl-variant of

the *N*-mesityl precatalyst to determine whether improved rates of benzoin formation may be reached.

From the ratio of rates of benzoin and deuterated adduct accumulation, there is some evidence to suggest that partitioning of the Breslow intermediate towards product is more favourable for triazolium catalysts. This may help to explain why benzoin yields are historically significantly higher for triazolium rather than thiazolium precatalysts.

Imidazolium and 4,5-dihydroimidazolium salts were ineffective as precatalysts for the benzoin condensation presumably as a result of their relatively low acidity under these conditions. Interestingly, the *ortho-N*-aryl effect mentioned above did result in the appearance of adduct for an *N*,*N'*-dimesityl substituted imidazolium ion, but did not yield product. This is likely due to the reduced acidity of the C(α)-H position, relative to triazolium and thiazolium derived adducts.

References

1   F. Wöhler and J. Liebig, *Ann. Pharm.*, 1832, **3**, 249.

2   A. Lapworth, *J. Chem. Soc.*, 1903, **83**, 995.

3   T. Ugai, S. Tanaka and S. Dokawa, *J. Pharm. Soc. Japan*, 1943, **63**, 269.

4   S. Mizuhara, R. Tamura and H. Arata, *Proc. Jpn. Acad.*, 1951, **87**, 302.

5   R. Breslow, *J. Am. Chem. Soc.*, 1958, **80**, 3719.

6   (a) H.-W. Wanzlick and H. J. Kleiner, *Angew. Chem.*, 1963, **75**, 1204; (b) For a review see: R. W. Alder, M. E. Blake, L. Chaker, J. N. Harvey, F. Paolini and J. Schütz, *Angew. Chem. Int. Ed.*, 2004, **43**, 5896.

7   (a) B. Lachmann, H. Steinmaus and H.-W. Wanzlick, *Tetrahedron*, 1971, **27**, 4085; (b) J. Castells, F. Lopez-Calahorra, F. Geijo, R. Perez-Dolz and M. Bassedas, *J. Heterocycl. Chem.*, 1986, **23**, 715.

8   J. Castells, F. López-Calahorra and L. Domingo, *J. Org. Chem.*, 1988, **53**, 4433.

9   Breslow's objections to the Castells mechanism were made clear in (a) R. Breslow and R. Kim, *Tetrahedron Lett.*, 1994, **35**, 699; and in no uncertain terms in (b) R. Breslow and C. Schmuck, *Tetrahedron Lett.*, 1996, **37**, 8241.

10   M.J. White and F.J. Leeper, *J. Org. Chem.*, 2001, **66**, 5124.

11   D.M. Lemal, R.A. Lovald and K.I. Kawano, *J. Am. Chem. Soc.*, 1964, **86**, 2518.

12   A. Berkessel, S. Elfert, K. Etzenbach-Effers and J. H. Teles, *Angew. Chem. Int. Ed.*, 2010, **49**, 7120.

13   D. A. DiRocco, K. M. Oberg and T. Rovis, *J. Am. Chem. Soc.*, 2012, **134**,6143.

14   A. Berkessel, S. Elfert, V. R. Yatham, J.-M. Neudörfl, N. E. Schlörer and J. H. Teles, *Angew. Chem. Int. Ed.*, 2012, **51**, 12370.

15   J. Kiss, R. D'Souza and H. Spiegelberg, *Helv. Chim. Acta*, 1968, **51**, 325.

16   J. J. Mieyal, G. Bantle, R. G. Votaw, I. A. Rosner and H. Z. Sable, *J. Biomol. Chem.*, 1971, **246**, 5213.

17   (a) A. A. Gallo and H. Z. Sable, *J. Biomol. Chem.*, 1976, **251**, 2564; (b) G. L. Barletta, Y. Zou, W. P. Huskey and F. Jordan, *J. Am. Chem. Soc.*, 1997, **119**, 2356.

18   M. W. Washabaugh and W. P. Jencks, *Biochemistry*, 1988, **27**, 5044.

19   (a) G. L. Barletta, Y. Zou, W. P. Huskey and F. Jordan, *J. Am. Chem. Soc.*, 1997, **119**, 2356; (b) M. W. Washabaugh, J. T. Stivers, K. A. Hickey, *J. Am. Chem. Soc.*, 1994, **116**, 7094.

20   J. Mahatthananchai and J. W. Bode, *Chem. Sci.*, 2012, **3**, 192.

21   (a) P.-C. Chiang, M. Rommel and J. W. Bode, *J. Am. Chem. Soc.*, 2009, **131**, 8714; (b) P.-C. Chiang, Y. Kim and J. W. Bode, *Chem. Commun.*, 2009, **129**, 3520.

22   Leeper notes that in the following references, a 9:1 NEt3:NEt3·HCl ratio was used, however, the 2:1 buffer ratio in Leeper's study and our own investigation gives a better buffer capacity. (a) F. Lópes-Calahorra and R. Rubires, *Tetrahedron*, 1995, **51**, 9713.

23   In Comprehensive Chemical Kinetics, Elsevier, Amsterdam, 1969, Eds. C. H. Bamford and C. F. H. Tipper, pp. 36-37.

24   O. R. Maguire, A. C. O'Donoghue, unpublished results.

25   E. M. Higgins, J. A. Sherwood, A. G. Lindsay, J. Armstrong, R. S. Massey, R. W. Alder and A. C. O'Donoghue, *Chem. Commun.*, 2011, **47**, 1559.

26   B. Maji, M. Breugst and H. Mayr, *Angew. Chem. Int. Ed.*, 2011, **50**, 6915.

27   (a) C. J. Collett, R. S. Massey, O. R. Maguire, A. S. Batsanov, A. C. O'Donoghue, A. D. Smith, *Chem. Sci.*, 2013, **4**, 1514; (b) C. J. Collett, A. D. Smith, Ph.D. Thesis, University of St. Andrews, St. Andrews, 2013.

28   M. Schedler, R. Frohlich, C. G. Daniluc and F. Glorius, *Eur. J. Org. Chem.*, 2012, 4164.

29   T. Soeta, Y. Tabatake, K. Inomata and Y. Ukaji, *Tetrahedron*, 2012, **68**, 894.

CHAPTER   5

Initial Rates Studies at Sub-Stoichiometric Precatalyst Concentrations

5.0   Foreword

The mechanistic studies of the benzoin condensation described in the previous chapter provide valuable information on the microscopic rate constants for a number of early steps involved in the proposed mechanistic cycle. This chapter focuses on our initial rates studies of the benzoin condensation performed using sub-stoichiometric concentrations of catalyst, and is divided into four sections. Section 5.1 summarises previous work relating to the determination of reaction order in the case of the benzoin condensation and Stetter reaction. Section 5.2 details the results of our initial rates experiments of thiazolium- and triazolium-catalysed benzoin condensations in triethylamine-buffered methanol at 50 °C. Reaction order with respect to aldehyde and precatalyst are probed. These results are discussed in Section 5.3 and our conclusions are summarised in Section 5.4.

5.1   Introduction

5.1.1   The 'initial rates method'

Several kinetic methodologies are available to enable the determination of a reaction rate law. One approach, used in the previous chapter, involves fitting the concentration of a reactant or product over extended reaction periods to characteristic first- or second-order plots. Alternatively, an 'initial rates method' may be used, which involves measuring the rate of reaction (v) at very short times (typically ≤10% conversion) before any significant changes in substrate concentration occur. Studying the initial rate (v_0) at several substrate concentrations allows the reaction order to be determined.

5.1.2   Steady-state kinetics of the benzoin condensation

Leeper and White have undertaken extensive kinetic studies of the thiazolium catalysed benzoin condensation.[1] The group's steady-state experiments involved a study of initial rates at a range of benzaldehyde 2**8** concentrations (0.1 – 1.7M) in excess of a constant catalytic amount of **247** (30 mM) in triethylamine-buffered (0.107 M NEt$_3$, 0.053 M NEt$_3$·HCl) methanol at 50 ºC. Using two separate methods of reaction monitoring ((i) *in-situ* UV-Vis spectroscopy and (ii) quenching followed by analysis by HPLC), the rate of reaction was found to be approximately first-order with respect to benzaldehyde, with both analytical methods giving essentially the same result (Figure 5.1).

Figure 5.1: **First-order dependence on benzaldehyde for the benzoin condensation catalysed by thiazolium salt (247)**
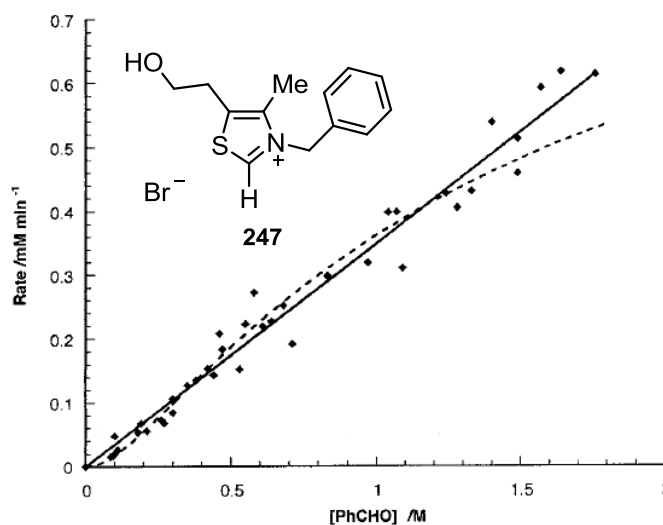
Leeper initially proposed three potential scenarios that may account for the near first-order dependence with respect to benzaldehyde (Scheme 4.8). In the first scenario, addition of the catalyst to benzaldehyde to form the 2-(hydroxybenzyl)thiazolium adduct **248** (step 1) may be rate-determining. Alternatively, deprotonation of **248** (step 2) may be rate-determining and its formation may occur as a rapid pre-equilibrium favouring starting materials, so that the equilibrium concentration of **248** is proportional to that of aldehyde. The final scenario requires that addition of the Breslow intermediate **249** to the second benzaldehyde molecule (step 3) be rate-determining, with step 1 occurring as a rapid pre-equilibrium favouring products (where catalyst is present almost entirely as 2-(hydroxybenzyl)thiazolium adduct).

Following the group's pre-steady-state NMR studies, Leeper evaluated whether the rate constants for the individual steps outlined in Scheme 4.8 accurately reflected the overall steady-state kinetics shown in Figure 5.1. Using Equation 5.1 (where constants a, b and c represent the microscopic rate constants determined in the pre-steady-state studies), the rate at each benzaldehyde concentration was calculated. A good fit to the apparent first-order relationship was obtained (dashed line), in agreement with the earlier description that all three steps were partially rate-determining. Leeper notes that factors were used to account for the 25 °C temperature difference between the two sets of experiments, although it is unclear precisely how these constants are calculated.

$$\text{rate} = \frac{k_{\text{cat}}[\text{PhCHO}]^2[\text{cat}][\text{base}]}{a+b[\text{PhCHO}]+c[\text{PhCHO}]^2} \qquad \textbf{Equation 5.1}$$

5.1.3   Steady-state kinetics of the intramolecular Stetter reaction

Rovis and co-workers have probed reaction order with respect to substrate and catalyst for the intramolecular Stetter reaction.[2] The disappearance of aldehyde **58** in the presence of base (KHMDS) (20 mol%) at 0 °C at several concentrations of chiral precatalyst **289** (2.5 – 10 mM) was monitored by gas chromatography (Scheme 5.1). Based on fits to first-order plots, the authors claim the reaction obeys first-order kinetics with respect to both aldehyde and catalyst.

Scheme 5.1:
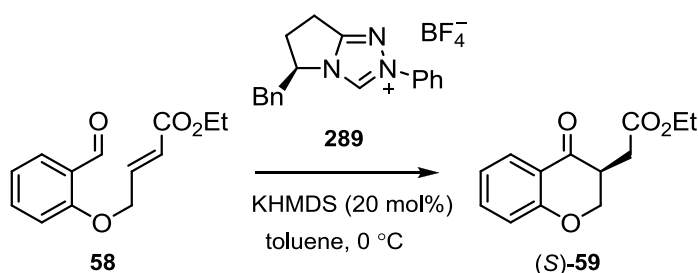
Collett and Smith, with whom we are collaborating on this project, have also studied the activities of a range of triazolium precatalysts **138 – 142**, **263** and **283** in the intramolecular Stetter reaction.[3,4] Using ^{1}H NMR spectroscopy, the extent of conversion for the reaction of aldehyde **58** to Stetter product **59** at 25 °C in triethylamine-buffered (0.107 M NEt$_3$, 0.053 M NEt$_3$·HCl) dichloromethane-d$_2$ was followed over time. The time for the reaction to reach 50% conversion was found to follow the order shown in Scheme 5.2. Electron-deficient precatalysts were found to result in superior rates of conversion.

Scheme 5.2:

	142	**263**	**138**	**139**	**141**	**283**	**140**
t$_{50\%}$ (min)	5	11	1320	1620	3540	3915	4720
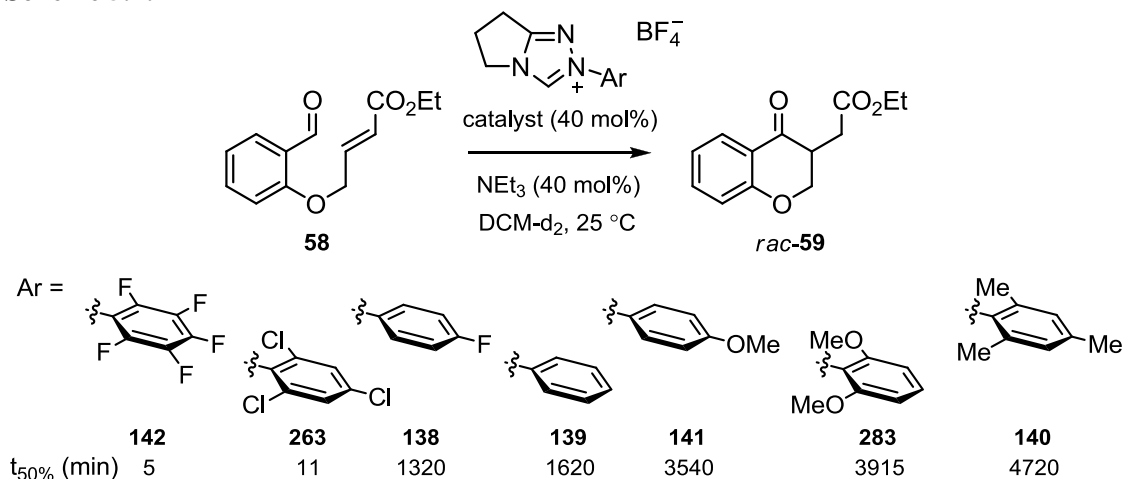
5.2 Results

5.2.1 3-Benzyl-5-(2-hydroxyethyl)-4-methylthiazolium chloride (53)
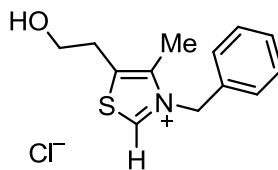
53

In order to determine reaction order with respect to benzaldehyde for the benzoin condensation catalysed by thiazolium salt **53**, a series of initial rates experiments were performed using a catalytic concentration of **53** at a range of initial benzaldehyde concentrations (0.32 – 1.6 M). Reaction order with respect to precatalyst was also probed by performing these experiments at three precatalyst concentrations (12 mM, 24 mM and 12 mM).

Reactions were carried out in 12.5 mL vials, incubated at 50 ± 0.01 ℃ in a thermostated water bath. Reactions were run on a 2.5 mL scale, and were initiated by the addition of a solution of precatalyst **53** (0.5 mL) to a pre-warmed solution containing appropriate concentrations of benzaldehyde **28** and triethylamine buffer (2 mL). The final concentrations of aldehyde and precatalyst were 0.32 – 1.6 M and 12 – 30 mM respectively. The final total concentration of triethylamine buffer was 0.16 M (0.107 M NEt$_3$, 0.053 NEt$_3$·HCl). At regular intervals, aliquots (12 μL) were taken and the reaction quenched by the addition of 1.5 mL acetonitrile. These samples were analysed by HPLC shortly afterwards, and where necessary refrigerated prior to analysis. Detection of benzoin **34** and benzaldehyde **28** was made by UV absorbance at 254 nm. Separation of peaks corresponding to benzoin and benzaldehyde was obtained using a reverse-phase X-bridge C18 column, with elution by acetonitrile-water (40 : 60) and flow rate 1 mL min^{-1} at 25 ℃. A representative set of chromatograms showing the formation of benzoin over the course of the reaction is shown in Figure 5.2. Benzaldehyde and benzoin eluted at approximately 2.9 and 4.2 min respectively. No signals corresponding to precatalyst **53** or benzoic acid could be detected, but as these compounds are charged they are likely to have eluted rapidly with the solvent front.

Figure 5.2: **Representative reverse phase HPLC chromatograms showing progress of the benzoin condensation of benzaldehyde (28) (0.64 M), catalysed by thiazolium salt (53) (12 mM) at 50 °C in triethylamine-buffered methanol**
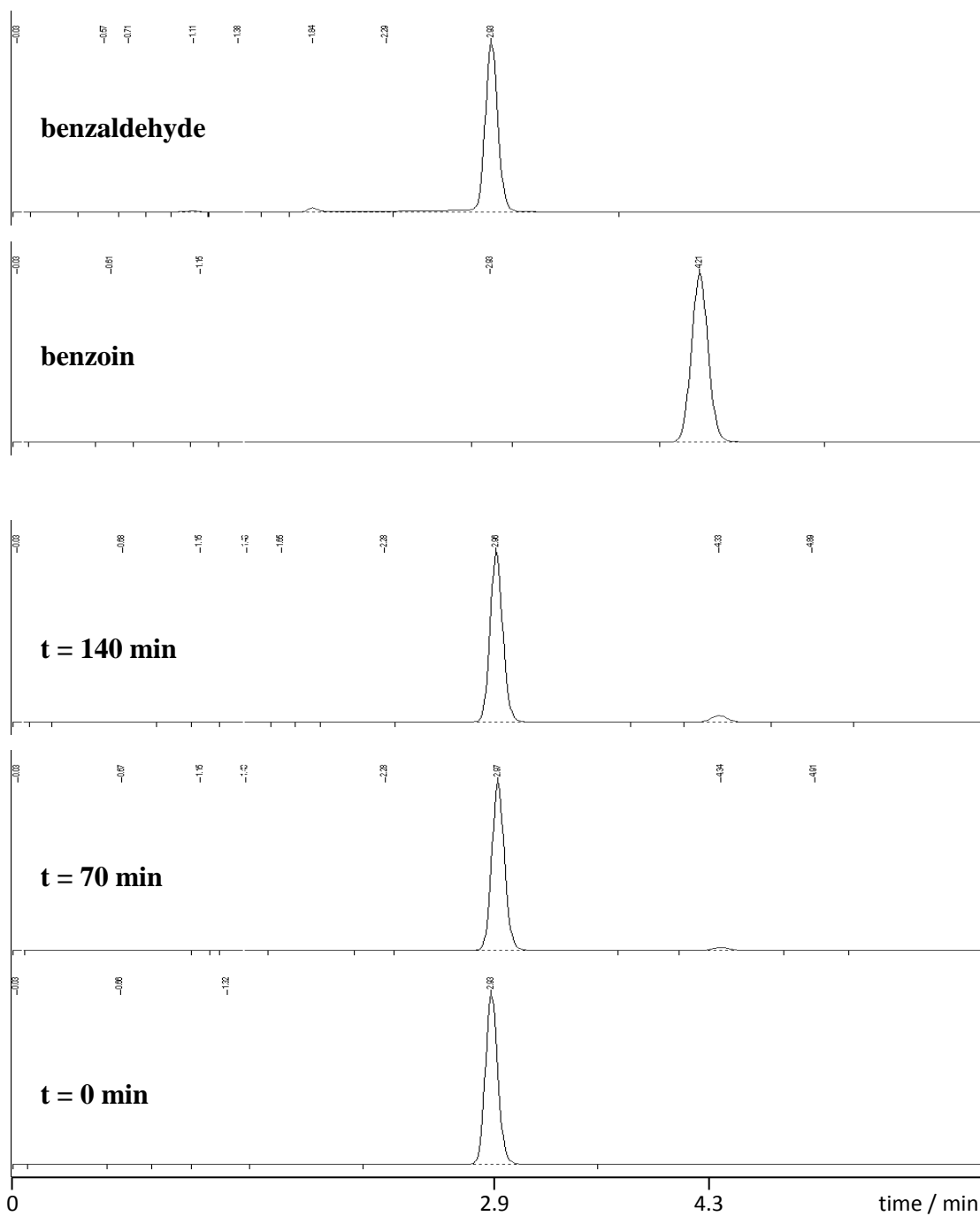
For an equimolar solution of benzaldehyde and benzoin, the value of x (area of benzoin peak / area of benzaldehyde peak) was found to equal 1.05. Assuming the concentration of hydroxybenzyl adduct is negligible under these conditions, the concentrations of benzaldehyde and benzoin may be calculated at each time point using Equations 5.2 and 5.3, where $A_{(PhCHO)}$ = area of benzaldehyde peak, and $A_{(benzoin)}$ = area of benzoin peak.

$$[PhCHO] = \frac{x \times A_{(PhCHO)} \, [PhCHO]_0}{x \times A_{(PhCHO)} + 2 \times A_{(benzoin)}} \qquad \textbf{Equation 5.2}$$

$$[benzoin] = \frac{A_{(benzoin)} \, [PhCHO]_0}{x \times A_{(PhCHO)} + 2 \times A_{(benzoin)}} \qquad \textbf{Equation 5.3}$$

Plots of benzoin concentration against time at three catalyst concentrations are shown in Figures 5.3 – 5.5. Initial rates of benzoin formation were obtained from the slopes of these plots, as described by Equation 5.4. The initial rate is defined as the period up to 10% conversion. Reaction data for the reaction catalysed by 30 mM thiazolium salt **53** is shown in Table 5.1. Reaction data for all other reactions are included in Appendix D.

$$v = \frac{d[benzoin]}{dt} = k_{cat}[PhCHO]^n = k_2[cat]^m[PhCHO]^n \qquad \textbf{Equation 5.4}$$

Figure 5.3: **Plots of benzoin concentration against time for the thiazolium (53) (30 mM) catalysed benzoin condensation, at initial benzaldehyde concentrations 0.32 M, 0.64 M, 0.96 M, 1.28 M, 1.60 M**

Figure 5.4: Plots of benzoin concentration against time for the thiazolium (53) (24 mM) catalysed benzoin condensation, at initial benzaldehyde concentrations 0.32 M, 0.64 M, 0.96 M, 1.28 M, 1.60 M

Figure 5.5: Plots of benzoin concentration against time for the thiazolium (53) (12 mM) catalysed benzoin condensation, at initial benzaldehyde concentrations 0.32 M, 0.64 M, 0.96 M, 1.28 M, 1.60 M
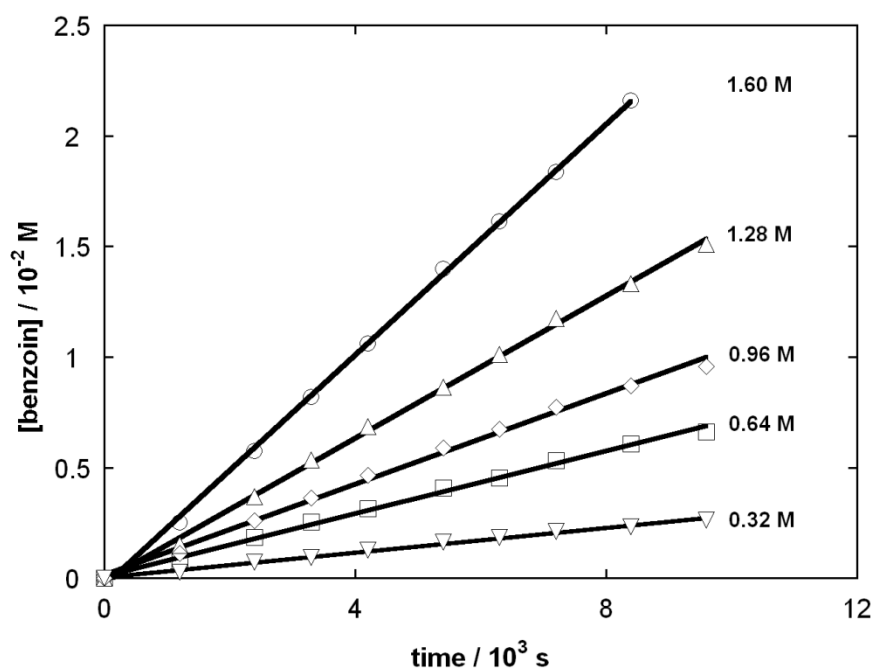
Table 5.1: Reaction data and initial rates of benzoin formation, catalysed by thiazolium salt (53) (30 mM) in 0.16 M triethylamine-buffered methanol (66% f_B) at 50 °C

$[\text{PhCHO}]_0$, M	time, s	A_{PhCHO}	A_{benzoin}	$[\text{PhCHO}]$, M	$[\text{benzoin}]$, M	v_0, M s^{-1} [a]
	0	1	0	0.320	0.00000	
	1200	2548305	7190	0.318	0.00086	
	2400	2380240	18915	0.315	0.00239	
	3300	2848893	31322	0.313	0.00328	
0.32	4200	2706125	38661	0.312	0.00424	9.39×10^{-7}
	5400	2209405	40028	0.309	0.00534	
	6300	2690529	55412	0.308	0.00604	
	7200	2616699	60907	0.306	0.00679	
	8400	2462373	64816	0.305	0.00764	
	0	1	0	0.640	0.00000	
	1200	1409241	6546	0.634	0.00281	
	2400	1364740	16570	0.626	0.00723	
	3300	1381861	23594	0.620	0.01008	
0.64	4200	1152260	25481	0.614	0.01293	3.07×10^{-6}
	5400	945469	26851	0.607	0.01642	
	6300	1496357	50743	0.601	0.01942	
	7200	1490278	57253	0.596	0.02182	
	8400	1449480	65115	0.590	0.02522	
	0	1	0	0.960	0.00000	
	1200	1847128	9119	0.951	0.00447	
	2400	1939313	23703	0.938	0.01092	
	3300	1610529	27875	0.929	0.01532	
0.96	4200	2264369	52282	0.920	0.02022	4.92×10^{-6}
	5400	1716073	52649	0.907	0.02650	
	6300	2422340	89424	0.897	0.03153	
	7200	2074903	84443	0.891	0.03453	
	8400	2096292	100020	0.880	0.03999	
	0	1	0	1.280	0.00000	
	1200	3596779	17665	1.268	0.00593	
	2400	3463488	42043	1.251	0.01446	
	3300	2739751	46923	1.240	0.02022	
1.28	4200	2625988	59252	1.227	0.02637	6.29×10^{-6}
	5400	2691332	79305	1.212	0.03401	
	6300	2787208	95788	1.201	0.03932	
	7200	2795055	114012	1.188	0.04614	
	8400	2543099	114943	1.179	0.05073	
	0	1	0	1.600	0.00000	
	1200	3307491	18438	1.583	0.00841	
	2400	3934153	52394	1.560	0.01979	
	3300	3212005	61181	1.544	0.02801	
1.60	4200	3736838	93560	1.527	0.03642	8.80×10^{-6}
	5400	3602856	118890	1.505	0.04731	
	6300	3500926	135273	1.490	0.05484	
	7200	3723676	165781	1.475	0.06254	
	8400	3612839	188801	1.455	0.07242	

(a) The initial rate of benzoin formation, v_0 (M^{-1} s^{-1}), was obtained from the slope of the plot of benzoin concentration against time in Figure 5.3.

Plots of initial rate against initial benzaldehyde concentration at each precatalyst concentration are shown in Figure 5.6. Reaction order with respect to benzaldehyde is essentially first-order in the range 0.32 – 1.60 M for all three precatalyst concentrations. Pseudo-first-order rate constants, k_{cat} (s^{-1}), were determined from the slopes of these plots and is summarised in Table 5.2.

Figure 5.6:   **First-order plots of initial rates against initial benzaldehyde concentration for reactions performed using thiazolium precatalyst (53) (12 mM, 24 mM and 30 mM)**
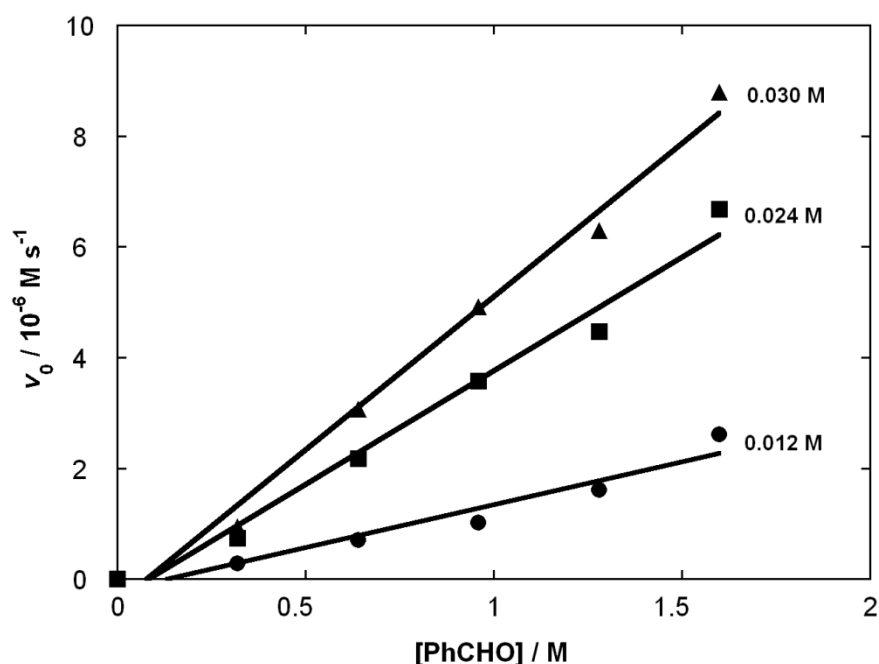
Table 5.2:   **Pseudo-first-order rate constants for the formation of benzoin from benzaldehyde, catalysed by thiazolium salt (53)**

[53], M	k_{cat}, s^{-1}
0.012	1.55×10^{-6}
0.024	4.11×10^{-6}
0.030	5.53×10^{-6}

A plot of k_{cat} against precatalyst concentration is shown in Figure 5.7. Reaction data suggests a first-order dependence with respect to precatalyst over the range of concentrations studied. A value for the second-order rate constant, $k_2 = 1.86 \times 10^{-4}$ M^{-1} s^{-1} was obtained from the slope of the plot.

Figure 5.7: **First-order plot of k_{cat} against concentration of thiazolium salt (53)**
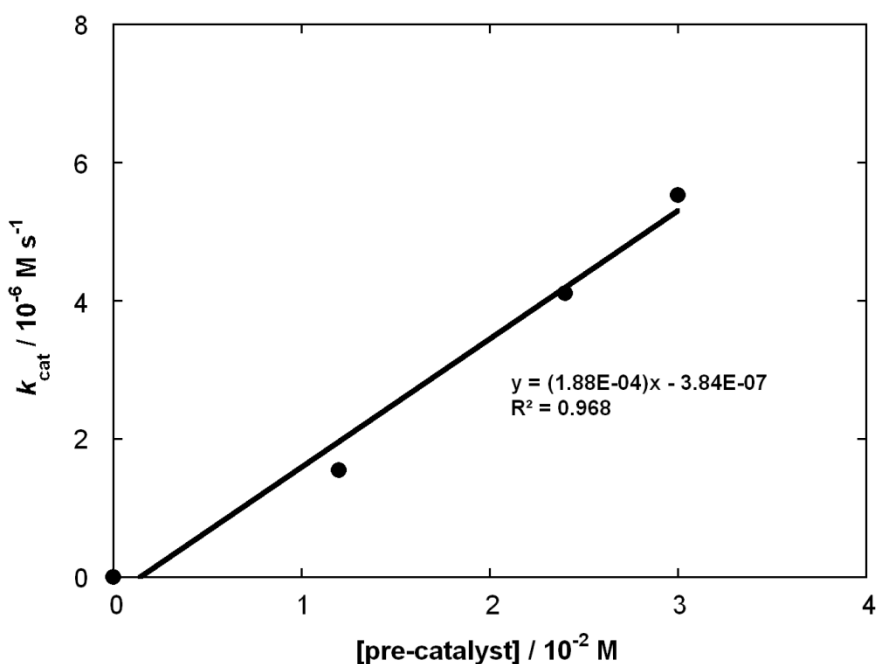
5.2.2 2-Phenyl-6,7-dihydro-5*H*-pyrrolo[2,1-c][1,2,4]triazol-2-ium tetrafluoroborate (139)
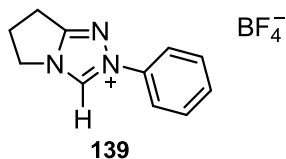
In order to determine reaction order with respect to benzaldehyde for the benzoin condensation catalysed by triazolium precatalyst **139**, a series of initial rates experiments were performed using a catalytic concentration of **139** at a range of initial benzaldehyde concentrations (0.16 – 1.60 M). Reaction order with respect to precatalyst was also probed by performing these experiments at three precatalyst concentrations (6 mM, 12 mM and 24 mM). The progress of the reaction was followed by HPLC, and experimental procedures were as described previously for thiazolium precatalyst **53**.

Plots of benzoin concentration against time at a range of initial benzaldehyde concentrations (0.16 M – 1.60 M) for three precatalyst concentrations are shown in Figures 5.8 – 5.10. Initial rates of benzoin formation were obtained from the slopes of these plots, as described by Equation 5.4.
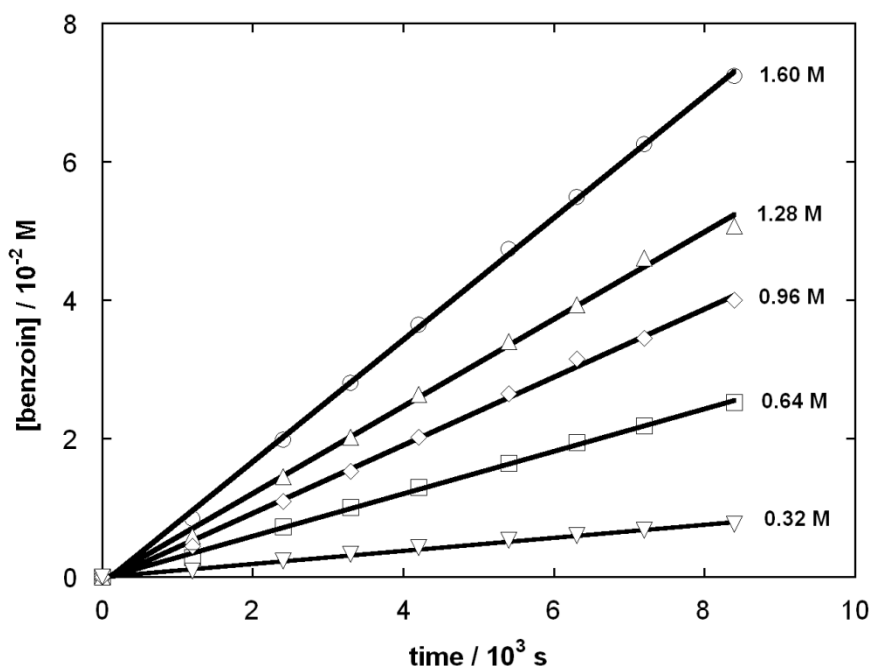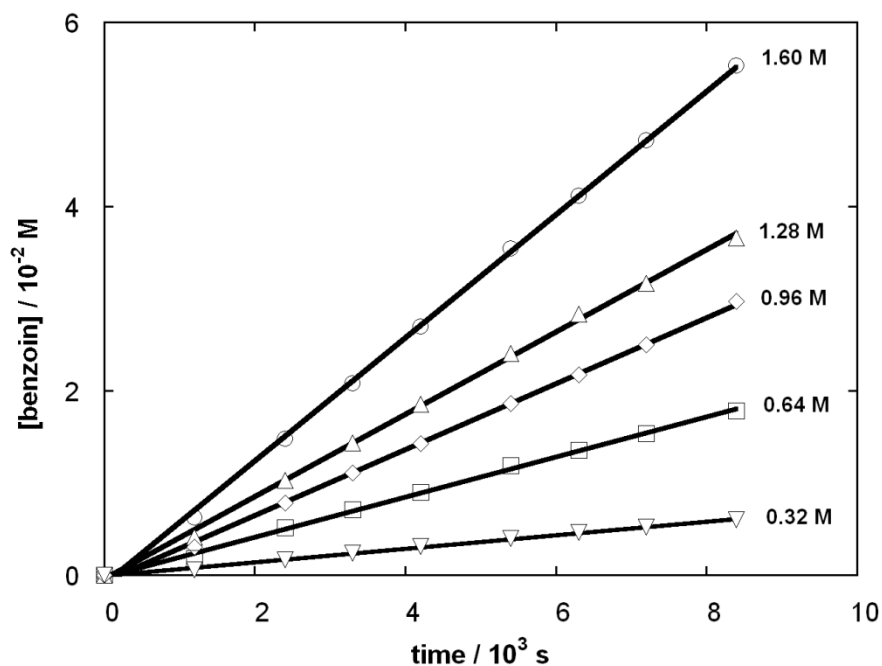
Figure 5.8: Plots of benzoin concentration against time for the triazolium (139) (24 mM) catalysed benzoin condensation, at initial benzaldehyde concentrations 0.16 M, 0.32 M, 0.64 M, 0.96 M, 1.28 M, 1.44 M, 1.60 M
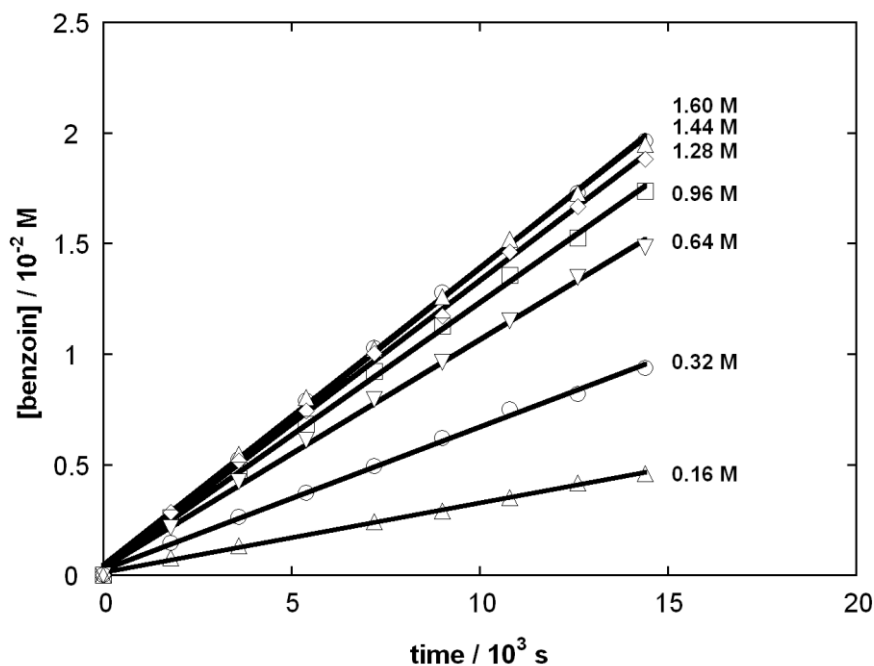
Figure 5.9: Plots of benzoin concentration against time for the triazolium (139) (12 mM) catalysed benzoin condensation, at initial benzaldehyde concentrations 0.16 M, 0.32 M, 0.64 M, 0.96 M, 1.28 M, 1.44 M, 1.60 M
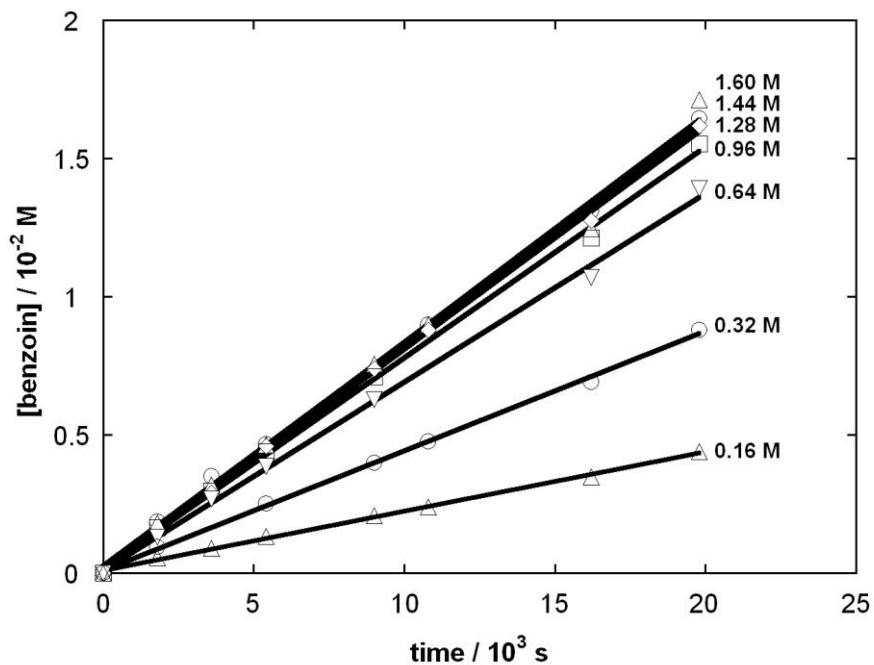
Figure 5.10: Plots of benzoin concentration against time for the triazolium (139) (6 mM) catalysed benzoin condensation, at initial benzaldehyde concentrations 0.16 M, 0.32 M, 0.64 M, 0.96 M, 1.28 M, 1.44 M, 1.60 M
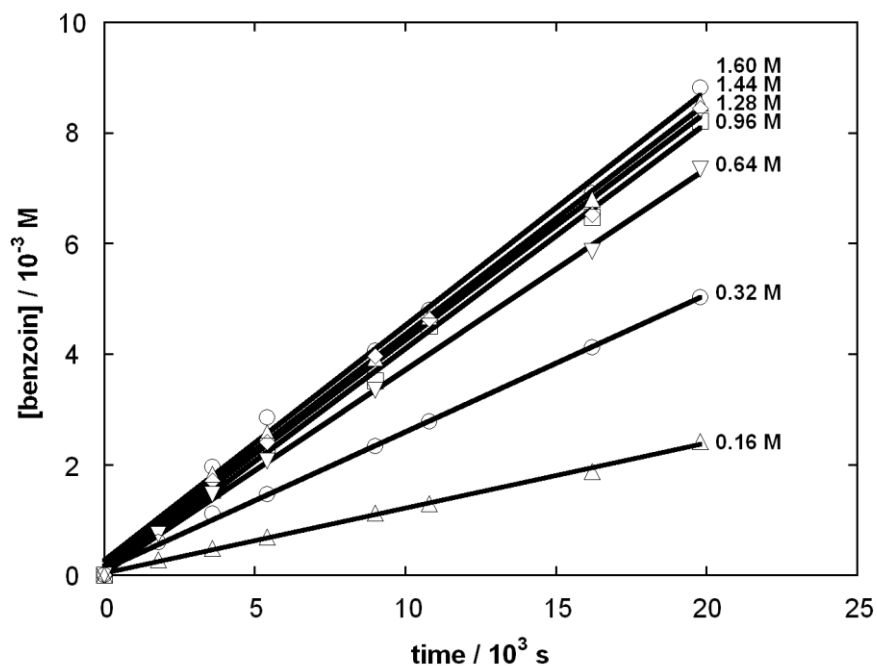

Plots of initial rate against initial benzaldehyde concentration at each precatalyst concentration are shown in Figure 5.11. Values of v_{max} are summarised in Table 5.3.

Figure 5.11: Plots of initial rate against initial benzaldehyde concentration for reactions performed using triazolium precatalyst (139) (6 mM, 12 mM and 24 mM)
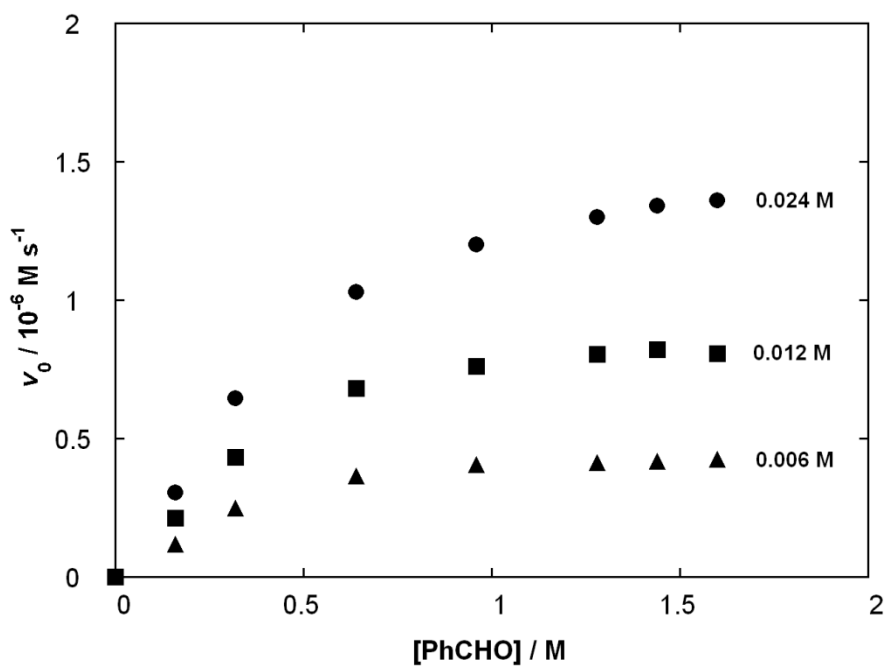
Table 5.3: Values of v_{max} estimated for the benzoin condensation, catalysed by triazolium ion (139)

[139], M	v_{max}, M s^{-1}
0.006	4.25×10^{-7}
0.012	8.11×10^{-7}
0.024	1.40×10^{-6}

To evaluate reaction order with respect to precatalyst, a plot of v_{max} against precatalyst concentration is shown in Figure 5.12. Reaction order with respect to catalyst is also first-order over the range of concentrations studied. An estimate for the second-order rate constant, $k_2 = 5.78 \times 10^{-5}$ M^{-1} s^{-1} was obtained from the slope of the plot. It is likely that the value of v_{max} reported for the reaction at 24 mM precatalyst **139** is slightly underestimated, as the plot of initial rate against aldehyde concentration has not fully levelled off in the aldehyde range studied.

Figure 5.12: Plot of v_{max} against concentration of triazolium salt (139)
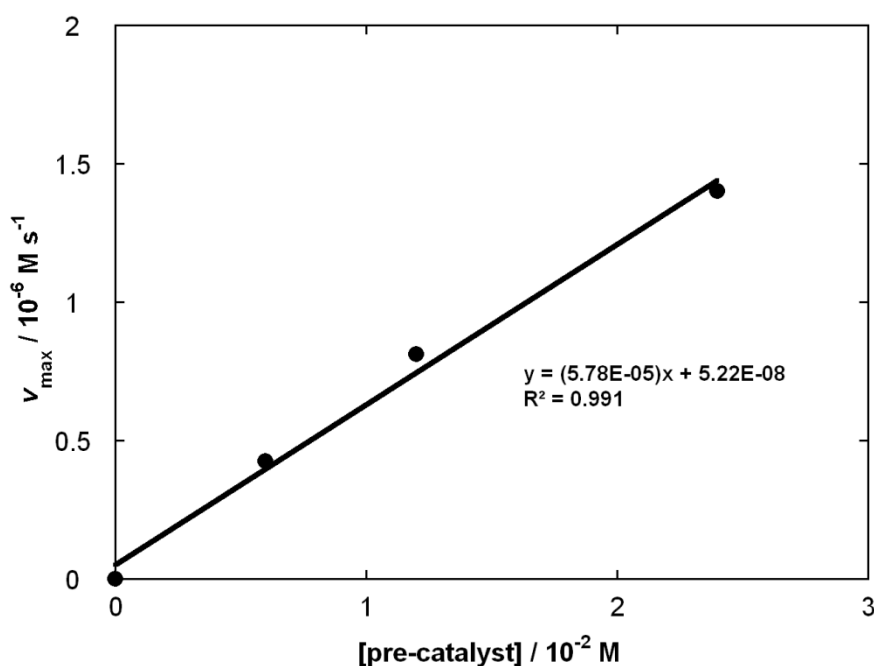
5.2.3   2-(4-Methoxyphenyl)-6,7-dihydro-5*H*-pyrrolo[2,1-c][1,2,4]triazol-2-ium tetrafluoroborate (141)
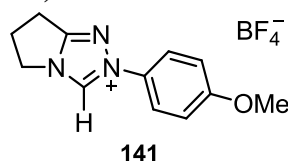
In order to determine reaction order with respect to benzaldehyde for the benzoin condensation catalysed by triazolium precatalyst **141**, a series of initial rates experiments were performed using a catalytic concentration of **141** at a range of initial benzaldehyde concentrations (0.32 – 1.6 M). Reaction order with respect to precatalyst was also probed by performing these experiments at two precatalyst concentrations (6 mM and 12 mM). The progress of the reaction was followed by HPLC, and experimental procedures were as described previously for thiazolium precatalyst **53**.

Plots of benzoin concentration against time at a range of initial benzaldehyde concentrations (0.16 M – 1.60 M) for two precatalyst concentrations are shown in Appendix D (Figures D1 and D2). Initial rates of benzoin formation were obtained from the slopes of these plots, as described by Equation 5.4. Plots of initial rate against initial benzaldehyde concentration at each precatalyst concentration are shown in Figure 5.13. Values of v_{max} are summarised in Table 5.4.

Figure 5.13:   **Plots of initial rate against initial benzaldehyde concentration for reactions performed using triazolium precatalyst (141) (6 mM and 12 mM)**
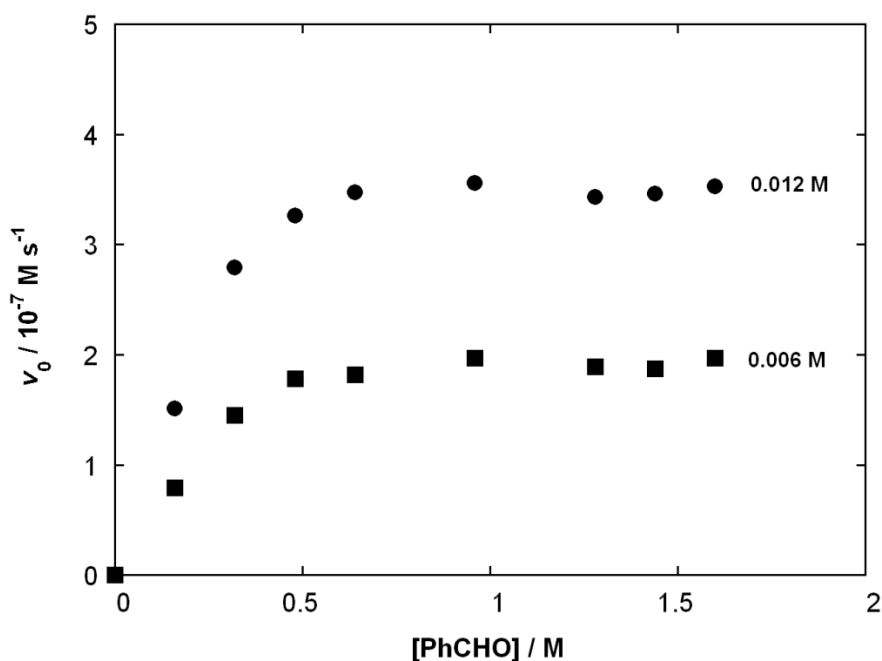
Table 5.4:   Values of v_{max} estimated for the benzoin condensation, catalysed by triazolium ion (141)

[141], M	v_{max}, M s^{-1}
0.006	1.90×10^{-7}
0.012	3.50×10^{-7}

To evaluate reaction order with respect to precatalyst, a plot of v_{max} against precatalyst concentration is shown in Figure 5.14. Reaction order with respect to precatalyst is also first-order over the range of concentrations studied. An estimate for the second-order rate constant, $k_2 = 2.92 \times 10^{-5}$ M^{-1} s^{-1} was obtained from the slope of the plot.

Figure 5.14:   Plot of v_{max} against concentration of triazolium salt (141)

y = (2.92E-05)x + 5.00E-09
R² = 0.998
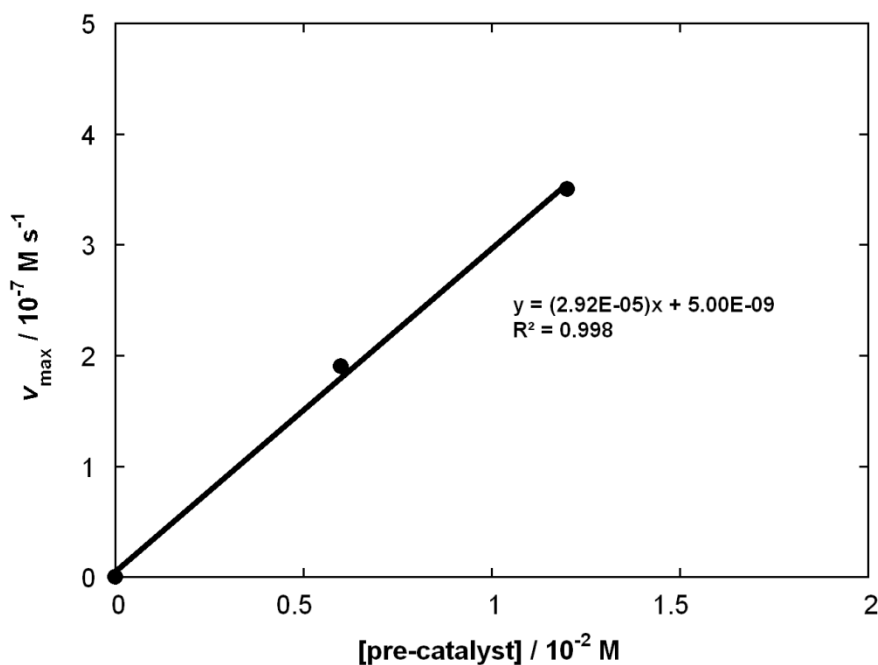
5.2.4 2-Mesityl-6,7-dihydro-5*H*-pyrrolo[2,1-c][1,2,4]triazol-2-ium tetrafluoroborate (140)

140
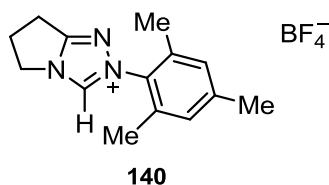
In order to determine reaction order with respect to benzaldehyde for the benzoin condensation catalysed by triazolium precatalyst **140**, a series of initial rates experiments were performed using a catalytic concentration of **140** (12 mM) at a range of initial benzaldehyde concentrations (0.16 – 1.60 M). The progress of the reaction was followed by HPLC, and experimental procedures were as described previously for thiazolium precatalyst **53**.

A plot of benzoin concentration against time at a range of initial benzaldehyde concentrations (0.16 – 1.60 M) is shown in Appendix D (Figure D3). Initial rates of benzoin formation were obtained from the slopes of these plots, as described by Equation 5.4. A plot of initial rate against initial benzaldehyde concentration is shown in Figure 5.15. From this plot, a value of $v_{max} = 5.58 \times 10^{-7}$ M s^{-1} was estimated.

Figure 5.15: **Plot of initial rate against initial benzaldehyde concentration using triazolium precatalyst (140) (12 mM)**
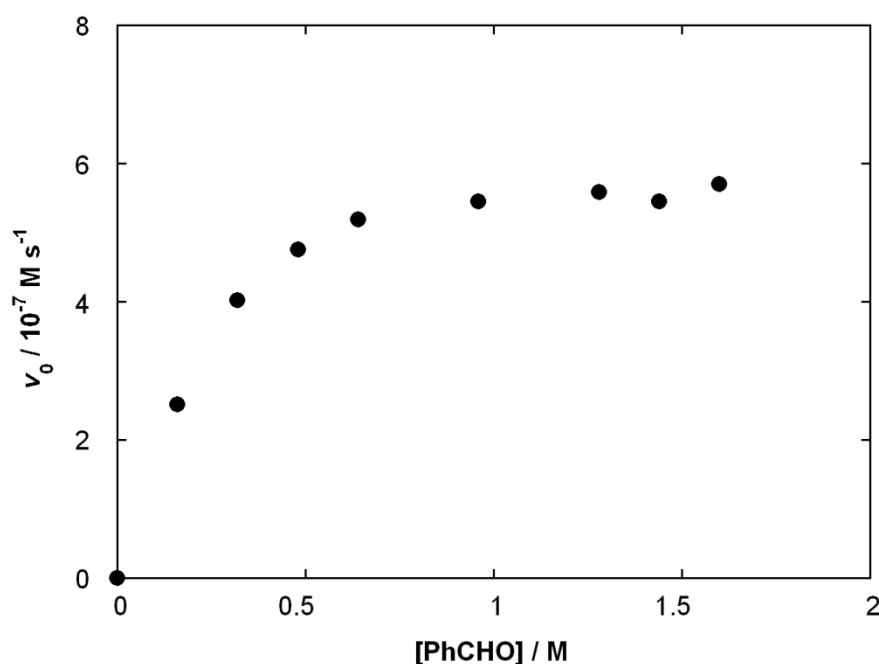
5.2.5   2-(4-Fluorophenyl)-6,7-dihydro-5*H*-pyrrolo[2,1-c][1,2,4]triazol-2-ium tetrafluoroborate (138)
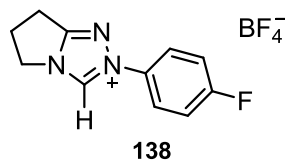
138

In order to determine reaction order with respect to benzaldehyde for the benzoin condensation catalysed by triazolium precatalyst **138**, a series of initial rates experiments were performed using a catalytic concentration of **138** (12 mM) at a range of initial benzaldehyde concentrations (0.16 – 1.60 M). The progress of the reaction was followed by HPLC, and experimental procedures were as described previously for thiazolium precatalyst **53**.

A plot of benzoin concentration against time at a range of initial benzaldehyde concentrations (0.16 – 1.60 M) is shown in Appendix D (Figure D4). Initial rates of benzoin formation were obtained from the slopes of these plots, as described by Equation 5.4. A plot of initial rate against initial benzaldehyde concentration is shown in Figure 5.16. From this plot, a value of $v_{max} = 1.36 \times 10^{-6}$ M s^{-1} was estimated.

Figure 5.16: **Plot of initial rate against initial benzaldehyde concentration using triazolium precatalyst (138) (12 mM)**
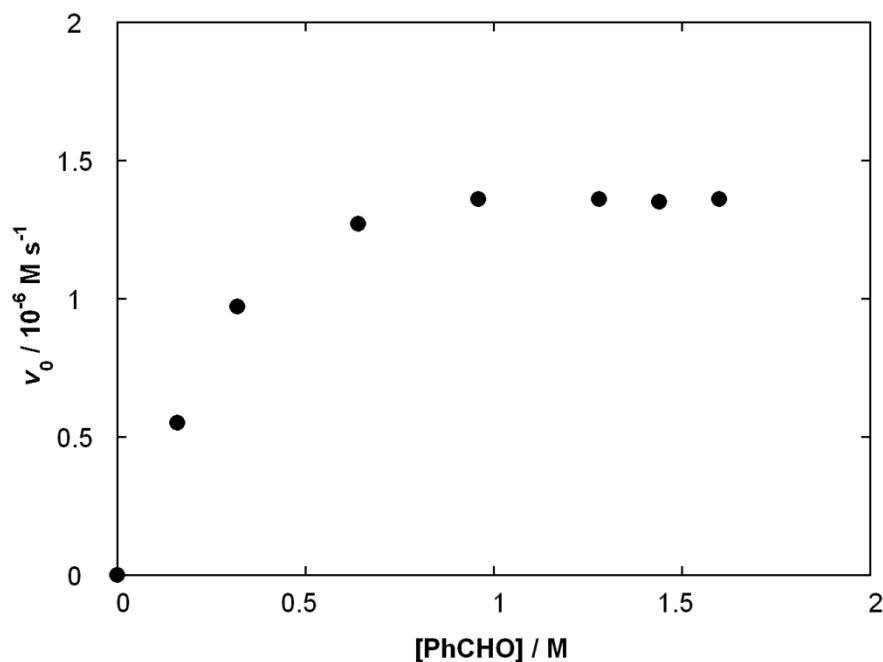
5.2.6   2-(4-Cyanophenyl-6,7-dihydro-5*H*-pyrrolo[2,1-c][1,2,4]triazol-2-ium tetrafluoroborate (137)
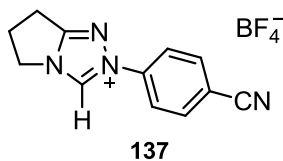
137

In order to determine reaction order with respect to benzaldehyde for the benzoin condensation catalysed by triazolium precatalyst **137**, a series of initial rates experiments were performed using a catalytic concentration of **137** (12 mM) at a range of initial benzaldehyde concentrations (0.16 – 1.60 M). The progress of the reaction was followed by HPLC, and experimental procedures were as described previously for thiazolium precatalyst **53**.

A plot of benzoin concentration against time at a range of initial benzaldehyde concentrations (0.16 – 1.60 M) is shown in Appendix D (Figure D5). Initial rates of benzoin formation were obtained from the slopes of these plots, as described by Equation 5.4. A plot of initial rate against initial benzaldehyde concentration is shown in Figure 5.17. From this plot, a value of $v_{max} = 8.36 \times 10^{-6}$ M s^{-1} was estimated.

Figure 5.17:   **Plot of initial rate against initial benzaldehyde concentration using triazolium precatalyst (137) (12 mM)**
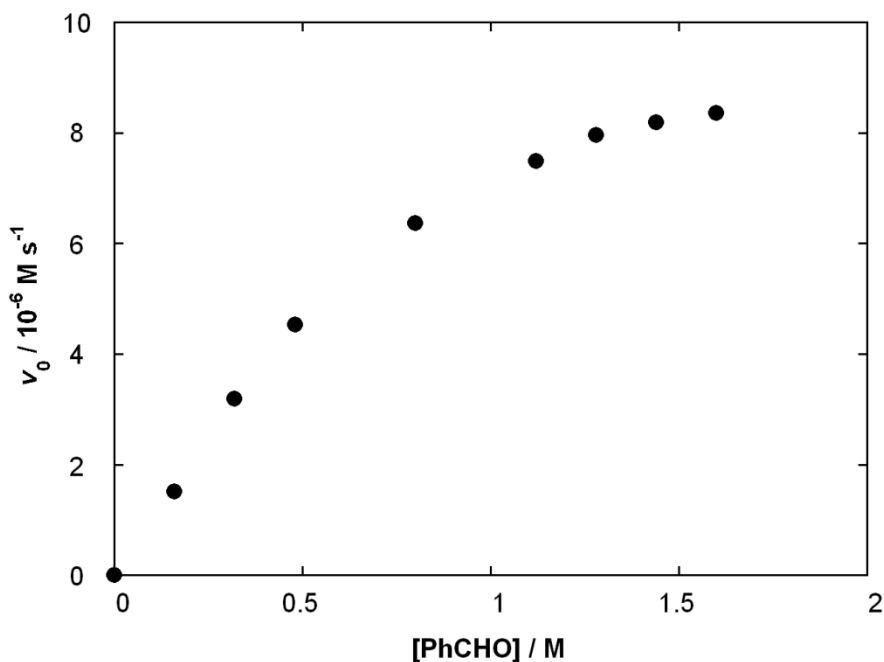
5.2.7   2-Pentafluorophenyl-6,7-dihydro-5*H*-pyrrolo[2,1-c][1,2,4]triazol-2-ium tetrafluoroborate (142)
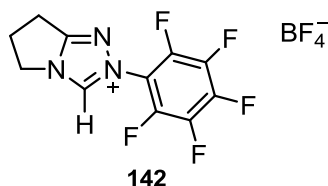
142

In order to determine reaction order with respect to benzaldehyde for the benzoin condensation catalysed by triazolium precatalyst **142**, a series of initial rates experiments were performed using a catalytic concentration of **142** (0.6 mM) at a range of initial benzaldehyde concentrations (0.16 – 1.60 M). The progress of the reaction was followed by HPLC, and experimental procedures were as described previously for thiazolium precatalyst **53**.

A plot of benzoin concentration against time at a range of initial benzaldehyde concentrations (0.16 – 1.60 M) is shown in Appendix D (Figure D6). Initial rates of benzoin formation were obtained from the slopes of these plots, as described by Equation 5.4. A plot of initial rate against initial benzaldehyde concentration is shown in Figure 5.18. From this plot, a value of $v_{max} = 1.45 \times 10^{-5}$ M s^{-1} was estimated for the reaction at 0.6 mM precatalyst concentration. Assuming a first-order dependence on precatalyst, as indicated by studies of **139** and **141**, a value of $v_{max} = 2.91 \times 10^{-4}$ M s^{-1} was estimated for the reaction at 12 mM, for comparison with other precatalysts.

Figure 5.18:   Plot of initial rate against initial benzaldehyde concentration using triazolium precatalyst (142) (0.6 mM)
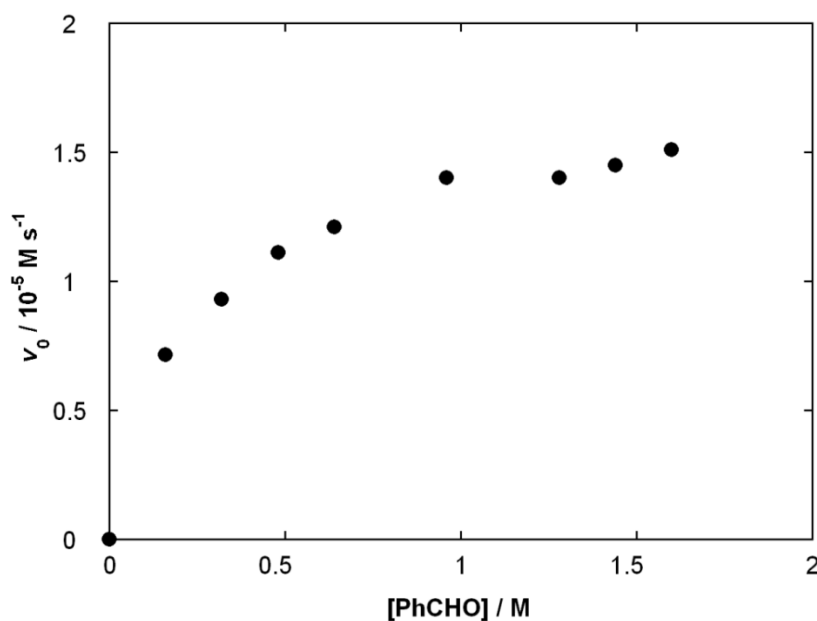
5.3   Discussion

5.3.1   Kinetics of the thiazolium-catalysed benzoin condensation

The self-condensation of benzaldehyde, catalysed by thiazolium salt **53**, shows a first-order dependence with respect to aldehyde across the full range of aldehyde concentrations studied. These results are consistent with the observations of Leeper and White, who observed first-order kinetics under similar conditions (Figure 5.1). Furthermore, our estimate of $k_{cat} = 5.53 \times 10^{-6}$ s^{-1} compares favourably with the value of $k_{cat} = 6 \times 10^{-6}$ s^{-1} determined by the authors at a precatalyst concentration of 30 mM. Our measurements of k_{cat} at several precatalyst concentrations suggest a first-order relationship with respect to precatalyst.

5.3.2   Kinetics of the triazolium-catalysed benzoin condensation

In contrast, triazolium precatalysts **137 – 142** display significantly different kinetics to the thiazolium precatalyst. For all triazolium salts studied, plots of initial rate against initial benzaldehyde concentration show two distinct regions: an initial first-order dependence on aldehyde at low benzaldehyde concentrations (~0.16 – 0.48 M), followed by a zero-order dependence at higher concentrations as the initial rate of catalysis reaches a maximum. One possible mechanistic explanation that may account for this profile is described below.

Scheme 5.3:
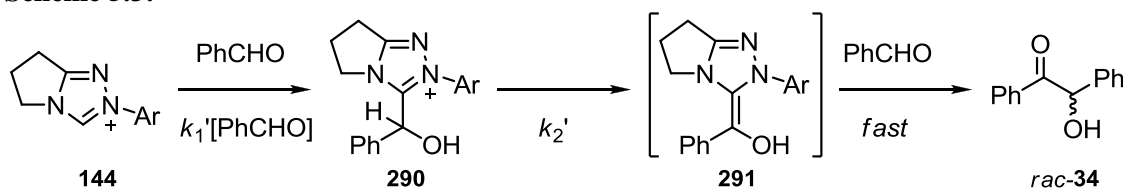
According to Scheme 5.3, the rate of adduct formation (k_1[PhCHO]) is dependent on aldehyde, whilst the rate of adduct deprotonation to give products (k_2) is not. At low benzaldehyde concentrations, the term for adduct formation may be significantly slower than for its deprotonation and would result in a first-order dependence of initial rate on starting benzaldehyde concentration. As the concentration of aldehyde increases, the term for the rate of adduct formation may exceed the rate of its

deprotonation – which occurs at a rate that is independent of aldehyde. From the stoichiometric studies by ^{1}H NMR spectroscopy described earlier, deprotonation of the adduct was found to be clearly rate determining

Similar initial-rates experiments performed by Collett and Smith on the Stetter reaction support these claims.[4] For the *N*-phenyl triazolium **139**-catalysed Stetter reaction of substrate **58** (Scheme 5.3), the initial rate of formation of **59** was measured as a function of aldehyde concentration. In the previous chapter we demonstrated that the presence of an *ortho*-alkoxyl substituent in the aldehyde substrate results in significantly faster rates of adduct formation than for unsubstituted benzaldehyde. Under the same buffer conditions, a zero-order dependence on aldehyde is observed across the full range of substrate concentrations (Figure 5.19). This is consistent with the notion that adduct formation has exceeded adduct deprotonation for this more reactive aldehyde.

Scheme 5.4:
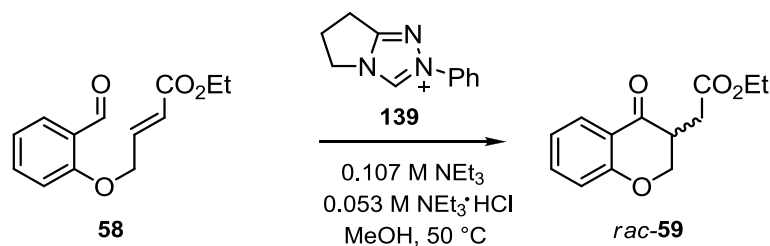
Figure 5.19: Plot of initial rate against initial concentration of aldehyde (58) for reactions performed using triazolium precatalyst (139) (10 mM, 20 mM and 40 mM)
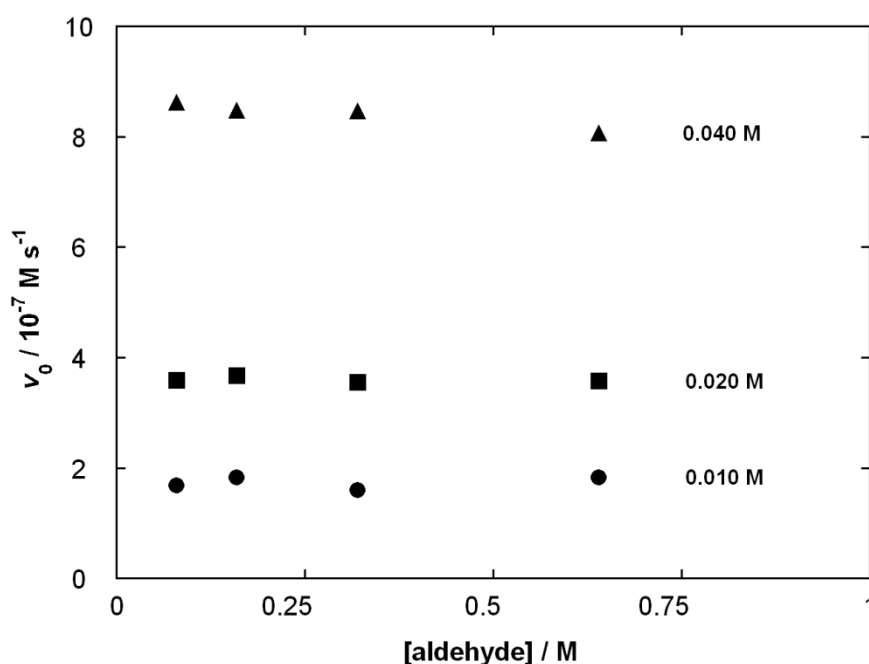
Within the series of triazolium precatalysts studied, a trend towards enhanced catalytic activity with increased electron-withdrawing character of the *N*-aryl ring is apparent. This is consistent with our *in situ* reaction studies under stoichiometric conditions, and supports the reactivity series in dichloromethane-d$_2$ obtained by Collett and Smith outlined in the introduction to this chapter (Scheme 5.2). A tentative Brønsted plot of log(v_{max}) against precatalyst pK_a is shown in Figure 5.20, for the benzoin condensation using 12 mM triazolium precatalyst. As mentioned previously, the pK_a values for triazolium ions **137** and **142** at the lower end of this plot may be up to 1 unit lower than the quoted values, and may partly explain the unrealistic slope of < -1.

Figure 5.20:   **Brønsted plot for triazolium salt-catalysed benzoin condensation**
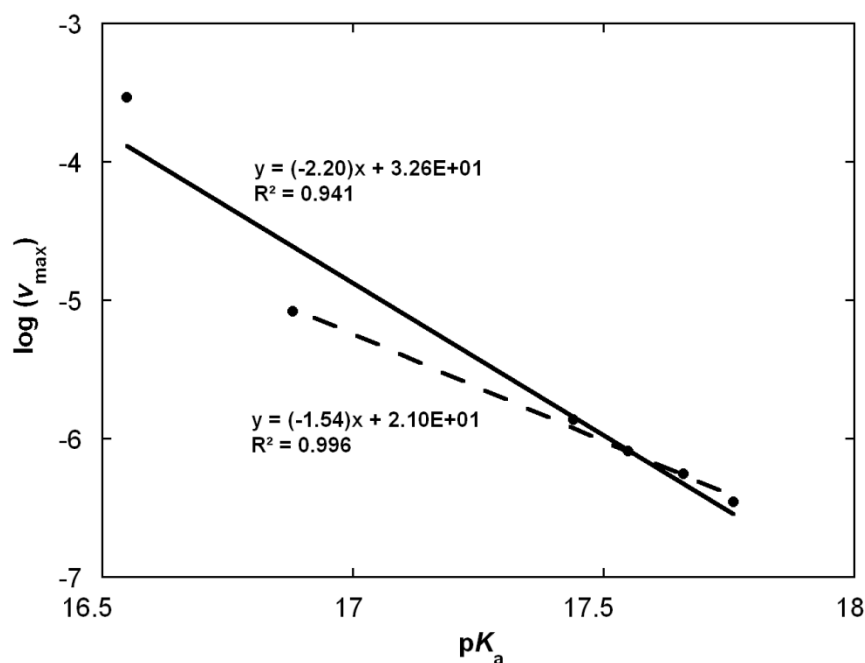
5.4   Summary

An initial-rates kinetic study of the thiazolium and triazolium-catalysed benzoin condensation was performed in triethylamine-buffered methanol at 50 °C. The concentration of benzoin was determined using an HPLC analysis method, from the relative integrals of the absorbances at 254 nm for aldehyde and product.

The thiazolium-catalysed reaction showed a first-order dependence with respect to benzaldehyde over the range studied (0.32 − 1.60 M), with a first-order rate constant ($k_{cat} = 5.53 \times 10^{-6}$ M^{-1} s^{-1}) for the reaction catalysed by 30 mM in good agreement with the value previously obtained by Leeper ($k_{cat} = 6 \times 10^{-6}$ M^{-1} s^{-1}) under the same conditions. An apparent first-order dependence on precatalyst was also observed, although additional experiments at higher concentrations may be necessary to firmly rule out a higher order dependence.

The triazolium precatalysts showed significantly altered behaviour, with a first-order dependence on aldehyde at low concentrations, proceeding to a zero-order dependence at higher concentrations. Triazolium precatalysts bearing electron withdrawing *N*-aryl substituents result in faster rates of benzoin formation, in agreement with catalytic studies of the Stetter reaction carried out by Collett and Smith. These combined observations are consistent with rate-determining deprotonation of the 3-(hydroxybenzyl)triazolium adduct at higher aldehyde concentrations in the benzoin condensation. Our studies also indicate a first-order dependence on triazolium precatalyst.

References

1   M.J. White and F.J. Leeper, *J. Org. Chem.*, 2001, **66**, 5124.

2   J. L. Moore, A. P. Silvestri, J. Read de Alaniz, D. A. DiRocco and T. Rovis, *Org. Lett.*, 2011, **13**, 1742.

3   C. J. Collett, R. S. Massey, O. R. Maguire, A. S. Batsanov, A. C. O'Donoghue and A. D. Smith, *Chem. Sci.*, 2013, **4**, 1514.

4   C. J. Collett, A. D. Smith, Ph.D. Thesis, 2013, University of St. Andrews, St. Andrews.

CHAPTER   6

Experimental

6.0   Foreword

This chapter details the experimental methods and equipment used in these investigations, and is divided into five sections. Section 6.1 describes general instrumentation and Section 6.2 gives details of chemical materials. Section 6.3 details the synthetic procedures used to obtain the catalysts and substrates. Section 6.4 and Section 6.5 describe the preparation of solutions and kinetic methods.

6.1   General Instrumentation

NMR: NMR samples were prepared in chloroform-d_1, deuterium oxide-d_2, dichloromethane-d_2, dimethyl sulfoxide-d_6, and methanol-d_4. ^{1}H and ^{13}C NMR chemical shifts are reported relative to residual solvent peaks as stated in Table 6.1.[1] Tetramethylsilane (TMS) was used as an internal reference in chloroform-d_1, dichloromethane-d_2 and methanol-d_4.

Table 6.1:   **NMR solvents and reference signals**

solvent	δ_H, ppm	δ_C, ppm
chloroform-d_1	7.26	77.2
deuterium oxide-d_1	4.79	-
dichloromethane-d_2	5.32	53.8
dimethyl sufoxide-d_6	2.50	39.5
methanol-d_4	3.31	49.0

Data are presented as follows: chemical shift (ppm), integration, multiplicity (br = broad, s = singlet, d = doublet, t = triplet, q = quartet, m = multiplet), coupling constants (Hz), and assignment. NMR spectra at 400, 500, 600 and 700 MHz were recorded on Varian Mercury-400, Bruker Avance-400, Varian Inova-500, Varian VNMRS-600 and Varian VNMRS-700 instruments.

EA: Elemental analyses were obtained from the Microanalytical Unit (Department of Chemistry, Durham University), and performed on an Exeter CE-440 Elemental Analyser.

MS: Low resolution mass spectrometry was performed on a Waters *TQD* mass spectrometer. High resolution mass spectrometry was performed on a Thermo-Finnigan *LTQ FT* mass spectrometer.

IR: Infrared spectra were obtained as neat samples on a Perkin Elmer Spectrum *RX I* FT-IR spectrometer.

Chromatography: Thin layer chromatography was performed using silica-backed Machery-Nagel Polygram SILG/UV$_{254}$ plates. Column chromatography was performed using silica gel.

LC-MS: Samples were run on a Waters Mass Directed Auto Preparation (MDAP) system using an XBridge C18 OBD 19 × 100 mm (i.d. = 5 μm) column. Separation was achieved using a water-methanol gradient method (Table 6.2) and flow rate 17 mL min^{-1}. Detection by mass spectrometry was by ES+.

Table 6.2:   Preparative LC-MS gradient

time, min	% water	% methanol	curve
0	90	10	0
0.2	90	10	6
0.7	90	10	6
11	5	95	6
14	5	95	6
14.5	90	10	6
16.5	90	10	1

6.2   Materials

NMR Solvents: Deuterium oxide-d$_2$ (99.9 atom % D), dichloromethane-d$_2$ (99.8 atom % D), dimethyl sulfoxide-d$_6$ (99.9 atom % D) and methanol-d$_4$ (99.8 atom % D) were purchased from Goss Scientific. Chloroform-d$_1$ (99.8 atom % D) was purchased from Sigma-Aldrich. Potassium deuteroxide (99.8 atom % D, 40 wt %) and deuterium chloride (99 atom % D, 35 wt %) were purchased from Apollo Scientific and Sigma-Aldrich respectively.

Azolium ion substrates: 3-Benzyl-5-(2-hydroxyethyl)-4-methylthiazolium chloride (**53**) and 3-mesityl-5,6,7,8-tetrahydro-4*H*-cycloheptathiazolium perchlorate (**151**) were purchased from Sigma-Aldrich and were used without further purification. Bridged *bis*-propyl *bis*-imidazolium diiodide (**152**) was donated by Prof. John Murphy (University of Strathclyde). 1,2,3-Triazolium ions **204 – 207** and imidazolium ions **208 – 210** were donated by Prof. Martin Albrecht (University College Dublin). Imidazolium and 4,5-dihydroimidazolium salts **70**, **74**, **156** and **275** were prepared by former members of our laboratory. Tetramethylammonium deuteriosulfate was donated by Prof. Tina Amyes (University of Buffalo).

Other reagents: Acetonitrile (HPLC grade) and methanol (HPLC grade) were purchased from Fisher Scientific. Benzaldehyde and triethylamine were purchased from Sigma-Aldrich and distilled prior to use. Mesitylhydrazine hydrochloride, was donated by Prof. Andrew Smith (University of St. Andrews). Unless stated, all other chemicals were reagent grade and used without further purification. Reactions involving air or moisture sensitive reagents were performed under an argon atmosphere using oven-dried glassware. Solvents were dried prior to use using an Innovative Technology Inc. solvent purification system.

6.3   Synthetic Procedures

6.3.1   Synthesis of 1,2,4-triazolium and imidazolium salts

6.3.1.1   2-Pentafluorophenyl-6,7-dihydro-5*H*-pyrrolo[2,1-c][1,2,4]triazol-2-ium tetrafluoroborate (142)
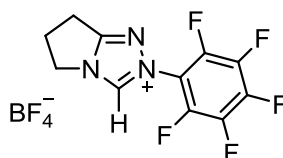
Based on a procedure by Rovis and co-workers,[2] trimethyloxonium tetrafluoroborate (3.22 g, 22 mmol) was added to a solution of 2-pyrrolidinone (1.85 g, 22 mmol) in dry dichloromethane (100 mL) and stirred for 24 h at r.t. under an inert atmosphere. Pentafluorophenylhydrazine (4.33 g, 22 mmol) was then added, and the solution stirred for a further 48 h at r.t. under an inert atmosphere. The solvent was removed under reduced pressure, and the residue dissolved in triethyl orthoformate (50 mL) and refluxed for 24 h. The solvent was removed under reduced pressure and precipitated and washed with ethyl acetate to yield the title compound as a white solid (1.13 g, 18%), with spectroscopic details in accordance with the literature. **m.p.** 250–252 °C {lit.[2] 248–253 °C}; **^{1}H NMR** (500 MHz, MeOD-d$_4$): δ_H 2.76 (2H, quintet, *J*=7.4, CH$_2$), 3.16 (2H, t, *J*=7.8, CH$_2$), 4.43 (2H, t, *J*=7.4, CH$_2$); **^{13}C NMR** (125 MHz, MeOD-d$_4$): δ_C 24.3 (CH$_2$), 29.2 (CH$_2$), 58.2 (CH$_2$), 113.6 (Cq), 139.7 (ArCN), 144.4 (2 × ArCF), 145.3 (ArCF), 146.4 (2 × ArCF), 167.5 (NCN); **^{19}F NMR** (400 MHz, CDCl$_3$): δ_F − 146.53 (2F, d, *J*=19.4, ArF), 147.51 (1F, t, *J*=21.5, ArF), −150.58 (br s, BF$_4$), −150.63 (q, BF$_4$), −159.64 (2F, t, *J*=19.0, ArF); ***m/z*** (ES+): 276 ([M–BF$_4$]$^+$, 100%); **HRMS** (ES+): [M–BF$_4$]$^+$ C$_{11}$H$_7$N$_3$F$_5$ requires 276.0566, found 276.0560.

6.3.1.2   2-Phenyl-6,7-dihydro-5*H*-pyrrolo[2,1-c][1,2,4]triazol-2-ium tetrafluoroborate (139)
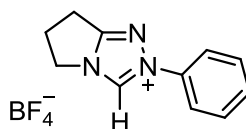
Based on a procedure by Rovis and co-workers,[2] trimethyloxonium tetrafluoroborate (9.05 g, 61 mmol) was added to a solution of 2-pyrrolidinone (4.72 g, 56 mmol) in dry dichloromethane (250 mL) and stirred for 24 h at r.t. under an inert atmosphere. Phenylhydrazine (6 mL, 61 mmol) was then added, and the solution stirred for a further 48 h at r.t. under an inert atmosphere. The solvent was removed under reduced pressure, and the residue dissolved in methanol (25 mL) and triethyl orthoformate (50 mL, 297 mmol) and refluxed for 24 h. The solvent was removed under reduced pressure and precipitated and washed with ethyl acetate to yield the title compound as a yellow solid (12.36 g, 81%), with spectroscopic details in accordance with the literature. **m.p.** 154–156 °C {lit.[3] 154–156 °C}; **^{1}H NMR** (700 MHz, D$_2$O): δ_H 2.75 (2H, q, *J*=7.6 Hz, CH$_2$), 3.13 (2H, t, *J*=7.7Hz, CH$_2$), 4.37 (2H, t, *J*=7.4 Hz, CH$_2$), 7.50–7.56 (3H, m, ArH), 7.66 (2H, dd, *J*=8.1 Hz, ArH), 9.98 (1H, s, NCH(N)); **^{13}C NMR** (176 MHz, D$_2$O): δ_C 21.3 (CH$_2$), 26.5 (CH$_2$), 47.3 (CH$_2$), 121.3 (2 × ArCH), 130.1 (2 × ArCH), 130.9 (ArCH), 135.3 (ArCN), 163.8 (NCN); ***m/z*** (ES+): 186 ([M–BF$_4$]$^+$, 100%); **EA** Calc. for C$_{11}$H$_{12}$N$_3$BF$_4$: %C 48.39, %H 4.43, %N 15.39; Found: %C 47.26, %H 4.44, %N 15.20.

6.3.1.3   2-Mesityl-6,7-dihydro-5*H*-pyrrolo[2,1-c][1,2,4]triazol-2-ium tetrafluoroborate (140)

Based on a procedure by Smith and co-workers,[4] trimethyloxonium tetrafluoroborate (0.87 g, 6 mmol) was added to a solution of 2-pyrrolidinone (0.5 g, 6 mmol) in anhydrous dichloromethane (30 mL) and stirred for 24 h at r.t. under an inert atmosphere. Mesitylhydrazine hydrochloride (1.50 g, 8 mmol) was dissolved in aqueous NaOH (1 M), and extracted into dichloromethane. This solution was immediately added to the reaction mixture, and stirred for a further 48 h at r.t. under an inert atmosphere. The solvent was removed under reduced pressure, and the residue dissolved in chlorobenzene (10 mL) and triethyl orthoformate (5 mL) and refluxed for

72 h. The solvent was removed under reduced pressure and precipitated and washed with ethyl acetate to yield the title compound as a pale brown solid (1.22 g, 66%) with spectroscopic details in accordance with the literature. **m.p.** 175–177 °C {lit.[4] 174–176 °C}; **^{1}H NMR** (400 MHz, CDCl$_3$): δ_H 2.06 (6H, s, 2 × CH$_3$), 2.36 (3H, s, CH$_3$), 2.89 (2H, m, CH$_2$), 3.25 (2H, t, *J*=7.7 Hz, CH$_2$), 4.70 (2H, t, *J*=7.4 Hz, CH$_2$), 6.99 (2H, s, 2 × ArCH), 9.51 (1H, s, NCH(N)); **^{13}C NMR** (101 MHz, CDCl$_3$): δ_C 17.4 (2 × CH$_3$), 21.4 (CH$_3$), 22.1 (CH$_2$), 26.8 (CH$_2$), 48.1 (CH$_2$), 129.8 (2 × ArCH), 132.0 (ArC), 135.3 (2 × ArC), 141.6 (ArC), 142.1 (ArCN), 162.9 (NCN); ***m/z*** (ES+): 228 ([M–BF$_4$]$^+$, 100%).

6.3.1.4 2-(4-Methoxyphenyl)-6,7-dihydro-5*H*-pyrrolo[2,1-c][1,2,4]triazol-2-ium tetrafluoroborate (141)
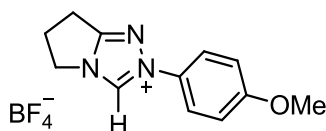
Based on a procedure by Smith and co-workers,[3] trimethyloxonium tetrafluoroborate (2.25 g, 15 mmol) was added to a solution of 2-pyrrolidinone (1.18 g, 14 mmol) in anhydrous dichloromethane (50 mL) and stirred for 24 h at r.t. under an inert atmosphere. 4-Methoxyphenylhydrazine hydrochloride (3.49 g, 20 mmol) was dissolved in aqueous NaOH (1 M), and extracted into dichloromethane. This solution was immediately added to the reaction mixture, and stirred for a further 48 h at r.t. under an inert atmosphere. The solvent was removed under reduced pressure, and the residue dissolved in methanol (15 mL) and triethyl orthoformate (40 mL) and refluxed for 24 h. The solvent was removed under reduced pressure and precipitated and washed with ethyl acetate to yield the title compound as an off-white solid (3.27 g, 72%), with spectroscopic details in accordance with the literature. **m.p.** 159–161 °C {lit.[3] 155–157}; **^{1}H NMR** (700 MHz, CDCl$_3$): δ_H 2.87 (2H, m, CH$_2$), 3.23 (2H, t, *J*=7.8 Hz, CH$_2$), 3.86 (3H, s, OCH$_3$), 4.62 (2H, t, *J*=7.4 Hz, CH$_2$), 7.01 (2H, d, *J*=9.1 Hz, ArH), 7.71 (2H, d, *J*=9.1 Hz, ArH), 9.97 (1H, s, NCH(N)); **^{13}C NMR** (176 MHz, CDCl$_3$): δ_C 22.0 (CH$_2$), 26.8 (CH$_2$), 47.8 (CH$_2$), 55.90 (OCH$_3$), 115.4 (2 × ArCH), 122.8 (2 × ArCH), 128.8 (ArCN), 137.1 (NCH(N)), 161.5 (ArCO), 162.5 (NCN); ***m/z*** (ES+): 216 ([M–BF$_4$]$^+$, 100%); **HRMS** (ES+): [M–BF$_4$]$^+$ C$_{12}$H$_{14}$N$_3$O requires 216.1137, found 216.1122.

6.3.1.5   2-(4-Fluorophenyl)-6,7-dihydro-5*H*-pyrrolo[2,1-c][1,2,4]triazol-2-ium tetrafluoroborate (138)
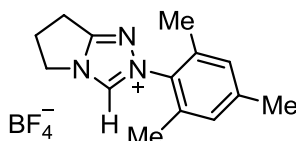

Based on a procedure by Rovis and co-workers,[2] trimethyloxonium tetrafluoroborate (2.25 g, 15 mmol) was added to a solution of 2-pyrrolidinone (1.18 g, 14 mmol) in anhydrous dichloromethane (50 mL) and stirred for 24 h at r.t. under an inert atmosphere. 4-Fluorophenylhydrazine hydrochloride (3.25 g, 20 mmol) was dissolved in aqueous NaOH (1 M), and extracted into dichloromethane. This solution was immediately added to the reaction mixture, and stirred for a further 48 h at r.t. under an inert atmosphere. The solvent was removed under reduced pressure, and the residue dissolved in methanol (15 mL) and triethyl orthoformate (40 mL, 238 mmol) and refluxed for 24 h. Solvent was removed under reduced pressure and precipitated and washed with ethyl acetate to yield the title compound as an off-white solid (2.37 g, 58%). **m.p.** 109–111 °C; **^{1}H NMR** (700 MHz, CDCl$_3$): δ_H 2.84 (2H, quintet, *J*=7.6 Hz, CH$_2$), 3.21 (2H, t, *J*=7.4 Hz, CH$_2$), 4.56 (2H, t, *J*=7.4 Hz, CH$_2$), 7.20 (2H, dd, *J*=9.2, 7.9 Hz, ArH), 7.78 (2H, dd, *J*=9.2, 4.5 Hz, ArH), 9.92 (1H, s, NCH(N)); **^{13}C NMR** (176 MHz, CDCl$_3$): δ_C 21.9 (CH$_2$), 26.8 (CH$_2$), 47.7 (CH$_2$), 117.3 (d, *J*=23.6 Hz, 2 × ArCH), 123.5 (d, *J*=9.1, 2 × ArCH), 132.0 (d, *J*=3.1 Hz, ArCN), 137.8 (NCH(N)), 162.9 (NCN), 164.3 (d, *J*=251.9 Hz, ArCF); **^{19}F NMR** (376 MHz, DMSO-*d$_6$*): δ_F − 110.7 (ArF), −148.6 (s, BF$_4$), −148.7 (s, BF$_4$); **v_{max}/cm^{-1}** (neat): 3135, 2357, 1595, 1528, 1514, 1389, 1230, 1030; **m/z** (ES+): 204 ([M–BF$_4$]$^+$, 100%); **HRMS** (ES+): [M–BF$_4$]$^+$ C$_{11}$H$_{11}$FN$_3$ requires 204.0937, found 204.0932.

6.3.1.6   2-(4-Cyanophenyl)-6,7-dihydro-5*H*-pyrrolo[2,1-c][1,2,4]triazol-2-ium tetrafluoroborate (137)

Based on a procedure by Rovis and co-workers,[2] trimethyloxonium tetrafluoroborate (0.87 g, 5.9 mmol) was added to a solution of 2-pyrrolidinone (0.50 g, 5.9 mmol) in anhydrous dichloromethane (30 mL) and stirred for 24 h at r.t. under an inert atmosphere. 4-Cyanophenylhydrazine hydrochloride (1.27 g, 7.5 mmol) was dissolved in aqueous NaOH (1 M), and extracted into dichloromethane. This solution was immediately added to the reaction mixture, and stirred for a further 48 h at r.t. under an

inert atmosphere. The solvent was removed under reduced pressure, and the residue dissolved in chlorobenzene (15 mL) and triethyl orthoformate (2.93 mL) and refluxed for 24 h. The solvent was removed under reduced pressure and precipitated and washed with toluene to yield the title compound as a pale brown solid (1.45 g, 81%). **m.p.** 125–127 °C; **^{1}H NMR** (700 MHz, D$_2$O): δ_H 2.92 (2H, quintet, *J*=7.6 Hz, CH$_2$), 3.31 (2H, t, *J*=7.6 Hz, CH$_2$), 4.57 (2H, t, *J*=7.5 Hz, CH$_2$), 8.02-8.10 (4H, m, ArH); **^{13}C NMR** (125 MHz, D$_2$O): δ_C 21.6 (CH$_2$), 26.7 (CH$_2$), 47.7 (CH$_2$), 113.5 (ArC), 118.4 (*para*-CN), 121.8 (2 × ArCH), 134.7 (2 × ArCH), 134.7 (ArCN), 138.8 (NCH(N)), 164.4 (NCN); ν_{max} /cm^{-1} (neat): 3142, 2360, 2244, 1606, 1585, 1523, 1382, 1292, 1222, 1054, 1026; *m/z* (ES+): 211 ([M–BF$_4$]$^+$, 100%); **HRMS** (ES+): [M–BF$_4$]$^+$ C$_{12}$H$_{11}$N$_4$ requires 211.0978, found 211.0979.

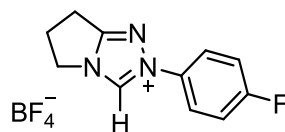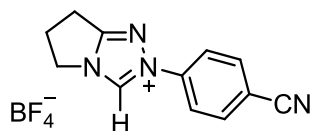### 6.3.1.7   2-(2-Pyridyl)-6,7-dihydro-5*H*-pyrrolo[2,1-c][1,2,4]triazol-2-ium tetrafluoroborate (143)
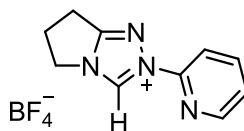
Based on a procedure by Rovis and co-workers,[2] trimethyloxonium tetrafluoroborate (6.11 g, 41 mmol) was added to a solution of 2-pyrrolidinone (3.19 g, 38 mmol) in anhydrous dichloromethane (200 mL) and stirred for 24 h at r.t. under an inert atmosphere. 2-Hydrazinopyridine (4.50 mL, 41 mmol) was then added, and the solution stirred for a further 48 h at r.t. under an inert atmosphere. The solvent was removed under reduced pressure, and the residue dissolved in methanol (25 mL) and triethyl orthoformate (50 mL, 297 mmol) and refluxed for 24 h. The solvent was removed under reduced pressure and recrystallised from cold methanol to yield the title compound as white crystals (0.89 g, 9%). **m.p.** 134–136 °C; **^{1}H NMR** (700 MHz, DMSO-d$_6$): δ_H 2.75 (2H, quintet, *J*=7.5 Hz, CH$_2$), 3.22 (2H, t, *J*=7.7 Hz, CH$_2$), 4.40 (2H, t, *J*=7.4 Hz, CH$_2$), 7.70 (1H, dd, *J*=7.6, 4.8 Hz, ArH), 8.01 (1H, d, *J*=8.2 Hz, ArH), 8.23 (1H, td, *J*=7.9, 1.7 Hz, ArH), 8.68 (1H, d, *J*=4.8 Hz, ArH), 10.81 (1H, s, NCH(N)); **^{13}C NMR** (176 MHz, DMSO-d$_6$): δ_C 21.3 (CH$_2$), 26.6 (CH$_2$), 47.1 (CH$_2$), 113.7 (ArCH), 126.0 (ArCH), 138.1 (NCH(N)), 141.0 (ArCH), 147.3 (ArCN), 149.3 (ArCH), 163.5 (NCN); ν_{max} /cm^{-1} (neat): 3196, 1594, 1573, 1513, 1469, 1421, 1386, 1298, 1286, 1194, 1046, 1034; *m/z* (ES+): 188 ([M+H–BF$_4$]$^+$, 100%), 187 ([M–BF$_4$]$^+$, 65%); **HRMS** (ES+): [M–BF$_4$]$^+$ C$_{10}$H$_{11}$N$_4$ requires 187.0984, found 187.0983.

6.3.1.8   1,3-Dipropylimidazolium iodide (153)
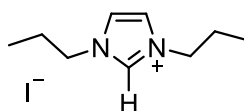
Based on a procedure by Thieuleux and co-workers,[5] a mixture of sodium hydride (6.11 g, 41 mmol) and imidazole (1.0 g, 15 mmol) in dry THF (30 mL) was stirred for 20 min at r.t. under an inert atmosphere. 1-Iodopropane (3.0 mL, 31 mmol) was added dropwise and the solution refluxed for 48 h. The solution was filtered and the precipitate washed with THF. The filtrate was evaporated under reduced pressure, and the residue dissolved in dichloromethane (30 mL) and filtered. The solution was washed with pentane (4 × 30 mL) and solvent removed under reduced pressure to yield the title compound as a brown oil (2.67 g, 64%), with spectroscopic details in accordance with the literature. ^{1}**H NMR** (700 MHz, CDCl$_3$): δ_H 1.01 (6H, t, *J*=7.4 Hz, 2 × CH$_3$), 2.00 (2H, m, 2 × CH$_2$), 4.34 (4H, t, *J*=7.3 Hz, 2 × NCH$_2$), 7.36 (2H, d, *J*=1.6 Hz, 2 × CH), 10.32 (1H, s, NCH(N)); ^{13}**C NMR** (176 MHz, CDCl$_3$): δ_C 10.9 (2 × CH$_3$), 23.9 (2 × CH$_2$), 51.9 (2 × CH$_2$), 122.1 (2 × CH), 137.1 (NCH(N)).

6.3.2 Synthesis of 3-(α-hydroxyaryl)triazolium adducts

6.3.2.1 2-Phenyl-3-(α-hydroxybenzyl)-6,7-dihydro-5*H*-pyrrolo[2,1-c][1,2,4]triazol-2-ium tetrafluoroborate (264)

To a solution of 2-phenyl-6,7-dihydro-5H-pyrrolo[2,1-c][1,2,4]triazol-2-ium tetrafluoroborate **139** (0.5 g, 1.83 mmol) and triethylamine (510 µL, 3.66 mmol) in dichloromethane (25 mL) was added benzaldehyde (186 µL, 1.83 mmol). After stirring at r.t. for 3 h, the solution was washed once with aqueous 0.1 M HCl (30 mL) and concentrated under reduced pressure. The crude product was diluted with a small amount of methanol for purification by preparative LC-MS as described in Section 6.1. The combined fractions were evaporated under reduced pressure to yield the title compound as a pale yellow oil (0.018 g, 3%). The analogous chloride salt could be recrystallised from a saturated solution of aqueous 0.1 M DCl inside an NMR tube. **^{1}H NMR** (500 MHz, MeOD-d$_4$): δ$_H$ 2.85 (2H, m, CH$_2$), 3.21 (2H, td, *J*=7.9, 2.8 Hz, CH$_2$), 4.44 (1H, dt, *J*=12.4, 7.5 Hz, C*H*H), 4.60 (1H, dt, *J*=12.4, 7.5 Hz, CH*H*), 6.21 (1H, s, CH), 7.19 (2H, d, *J*=7.7 Hz, ArH), 7.28–7.34 (3H, m, ArH), 7.46 (2H, d, *J*=8.3 Hz, ArH), 7.53 (2H, t, *J*=7.8 Hz, ArH), 7.61 (1H, t, *J*=7.5 Hz, ArH); **^{13}C NMR** (125 MHz, MeOD-d$_4$): δ$_C$ 22.3 (CH$_2$), 27.9 (CH$_2$), 50.1 (CH$_2$), 69.2 (CH), 127.1 (2 × ArCH), 128.2 (2 × ArCH), 130.1 (2 × ArCH), 130.5 (ArCH), 130.9 (2 × ArCH), 132.6 (ArCH), 136.7 (ArCN), 137.9 (ArCq), 153.5 (NCN), 164.0 (NCN); **v$_{max}$** /cm^{-1} (neat): 1589, 1496, 1455, 1390, 1342, 1192, 1046, 764, 693; ***m/z*** (ES+): 292 ([M–BF$_4$]$^+$, 100%); **HRMS** (ES+): [M–BF$_4$]$^+$ C$_{18}$H$_{18}$N$_3$O requires 292.1450, found 292.1461.

6.3.2.2 2-Phenyl-3-(α-hydroxy-parafluorobenzyl)-6,7-dihydro-5*H*-pyrrolo[2,1-c][1,2,4]triazol-2-ium tetrafluoroborate (269)
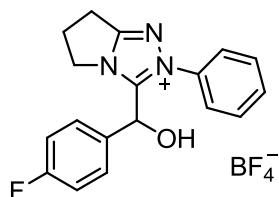
To a solution of 2-phenyl-6,7-dihydro-5H-pyrrolo[2,1-c][1,2,4]triazol-2-ium tetrafluoroborate **139** (0.5 g, 1.83 mmol) and triethylamine (510 µL, 3.66 mmol) in dichloromethane (25 mL) was added 4-fluorobenzaldehyde (196 µL, 1.83 mmol). After stirring at r.t. for 3 h, the solution was washed once with aqueous 0.1 M HCl (30 mL) and concentrated under reduced pressure. The crude product was diluted with a small amount of methanol for purification by preparative LC-MS as described in Section 6.1. The combined fractions were evaporated under reduced pressure to yield the title compound as a pale yellow oil (0.015 g, 2%). The analogous chloride salt could be recrystallised from a saturated solution of aqueous 0.1 M DCl inside an NMR tube. **^{1}H NMR** (400 MHz, MeOD-d$_4$): δ$_H$ 2.87 (2H, m, CH$_2$), 3.22 (2H, td, *J*=7.9, 2.7 Hz, CH$_2$), 4.45 (1H, dt, *J*=12.4, 7.5 Hz, C*H*H), 4.61 (1H, dt, *J*=12.4, 7.5 Hz, CH*H*), 6.25 (1H, s, CH), 7.20 (2H, d, *J*=7.7 Hz, ArH), 7.29–7.35 (3H, m, ArH), 7.47 (2H, d, *J*=8.3 Hz, ArH), 7.54 (2H, t, *J*=7.8 Hz, ArH), 7.62 (1H, t, *J*=7.5 Hz, ArH); **^{13}C NMR** (101 MHz, MeOD-d$_4$): δ$_C$ 22.4 (CH$_2$), 28.0 (CH$_2$), 50.2 (CH$_2$), 68.6 (CH), 116.9 (d, *J*=22.2 Hz, 2 × ArCH), 127.2 (2 × ArCH), 130.5 (d, *J*=8.6 Hz, 2 × ArCH), 131.0 (2 × ArCH), 132.7 (ArCH), 134.1 (d, *J*=8.6 Hz, ArCq), 136.7 (ArCN), 153.4 (NCN), 164.0 (NCN); **^{19}F NMR** (658 MHz, D$_2$O): δ$_F$ −112.1 (ArF), −150.7 (s, BF$_4$), −150.8 (s, BF$_4$); **ν$_{max}$** /cm^{-1} (neat): 3368, 1602, 1509, 1456, 1288, 1225, 1161, 1049, 769, 694; **m/z** (ES+): 311 ([M+H–BF$_4$]$^+$, 100%), 310 ([M–BF$_4$]$^+$, 50%); **HRMS** (ES+): [M–BF$_4$]$^+$ C$_{18}$H$_{17}$N$_3$OF requires 310.1356, found 310.1366.

6.3.2.3   2-Phenyl-3-(α-hydroxy-paramethylbenzyl)-6,7-dihydro-5*H*-pyrrolo[2,1-c][1,2,4]triazol-2-ium tetrafluoroborate (270)

To a solution of 2-phenyl-6,7-dihydro-5H-pyrrolo[2,1-c][1,2,4]triazol-2-ium tetrafluoroborate **139** (0.5 g, 1.83 mmol) and triethylamine (510 μL, 3.66 mmol) in dichloromethane (25 mL) was added 4-methylbenzaldehyde (217 μL, 1.83 mmol). After stirring at r.t. for 3 h, the solution was washed once with aqueous 0.1 M HCl (30 mL) and concentrated under reduced pressure. The crude product was diluted with a small amount of methanol for purification by preparative LC-MS as described in Section 6.1. The combined fractions were evaporated under reduced pressure to yield the title compound as a pale yellow oil (0.020 g, 3%). The analogous chloride salt could be recrystallised from a saturated solution of aqueous 0.1 M DCl inside an NMR tube. **^{1}H NMR** (500 MHz, MeOD-d$_4$): δ$_H$ 2.30 (3H, s, CH$_3$), 2.87 (2H, m, CH$_2$), 3.22 (2H, td, *J*=7.8, 3.7 Hz, CH$_2$), 4.44 (1H, dt, *J*=12.4, 7.5 Hz, C*H*H), 4.61 (1H, dt, *J*=12.4, 7.5 Hz, CH*H*), 6.17 (1H, s, CH), 7.07 (2H, d, *J*=8.1 Hz, ArH), 7.13 (2H, d, *J*=7.9 Hz, ArH), 7.48 (2H, d, *J*=8.2 Hz, ArH), 7.55 (2H, t, *J*=7.9 Hz, ArH), 7.62 (1H, t, *J*=7.6 Hz, ArH); **^{13}C NMR** (176 MHz, MeOD-d$_4$): δ$_C$ 21.2 (CH$_3$), 22.4 (CH$_2$), 28.0 (CH$_2$), 50.1 (CH$_2$), 69.0 (CH), 127.1 (2 × ArCH), 128.1 (2 × ArCH), 130.7 (2 × ArCH), 131.0 (2 × ArCH), 132.6 (ArCH), 134.9 (ArCCH$_3$), 136.8 (ArCN), 140.8 (ArCq), 153.7 (NCN), 164.0 (NCN); **ν$_{max}$** /cm^{-1} (neat): 3510, 3423, 3100, 1605, 1503, 1230, 1122, 1095, 982, 785, 700; **m/z** (ES+): 307 ([M+H–BF$_4$]$^+$, 100%), 306 ([M–BF$_4$]$^+$, 85%); **HRMS** (ES+): [M–BF$_4$]$^+$ C$_{19}$H$_{20}$N$_3$O requires 306.1606, found 306.1615.

6.3.2.4 2-Phenyl-3-(α-hydroxy-orthomethoxybenzyl)-6,7-dihydro-5*H*-pyrrolo[2,1-c][1,2,4]triazol-2-ium tetrafluoroborate (272)
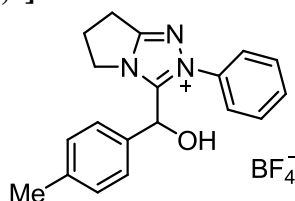

To a solution of 2-phenyl-6,7-dihydro-5H-pyrrolo[2,1-c][1,2,4]triazol-2-ium tetrafluoroborate **139** (0.3 g, 1.10 mmol) and triethylamine (306 µL, 2.20 mmol) in dichloromethane (25 mL) was added 2-methoxybenzaldehyde (0.15 g, 1.10 mmol). After stirring at r.t. for 3 h, the solution was washed once with aqueous 0.1 M HCl (30 mL) and concentrated under reduced pressure. The crude product was purified by column chromatography (5:2 chloroform : hexane). The combined fractions were evaporated under reduced pressure to yield the title compound as an orange solid (0.12 g, 24%). **m.p.** 72–74 °C. **^{1}H NMR** (600 MHz, MeOD-d$_4$): δ$_H$ 2.74 – 2.89 (2H, m, CH$_2$), 3.20 (2H, t, *J*=8.2 Hz, CH$_2$), 3.59 (3H, s, CH$_3$), 4.15 (1H, m, C*H*H), 4.50 (1H, m, CH*H*), 6.29 (1H, s, CH), 6.93 (2H, dd, *J*=8.1 Hz, ArH), 7.30 (1H, td, *J*=7.9, 1.7 Hz, ArH), 7.38 (1H, dd, *J*=7.6, 1.3 Hz, ArH), 7.53 (4H, d, *J*=4.2 Hz, ArH), 7.56 – 7.61 (1H, m, ArH); **^{13}C NMR** (151 MHz, MeOD-d$_4$): δ$_C$ 22.4 (CH$_2$), 28.1 (CH$_2$), 49.3 (CH$_2$), 56.4 (CH$_3$), 64.2 (CH), 112.0 (ArCH), 121.9 (ArCH), 125.2 (ArCq), 126.8 (2 × ArCH), 129.1 (ArCH), 130.8 (2 × ArCH), 132.0 (ArCH), 132.4 (ArCH), 136.9 (ArCN), 153.4 (NCN), 157.3 (ArCO), 163.6 (NCN); **v$_{max}$** /cm^{-1} (neat): 3124, 1599, 1491, 1466, 1395, 1287, 1245, 1046, 1019, 759, 695; **m/z** (ES+): 323 ([M+H–BF$_4$]$^+$, 100%), 322 ([M–BF$_4$] $^+$, 40%); **HRMS** (ES+): [M–BF$_4$]$^+$ C$_{18}$H$_{17}$N$_3$OF requires 322.1556, found 322.1566.

6.3.2.5 2-Mesityl-3-(α-hydroxybenzyl)-6,7-dihydro-5*H*-pyrrolo[2,1-c][1,2,4]triazol-2-ium tetrafluoroborate (271)
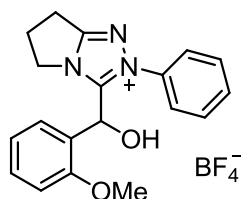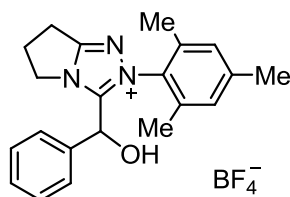

To a solution of 2-mesityl-6,7-dihydro-5H-pyrrolo[2,1-c][1,2,4]triazol-2-ium tetrafluoroborate **140** (0.5 g, 1.83 mmol) and triethylamine (510 μL, 3.66 mmol) in dichloromethane (25 mL) was added benzaldehyde (186 μL, 1.83 mmol). After stirring at r.t. for 3 h, the solution was washed once with aqueous 0.1 M HCl (30 mL) and concentrated under reduced pressure. The crude product was diluted with a small amount of methanol for purification by preparative LC-MS as described in Section 6.1. The combined fractions were evaporated under reduced pressure to yield the title compound as a brown oil (0.067 g, 9%). **^{1}H NMR** (500 MHz, MeOD-d$_4$): δ_H 1.38 (3H, s, CH$_3$), 2.15 (3H, s, CH$_3$), 2.38 (3H, s, CH$_3$), 2.92 (2H, m, CH$_2$), 3.24 (2H, t, *J*=7.9 Hz, CH$_2$), 4.70 (1H, dt, *J*=12.4, 7.5 Hz, C*H*H), 4.78 (1H, dt, *J*=12.4, 7.5 Hz, CH*H*), 6.81 (1H, s, CH), 6.92 (1H, s, ArH), 7.08 (2H, dd, *J*=7.9, 1.4 Hz, ArH), 7.17 (1H, s, ArH), 7.30 (2H, t, *J*=7.8 Hz, ArH), 7.37 (1H, T *J*=7.5 Hz, ArH); **^{13}C NMR** (126 MHz, MeOD-d$_4$): δ_C 17.0 (CH$_3$), 17.4 (CH$_3$), 21.2 (CH$_3$), 22.5 (CH$_2$), 27.9 (CH$_2$), 50.5 (CH$_2$), 69.8 (CH), 127.3 (2 × ArCH), 129.0 (2 × ArCH), 129.6 (2 × ArCH), 129.8 (ArCH), 130.9 (ArC), 135.0 (ArC), 136.5 (ArC), 142.7 (ArC), 153.0 (NCN), 163.6 (NCN); **ν_{max}** /cm^{-1} (neat): 3450, 1591, 1454, 1383, 1284, 1048, 854, 738, 698; **_m/z_** (ES+): 335 ([M+H–BF$_4$]$^+$, 100%), 334 ([M–BF$_4$]$^+$, 47%); **HRMS** (ES+): [M–BF$_4$]$^+$ C$_{21}$H$_{24}$N$_3$O requires 334.1919, found 334.1923.

6.3.3 Synthesis of reference acyloins

6.3.3.1 (±)-1-Hydroxy-1,2-bis(2-methoxyphenyl)ethanone (292)
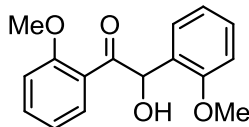
2-Methoxybenzaldehyde (0.54 g, 4 mmol), triethylamine (0.28 mL, 2 mmol) and triazolium ion **142** (0.15 g, 0.4 mmol) were refluxed in methanol (10 mL) for 48 h. Solvent was removed under reduced pressure and the product purified by column chromatography (hexane : ethyl acetate, gradient). The title compound was recrystallised from methanol to give a white solid, with spectroscopic properties in accordance with the literature. **m.p.** 94–96 °C {lit.[6] 96–98 °C}; **^{1}H NMR** (600 MHz, MeOD-d$_4$): δ_H 3.68 (3H, s, CH$_3$), 3.76 (3H, s, CH$_3$), 6.18 (1H, s, C*H*(OH)), 6.83 (2H, m, CH*H*), 6.90 (1H, td, *J*=7.5, 1.0 Hz, ArH), 6.91 (1H, d, *J*=8.4 Hz, ArH), 7.18 (2H, m, ArH), 7.38 (1H, td, *J*=7.9, 1.8 Hz, ArH), 7.49 (1H, dd, *J*=7.7, 1.8 Hz, ArH); **^{13}C NMR** (151 MHz, MeOD-d$_4$): δ_C 55.7 (CH$_3$), 55.9 (CH$_3$), 76.4 (CH(OH)), 111.9 (ArCH), 112.4 (ArCH), 121.4 (2 × ArCH), 127.6 (ArC), 128.6 (ArC), 130.7 (ArCH), 130.8 (ArCH), 131.2 (ArCH), 134.6 (ArCH), 158.7 (ArCO), 159.4 (ArCO), 203.5 (C=O).

6.3.3.2 (±)-1-Hydroxy-1,2-bis(4-fluorophenyl)ethanone (293)
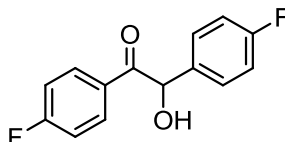
4-Fluorobenzaldehyde (1.05 mL, 5 mmol), triethylamine (0.28 mL, 2 mmol) and triazolium ion **142** (0.15 g, 0.4 mmol) were refluxed in methanol (10 mL) for 72 h. Solvent was removed under reduced pressure and the product purified by column chromatography (4:3 dichloromethane : hexane). The title compound was recrystallised from methanol to give a yellow solid, with spectroscopic properties in accordance with the literature. **m.p.** 81–84 °C {lit.[7] 84–86 °C}; **^{1}H NMR** (400 MHz, MeOD-d$_4$): δ_H 6.09 (1H, s, C*H*(OH)), 7.04 (2H, dd, *J*=8.8, 8.8 Hz, 2 × ArH), 7.14 (2H, dd, *J*=8.8, 8.8 Hz, 2 × ArH), 7.45 (2H, dd, *J*=8.8, 5.4 Hz, 2 × ArH), 8.05 (2H, dd, *J*=8.8, 5.4 Hz, 2 × ArH); **^{13}C NMR** (101 MHz, MeOD-d$_4$): δ_C 76.7 (CH), 116.6 (d, *J*=21.8 Hz, 2 × ArCH), 116.6 (d, *J*=22.3 Hz, 2 × ArCH), 130.8 (d, *J*=8.4 Hz, 2 × ArCH), 132.4 (ArCq), 133.0 (d, *J*=9.5 Hz, 2 × ArCH), 136.6 (ArCq), 164.0 (d, ^{1}*J*=246.1 Hz, ArCF), 167.1 (d, ^{1}*J*=254.1 Hz, ArCF), 198.8 (C=O); **^{19}F NMR** (376 MHz, MeOD-d$_4$): δ_F −107.6, −116.6.

6.4   Preparation of Solutions

6.4.1   Measurement of azolium ion acidities

Solutions of DCl and KOD in D_2O were prepared by dilution of the commercially available stock solutions, followed by titration against standard solutions of KOH or HCl respectively.

Acetate buffers in D_2O were prepared by mixing stock solutions of potassium acetate and DCl with KCl where necessary, to give buffer solutions at different free base ratios at $I = 1.0$ (KCl).

Stock solutions of K_2DPO_4 and KD_2PO_4 in D_2O were obtained from dibasic and monobasic potassium phosphate, where the hydrogen atoms had been exchanged for deuterium. The deuterated salts were obtained from the analogous protonated salts by dissolving in D_2O, followed by removal of solvent under reduced pressure. This process was repeated five times and on the sixth iteration dried vigorously under vacuum. Phosphate buffers in D_2O were prepared by mixing stock solutions of K_2DPO_4 and KD_2PO_4 with KCl where necessary, to give buffer solutions at different free base ratios at $I = 1.0$ (KCl).

6.4.2   Studies of the NHC-catalysed benzoin condensation

Solutions of triethylamine buffer in methanol-d_4 were prepared from distilled triethylamine and dried triethylamine hydrochloride. For the adduct dissociation studies, dried triethylamine deuterochloride was used as the acid component. The deuterated salt was obtained by exchange of the corresponding hydrochloride salt, as described above. Solutions were prepared immediately prior to use.

6.5 Kinetic Methods

6.5.1 Measurement of p*H,* p*D* and determination of hydroxide ion activity coefficient (γ_{HO})

p*H*s of buffered solutions were determined at 25 ºC using a MeterLab^{TM} PHM 290 p*H*-Stat Controller equipped with a radiometer combination electrode filled with saturated KCl solution. The apparatus could be standardised between p*H* 4 − 7, p*H* 7 − 10 or p*H* 10 − 12.45 to encompass the p*H* of the buffer solution. Saturated calcium hydroxide solution was used to standardise the electrode at p*H* 12.45.[8] The p*D* was calculated by adding 0.4 to the reading on the p*H* meter.[9]

The activity coefficient for hydroxide ion (γ_{HO}) was determined from the fit of the observed p*H* of a series of titrimetrically-known solutions of KOH at 25 °C and constant ionic strength I = 1.0 (KCl) to Equation 6.1, where pK_W = 14. Two electrodes were used during this project: (i) a value of γ_{HO} = 0.73 had previously been determined for the first; (ii) a value of γ_{HO} = 0.72 was determined for the latter (this data is shown in Table 6.3 and Figure 6.1).

$$10^{(pH - pK_W)} = \gamma_{OH}[OH^-] \qquad \textbf{Equation 6.1}$$

Table 6.3: **Dependence of p*H* on hydroxide ion (determination of γ_{HO}) at 25 °C and *I* = 1.0 (KCl)**

[HO⁻], M	p*H*	$10^{(pH - 14)}$
0.01	11.89	0.0078
0.02	12.16	0.0145
0.04	12.45	0.0282
0.06	12.64	0.0437
0.08	12.76	0.0575
0.10	12.86	0.0724

Figure 6.1: **Determination of the activity coefficient for hydroxide ion (γ_{OH})**
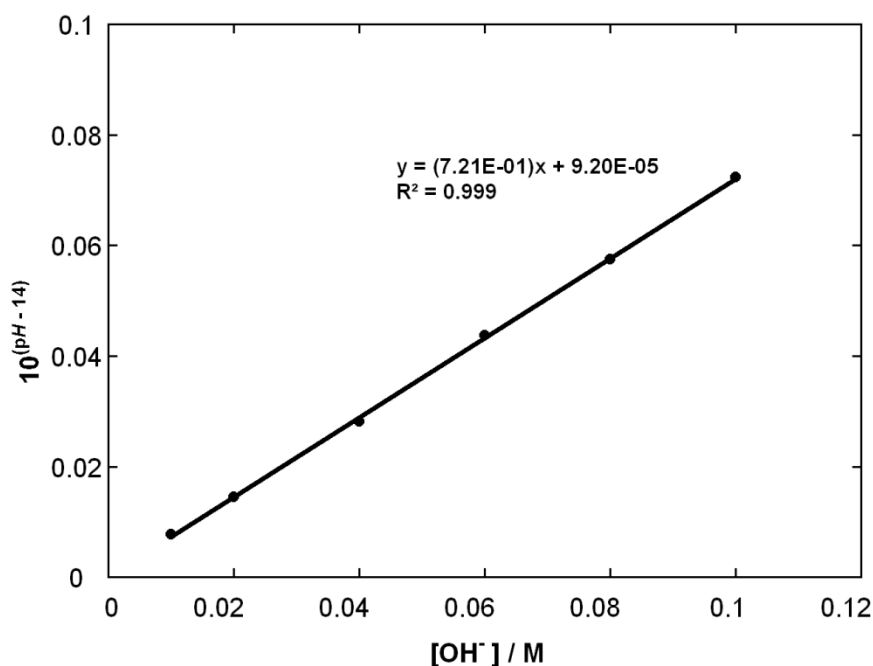
6.5.2 NMR conditions

For exchange reactions of azolium ions, ^{1}H NMR spectra were typically recorded on a Varian 400 spectrometer with a relaxation delay of 20 s, sweep width of 8298.8 Hz, acquisition time of 4 s and 90° pulse angle. Spectra were run with 32 transients (total running time ~12 min). For exchange reactions thermostated in the NMR instrument at 25 °C, ^{1}H NMR spectra were recorded on a Varian 500 spectrometer with a relaxation delay of 20 s, sweep width of 10000.0 Hz, acquisition time of 4 s and 90° pulse angle. Spectra were run with 32 transients (total running time ~12 min). ^{1}H NMR spectral baselines were subject to a first-order drift correction before integration of the peak areas.

For studies of adduct decomposition, ^{1}H NMR spectra were recorded on an Oxford Varian Inova 500 spectrometer thermostated at 25 °C, with a relaxation delay of 2 s, sweep width of 10000.0 Hz, acquisition time of 2 s and 45° pulse angle. Spectra were run with 32 transients (total running time ~2 min). Measurement times were taken from the mid-point of the acquisition.

For studies of the benzoin condensation, ^{1}H NMR spectra were recorded on an Oxford Varian Inova 500 spectrometer thermostated at 25 °C, with a relaxation delay of 5 s,

sweep width of 10000.0 Hz, acquisition time of 2 s and 45° pulse angle. Spectra were run with 32 transients (total running time ~4 min). Measurement times were taken from the mid-point of the acquisition.

In all cases, ^{1}H NMR spectral baselines were subject to a first-order drift correction before integration of the peak areas. Substrate peak areas were compared with the peak of the internal standard (tetramethylammonium tetrafluroroborate or TMS) that was set to an arbitrary figure of 1000.

References

1   G. R. Fulmer, A. J. M. Miller, N. H. Sherden, H. E. Gottlieb, A. Nudelman, B. M. Stolts, J. E. Bercaw and K. I. Goldberg, *Organometallics*, 2010, **29**, 2176.
2   M. S. Kerr, J. Read de Alaniz and T. Rovis, *J. Org. Chem.*, 2005, **70**, 5725.
3   J. E. Thomson, C. D. Campbell, C. Concellon, N. Duguet, K. Rix, A. M. Z. Slawin and A. D. Smith, *J. Org. Chem.*, 2008, **73**, 2784.
4   K. B. Ling and A. D. Smith, *Chem. Commun.*, 2011, **47**, 373.
5   M. Bouhrara, E. Jeanneau, L. Veyre, C. Copéret and C. Thieuleux, *Dalton Trans.*, 2011, **40**, 2995.
6   J. Broeker, M. Knollmueller and P. Gaertner, *Tetrahedron: Asymmetry*, 2006, **17**, 2413.
7   B. Procuranti and S. J. Connon, *Chem. Commun.*, 2007, 1421.
8   Y.-R. Zhang, L. He, X. Wu, P.-L. Shao and S. Ye, *Org. Lett.*, 2007, **10**, 277.
9   P. K. Glasoe and F. A. Long, *J. Phys. Chem.*, 1960, **64**, 188.

CHAPTER 7

Conclusions and Future Work

Following the groundbreaking developments in the isolation of stable carbenes achieved by Arduengo and Bertrand, N-heterocyclic carbenes have risen to prominence as ligands in organometallic chemistry and as versatile organocatalysts for a broad range of transformations. Recent advances have found triazol-3-ylidenes derived from triazolium ion precatalysts to be particularly effective for reactions that proceed *via* azolium homoenolate and enolate intermediates, and these species are the primary focus of our investigations.

In almost all NHC-catalysed transformations, the active NHC is generated *in situ* from the parent azolium ion by deprotonation, and knowledge of the acidity of these azolium ion precatalysts is highly desirable. Surprisingly however, literature reports of triazolium ion acidities are scarce. We have used a kinetic method to determine kinetic acidities towards deuteroxide ion and aqueous pK_a values in a systematic study of *N*-aryl substituted triazolium ions.

For a homologous series of triazolium salts **137 – 143**, deuterium exchange reactions at the C(3)-H position were followed by ^{1}H NMR spectroscopy in aqueous solution at 25 °C. Pseudo-first-order rate constants for exchange, k_{ex} (s^{-1}), were determined at a range of pDs at constant ionic strength, $I = 1.0$ (KCl). These values of k_{ex} were used to construct pD-rate profiles for exchange, from which second-order rate constants for deuteroxide ion-catalysed exchange, k_{DO} (M^{-1} s^{-1}), could be obtained. Values of k_{DO} were obtained in the range $1.75 \times 10^7 – 2.84 \times 10^8$ M^{-1} s^{-1}, with more electron-deficient *N*-aryl substituents affording the greatest kinetic acidities. The 16-fold span measured for the series is small given the broad electronic properties of the substituents studied, which may reflect the dual carbene/ylide resonance structure of the transition state for deprotonation. In contrast, k_{DO} values determined for these triazolium ions are 10^3- and 10^5-fold larger than those of thiazolium and imidazolium ions, respectively, highlighting the large effect of the additional electron-withdrawing azolium ring nitrogen.

The presence of the additional ring nitrogen was also found to result in an altered dependence of k_{ex} at lower pDs for triazolium salt **142**. This behaviour is consistent with protonation at N(1) to generate a dicationic triazolium ion, with an estimate of p$K_a^{N(1)} = -0.2$, consistent with other dicationic nitrogen species. A second-order rate constant for deuteroxide catalysed exchange at the C(3)-H position of this dicationic

species was estimated to lie just above the diffusional limit. The fact that N(1)-protonation is observed for the most acidic of the series is surprising, considering the highly electron-withdrawing nature of the N-C_6F_5 substituent. It is possible that protonation at N(1) may decrease an unfavourable electrostatic interaction between the lone pairs on N(1) and on the *ortho* halogen. The pD-rate profiles of other triazolium ions incorporating substituents bearing lone pairs at the *ortho,ortho* aryl positions should be studied alongside the analogous *meta,meta* structures in order to probe this hypothesis.

Using a secondary isotope effect of $k_{DO}/k_{HO} = 2.4$, second-order rate constants for deprotonation by hydroxide ion k_{HO} (M^{-1} s^{-1}) were obtained from values of k_{DO}. Buffer catalysis experiments show that general base catalysis is not observed for H/D-exchange of triazolium salt **138**. A value for the reverse rate constant for carbene protonation equal to the rate constant for solvent reorganisation ($k_p = k_{reorg} = 10^{11}$ s^{-1}) could therefore be estimated for triazolium ions where $k_{DO} \leq 8.66 \times 10^7$ M^{-1} s^{-1}. As the acid dissociation constant K_a may be written in terms of the rate constant for azolium ion deprotonation and carbene protonation, carbon acid pK_a values in the range 16.5 – 17.8 could be estimated. For the two most acidic triazolium ions, for which the extent of general base catalysis could not be determined, estimated values of pK_a should be no more than 1 unit lower than the quoted value.

In a parallel investigation, kinetic acidities and carbon acid pK_a estimates for the conjugate acids of six 'mesoionic' triazol-4-ylidenes and imidazol-4(5)-ylidenes were determined. These species have gained considerable interest as strong ligand donors in organometallic chemistry and as organocatalysts in their own right. Ligand donor studies have shown these species to be more basic than 'classical' NHCs, however, no experimental measurements of pK_a have been reported to the best of our knowledge.

For 1,2,3-triazolium salts **204 – 207** bearing alkyl and aryl substituents, k_{DO} values in the range $4.61 \times 10^{-2} – 2.10 \times 10^2$ M^{-1} s^{-1} were obtained. Kinetic acidities at the C(5)-H position of these species are around 10^5-fold smaller than at the C(3)-H position for structurally similar 1,2,4-triazolium ions, as a result of the stabilisation gained from relocation of the electron-withdrawing nitrogen atom away from the site of deprotonation. Aryl substituents resulted in increased kinetic acidities of up to 270-fold, whereas the effect of counterion was negligible. The absence of general base catalysis

for the most acidic of these substrates implies that solvent reorganisation is also rate determining for these species. Following the treatment described above, carbon acid pK_a values could be estimated for these species in the range 23.1 – 26.7.

Studies of imidazolium salts **208 – 210** proved to be less straightforward, and a clear first-order dependence on deuteroxide ion was not observed in solutions of KOD at $I =$ 1.0 (KCl). We have proposed a number of possible alternative pathways for H/D-exchange which could account for this higher order dependence. ^{1}H NMR spectroscopic evidence requires that the fraction of hydrate be small and undetectable. At lower pDs the fraction of hydrate present in solution would be significantly lower. However, due to the slow rates of exchange predicted for these species at lower pDs it was not possible to follow exchange in buffered solution on the timescale of these investigations. Given a longer period of study, it may be possible to obtain a value of k_{DO} at a suitable pD range (*e.g.* using quinuclidinone buffers) where hydrate formation is supressed. It would also be beneficial to prepare methyl or alkoxy analogues of this hydrate in an attempt to estimate rate constants for deuteroxide ion-catalysed exchange of this species.

Despite this, second-order rate constants for deuteroxide ion-catalysed exchange, k^2_{DO} (M^{-1} s^{-1}) in the range 1.27×10^{-5} – 7.17×10^{-5} M^{-1} s^{-1} were determined. These k_{DO} values are amongst the least acidic azolium ions studied using this kinetic method. Aryl substituents were found to result in an increase in kinetic acidity, whilst the effect of *N*-alkyl substituent was negligible.

Despite the widespread use of NHCs in organocatalysis, the product distributions of the reactions highlighted in the introduction to this thesis differ dramatically with variation of the catalyst family. Furthermore, studies of triazol-3-ylidene-catalysed transformations show that the *N*-aryl substituent plays a decisive role in dictating catalyst reactivity. To better understand the role of the *N*-aryl substituent and differences between azolium precatalyst families, we have undertaken an in-depth mechanistic study of the benzoin condensation, focusing particularly on the role of the intermediate 3-(hydroxyaryl)azolium species.

The appearance and consumption of reactants, intermediates and products in the NHC-catalysed benzoin condensation was monitored *in situ* by ^{1}H NMR spectroscopy, at 25

°C in triethylamine-buffered methanol-d$_4$. Under these conditions, the only intermediate observed over the course of the reaction was the 3-(hydroxyaryl)azolium adduct. Several examples of these adducts (**264** and **269** – **272**) derived from *N*-phenyl substituted triazol-3-ylidenes have been isolated, and structures unambiguously confirmed by NMR and crystallographic techniques. Formation of adduct from aldehyde and catalyst was shown to be reversible, irrespective of *N*-aryl substituent, and equilibrium constants for this initial step were determined. Our results show that *N*-mesityl architectures significantly increase the equilibrium constant for this addition step, K_1 (M^{-1}), by over 10-fold. Through collaboration with another group, there is evidence to suggest that this effect is not limited to *N*-mesityl substituents – a number of 2,6-substituted aryl substituents (*e.g.* C$_6$F$_5$) will increase the stability of this adduct. From the available crystallographic data, we propose that 2,6-substitutents enforce an orthogonal *N*-aryl ring orientation on the NHC, which may better accommodate the 3-hydroxybenzyl group relative to unsubstituted aryl rings. Interestingly, a second K_1-enhancing substituent effect resulting from the presence of 2-alkoxyl groups on the aromatic aldehyde is also apparent, increasing the equilibrium concentration of adduct by a similar magnitude. We have attributed this effect to the possible formation of an intramolecular hydrogen bond between the 2-alkoxyl group and the C(α)-hydroxyl substituent.

By fitting parts of the concentration profile to first-order plots and from global fitting, pseudo-first-order rate constants for the second step in the benzoin condensation – deprotonation of the 3-(hydroxyaryl)triazolium adduct, k_2 (s^{-1}), were estimated. Systematic variation of substituents on the aldehyde and catalyst indicate that electron-withdrawing substituents will increase the rate of this step, presumably as a result of the increase in acidity of the C(α)-H position. There is some evidence to suggest that the presence of an *ortho* alkoxyl substituent may enhance the rate of deprotonation of this species, potentially *via* intramolecular deprotonation.

We may conclude that electron-withdrawing *N*-aryl substituents with 2,6-substitution patterns will provide optimum rates of catalysis in the benzoin condensation by enhancing both the concentration of adduct at equilibrium, and the rate of its deprotonation. Unfortunately, the *N*-C$_6$F$_5$ substituted triazolium precatalyst **142** was too fast to study under the conditions employed in these investigations, and it would be

beneficial to undertake a similar study under milder conditions (*e.g.* lower f_B buffer or lower temperature). The preparation of an N-$C_6(CF_3)_3H_2$ substituted triazolium precatalyst would also merit investigation, as this may also fulfil the requirements for an ideal catalyst as described above.

We have also undertaken a more synthetically relevant initial rates kinetic study of the benzoin condensation at catalytic concentrations of azolium ion precatalyst. An HPLC analysis method was used to determine the concentrations of benzoin and benzaldehyde over the course of the reaction in triethylamine-buffered methanol at 50 °C. The reaction catalysed by thiazolium salt **53** is essentially first-order with respect to aldehyde over the full range of benzaldehyde concentrations studied (0.32 – 1.60 M). Using a concentration of 30 mM precatalyst, the reaction occurs with a pseudo-first-order rate constant of $k_{cat} = 5.53 \times 10^{-6}$ s^{-1}, in good agreement with a value obtained by Leeper of $k_{cat} = 6 \times 10^{-6}$ s^{-1} under the same conditions.

In contrast, for a range of N-substituted triazolium precatalysts **137 – 142** the reaction displays a first-order dependence at low aldehyde concentrations, before changing to a zero-order dependence at higher benzaldehyde concentrations. Variation of the precatalyst N-substituent shows that the maximum rate of catalysis reached in this zero-order region is increased if electron-withdrawing substituents on the N-aryl ring are used. This is consistent with a rate-determining adduct deprotonation step at higher concentrations, enhanced by electron-withdrawing substituents on the N-aryl ring, as indicated by the kinetic experiments at stoichiometric concentrations of catalyst and aldehyde.

To confirm this mechanistic interpretation, it may be beneficial to perform analogous experiments using α-deuteriobenzaldehyde instead of benzaldehyde. If the maximum rate of catalysis is limited by the rate of adduct deprotonation at higher aldehyde concentrations, a significant primary kinetic isotope effect should be observed in this zero-order region. Additionally, an inverse secondary isotope effect may be observed in the initial first-order region at lower aldehyde concentrations, as addition of NHC to the sp^2-hybridised carbonyl group results in a change to sp^3-hybridisation at the α-position in the adduct.

Acknowledgements

Above all, I'd sincerely like to thank my supervisor, AnnMarie O'Donoghue, for her expert knowledge and guidance over the past three years and eight months. She has been a helpful and kind supervisor. I'd also like to thank Andy Smith and Chris Collett at the University of St. Andrews, who have been great to work with, and their hard work has helped us achieve so much with this project.

Thank you to Oliver Maguire and David Jasiewicz for their efforts on projects relating to this work during 4th year/summer work. Thanks also to the academic and technical staff who helped to obtain all of the HPLC, NMR and X-ray crystallography data: Aileen Congreve, Ellie Hurst, Catherine Heffernan, Alan Kenwright, Ian McKeague, Juan Aguilar and Andrei Batsanov.

I would also like to thank Casey Lam, who has been a great friend and co-worker from the very first day. Working in CG115 has been consistently entertaining, thanks to the members named above and Richard Delley, Rob Goodwill, Ffion Abraham, Louis Conway, Chris Goodall, Anita Savanur, Lucy Hodge, Gordon Hack, David Wong-Pascua, Chris Bramley and Jacob Grant.

Finally, I'd like to thank my mum and dad for their love and encouragement.

APPENDIX

APPENDIX A

A1   Determination of pseudo first-order rate constants for exchange (k_{ex})

Table A1:   **Reaction data and first-order rate constants for exchange of the C(3)-H of triazolium salt (138) for deuterium in solutions of DCl in D_2O at 25 ºC and $I = 1.0$ (KCl).**

[DCl], M	[DO⁻], M	time, s	$f(s)$	$\ln f(s)$	k_{ex}, s⁻¹
1.0	2.49×10^{-15} (pD 0.13)	0	1.000	0.000	4.93×10^{-7}
		339480	0.838	-0.177	
		433260	0.821	-0.198	
		516660	0.784	-0.244	
		596520	0.766	-0.267	
		856260	0.673	-0.396	
		1201740	0.570	-0.562	
		1372620	0.500	-0.692	
		1535400	0.491	-0.712	
		1803660	0.401	-0.913	
		2323560	0.322	-1.133	
0.5	4.37×10^{-15} (pD 0.37)	0	1.000	0.000	6.87×10^{-7}
		68340	0.927	-0.075	
		93120	0.918	-0.085	
		151560	0.897	-0.109	
		341640	0.764	-0.269	
		436140	0.723	-0.324	
		592620	0.648	-0.434	
		771600	0.573	-0.557	
		1041780	0.496	-0.702	
		1189380	0.423	-0.860	
		1462020	0.360	-1.021	
		2247960	0.210	-2.560	
0.1	2.11×10^{-14} (pD 1.06)	0	1.000	0.000	2.18×10^{-6}
		55980	0.912	-0.092	
		141720	0.730	-0.315	
		171060	0.728	-0.318	
		227940	0.620	-0.478	
		253440	0.598	-0.515	
		409260	0.419	-0.870	
		505800	0.337	-1.088	
		683700	0.229	-1.475	
0.015	1.37×10^{-13} (pD 1.87)	0	1.000	0.000	1.25×10^{-5}
		15240	0.828	-0.189	
		24240	0.755	-0.281	
		34740	0.676	-0.392	
		44040	0.598	-0.515	
		74280	0.409	-0.893	
		78180	0.375	-0.981	
		85140	0.346	-1.060	

		0	1.000	0.000	
		62700	0.348	-1.054	
0.01	1.98×10^{-13}	72900	0.293	-1.226	1.64×10^{-5}
	(pD 2.03)	87960	0.229	-1.475	
		98760	0.194	-1.641	
		109680	0.160	-1.833	
		146940	0.091	-2.396	
		0	1.000	0.000	
		13020	0.769	-0.263	
0.008	2.50×10^{-13}	21420	0.645	-0.439	2.23×10^{-5}
	(pD 2.13)	33120	0.506	-0.682	
		39900	0.435	-0.833	
		44700	0.389	-0.945	
		79020	0.171	-1.765	
		0	1.000	0.000	
		8580	0.810	-0.211	
0.006	3.44×10^{-13}	22740	0.537	-0.622	2.96×10^{-5}
	(pD 2.27)	38340	0.325	-1.122	
		43440	0.293	-1.227	
		46380	0.260	-1.346	
		76440	0.111	-2.197	
		80340	0.094	-2.367	
		87300	0.076	-2.572	
		0	1.000	0.000	
		8340	0.737	-0.306	
0.004	4.86×10^{-13}	19980	0.455	-0.787	4.06×10^{-5}
	(pD 2.42)	35880	0.226	-1.487	
		45360	0.156	-1.859	
		48360	0.139	-1.976	
		73800	0.052	-2.959	
		0	1.000	0.000	
		2160	0.796	-0.228	
0.001	1.37×10^{-12}	5520	0.532	-0.631	1.20×10^{-4}
	(pD 2.87)	7560	0.408	-0.896	
		9840	0.319	-1.143	
		11820	0.249	-1.389	
		14820	0.169	-1.779	
		0	1.000	0.000	
		120	0.777	-0.252	
10% f_B	2.12×10^{-11}	240	0.643	-0.442	1.81×10^{-3}
acetic acid	(pD 4.06)	360	0.505	-0.683	
buffer		540	0.362	-1.016	
		720	0.261	-1.344	
		960	0.168	-1.782	
		1260	0.103	-2.272	

(a) Concentration of deuteroxide ion calculated using Equation 2.6. (b) Fraction of substrate remaining f(s) calculated using Equation 2.4. (c) Pseudo-first-order rate constant for exchange, k_{ex} (s^{-1}), obtained from the slope of the plot of ln f(s) against time in Figures A1 – A3.

Figure A1: Semilogarithmic plots of the fraction of unexchanged substrate against time for the deuterium exchange reaction of (138) in solutions of DCl in D_2O at 25 ºC and $I = 1.0$ (KCl).

Figure A2: Semilogarithmic plots of the fraction of unexchanged substrate against time for the deuterium exchange reaction of (138) in solutions of DCl in D_2O at 25 ºC and $I = 1.0$ (KCl).

Figure A3: **Semilogarithmic plots of the fraction of unexchanged substrate against time for the deuterium exchange reaction of (138) in solutions of DCl in D$_2$O at 25 ºC and *I* = 1.0 (KCl).**

Table A2: **Reaction data and first-order rate constants for exchange of the C(3)-H of triazolium salt (139) for deuterium in solutions of DCl in D$_2$O at 25 ºC and *I* = 1.0 (KCl).**

[DCl], M	[DO⁻], M	time, s	*f*(s)	ln *f*(s)	k_{ex}, s⁻¹
		0	1.000	0.000	
		161640	0.934	-0.068	
1.0	2.49 × 10⁻¹⁵	329280	0.880	-0.128	3.41 × 10⁻⁷
	(p*D* 0.13)	596820	0.798	-0.226	
		780240	0.758	-0.277	
		1889100	0.507	-0.680	
		4314720	0.232	-1.462	
		5178000	0.166	-1.795	
		0	1.000	0.000	
		2580	0.795	-0.230	
0.001	1.34 × 10⁻¹²	5280	0.611	-0.493	9.46 × 10⁻⁵
	(p*D* 2.86)	7500	0.495	-0.703	
		9780	0.401	-0.914	
		11700	0.332	-1.101	
		14640	0.252	-1.380	
		0	1.000	0.000	
		240	0.740	-0.302	
10% f_B	2.12 × 10⁻¹¹	480	0.518	-0.657	1.45 × 10⁻³
acetic acid	(p*D* 4.06)	720	0.359	-1.023	
buffer		960	0.255	-1.368	
		1200	0.176	-1.735	
		1380	0.140	-1.968	

(a) Concentration of deuteroxide ion calculated using Equation 2.6. (b) Fraction of substrate remaining *f*(s) calculated using Equation 2.4. (c) Pseudo-first-order rate constant for exchange, k_{ex} (s⁻¹), obtained from the slope of the plot of ln *f*(s) against time in Figures A4 – A5.
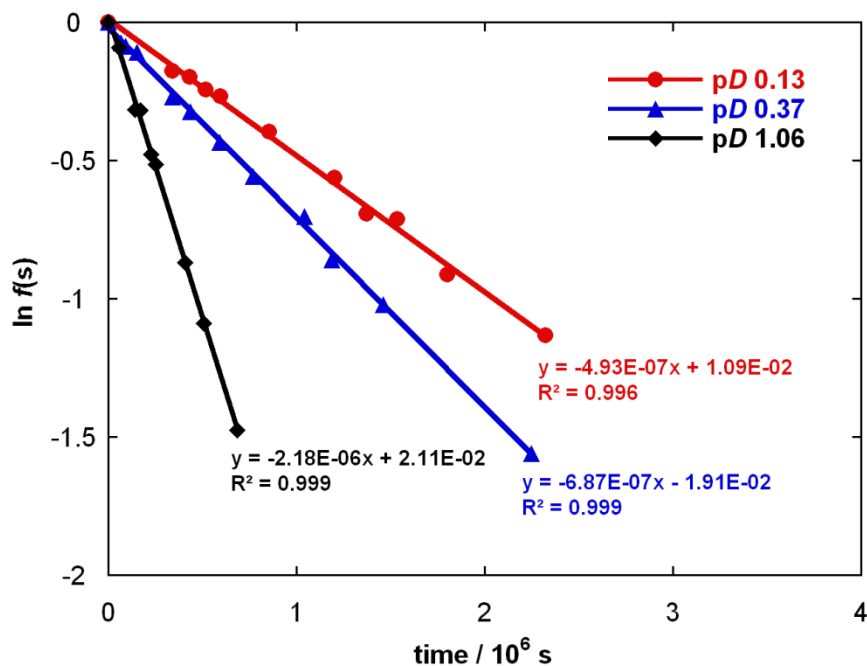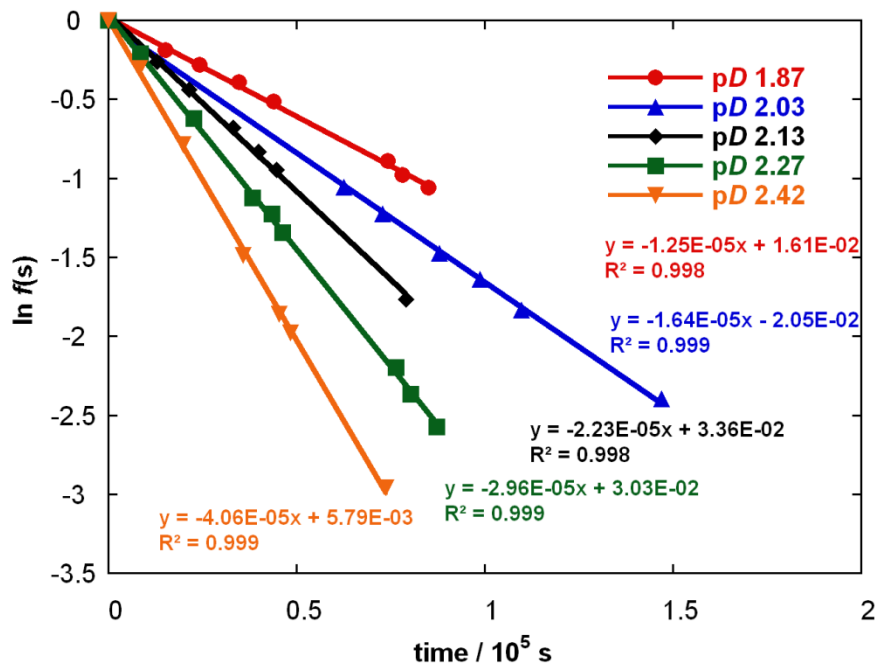
Figure A4: **Semilogarithmic plots of the fraction of unexchanged substrate against time for the deuterium exchange reaction of (139) in solutions of DCl in D_2O at 25 ºC and $I = 1.0$ (KCl).**

Figure A5: **Semilogarithmic plots of the fraction of unexchanged substrate against time for the deuterium exchange reaction of (139) in solutions of DCl in D_2O at 25 ºC and $I = 1.0$ (KCl).**
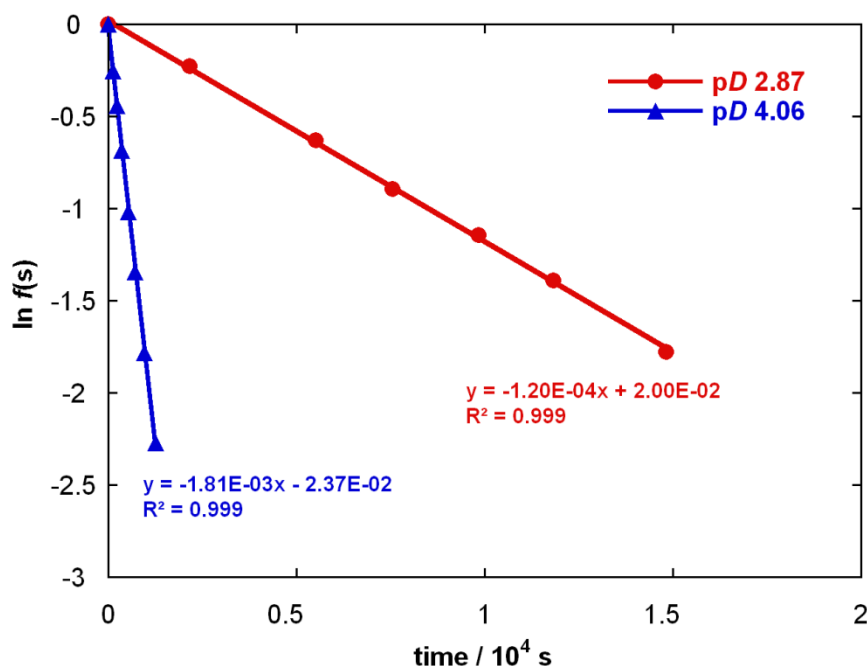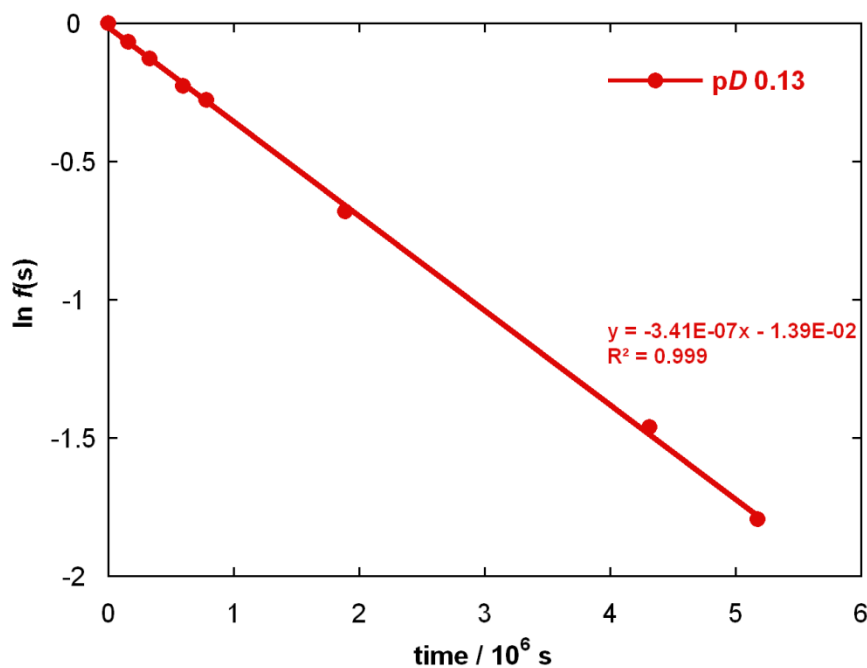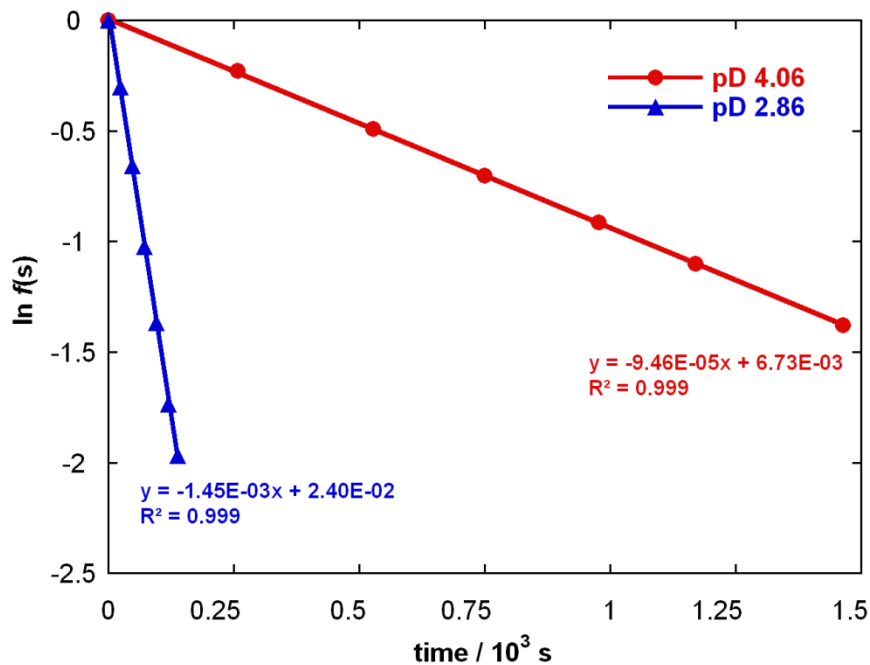
Table A3: **Reaction data and first-order rate constants for exchange of the C(3)-H of triazolium salt (140) for deuterium in solutions of DCl in D_2O at 25 ºC and I = 1.0 (KCl).**

[DCl], M	[DO⁻], M	time, s	$f(s)$	ln $f(s)$	k_{ex}, s⁻¹
		0	1.000	0.000	
		273960	0.946	-0.055	
1.0	2.49×10^{-15}	626280	0.848	-0.165	2.67×10^{-7}
	(p*D* 0.13)	805440	0.798	-0.225	
		2091960	0.554	-0.590	
		4341960	0.316	-1.151	
		5203020	0.251	-1.384	
		0	1.000	0.000	
		7500	0.963	-0.037	
0.02	1.04×10^{-13}	20580	0.902	-0.103	5.66×10^{-6}
	(p*D* 1.75)	80400	0.638	-0.449	
		122940	0.499	-0.696	
		176940	0.372	-0.988	
		208440	0.303	-1.193	
		302700	0.180	-1.712	
		356100	0.135	-2.004	
		0	1.000	0.000	
		7320	0.913	-0.091	
0.01	1.98×10^{-13}	24480	0.762	-0.272	1.09×10^{-5}
	(p*D* 2.03)	48060	0.576	-0.552	
		79260	0.413	-0.885	
		105720	0.312	-1.164	
		122160	0.259	-1.352	
		175800	0.146	-1.924	
		0	1.000	0.000	
		6600	0.918	-0.085	
0.008	2.49×10^{-13}	21780	0.743	-0.297	1.37×10^{-5}
	(p*D* 2.13)	35940	0.607	-0.499	
		48600	0.514	-0.666	
		77580	0.349	-1.052	
		98160	0.262	-1.340	
		119940	0.194	-1.639	
		0	1.000	0.000	
		6540	0.900	-0.105	
0.006	3.44×10^{-13}	18660	0.717	-0.333	1.77×10^{-5}
	(p*D* 2.27)	30360	0.605	-0.503	
		45060	0.455	-0.788	
		77220	0.257	-1.360	
		90600	0.207	-1.576	
		104580	0.158	-1.847	
		119640	0.121	-2.116	
		0	1.000	0.000	
		7620	0.833	-0.183	
0.004	4.86×10^{-13}	19020	0.626	-0.468	2.49×10^{-5}
	(p*D* 2.42)	29160	0.478	-0.738	
		39780	0.372	-0.989	
		47400	0.303	-1.195	
		76080	0.151	-1.888	
		83880	0.123	-2.093	

		0	1.000	0.000	
0.001	1.37×10^{-12}	2160	0.857	-0.154	7.09×10^{-5}
	(pD 2.87)	5100	0.693	-0.367	
		7920	0.575	-0.554	
		10260	0.481	-0.732	
		12180	0.423	-0.859	
		15120	0.341	-1.077	
		0	1.000	0.000	
		120	0.874	-0.134	
10% f_B	2.12×10^{-11}	240	0.781	-0.248	1.08×10^{-3}
acetic acid	(pD 4.06)	360	0.688	-0.375	
buffer		480	0.596	-0.518	
		600	0.527	-0.641	
		720	0.464	-0.768	
		840	0.404	-0.907	

(a) Concentration of deuteroxide ion calculated using Equation 2.6. (b) Fraction of substrate remaining f(s) calculated using Equation 2.4. (c) Pseudo-first-order rate constant for exchange, k_{ex} (s^{-1}), obtained from the slope of the plot of ln f(s) against time in Figures A6 – A8.

Figure A6: **Semilogarithmic plots of the fraction of unexchanged substrate against time for the deuterium exchange reaction of (140) in solutions of DCl in D$_2$O at 25 ºC and I = 1.0 (KCl).**

Figure A7: Semilogarithmic plots of the fraction of unexchanged substrate against time for the deuterium exchange reaction of (140) in solutions of DCl in D_2O at 25 ºC and $I = 1.0$ (KCl).

Figure A8: Semilogarithmic plots of the fraction of unexchanged substrate against time for the deuterium exchange reaction of (140) in solutions of DCl in D_2O at 25 ºC and $I = 1.0$ (KCl).

Table A4: **Reaction data and first-order rate constants for exchange of the C(3)-H of triazolium salt (141) for deuterium in solutions of DCl in D_2O at 25 ºC and $I = 1.0$ (KCl).**

[DCl], M	[DO⁻], M	time, s	$f(s)$	ln $f(s)$	k_{ex}, s⁻¹
1.0	2.49×10^{-15} (pD 0.13)	0	1.000	0.000	2.02×10^{-7}
		164400	0.980	-0.021	
		779880	0.873	-0.135	
		3086820	0.547	-0.603	
		4473000	0.411	-0.890	
		5174340	0.353	-1.041	
0.5	4.37×10^{-15} (pD 0.37)	0	1.000	0.000	3.10×10^{-7}
		168060	0.932	-0.071	
		327900	0.896	-0.110	
		584460	0.823	-0.195	
		751980	0.767	-0.265	
		1037220	0.714	-0.338	
		1197120	0.669	-0.402	
		1623360	0.589	-0.529	
		3115140	0.380	-0.969	
0.001	1.40×10^{-12} (pD 2.88)	0	1.000	0.000	6.08×10^{-5}
		2640	0.861	-0.149	
		5340	0.721	-0.327	
		8340	0.608	-0.498	
		10560	0.528	-0.638	
		12480	0.477	-0.741	
		15360	0.390	-0.940	

(a) Concentration of deuteroxide ion calculated using Equation 2.6. (b) Fraction of substrate remaining $f(s)$ calculated using Equation 2.4. (c) Pseudo-first-order rate constant for exchange, k_{ex} (s⁻¹), obtained from the slope of the plot of ln $f(s)$ against time in Figures A9 – A10.

Figure A9: **Semilogarithmic plots of the fraction of unexchanged substrate against time for the deuterium exchange reaction of (141) in solutions of DCl in D_2O at 25 ºC and $I = 1.0$ (KCl).**
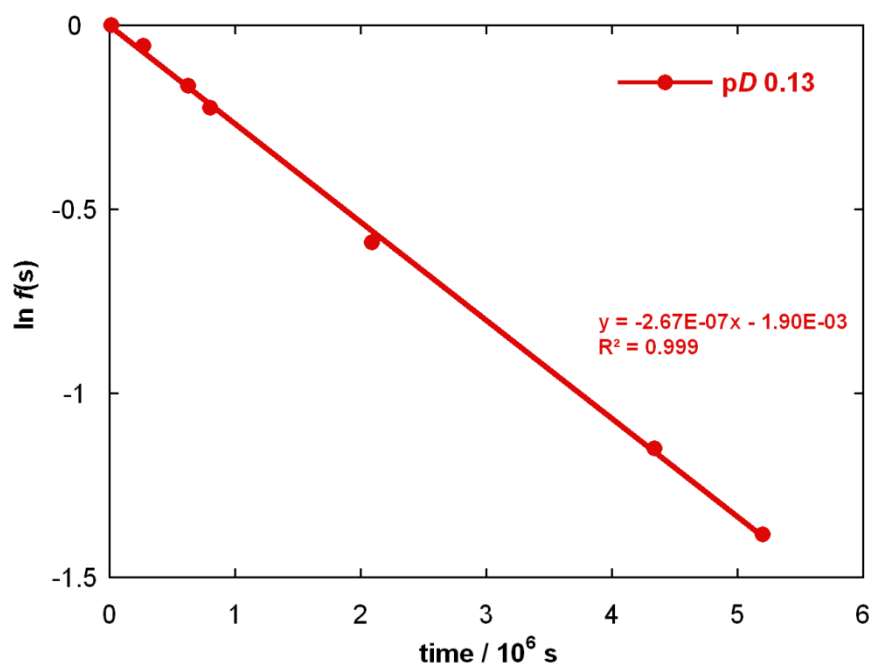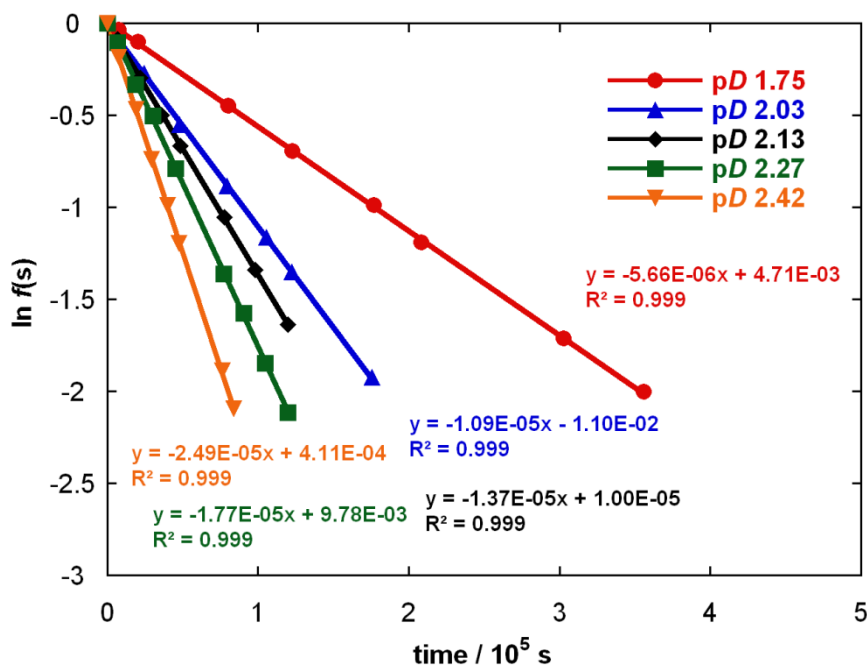
Figure A10: Semilogarithmic plots of the fraction of unexchanged substrate against time for the deuterium exchange reaction of (141) in solutions of DCl in D_2O at 25 ºC and $I = 1.0$ (KCl).
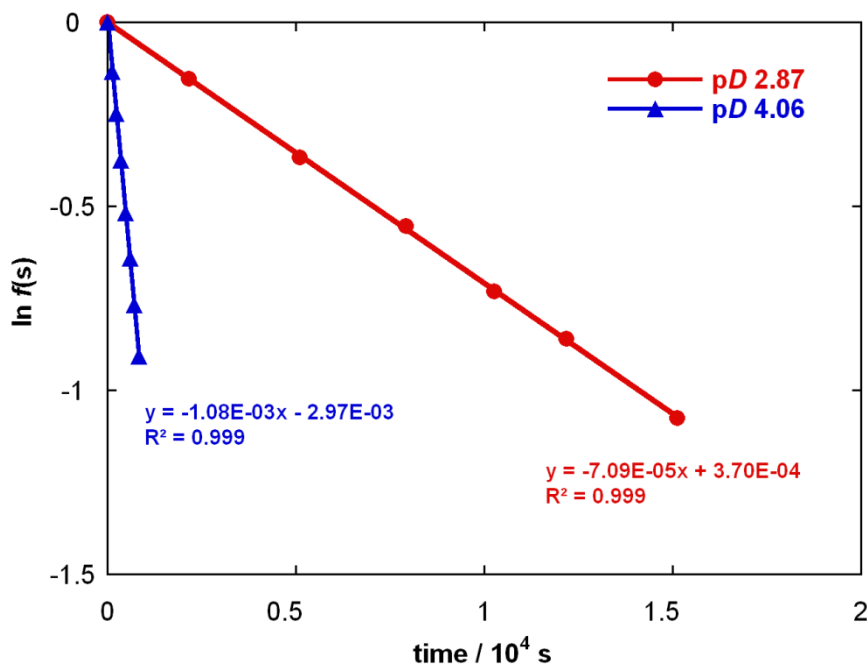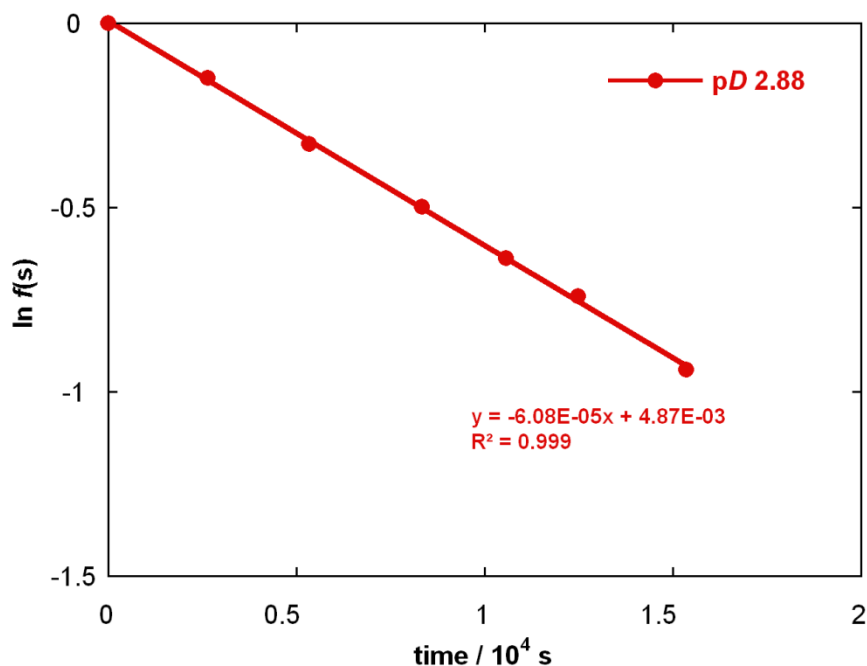

Table A5: Reaction data and first-order rate constants for exchange of the C(3)-H of triazolium salt (142) for deuterium in solutions of DCl in D_2O at 25 ºC and $I = 1.0$ (KCl).

[DCl], M	[DO⁻], M	time, s	$f(s)$	$\ln f(s)$	k_{ex}, s⁻¹
2.0 [b]	1.22×10^{-15} (pD -0.18)	0	1.000	0.000	1.66×10^{-5}
		18060	0.744	-0.296	
		58620	0.379	-0.970	
		70680	0.311	-1.168	
		83760	0.249	-1.389	
1.244 [c]	1.72×10^{-15} (pD -0.03)	0	1.000	0.000	3.28×10^{-5}
		7260	0.793	-0.232	
		14280	0.634	-0.456	
		19380	0.528	-0.638	
		27300	0.410	-0.893	
1.0	2.49×10^{-15} (pD 0.13)	0	1.000	0.000	4.15×10^{-5}
		3900	0.825	-0.192	
		10800	0.623	-0.473	
		18420	0.460	-0.776	
		25380	0.351	-1.046	
		33960	0.243	-1.414	
		46560	0.143	-1.946	
		49440	0.126	-2.072	
0.5	4.37×10^{-15} (pD 0.37)	0	1.000	0.000	5.03×10^{-5}
		6780	0.705	-0.349	
		10500	0.591	-0.527	
		17280	0.421	-0.864	
		21120	0.338	-1.084	
		27000	0.256	-1.362	

		31140	0.211	-1.555	
		41220	0.125	-2.082	
		0	1.000	0.000	
		6720	0.650	-0.431	
0.2	1.03×10^{-14}	13440	0.440	-0.821	6.00×10^{-5}
	(pD 0.75)	17400	0.348	-1.054	
		24480	0.226	-1.489	
		28920	0.177	-1.732	
		31080	0.153	-1.875	
		39060	0.094	-2.360	
		0	1.000	0.000	
		4590	0.746	-0.293	
0.1	2.12×10^{-14}	9600	0.526	-0.642	6.58×10^{-5}
	(pD 1.06)	13680	0.412	-0.887	
		22380	0.219	-1.520	
		27600	0.161	-1.824	
		31020	0.132	-2.024	
		33060	0.115	-2.166	
		0	1.000	0.000	
		3780	0.726	-0.320	
0.05	4.23×10^{-14}	10380	0.408	-0.897	8.71×10^{-5}
	(pD 1.36)	14940	0.266	-1.326	
		18000	0.209	-1.563	
		21480	0.154	-1.869	
		24060	0.124	-2.085	
		0	1.000	0.000	
		3600	0.668	-0.404	
0.03	6.56×10^{-14}	8700	0.371	-0.992	1.12×10^{-4}
	(pD 1.55)	11460	0.273	-1.297	
		13200	0.226	-1.489	
		15540	0.180	-1.716	
		18360	0.125	-2.083	
		19860	0.109	-2.220	

(a) Concentration of deuteroxide ion calculated using Equation 2.6. (b) Fraction of substrate remaining f(s) calculated using Equation 2.4. (c) Pseudo-first-order rate constant for exchange, k_{ex} (s^{-1}), obtained from the slope of the plot of ln f(s) against time in Figure A11 – A12. (b) Ionic strength $I = 2.0$. (c) Ionic strength $I = 1.244$.
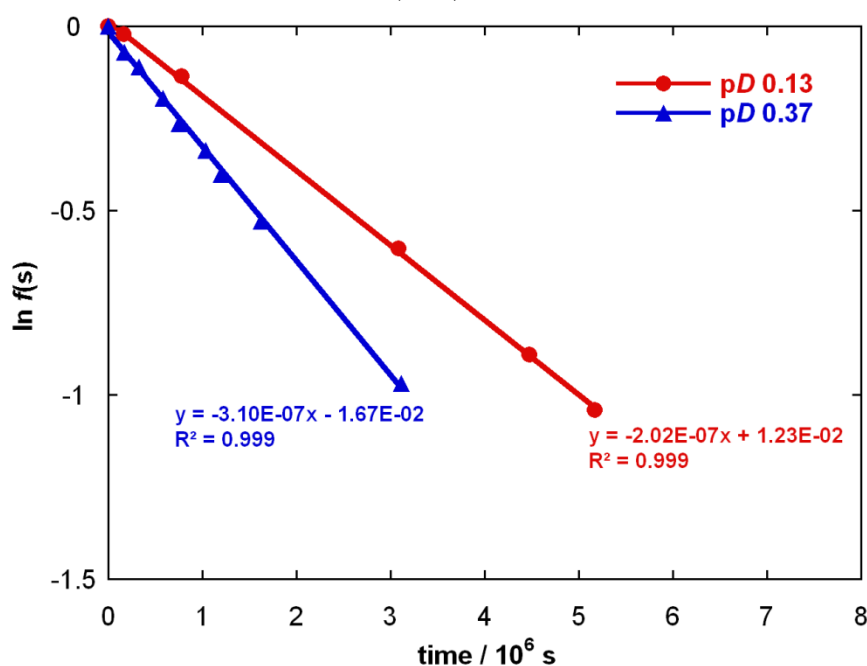
Figure A11: Semilogarithmic plots of the fraction of unexchanged substrate against time for the deuterium exchange reaction of (142) in solutions of DCl in D_2O at 25 ºC and $I = 1.0$ (KCl).
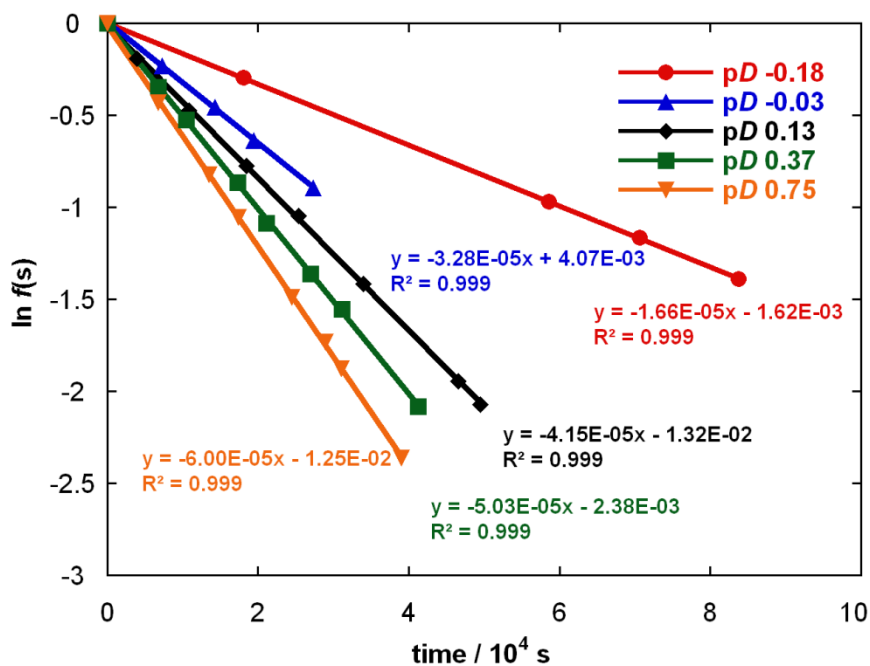

Figure A12: Semilogarithmic plots of the fraction of unexchanged substrate against time for the deuterium exchange reaction of (142) in solutions of DCl in D_2O at 25 ºC and $I = 1.0$ (KCl).
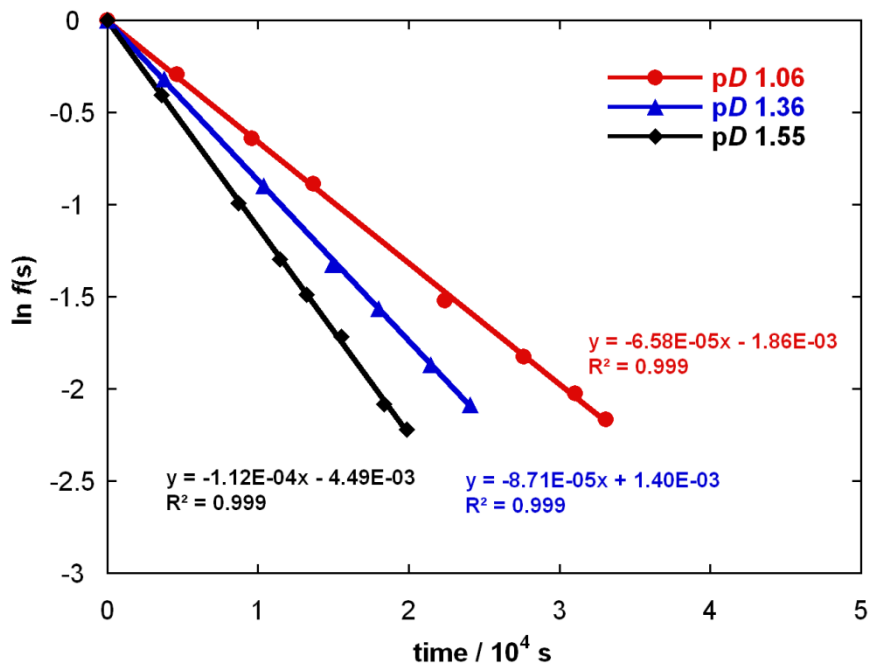
Table A6: Reaction data and first-order rate constants for exchange of the C(3)-H of triazolium salt (143) for deuterium in solutions of DCl in D_2O at 25 ºC and $I = 1.0$ (KCl).

[DCl], M	[DO⁻], M	time, s	$f(s)$	$\ln f(s)$	k_{ex}, s⁻¹
1.0	2.16×10^{-15} (pD 0.08)	0	1.000	0.000	6.92×10^{-5}
		6660	0.618	-0.481	
		12000	0.394	-0.931	
		17400	0.274	-1.295	
		26580	0.163	-1.813	
		31740	0.107	-2.237	
0.5	4.22×10^{-15} (pD 0.37)	0	1.000	0.000	4.27×10^{-5}
		8460	0.712	-0.340	
		16800	0.505	-0.683	
		23100	0.369	-0.998	
		28980	0.291	-1.235	
		37680	0.201	-1.606	
		44100	0.156	-1.860	
0.2	1.03×10^{-14} (pD 0.76)	0	1.000	0.000	2.22×10^{-5}
		14460	0.706	-0.348	
		28860	0.514	-0.666	
		39720	0.421	-0.864	
		47280	0.353	-1.040	
		85320	0.147	-1.920	
		99240	0.110	-2.210	
0.1	1.93×10^{-14} (pD 1.03)	0	1.000	0.000	1.40×10^{-5}
		16860	0.782	-0.246	
		57360	0.465	-0.765	
		76620	0.336	-1.090	
		92280	0.287	-1.248	
		102540	0.234	-1.454	
		144300	0.137	-1.987	
		166260	0.095	-2.357	
0.05	3.93×10^{-14} (pD 1.34)	0	1.000	0.000	1.11×10^{-5}
		12960	0.855	-0.157	
		40260	0.649	-0.433	
		85500	0.401	-0.913	
		108360	0.295	-1.220	
		129540	0.239	-1.430	
		180360	0.133	-2.016	
0.025	8.22×10^{-14} (pD 1.66)	0	1.000	0.000	1.39×10^{-5}
		23520	0.746	-0.292	
		40920	0.568	-0.566	
		86880	0.294	-1.224	
		101760	0.235	-1.447	
		116160	0.203	-1.595	
		131100	0.164	-1.806	
		176220	0.088	-2.428	
0.02	1.01×10^{-13} (pD 1.75)	0	1.000	0.000	1.57×10^{-5}
		21300	0.724	-0.323	
		67200	0.342	-1.074	
		82080	0.267	-1.320	
		95820	0.218	-1.524	

		111600	0.175	-1.742	
		157320	0.084	-2.474	
		0	1.000	0.000	
		38760	0.506	-0.681	
0.015	1.36×10^{-13}	53820	0.382	-0.963	1.83×10^{-5}
	(pD 1.88)	66600	0.308	-1.179	
		83280	0.222	-1.504	
		128940	0.095	-2.358	
		0	1.000	0.000	
		11160	0.767	-0.265	
0.01	2.02×10^{-13}	24420	0.549	-0.600	2.47×10^{-5}
	(pD 2.05)	43620	0.330	-1.109	
		89280	0.109	-2.213	
		98520	0.089	-2.414	
		0	1.000	0.000	
		7800	0.704	-0.352	
0.005	3.67×10^{-13}	14340	0.541	-0.615	4.20×10^{-5}
	(pD 2.31)	21540	0.411	-0.889	
		30420	0.270	-1.310	
		38220	0.201	-1.606	
		0	1.000	0.000	
		120	0.823	-0.195	
10% f_B	1.97×10^{-11}	255	0.651	-0.430	1.88×10^{-3}
acetic acid	(pD 4.04)	360	0.530	-0.635	
buffer		480	0.408	-0.896	
		600	0.324	-1.128	
		735	0.253	-1.374	
		840	0.214	-1.543	
		960	0.168	-1.785	

(a) Concentration of deuteroxide ion calculated using Equation 2.6. (b) Fraction of substrate remaining f(s) calculated using Equation 2.4. (c) Pseudo-first-order rate constant for exchange, k_{ex} (s^{-1}), obtained from the slope of the plot of ln f(s) against time in Figures A13 – A14.

Figure A13: Semilogarithmic plots of the fraction of unexchanged substrate against time for the deuterium exchange reaction of (143) in solutions of DCl in D_2O at 25 ºC and I = 1.0 (KCl).
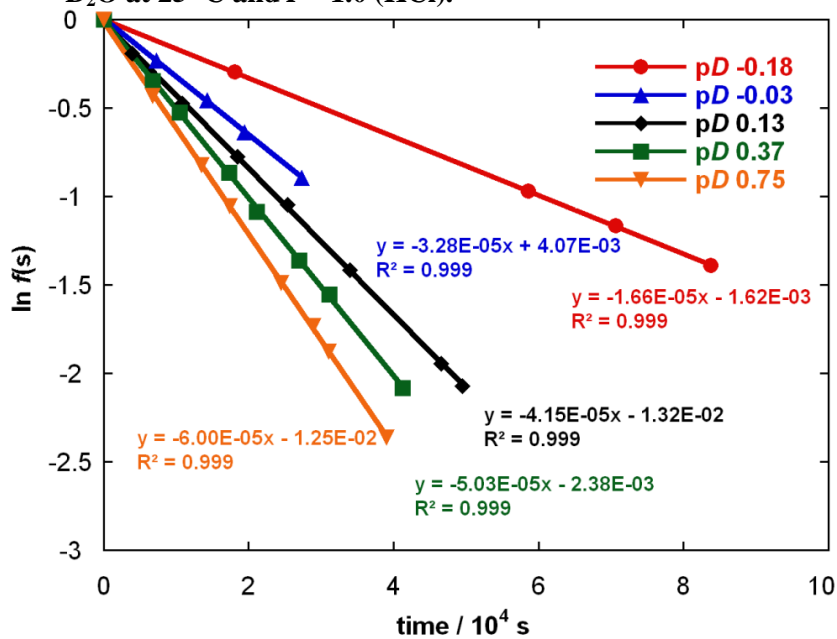

Figure A14: Semilogarithmic plots of the fraction of unexchanged substrate against time for the deuterium exchange reaction of (143) in solutions of DCl in D_2O at 25 ºC and I = 1.0 (KCl).
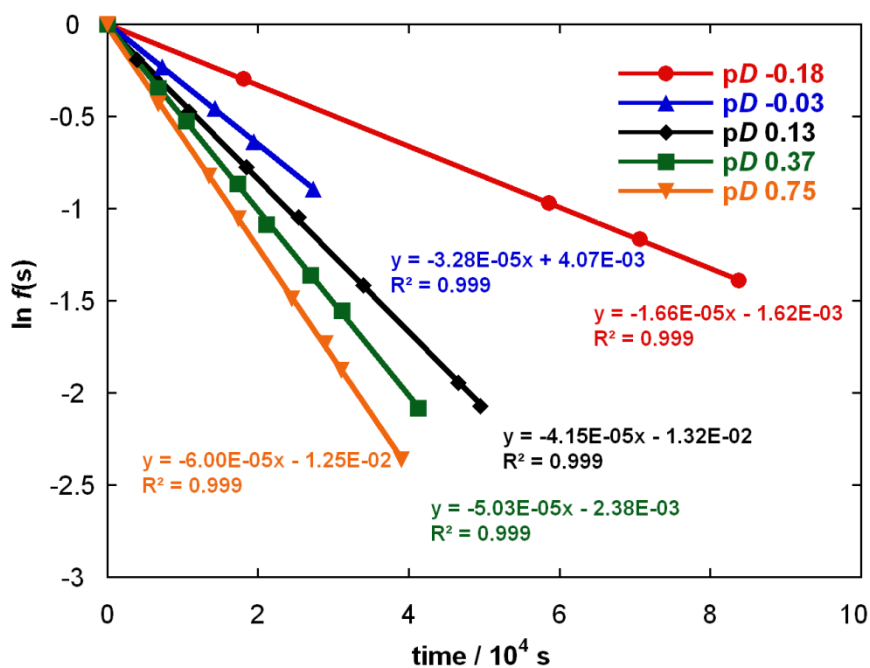
Table A7: **Reaction data and first-order rate constants for exchange of the C(3)-H of triazolium salt (53) for deuterium in solutions of acetic acid buffer (250 mM) in D$_2$O at 25 ºC and I = 1.0 (KCl).**

f_B	[DO$^-$], M	time, s	f(s)	ln f(s)	k_{ex}, s^{-1}
10%	2.17×10^{-11} (pD 4.07)	0	1.000	0.000	7.63×10^{-6}
		11160	0.902	-0.103	
		31260	0.760	-0.275	
		74520	0.551	-0.596	
		96360	0.465	-0.766	
		119820	0.393	-0.934	
		158220	0.299	-1.209	
		180360	0.246	-1.401	
30%	9.05×10^{-11} (pD 4.69)	0	1.000	0.000	2.99×10^{-5}
		3840	0.889	-0.118	
		9960	0.738	-0.304	
		16680	0.611	-0.493	
		21900	0.520	-0.654	
		25380	0.469	-0.757	
		62640	0.151	-1.889	
		69840	0.125	-2.079	
50%	2.17×10^{-10} (pD 5.07)	0	1.000	0.000	7.25×10^{-5}
		2940	0.861	-0.149	
		4980	0.740	-0.301	
		8580	0.568	-0.565	
		12660	0.426	-0.854	
		16140	0.329	-1.113	
		22560	0.210	-1.561	
		26760	0.145	-1.934	
70%	5.33×10^{-10} (pD 5.46)	0	1.000	0.000	1.71×10^{-4}
		960	0.847	-0.166	
		2100	0.692	-0.368	
		3120	0.604	-0.504	
		4980	0.436	-0.831	
		7320	0.287	-1.249	
		11280	0.144	-1.936	
		13800	0.096	-2.344	
90%	2.07×10^{-9} (pD 6.05)	0	1.000	0.000	6.31×10^{-4}
		300	0.870	-0.140	
		600	0.732	-0.312	
		900	0.578	-0.549	
		1200	0.477	-0.740	
		1500	0.400	-0.915	
		1800	0.329	-1.113	
		2580	0.203	-1.594	

(a) Concentration of deuteroxide ion calculated using Equation 2.6. (b) Fraction of substrate remaining f(s) calculated using Equation 2.4. (c) Pseudo-first-order rate constant for exchange, k_{ex} (s^{-1}), obtained from the slope of the plot of ln f(s) against time in Figure A15.

Figure A15: **Semilogarithmic plots of the fraction of unexchanged substrate against time for the deuterium exchange reaction of (53) in solutions of acetic acid buffer (250 mM) in D_2O at 25 °C and I = 1.0 (KCl).**
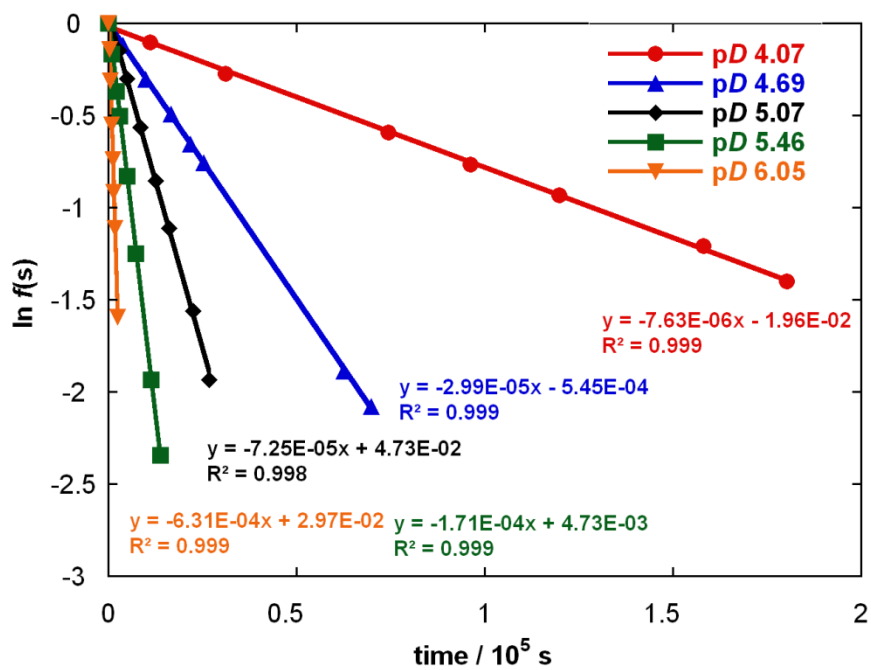
Table A8: **Reaction data and first-order rate constants for exchange of the C(3)-H of triazolium salt (151) for deuterium in solutions of acetic acid buffer (250 mM) in D_2O at 25 ºC and I = 1.0 (KCl).**

f_B	[DO⁻], M	time, s	f(s)	ln f(s)	k_{ex}, s⁻¹
10%	2.52×10^{-11} (pD 4.13)	0	1.000	0.000	1.30×10^{-5}
		42600	0.627	-0.468	
		60120	0.488	-0.718	
		77160	0.384	-0.956	
		132180	0.181	-1.711	
		151500	0.147	-1.917	
30%	8.95×10^{-11} (pD 4.68)	0	1.000	0.000	4.42×10^{-5}
		3480	0.824	-0.194	
		7020	0.773	-0.258	
		13380	0.534	-0.628	
		18720	0.434	-0.835	
		23100	0.362	-1.016	
50%	2.30×10^{-10} (pD 5.09)	0	1.000	0.000	1.09×10^{-4}
		2700	0.751	-0.286	
		5100	0.541	-0.615	
		7860	0.391	-0.938	
		10860	0.305	-1.188	
		12240	0.266	-1.325	
		17880	0.139	-1.975	
70%	5.45×10^{-10} (pD 5.45)	0	1.000	0.000	2.72×10^{-4}
		900	0.773	-0.257	
		1800	0.589	-0.529	
		3360	0.384	-0.958	
		4680	0.272	-1.304	
		5340	0.238	-1.435	

(a) Concentration of deuteroxide ion calculated using Equation 2.6. (b) Fraction of substrate remaining f(s) calculated using Equation 2.4. (c) Pseudo-first-order rate constant for exchange, k_{ex} (s⁻¹), obtained from the slope of the plot of ln f(s) against time in Figure A16.

Figure A16: **Semilogarithmic plots of the fraction of unexchanged substrate against time for the deuterium exchange reaction of (151) in solutions of acetic acid buffer (250 mM) in D_2O at 25 ºC and I = 1.0 (KCl).**
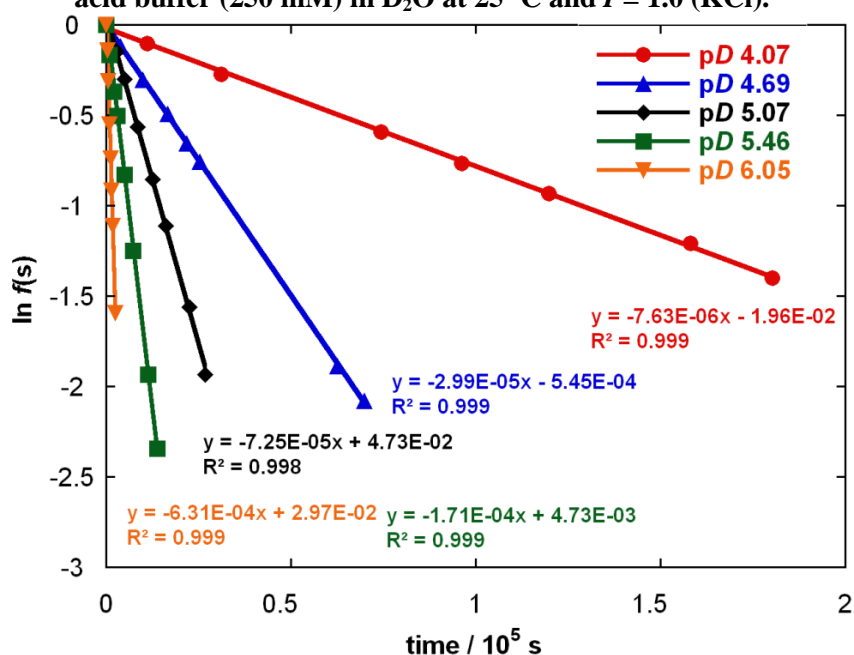
Table A9: **Reaction data and first-order rate constants for exchange of the two C(2)-H groups of triazolium salt (152) for deuterium in solutions of acetic acid buffer (250 mM) in D_2O at 25 ºC and $I = 1.0$ (KCl).**

f_B	[DO⁻], M	time, s	$f(s)$	ln $f(s)$	k_{ex}, s⁻¹
10%	2.17×10^{-11} (pD 4.07)	0	1.000	0.000	3.40×10^{-7}
		11100	0.977	-0.023	
		77760	0.971	-0.030	
		250200	0.915	-0.089	
		353400	0.879	-0.128	
		422400	0.855	-0.156	
		702060	0.783	-0.245	
30%	9.05×10^{-11} (pD 4.69)	0	1.000	0.000	1.26×10^{-6}
		80940	0.907	-0.098	
		172620	0.807	-0.214	
		352740	0.650	-0.431	
		421740	0.595	-0.519	
		701760	0.412	-0.887	
		884520	0.334	-1.095	
		1129080	0.241	-1.425	
50%	2.17×10^{-10} (pD 5.07)	0	1.000	0.000	3.05×10^{-6}
		19140	0.938	-0.064	
		80520	0.776	-0.253	
		169200	0.600	-0.511	
		352380	0.333	-1.101	
		421020	0.273	-1.298	
		535860	0.190	-1.658	
		701100	0.121	-2.116	
70%	5.33×10^{-10} (pD 5.46)	0	1.000	0.000	7.52×10^{-6}
		10440	0.928	-0.075	
		41220	0.747	-0.292	
		79740	0.557	-0.585	
		101640	0.468	-0.758	
		168180	0.283	-1.261	
		192900	0.232	-1.459	
		258900	0.145	-1.930	
90%	2.07×10^{-9} (pD 6.05)	0	1.000	0.000	2.84×10^{-5}
		10140	0.746	-0.293	
		19320	0.570	-0.562	
		30780	0.405	-0.903	
		43080	0.292	-1.231	
		81420	0.098	-2.320	

(a) Concentration of deuteroxide ion calculated using Equation 2.6. (b) Fraction of substrate remaining $f(s)$ calculated using Equation 2.4. (c) Pseudo-first-order rate constant for exchange, k_{ex} (s⁻¹), obtained from the slope of the plot of ln $f(s)$ against time in Figure A18.

Figure A17: **Semilogarithmic plots of the fraction of unexchanged substrate against time for the deuterium exchange reaction of (152) in solutions of acetic acid buffer (250 mM) in D₂O at 25 ºC and *I* = 1.0 (KCl).**
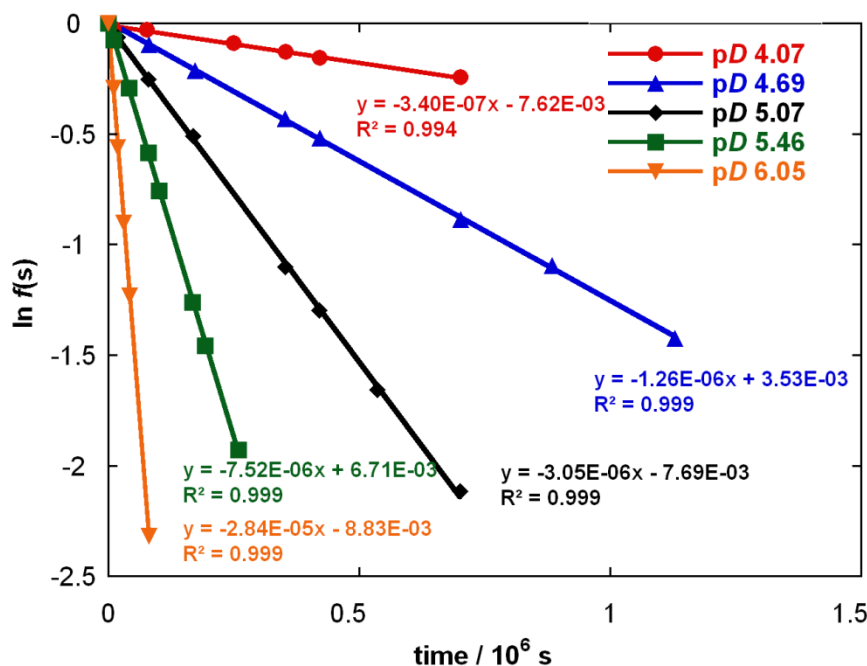

Table A10: **Reaction data and first-order rate constants for exchange of the C(2)-H of imidazolium salt (153) for deuterium in solutions of acetic acid buffer (250 mM) in D₂O at 25 ºC and *I* = 1.0 (KCl).**

f_B	[DO⁻], M	time, s	$f(s)$	ln $f(s)$	k_{ex}, s⁻¹
		0	1.000	0.000	
		1904760	0.883	-0.124	
60%	3.57×10^{-10}	3631020	0.774	-0.256	6.31×10^{-8}
	(p*D* 5.28)	4859460	0.725	-0.321	
		6047400	0.684	-0.380	
		8469840	0.584	-0.538	
		0	1.000	0.000	
		1198800	0.884	-0.123	
70%	5.52×10^{-10}	1977360	0.827	-0.190	9.55×10^{-8}
	(p*D* 5.47)	3014160	0.776	-0.254	
		4413480	0.637	-0.451	
		6120060	0.545	-0.608	
		8540100	0.449	-0.800	
		0	1.000	0.000	
		684720	0.878	-0.131	
80%	9.82×10^{-10}	1199940	0.803	-0.219	1.72×10^{-7}
	(p*D* 5.72)	1977960	0.721	-0.327	
		2491980	0.637	-0.451	
		3708840	0.528	-0.638	
		4419780	0.459	-0.779	
		6124380	0.349	-1.054	

		0	1.000	0.000	
90%	2.10×10^{-9}	152100	0.946	-0.055	3.74×10^{-7}
	(pD 6.05)	572700	0.808	-0.213	
		1271340	0.621	-0.476	
		2049120	0.455	-0.787	
		2563380	0.378	-0.974	
		3091080	0.320	-1.140	
		3780180	0.243	-1.413	

(a) Concentration of deuteroxide ion calculated using Equation 2.6. (b) Fraction of substrate remaining f(s) calculated using Equation 2.4. (c) Pseudo-first-order rate constant for exchange, k_{ex} (s^{-1}), obtained from the slope of the plot of ln f(s) against time in Figure A17.

Figure A18: **Semilogarithmic plots of the fraction of unexchanged substrate against time for the deuterium exchange reaction of (153) in solutions of acetic acid buffer (250 mM) in D$_2$O at 25 ºC and I = 1.0 (KCl).**

Legend:
- pD 5.28
- pD 5.47
- pD 5.72
- pD 6.05

y = -6.31E-08x - 7.96E-03
R² = 0.997

y = -9.55E-08x - 1.56E-03
R² = 0.994

y = -1.72E-07x - 6.98E-03
R² = 0.999

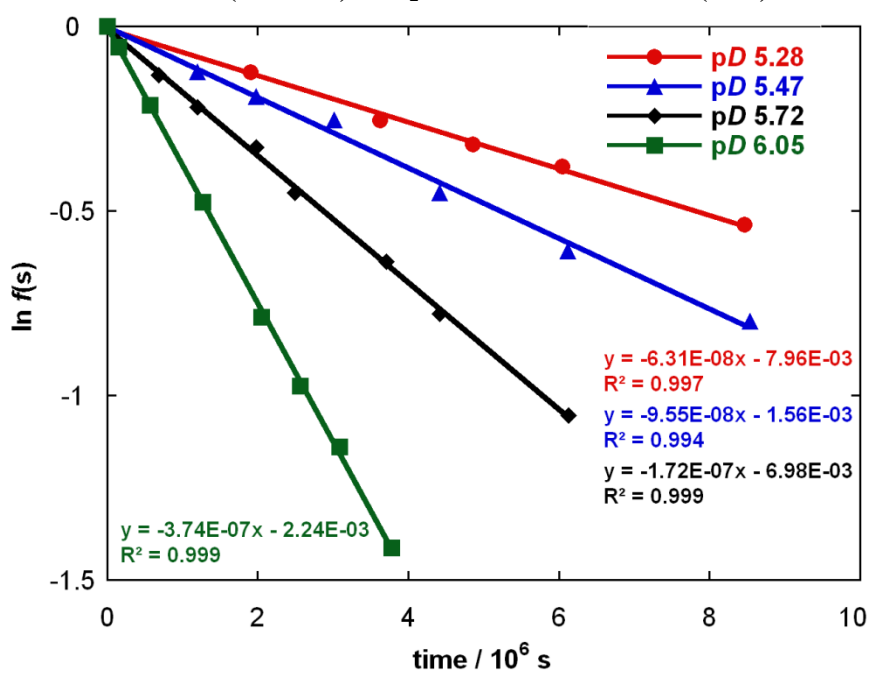y = -3.74E-07x - 2.24E-03
R² = 0.999

Table A11: **Reaction data and first-order rate constants for exchange of the C(5)-H of 1,2,3-triazolium salt (204) for deuterium in solutions of KOD in D_2O at 25 ºC and I = 1.0 (KCl).**

[DO⁻], M	time, s	f(s) [a]	ln f(s)	k_{ex}, s⁻¹ [b]
	0	1.000	0.000	
	900	0.717	-0.333	
0.01	2340	0.357	-1.029	4.20×10^{-4}
	3000	0.278	-1.281	
	3900	0.192	-1.650	
	4800	0.134	-2.007	
	6000	0.082	-2.502	
	0	1.000	0.000	
0.02	600	0.573	0.558	
	1200	0.340	-1.078	9.06×10^{-4}
	1800	0.194	-1.641	
	2700	0.085	-2.468	
	3000	0.067	-2.707	
	0	1.000	0.000	
	300	0.729	-0.317	
0.03	600	0.459	-0.780	1.33×10^{-3}
	900	0.314	-1.160	
	1200	0.208	-1.569	
	2100	0.063	-2.760	
	0	1.000	0.000	
	240	0.662	-0.412	
0.04	420	0.480	-0.734	2.27×10^{-3}
	600	0.331	-1.105	
	780	0.248	-1.396	
	960	0.176	-1.735	
	1140	0.129	-2.051	
	0	1.000	0.000	
	180	0.667	-0.405	
0.05	360	0.462	-0.772	1.81×10^{-3}
	540	0.294	-1.223	
	840	0.174	-1.916	
	1020	0.100	-2.300	

(a) Fraction of substrate remaining f(s) calculated using Equation 2.4. (b) Pseudo-first-order rate constant for exchange, k_{ex} (s⁻¹), obtained from the slope of the plot of ln f(s) against time in Figure A19.

Figure A19: Semilogarithmic plots of the fraction of unexchanged substrate against time for the deuterium exchange reaction of (204) in solutions of KOD in D_2O at 25 ºC and $I = 1.0$ (KCl).
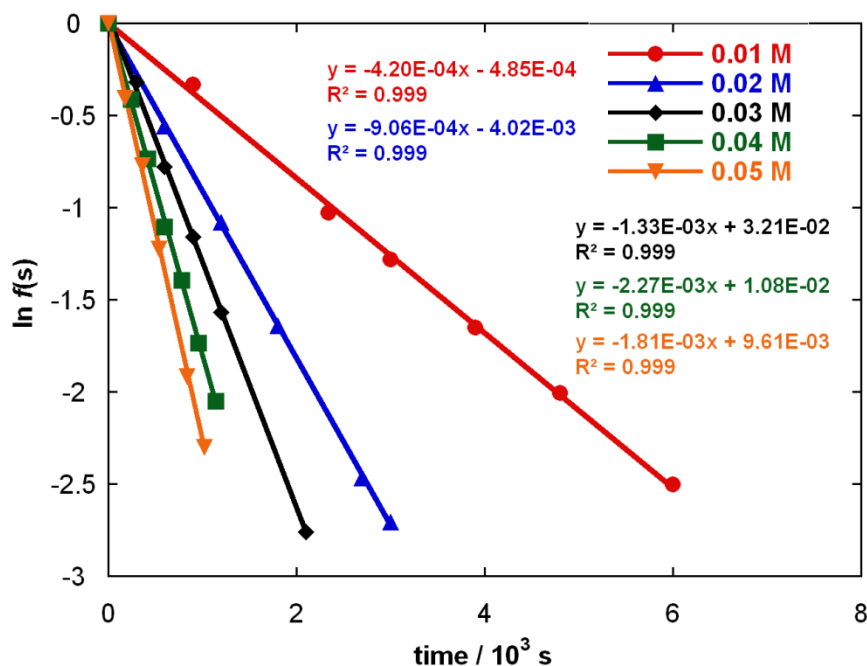

Table A12: Reaction data and first-order rate constants for exchange of the C(5)-H of 1,2,3-triazolium salt (205) for deuterium in solutions of phosphate buffer (250 mM) in D_2O at 25 ºC and $I = 1.0$ (KCl).

f_B	[DO⁻], M [a]	time, s	$f(s)$ [b]	$\ln f(s)$	k_{ex}, s⁻¹ [c]
		0	1.000	0.000	
		416580	0.918	-0.085	
40%	2.07×10^{-8}	698700	0.848	-0.164	2.42×10^{-7}
	(pD 7.05)	1275240	0.738	-0.304	
		1621920	0.670	-0.400	
		2317800	0.567	-0.568	
		2836440	0.505	-0.682	
		3508380	0.433	-0.837	
		0	1.000	0.000	
		341760	0.906	-0.099	
50%	2.93×10^{-8}	951240	0.723	-0.325	3.38×10^{-7}
	(pD 7.20)	1558260	0.598	-0.514	
		2155620	0.486	-0.721	
		2850480	0.387	-0.949	
		3382680	0.318	-1.145	
		0	1.000	0.000	
		257640	0.759	-0.276	
70%	7.88×10^{-8}	428220	0.652	-0.428	9.53×10^{-7}
	(pD 7.63)	690300	0.513	-0.667	
		1028580	0.380	-0.967	
		1281300	0.290	-1.236	
		1625580	0.208	-1.570	

		0	1.000	0.000	
90%	2.38×10^{-7}	96600	0.756	-0.280	2.95×10^{-6}
	(p*D* 8.11)	176040	0.590	-0.528	
		261660	0.480	-0.734	
		350820	0.355	-1.034	
		442620	0.273	-1.299	
		521040	0.217	-1.529	
		608100	0.166	-1.796	

(a) Concentration of deuteroxide ion calculated using Equation 2.6. (b) Fraction of substrate remaining *f*(s) calculated using Equation 2.4. (c) Pseudo-first-order rate constant for exchange, k_{ex} (s^{-1}), obtained from the slope of the plot of ln *f*(s) against time in Figure A20.

Figure A20: **Semilogarithmic plots of the fraction of unexchanged substrate against time for the deuterium exchange reaction of (205) in solutions of phosphate buffer (250 mM) in D$_2$O at 25 °C and *I* = 1.0 (KCl).**

$y = -2.42E{-}07x + 3.27E{-}03$
$R^2 = 0.999$

$y = -3.38E{-}07x + 6.91E{-}03$
$R^2 = 0.999$

$y = -2.95E{-}06x + 5.72E{-}03$
$R^2 = 0.999$

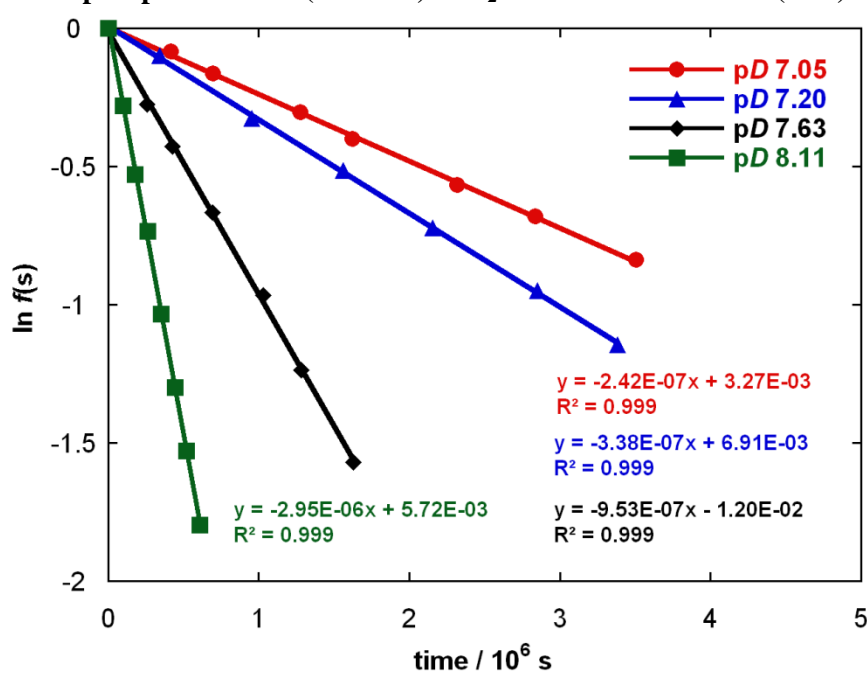$y = -9.53E{-}07x - 1.20E{-}02$
$R^2 = 0.999$

Table A13: **Reaction data and first-order rate constants for exchange of the C(5)-H of 1,2,3-triazolium salt (206) for deuterium in solutions of phosphate buffer (250 mM) in D$_2$O at 25 ºC and I = 1.0 (KCl).**

f_B	[DO$^-$], M	time, s	f(s)	ln f(s)	k_{ex}, s^{-1}
10%	1.96×10^{-9} (pD 6.02)	0	1.000	0.000	2.04×10^{-8}
		1718640	0.971	-0.029	
		3207240	0.927	-0.075	
		3972300	0.917	-0.086	
		5547540	0.888	-0.118	
		7246800	0.867	-0.143	
30%	8.17×10^{-9} (pD 6.64)	0	1.000	0.000	8.64×10^{-8}
		1144260	0.906	-0.099	
		1717740	0.851	-0.162	
		2933460	0.765	-0.268	
		3969540	0.716	-0.334	
		4912020	0.655	-0.423	
		6668520	0.557	-0.585	
50%	2.58×10^{-8} (pD 7.14)	0	1.000	0.000	3.42×10^{-7}
		619140	0.826	-0.191	
		1049940	0.720	-0.329	
		1456740	0.609	-0.496	
		2080380	0.501	-0.691	
		2922240	0.361	-1.019	
		3891600	0.272	-1.303	
70%	5.92×10^{-8} (pD 7.50)	0	1.000	0.000	7.21×10^{-7}
		153720	0.917	-0.086	
		417180	0.762	-0.272	
		665220	0.638	-0.450	
		1047720	0.478	-0.738	
		1394040	0.373	-0.986	
		1908480	0.256	-1.362	

(a) Concentration of deuteroxide ion calculated using Equation 2.6. (b) Fraction of substrate remaining f(s) calculated using Equation 2.4. (c) Pseudo-first-order rate constant for exchange, k_{ex} (s^{-1}), obtained from the slope of the plot of ln f(s) against time in Figure A21.

Figure A21: Semilogarithmic plots of the fraction of unexchanged substrate against time for the deuterium exchange reaction of (206) in solutions of phosphate buffer (250 mM) in D_2O at 25 °C and $I = 1.0$ (KCl).
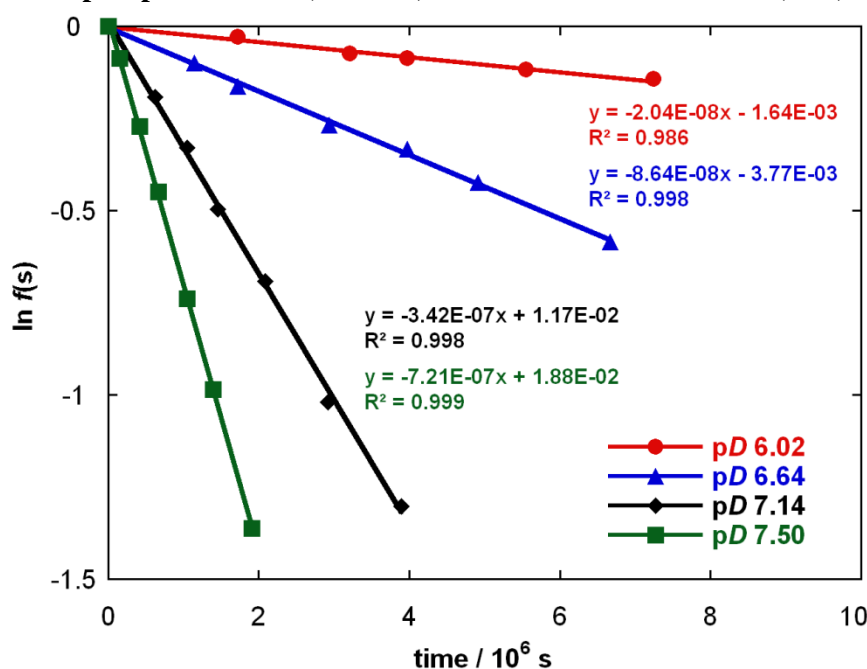

Table A14: Reaction data and first-order rate constants for exchange of the C(5)-H of 1,2,3-triazolium salt (207) for deuterium in solutions of phosphate buffer (250 mM) in D_2O at 25 °C and $I = 1.0$ (KCl).

f_B	[DO⁻], M	time, s	$f(s)$	$\ln f(s)$	k_{ex}, s⁻¹
10%	1.96×10^{-9} (pD 6.02)	0	1.000	0.000	3.06×10^{-7}
		174840	0.939	-0.062	
		368220	0.868	-0.142	
		523980	0.827	-0.190	
		1045440	0.691	-0.370	
		1487280	0.622	-0.475	
		2011320	0.528	-0.639	
		2609520	0.447	-0.804	
30%	8.17×10^{-9} (pD 6.64)	0	1.000	0.000	1.37×10^{-6}
		136020	0.826	-0.191	
		263280	0.710	-0.343	
		418200	0.573	-0.556	
		585840	0.452	-0.793	
		753420	0.366	-1.006	
		1107120	0.218	-1.525	
50%	2.58×10^{-8} (pD 7.14)	0	1.000	0.000	5.16×10^{-6}
		62280	0.723	-0.325	
		96480	0.608	-0.498	
		139140	0.488	-0.717	
		176760	0.403	-0.910	
		237660	0.299	-1.206	
		265260	0.251	-1.384	
		331860	0.180	-1.716	

		0	1.000	0.000	
70%	6.20×10^{-8}	13200	0.822	-0.196	1.28×10^{-5}
	(pD 7.52)	52620	0.488	-0.718	
		70740	0.383	-0.959	
		99780	0.271	-1.305	
		136920	0.170	-1.770	
		154560	0.134	-2.011	
		166440	0.117	-2.147	

(a) Concentration of deuteroxide ion calculated using Equation 2.6. (b) Fraction of substrate remaining f(s) calculated using Equation 2.4. (c) Pseudo-first-order rate constant for exchange, k_{ex} (s^{-1}), obtained from the slope of the plot of ln f(s) against time in Figure A22.

Figure A22: **Semilogarithmic plots of the fraction of unexchanged substrate against time for the deuterium exchange reaction of (207) in solutions of phosphate buffer (250 mM) in D$_2$O at 25 ºC and I = 1.0 (KCl).**
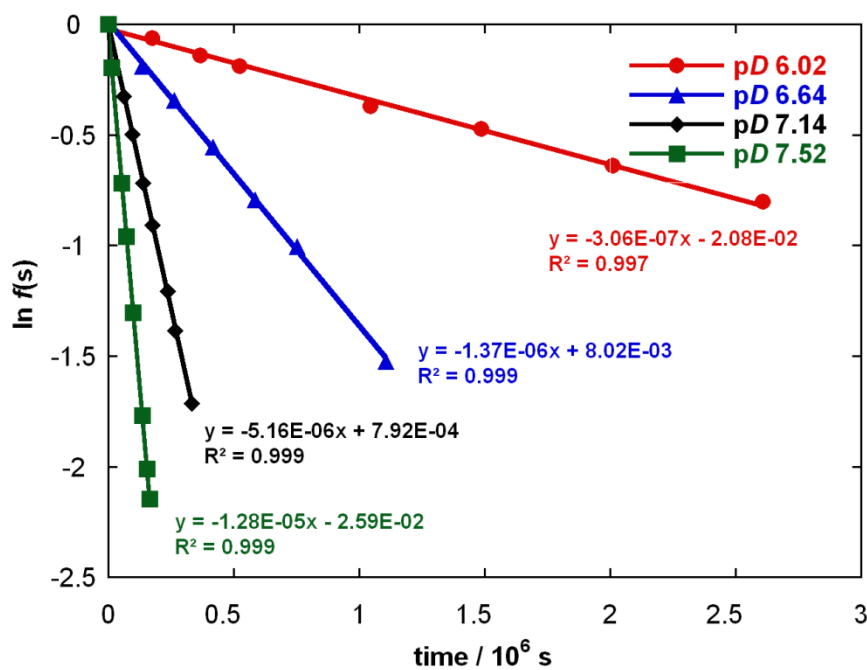
Table A15: **Reaction data and pseudo-first-order rate constants for exchange, k_{ex} (s^{-1}), of the C(5)-H of 1,2,3-triazolium ion (207) for deuterium in 70% f_B phosphate buffered solutions of D$_2$O at 25 ºC and $I = 1.0$ (KCl).**

[buffer]$_{tot}$, M [a]	[DO$^-$], M [b]	time, s	f(s) [c]	ln f(s)	k_{ex}, s^{-1} [d]
0.10	5.78×10^{-8} (pD 7.49)	0	1.000	0.000	1.16×10^{-5}
		22140	0.769	-0.263	
		72360	0.419	-0.870	
		82620	0.377	-0.975	
		96720	0.315	-1.156	
		152100	0.172	-1.759	
		164340	0.147	-1.918	
		180300	0.121	-2.115	
0.20	6.05×10^{-8} (pD 7.51)	0	1.000	0.000	1.32×10^{-5}
		22020	0.754	-0.282	
		72360	0.381	-0.965	
		82560	0.331	-1.104	
		95940	0.271	-1.307	
		151980	0.132	-2.026	
		164040	0.118	-2.134	
0.25	6.20×10^{-8} (pD 7.52)	0	1.000	0.000	1.28×10^{-5}
		13200	0.822	-0.196	
		52620	0.488	-0.718	
		70740	0.383	-0.959	
		99780	0.271	-1.305	
		136920	0.170	-1.770	
		154560	0.134	-2.011	
		166440	0.117	-2.147	
0.30	6.64×10^{-8} (pD 7.55)	0	1.000	0.000	1.45×10^{-5}
		23040	0.737	-0.305	
		71940	0.365	-1.008	
		83580	0.314	-1.157	
		97020	0.258	-1.356	
		153000	0.107	-2.232	
0.40	7.11×10^{-8} (pD 7.58)	0	1.000	0.000	1.57×10^{-5}
		23040	0.699	-0.358	
		72000	0.320	-1.138	
		83700	0.268	-1.316	
		97020	0.217	-1.528	
		153060	0.091	-2.396	

(a) Total concentration of phosphate buffer [DPO$_4$$^{2-}$(K$^+$)$_2$]+[D$_2PO_4$$^-K^+$]; (b) Concentration of deuteroxide ion calculated using Equation 2.6, where γ_{DO} = 0.72; (c) Fraction of unexchanged substrate remaining, f(s), calculated using Equation 2.4; (d) Pseudo-first-order rate constant for exchange, k_{ex} (s^{-1}), obtained from the slope of the plot of ln f(s) against time in Figure A23.

Figure A23: Semilogarithmic plots of the fraction of unexchanged substrate against time for the H/D exchange reaction of triazolium ion (207) in phosphate buffer solutions (70% f_B) at buffer base concentrations 0.070 M (○), 0.140 M (□), 0.175 M (◇), 0.210 M (△) and 0.280 M (▽) in D_2O at 25 ºC and I = 1.0 (KCl).
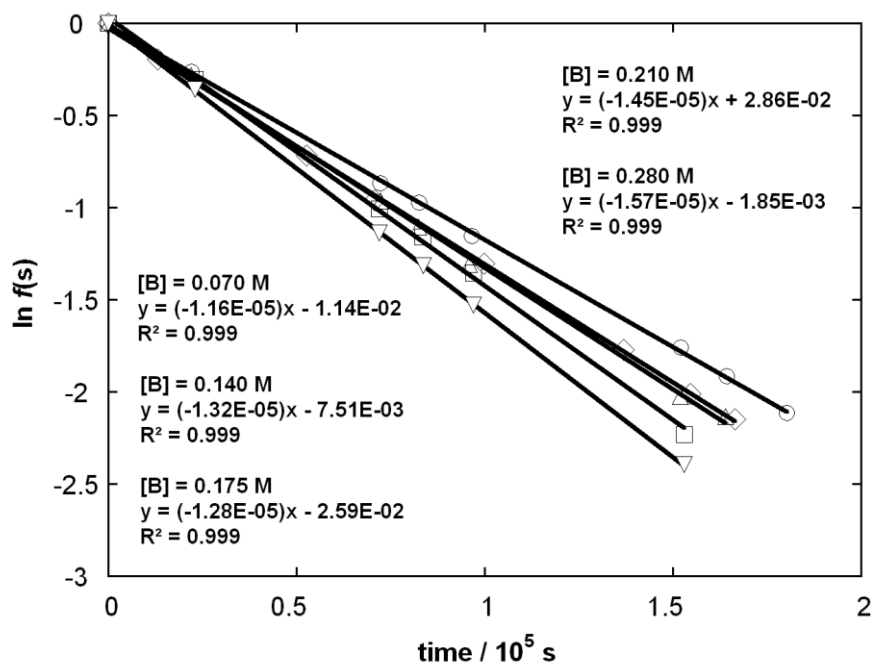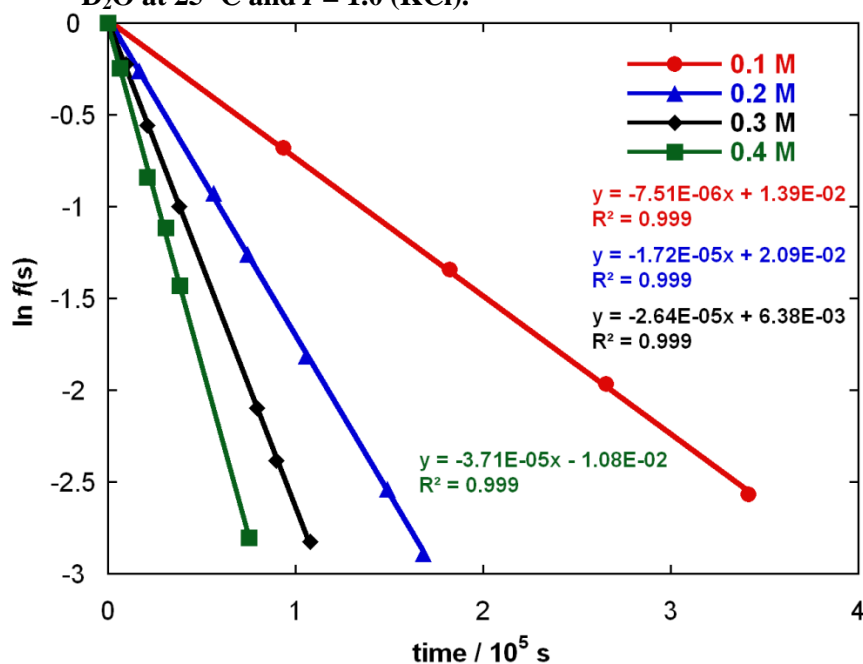
Table A16: Reaction data and first-order rate constants for exchange of the C(4/5)-H of imidazolium salt (208) for deuterium in solutions of KOD in D_2O at 25 °C and $I = 1.0$ (KCl).

[DO⁻], M	time, s	$f(s)$ [a]	ln $f(s)$	k_{ex}, s⁻¹ [b]
	0	1.000	0.000	
	93480	0.507	-0.680	
0.1	182220	0.261	-1.343	7.51×10^{-6}
	265680	0.140	-1.968	
	341640	0.077	-2.569	
	0	1.000	0.000	
	16620	0.770	-0.261	
0.2	56460	0.396	-0.927	1.72×10^{-5}
	74520	0.284	-1.260	
	105840	0.163	-1.814	
	149040	0.079	-2.540	
	168120	0.056	-2.890	
	0	1.000	0.000	
	9480	0.800	-0.223	
0.3	20940	0.574	-0.556	2.64×10^{-5}
	37980	0.369	-0.998	
	79680	0.123	-2.098	
	89940	0.092	-2.382	
	108000	0.059	-2.827	
	0	1.000	0.000	
	6300	0.783	-0.244	
0.4	21000	0.432	-0.839	3.71×10^{-5}
	30900	0.327	-1.117	
	38400	0.239	-1.430	
	75240	0.061	-2.805	

(a) Fraction of substrate remaining $f(s)$ calculated using Equation 2.4. (b) Pseudo-first-order rate constant for exchange, k_{ex} (s⁻¹), obtained from the slope of the plot of ln $f(s)$ against time in Figure A24.

Figure A24: Semilogarithmic plots of the fraction of unexchanged substrate against time for the deuterium exchange reaction of (208) in solutions of KOD in D_2O at 25 °C and $I = 1.0$ (KCl).
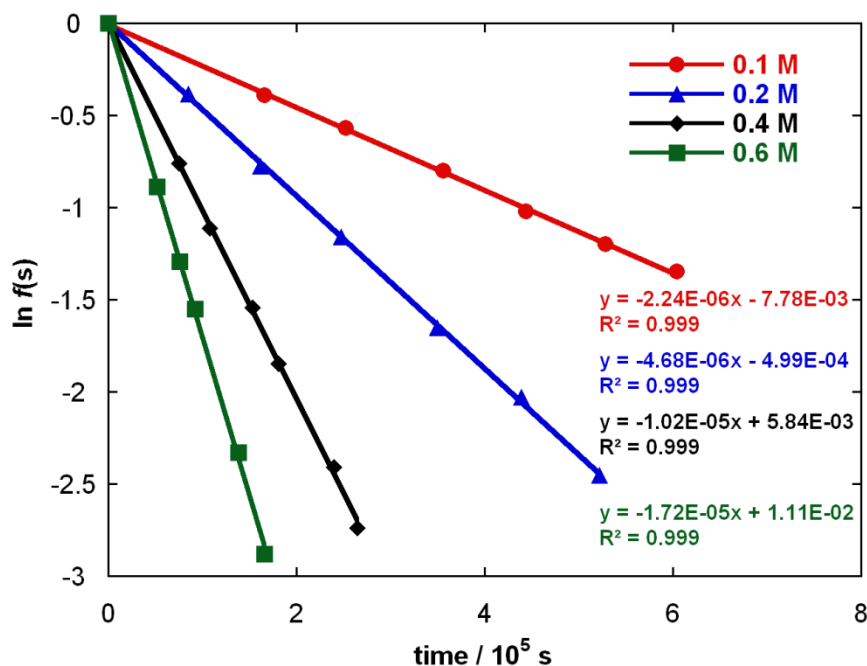
Table A17: **Reaction data and first-order rate constants for exchange of the C(4/5)-H of imidazolium salt (209) for deuterium in solutions of KOD in D_2O at 25 ºC and I = 1.0 (KCl).**

[DO⁻], M	time, s	f(s) [a]	ln f(s)	k_{ex}, s⁻¹ [b]
	0	1.000	0.000	
	166020	0.676	-0.391	
0.1	252480	0.566	-0.569	2.24×10^{-6}
	356280	0.450	-0.799	
	444000	0.360	-1.023	
	528180	0.302	-1.198	
	604560	0.260	-1.349	
	0	1.000	0.000	
	85260	0.770	-0.383	
0.2	161460	0.396	-0.774	4.68×10^{-6}
	247800	0.284	-1.161	
	349500	0.163	-1.651	
	439140	0.079	-2.030	
	522420	0.056	-2.452	
	0	1.000	0.000	
	75300	0.467	-0.760	
0.4	108000	0.329	-1.113	1.02×10^{-5}
	153600	0.214	-1.542	
	180840	0.157	-1.848	
	240060	0.090	-2.410	
	264480	0.065	-2.739	
	0	1.000	0.000	
	51960	0.411	-0.889	
0.6	76080	0.275	-1.293	1.72×10^{-5}
	91980	0.212	-1.551	
	138600	0.097	-2.330	
	165780	0.056	-2.879	

(a) Fraction of substrate remaining f(s) calculated using Equation 2.4. (b) Pseudo-first-order rate constant for exchange, k_{ex} (s⁻¹), obtained from the slope of the plot of ln f(s) against time in Figure 2.4 – 2.6.

Figure A25: Semilogarithmic plots of the fraction of unexchanged substrate against time for the deuterium exchange reaction of (209) in solutions of KOD in D_2O at 25 °C and $I = 1.0$ (KCl).

Table A18: Reaction data and first-order rate constants for exchange of the C(4)-H and C(5)-H of imidazolium salt (210) for deuterium in solutions of KOD in D_2O at 25 °C and $I = 1.0$ (KCl).

[DO$^-$], M	time, s	f(C4) [a]	ln f(C4)	f(C5) [a]	ln f(C5)	k_{ex}, s^{-1} [b]
	0	1.000	0.000	1.000	0.000	
	91500	0.702	-0.355	0.743	-0.297	
0.2	250080	0.350	-1.050	0.438	-0.825	C(4): 3.83×10^{-6}
	340440	0.266	-1.326	0.350	-1.050	C(5): 2.99×10^{-6}
	418380	0.196	-1.632	0.275	-1.292	
	557760	0.119	-2.130	0.190	-1.663	
	0	1.000	0.000	1.000	0.000	
	48600	0.614	-0.488	0.678	-0.388	
0.4	86400	0.424	-0.858	0.512	-0.670	C(4): 8.93×10^{-6}
	100860	0.398	-0.922	0.486	-0.722	C(5): 6.88×10^{-6}
	141000	0.275	-1.292	0.369	-0.997	
	179640	0.199	-1.616	0.283	-1.261	
	239280	0.114	-2.172	0.188	-1.674	
	0	1.000	0.000	1.000	0.000	
	20100	0.627	-0.467	0.692	-0.368	
0.8	35520	0.458	-0.780	0.532	-0.630	C(4): 2.23×10^{-5}
	50940	0.309	-1.175	0.404	-0.907	C(5): 1.76×10^{-5}
	81180	0.160	-1.833	0.232	-1.461	
	100200	0.104	-2.259	0.166	-1.794	
	116040	0.077	-2.568	0.133	-2.015	
	0	1.000	0.000	1.000	0.000	
1.0	22620	0.454	-0.789	0.529	-0.637	C(4): 2.97×10^{-5}
	49800	0.211	-1.554	0.289	-1.240	C(5): 2.38×10^{-5}
	79980	0.091	-2.399	0.146	-1.924	

(a) Fraction of substrate remaining f(s) calculated using Equation 2.4. (b) Pseudo-first-order rate constant for exchange, k_{ex} (s^{-1}), obtained from the slope of the plot of ln f(s) against time in Figures A26 – A27.
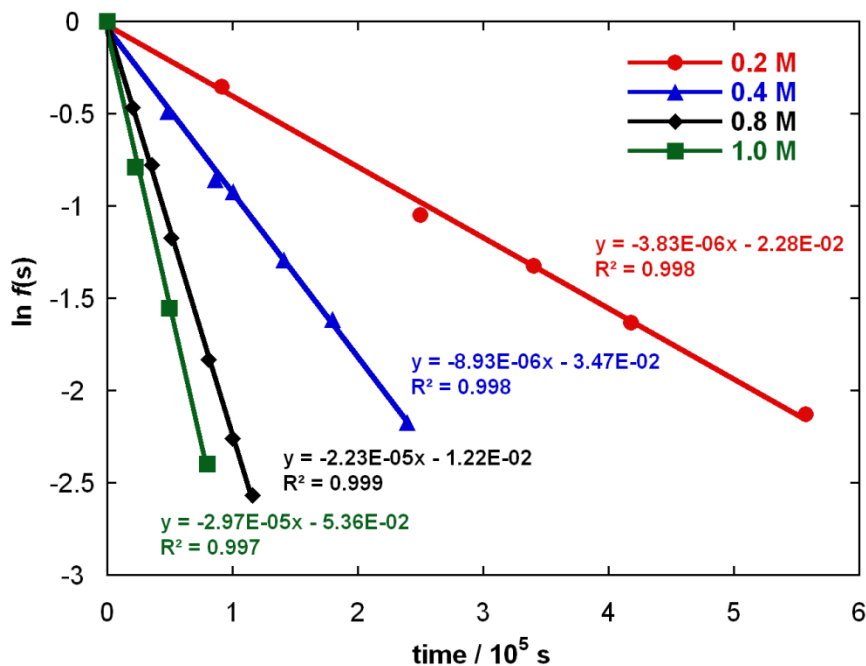
Figure A26: **Semilogarithmic plots of the fraction of unexchanged substrate against time for the deuterium exchange reaction of the C(4)-H of (210) in solutions of KOD in D_2O at 25 ºC and $I = 1.0$ (KCl).**

Figure A27: **Semilogarithmic plots of the fraction of unexchanged substrate against time for the deuterium exchange reaction of the C(5)-H of (210) in solutions of KOD in D_2O at 25 ºC and $I = 1.0$ (KCl).**
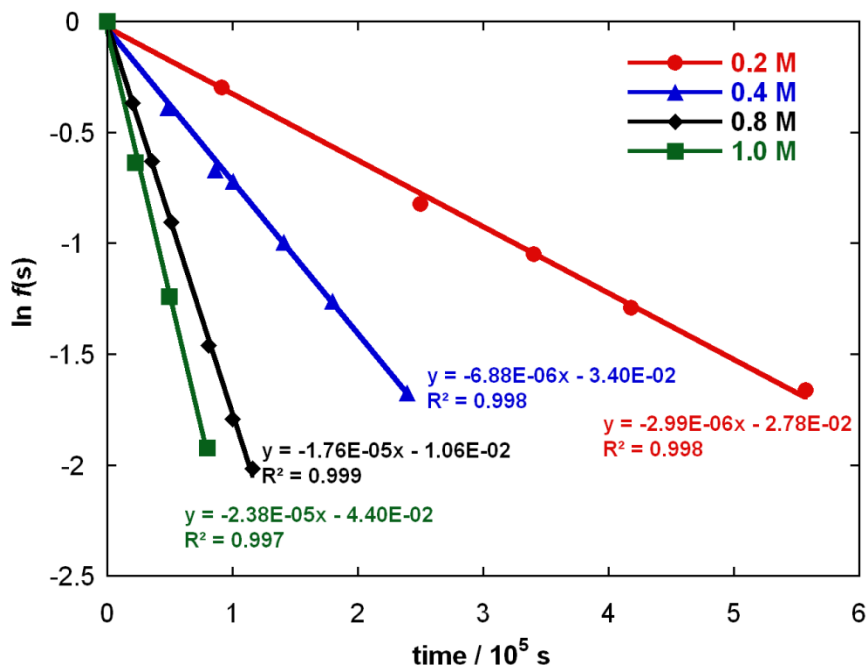
A2   Determination of error

First-order rate constants for deuterium exchange (k_{ex})

The maximum percentage error in k_{ex} is estimated to be 6%, based on the standard error reported in the fit of ln f(s) against time for the exchange reaction of triazolium salt **139**, measured at pD 2.37. This particular plot had the smallest (*i.e.* worst) value of R^2 (0.985). Typically, errors in the range $2 - 3\%$ were reported.

Second-order rate constants for deuteroxide ion-catalysed exchange (k_{DO}) and pK_a

In the treatment that follows, we have assumed that the error in the value of k_{DO} (s_{DO}) is equal to the standard error in the value of ($k_{DO} \times K_W / \gamma_{DO}$) reported from the fits of log $k_{ex} -$ pD data to Equation 2.9 or Equations 2.13/2.15. The standard error in ($k_{DO} \times K_W / \gamma_{DO}$) ranged from $1.3 - 7.1\%$ and we have assumed that the overall error in ($k_{DO} \times K_W / \gamma_{DO}$) reflects that in k_{DO} as the errors in K_W and γ_{DO} are small (<1%).[1]

The second-order rate constants for deprotonation by hydroxide ion were calculated assuming the secondary solvent isotope relationship $k_{DO}/k_{HO} = 2.4$. The standard deviation in k_{HO} (s_{HO}) was calculated using Equation A1, taking into account the error in k_{DO} (s_{DO}), and the error in the solvent isotope effect (2.4 ± 0.063).[2]

$$s_{HO} = k_{HO} \times \sqrt{\left(\frac{0.0631}{2.40}\right)^2 + \left(\frac{s_{DO}}{k_{DO}}\right)^2} \qquad \textbf{Equation A1}$$

As described in Chapters 2 and 3, values of pK_a for all azolium ions were calculated using Equation 2.20 (shown in thesis). The standard error of the ratio k_{HOH}/k_{HO} (s_r), obtained by Equation A2, takes into account the error in k_{HOH} ($1 \times 10^{11} \pm 1 \times 10^{10}$).[3]

$$pK_a = pK_W + \log_{10}\left(\frac{k_{HOH}}{k_{HO}}\right) \qquad \textbf{Equation 2.20}$$

$$s_r = \frac{k_{HOH}}{k_{HO}} \times \sqrt{\left(\frac{1 \times 10^{10}}{1 \times 10^{11}}\right)^2 + \left(\frac{s_{HO}}{k_{HO}}\right)^2} \qquad \textbf{Equation A2}$$

The standard error in pK_a (s_{pKa}) was calculated using Equation A3. The error in pK_W is negligible[1] and is excluded from this treatment.

$$s_{pKa} = 0.434 \times \frac{s_r}{(k_{HOH}/k_{HO})} \qquad \textbf{Equation A3}$$

APPENDIX B

B1   Concentration profiles for triazolium ion-catalysed reactions

Figure B1:   Concentration profile for the self-condensation of 4-fluorobenzaldehyde (266) (0.08 M), catalysed by *N*-C$_6$H$_4$F triazolium precatalyst (138) (0.08 M), in 0.107 M NEt$_3$ and 0.107 M NEt$_3$·DCl in methanol-d$_4$.
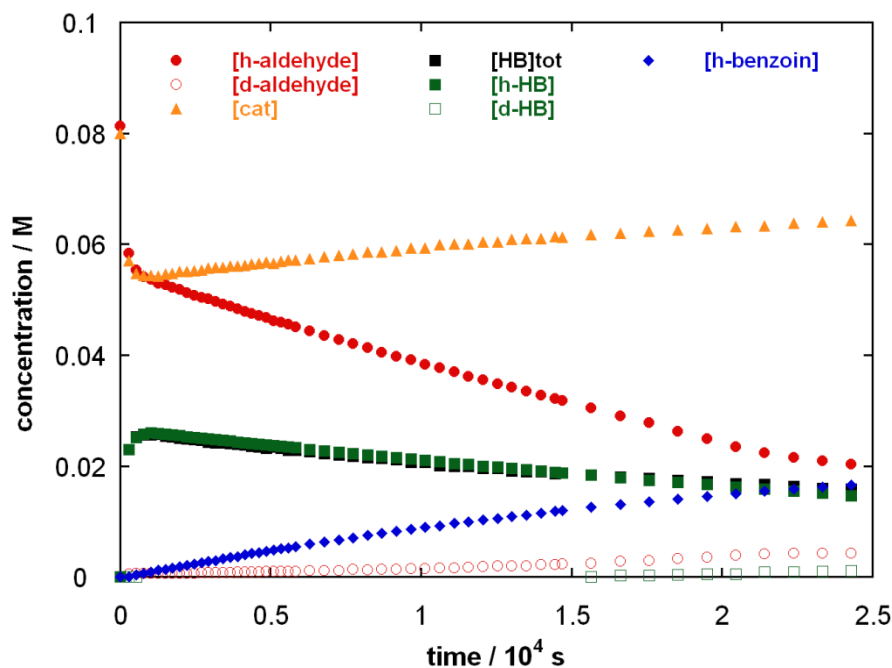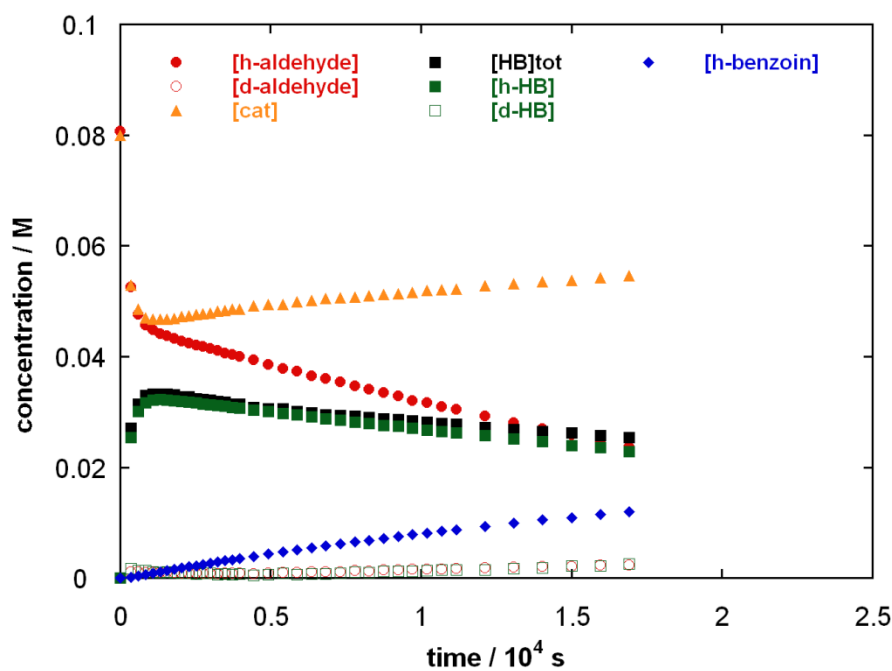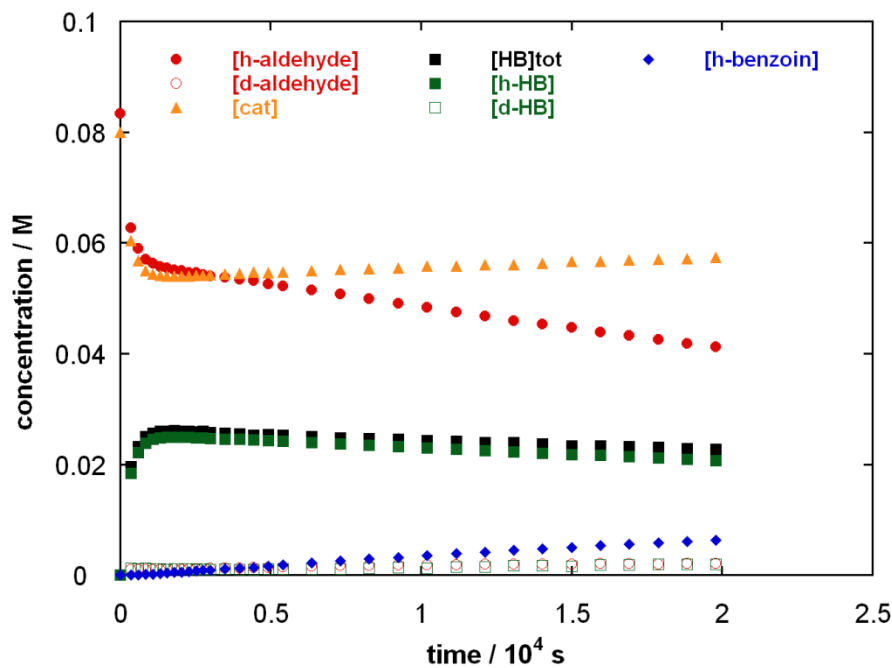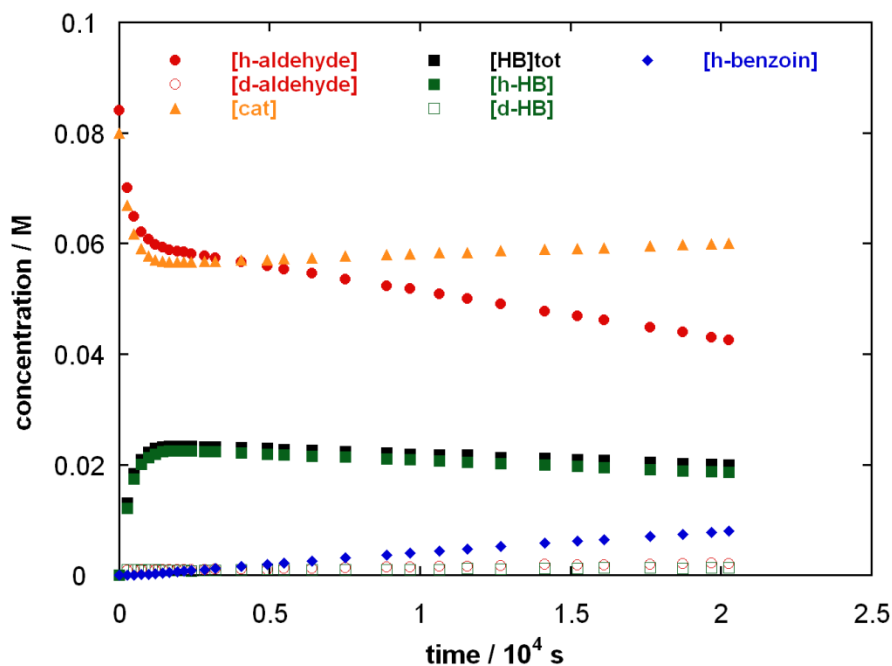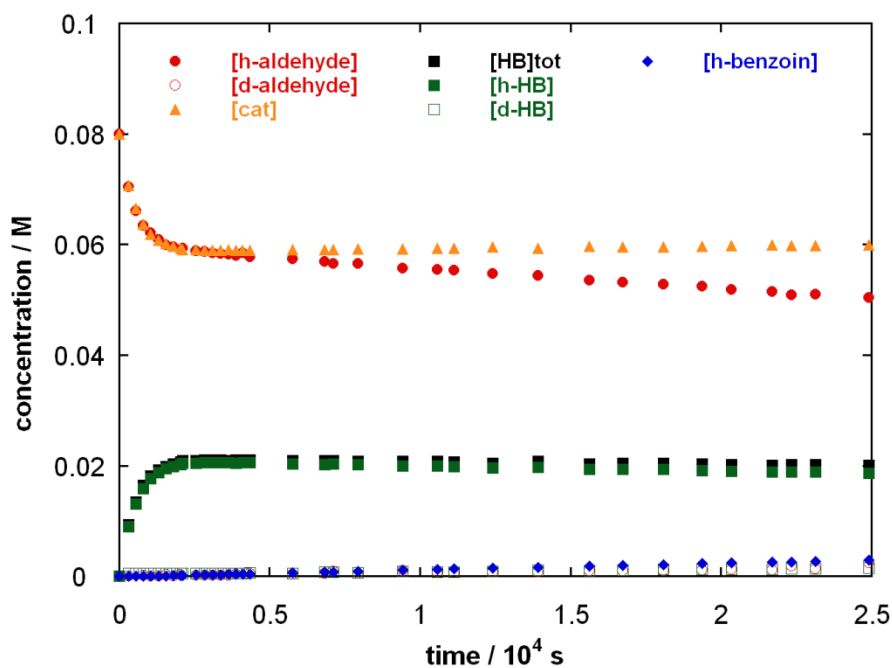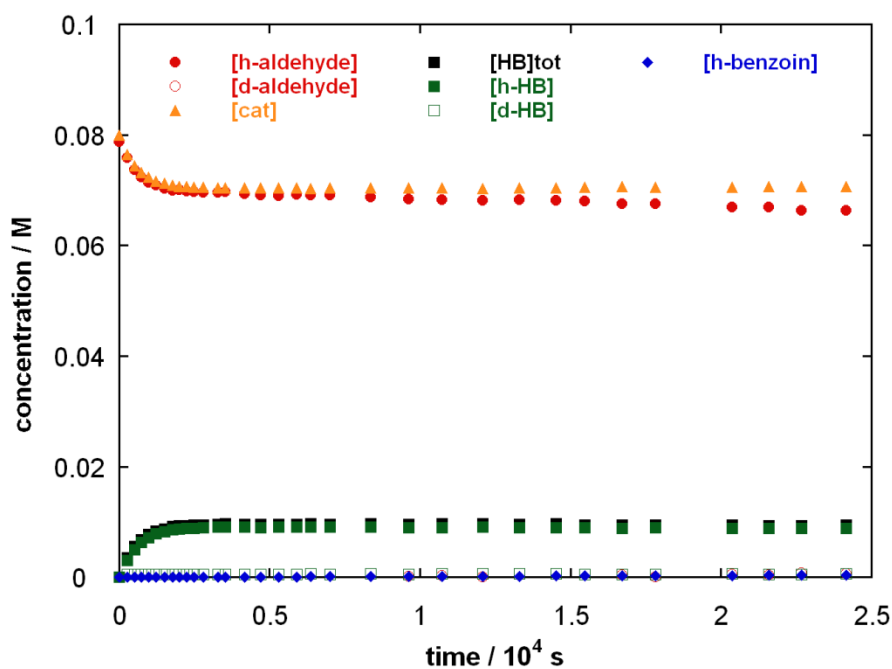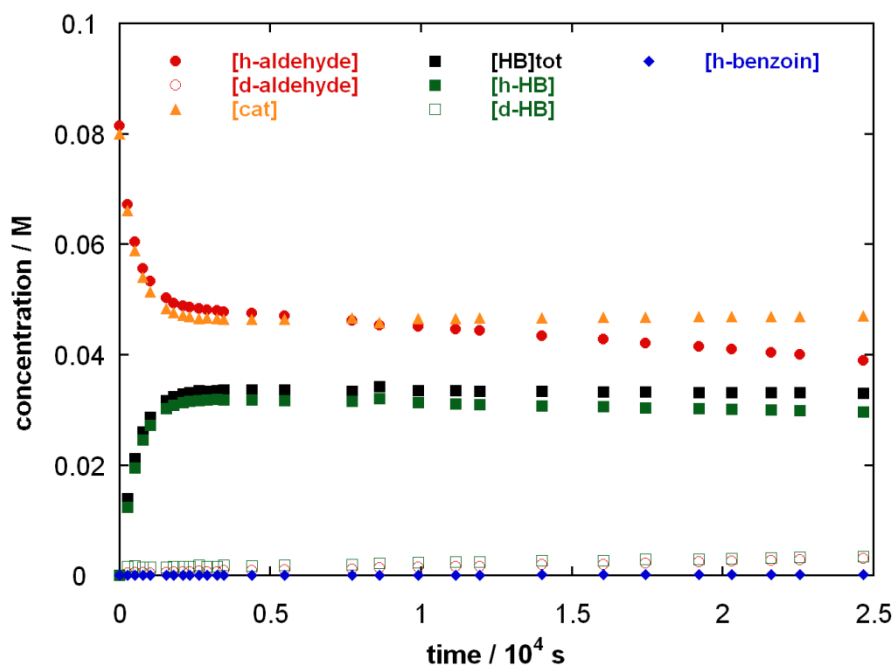

Figure B2:   Concentration profile for the self-condensation of benzaldehyde (28) (0.08 M), catalysed by *N*-C$_6$H$_4$F triazolium precatalyst (138) (0.08 M), in 0.107 M NEt$_3$ and 0.107 M NEt$_3$·DCl in methanol-d$_4$.

Figure B3: **Concentration profile for the self-condensation of 4-methylbenzaldehyde (267) (0.08 M), catalysed by *N*-C$_6$H$_4$F triazolium precatalyst (138) (0.08 M), in 0.107 M NEt$_3$ and 0.107 M NEt$_3$·DCl in methanol-d$_4$.**
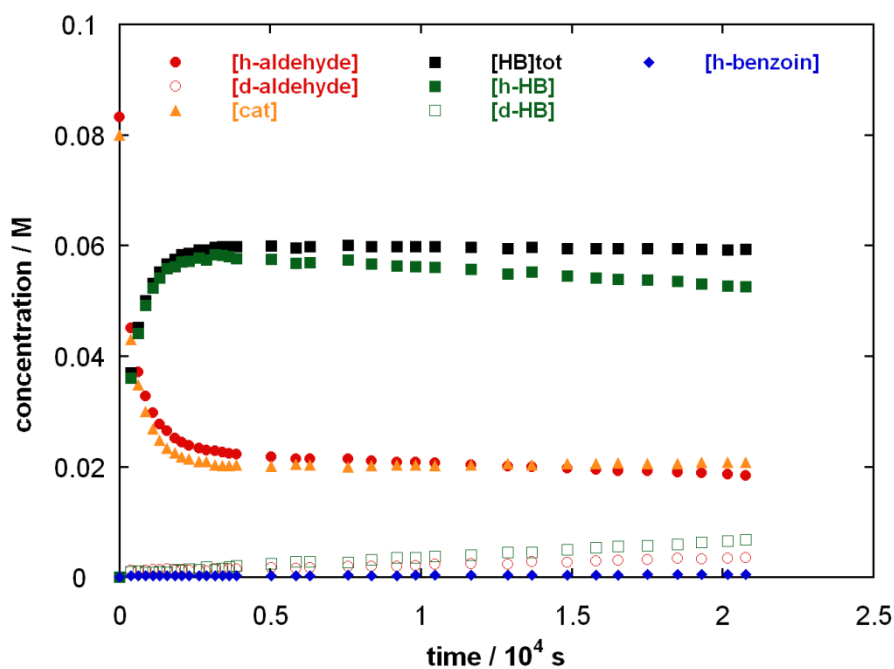

Figure B4: **Concentration profile for the self-condensation of 4-fluorobenzaldehyde (266) (0.08 M), catalysed by *N*-phenyl triazolium precatalyst (139) (0.08 M), in 0.107 M NEt$_3$ and 0.107 M NEt$_3$·DCl in methanol-d$_4$.**
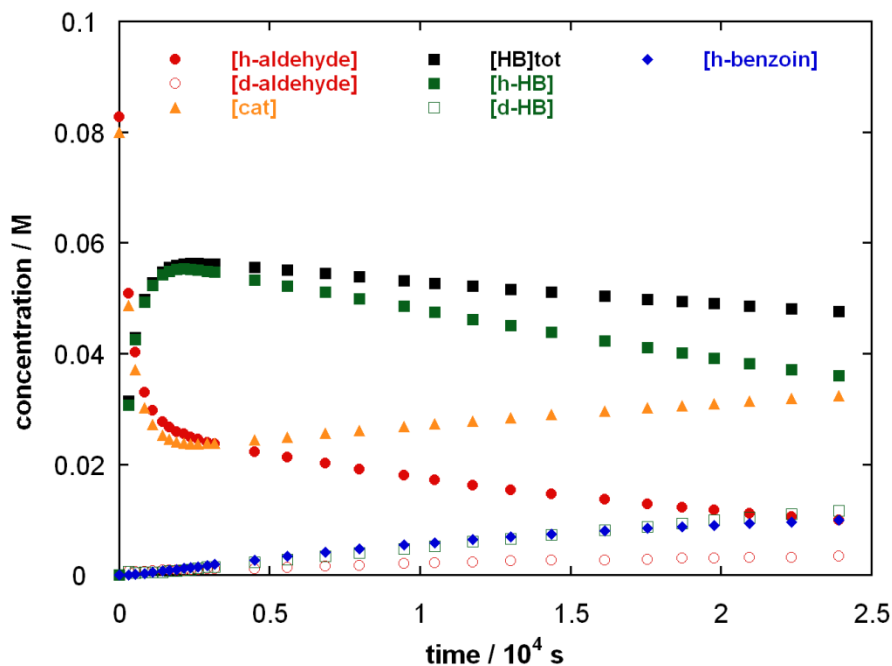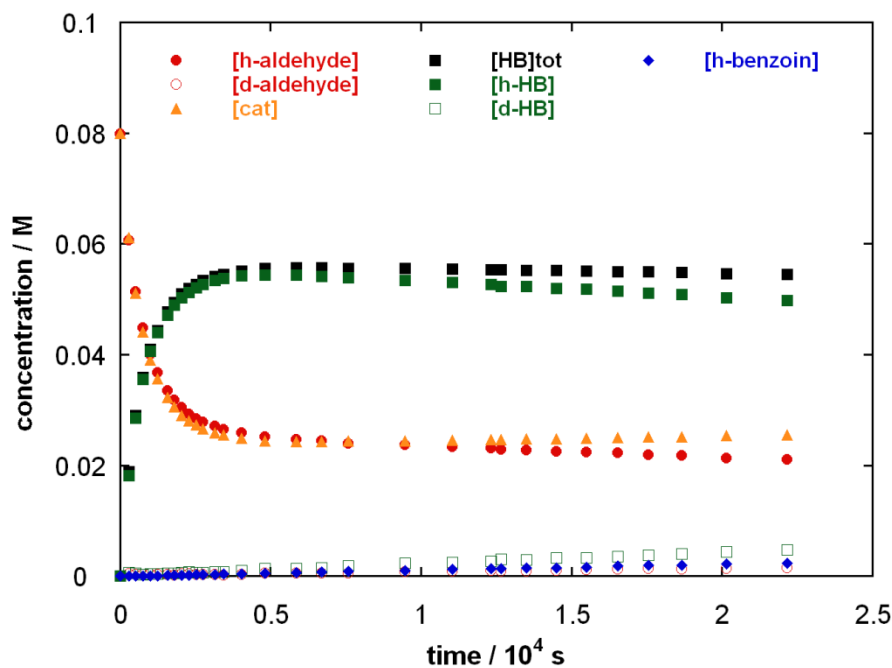
Figure B5: **Concentration profile for the self-condensation of 4-methylbenzaldehyde (267) (0.08 M), catalysed by *N*-phenyl triazolium precatalyst (139) (0.08 M), in 0.107 M NEt$_3$ and 0.107 M NEt$_3$·DCl in methanol-d$_4$.**

Figure B6: **Concentration profile for the self-condensation of 4-methoxybenzaldehyde (273) (0.08 M), catalysed by *N*-phenyl triazolium precatalyst (139) (0.08 M), in 0.107 M NEt$_3$ and 0.107 M NEt$_3$·DCl in methanol-d$_4$.**

Figure B7: **Concentration profile for the self-condensation of 2-methylbenzaldehyde (274) (0.08 M), catalysed by *N*-phenyl triazolium precatalyst (139) (0.08 M), in 0.107 M NEt₃ and 0.107 M NEt₃·DCl in methanol-d₄.**

Figure B8: **Concentration profile for the self-condensation of 2-methoxybenzaldehyde (268) (0.08 M), catalysed by *N*-phenyl triazolium precatalyst (139) (0.08 M), in 0.107 M NEt₃ and 0.107 M NEt₃·DCl in methanol-d₄.**
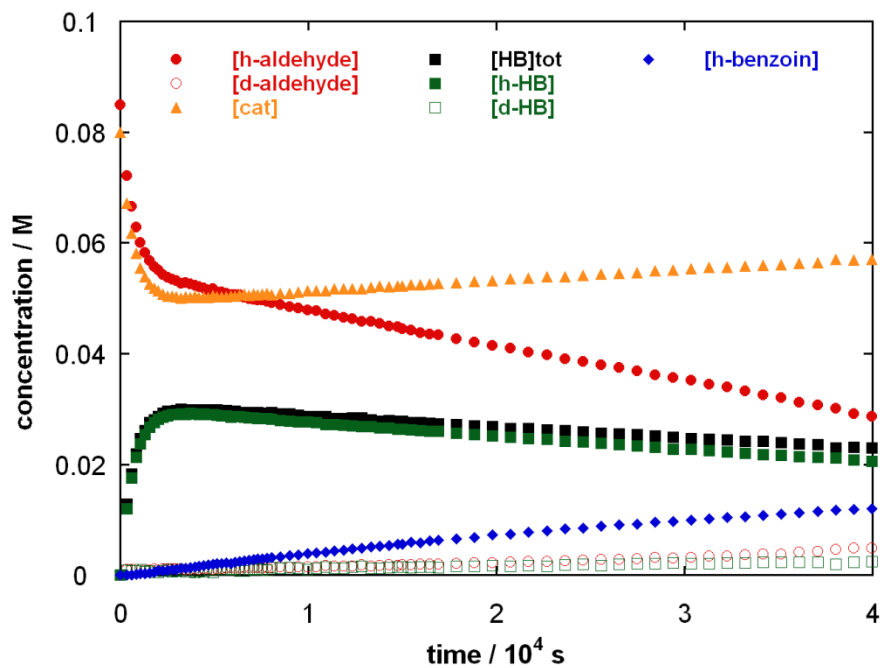
Figure B9: **Concentration profile for the self-condensation of 4-fluorobenzaldehyde (266) (0.08 M), catalysed by *N*-mesityl triazolium precatalyst (140) (0.08 M), in 0.107 M NEt$_3$ and 0.107 M NEt$_3$·DCl in methanol-d$_4$.**
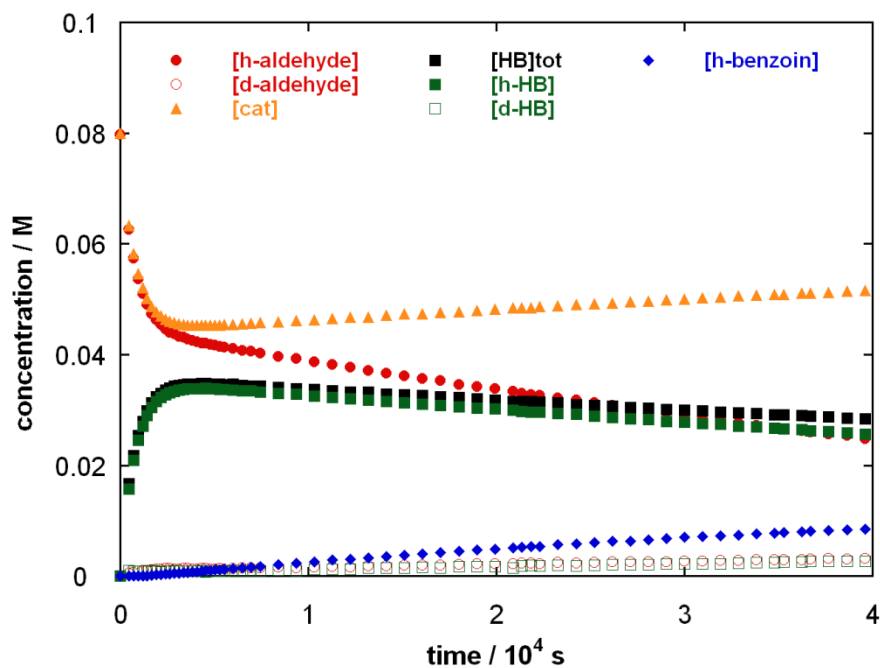

Figure B10: **Concentration profile for the self-condensation of 4-methylbenzaldehyde (267) (0.08 M), catalysed by *N*-mesityl triazolium precatalyst (140) (0.08 M), in 0.107 M NEt$_3$ and 0.107 M NEt$_3$·DCl in methanol-d$_4$.**

Figure B11: Concentration profile for the self-condensation of 4-fluorobenzaldehyde (266) (0.08 M), catalysed by *N*-C$_6$H$_4$OMe triazolium precatalyst (141) (0.08 M), in 0.107 M NEt$_3$ and 0.107 M NEt$_3$·DCl in methanol-d$_4$.

Figure B12: Concentration profile for the self-condensation of benzaldehyde (28) (0.08 M), catalysed by *N*-C$_6$H$_4$OMe triazolium precatalyst (141) (0.08 M), in 0.107 M NEt$_3$ and 0.107 M NEt$_3$·DCl in methanol-d$_4$.

Figure B13: Concentration profile for the self-condensation of 4-methylbenzaldehyde (267) (0.08 M), catalysed by N-C_6H_4OMe triazolium precatalyst (141) (0.08 M), in 0.107 M NEt_3 and 0.107 M $NEt_3 \cdot DCl$ in methanol-d_4.
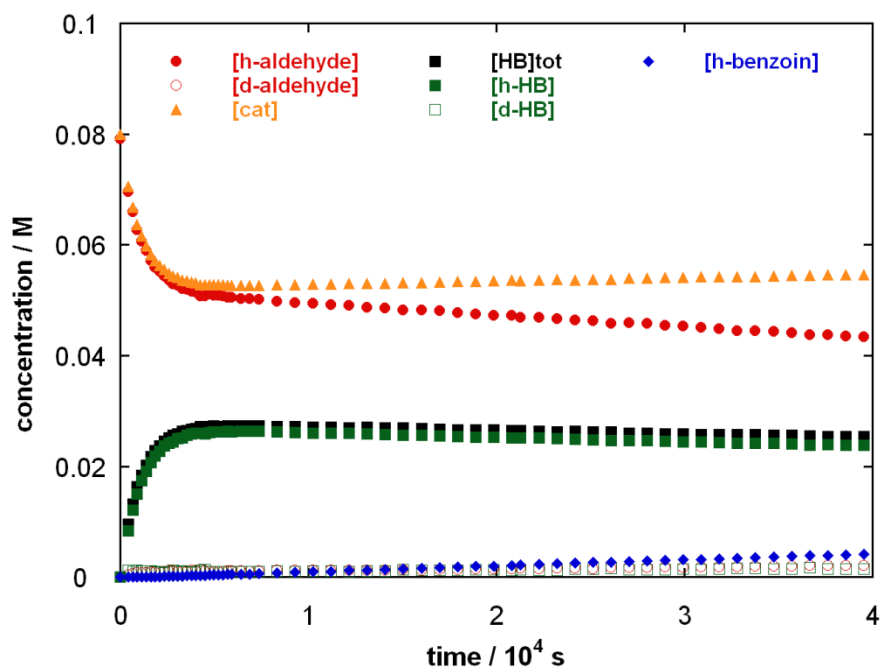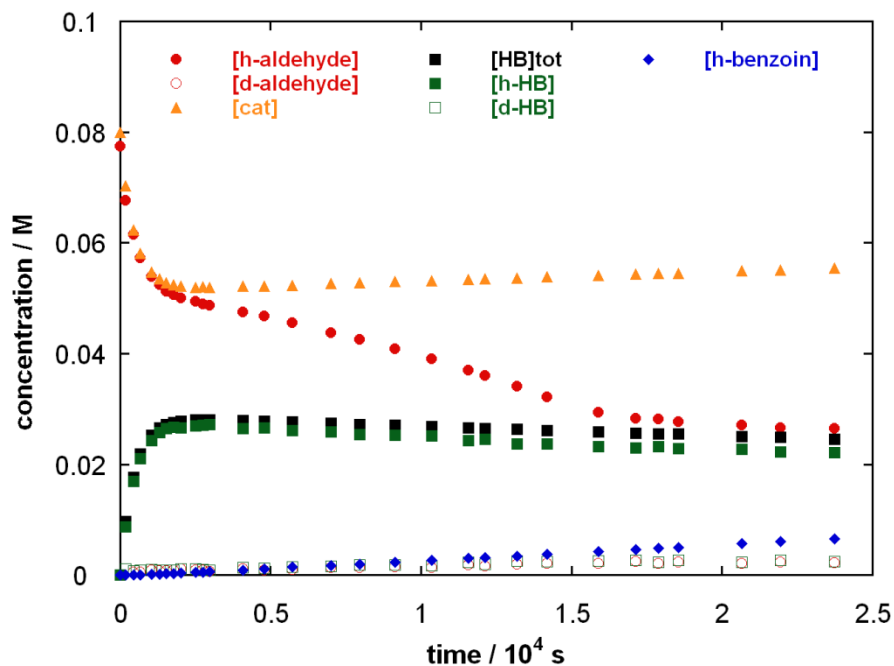

Figure B14: Concentration profile for the self-condensation of benzaldehyde (28) (0.08 M), catalysed by N-pyridyl triazolium precatalyst (143) (0.08 M), in 0.107 M NEt_3 and 0.107 M $NEt_3 \cdot DCl$ in methanol-d_4.

APPENDIX C

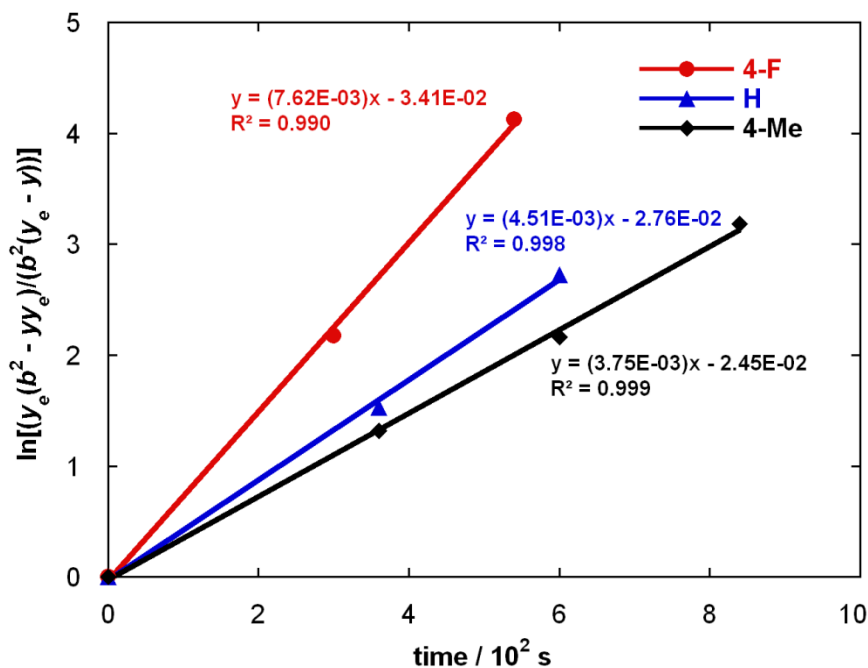### C1   'Manual' fitting to obtain estimates of k_1

Figure C1:   Semilogarithmic plots of $[y_e(b^2 - yy_e)/(b^2(y_e - y))]$ against time for the reactions of a range of substituted benzaldehydes with N-C$_6$H$_4$F triazolium precatalyst (**138**)

Figure C2:   Semilogarithmic plots of $[y_e(b^2 - yy_e)/(b^2(y_e - y))]$ against time for the reactions of a range of substituted benzaldehydes with N-mesityl triazolium precatalyst (**140**)
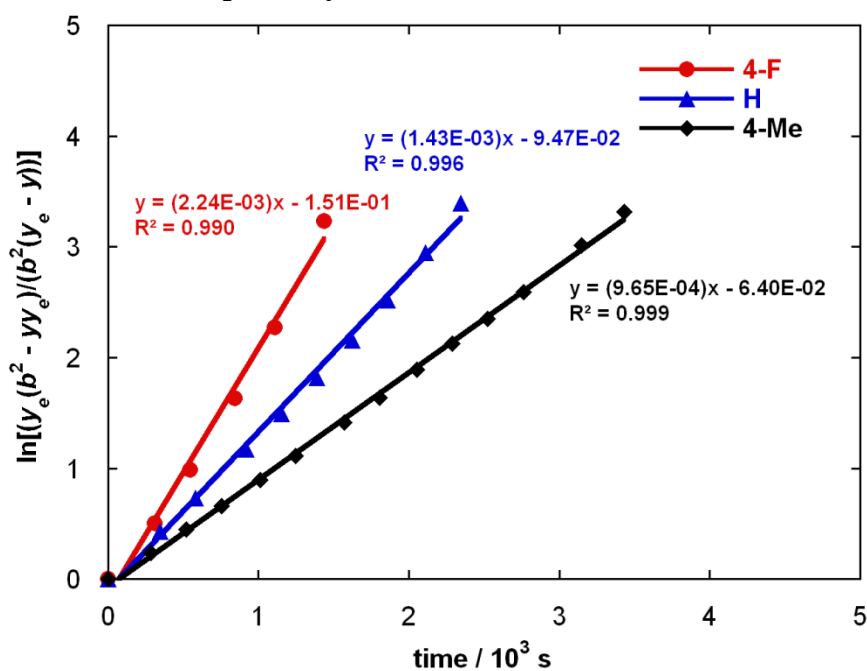
Figure C3: **Semilogarithmic plots of $[y_e(b^2 - yy_e)/(b^2(y_e - y))]$ against time for the reactions of a range of substituted benzaldehydes with N-C$_6$H$_4$OMe triazolium precatalyst (141)**
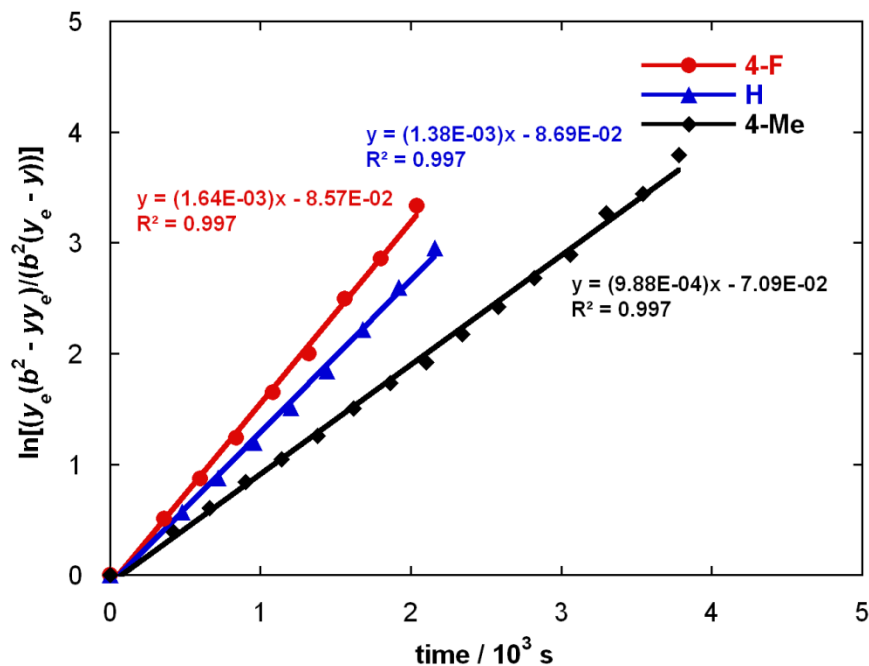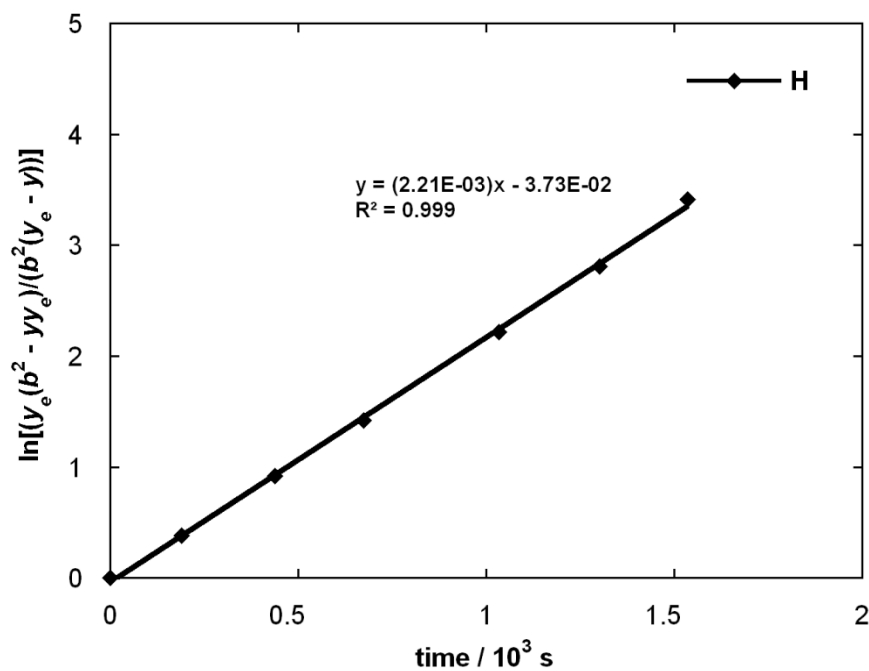

Figure C4: **Semilogarithmic plots of $[y_e(b^2 - yy_e)/(b^2(y_e - y))]$ against time for the reactions of benzaldehyde with N-pyridyl triazolium precatalyst (143)**

C2 'Manual' fitting to obtain estimates of k_{-1}

Figure C5: Semilogarithmic plot of $[(ax_e + x(a - x_e))/(a(x_e - x))]$ against time for the reaction of adduct (270) in 0.107 M NEt$_3$ and 0.053 M NEt$_3$·DCl in methanol-d$_4$ at 25 ºC
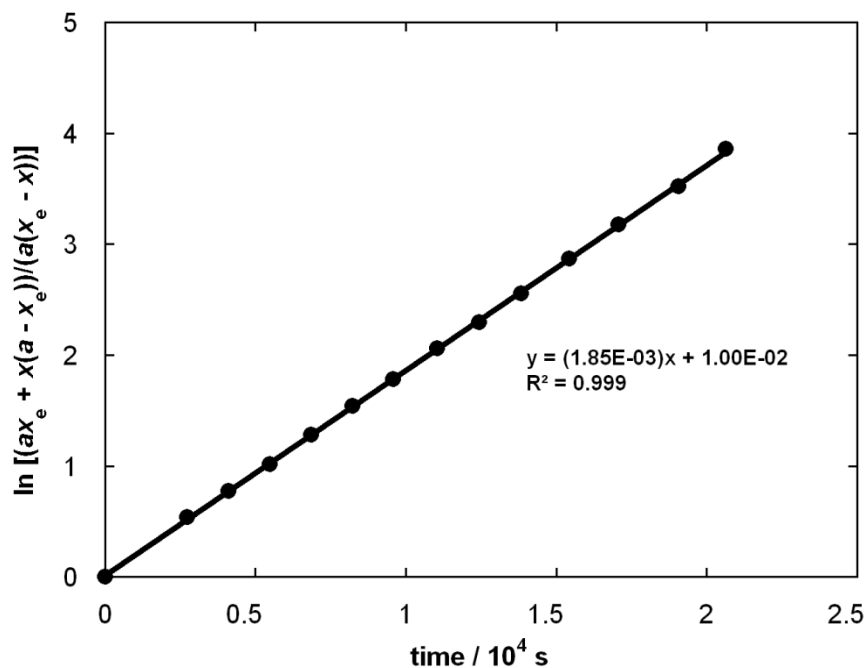

Figure C6: Semilogarithmic plot of $[(ax_e + x(a - x_e))/(a(x_e - x))]$ against time for the reaction of adduct (269) in 0.107 M NEt$_3$ and 0.053 M NEt$_3$·DCl in methanol-d$_4$ at 25 ºC
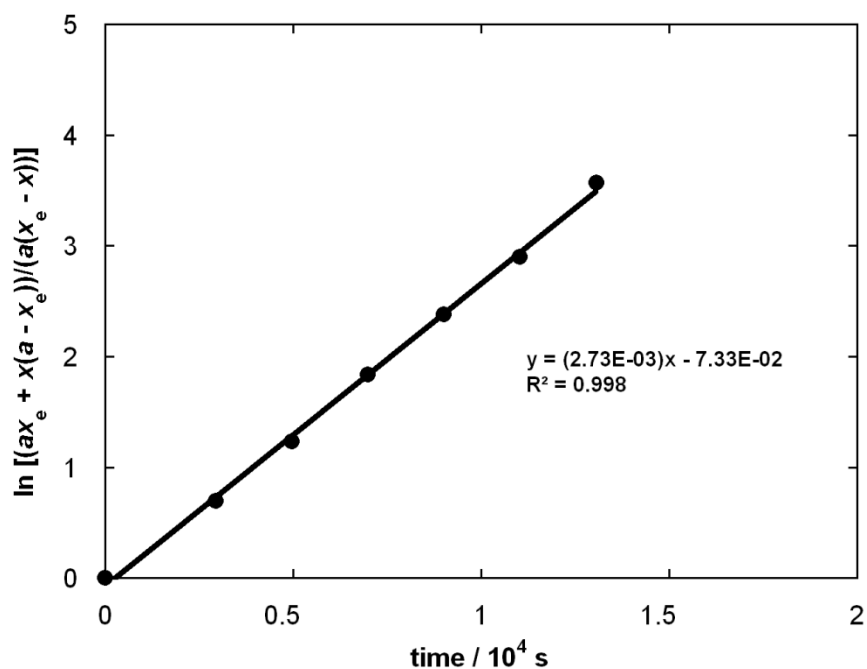
Figure C7: Semilogarithmic plot of $[(ax_e + x(a - x_e))/(a(x_e - x))]$ against time for the reaction of adduct (272) in 0.107 M NEt$_3$ and 0.053 M NEt$_3$·DCl in methanol-d$_4$ at 25 ºC
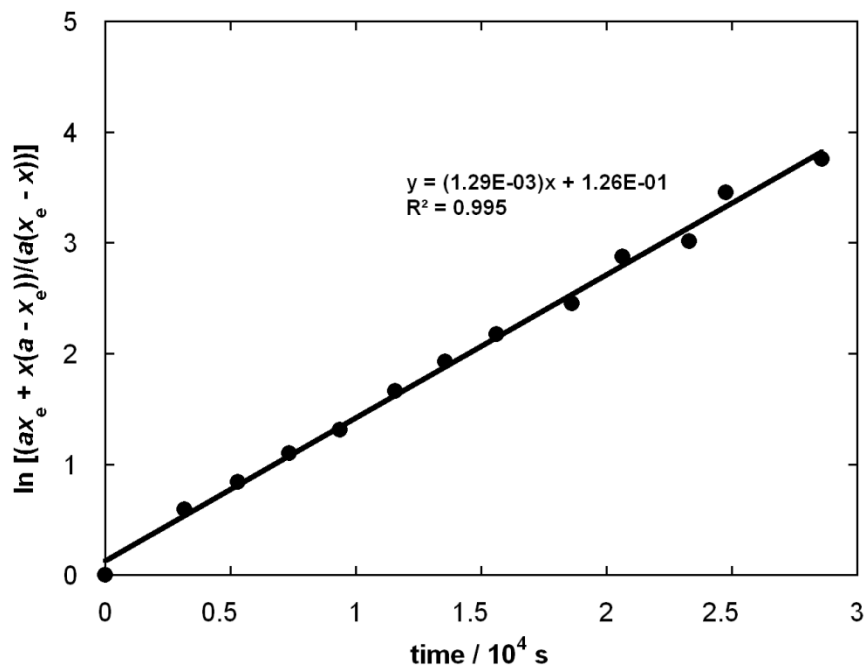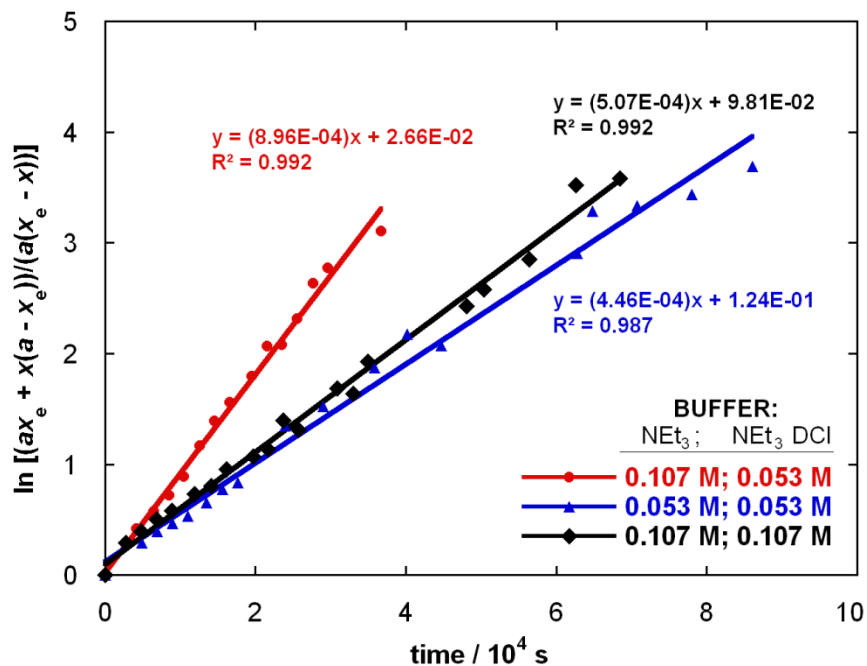

Figure C8: Semilogarithmic plot of $[(ax_e + x(a - x_e))/(a(x_e - x))]$ against time for the reaction of adduct (271) in three triethylamine-buffered solutions in methanol-d$_4$ at 25 ºC

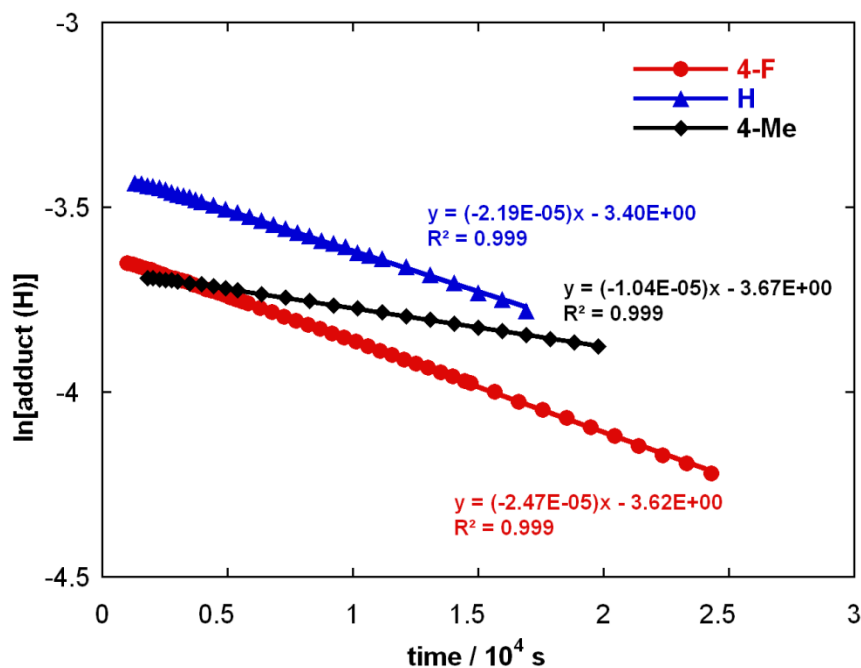## C3   'Manual' fitting to obtain estimates of k_2

Figure C9:   Semilogarithmic plot of [adduct (H)] against time for the reactions of a range of substituted benzaldehydes with *N*-C$_6$H$_4$F triazolium precatalyst (138)

Figure C10:   Semilogarithmic plot of [adduct (H)] against time for the reactions of a range of substituted benzaldehydes with *N*-mesityl triazolium precatalyst (140)
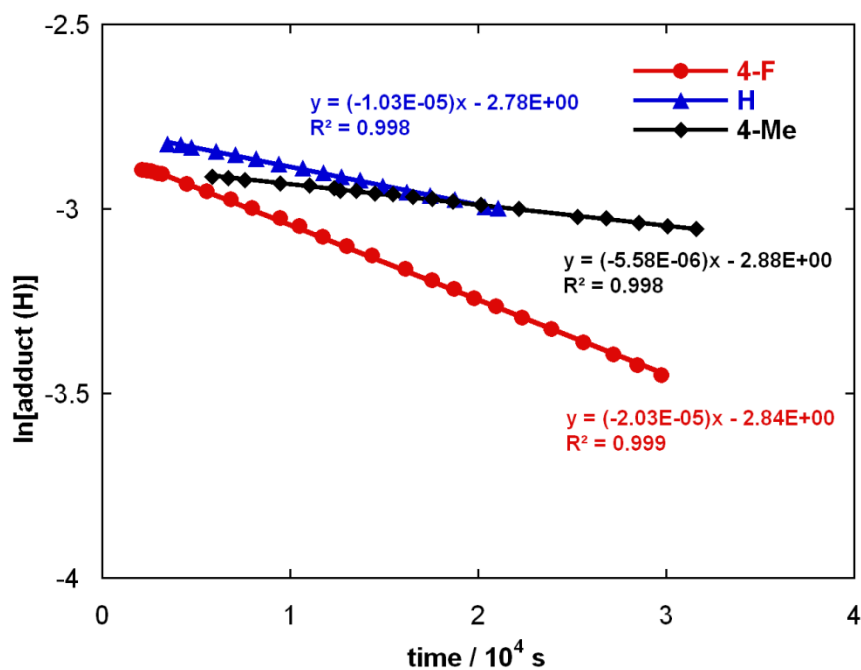
Figure C11: **Semilogarithmic plot of [adduct (H)] against time for the reactions of a range of substituted benzaldehydes with *N*-C$_6$H$_4$OMe triazolium precatalyst (141)**
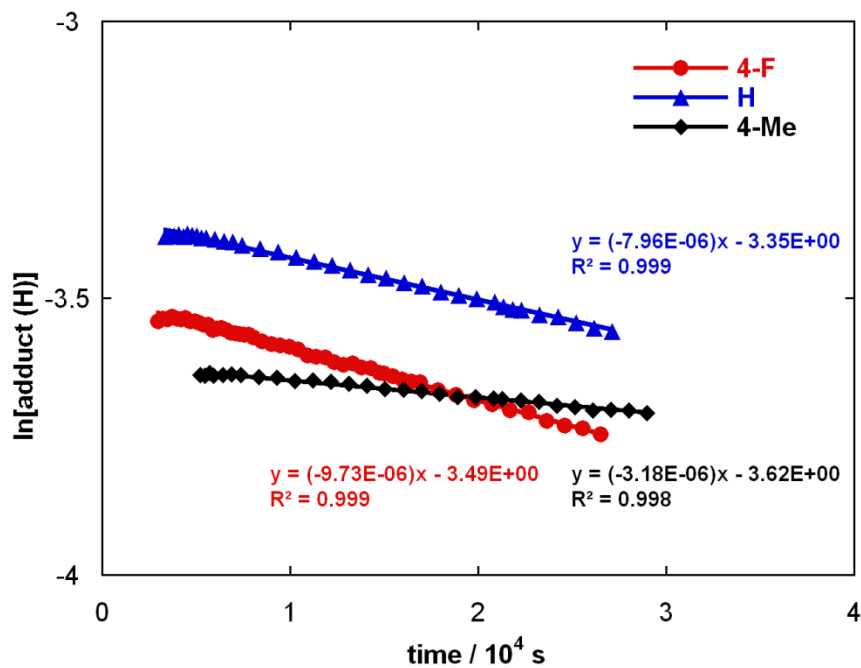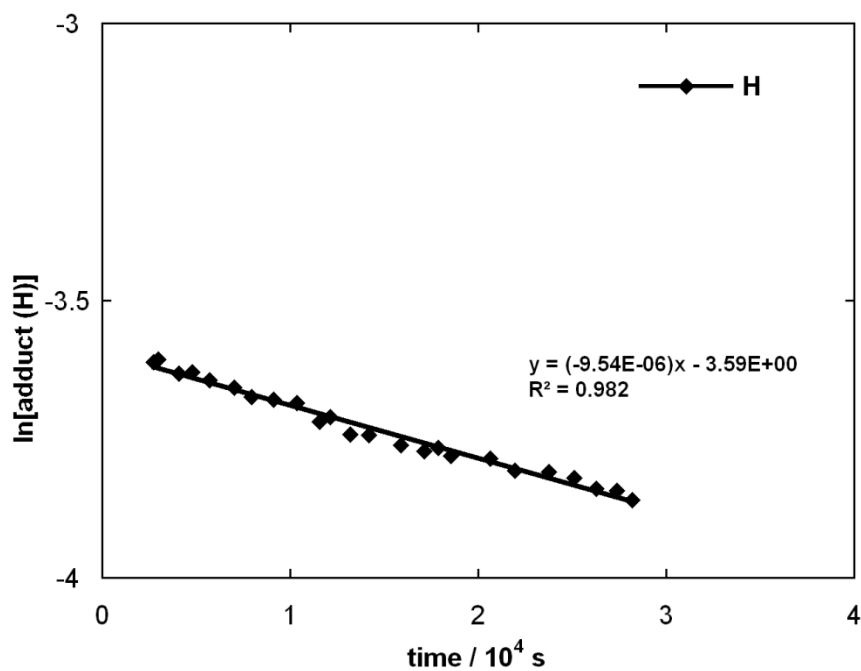

Figure C12: **Semilogarithmic plot of [adduct (H)] against time for the reaction of benzaldehyde with *N*-pyridyl triazolium precatalyst (143)**

C4   Rates of product formation

Figure C13:   **Plots of acyloin concentration against time for a range of substituted benzaldehydes with *N*-C$_6$H$_4$F triazolium precatalyst (138)**

Plot legend: 4-F, H, 4-Me

$y = (9.71E\text{-}07)x - 1.08E\text{-}04$
$R^2 = 0.999$

$y = (8.41E\text{-}07)x + 8.93E\text{-}05$
$R^2 = 0.998$

$y = (3.71E\text{-}07)x - 2.11E\text{-}04$
$R^2 = 0.999$

x-axis: time / 10^3 s
y-axis: [benzoin] / 10^{-3} M

Figure C14:   **Plots of acyloin concentration against time for a range of substituted benzaldehydes with *N*-mesityl triazolium precatalyst (140)**

Plot legend: 4-F, H, 4-Me

$y = (5.87E\text{-}07)x - 1.26E\text{-}05$
$R^2 = 0.998$

$y = (2.38E\text{-}07)x + 8.13E\text{-}05$
$R^2 = 0.997$

$y = (1.00E\text{-}07)x + 8.56E\text{-}05$
$R^2 = 0.997$

x-axis: time / 10^4 s
y-axis: [benzoin] / 10^{-3} M

Figure C15: **Plots of acyloin concentration against time for a range of substituted benzaldehydes with *N*-C$_6$H$_4$OMe triazolium precatalyst (141)**

Figure C16: **Plots of benzoin concentration against time for the reaction of benzaldehyde with *N*-pyridyl triazolium precatalyst (143)**

C5   Rates of formation of deuterated adduct

Figure C17:   Plots of deuterated adduct concentration against time for a range of substituted benzaldehydes with N-C_6H_4F triazolium precatalyst (138)
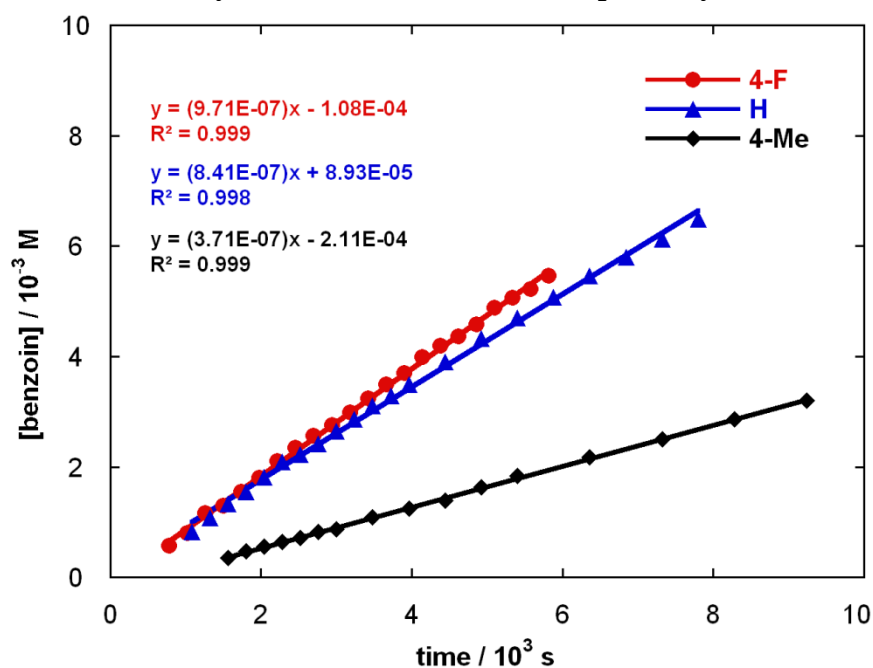

Figure C18:   Plots of acyloin concentration against time for a range of substituted benzaldehydes with N-mesityl triazolium precatalyst (140)
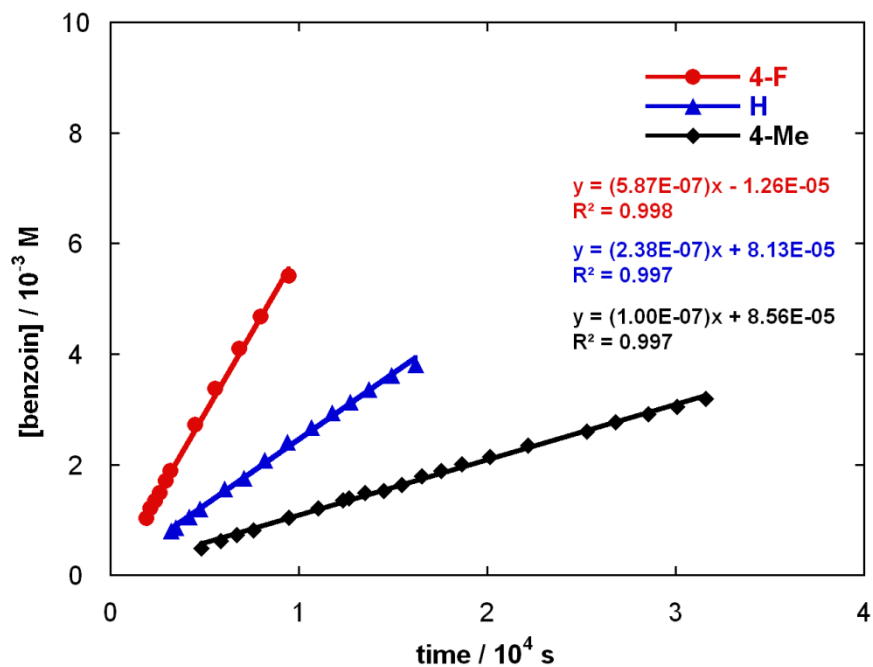
Figure C19: Plots of acyloin concentration against time for a range of substituted benzaldehydes with *N*-C$_6$H$_4$OMe triazolium precatalyst (141)
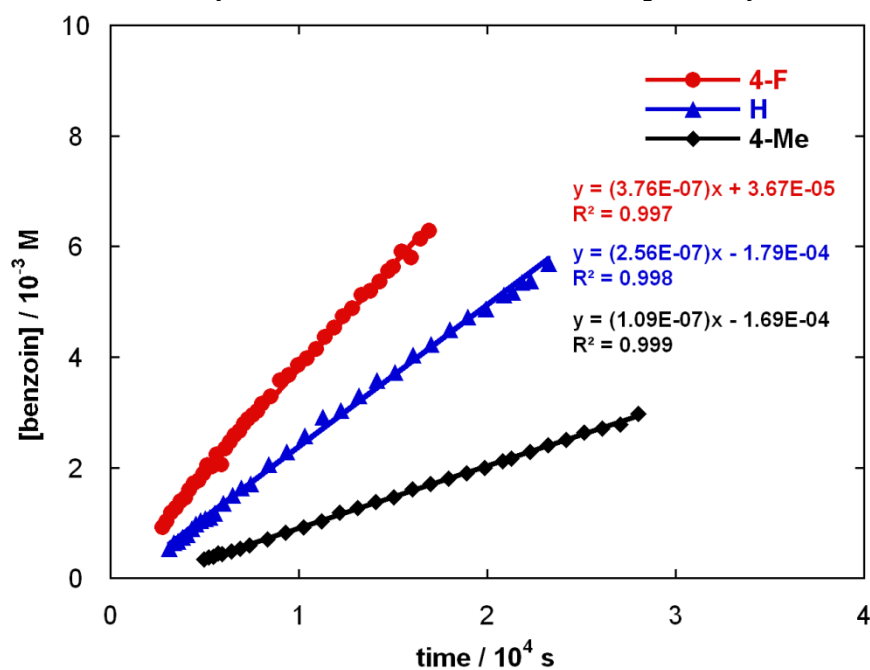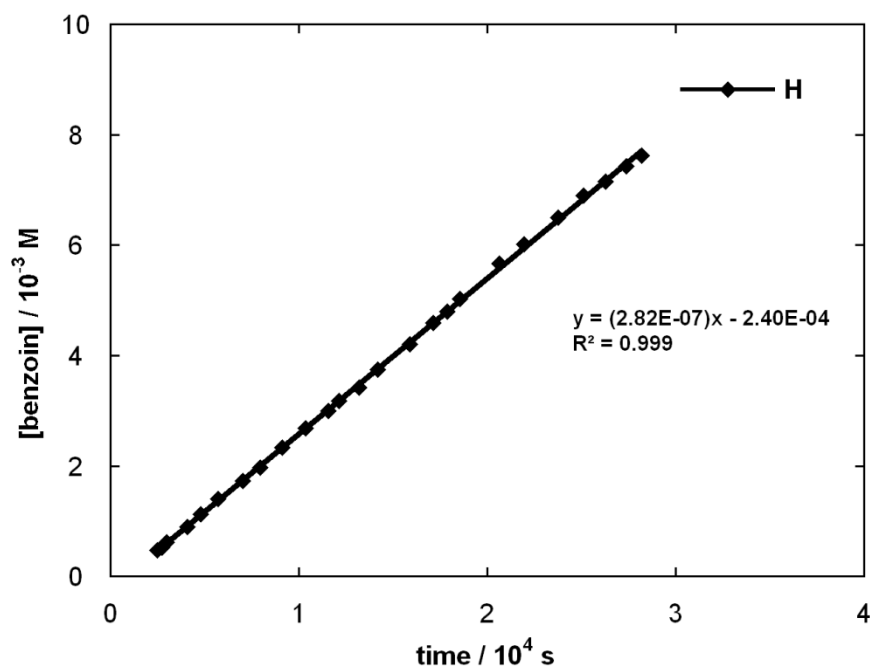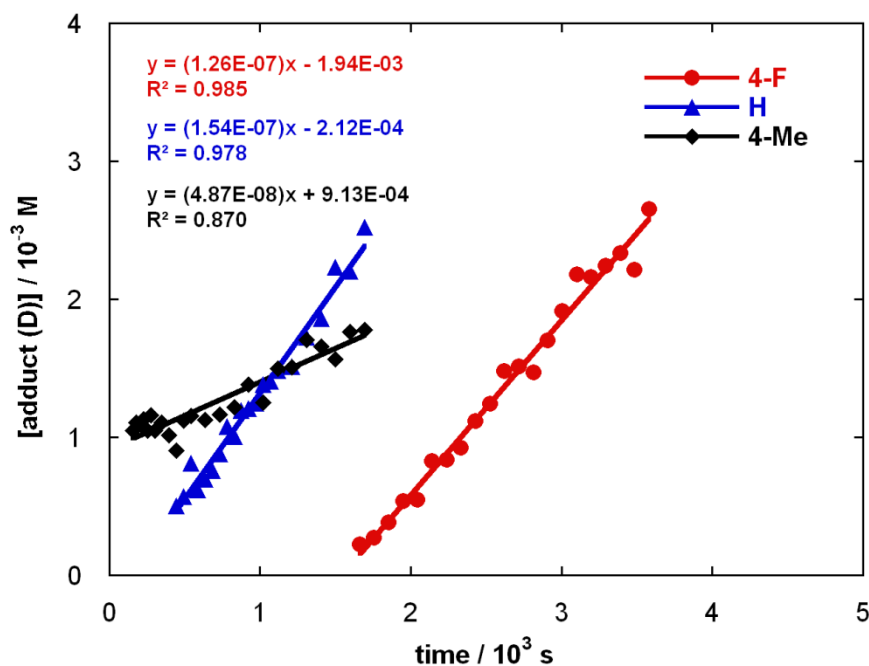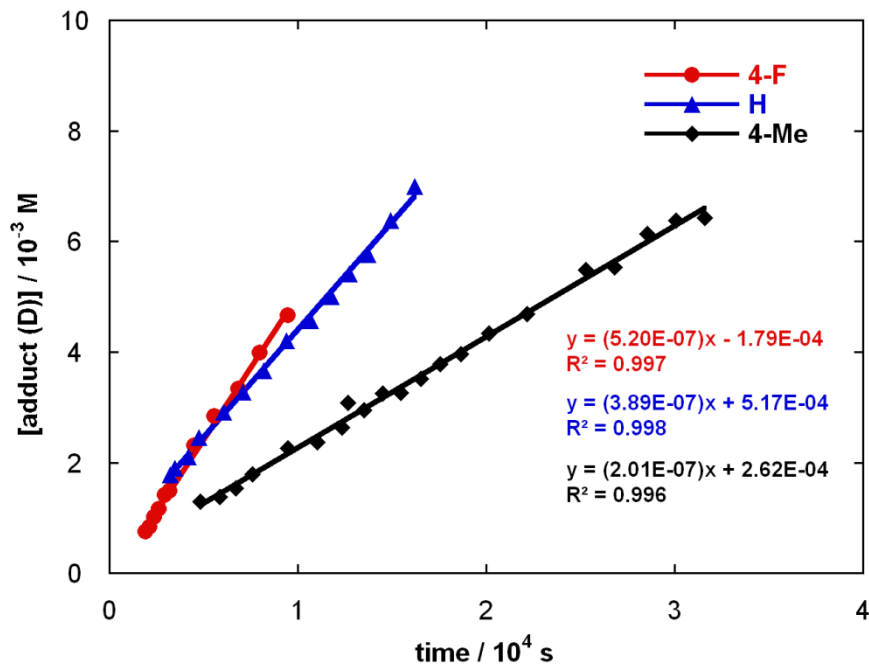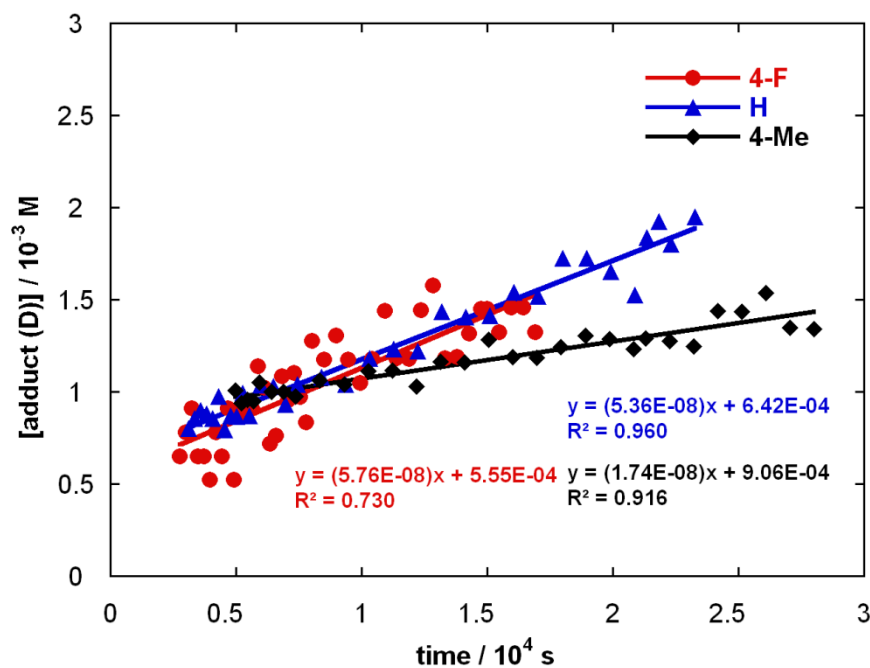

Figure C20: Plots of benzoin concentration against time for the reaction of benzaldehyde with *N*-pyridyl triazolium precatalyst (143)
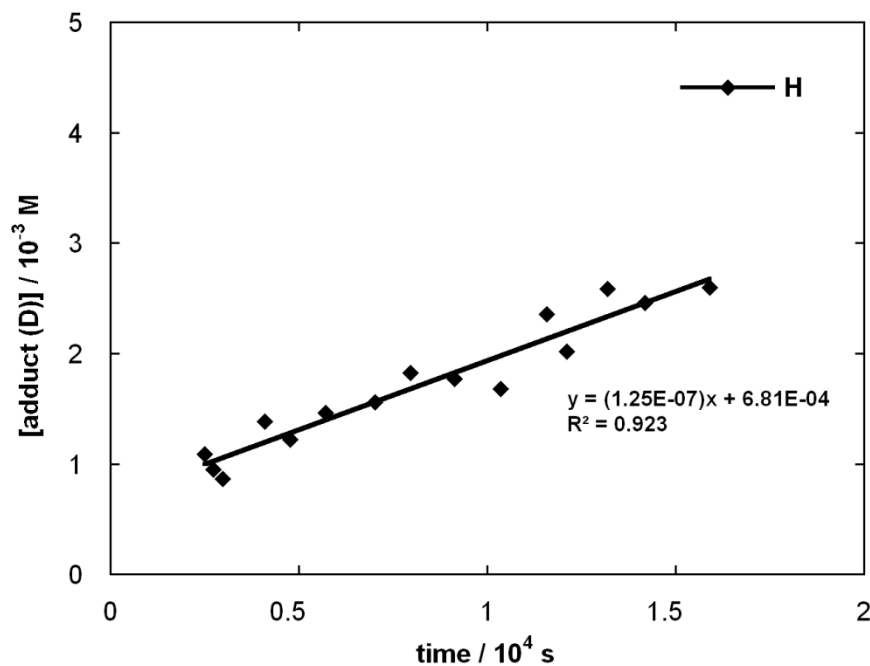
C6 Global fitting

Shown on the same scale.

Figure C21: Concentration profile for the self-condensation of *para*-fluorobenzaldehyde (266) (0.08 M), catalysed by *N*-C$_6$H$_4$F triazolium precatalyst (138) (0.08 M), in 0.107 M NEt$_3$ and 0.107 M NEt$_3$·DCl in methanol-d$_4$, fitted using Berkeley Madonna global fitting software

Figure C22: Concentration profile for the self-condensation of benzaldehyde (28) (0.08 M), catalysed by *N*-C$_6$H$_4$F triazolium precatalyst (138) (0.08 M), in 0.107 M NEt$_3$ and 0.107 M NEt$_3$·DCl in methanol-d$_4$, fitted using Berkeley Madonna global fitting software

Figure C23: Concentration profile for the self-condensation of *para*-methylbenzaldehyde (267) (0.08 M), catalysed by *N*-C$_6$H$_4$F triazolium precatalyst (138) (0.08 M), in 0.107 M NEt$_3$ and 0.107 M NEt$_3$·DCl in methanol-d$_4$, fitted using Berkeley Madonna global fitting software

Figure C24: Concentration profile for the self-condensation of *para*-fluorobenzaldehyde (266) (0.08 M), catalysed by *N*-phenyl triazolium precatalyst (139) (0.08 M), in 0.107 M NEt$_3$ and 0.107 M NEt$_3$·DCl in methanol-d$_4$, fitted using Berkeley Madonna global fitting software

Figure C25: Concentration profile for the self-condensation of *para*-methylbenzaldehyde (267) (0.08 M), catalysed by *N*-phenyl triazolium precatalyst (139) (0.08 M), in 0.107 M NEt$_3$ and 0.107 M NEt$_3$·DCl in methanol-d$_4$, fitted using Berkeley Madonna global fitting software

Figure C26: Concentration profile for the self-condensation of *para*-methoxybenzaldehyde (273) (0.08 M), catalysed by *N*-phenyl triazolium precatalyst (139) (0.08 M), in 0.107 M NEt$_3$ and 0.107 M NEt$_3$·DCl in methanol-d$_4$, fitted using Berkeley Madonna global fitting software

Figure C27: Concentration profile for the self-condensation of *ortho*-methylbenzaldehyde (274) (0.08 M), catalysed by *N*-phenyl triazolium precatalyst (139) (0.08 M), in 0.107 M NEt_3 and 0.107 M $NEt_3·DCl$ in methanol-d_4, fitted using Berkeley Madonna global fitting software
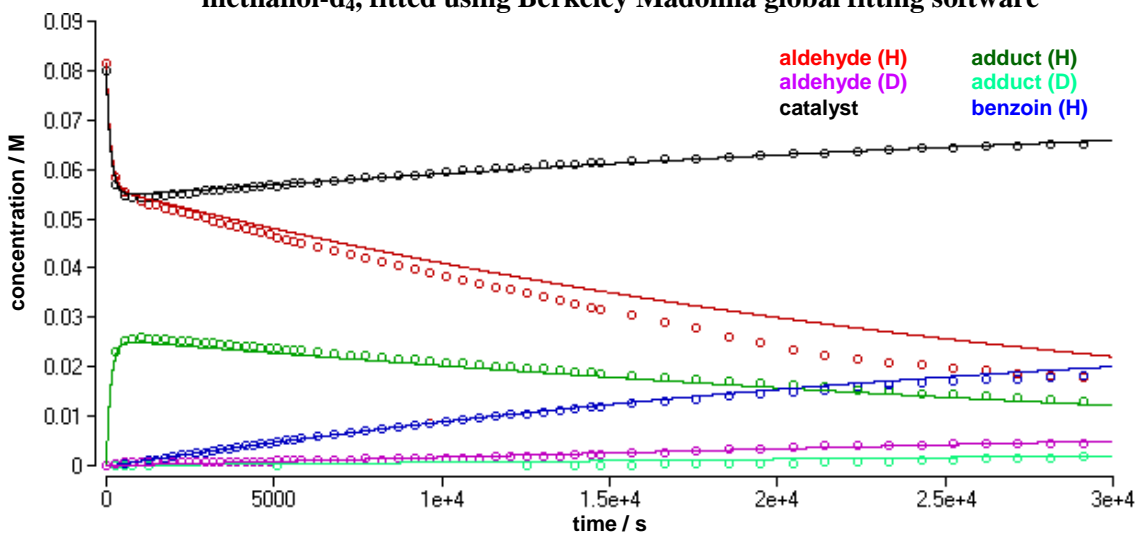

Figure C28: Concentration profile for the self-condensation of *ortho*-methoxybenzaldehyde (268) (0.08 M), catalysed by *N*-phenyl triazolium precatalyst (139) (0.08 M), in 0.107 M NEt_3 and 0.107 M $NEt_3·DCl$ in methanol-d_4, fitted using Berkeley Madonna global fitting software
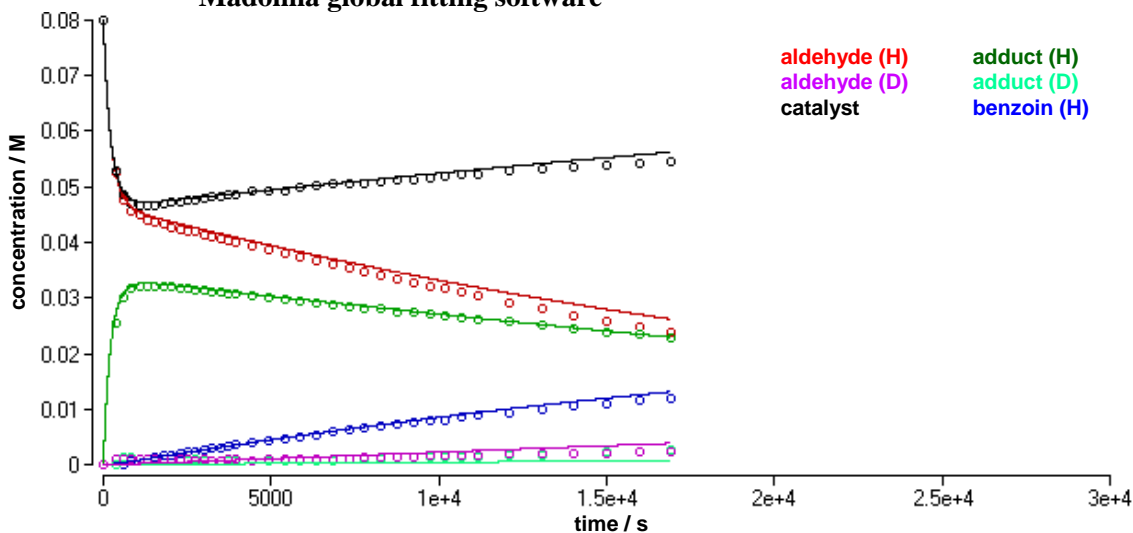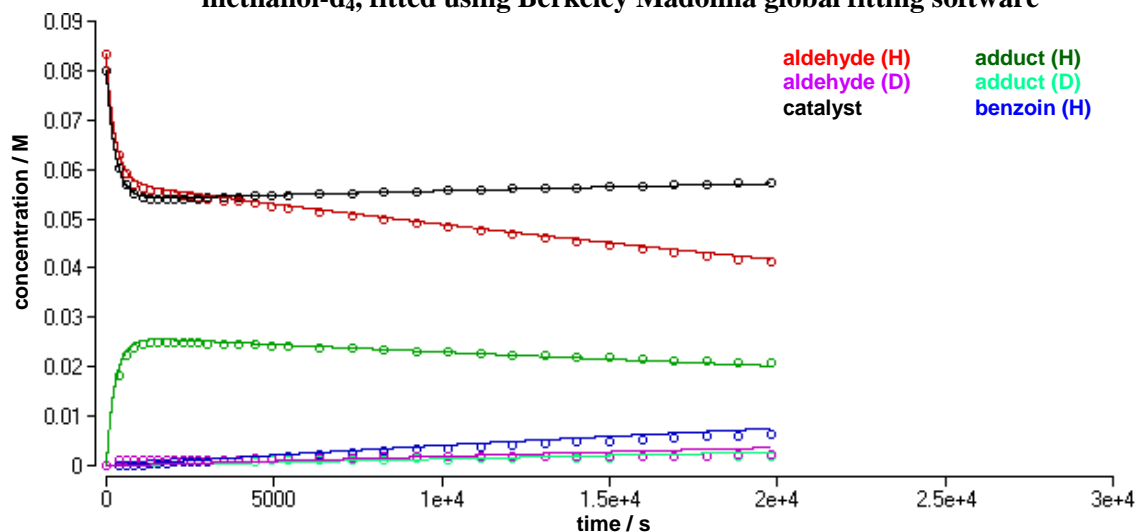
Figure C29: Concentration profile for the self-condensation of *para*-fluorobenzaldehyde (266) (0.08 M), catalysed by *N*-mesityl triazolium precatalyst (140) (0.08 M), in 0.107 M NEt$_3$ and 0.107 M NEt$_3$·DCl in methanol-d$_4$, fitted using Berkeley Madonna global fitting software
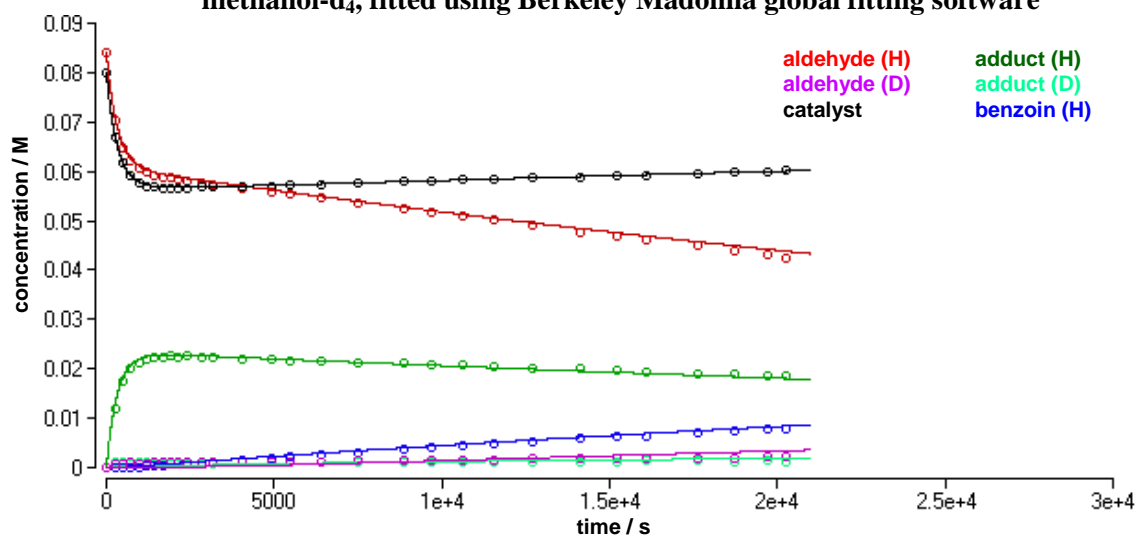

Figure C30: Concentration profile for the self-condensation of *para*-methylbenzaldehyde (267) (0.08 M), catalysed by *N*-mesityl triazolium precatalyst (140) (0.08 M), in 0.107 M NEt$_3$ and 0.107 M NEt$_3$·DCl in methanol-d$_4$, fitted using Berkeley Madonna global fitting software

Figure C31: Concentration profile for the self-condensation of *para*-fluorobenzaldehyde (266) (0.08 M), catalysed by *N*-C$_6$H$_4$OMe triazolium precatalyst (141) (0.08 M), in 0.107 M NEt$_3$ and 0.107 M NEt$_3$·DCl in methanol-d$_4$, fitted using Berkeley Madonna global fitting software

Figure C32: Concentration profile for the self-condensation of benzaldehyde (28) (0.08 M), catalysed by *N*-C$_6$H$_4$OMe triazolium precatalyst (141) (0.08 M), in 0.107 M NEt$_3$ and 0.107 M NEt$_3$·DCl in methanol-d$_4$, fitted using Berkeley Madonna global fitting software
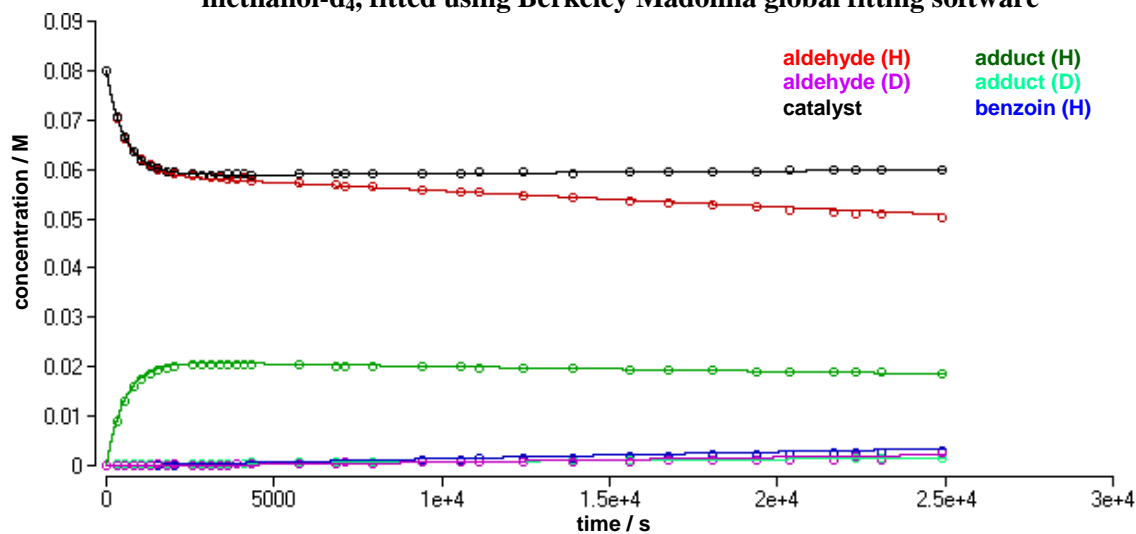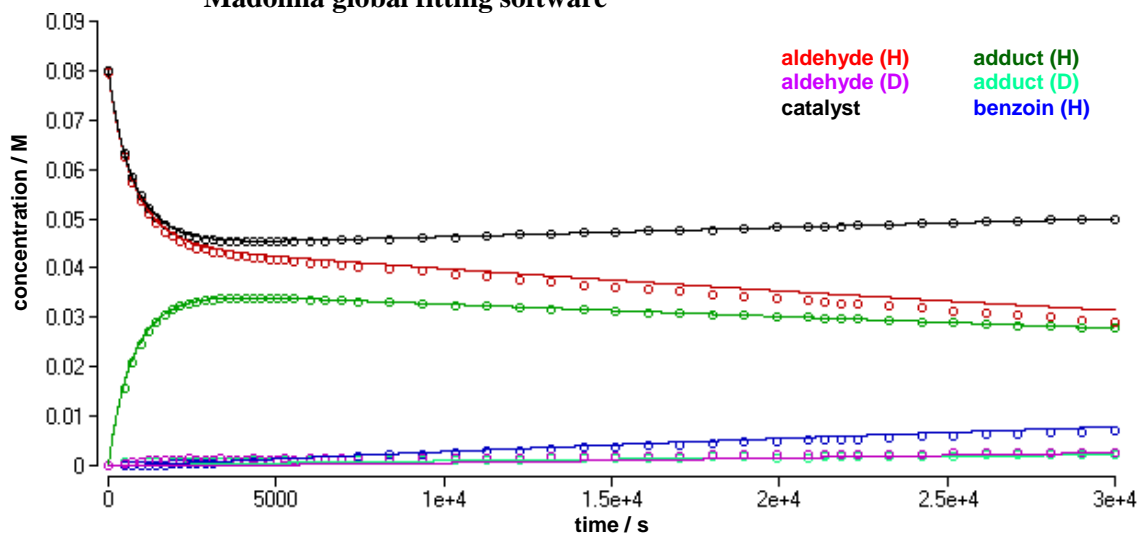
Figure C33: Concentration profile for the self-condensation of *para*-methylbenzaldehyde (267) (0.08 M), catalysed by *N*-C$_6$H$_4$OMe triazolium precatalyst (141) (0.08 M), in 0.107 M NEt$_3$ and 0.107 M NEt$_3$·DCl in methanol-d$_4$, fitted using Berkeley Madonna global fitting software
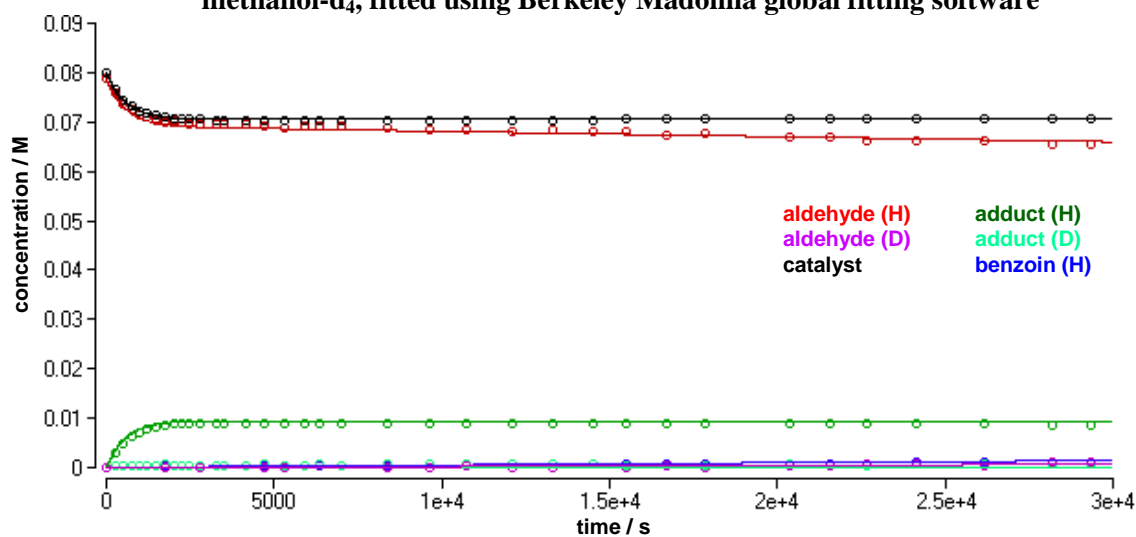

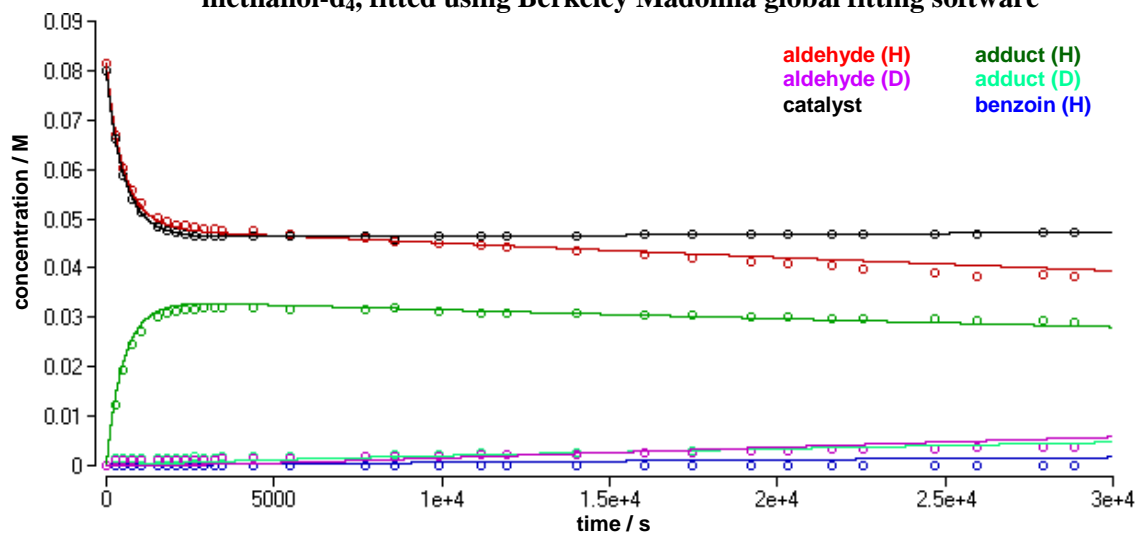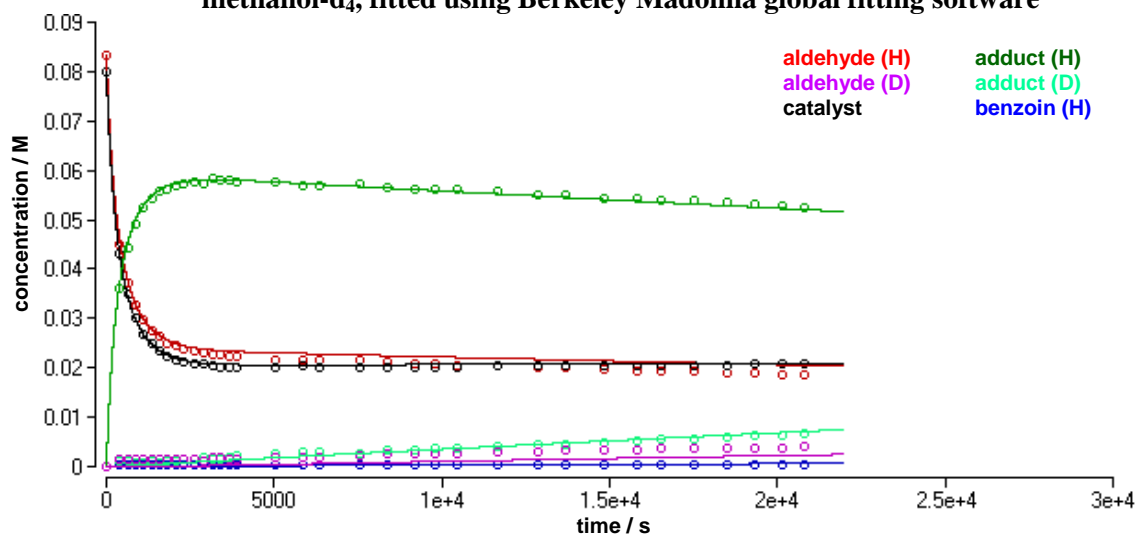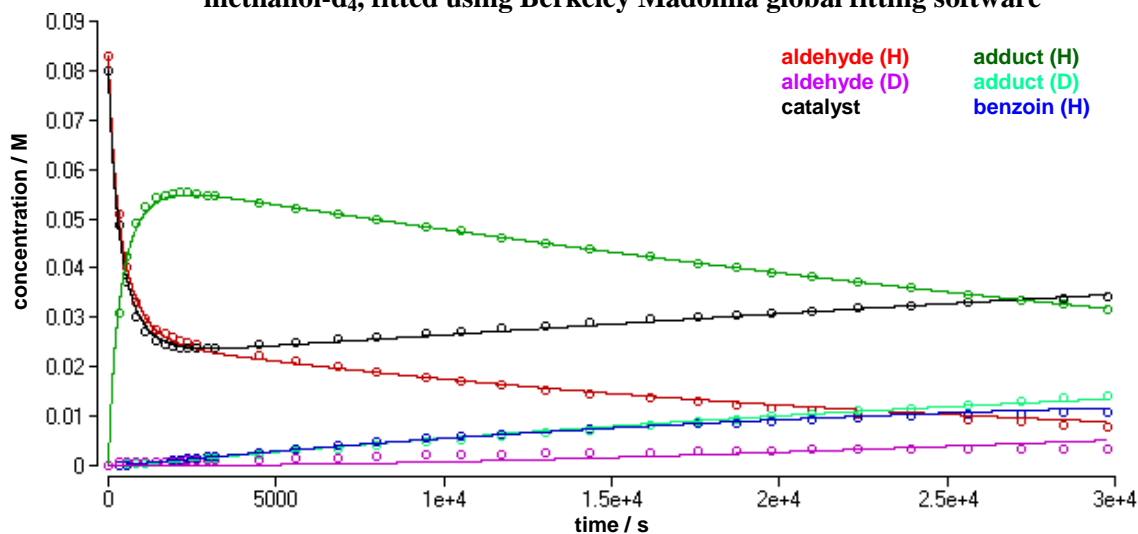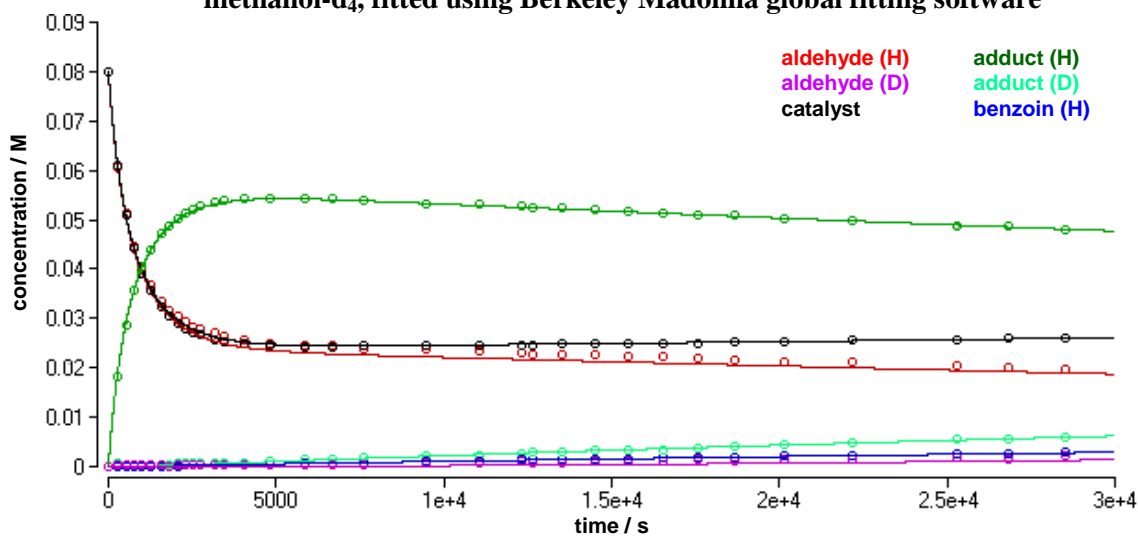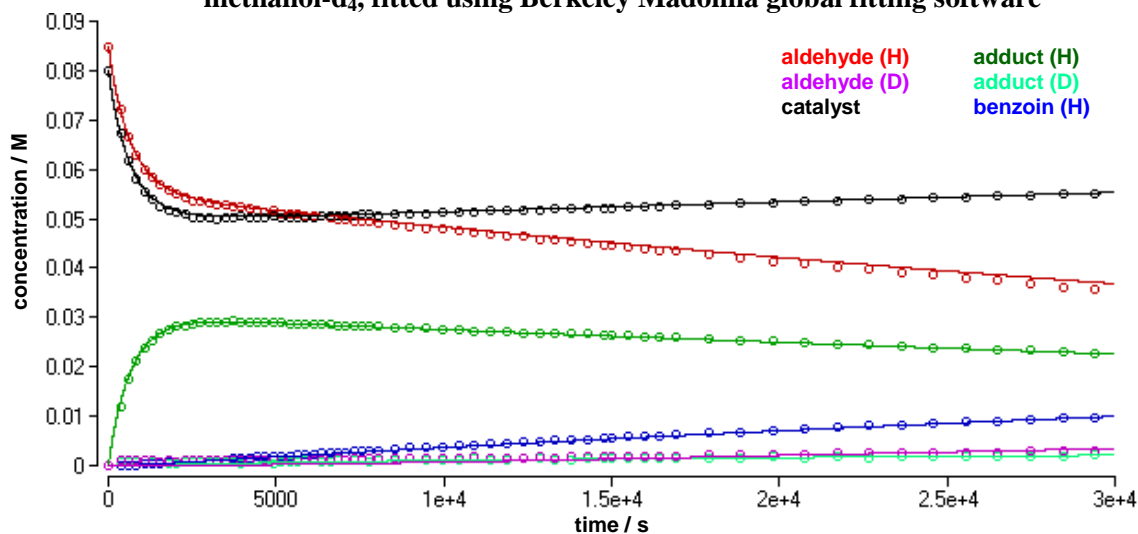**Figure C34:** Concentration profile for the self-condensation of benzaldehyde (28) (0.08 M), catalysed by *N*-pyridyl triazolium precatalyst (143) (0.08 M), in 0.107 M NEt$_3$ and 0.107 M NEt$_3$·DCl in methanol-d$_4$, fitted using Berkeley Madonna global fitting software
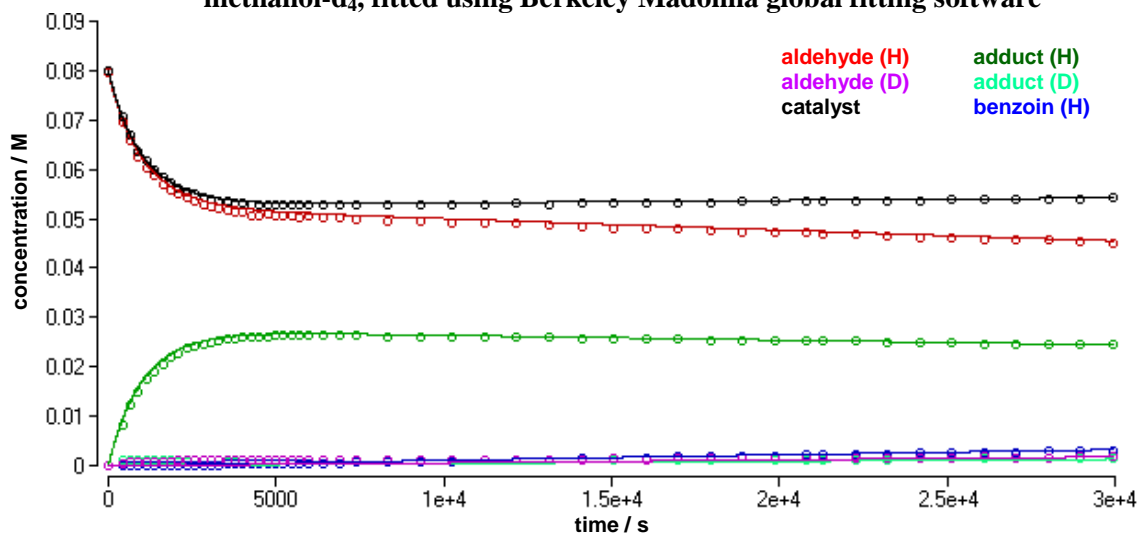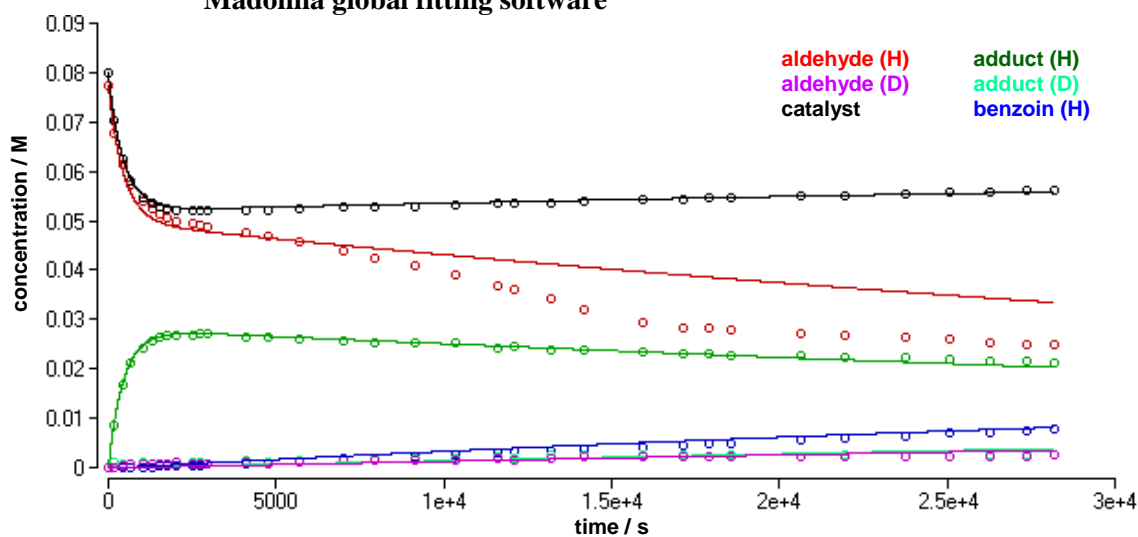
APPENDIX D

D1   Measurement of initial rates of reaction (v_0)

Table D1:   Reaction data and initial rates of benzoin formation, catalysed by thiazolium salt (53) (24 mM) in 0.16 M triethylamine-buffered methanol (66% f_B) at 50 °C.

$[PhCHO]_0$, M	time, s	A_{PhCHO}	$A_{benzoin}$	[PhCHO], M	[benzoin], M	v_0, M s^{-1} [a]
	0	1	0	0.320	0.00000	
	1200	3048438	6125	0.319	0.00061	
	2400	2545503	14074	0.317	0.00167	
	3300	2270097	18045	0.315	0.00239	
0.32	4200	2719212	28528	0.314	0.00313	7.40×10^{-7}
	5400	2485651	33138	0.312	0.00396	
	6300	2390364	37572	0.311	0.00465	
	7200	2565974	45582	0.310	0.00524	
	8400	2360545	48556	0.308	0.00603	
	0	1	0	0.640	0.00000	
	1200	1215710	3716	0.636	0.00185	
	2400	1510742	12963	0.630	0.00515	
	3300	1320120	15697	0.626	0.00709	
0.64	4200	1434747	21730	0.622	0.00897	2.17×10^{-6}
	5400	1525484	30805	0.616	0.01185	
	6300	1283070	29743	0.613	0.01353	
	7200	1250170	33208	0.609	0.01541	
	8400	1428125	44330	0.604	0.01786	
	0	1	0	0.960	0.00000	
	1200	2039269	6900	0.954	0.00307	
	2400	1836914	16045	0.944	0.00786	
	3300	3046600	37785	0.938	0.01108	
0.96	4200	2222598	35782	0.931	0.01428	3.58×10^{-6}
	5400	2240301	47594	0.923	0.01867	
	6300	2014817	50112	0.917	0.02171	
	7200	2177032	62764	0.910	0.02499	
	8400	1867098	64760	0.901	0.02975	
	0	1	0	1.280	0.00000	
	1200	2449786	8324	1.272	0.00412	
	2400	2785797	23876	1.259	0.01028	
	3300	3077674	37142	1.251	0.01438	
1.28	4200	2729644	42861	1.243	0.01859	4.47×10^{-6}
	5400	2715919	55784	1.232	0.02410	
	6300	3197466	77808	1.223	0.02835	
	7200	3330458	91003	1.217	0.03166	
	8400	2649333	84362	1.207	0.03660	
	0	1	0	1.600	0.00000	
	1200	3360229	13935	1.587	0.00627	
	2400	3275503	32432	1.570	0.01481	
	3300	3083531	43187	1.558	0.02079	
1.60	4200	3170843	58073	1.546	0.02697	6.68×10^{-6}
	5400	4072840	99224	1.529	0.03548	
	6300	4079768	116196	1.518	0.04117	
	7200	4133466	135930	1.506	0.04716	
	8400	3664093	142859	1.489	0.05530	

(a) The initial rate of benzoin formation, v_0 (M^{-1} s^{-1}), was obtained from the slope of the plot of benzoin concentration against time in Figure 5.4.

Table D2: Reaction data and initial rates of benzoin formation, catalysed by thiazolium salt (53) (12 mM) in 0.16 M triethylamine-buffered methanol (66% f_B) at 50 °C.

[PhCHO]$_0$, M	time, s	A_{PhCHO}	$A_{benzoin}$	[PhCHO], M	[benzoin], M	v_0, M s^{-1} [a]
	0	1	0	0.320	0.00000	
	1200	4089635	3853	0.319	0.00029	
	2400	2617637	6146	0.319	0.00071	
	3300	2261509	7078	0.318	0.00095	
	4200	2648769	11109	0.317	0.00127	
0.32	5400	2528989	13617	0.317	0.00162	2.80×10^{-7}
	6300	2914627	17759	0.316	0.00184	
	7200	2993442	20966	0.316	0.00211	
	8400	2934447	22875	0.315	0.00234	
	9600	2901303	25371	0.315	0.00262	
	0	1	0	0.640	0.00000	
	1200	1261443	1591	0.638	0.00077	
	2400	1288067	3898	0.636	0.00183	
	3300	1332267	5571	0.635	0.00253	
	4200	1164125	6067	0.634	0.00315	
0.64	5400	1331151	9029	0.632	0.00408	7.06×10^{-7}
	6300	1327170	10003	0.631	0.00453	
	7200	1460332	12923	0.629	0.00530	
	8400	1623852	16476	0.628	0.00607	
	9600	1496361	16566	0.627	0.00661	
	0	1	0	0.960	0.00000	
	1200	2620732	3236	0.958	0.00113	
	2400	2395678	6882	0.955	0.00261	
	3300	2200434	8769	0.953	0.00362	
	4200	2239358	11525	0.951	0.00466	
0.96	5400	1930693	12593	0.948	0.00589	1.02×10^{-6}
	6300	2360240	17643	0.947	0.00674	
	7200	2255081	19401	0.945	0.00774	
	8400	1999902	19398	0.943	0.00871	
	9600	2327694	24841	0.941	0.00956	
	0	1	0	1.280	0.00000	
	1200	2870776	3553	1.277	0.00151	
	2400	2570612	7824	1.273	0.00369	
	3300	2642066	11709	1.269	0.00536	
	4200	3316016	18855	1.266	0.00686	
1.28	5400	2711623	19509	1.263	0.00865	1.61×10^{-6}
	6300	2668768	22494	1.260	0.01011	
	7200	3009879	29580	1.256	0.01176	
	8400	3658421	40826	1.253	0.01332	
	9600	2942948	37374	1.250	0.01512	
	0	1	0	1.600	0.00000	
	1200	3367906	5572	1.595	0.00251	
	2400	3402851	12907	1.589	0.00574	
	3300	3692804	20038	1.584	0.00818	
1.60	4200	3266756	23017	1.579	0.01059	2.61×10^{-6}
	5400	4021005	37576	1.572	0.01399	
	6300	4347864	46965	1.568	0.01613	
	7200	3982480	49101	1.563	0.01836	
	8400	3873705	56435	1.557	0.02160	

(a) The initial rate of benzoin formation, v_0 (M^{-1} s^{-1}), was obtained from the slope of the plot of benzoin concentration against time in Figure 5.5.

Table D3: Reaction data and initial rates of benzoin formation, catalysed by triazolium salt (139) (24 mM) in 0.16 M triethylamine-buffered methanol (66% f_B) at 50 °C.

[PhCHO]$_0$, M	time, s	A_{PhCHO}	$A_{benzoin}$	[PhCHO], M	[benzoin], M	v_0, M s^{-1} [a]
0.16	0	1	0	0.160	0.00000	
	1800	1464527	7792	0.158	0.00080	
	3600	1267043	11352	0.157	0.00134	
	7200	1338410	21795	0.155	0.00241	
	9000	1234961	24432	0.154	0.00291	3.13×10^{-7}
	10800	1321923	31867	0.153	0.00351	
	12600	1232249	35589	0.152	0.00417	
	14400	1442571	45943	0.151	0.00458	
0.32	0	1	0	0.320	0.00000	
	1800	1077340	5158	0.317	0.00145	
	3600	1408141	12390	0.315	0.00264	
	5400	1368637	17144	0.313	0.00373	
	7200	1699697	28346	0.310	0.00493	6.76×10^{-7}
	9000	1283427	27190	0.308	0.00620	
	10800	1248861	32133	0.305	0.00748	
	12600	1163626	32881	0.304	0.00817	
	14400	1411367	46065	0.301	0.00937	
0.64	0	1	0	0.640	0.00000	
	1800	424308	1498	0.636	0.00214	
	3600	594307	4189	0.632	0.00424	
	5400	678796	6926	0.628	0.00610	
	7200	653037	8737	0.624	0.00795	1.03×10^{-6}
	9000	676979	11028	0.621	0.00963	
	10800	794659	15564	0.617	0.01151	
	12600	780418	18006	0.613	0.01347	
	14400	695281	17748	0.610	0.01484	
0.96	0	1	0	0.960	0.00000	
	1800	1203419	3442	0.955	0.00260	
	3600	903519	4723	0.951	0.00473	
	5400	853478	6462	0.946	0.00682	
	7200	2159474	22189	0.942	0.00921	1.20×10^{-6}
	9000	1162182	14662	0.937	0.01126	
	10800	1496355	22852	0.933	0.01357	
	12600	1204386	20772	0.929	0.01527	
	14400	1153168	22712	0.925	0.01736	
1.28	0	1	0	1.280	0.00000	
	1800	1571547	3683	1.274	0.00284	
	3600	1813265	7724	1.270	0.00515	
	5400	1101633	6800	1.265	0.00744	
	7200	3112260	25966	1.260	0.01001	1.30×10^{-6}
	9000	1268717	12438	1.257	0.01173	
	10800	1357705	16660	1.251	0.01462	
	12600	1378121	19364	1.247	0.01668	
	14400	1532640	24376	1.242	0.01882	
1.44	0	1	0	1.440	0.00000	
	3600	1748129	7042	1.429	0.00548	
	5400	1879657	11135	1.424	0.00803	
	7200	2215806	16793	1.420	0.01025	
	9000	1398507	13074	1.415	0.01260	1.34×10^{-6}
	10800	1801747	20371	1.410	0.01518	
	12600	2037915	26286	1.405	0.01727	
	14400	2436171	35575	1.401	0.01948	

	0	1	0	1.600	0.00000	
	1800	1529919	2582	1.595	0.00256	
	3600	1723728	5962	1.590	0.00524	
	5400	1925285	10051	1.584	0.00788	
1.60	7200	1818671	12432	1.579	0.01028	1.36×10^{-6}
	9000	1683077	14340	1.574	0.01278	
	12600	1642636	19033	1.565	0.01728	
	14400	1923111	25385	1.561	0.01962	

(a) The initial rate of benzoin formation, v_0 (M^{-1} s^{-1}), was obtained from the slope of the plot of benzoin concentration against time in Figure 5.8.

Table D4: **Reaction data and initial rates of benzoin formation, catalysed by triazolium salt (139) (12 mM) in 0.16 M triethylamine-buffered methanol (66% f_B) at 50 °C.**

[PhCHO]$_0$, M	time, s	A_{PhCHO}	$A_{benzoin}$	[PhCHO], M	[benzoin], M	v_0, M s^{-1} [a]
	0	1	0	0.160	0.00000	
	1800	1127240	4178	0.159	0.00056	
	3600	960391	5710	0.158	0.00090	
	5400	1000149	8800	0.157	0.00132	
0.16	9000	1079324	15178	0.156	0.00209	2.14×10^{-7}
	10800	1345814	21744	0.155	0.00239	
	16200	1119943	26696	0.153	0.00348	
	19800	1268988	38869	0.151	0.00441	
	0	1	0	0.320	0.00000	
	1800	1331941	4111	0.318	0.00094	
	5400	1256635	10593	0.315	0.00253	
0.32	9000	1076590	14472	0.312	0.00399	4.33×10^{-7}
	10800	1344210	21669	0.310	0.00477	
	16200	1257781	29799	0.306	0.00691	
	19800	1328294	40533	0.302	0.00879	
	0	1	0	0.640	0.00000	
	1800	1962751	4227	0.637	0.00131	
	3600	2158401	9603	0.635	0.00269	
0.64	5400	1970114	12623	0.632	0.00389	6.82×10^{-7}
	9000	2718276	28539	0.627	0.00627	
	16200	2448240	44497	0.619	0.01071	
	19800	2641928	62995	0.612	0.01390	
	0	1	0	0.960	0.00000	
	1800	1014998	1847	0.957	0.00166	
	3600	793499	2595	0.954	0.00297	
0.96	5400	718072	3481	0.951	0.00439	7.62×10^{-7}
	9000	841947	6644	0.946	0.00711	
	16200	1072136	14587	0.936	0.01213	
	19800	1039490	18240	0.929	0.01552	
	0	1	0	1.280	0.00000	
	3600	851583	2045	1.274	0.00291	
	5400	822767	3117	1.271	0.00459	
1.28	9000	1432671	8782	1.265	0.00739	
	10800	1130709	8275	1.262	0.00880	
	16200	1452514	15514	1.254	0.01276	8.04×10^{-7}
	19800	1259717	17155	1.248	0.01618	

[PhCHO]₀, M	time, s	A_{PhCHO}	$A_{benzoin}$	[PhCHO], M	[benzoin], M	v_0, M s⁻¹ ᵃ
	0	1	0	1.440	0.00000	
	1800	1075984	1427	1.436	0.00181	
	3600	835615	1949	1.434	0.00319	
	5400	1393888	4744	1.431	0.00464	
1.44	9000	1244496	6946	1.425	0.00757	8.21×10^{-7}
	10800	2804487	18591	1.422	0.00898	
	16200	1326628	12260	1.415	0.01246	
	19800	1583979	20274	1.406	0.01714	
	0	1	0	1.600	0.00000	
	1800	1486386	1815	1.596	0.00186	
	3600	1307070	3029	1.593	0.00352	
	5400	1504372	4625	1.591	0.00466	
1.60	9000	1120923	5379	1.586	0.00725	8.07×10^{-7}
	10800	1038324	6188	1.582	0.00898	
	16200	3316836	28986	1.574	0.01310	
	19800	1723210	18991	1.567	0.01645	

(a) The initial rate of benzoin formation, v_0 (M⁻¹ s⁻¹), was obtained from the slope of the plot of benzoin concentration against time in Figure 5.9.

Table D5: **Reaction data and initial rates of benzoin formation, catalysed by triazolium salt (139) (6 mM) in 0.16 M triethylamine-buffered methanol (66% f_B) at 50 °C.**

[PhCHO]₀, M	time, s	A_{PhCHO}	$A_{benzoin}$	[PhCHO], M	[benzoin], M	v_0, M s⁻¹ ᵃ
	0	1	0	0.160	0.000000	
	1800	2292953	4144	0.159	0.000274	
	3600	2251713	7118	0.159	0.000479	
	5400	2462060	11220	0.159	0.000688	
0.16	9000	2231951	16669	0.158	0.001122	1.18×10^{-7}
	10800	2493196	21564	0.157	0.001297	
	16200	2468415	31106	0.156	0.001875	
	19800	2490332	40792	0.155	0.002421	
	0	1	0	0.320	0.000000	
	1800	914228	1796	0.319	0.000596	
	3600	1048343	3860	0.318	0.001114	
	5400	1130326	5485	0.317	0.001465	
0.32	9000	1321311	10265	0.315	0.002333	2.48×10^{-7}
	10800	1409536	13077	0.314	0.002778	
	16200	1135312	15743	0.312	0.004117	
	19800	1188189	20218	0.310	0.005023	
	0	1	0	0.640	0.000000	
	1800	2213909	2691	0.639	0.000739	
	3600	2280487	5505	0.637	0.001465	
0.64	5400	2406983	8209	0.636	0.002065	3.64×10^{-7}
	9000	2368797	13138	0.633	0.003345	
	16200	2567378	25141	0.628	0.005859	
	19800	2500140	30859	0.625	0.007350	
	0	1	0	0.960	0.000000	
	3600	617009	1037	0.957	0.001532	
	5400	668785	1713	0.955	0.002330	
	9000	698087	2708	0.953	0.003521	
0.96	10800	1134156	5649	0.951	0.004511	4.07×10^{-7}
	16200	974416	7000	0.947	0.006479	
	19800	495828	4530	0.944	0.008210	

[PhCHO]₀, M	time, s	A_PhCHO	A_benzoin	[PhCHO], M	[benzoin], M	v₀, M s⁻¹
	0	1	0	1.280	0.000000	
	3600	1404999	1969	1.277	0.001704	
	5400	1375015	2721	1.275	0.002403	
1.28	9000	1325822	4330	1.272	0.003957	4.13×10^{-7}
	10800	954237	3644	1.271	0.004622	
	16200	1241001	6716	1.267	0.006530	
	19800	1169157	8200	1.263	0.008437	
	0	1	0	1.440	0.000000	
	3600	1380288	1840	1.436	0.001824	
	5400	1328662	2501	1.435	0.002572	
1.44	9000	1661804	4782	1.432	0.003925	4.18×10^{-7}
	10800	1385280	4757	1.431	0.004679	
	16200	1505939	7533	1.426	0.006795	
	19800	1366611	8609	1.423	0.008537	
	0	1	0	1.600	0.000000	
	3600	1087550	1404	1.596	0.001962	
	5400	1620624	3043	1.694	0.002851	
1.44	9000	1287851	3452	1.592	0.004064	4.25×10^{-7}
	10800	1657941	5253	1.590	0.004799	
	16200	1941723	8876	1.586	0.006906	
	19800	1230481	7198	1.582	0.008816	

(a) The initial rate of benzoin formation, v_0 (M⁻¹ s⁻¹), was obtained from the slope of the plot of benzoin concentration against time in Figure 5.10.

Table D6: **Reaction data and initial rates of benzoin formation, catalysed by triazolium salt (141) (12 mM) in 0.16 M triethylamine-buffered methanol (66% f_B) at 50 °C.**

[PhCHO]₀, M	time, s	A_PhCHO	A_benzoin	[PhCHO], M	[benzoin], M	v₀, M s⁻¹ ᵃ
	0	1	0	0.160	0.00000	
	2400	1357235	3491	0.159	0.00039	
	4800	1687585	8996	0.158	0.00080	
0.16	7200	2010026	15206	0.158	0.00114	1.51×10^{-7}
	9600	1826355	19211	0.157	0.00157	
	12000	2131569	26493	0.156	0.00185	
	14400	2099425	31603	0.156	0.00223	
	16800	1803153	30921	0.155	0.00253	
	0	1	0	0.320	0.00000	
	2400	2263867	5412	0.319	0.00073	
	4800	2170347	10370	0.317	0.00144	
0.32	7200	2328065	17724	0.315	0.00229	2.79×10^{-7}
	9600	2026237	19021	0.314	0.00281	
	12000	2055596	23608	0.313	0.00343	
	14400	2573422	34760	0.312	0.00401	
	16800	1691993	27186	0.310	0.00475	
	0	1	0	0.480	0.00000	
	2400	2579849	4695	0.478	0.00083	
	4800	2407880	8745	0.477	0.00165	
0.48	7200	2671867	15253	0.475	0.00258	3.26×10^{-7}
	9600	2185462	16529	0.473	0.00341	
	12000	2613674	23441	0.472	0.00403	
	14400	2006961	21532	0.470	0.00481	
	16800	2414026	29176	0.469	0.00540	

[PhCHO]₀, M	time, s	A_{PhCHO}	$A_{benzoin}$	[PhCHO], M	[benzoin], M	v_0, M s⁻¹
	0	1	0	0.640	0.00000	
	2400	2129706	3349	0.638	0.00096	
	4800	2438234	8070	0.636	0.00200	
0.64	7200	2116715	9911	0.634	0.00283	3.47×10^{-7}
	9600	2048407	12647	0.633	0.00372	
	12000	2692347	19879	0.631	0.00444	
	14400	2613579	22578	0.630	0.00518	
	16800	2092248	20344	0.628	0.00582	
	0	1	0	0.960	0.00000	
	2400	3909033	3994	0.958	0.00093	
	4800	3599960	8285	0.956	0.00210	
0.96	7200	4434974	13827	0.954	0.00283	3.56×10^{-7}
	9600	4059903	16726	0.953	0.00374	
	12000	3396525	15341	0.952	0.00409	
	14400	3572467	21819	0.949	0.00552	
	16800	3798276	25226	0.948	0.00600	
	0	1	0	1.280	0.00000	
	2400	5265225	5141	1.278	0.00119	
	4800	4694081	6585	1.277	0.00171	
1.28	7200	5499779	12435	1.275	0.00274	3.43×10^{-7}
	9600	4844869	14089	1.273	0.00353	
	12000	4563671	15936	1.272	0.00423	
	14400	4859732	20262	1.270	0.00504	
	0	1	0	1.440	0.00000	
	2400	1274803	891	1.438	0.00096	
	4800	1294019	1658	1.436	0.00175	
1.44	7200	1654004	3243	1.435	0.00268	3.46×10^{-7}
	9600	1320452	3552	1.433	0.00367	
	12000	1689081	5084	1.432	0.00410	
	14400	1133743	4170	1.430	0.00501	
	0	1	0	1.600	0.00000	
	2400	1553473	870	1.598	0.00085	
	4800	2019987	2267	1.597	0.00171	
1.60	7200	1521216	2698	1.595	0.00269	3.53×10^{-7}
	9600	1860905	4227	1.593	0.00345	
	12000	1821032	5316	1.591	0.00442	

(a) The initial rate of benzoin formation, v_0 (M⁻¹ s⁻¹), was obtained from the slope of the plot of benzoin concentration against time in Figure D1.

Table D7: **Reaction data and initial rates of benzoin formation, catalysed by triazolium salt (141) (6 mM) in 0.16 M triethylamine-buffered methanol (66% f_B) at 50 °C.**

[PhCHO]₀, M	time, s	A_{PhCHO}	$A_{benzoin}$	[PhCHO], M	[benzoin], M	v_0, M s⁻¹ [a]
	0	1	0	0.160	0.000000	
	2400	1512317	2116	0.160	0.000213	
	4800	1840595	4955	0.159	0.000408	
	7200	2226508	8975	0.159	0.000610	
0.16	9600	1699218	9094	0.158	0.000807	7.90×10^{-8}
	12000	1194081	7863	0.158	0.000991	
	14400	2058669	15838	0.158	0.001155	
	16800	1818055	16062	0.157	0.001324	

	0	1	0	0.320	0.000000	
	2400	1364627	1817	0.319	0.000405	
	4800	2888044	7651	0.318	0.000803	
	7200	2468413	9134	0.318	0.001120	
0.32	9600	2577578	12799	0.317	0.001499	1.45×10^{-7}
	12000	2632310	16092	0.316	0.001842	
	14400	2525157	18123	0.316	0.002158	
	16800	2726414	22004	0.315	0.002422	
	0	1	0	0.480	0.000000	
	2400	1737665	1576	0.479	0.000414	
	4800	2171017	4044	0.478	0.000849	
0.48	7200	2084262	5879	0.477	0.001283	1.78×10^{-7}
	9600	2323181	8094	0.477	0.001582	
	12000	1907709	8915	0.476	0.002117	
	14400	2051552	11837	0.475	0.002609	
	0	1	0	0.640	0.000000	
	2400	2231737	1818	0.639	0.000496	
	4800	1939826	2857	0.638	0.000895	
0.64	7200	1929554	4501	0.637	0.001416	1.82×10^{-7}
	9600	2208474	6369	0.637	0.001748	
	12000	1937299	7275	0.635	0.002273	
	14400	1988178	8565	0.635	0.002604	
	0	1	0	0.960	0.000000	
	2400	3350639	1903	0.959	0.000519	
	4800	3390845	3844	0.958	0.001034	
0.96	7200	2432641	4184	0.957	0.001567	1.97×10^{-7}
	9600	3417977	7503	0.956	0.001999	
	12000	3691438	9760	0.955	0.002405	
	14400	3365379	10498	0.954	0.002835	
	0	1	0	1.280	0.000000	
	2400	4777685	1910	1.279	0.000487	
	4800	5573762	4727	1.278	0.001032	
1.28	7200	3372789	4129	1.277	0.001489	1.89×10^{-7}
	9600	4880734	7562	1.276	0.001883	
	12000	4714471	8863	1.275	0.002284	
	14400	5311222	12007	1.275	0.002744	
	0	1	0	1.440	0.000000	
	2400	1236103	548	1.439	0.000607	
	4800	1622944	1286	1.438	0.001085	
1.44	7200	1276723	1444	1.437	0.001548	1.87×10^{-7}
	9600	1129553	1542	1.436	0.001867	
	12000	1328405	2312	1.435	0.002379	
	14400	1512754	3042	1.435	0.002747	
	0	1	0	1.600	0.000000	
	2400	1938721	774	1.599	0.000608	
	4800	2069215	1448	1.598	0.001065	
1.60	9600	1745579	2196	1.596	0.001912	1.97×10^{-7}
	12000	1427131	2329	1.595	0.002479	
	14400	1534787	2920	1.594	0.002889	

(a) The initial rate of benzoin formation, v_0 (M^{-1} s^{-1}), was obtained from the slope of the plot of benzoin concentration against time in Figure D2.

Figure D1: **Plots of benzoin concentration against time for the triazolium (141) (12 mM) catalysed benzoin condensation, at initial benzaldehyde concentrations 0.16 M, 0.32 M, 0.48 M, 0.64 M, 0.96 M, 1.28 M, 1.44 M and 1.60 M.**

Figure D2: **Plots of benzoin concentration against time for the triazolium (141) (6 mM) catalysed benzoin condensation, at initial benzaldehyde concentrations 0.16 M, 0.32 M, 0.48 M, 0.64 M, 0.96 M, 1.28 M, 1.44 M and 1.60 M.**
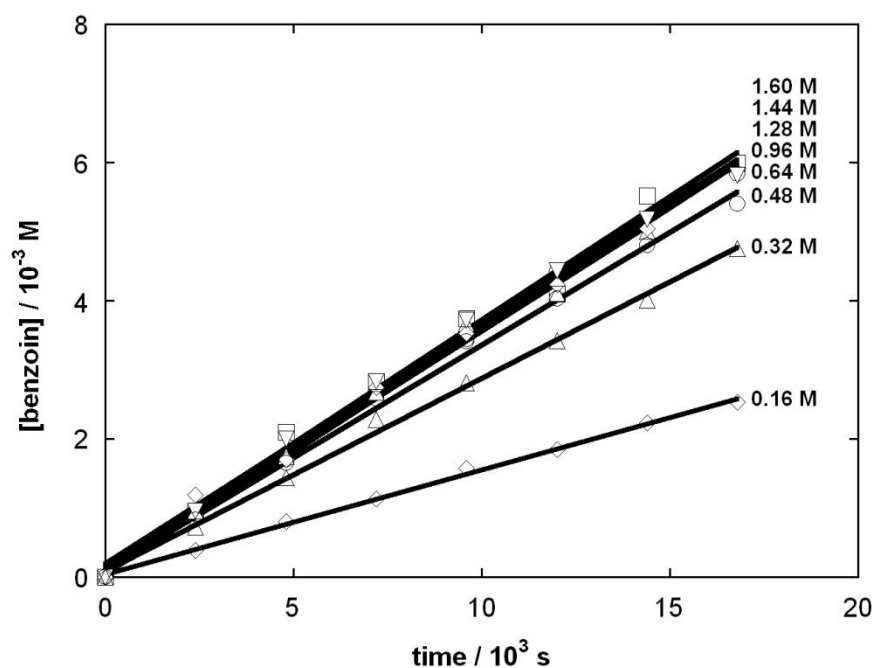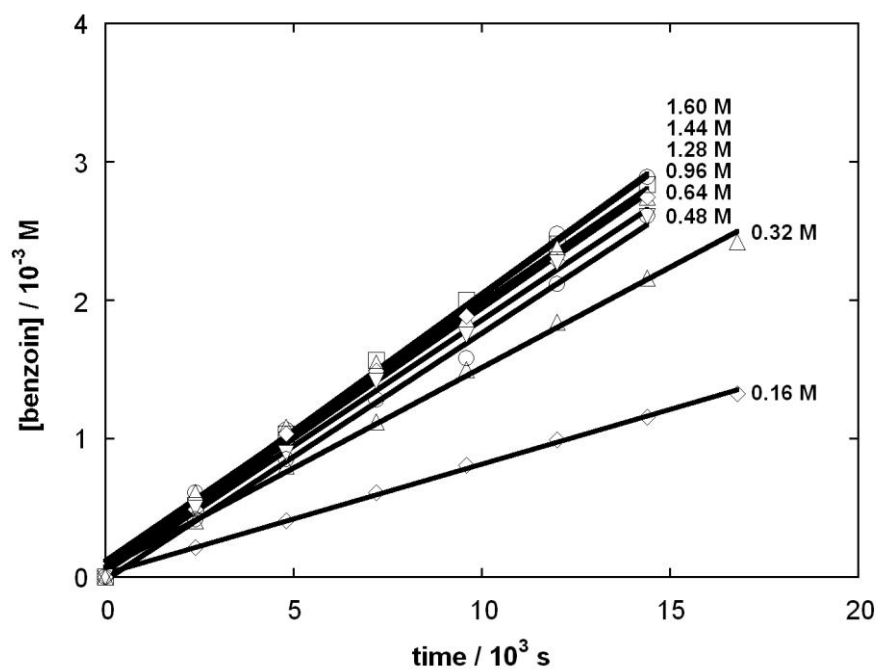
Table D8: Reaction data and initial rates of benzoin formation, catalysed by triazolium salt (140) (12 mM) in 0.16 M triethylamine-buffered methanol (66% f_B) at 50 °C.

[PhCHO]$_0$, M	time, s	A_{PhCHO}	$A_{benzoin}$	[PhCHO], M	[benzoin], M	v_0, M s^{-1} [a]
0.16	0	1	0	0.160	0.00000	
	1500	3336740	8990	0.159	0.00041	
	3000	3471325	17804	0.158	0.00077	
	5100	3172524	28738	0.157	0.00136	
	6600	2410637	28368	0.156	0.00175	2.51×10^{-7}
	8700	2816921	42959	0.155	0.00226	
	10200	3677216	65294	0.155	0.00262	
	11700	3476491	68259	0.154	0.00288	
	13200	3732094	85599	0.153	0.00335	
0.32	0	1	0	0.320	0.00000	
	1500	4807998	10110	0.319	0.00064	
	3000	4522753	19709	0.317	0.00132	
	5100	4456275	31378	0.316	0.00212	
	6600	4133790	38237	0.314	0.00277	4.02×10^{-7}
	8700	4258524	50404	0.313	0.00353	
	10200	4897249	68593	0.312	0.00416	
	11700	4445527	71351	0.311	0.00475	
	13200	4606029	83590	0.309	0.00535	
0.48	0	1	0	0.480	0.00000	
	1500	3429319	5585	0.479	0.00074	
	3000	3777271	12550	0.477	0.00151	
	5100	3672018	20725	0.475	0.00255	
	6600	3561366	25762	0.473	0.00326	4.76×10^{-7}
	8700	3975502	38702	0.471	0.00437	
	10200	3842660	41544	0.470	0.00484	
	11700	3910086	49233	0.469	0.00562	
	13200	3592336	50638	0.467	0.00628	
0.64	0	1	0	0.640	0.00000	
	1500	4193840	5579	0.638	0.00081	
	3000	5330597	14334	0.637	0.00163	
	5100	3812121	17843	0.634	0.00283	
	6600	4480430	26471	0.633	0.00356	5.19×10^{-7}
	8700	4931956	39051	0.630	0.00475	
	10200	4506102	41587	0.629	0.00553	
	11700	4233166	42786	0.628	0.00604	
	13200	5632245	64066	0.626	0.00679	
0.96	0	1	0	0.960	0.00000	
	1500	2025854	1751	0.958	0.00079	
	3000	2257909	4527	0.956	0.00183	
	5100	2266051	7267	0.954	0.00291	
	6600	2287390	9490	0.952	0.00376	5.45×10^{-7}
	8700	1984550	10435	0.950	0.00476	
	10200	2555163	15522	0.949	0.00549	
	11700	2484328	18062	0.947	0.00656	
	13200	2543196	20384	0.946	0.00722	
1.28	0	1	0	1.280	0.00000	
	1500	2705244	2077	1.278	0.00094	
	3000	2827988	4137	1.276	0.00178	
	5100	3429897	7955	1.274	0.00282	
	6600	2558184	8505	1.272	0.00403	5.59×10^{-7}
	8700	2724294	11259	1.270	0.00500	
	10200	3221098	15327	1.269	0.00575	
	11700	3050772	16894	1.267	0.00668	

	13200	2944229	17886	1.265	0.00732	
1.44	0	1	0	1.440	0.00000	
	1500	3263349	2272	1.438	0.00095	
	3000	3195452	4316	1.436	0.00185	
	5100	3287273	7326	1.434	0.00304	5.45×10^{-7}
	8700	3082439	11132	1.430	0.00492	
	10200	3549584	15153	1.428	0.00581	
	11700	3213622	15107	1.427	0.00639	
	13200	3156331	16970	1.425	0.00730	
1.60	0	1	0	1.600	0.00000	
	1500	3392593	1080	1.599	0.00048	
	3000	3362423	3782	1.597	0.00171	
	5100	3619007	6734	1.594	0.00283	
	6600	3361340	8765	1.592	0.00395	5.70×10^{-7}
	8700	3148867	10948	1.589	0.00526	
	10200	4114623	15412	1.589	0.00567	
	11700	3879808	17002	1.587	0.00662	
	13200	4181312	19998	1.586	0.00722	

(a) The initial rate of benzoin formation, v_0 (M^{-1} s^{-1}), was obtained from the slope of the plot of benzoin concentration against time in Figure D3.

Figure D3: **Plots of benzoin concentration against time for the triazolium (140) (12 mM) catalysed benzoin condensation, at initial benzaldehyde concentrations 0.16 M, 0.32 M, 0.48 M, 0.64 M, 0.96 M, 1.28 M, 1.44 M and 1.60 M.**
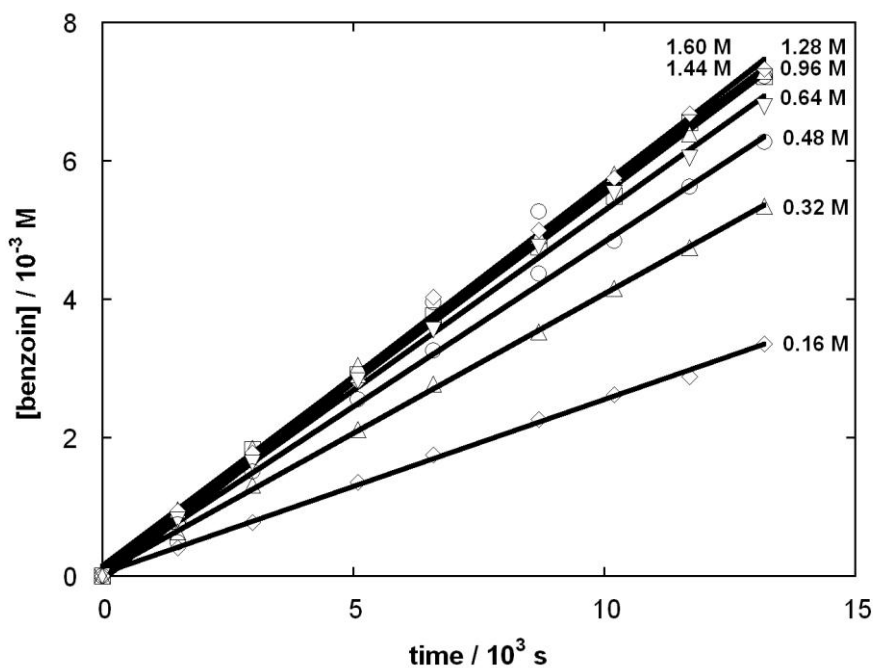
Table D9: Reaction data and initial rates of benzoin formation, catalysed by triazolium salt (138) (12 mM) in 0.16 M triethylamine-buffered methanol (66% f_B) at 50 °C.

[PhCHO]$_0$, M	time, s	A_{PhCHO}	$A_{benzoin}$	[PhCHO], M	[benzoin], M	v_0, M s^{-1} [a]
	0	1	0	0.160	0.00000	
	1800	2680891	19840	0.158	0.00111	
	3600	1947288	28708	0.156	0.00219	
0.16	5400	2042586	43907	0.154	0.00315	5.52×10^{-7}
	7200	2631656	73571	0.152	0.00405	
	9000	2221867	77866	0.150	0.00501	
	0	1	0	0.320	0.00000	
	1800	4833999	30115	0.316	0.00188	
	3600	4858884	59156	0.313	0.00363	
0.32	5400	5213438	96473	0.309	0.00545	9.72×10^{-7}
	7200	4842297	118150	0.306	0.00711	
	9000	4122680	125108	0.303	0.00874	
	0	1	0	0.640	0.00000	
	1800	3832244	16138	0.635	0.00255	
	3600	3987862	32766	0.630	0.00493	
0.64	5400	2766674	33065	0.626	0.00712	1.27×10^{-6}
	7200	3642867	57240	0.621	0.00930	
	9000	3453551	67586	0.617	0.01150	
	0	1	0	0.960	0.00000	
	1800	6025407	18747	0.954	0.00283	
	3600	4941113	28449	0.950	0.00521	
0.96	5400	4282378	36035	0.945	0.00757	1.36×10^{-6}
	7200	5581296	62972	0.940	0.01010	
	9000	5544883	76438	0.935	0.01228	
	0	1	0	1.280	0.00000	
	1800	2019804	4519	1.275	0.00272	
	3600	1872623	8013	1.270	0.00517	
1.28	5400	2296351	14582	1.265	0.00765	1.36×10^{-6}
	7200	1873672	15387	1.260	0.00986	
	9000	1851301	19036	1.255	0.01229	
	0	1	0	1.440	0.00000	
	1800	1588434	3050	1.435	0.00262	
	3600	2036267	7782	1.430	0.00520	
1.44	5400	2329154	12717	1.425	0.00741	1.35×10^{-6}
	7200	2307036	16657	1.420	0.00977	
	0	1	0	1.600	0.00000	
	1800	2272970	4314	1.594	0.00288	
	3600	1780993	6087	1.590	0.00517	
1.60	5400	2579114	12678	1.585	0.00742	1.35×10^{-6}
	7200	1550639	10152	1.580	0.00985	

(a) The initial rate v_0 was obtained from the slope of the plot of [benzoin] against time in Figure D4.

Figure D4: **Plots of benzoin concentration against time for the triazolium (138) (12 mM) catalysed benzoin condensation, at initial benzaldehyde concentrations 0.16 M, 0.32 M, 0.64 M, 0.96 M, 1.28 M, 1.44 M, 1.60 M.**
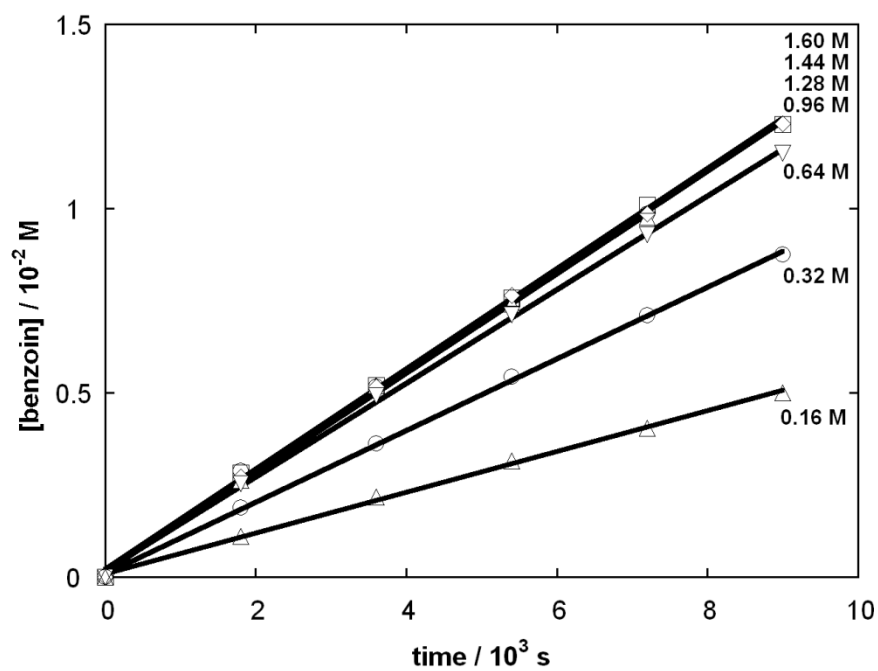
Table D10: Reaction data and initial rates of benzoin formation, catalysed by triazolium salt (137) (12 mM) in 0.16 M triethylamine-buffered methanol (66% f_B) at 50 °C.

[PhCHO]$_0$, M	time, s	A_{PhCHO}	$A_{benzoin}$	[PhCHO], M	[benzoin], M	v_0, M s^{-1} [a]
0.16	0	1	0	0.160	0.00000	
	600	1842049	12248	0.158	0.00100	
	1320	1794659	26186	0.156	0.00216	
	1800	2394353	49407	0.154	0.00303	
	2400	1862779	50340	0.152	0.00392	1.51×10^{-6}
	2700	2124108	63908	0.151	0.00434	
	3000	2040893	67400	0.151	0.00473	
	3600	2008119	77705	0.149	0.00549	
	4200	1874149	84352	0.147	0.00632	
0.32	0	1	0	0.320	0.00000	
	480	2237371	12385	0.317	0.00167	
	1200	2176023	30375	0.312	0.00414	
	1680	2448471	49036	0.308	0.00588	
	2280	1996949	52946	0.305	0.00769	3.19×10^{-6}
	2580	2235973	67022	0.303	0.00864	
	2880	2294206	76903	0.301	0.00960	
	3480	1744284	69548	0.297	0.01129	
	4080	2376254	109455	0.294	0.01291	
0.48	0	1	0	0.480	0.00000	
	360	3733822	13916	0.477	0.00169	
	1080	3645202	46981	0.468	0.00575	
	2160	3574105	85848	0.459	0.01050	
	2460	3029235	81677	0.457	0.01172	4.53×10^{-6}
	2760	3046875	90571	0.454	0.01286	
	3360	3435358	124867	0.449	0.01554	
	3960	3041864	128363	0.444	0.01786	
0.80	0	1	0	0.800	0.00000	
	300	1387235	3582	0.796	0.00196	
	780	1322034	9861	0.789	0.00560	
	1200	1247650	14317	0.783	0.00856	
	1500	1630932	22369	0.780	0.01018	6.36×10^{-6}
	1920	1806764	31312	0.774	0.01278	
	2400	1529417	32669	0.769	0.01564	
	2700	1291581	30701	0.765	0.01733	
	3000	1652016	43667	0.762	0.01917	
1.12	0	1	0	1.120	0.00000	
	300	1680081	3616	1.115	0.00229	
	780	1909936	10907	1.108	0.00603	
	1200	2237495	20498	1.101	0.00960	
	1500	1914280	21892	1.096	0.01194	7.49×10^{-6}
	1920	1945115	27198	1.091	0.01453	
	2400	1934441	33990	1.084	0.01814	
	2700	2206276	43365	1.080	0.02021	
	3000	2316466	51273	1.075	0.02265	
1.28	0	1	0	1.280	0.00000	
	600	2039677	8191	1.270	0.00486	
	900	2111366	13053	1.265	0.00745	
	1200	2779772	22053	1.261	0.00953	
	1500	2362474	24224	1.255	0.01226	7.93×10^{-6}
	1800	3048339	36990	1.251	0.01446	
	2100	2601376	35738	1.247	0.01632	
	2400	2369431	38744	1.241	0.01933	

	0	1	0	1.440	0.00000
	300	2257772	5158	1.434	0.00312
	600	2149035	8064	1.430	0.00511
	900	2865928	15939	1.425	0.00755
1.44	1200	3330382	25693	1.419	0.01043	8.19×10^{-6}
	1500	2969281	27702	1.415	0.01257
	1800	2894106	31543	1.411	0.01464
	2100	2935356	39180	1.404	0.01785
	2400	3403768	50534	1.400	0.01980
	0	1	0	1.600	0.00000
	300	2908400	4932	1.595	0.00258
	600	3102320	10749	1.590	0.00525
	900	3147457	16269	1.584	0.00780
1.60	1200	2611893	18226	1.579	0.01049	8.36×10^{-6}
	1500	3358514	29606	1.574	0.01321
	1800	3592518	37208	1.569	0.01548
	2100	3698030	43900	1.565	0.01769
	2400	3368442	44881	1.560	0.01980

(a) The initial rate v_0 was obtained from the slope of the plot of [benzoin] against time in Figure D5.

Figure D5: **Plots of benzoin concentration against time for the triazolium (137) (12 mM) catalysed benzoin condensation, at initial benzaldehyde concentrations 0.16 M, 0.32 M, 0.48 M, 0.80 M, 1.12 M, 1.28 M, 1.44 M and 1.60 M.**
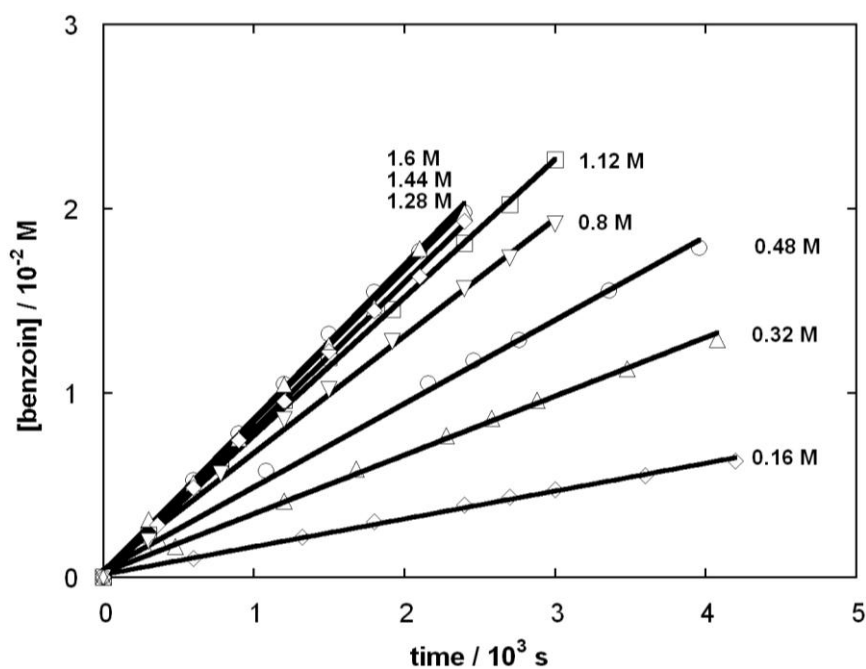
Table D11: **Reaction data and initial rates of benzoin formation, catalysed by triazolium salt (142) (0.6 mM) in 0.16 M triethylamine-buffered methanol (66% f_B) at 50 °C.**

[PhCHO]$_0$, M	time, s	A_{PhCHO}	$A_{benzoin}$	[PhCHO], M	[benzoin], M	v_0, M s^{-1} [a]
	0	1	0	0.160	0.00000	
	90	2694262	13899	0.158	0.00078	
	180	3034047	28860	0.157	0.00142	
	270	2660026	37717	0.156	0.00210	
0.16	360	2972236	56225	0.154	0.00278	7.14×10^{-6}
	450	3050756	71312	0.153	0.00341	
	540	2958669	83416	0.152	0.00408	
	630	3013873	97510	0.151	0.00464	
	720	3050184	108641	0.150	0.00508	
	0	1	0	0.320	0.00000	
	90	3138858	7900	0.318	0.00076	
	180	1986110	10860	0.317	0.00165	
	270	4077826	35128	0.315	0.00258	
0.32	360	3475726	41141	0.313	0.00353	9.31×10^{-6}
	450	4447142	63248	0.312	0.00422	
	540	4509076	78900	0.310	0.00516	
	630	4832027	96184	0.308	0.00584	
	720	4328910	97656	0.307	0.00659	
	0	1	0	0.480	0.00000	
	60	3232968	4222	0.479	0.00060	
	120	3844589	11883	0.477	0.00140	
	180	3882284	18916	0.476	0.00221	
	270	3214124	22587	0.474	0.00317	
0.48	360	2929864	27059	0.472	0.00415	1.11×10^{-5}
	450	3923017	44999	0.470	0.00513	
	540	3429502	47897	0.468	0.00622	
	630	3720130	60749	0.466	0.00724	
	720	3894930	68626	0.464	0.00779	
	0	1	0	0.640	0.00000	
	60	4064085	4794	0.639	0.00072	
	120	3762780	10169	0.637	0.00164	
	180	4232824	17709	0.635	0.00253	
	270	3978316	23312	0.633	0.00353	
0.64	360	4685185	36191	0.631	0.00464	1.21×10^{-5}
	450	4380894	41849	0.629	0.00572	
	540	3647333	41383	0.626	0.00677	
	630	4823703	62419	0.625	0.00770	
	720	5221807	76744	0.623	0.00871	
	0	1	0	0.960	0.00000	
	60	2057013	2612	0.958	0.00116	
	120	2339607	4830	0.956	0.00188	
	180	1642880	4758	0.955	0.00263	
	240	1914086	7225	0.953	0.00343	
0.96	300	2655586	12969	0.951	0.00442	1.40×10^{-8}
	360	1752575	9742	0.950	0.00503	
	420	2076524	14249	0.948	0.00619	
	480	1749811	13254	0.946	0.00683	
	540	2494269	21331	0.945	0.00769	

	0	1	0	1.280	0.00000	
	60	3219382	1976	1.279	0.00075	
	120	2671822	3521	1.277	0.00160	
	180	2749713	5285	1.275	0.00233	
	240	2657801	7464	1.273	0.00341	
1.28	300	2908197	9812	1.272	0.00409	1.40×10^{-5}
	360	2915845	11781	1.270	0.00489	
	420	2911768	14239	1.268	0.00591	
	480	2578013	13491	1.267	0.00632	
	540	2989405	18722	1.265	0.00754	
	600	2879830	20193	1.263	0.00844	
	0	1	0	1.440	0.00000	
	60	3194026	2487	1.438	0.00107	
	120	3579256	5066	1.436	0.00194	
	180	3085535	6227	1.434	0.00276	
	240	3362287	8613	1.433	0.00350	
1.44	300	2602394	8455	1.431	0.00443	1.45×10^{-5}
	360	3619134	14233	1.429	0.00535	
	420	3001725	13565	1.428	0.00614	
	480	3145559	16546	1.426	0.00714	
	540	3579632	20784	1.424	0.00788	
	600	3311412	21542	1.422	0.00881	
	0	1	0	1.600	0.00000	
	60	3376952	2384	1.598	0.00107	
	120	3842313	4293	1.597	0.00170	
	180	3141597	5981	1.594	0.00289	
	240	3423092	8157	1.593	0.00361	
1.60	300	3150498	9931	1.590	0.00477	1.51×10^{-5}
	420	3491826	14511	1.587	0.00628	
	480	3108643	15074	1.585	0.00732	
	540	4091982	22536	1.583	0.00831	
	600	3757449	22774	1.582	0.00913	

(a) The initial rate v_0 was obtained from the slope of the plot of [benzoin] against time in Figure D6.

Figure D6: **Plots of benzoin concentration against time for the triazolium (142) (0.6 mM) catalysed benzoin condensation, at initial benzaldehyde concentrations 0.16 M, 0.32 M, 0.48 M, 0.64 M, 0.96 M, 1.28 M, 1.44 M and 1.60 M.**
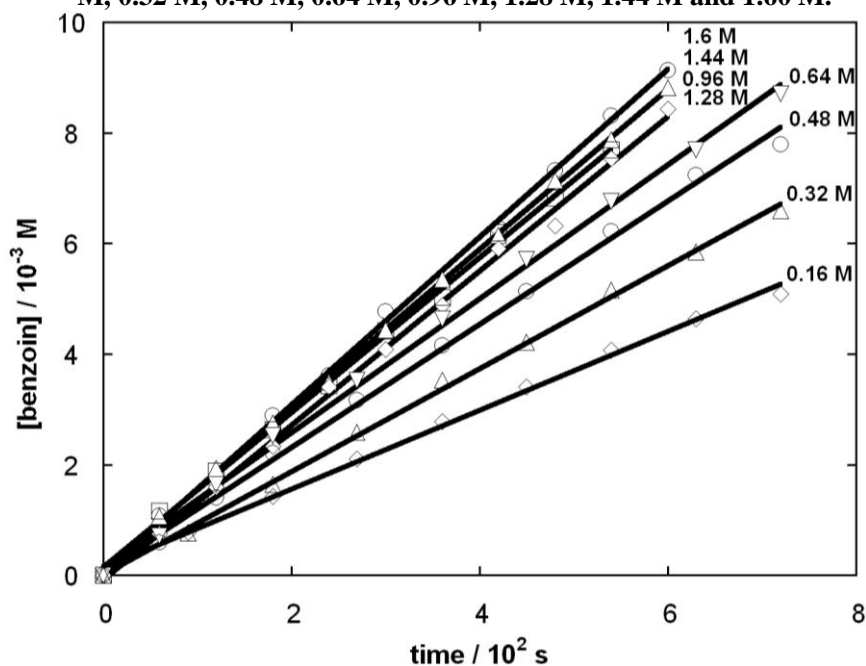
References

1   H. S. Harned and R. A. Robinson, *Trans. Faraday Soc.*, 1940, **36**. 937.
2   V. Gold and S. Grist, *J. Chem. Soc., Perkin Trans. 2*, 1972, 89.
3   U. Kaatze, *J. Chem. Eng. Data*, 1989, **34**, 371.